Reliability analysis and optimal design under uncertainty - Focus on adaptive surrogate-based approaches

Jean-Marc Bourinet

UNIVERSITÉ CLERMONT AUVERGNE

MÉMOIRE D'HABILITATION À DIRIGER DES RECHERCHES

Reliability analysis and optimal design under uncertainty – Focus on adaptive surrogate-based approaches

Jean-Marc Bourinet

SIGMA Clermont, Institut Pascal, UMR CNRS 6602

présentée et soutenue publiquement le 29 janvier 2018 devant le jury composé de :

Rapporteurs :

Armen Der Kiureghian	Professeur émérite, UC Berkeley, USA
Rodolphe Le Riche	Directeur de recherche CNRS, Ecole des Mines de Saint Etienne
Fabrice Poirion	Maître de Recherche, ONERA Chatillon

Examinateurs :

Michel Fogli	Professeur émérite, Polytech Clermont-Ferrand
Bruno Sudret	Professeur, ETH Zurich, Suisse

Président et examinateur :

Maurice Lemaire	Professeur émérite, SIGMA Clermont

Acknowledgments

This report gives an overview of my research work carried out since my move to academia in 2004. I would like to thank here several people to whom I am indebted for their support and contributions to my academic career.

I would like first to express my deep gratitude to Maurice Lemaire for his important role in my career transition. I met Maurice in the late nineties when reliability was such an exotic word that I could not even believe that one day I would make this topic the main line of my research. Thank you, Maurice, for offering me this chance to work in such an exciting field, and making my career transition as smooth as possible at IFMA. I owe you so much. Your passion for structural reliability, your scientific rigor, your openness to new ideas and new challenges and your motivation to pass on this passion to others, including students, have been great sources of inspiration for me.

In my quest to deepen my understanding of structural reliability, I followed Maurice's suggestion and contacted Armen Der Kiureghian for a sabbatical stay under his guidance, while I was still working as an engineer for DGA. Thank you, Armen, for offering me the opportunity to work with you at UC Berkeley during 2001 and to have such a rewarding time there. Your enthusiasm to share your experience and wealth of knowledge, your clarity of thinking and your drive to attain perfection have had a deep impact on my ways of thinking and working; they are and always will be perfect models to reach. I consider myself so fortunate to have been able to work with you.

I would like to thank the members of my HDR committee, Armen Der Kiureghian, Rodolphe Le Riche and Fabrice Poirion, for spending their precious time to assess my (quite long) manuscript and for participating in the final oral examination of my work.

My research works would have not been possible without the collaboration of several other researchers, who have had an important role in my academic achievements. I would like to thank Michel Fogli for his collaboration in the scope of the PhD works of Claudine Noirfalise, Attibaud Kouassi and Mathieu Sallin, and more broadly for his invaluable advice, especially on problems involving random processes and fields. My research has also benefited from fruitful exchanges with Bruno Sudret, in the scope of the PhD works of Vincent Dubourg and Maliki Moustapha, and in other contexts. Thank you Bruno for the enriching discussions, the innovative ideas and the high level scientific guidance you provided in the works we co-supervised. I always enjoyed our productive collaborations and I look forward to initiating new ones in the future.

My research works owes much to the contribution of the PhD students I have co-supervised in the past or of those I am still co-supervising, namely and in order of appearance in my academic career: Lukáš, François, Claudine, Cécile, Vincent, Maliki, Attibaud, Mathieu and Vincent. This report gives a broad overview of the PhD works defended so far. I would like to thank each of you for the always stimulating exchanges and your efforts to explore new ideas.

I have also had the opportunity to collaborate with some colleagues from abroad. I would like first to thank Carsten Proppe from the Karlsruhe Institute of Technology for the collaborations we initiated, and especially the nice summer schools we co-organized. For all those who attended the last one, you probably remember it well. Be patient, the next one is expected to be held in 2019! Thank you also to Samy Missoum and Tom Lahmer for their collaborations through the short-term visits of some of their respective PhD students: Anirban Basudhar and Sylvain Lacaze from the University of Arizona and Maria Steiner from Bauhaus-Universität Weimar. Thank you Anirban, Sylvain and Maria for the great jobs you performed here in Clermont Ferrand.

My research works benefited from several financial supports, which I would like to gratefully acknowledge. My thanks go to Maurice Pendola and Thierry Yalamas from Phimeca Engineering, for the long term and fruitful collaboration we established. I would like also to thank DGA, DCNS (Mikaël Cazuguel) and NEXTER Systems (Bruno Colin).

Several other people have contributed more or less directly to my research or my choices along my career. Hopefully without forgetting a single person I would like to thank :

- My former colleagues at DGA who introduced me to the fields of buckling and damage tolerance. Bernard Auroire was the first to advise me to discover structural reliability. Bernard, I also much appreciated your willingness to always explore new ideas and to push me to carry out in-depth analyses. Thank you also to Alexandre Lahousse, Jean-Fred Bègue and Damien Théret for sharing their experiences in damage tolerance.

- The following academic researchers: Bruno Cochelin (for his precious help and advice about the asymptotic numerical method), Anthony Gravouil (for passing on to us his XFEM code and for helping us in its usage), Alain Combescure (for the great source of inspiration in all our buckling analyses).

- Pierre Bernard for his insightful advice in the scope of Cécile's PhD work.

- My close colleagues in the UQ group, including Nicolas, Cécile, Pierre and David, for the fruitful scientific exchanges and all the good moments spent together and, more broadly, all my other colleagues at SIGMA Clermont and Institut Pascal.

- Frédéric Dedieu for the installation and management of the computational resources and Christophe Dumonet for his help in the construction and maintenance of FERUM website.

- Marion Lucazeau and Jacqueline Madebène for facilitating the treatment of all the necessary administrative tasks related to my research activities.

- David Turner for his meticulous proofreading of the English in this report.

Lastly and on a more personal note, my greatest gratitude goes to you, Isabelle, for your patience and the many sacrifices you endured during the time needed to write this report. I promise you, Eliott and Jade, to spend more of my time with you from now on (the swing to install was relegated to the garage for months but now it is standing upright on the lawn). Finally, I would also like to express my deep gratitude to my parents who transmitted me the value of learning when I was growing up.

Contents

Introduction

Foreword

This document is written as a requirement of the Habilitation à Diriger des Recherches (HDR), which allows researchers to supervise PhD works as principal advisors in France. It summarizes my research activities since 2004, when I joined SIGMA Clermont (formerly IFMA) as an assistant professor. My academic achievements are listed in Appendix B and the list of my publications is given in Appendix C. My interest in uncertainty quantification came after my PhD degree in structural mechanics, which was obtained in 1996 at École Centrale de Nantes. I discovered this new field when I was serving as a structural engineer for the Armaments Procurement Agency of the French Ministry of Defense (DGA) from 1997 to 2004, through fruitful exchanges with Prof. Maurice Lemaire at IFMA, who introduced me more specifically to structural reliability. The catalyst for my academic career was my research period at UC Berkeley in 2001 under the supervision of Prof. Armen Der Kiureghian, who encouraged me to further explore this field which was new to me. My enthusiasm for reliability assessment, extended later to the wider scope of uncertainty quantification, has continued to grow since then.

Context

The design of optimal and reliable systems is an objective which is pursued in several fields of engineering. Optimality is expressed in terms of a system cost which needs to be minimized, including the partial costs involved at each instant of the system's life, e.g. construction costs, maintenance costs and costs resulting from potential failures. In addition, the system is expected to satisfy performance requirements considering all the criteria which could cause it to fail. In a probabilistic framework this performance is assessed through a failure probability w.r.t. such criteria, accounting for all sources of uncertainty in the problem inputs. The tradeoff to make between optimality and safety constitutes nowadays one the greatest challenges to solve in the engineering field. The set of works presented in this document brings contributions to the *efficient* solving of the above-defined problem, by addressing either the calculation of the system failure probability (problem referred to as *reliability assessment*) or the finding of its optimal design under constraints expressed in terms of this failure probability (problem referred to as *reliability-based design optimization*).

The probabilistic model has a prominent role in the analysis. The type of model, along with its parameters, must be carefully selected, since it greatly impacts the results of the uncertainty propagation analysis. If statistical data concerning the inputs are available in sufficient quantity, a trustworthy probabilistic model can be identified and used in the analysis. Such a situation is considered in works presented in Chapter III in the specific context of buckling and crack propagation, by using data either available in the literature (Virkler data set for crack extension, imperfection data bank for shape im-

perfections in cylindrical shells) or provided by industrial partners (load sequences in a fleet of fighter aircraft). As detailed in this report, the choice of a given probabilistic model may have consequences in terms of applicable methods for reliability assessment and the accuracy of the obtained results.

Another important aspect of the analysis is the computational time required for the evaluation of the failure criteria. In all fields of engineering highly accurate numerical solutions can be obtained, most often by means of costly-to-evaluate methods, e.g. finite element solutions in structural mechanics. The computational burden associated with the use of such numerical models needs to be addressed for the efficient solving of uncertainty propagation problems. The several calls to this model, necessary e.g. in a crude Monte Carlo approach, are most often incompatible with the available computational resources. As a consequence, we need to consider approaches which require as few calls to the costly-to-evaluate model as possible. Surrogate models, as investigated in Chapter II, are one solution which has become increasingly popular over the years, with limits in terms of input space dimensionality and model complexity that can be handled in current approaches. In this report we focus on support vector machine and kriging surrogate models, which have been used in adaptive methods for reliability assessment and design under uncertainty as efficient alternatives to other, more expensive, techniques.

Outline

The document is organized in three chapters as described below, with highlights on my contributions.

Chapter I concerns methods which are well established in reliability. My objective has been to make a clear and almost self-contained presentation of the main available methods with unified notations. All these methods were applied in the works I supervised, which are described later in Chapter II and mainly in Chapter III. My contributions to these methods concern sensitivities of failure probability w.r.t. distribution parameters, exact sensitivities in FORM with the Nataf model, including those regarding correlation, and sensitivities in the standard normal space with subset simulation. I am also providing the reader with a comparison between subset simulation and the cross-entropy method applied to variates of the standard normal space on a set of selected examples, which illustrates the performances of each method.

Chapter II gives a presentation of kernel-based techniques used as surrogates of costly-to-evaluate models involved in failure criteria. These surrogate models are used for the purpose of reliability assessment and reliability-based design optimization in adaptive approaches. This type of approach starts from an initial set of evaluated points in the input space and then sequentially selects a few new points to evaluate, with updates to the surrogate model until a sufficient accuracy is reached. Two surrogate techniques are presented in this document: support vector machines (SVMs) and kriging, whose juxtaposition will hopefully help the reader in understanding the connections between them, in addition to the well-known and shared concept of kernel.

- In Chapter II SVMs are presented for the usual linear case, both in classification and regression. The formulations are then extended to nonlinear models by means of kernels. The settings of SVMs are placed in the framework of regularization, which clearly states the target objective for the accuracy of the constructed models: a tradeoff between the simplest model possible but close enough to the available data. The mathematical formalism has been kept minimal, albeit hopefully sufficiently rigorous, in order to express the key ideas without too heavy notations and mathematical proofs. I am also addressing the tuning of SVM models, which is, in my opinion, the key to accurate approximate models. This tuning can be achieved by the minimization of approximations of the leave-one-out errors available for SVM both in classification and regression. SVMs in classification were explored in the PhD work of Deheeger (2008) in an adaptive approach for reliability assessment, as described in this chapter (referred to as ^{2}SMART method). I have further explored adaptive surrogates based on

SVMs used in regression, again for reliability assessment (referred to as ASVR method). In this latter method the minimization of the leave-one-out errors of the surrogates is performed by stochastic optimization. This chapter gives the main algorithms and a comparison of results between the ^{2}SMART and ASVR methods, also including those obtained using other methods.

- The main elements of kriging are then recalled in the second part of Chapter II, including training on noisy data with the so-called nugget effect. Noisy kriging allows us to make the connection between kriging and SVMs. It is shown that the kriging mean predictor and the least squares support vector regressor are equivalent in their formulations. The chapter is concluded by a presentation of the RBDO approach proposed in the PhD work of Dubourg (2011) and the quantile-based RBDO approach proposed in the PhD work of Moustapha (2016), both based on sequential constructions of kriging surrogate models in the so-called augmented reliability space. The two methods take advantage of the kriging variance of the constructed models. The RBDO approach of Dubourg is illustrated in Chapter III in the context of the optimal design of a submarine pressure hull.

Chapter III compiles some results obtained in two specific fields of structural mechanics, namely buckling and crack propagation, which are known for their uncertain character as observed in experimental works. Several types of challenge were addressed in the selected problems, e.g. identification of a probabilistic model from statistical data; reliability assessment not so easy to carry out due to the reliability problem formulation or intricacy of the limit-state surface; high computational cost of the numerical model involved in the analysis.

Regarding the buckling of shells with shape imperfections, the PhD works of Noirfalise (2009) and Dubourg (2011) were both based on nonlinear finite element solutions obtained by means of the asymptotic numerical method, as an alternative to more conventional incremental-iterative methods.

- In the presented work of Noirfalise, the purpose is to model the shape imperfections in a cylindrical shell by a random field considered as the input of a reliability problem. The two proposed models, based on a Fourier representation with random coefficients and a Karhunen-Loève series expansion, are identified from real data extracted from the imperfection data bank of Delft University. Subset simulation is applied for failure probability estimation.

- The first problem addressed by Dubourg aims to estimate the failure probability of a shell roof subjected to buckling with random shape imperfections and space-variant material/thickness properties. The studied reliability problem with random fields as inputs was solved using subset simulation and FORM. This latter method, applicable here, revealed the existence of multiple most probable failure points of equal importance.

- In the second problem studied by Dubourg the objective is to find the optimal design of a single bay reference structure representative of a submarine pressure hull under a reliability constraint. This RBDO problem is efficiently solved using the proposed adaptive method, based on kriging surrogate models and presented in Chapter II.

Random crack propagation was studied in scope of the PhD works of Nešpůrek (2010) and Mattrand (2011). Two selected problems are presented in Chapter III:

- The first problem investigates the randomization of the Paris-Erdogan crack growth law under constant-amplitude fatigue loading. The reliability problems are analyzed using FORM and some of the results are compared with the experimental data of Virkler et al. The problem is found to be quite sensitive to the correlation between the two parameters C and m of the crack growth law, depending on the random model which is selected as the input. The reliability problem is additionally found to be highly sensitive to the small errors between the crack extensions given by the model and those found experimentally, which has been the source of a controversial interpretation in the literature.

- In the second presented problem, investigated by Mattrand, the focus is put on crack propagation under random loading. The PREFFAS crack closure model is used in this work, in order to account for load interactions during crack growth, such as retardations and accelerations. Markov chains and hidden Markov models are proposed as candidates for the modeling of random loads recorded in-flight in a fleet of fighter aircraft. After their identification these models are used for the purpose of reliability assessment. The formulated problems differ from those conventionally solved in structural reliability, due the use of such Markov models. Results are obtained by means of the cross-entropy method as an efficient alternative to a crude Monte Carlo approach.

I

Rare-event probability estimation

Overview: *This chapter presents the main techniques used to estimate the probabilities of rare failure events and their sensitivities. The first class of methods is the so-called approximation methods (FORM and SORM), which are well known in structural reliability. FORM was applied in several PhD works I co-supervised with Profs. Lemaire, Fogli and Sudret (Noirfalise, 2009; Nešpůrek, 2010; Dubourg, 2011; Kouassi, 2017). Simulation methods are introduced next, with crude Monte Carlo presented first. For better efficiency in the context of low failure probabilities, several techniques are available, among which subset simulation and importance sampling. Subset simulation was applied in all the works I co-supervised except the one Nešpůrek (2010) that was carried out before this method was brought to my attention by Deheeger. This method was applied either directly to the physical model involved in the failure criterion or to a surrogate of this model such as developed in Chapter II. A specific form of importance sampling known as the cross-entropy method is also presented. This technique was used by Mattrand (2011) in the specific context of Markov models, as described in Chapter III. The chapter concludes with a section concerning the failure probability sensitivities* w.r.t. *random inputs and distribution parameters.*

Contributions: *This chapter presents all the methods with unified notations. I implemented all the presented methods in the open-source code FERUM (Bourinet et al., 2009) under Matlab, starting from the basis of this code developed at UCB Berkeley until 2003 (Der Kiureghian et al., 2006). I contributed to the computation of the failure probability sensitivities* w.r.t. *distribution parameters in the context of FORM with the Nataf transformation (Bourinet, 2017a; Bourinet, 2017a), including sensitivities to correlation, see Section I–4.2.2. The computation of these sensitivities is part of the current release of FERUM. Sensitivities expressed in the standard normal space* w.r.t. *means and standard deviations of the associated standard normal variates are proposed in Section I–4.3.3, and this is a new idea to the best of my knowledge. Another contribution is the fair comparison made between subset simulation and the cross-entropy method applied in the standard normal space, see Section I–3.4.*

Credits: *This chapter has excerpts from the paper of Bourinet and Lemaire (2008) and the book chapter of Bourinet (2017a) in Section I–4.2.2.*

I–1 Introduction

The scope of this chapter will be restricted to *time-invariant* reliability problems as defined in the structural reliability literature (see, e.g., Ditlevsen and Madsen, 2007; Lemaire et al., 2010) a.k.a. *static* simulation problems or models by some authors (see, e.g., Homem-de-Mello and Rubinstein, 2002; Cancela et al., 2009), in which time is not an explicit variable.

We consider a finite set of uncertain scalar parameters modeled by a random vector $\mathbf{X} = (X_1, \ldots, X_n)^{\mathrm{T}}$ defined by its joint continuous probability density function (PDF) $f_{\mathbf{X}} : \mathbb{R}^n \to \mathbb{R}_{\geq 0}, \mathbf{x} \mapsto f_{\mathbf{X}}(\mathbf{x})$, whose support[1] $\mathcal{D}_{f_{\mathbf{X}}}$ is denoted by $\mathcal{X}$ and where $\mathbf{x} = (x_1, \ldots, x_n)^{\mathrm{T}}$.

We assume that the performance of a given physical system is defined by a deterministic scalar function $g : \mathcal{D}_g \subseteq \mathbb{R}^n \to \mathbb{R}, \mathbf{x} \mapsto g(\mathbf{x})$, known as the *limit-state function* (LSF) or *performance function*, where $\mathcal{D}_g$ is the domain of definition of g, assumed to verify $\mathcal{D}_g \supseteq \mathcal{D}_{f_{\mathbf{X}}} = \mathcal{X}$. As an illustration, if we are interested in the exceedance of a given threshold level y_{th} by some response $s(\mathbf{x})$ of the system, the LSF takes the form $g(\mathbf{x}) = y_{\mathrm{th}} - s(\mathbf{x})$ for any given $\mathbf{x} \in \mathcal{D}_g$.

The hypersurface $\mathcal{F}_{\mathbf{x}}^0 = \{\mathbf{x} \in \mathcal{D}_g : g(\mathbf{x}) = 0\}$ is called the *limit-state surface* (LSS). It divides $\mathcal{D}_g$ into a *failure domain* conventionally defined as $\mathcal{F}_{\mathbf{x}} = \{\mathbf{x} \in \mathcal{D}_g : g(\mathbf{x}) \leq 0\}$ and a *safe domain* $\overline{\mathcal{F}}_{\mathbf{x}}$ defined as the complement of $\mathcal{F}_{\mathbf{x}}$ in $\mathcal{D}_g$, see Figure I.1b.

[1] The support $\mathcal{D}_{f_{\mathbf{X}}}$ of a PDF $f_{\mathbf{X}}$ is the set of points over which this PDF is not equal to zero: $\mathcal{D}_{f_{\mathbf{X}}} = \{\mathbf{x} : f_{\mathbf{X}}(\mathbf{x}) > 0\}$.

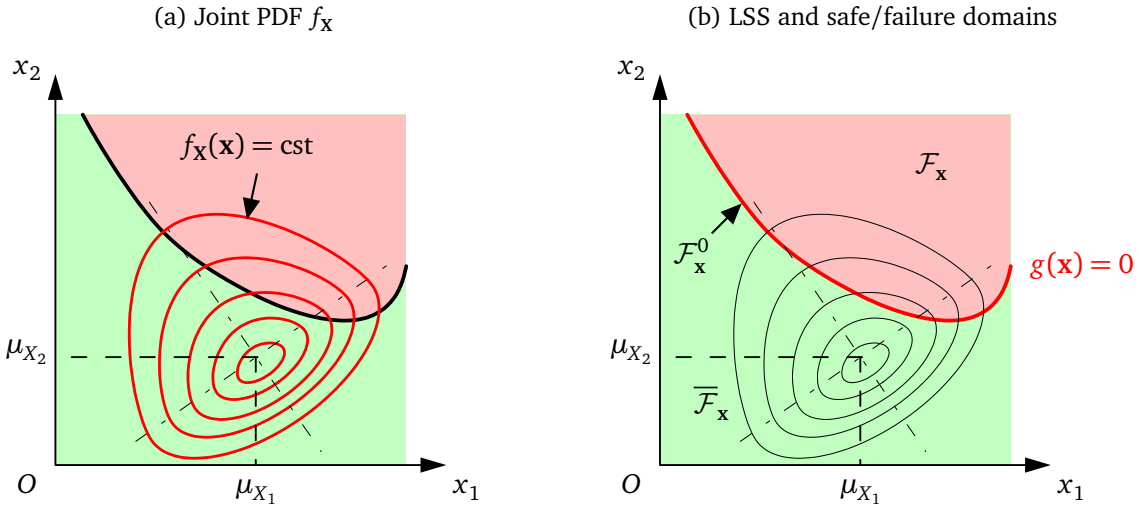

Figure I.1 – Joint PDF $f_{\mathbf{X}}$, limit-state surface $\mathcal{F}^0_{\mathbf{x}}$, safe domain $\overline{\mathcal{F}}_{\mathbf{x}}$ and failure domain $\mathcal{F}_{\mathbf{x}}$.

It is important to point out that the LSF g can only be evaluated pointwise and, as a consequence, the LSS $\mathcal{F}^0_{\mathbf{x}}$ cannot be explicitly defined. The LSF g will be assumed to be expensive to evaluate for any realization $\mathbf{x} \in \mathcal{X}$ of $\mathbf{X}$. Each evaluation of g may require the solution of a large system of equations, e.g. finite element models in structural mechanics. The formulation is restricted here to a single function g but this function may represent a combination of several failure criteria in more general settings, such as studied in system reliability (union or intersection of failure events, or any more general systems based e.g. on the union of minimal cutsets).

The probability p_{f} that the system fails w.r.t. the above defined LSF g is given by the following n-fold integral:

$$p_{\mathrm{f}} = \mathbb{P}(E) = \int_{g(\mathbf{x}) \leq 0} f_{\mathbf{X}}(\mathbf{x})\,\mathrm{d}\mathbf{x} = \int_{\mathcal{X}} \mathbb{1}_{\mathcal{F}_{\mathbf{x}}}(\mathbf{x})\, f_{\mathbf{X}}(\mathbf{x})\,\mathrm{d}\mathbf{x}\,, \tag{I.1}$$

where $E = \{g(\mathbf{X}) \leq 0\}$ is the failure event, $\mathbb{1}_{\mathcal{D}}(\cdot)$ denotes the *indicator function* of domain $\mathcal{D}$ such that $\mathbb{1}_{\mathcal{D}}(\mathbf{x}) = 1$ if $\mathbf{x} \in \mathcal{D}$, $\mathbb{1}_{\mathcal{D}}(\mathbf{x}) = 0$ otherwise, and $\mathrm{d}\mathbf{x} = \mathrm{d}x_1 \ldots \mathrm{d}x_n$.

The *reliability* R of the system is defined as the probability of the complementary event of E: $R = \mathbb{P}\left(\overline{E}\right) = 1 - p_{\mathrm{f}}$. We will assume that the *failure probability* p_{f} is small ($p_{\mathrm{f}} \ll 1$), i.e. that the failure event E is rare. Such a situation is frequent in many domains, where the safety level is required to be high.

I–1.1 Mapping to the multivariate standard normal space

This section addresses two important interrelated points in reliability assessment: could Eq. (I.1) be solved in another space than $\mathcal{X}$ by means of a suitable mapping, to be defined in order to make calculations more tractable (this will enable us to introduce the so-called *standard normal space*) and, if so, how can we practically define this mapping such that the new reliability assessment problem to solve is set up in accordance with the statistical information known about the joint PDF $f_{\mathbf{X}}$. We will assume that both the marginal and conditional CDFs of $\mathbf{X}$ are strictly continuous, i.e. there should not be probability masses associated with any outcome of $\mathbf{X}$.

A central idea of structural reliability is to rewrite the reliability problem defined in Eq. (I.1) in the standard Gaussian context. To do so, a diffeomorphism [2] $T : \mathcal{X} \to \mathbb{R}^n, \mathbf{x} = (x_1, \dots, x_n)^{\mathrm{T}} \mapsto \mathbf{u} = (u_1, \dots, u_n)^{\mathrm{T}} = T(\mathbf{x})$ (referred to as *isoprobabilistic transformation* in the following) is constructed such that the following equalities (in distribution) hold:

$$\mathbf{U} = T(\mathbf{X}) \Leftrightarrow \mathbf{X} = T^{-1}(\mathbf{U}) \,, \tag{I.2}$$

where $\mathbf{U} = (U_1, \dots, U_n)^{\mathrm{T}}$ is a n-dimensional standard Gaussian vector whose joint PDF $\varphi_n(\cdot)$ is given, for any $\mathbf{u} = (u_1, \dots, u_n)^{\mathrm{T}} \in \mathbb{R}^n$, by:

$$\varphi_n(\mathbf{u}) = \frac{1}{(2\pi)^{n/2}} \exp\left(-\frac{\|\mathbf{u}\|^2}{2}\right) , \tag{I.3}$$

where $\|\mathbf{u}\|^2 = \mathbf{u}^{\mathrm{T}}\mathbf{u} = u_1^2 + \cdots + u_n^2$ and $\|\cdot\|$ represents the canonical Euclidean norm on $\mathbb{R}^n$.

In the image space $\mathbb{R}^n$ referred to as *standard normal space*, the LSF is a mapping $G : \mathbb{R}^n \to \mathbb{R}, \mathbf{u} \mapsto G(\mathbf{u})$ such that, for any $\mathbf{u} \in \mathbb{R}^n$:

$$G(\mathbf{u}) = (g \circ T^{-1})(\mathbf{u}) \,. \tag{I.4}$$

The reformulated problem is obtained by performing the change of variable $\mathbf{x} = T(\mathbf{u})$ in Eq. (I.1), which is justified by the fact that T is a diffeomorphism. Its expression writes:

$$p_{\mathrm{f}} = \mathbb{P}(E) = \int_{G(\mathbf{u}) \leq 0} \varphi_n(\mathbf{u}) \, \mathrm{d}\mathbf{u} = \int_{\mathbb{R}^n} \mathbb{1}_{\mathcal{F}_{\mathbf{u}}}(\mathbf{u}) \, \varphi_n(\mathbf{u}) \, \mathrm{d}\mathbf{u} \,, \tag{I.5}$$

where $\mathcal{F}_{\mathbf{u}} = \{\mathbf{u} \in \mathbb{R}^n : G(\mathbf{u}) \leq 0\}$ is the failure domain in the standard normal space and $\mathrm{d}\mathbf{u} = \mathrm{d}u_1 \dots \mathrm{d}u_n$.

This formulation in the standard normal space $\mathbb{R}^n$, also referred to as $\mathbf{u}$-space, presents the following properties, which are exploited by the FORM and SORM approximation methods presented later in Section I–2:

- The $\mathbf{u}$-space is normalized (same standard normal distribution for each component U_i) and rotationally symmetric.
- If we consider a given point P^* in the $\mathbf{u}$-space specified by its coordinates $\mathbf{u}^* = (u_1^*, u_2^*)^{\mathrm{T}}$, the joint PDF φ_n is characterized by an exponential decay with the square of the distance from the origin (i.e. $\|u\|^2$) along the radial direction (see blue cross-section in Figure I.2). An exponential decay also appears in the orthoradial direction when we move away from P^* in the hyperplane $\{\mathbf{u} \in \mathbb{R}^n : \beta - \boldsymbol{\alpha}^{\mathrm{T}}\mathbf{u} = 0\}$ where $\beta = \boldsymbol{\alpha}^{\mathrm{T}}\mathbf{u}^*$ (see red cross-section in Figure I.2).
- The probability in the half-space $\{\mathbf{u} \in \mathbb{R}^n : \beta - \boldsymbol{\alpha}^{\mathrm{T}}\mathbf{u} \leq 0\}$ is equal to $\Phi(-\beta)$ where $\Phi(\cdot)$ is the univariate standard normal CDF.

The transformation T from the physical input space $\mathcal{X}$ to the standard normal space $\mathbb{R}^n$ is constructed in accordance with the level of information that is given about the random vector $\mathbf{X}$. Complete knowledge of the joint PDF $f_{\mathbf{X}}$ is rare, and some simplifying assumptions are often made due to the available amount of statistical data. The marginal distributions of $\mathbf{X}$ are assumed to be known through their PDFs f_{X_i} or CDFs F_{X_i} for $i = 1, \dots, n$. Statistical independence between some or all the X_i-components of $\mathbf{X}$ is often encountered, and this specific case is first presented. The case of known linear correlations between X_i-components is then considered. This latter case is often a practical choice in the case of limited statistical information. More general situations based on other measures of dependence, e.g. defined in terms of a given copula, may be considered. Such models are not addressed within the scope of this report. The transformations corresponding to the following cases are considered in Section I–1.3:

[2] A diffeomorphism is a globally bijective (i.e. surjective and injective, or onto and one-to-one) mapping which is continuously-differentiable and has a continuously-differentiable inverse.

- statistical independence between the X_i-components and knowledge of their marginal distributions (marginal PDFs f_{X_i} or CDFs F_{X_i} for $i = 1, \ldots, n$),
- knowledge of linear correlations between X_i-components in addition to their marginal distributions (marginal PDFs f_{X_i} or CDFs F_{X_i} for $i = 1, \ldots, n$),
- complete knowledge of the joint PDF $f_{\mathbf{X}}$.

These transformations are presented in the context of *copulas*, which constitute a useful and general tool to express the dependence between random inputs. To this end, some basic definitions and important results are given in Section I–1.2.

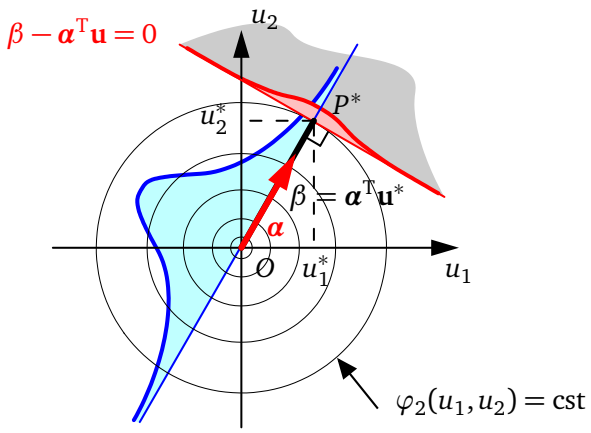

Figure I.2 – Standard normal space.

I–1.2 Copulas and correlation

This section introduces copulas for their practical use in the modeling of dependencies between random inputs. For a detailed presentation of copulas and their mathematical basis, the reader is invited to refer to general textbooks (see, e.g., Nelsen, 1999). From a practical point of view, a copula C is a joint CDF on $[0,1]^n$ with uniformly-distributed marginals (on $[0,1]$). From Sklar's Theorem (Sklar, 1959) recalled hereafter, it clearly appears that a copula represents the complementary information needed to define the joint CDF of a random vector $\mathbf{X}$ in addition to the information given by its marginals (here marginal CDFs F_{X_i}).

Theorem I–1.1 (Sklar's Theorem) *Let $F_{\mathbf{X}}$ be a n-dimensional joint CDF with given marginal CDF F_{X_i} for $i = 1, \ldots, n$. Then there exists a n-dimensional copula C such that, for all $\mathbf{x} = (x_1, \ldots, x_n)^{\mathrm{T}} \in [-\infty, +\infty]^n$:*

$$F_{\mathbf{X}}(\mathbf{x}) = F_{\mathbf{X}}(x_1, \ldots, x_n) = C\left(F_{X_1}(x_1), \ldots, F_{X_n}(x_n)\right) . \tag{I.6}$$

In addition, if the marginal CDFs $F_{X_1}, \ldots, F_{X_n}$ are continuous, then C is unique.

As a corollary of Sklar's Theorem, if we consider a given n-dimensional joint CDF $F_{\mathbf{X}}$ with continuous marginal CDFs, we can express the copula C as follows, for any $\mathbf{u} = (u_1, \ldots, u_n)^{\mathrm{T}} \in [0,1]^n$:

$$C(u_1, \ldots, u_n) = F_{\mathbf{X}}\left(F_{X_1}^{-1}(u_1), \ldots, F_{X_n}^{-1}(u_n)\right) , \tag{I.7}$$

where $F_{X_i}^{-1}$ denotes the inverse of the marginal CDF F_{X_i} for $i = 1, \ldots, n$.

From Sklar's Theorem, it is also possible to express the joint PDF $f_{\mathbf{X}}$ for a given copula C, knowing the marginal PDFs f_{X_i} of $\mathbf{X}$ for $i = 1, \ldots, n$:

$$f_{\mathbf{X}}(\mathbf{x}) = f_{\mathbf{X}}(x_1, \ldots, x_n) = c\left(F_{X_1}(x_1), \ldots, F_{X_n}(x_n)\right) \prod_{i=1}^{n} f_{X_i}(x_i) \ , \tag{I.8}$$

where $c(u_1, \ldots, u_n) = \dfrac{\partial^n C(u_1, \ldots, u_n)}{\partial u_1 \ldots \partial u_n}$ is the density of copula C.

Several copulas are available for modeling dependencies, e.g. normal, Student, Frank, Clayton and Gumbel, among others. Only the definitions of the independent and normal copulas are given in this report, since they are used in the construction of the isoprobabilistic transformation T in Section I–1.3. We also recall a few important results concerning copulas (Lebrun and Dutfoy, 2009b, p. 578). These results are useful in the following for the definition of T.

Definition The n-dimensional *independent copula* is given by:

$$C(u_1, \ldots, u_n) = C_{\text{ind}}(u_1, \ldots, u_n) = \prod_{i=1}^{n} u_i \ . \tag{I.9}$$

Definition Let $\Phi_n(\cdot; \mathbf{R}_0)$ denote the n-dimensional standard normal CDF with linear correlation matrix $\mathbf{R}_0$. Then

$$C(u_1, \ldots, u_n) = C_{\mathcal{N}_n}(u_1, \ldots, u_n; \mathbf{R}_0) = \Phi_n\left(\Phi^{-1}(u_1), \ldots, \Phi^{-1}(u_n); \mathbf{R}_0\right) \tag{I.10}$$

is the n-dimensional *normal copula* (or Gaussian copula) parameterized by the linear correlation matrix $\mathbf{R}_0$.

Theorem I–1.2 *Let $\mathbf{X} = (X_1, \ldots, X_n)^{\mathrm{T}}$ be a vector of continuous random variables with copula C. If $\alpha_1, \ldots, \alpha_n$ are strictly increasing functions on the respective supports of X_i components, then C is also the copula of $(\alpha_1(X_1), \ldots, \alpha_n(X_n))^{\mathrm{T}}$.*

CDF of random vector $(X_1, \ldots, X_k)^{\mathrm{T}}$. Let $\mathbf{X} = (X_1, \ldots, X_n)^{\mathrm{T}}$ be a vector of continuous random variables defined by its copula C and its marginal CDFs F_{X_i} for $i = 1, \ldots, n$. The CDF of the k-dimensional random vector $(X_1, \ldots, X_k)^{\mathrm{T}}$ is given for $k \leq n$ by:

$$F_{X_1, \ldots, X_k}(x_1, \ldots, x_k) = C_{1, \ldots, k}\left(F_{X_1}(x_1), \ldots, F_{X_k}(x_k)\right) \ , \tag{I.11}$$

where $C_{1, \ldots, k}(u_1, \ldots, u_k) = C(u_1, \ldots, u_k, 1, \ldots, 1)$.

Conditional CDF of $X_k | X_1, \ldots, X_{k-1}$. Let $\mathbf{X} = (X_1, \ldots, X_n)^{\mathrm{T}}$ be a vector of continuous random variables defined by its copula C and its marginal CDFs F_{X_i} for $i = 1, \ldots, n$. The CDF of the conditional random variable $X_k | X_1, \ldots, X_{k-1}$ is given for $k \leq n$ by:

$$F_{X_k | X_1, \ldots, X_{k-1}}(x_k | x_1, \ldots, x_{k-1}) = C_{k|1, \ldots, k-1}\left(F_{X_k}(x_k) | F_{X_1}(x_1), \ldots, F_{X_{k-1}}(x_{k-1})\right) \ , \tag{I.12}$$

where $C_{k|1, \ldots, k-1}(u_k | u_1, \ldots, u_{k-1}) = \dfrac{\partial^{k-1} C_{1, \ldots, k}(u_1, \ldots, u_k)}{\partial u_1 \ldots \partial u_{k-1}} \Big/ \dfrac{\partial^{k-1} C_{1, \ldots, k-1}(u_1, \ldots, u_{k-1})}{\partial u_1 \ldots \partial u_{k-1}}$.

In addition to the basics of copula modeling, we present a brief review of some scalar and bivariate measures of dependence (see, e.g., Nelsen, 1999; Lebrun, 2013, for more details, including the definitions of measures of concordance, dependence and association). It is important to stress that dependences defined in terms of copulas are more informative than such scalar measures, and as a consequence we cannot in general define a dependence structure only in terms of these scalar measures.

A first and usual measure used to describe the dependence between two random variables X_i and X_j is *linear correlation* (or Pearson's correlation), defined in terms of the following coefficient:

$$\begin{aligned}\rho_{ij} = \rho(X_i, X_j) &= \frac{\mathrm{Cov}\left[X_i, X_j\right]}{\sqrt{\mathrm{Var}\left[X_i\right]}\sqrt{\mathrm{Var}\left[X_j\right]}} \\ &= \frac{1}{\sqrt{\mathrm{Var}\left[X_i\right]}\sqrt{\mathrm{Var}\left[X_j\right]}} \int_0^1 \int_0^1 \left[C\left(u_i, u_j\right) - u_i u_j\right] \mathrm{d}F_{X_i}^{-1}(u_i)\, \mathrm{d}F_{X_j}^{-1}\left(u_j\right) ,\end{aligned} \tag{I.13}$$

where $\mathrm{Cov}\left[X_i, X_j\right] = \mathbb{E}\left[\left(X_i - \mathbb{E}\left[X_i\right]\right)\left(X_j - \mathbb{E}\left[X_j\right]\right)\right]$ is the covariance between X_i and X_j, and $\mathrm{Var}\left[X_i\right]$, $\mathrm{Var}\left[X_j\right]$ are the respective variances of X_i, X_j (assumed to be finite and nonzero).

From Eq. (I.13), it is found that linear correlation is not a function of the copula only, but also of the marginal CDFs of X. The direct consequence is that linear correlation is not independent of the marginal distributions. This scalar measure is nevertheless well suited to joint normal or elliptical distributions, provided the second moments exist. The dependence structure of more general distributions cannot, however, be represented by such a unique scalar for each pair of inputs, and using linear correlation in such situations could be misleading. Recourse to better-suited scalar measures is recommended for non-elliptical distributions, such as Spearman's rank correlation ρ_S given in Eq. (I.14) and Kendall's τ given in Eq. (I.15), where C denotes the bivariate copula of $\left(X_i, X_j\right)^{\mathrm{T}}$:

$$\rho_S = \rho\left(F_{X_i}(X_i), F_{X_j}\left(X_j\right)\right) = 12 \int_0^1 \int_0^1 \left[C\left(u_i, u_j\right) - u_i u_j\right] \mathrm{d}u_i \mathrm{d}u_j , \tag{I.14}$$

$$\tau = 4 \int_0^1 \int_0^1 C\left(u_i, u_j\right) \mathrm{d}C\left(u_i, u_j\right) . \tag{I.15}$$

I–1.3 Isoprobabilistic transformations

I–1.3.1 Independent random inputs

In this first case, we make the following assumptions about the random vector $\mathbf{X} = (X_1, \ldots, X_n)^{\mathrm{T}}$:

- the n marginal distributions of $\mathbf{X}$ are known through their PDFs f_{X_i} or CDFs F_{X_i} for $i = 1, \ldots, n$,
- the X_i-components of $\mathbf{X}$ are mutually independent.

In order to construct the isoprobabilistic transformation T, each component X_i of $\mathbf{X}$ is first mapped into a uniform random variable V_i on $[0,1]$ using its CDF F_{X_i}. This uniform random variable V_i is then mapped into a standard normal variable U_i using the inverse CDF of the standard normal distribution.

The isoprobabilistic transformation T is therefore defined as the following composed application:

$$\begin{array}{rccccc} T = T_{vu} \circ T_{xv} : & \mathcal{X} & \to & [0,1]^n & \to & \mathbb{R}^n \\ & \mathbf{x} & \mapsto & \mathbf{v} = T_{xv}(\mathbf{x}) & \mapsto & \mathbf{u} = T_{vu}(\mathbf{v}) \end{array} \tag{I.16}$$

where $\mathbf{x} = (x_1, \ldots, x_n)^{\mathrm{T}}$, $\mathbf{v} = (v_1, \ldots, v_n)^{\mathrm{T}}$, $\mathbf{u} = (u_1, \ldots, u_n)^{\mathrm{T}}$, and where, for $i = 1, \ldots, n$:

$$v_i = F_{X_i}(x_i) \quad , \quad u_i = \Phi^{-1}(v_i) . \tag{I.17}$$

The joint CDF of $\mathbf{X}$ is given from Theorem I–1.1 by:

$$\begin{aligned} F_{\mathbf{X}}(\mathbf{x}) = F_{\mathbf{X}}(x_1, \ldots, x_n) &= C_{\mathbf{X}}\left(F_{X_1}(x_1), \ldots, F_{X_n}(x_n)\right) \\ &= \prod_{i=1}^{n} F_{X_i}(x_i) , \end{aligned} \tag{I.18}$$

where $C_{\mathbf{X}}$ is the independent copula C_{ind}, i.e. such that $C_{\text{ind}}(u_1,\dots,u_n)=\prod_{i=1}^n u_i$, see Eq. (I.9).

From Eq. (I.8), the joint PDF of $\mathbf{X}$ simply reads:

$$\begin{aligned} f_{\mathbf{X}}(\mathbf{x}) = f_{\mathbf{X}}(x_1,\dots,x_n) &= c_{\mathbf{X}}\left(F_{X_1}(x_1),\dots,F_{X_n}(x_n)\right)\prod_{i=1}^n f_{X_i}(x_i) \\ &= \prod_{i=1}^n f_{X_i}(x_i)\ , \end{aligned} \tag{I.19}$$

where $c_{\mathbf{X}}$ is the density of the independent copula given by $c_{\text{ind}}(u_1,\dots,u_n)=1$.

The joint PDF in the $\mathbf{u}$-space $\mathbb{R}^n$ is obtained as a direct application of the invariance of the copula $C_{\mathbf{X}}$ by the n strictly increasing transformations $\left(\Phi^{-1}\circ F_{X_i}\right)(\cdot)$ for $i=1,\dots,n$, see Theorem I–1.2. We therefore have $C_{\mathbf{U}}=C_{\mathbf{X}}$ and $c_{\mathbf{U}}=c_{\mathbf{X}}$, and we can write:

$$\begin{aligned} f_{\mathbf{U}}(\mathbf{u}) = f_{\mathbf{U}}(u_1,\dots,u_n) &= c_{\mathbf{U}}(\Phi(u_1),\dots,\Phi(u_n))\prod_{i=1}^n \varphi(u_i) \\ &= \prod_{i=1}^n \varphi(u_i)\ , \end{aligned} \tag{I.20}$$

where $\varphi(\cdot)$ denotes the univariate standard normal PDF, which confirms that $f_{\mathbf{U}}(\mathbf{u})$ is the n-dimensional standard normal PDF $\varphi_n(\mathbf{u})=\prod_{i=1}^n\varphi(u_i)$.

I–1.3.2 Nataf transformation

We now make the following assumptions about the random vector $\mathbf{X}=(X_1,\dots,X_n)^{\mathrm{T}}$:

- the n marginal distributions of $\mathbf{X}$ are known through their PDFs f_{X_i} or CDFs F_{X_i} for $i=1,\dots,n$,
- the linear correlation coefficients $\rho_{ij}=\rho\left(X_i,X_j\right)$ of $\left(X_i,X_j\right)$-pairs are known for $i,j=1,\dots,n$. $\mathbf{R}=\left[\rho_{ij}\right]_{1\le i,j\le n}$ will denote the matrix of linear correlation coefficients.

The isoprobabilistic transformation T under such assumptions is known as the *Nataf transformation* (Nataf, 1962). This transformation was introduced into structural reliability by Liu and Der Kiureghian (1986). Its presentation in the framework of copulas is due to Lebrun and Dutfoy (2009a), from which the text of this section is inspired. In the Nataf transformation, each component X_i of $\mathbf{X}$ is first mapped into a uniform random variable V_i on $[0,1]$ using its CDF F_{X_i}. These uniform random variables V_i are then mapped into correlated standard normal variables Z_i using the inverse CDF of the standard normal distribution, i.e. such that $\mathbf{Z}=(Z_1,\dots,Z_n)^{\mathrm{T}}\sim\mathcal{N}(\mathbf{0},\mathbf{R}_0)$ where $\mathbf{R}_0$ denotes the correlation matrix of the random vector $\mathbf{Z}$. The correlated standard normal variables Z_i are finally mapped into independent standard normal variables U_i using a linear transformation denoted T_{zu}.

The isoprobabilistic transformation T is therefore defined as the following composed application:

$$\begin{array}{rccccccc} T=T_{zu}\circ T_{vz}\circ T_{xv}: & \mathcal{X} & \to & [0,1]^n & \to & \mathbb{R}^n & \to & \mathbb{R}^n \\ & \mathbf{x} & \mapsto & \mathbf{v}=T_{xv}(\mathbf{x}) & \mapsto & \mathbf{z}=T_{vz}(\mathbf{v}) & \mapsto & \mathbf{u}=T_{zu}(\mathbf{z}) \end{array} \tag{I.21}$$

where $\mathbf{x}=(x_1,\dots,x_n)^{\mathrm{T}}$, $\mathbf{v}=(v_1,\dots,v_n)^{\mathrm{T}}$, $\mathbf{z}=(z_1,\dots,z_n)^{\mathrm{T}}$, $\mathbf{u}=(u_1,\dots,u_n)^{\mathrm{T}}$, and where, for $i=1,\dots,n$:

$$v_i=F_{X_i}(x_i)\quad,\quad z_i=\Phi^{-1}(v_i)\ . \tag{I.22}$$

For the construction of T_{zu}, we assume a linear relation between $\mathbf{z}$ and $\mathbf{u}$ in the form $\mathbf{z} = \mathbf{A}\mathbf{u}$. The correlation matrix $\mathbf{R}_0$ can be written as follows:

$$\begin{aligned}\mathbf{R}_0 = \left[\mathrm{Cov}\left[Z_i, Z_j\right]\right]_{1\leq i,j\leq n} &= \mathbb{E}\left[\mathbf{Z}\mathbf{Z}^{\mathrm{T}}\right] - \mathbb{E}\left[\mathbf{Z}\right]\mathbb{E}\left[\mathbf{Z}^{\mathrm{T}}\right] \\ &= \mathbf{A}\,\mathbb{E}\left[\mathbf{U}\mathbf{U}^{\mathrm{T}}\right]\mathbf{A}^{\mathrm{T}} \\ &= \mathbf{A}\mathbf{A}^{\mathrm{T}}\,.\end{aligned} \tag{I.23}$$

From Eq. (I.23), it appears that $\mathbf{A}$ can be chosen as the lower-triangular matrix $\mathbf{L}_0$ of the Cholesky decomposition of matrix $\mathbf{R}_0$ (assumed positive definite) such that:

$$\mathbf{R}_0 = \mathbf{L}_0\mathbf{L}_0^{\mathrm{T}}\,, \tag{I.24}$$

which defines the transformation T_{zu}:

$$\begin{array}{rccl} T_{zu}: & \mathbb{R}^n & \to & \mathbb{R}^n \\ & \mathbf{z} & \mapsto & \mathbf{u} = T_{zu}(\mathbf{z}) = \mathbf{L}_0^{-1}\mathbf{z} \end{array} \tag{I.25}$$

As described in Lebrun and Dutfoy (2009a), the underlying assumption of the Nataf transformation is that the copula $C_{\mathbf{Z}}$ of the random vector $\mathbf{Z}$ (or equivalently the copula $C_{\mathbf{X}}$ of $\mathbf{X}$) is the n-dimensional normal copula parameterized by the correlation matrix $\mathbf{R}_0$.

The joint CDF of $\mathbf{Z}$ is therefore assumed to be given by:

$$\begin{aligned}F_{\mathbf{Z}}(\mathbf{z}) = F_{\mathbf{Z}}(z_1,\ldots,z_n) &= C_{\mathbf{Z}}(\Phi(z_1),\ldots,\Phi(z_n)) \\ &= C_{\mathcal{N}_n}(\Phi(z_1),\ldots,\Phi(z_n);\mathbf{R}_0) \\ &= \Phi_n(z_1,\ldots,z_n;\mathbf{R}_0)\,,\end{aligned} \tag{I.26}$$

where $C_{\mathbf{Z}}$ is the n-dimensional normal copula $C_{\mathcal{N}_n}$ parameterized by the correlation matrix $\mathbf{R}_0$, see Eq. (I.10).

From Eq. (I.8), the joint PDF of $\mathbf{Z}$ reads:

$$\begin{aligned}f_{\mathbf{Z}}(\mathbf{z}) = f_{\mathbf{Z}}(z_1,\ldots,z_n) &= c_{\mathbf{Z}}(\Phi(z_1),\ldots,\Phi(z_n))\prod_{i=1}^{n}\varphi(z_i) \\ &= c_{\mathcal{N}_n}(\Phi(z_1),\ldots,\Phi(z_n);\mathbf{R}_0)\prod_{i=1}^{n}\varphi(z_i) \\ &= \varphi_n(z_1,\ldots,z_n;\mathbf{R}_0)\,,\end{aligned} \tag{I.27}$$

where $c_{\mathbf{Z}}$ is the density of a n-dimensional normal copula parameterized by the correlation matrix $\mathbf{R}_0$, whose expression is:

$$c_{\mathcal{N}_n}(u_1,\ldots,u_n;\mathbf{R}_0) = \frac{\varphi_n\left(\Phi^{-1}(u_1),\ldots,\Phi^{-1}(u_n);\mathbf{R}_0\right)}{\prod_{i=1}^{n}\varphi\left(\Phi^{-1}(u_i)\right)}\,, \tag{I.28}$$

where $\varphi_n(\cdot;\mathbf{R}_0)$ is the n-dimensional standard normal PDF with linear correlation matrix $\mathbf{R}_0$.

The joint PDF in the $\mathbf{x}$-space $\mathcal{X}$ is obtained as a direct application of the invariance of the copula $C_{\mathbf{Z}}$ by the n strictly increasing transformations $\left(F_{X_i}^{-1}\circ\Phi\right)(\cdot)$ for $i = 1,\ldots,n$, see Theorem I–1.2. We therefore have $C_{\mathbf{X}} = C_{\mathbf{Z}}$ and $c_{\mathbf{X}} = c_{\mathbf{Z}}$. The joint PDF of $\mathbf{X}$ is therefore given by the following expression:

$$\begin{aligned}f_{\mathbf{X}}(\mathbf{x}) = f_{\mathbf{X}}(x_1,\ldots,x_n) &= c_{\mathbf{X}}\left(F_{X_1}(x_1),\ldots,F_{X_n}(x_n)\right)\prod_{i=1}^{n}f_{X_i}(x_i) \\ &= \frac{\varphi_n(z_1,\ldots,z_n;\mathbf{R}_0)}{\prod_{i=1}^{n}\varphi(z_i)}\prod_{i=1}^{n}f_{X_i}(x_i)\,,\end{aligned} \tag{I.29}$$

which is the expression given in Eq. (11) in the paper of Liu and Der Kiureghian (1986).

The $\mathbf{R}_0$ matrix has not been explicited yet. The elements $\rho_{0,ij}$ of this matrix are defined in terms of the given linear correlation coefficients $\rho_{ij} = \rho\left(X_i, X_j\right)$ of X_i and X_j components of $\mathbf{X}$. They are obtained from the following equation, for $i, j = 1, \ldots, n$, in which we use the bivariate form of the joint PDF expressed in Eq. (I.29):

$$\begin{aligned}
\rho_{ij} &= \mathbb{E}\left[\left(\frac{X_i - \mu_i}{\sigma_i}\right)\left(\frac{X_j - \mu_j}{\sigma_j}\right)\right] \\
&= \int_{\mathcal{X}_j}\int_{\mathcal{X}_i}\left(\frac{x_i - \mu_i}{\sigma_i}\right)\left(\frac{x_j - \mu_j}{\sigma_j}\right)\frac{\varphi_2\left(z_i, z_j; \rho_{0,ij}\right)}{\varphi\left(z_i\right)\varphi\left(z_j\right)} f_{X_i}\left(x_i\right) f_{X_j}\left(x_j\right) \mathrm{d}x_i \mathrm{d}x_j \\
&= \int_{\mathbb{R}}\int_{\mathbb{R}} h\left(z_i, z_j, \mu_i, \mu_j, \sigma_i, \sigma_j\right)\, \varphi_2\left(z_i, z_j; \rho_{0,ij}\right) \mathrm{d}z_i \mathrm{d}z_j \,,
\end{aligned} \tag{I.30}$$

where $\mathcal{X}_i$ and $\mathcal{X}_j$ denote the respective supports of the i^{th} and j^{th} components of the random vector $\mathbf{X}$, μ_i and μ_j their respective means, and σ_i and σ_j their respective standard deviations,

where $h\left(z_i, z_j, \mu_i, \mu_j, \sigma_i, \sigma_j\right) = \left(\frac{F_{X_i}^{-1}\left(\Phi\left(z_i\right)\right) - \mu_i}{\sigma_i}\right)\left(\frac{F_{X_j}^{-1}\left(\Phi\left(z_j\right)\right) - \mu_j}{\sigma_j}\right)$, and where

$$\varphi_2\left(z_i, z_j; \rho_{0,ij}\right) = \varphi_2\left(z_i, z_j; \begin{bmatrix} 1 & \rho_{0,ij} \\ \rho_{0,ij} & 1 \end{bmatrix}\right) = \frac{1}{2\pi\sqrt{1-\rho_{0,ij}^2}} \exp\left(-\frac{z_i^2 - 2\rho_{0,ij} z_i z_j + z_j^2}{2\left(1-\rho_{0,ij}^2\right)}\right).$$

The Nataf transformation is valid if Eq. (I.30) admits solutions for all $i, j = 1, \ldots, n$ and if the linear correlation matrix $\mathbf{R}_0$ is positive definite. Such a situation is often met in applications of practical interest, as reported by Liu and Der Kiureghian (1986). Finding $\rho_{0,ij}$ solutions of the integral relation defined in Eq. (I.30) is in general tedious, and for this reason approximate formulas for $\rho_{0,ij}$ were derived by Liu and Der Kiureghian (1986) for most common statistical distributions. These formulas are in general obtained by least squares fitting and therefore approximate, except for a few pairs of distributions. An alternative solution consists of calculating $\rho_{0,ij}$ for $i, j = 1, \ldots, n$ and $i > j$ by numerical integration, as implemented in FERUM 4.x (Bourinet et al., 2009). Such calculations are performed only once to define the transformation T and they are fast with currently available computers. Coefficients $\rho_{0,ij}$ of the $\mathbf{R}_0$ matrix are obtained by 2D numerical integration as solutions[3] of the following equation for $i, j = 1, \ldots, n$ and $i > j$:

$$\rho_{ij} = \sum_{k=1}^{n_i}\sum_{l=1}^{n_j} \omega_k \omega_l\, h\left(z_k, \mu_i, \sigma_i, z_l, \mu_j, \sigma_j\right)\, \varphi_2\left(z_k, z_l, \rho_{0,ij}\right) \,, \tag{I.31}$$

where (z_k, z_l) are the $n_i \times n_j$ integration points and $\omega_k \omega_l$ their respective weights. A Gaussian quadrature rule is applied over the truncated domain $[-6, 6] \times [-6, 6]$. Special attention must be paid to strongly-correlated random variables for accurate $\rho_{0,ij}$ values. A practical rule adopted in FERUM 4.x consists of increasing the number of integration points along each dimension with correlation, ranging from $n_i = n_j = 32$ points along each dimension for absolute correlation values lower than 0.9 to $1,024$ points for absolute values larger than 0.9995.

[3] It is important to point out that the unknown $\rho_{0,ij}$ in Eq. (I.31) is in the right-hand side of the equation, which requires an iterative solution for each pair (i, j).

In many engineering problems, the joint PDF $f_{\mathbf{X}}$ is often out of reach and the available statistical information is often limited to marginal distributions of $\mathbf{X}$ and, in some cases, linear correlations between its components. This explains why the Nataf transformation is so popular in the structural reliability literature, even if the assumption of normal copula may be questionable, as raised by Lebrun and Dutfoy (2009a). Note that all the works presented in this report are based on this transformation.

I–1.3.3 Rosenblatt transformation

We now assume that the random vector $\mathbf{X} = (X_1, \ldots, X_n)^{\mathrm{T}}$ is known through its joint distribution, e.g. its joint CDF $F_{\mathbf{X}}$.

In such a case, the isoprobabilistic transformation applied is known as the *Rosenblatt transformation* (Rosenblatt, 1952), see the paper from Hohenbichler and Rackwitz (1981) for its introduction in structural reliability. Based on the joint CDF $F_{\mathbf{X}}$, the random vector $\mathbf{X}$ is first mapped into a uniformly distributed random vector $\mathbf{V} = (V_1, \ldots, V_n)^{\mathrm{T}}$ over $[0,1]^n$ with independent copula (see demonstration by Ditlevsen and Madsen, 2007, p. 123). The uniform random variables V_i are then mapped into independent standard normal variables U_i using the inverse CDF of the standard normal distribution.

The isoprobabilistic transformation T is defined as the following composed application:

$$\begin{array}{rccccc} T = T_{vu} \circ T_{xv} : & \mathcal{X} & \to & [0,1]^n & \to & \mathbb{R}^n \\ & \mathbf{x} & \mapsto & \mathbf{v} = T_{xv}(\mathbf{x}) & \mapsto & \mathbf{u} = T_{vu}(\mathbf{v}) \end{array} \tag{I.32}$$

where $\mathbf{x} = (x_1, \ldots, x_n)^{\mathrm{T}}$, $\mathbf{v} = (v_1, \ldots, v_n)^{\mathrm{T}}$, $\mathbf{u} = (u_1, \ldots, u_n)^{\mathrm{T}}$,
and where $u_i = \Phi^{-1}(v_i)$ for $i = 1, \ldots, n$.

One possible choice for the transformations T_{xv} is given in Eq. (I.33). Note that there exist $n!$ different choices due to the variable ordering in the conditional expressions.

$$\begin{aligned} v_1 &= F_{X_1}(x_1) \\ v_2 &= F_{X_2|X_1}(x_2|x_1) \\ v_3 &= F_{X_3|X_1,X_2}(x_3|x_1,x_2) \\ &\ldots \\ v_n &= F_{X_n|X_1,\ldots,X_{n-1}}(x_n|x_1,\ldots,x_{n-1}) \end{aligned} \tag{I.33}$$

It is important to notice that the definition of T_{xv} necessitates a knowledge of the conditional CDFs of $X_k|X_1, \ldots, X_{k-1}$ for $k = 2, \ldots, n$. When the joint distribution of $\mathbf{X}$ is defined by its copula C and its marginal CDFs F_{X_i} for $i = 1, \ldots, n$, the Rosenblatt transformation T is computationally tractable by using the conditional expression obtained in Eq. (I.12). The definition of the inverse T^{-1} of the Rosenblatt transformation (needed in approximation methods such as FORM and SORM, addressed in Section I–2) may however require substantial efforts.

As a final remark, the dependence of the FORM results on the variable ordering in the conditional expressions of Eq. (I.33) has been studied in several works, see e.g. the example based on the bivariate exponential CDF $F_{\mathbf{X}}(\mathbf{x}) = F_{\mathbf{X}}(x_1, x_2) = 1 - \exp(-x_1) - \exp(-x_2) - \exp(-x_1 - x_2 - x_1 x_2)$ in Ditlevsen and Madsen (2007) and Lemaire et al. (2010). As pointed out by Lebrun (2013), it is important to mention that, despite differences in terms of FORM results, the exact failure probability remains unchanged, whatever the order of variables we choose in the Rosenblatt transformation.

I–2 MPFP-based methods

I–2.1 First-order reliability method (FORM)

I–2.1.1 Problem statement

The *first-order reliability method* (FORM) aims at finding the point P^* of the LSS $\mathcal{F}_{\mathbf{u}}^0$ that is the closest to the origin O in the standard normal space, i.e. the point in the failure domain $\mathcal{F}_{\mathbf{u}}$ with the largest PDF value (see, e.g., Ditlevsen and Madsen, 2007; Lemaire et al., 2010), cf. Figure I.3. This point, known as the *most probable failure point* (MPFP) (also called *design point*) in structural reliability, is the solution of the following quadratic optimization problem under nonlinear constraint:

$$\mathbf{u}^* = \underset{\mathbf{u}\in\mathbb{R}^n}{\arg\min}\ \frac{1}{2}\mathbf{u}^{\mathrm{T}}\mathbf{u} \ \text{ s.t. } \ G(\mathbf{u}) = 0\,, \tag{I.34}$$

where $\mathbf{u}^*$ is the coordinate vector of P^* in the standard normal space $\mathbb{R}^n$.

The so-called Hasofer-Lind *reliability index* β_{HL} is given by:

$$\beta_{\mathrm{HL}} = \beta = \boldsymbol{\alpha}^{\mathrm{T}}\mathbf{u}^*\,, \tag{I.35}$$

where $\boldsymbol{\alpha}$ is a unit vector such that $\boldsymbol{\alpha} = -\nabla G(\mathbf{u}^*)/\|\nabla G(\mathbf{u}^*)\|$ and ∇ is the gradient operator. In general, the origin O of the standard normal space belongs to the safe domain. As a consequence, β is positive and represents the Euclidean distance from the MPFP P^* to the origin O of the standard normal space, and $\boldsymbol{\alpha}$ is the unit vector of the (O, P^*) axis, see Figure I.3.

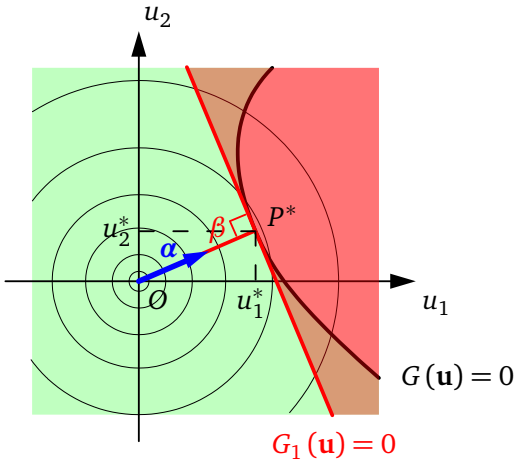

Figure I.3 – FORM approximation.

Under the assumption that the LSF is continuous, smooth and differentiable in the neighborhood of the MPFP, we define the linear approximation of G at the MPFP P^* (first-order Taylor polynomial of G at $\mathbf{u}^*$), which is given by the following expression:

$$G_1(\mathbf{u}) = \nabla G(\mathbf{u}^*)^{\mathrm{T}}(\mathbf{u} - \mathbf{u}^*)\,, \tag{I.36}$$

in which the term $G(\mathbf{u}^*)$ has been dropped since it is equal to zero (the MPFP P^* belongs to the LSS $\mathcal{F}_{\mathbf{u}}^0$).

The FORM method consists in approximating the unknown probability p_{f} defined in Eq. (I.5) by the following n-dimensional integral:

$$p_{\mathrm{f}}^{\mathrm{FORM}} = \int_{\mathbb{R}^n} \mathbb{1}_{\mathcal{F}_{\mathbf{u}1}}(\mathbf{u})\,\varphi_n(\mathbf{u})\,\mathrm{d}\mathbf{u}\,, \tag{I.37}$$

where $\mathcal{F}_{\mathbf{u}1} = \{\mathbf{u} \in \mathbb{R}^n : G_1(\mathbf{u}) \leq 0\} = \left\{\mathbf{u} \in \mathbb{R}^n : \beta - \boldsymbol{\alpha}^{\mathrm{T}}\mathbf{u} \leq 0\right\}$.

This integral can be evaluated in a closed form, and a simple calculation gives:

$$p_{\mathrm{f}}^{\mathrm{FORM}} = \Phi(-\beta) \ , \tag{I.38}$$

where Φ denotes the one-dimensional standard normal CDF.

I–2.1.2 Solving the constrained optimization problem

The main computational task of the FORM method is to search for the supposedly unique MPFP using a suitable optimization algorithm. Several methods are available to solve the optimization problem in Eq. (I.34), including general algorithms such as the usual sequential quadratic programming (SQP) algorithm, or others which have been specifically tailored to solve Eq. (I.34), e.g. the HLRF algorithm (Hasofer and Lind, 1974; Rackwitz and Fiessler, 1978) and the i-HLRF algorithm (Zhang and Der Kiureghian, 1994). The reader may refer to Lemaire et al. (2010, Chap. 5) for an overview of these algorithms and to Liu and Der Kiureghian (1991) for a comparison of the performances of the SQP, the HLRF and a few other algorithms.

Most of the existing algorithms share the same basis: they are iterative until some convergence criteria are met and, at each iteration of the algorithm, a search direction is determined along with a step length in that direction. Their performances are usually evaluated based on the following criteria: types of problems that can be solved, convergence to the solution with a prescribed accuracy, convergence rate of the algorithm, ability of the algorithm to scale with the dimension n of the problem.

From a practical viewpoint, all the above-mentioned algorithms require an evaluation of the gradient of the LSF at each iteration. The LSF gradient involves those of one or more outputs of a numerical model (e.g. a FE model) w.r.t. its inputs, considered as random. The gradients (or sensitivities to input parameters) are in general not directly accessible from the numerical codes, except in a very few cases and under some often restrictive assumptions, e.g. model linearity. If these sensitivities are available e.g. by direct differentiation of the equations governing the response(s), they can make FORM very efficient, see the early paper of Zhang and Der Kiureghian (1993) for the application of the so-called *direct differentiation method* to the dynamic response of structures with inelastic materials and the report by Haukaas and Der Kiureghian (2004) for more details on such approaches in the context of FE analyses. In the most general case, these sensitivities are inaccessible (case of nonintrusive approaches in reliability assessment) and they need to be assessed by finite differences, with the dilemma of choosing very small or sufficiently large perturbation steps in the finite difference scheme:

- If the applied perturbations are too small, the numerical model is often unable to evaluate outputs with sufficient accuracy (this could be interpreted as noisy outputs from the code) and the calculated sensitivities are therefore not representative of the level of perturbation applied to the model inputs.
- If large perturbations are selected, the output values are well separated from each other but the calculated sensitivities are no longer representative of first-order derivatives.

The selection of suitable perturbation steps, usually expressed as ratios of random input standard deviations, has considerable consequences on the convergence and convergence rate of the optimization algorithms used to solve Eq. (I.34). The tuning of such perturbation steps in a finite difference scheme may require considerable efforts in engineering applications of practical interest.

The FORM results presented in this report are based on the i-HLRF algorithm. This algorithm was implemented in FERUM 4.x so as to take advantage of independent tasks in multicore computational platforms (distributed LSF evaluations to assess the gradient by finite differences and to determine an optimal step size by means of the Goldstein-Armijo approximate line search rule).

I–2.1.3 Remarks about the accuracy of the FORM solution

It is important to emphasize that the approximation of p_f given in Eq. (I.38) is under the assumption of a unique MPFP P^* and a linear (or weakly nonlinear) LSS $\mathcal{F}^0_{\mathbf{u}}$. If these assumptions are not fulfilled, the FORM approximation could be a fairly crude one with a large bias w.r.t. the true failure probability.

The uniqueness of the MPFP is often encountered in practice. Note that such an assumption cannot be checked beforehand, and it is also hard to verify it when a FORM solution has been obtained. Some engineering reliability assessment problems may, however, exhibit several zones of similar importance (and therefore multiple MPFPs), as presented in Section III–1.4. In the FORM context, the method proposed by Der Kiureghian and Dakessian (1998) aims at solving such problems. In essence, the method consists in repeating the FORM analysis with a modified LSF which triggers the search outside the zone where a MPFP has been found. Assuming that K MPFPs have already been identified (the first one being obtained e.g. with the i-HLRF algorithm), the FORM analysis performed next uses the following modified LSF $G_{\text{bulge},K+1}$ in the standard normal space, which consists in adding bulges centered at each of the K obtained MPFPs, see examples of corresponding LSS in Figure I.4:

$$G_{\text{bulge},K+1}(\mathbf{u}) = G(\mathbf{u}) + \sum_{k=1}^{K} \mathbb{1}_{\mathcal{B}_k}(\mathbf{u})\, s_k \left(r_k^2 - \|\mathbf{u}-\mathbf{u}_k^*\|^2\right)^2 , \tag{I.39}$$

where $\mathbf{u}_k^*$ and β_k are the MPFP and reliability index of the k^{th} MPFP, $\mathcal{B}_k$ is the ball of radius r_k centered on the k^{th} MPFP, i.e. such that $\mathcal{B}_k = \left\{\mathbf{u} \in \mathbb{R}^n : \|\mathbf{u}-\mathbf{u}_k^*\| \leq r_k\right\}$, and where r_k is the radius of the bulge and s_k a parameter that controls its height, defined as follows:

$$r_k = \gamma\beta_k \quad , \quad s_k = \frac{\delta\beta_k \|\nabla G(\mathbf{u}_k^*)\|}{\left[(\gamma\beta_k)^2 - (\delta\beta_k)^2\right]^2} , \tag{I.40}$$

where δ and γ are user-defined parameters such that $0 < \delta < \gamma$.

This procedure is repeated until a spurious MPFP is obtained. Such points appear in the foot of one of the created bulges and they correspond to artificially-created minimal distance points, see Figure I.4c. To make the method more efficient, it is suggested by Der Kiureghian and Dakessian (1998) to start the FORM algorithm from an initial point $\mathbf{u}_{0,K+1}$, defined as follows to search for the $(K+1)^{\text{th}}$ MPFP:

$$\mathbf{u}_{0,K+1} = -\epsilon \sum_{k=1}^{K} \mathbf{u}_k^* , \tag{I.41}$$

where ϵ is a user-defined parameter in the range 0.2-0.5.

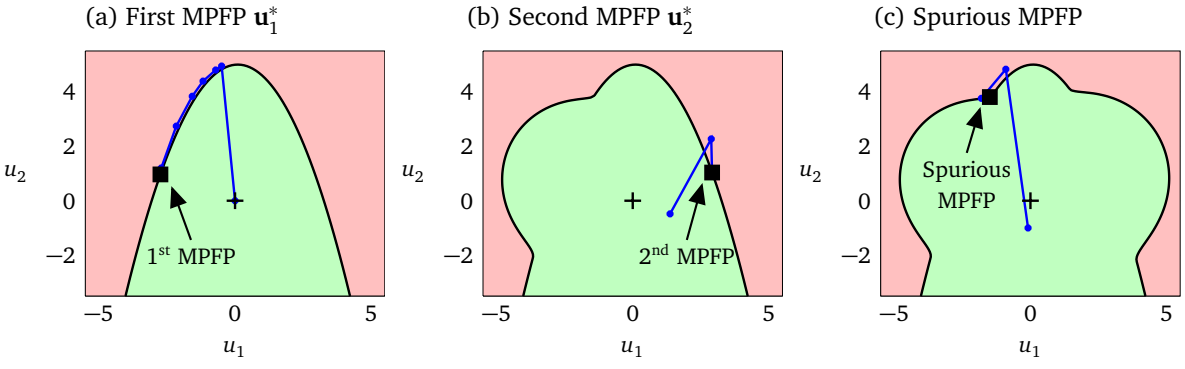

Figure I.4 – Successive use of bulges to find multiple MPFPs (Der Kiureghian and Dakessian, 1998, Example 1). Selected parameters: $\delta = 0.75$, $\gamma = 1.1$, $\epsilon = 0.5$.

Regarding a potential nonlinearity of the LSS, the FORM approximation may be corrected by a subsequent recourse to one of the second-order reliability methods presented in the next section (either curvature-fitting or point-fitting SORM).

I–2.2 Second-order reliability method (SORM)

I–2.2.1 Curvature-fitting SORM

We assume that the LSF is continuous, smooth and at least twice differentiable in the neighborhood of the MPFP obtained by a FORM analysis. In the *second-order reliability method* (SORM) based on *curvature-fitting* (SORM-cf), we consider the quadratic approximation of G at the MPFP P^* (or second-order Taylor polynomial of G at $\mathbf{u}^*$) given by:

$$G_2(\mathbf{u}) = \nabla G(\mathbf{u}^*)^{\mathrm{T}}(\mathbf{u}-\mathbf{u}^*) + \frac{1}{2}(\mathbf{u}-\mathbf{u}^*)^{\mathrm{T}}\nabla^2 G(\mathbf{u}^*)(\mathbf{u}-\mathbf{u}^*)\,, \tag{I.42}$$

where ∇^2 denotes the Hessian operator. The SORM-cf approximation of the unknown probability p_{f} defined in Eq. (I.5) is expressed as the following n-dimensional integral:

$$p_{\mathrm{f}}^{\text{SORM-cf}} = \int_{\mathbb{R}^n} \mathbb{1}_{\mathcal{F}_{\mathbf{u}2}}(\mathbf{u})\,\varphi_n(\mathbf{u})\,\mathrm{d}\mathbf{u}\,, \tag{I.43}$$

where $\mathcal{F}_{\mathbf{u}2} = \{\mathbf{u}\in\mathbb{R}^n : G_2(\mathbf{u}) \le 0\}$.

In order to make the calculation of this integral tractable, the quadratic approximation defined in Eq. (I.42) is usually expressed in another set of axes by means of the following composed orthonormal transformations (Der Kiureghian, 1999).

The first, $\mathbf{u}\mapsto\mathbf{u}' = \left(u_1',\ldots,u_n'\right)^{\mathrm{T}} = \mathbf{R}_1\mathbf{u}$, is constructed such that the last coordinate axis u_n' coincides with the direction (O,P^*), e.g. by means of a Gram-Schmidt algorithm. In the new space, Eq. (I.42) is rewritten as follows, in which the factor terms of $\left(u_n'-\beta\right)$ are dropped in relation to the remaining terms:

$$\frac{G_2\left(\mathbf{R}_1^{-1}(\mathbf{u}')\right)}{\|\nabla G(\mathbf{u}^*)\|} \approx \beta - u_n' + \frac{1}{2}\widetilde{\mathbf{u}}'^{\mathrm{T}}\widetilde{\mathbf{A}}\widetilde{\mathbf{u}}'\,, \tag{I.44}$$

where $\widetilde{\mathbf{u}}' = \left(u_1',\ldots,u_{n-1}'\right)^{\mathrm{T}}$ and $\widetilde{\mathbf{A}}$ is the sub-matrix composed of the first $(n-1)$ rows and colums of $\mathbf{A} = \mathbf{R}_1\nabla^2 G(\mathbf{u}^*)\mathbf{R}_1^{\mathrm{T}}/\|\nabla G(\mathbf{u}^*)\|$.

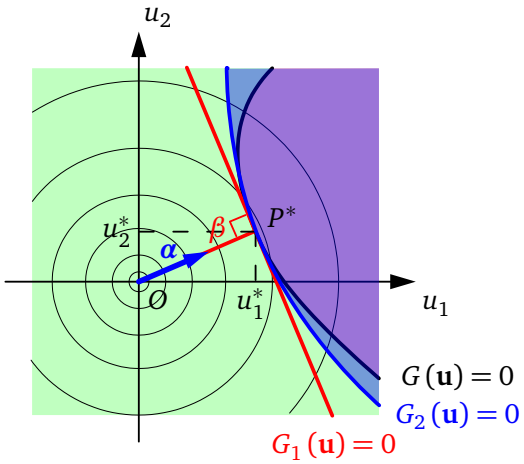

Figure I.5 – SORM-cf approximation.

A rotation around axis u'_n is then applied to be in the principal coordinates of the parabolic approximation of the LSS. Let us denote this rotation $\widetilde{\mathbf{u}}' \mapsto \widetilde{\mathbf{u}}'' = \widetilde{\mathbf{R}}_2 \widetilde{\mathbf{u}}'$ where $\widetilde{\mathbf{u}}'' = \left(u''_1, \ldots, u''_{n-1}\right)^{\mathrm{T}}$, defined such that $\widetilde{\mathbf{R}}_2 \widetilde{\mathbf{A}} \widetilde{\mathbf{R}}_2^{\mathrm{T}} = \mathrm{diag}\left(\kappa_i\right)$. The rotation matrix $\widetilde{\mathbf{R}}_2$ represents the eigenmatrix of $\widetilde{\mathbf{A}}$, and the $(n-1)$ principal curvatures $\kappa_1, \ldots, \kappa_{n-1}$ are the corresponding eigenvalues. In this rotated space, Eq. (I.44) takes the following canonical form:

$$\frac{G_2\left(\mathbf{R}_1^{-1}\left(\mathbf{R}_2^{-1}\left(\mathbf{u}''\right)\right)\right)}{\left\|\nabla G\left(\mathbf{u}^*\right)\right\|} \approx \beta - u''_n + \sum_{i=1}^{n-1} \kappa_i u''^2_i \,, \tag{I.45}$$

where $\mathbf{u}'' = \left(u''_1, \ldots, u''_n\right)^{\mathrm{T}}$ and $\mathbf{R}_2 = \begin{bmatrix} \widetilde{\mathbf{R}}_2 & \mathbf{0} \\ \mathbf{0}^{\mathrm{T}} & 1 \end{bmatrix}$.

Eq. (I.43) can then be rewritten in the following form:

$$p_{\mathrm{f}}^{\text{SORM-cf}} \approx \int_{\mathbb{R}^n} \mathbb{1}_{\mathcal{F}_{\mathbf{u}''2}}\left(\mathbf{u}''\right) \varphi_n\left(\mathbf{u}''\right) \mathrm{d}\mathbf{u}'' \,, \tag{I.46}$$

where $\mathcal{F}_{\mathbf{u}''2} = \left\{\mathbf{u}'' \in \mathbb{R}^n : \beta - u''_n + \sum_{i=1}^{n-1} \kappa_i u''^2_i \leq 0\right\}$.

Several formulas can be found in the literature to approximate this integral. The best known are those established by Breitung (1984), Tvedt (1988), and Hohenbichler and Rackwitz (1988). Only the SORM approximation given by the asymptotic formula of Hohenbichler and Rackwitz is recalled here:

$$p_{\mathrm{f}}^{\text{SORM-cf}} \approx \Phi\left(-\beta\right) \prod_{i=1}^{n-1} \frac{1}{\sqrt{1 + \psi\left(\beta\right)\kappa_i}} \quad \left(\beta \to \infty\right) \,, \tag{I.47}$$

where $\psi\left(\beta\right) = \varphi\left(\beta\right) / \Phi\left(-\beta\right)$, assuming that $\kappa_i > -1/\psi\left(\beta\right)$ for all $i \in \{1, \ldots, (n-1)\}$.

It is important to point out that the SORM-cf method requires the evaluation of the *Hessian matrix* at P^* used for the definition of $\widetilde{\mathbf{A}}$. This Hessian matrix $\nabla^2 G\left(\mathbf{u}^*\right)$ is computed numerically by finite differences in FERUM 4.x by means of $n + n\left(n+1\right)/2$ calls to the LSF. All these calls are independent and therefore run in parallel by FERUM.

I–2.2.2 Point-fitting SORM

An alternative method proposed by Der Kiureghian et al. (1987) and known as *point-fitting* SORM (SORM-pf) consists in approximating the LSS by a piece-wise paraboloid surface which must be tangent to the LSS at the MPFP and interpolates the LSS at a set of fitting points. This method is advantageous for slightly noisy LSF, such as those resulting from calls to a FE code for which the computation of the Hessian matrix by finite differences cannot be achieved with sufficient accuracy, for high-dimensional problems, i.e. large n, or when the computation of curvatures fails.

The method works in a rotated standard normal space such that the last coordinate axis u'_n coincides with the direction (O, P^*), as defined in the SORM-cf method (note that this choice of axes is made regardless of the orientation of the principal directions of the LSS, whose determination would require us to calculate the Hessian of G at the MPFP). The orthogonal transformation to this new space is, as previously described, defined by $\mathbf{u}' = \mathbf{R}_1 \mathbf{u}$, where $\mathbf{u}'$ denotes the coordinate vector in the new space.

For each coordinate u'_i, $i = 1, \ldots, n-1$, the objective is to find two fitting points of the LSS with coordinates $(-k\beta, u'_{n,-i})$ and $(k\beta, u'_{n,+i})$, where β is the reliability index and k is a preselected parameter which controls the distance of these points from the (O, P^*) axis, see Figure I.6. The ordinates $u'_{n,-i}$ and $u'_{n,+i}$ of these two points are solutions of the following equation:

$$G\left(\mathbf{R}_1^{-1}\mathbf{u}'\right) = 0 \,, \tag{I.48}$$

where $\mathbf{u}' = \left(0,\ldots,0,u'_i,0,\ldots,0,u'_n\right)^{\mathrm{T}}$ and $u'_i = \pm k\beta$, $u'_n = u'_{n,\pm i}$. The corresponding optimization problem is solved in FERUM 4.x using a vectorized version of the Matlab fzero function, which allows the $2\,(n-1)$ independent searches to be run in parallel.

Two semi-parabolas can then be defined in the $\left(u'_i,u'_n\right)$ plane, which are tangent to the LSS at P^* and pass through the fitting points, see Figure I.6. The corresponding curvatures at P^* are given by $\kappa_{\pm i} = 2(u'_{n,\pm i} - \beta)/\,(k\beta)^2$ and the Hohenbicher and Rackwitz approximation reads:

$$p_{\mathrm{f}}^{\text{SORM-pf}} \approx \Phi\,(-\beta) \prod_{i=1}^{n-1} \frac{1}{2}\left(\frac{1}{\sqrt{1+\kappa_{-i}\psi\,(\beta)}} + \frac{1}{\sqrt{1+\kappa_{+i}\psi\,(\beta)}} \right) . \tag{I.49}$$

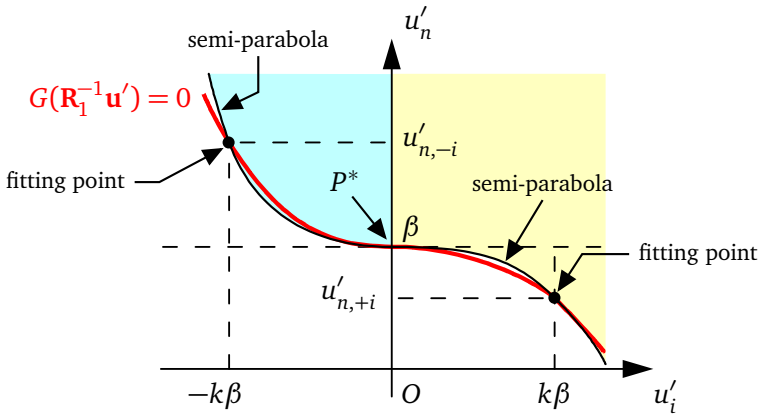

Figure I.6 – Concept of SORM-pf approximation in the (u'_i,u'_n) plane.

I–3 Simulation methods

This section presents the main basis of some popular *sampling methods*, which are often used for the reliability assessment of rare events. The common idea of all these method is to generate samples in the outcome space, e.g. random realizations from the joint PDF $f_{\mathbf{X}}$ in a crude Monte Carlo simulation, in order to find an estimate of the failure probability p_{f}. The goal is to construct an *estimator* $\widehat{p}_{\mathrm{f}}$ that is close to the unknown failure probability p_{f} for any generated sample. This "proximity" to the true and unknown quantity p_{f} is defined in terms of the following important properties of the estimator $\widehat{p}_{\mathrm{f}}$: *bias* of $\widehat{p}_{\mathrm{f}}$ w.r.t. the true and unknown probability p_{f} (the objective is to have an unbiased estimator such that $\mathbb{E}[\widehat{p}_{\mathrm{f}}] = p_{\mathrm{f}}$), and *variance* $\mathrm{Var}[\widehat{p}_{\mathrm{f}}]$ (the objective is to construct an estimator with the lowest achievable variance in order to obtain an estimate close to the unknown value p_{f} for any sample set that is drawn). Note that other properties, such as consistency and efficiency, are also of interest for the characterization of $\widehat{p}_{\mathrm{f}}$.

The well-known Monte Carlo method, applied in numerous fields of physics and engineering, is introduced first in Section I–3.1. For improved efficiency in the context of rare events, two *variance reduction* techniques are then presented: subset simulation, proposed by Au and Beck (2001) in Section I–3.2, and importance sampling, through its adaptive variant known as the cross-entropy method (Rubinstein, 1999) in Section I–3.3. The objective of variance reduction techniques is to retain most of the advantages of the Monte Carlo method (sampling in the outcome space, no assumption about the complexity of the LSF and independence w.r.t. the dimension n of the outcome space) with a lower variance of the estimator $\widehat{p}_{\mathrm{f}}$ for a fixed computational budget. For complementary details about the

sampling methods addressed in this section and some of the related useful techniques (e.g. random number generation and Markov chains), the reader may refer to general textbooks such as those of Robert and Casella (2004), Rubinstein and Kroese (2007), and Kroese et al. (2011).

I–3.1 Crude Monte Carlo (MC) simulation

In order to define the estimator of p_f in a *crude Monte Carlo* (MC) simulation, Eq. (I.1) is rewritten as:

$$p_\mathrm{f} = \mathbb{P}(E) = \int_{\mathcal{X}} \mathbb{1}_{\mathcal{F}_\mathrm{x}}(\mathbf{x})\, f_\mathbf{X}(\mathbf{x})\, \mathrm{d}\mathbf{x} = \mathbb{E}_{f_\mathrm{x}}\left[\mathbb{1}_{\mathcal{F}_\mathrm{x}}(\mathbf{X})\right], \tag{I.50}$$

where $\mathbb{E}_h$ denotes the mathematical expectation operator w.r.t. a given PDF h.

The crude MC estimator of p_f is simply derived from Eq. (I.50) as the sample mean of the failure indicator function:

$$\widehat{p}_\mathrm{f}^{\,\mathrm{MC}} = \frac{1}{N}\sum_{j=1}^{N} \mathbb{1}_{\mathcal{F}_\mathrm{x}}\left(\mathbf{X}^{(j)}\right), \tag{I.51}$$

where $\{\mathbf{X}^{(j)}, 1 \le j \le N\}$ are N independent copies of the random vector $\mathbf{X}$, i.e. $\mathbf{X}^{(1)}, \ldots, \mathbf{X}^{(N)} \overset{\text{i.i.d.}}{\sim} f_\mathbf{X}$, and N denotes the sample size.

From simple calculations, we can find that the coefficient of variation (c.o.v.) of the crude MC estimator $\widehat{p}_\mathrm{f}^{\,\mathrm{MC}}$ writes as follows:

$$\delta_{\widehat{p}_\mathrm{f}^{\,\mathrm{MC}}} = \frac{\sqrt{\mathrm{Var}\left[\widehat{p}_\mathrm{f}^{\,\mathrm{MC}}\right]}}{\mathbb{E}\left[\widehat{p}_\mathrm{f}^{\,\mathrm{MC}}\right]} = \frac{\sqrt{\dfrac{p_\mathrm{f}(1-p_\mathrm{f})}{N}}}{p_\mathrm{f}} = \sqrt{\frac{1-p_\mathrm{f}}{N p_\mathrm{f}}}\,. \tag{I.52}$$

From Eq. (I.52), it can be noticed that the convergence speed of a crude MC simulation is a function of N (the c.o.v. of $\widehat{p}_\mathrm{f}^{\,\mathrm{MC}}$ is proportional to $1/\sqrt{N}$). As an illustration, a 10% c.o.v. on $\widehat{p}_\mathrm{f}^{\,\mathrm{MC}}$ by crude MC requires a sample size N approximately equal to $100/p_\mathrm{f}$ in the case of a rare event ($p_\mathrm{f} \ll 1$). Crude MC hence appears inefficient for estimating probabilities of rare events. The efficiency can, however, be enhanced by means of variance reduction techniques such as those presented in Sections I–3.2 and I–3.3. It is also important to mention that the c.o.v. of $\widehat{p}_\mathrm{f}^{\,\mathrm{MC}}$ is independent of the dimension n of the problem. This independence w.r.t. the dimension is a key advantage of the crude MC approach over other techniques. Last but not least, it is of paramount importance to remember that the crude MC method works regardless of the complexity of the LSF, which is also an advantage over approximation methods presented in Section I–2 or approaches based on surrogate models such as those addressed in Chapter II.

The crude MC method is implemented in FERUM 4.x and takes full advantage of the independence of $\left\{\mathbf{X}^{(j)}, 1 \le j \le N\right\}$, which allows the respective calls to the LSF to be sent in parallel.

I–3.2 Subset simulation (SS)

This section describes the *subset simulation* (SS) method developed by Au and Beck (2001) which has become popular over the years in the structural reliability community. Methods with a very similar basis have been proposed in the statistical community, starting with the seminal work of Kahn and Harris (1951) in the setting of particle transmission. Such methods are also known as *adaptive multilevel splitting* (Cérou and Guyader, 2007; Botev and Kroese, 2012). These methods were developed in a framework that may differ from the specific one of structural reliability, e.g. such as the classical context of Markovian processes (Cérou and Guyader, 2007).

I–3.2.1 Conceptual idea of subset simulation

The conceptual idea of subset simulation (SS) is to represent the small probability of a rare failure event E as a product of larger and sequentially-estimated probabilities of wisely-selected *intermediate events* E_s, $s = 1, \ldots, m$. These m intermediate events are *nested* such that $E_m \subset E_{m-1} \subset \cdots \subset E_2 \subset E_1$ where $E_m = E$. From the inclusion rule and by successive conditioning we can write:

$$\begin{aligned} p_\mathrm{f} = \mathbb{P}(E) = \mathbb{P}(E_m) &= \mathbb{P}(E_m|E_{m-1})\,\mathbb{P}(E_{m-1}) \\ &= \ldots \\ &= \mathbb{P}(E_m|E_{m-1})\,\mathbb{P}(E_{m-1}|E_{m-2}) \ldots \mathbb{P}(E_2|E_1)\,\mathbb{P}(E_1) \\ &= \prod_{s=1}^{m} p_s \,, \end{aligned} \tag{I.53}$$

where p_1 denotes the probability of E_1, and $p_s = \mathbb{P}(E_s|E_{s-1})$ the conditional probability of E_s given E_{s-1} for $s = 2, \ldots, m$. Hence, p_f appears as the product of m probabilities, each of which is necessarily larger than p_f and therefore easier to estimate than p_f by sampling.

We will here assume a component-wise independence of the input random vector for the subsequent application of the Metropolis algorithm modified by Au and Beck (2001) (m-M), see Section I–3.2.3. This can be conveniently achieved by considering the reliability assessment problem in the standard normal space, see Eq. (I.5), wherein $\varphi_n(\mathbf{u}) = \prod_{i=1}^{n} \varphi(u_i)$. All the components U_i for $i = 1, \ldots, n$ have the same univariate standard normal distribution, which moreover greatly simplifies the choice of the proposal multivariate PDF used for Monte Carlo Markov chain sampling and the tuning of the algorithm parameters.

We define the following set of nested *intermediate failure domains* in the standard normal space, for $s = 1, \ldots, m$, see Figure I.7:

$$\mathcal{F}_{\mathbf{u},s} = \{\mathbf{u} \in \mathbb{R}^n : G(\mathbf{u}) \leq y_s\} \,, \tag{I.54}$$

where y_s represents intermediate levels of the LSF such that $y_m = 0$ and $y_m < y_{m-1} < \ldots < y_1$. The intermediate events E_s are such that $E_s = \{G(\mathbf{U}) \leq y_s\}$ for $s = 1, \ldots, m$. They correspond to the intermediate failure domains $\mathcal{F}_{\mathbf{u},s}$ and they meet the previously defined inclusion rule $E_m \subset E_{m-1} \subset \cdots \subset E_2 \subset E_1$.

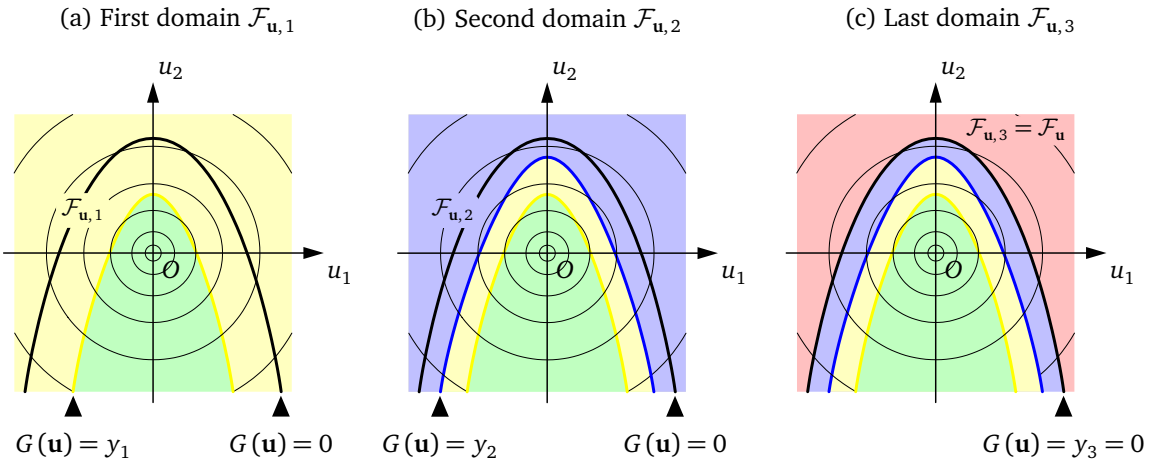

Figure I.7 – Intermediate failure domains $\mathcal{F}_{\mathbf{u},s}$ for $s = 1, \ldots, m$ (here $m = 3$).

I–3.2.2 Description of SS algorithm

The rare event estimation problem formulated in Eq. (I.5) is replaced by a sequence of m problems with larger probabilities to estimate w.r.t. the intermediate levels y_s, for $s = 1$:

$$p_1 = \mathbb{P}(E_1) = \mathbb{E}_{\varphi_n}\left[\mathbb{1}_{\mathcal{F}_{\mathbf{u},1}}(\mathbf{U})\right], \tag{I.55}$$

and, for $s = 2, \ldots, m$:

$$p_s = \mathbb{P}(E_s|E_{s-1}) = \mathbb{E}_{\varphi_n(\cdot|E_{s-1})}\left[\mathbb{1}_{\mathcal{F}_{\mathbf{u},s}}(\mathbf{U})\right]. \tag{I.56}$$

Estimators of these probabilities are given by the fraction of independent samples (for $s = 1$) or conditional independent samples (for $s > 1$) that cause failure w.r.t. the selected intermediate level y_s, respectively for $s = 1$:

$$\widehat{p}_1 = \frac{1}{N}\sum_{j=1}^{N}\mathbb{1}_{\mathcal{F}_{\mathbf{u},1}}\left(\mathbf{U}_1^{(j)}\right) \text{ where } \mathbf{U}_1^{(1)}, \ldots, \mathbf{U}_1^{(N)} \overset{\text{i.i.d.}}{\sim} \varphi_n, \tag{I.57}$$

and for $s = 2, \ldots, m$:

$$\widehat{p}_s = \frac{1}{N}\sum_{j=1}^{N}\mathbb{1}_{\mathcal{F}_{\mathbf{u},s}}\left(\mathbf{U}_s^{(j)}\right) \text{ where } \mathbf{U}_s^{(1)}, \ldots, \mathbf{U}_s^{(N)} \overset{\text{i.i.d.}}{\sim} \varphi_n(\cdot|E_{s-1}), \tag{I.58}$$

where N denotes the sample size (same value used at each level y_s) and where the conditional PDF $\varphi_n(\cdot|E_{s-1})$ is defined as follows, for $s = 2, \ldots, m$:

$$\varphi_n(\mathbf{u}|E_{s-1}) = \frac{\varphi_n(\mathbf{u})\,\mathbb{1}_{\mathcal{F}_{\mathbf{u},s-1}}(\mathbf{u})}{\mathbb{P}(E_{s-1})}. \tag{I.59}$$

In SS, the intermediate levels y_s are selected such that, by construction, all the estimates $\widehat{p}_s$ for $s = 1, \ldots, (m-1)$ are set equal to p_0, where p_0 is a prescribed probability level (a usual choice is $p_0 = 0.1$). Note that targeting equal probability levels in terms of conditional probabilities corresponds to the optimal choice for a minimal asymptotic variance of $\widehat{p}_{\mathrm{f}}^{\mathrm{SS}} = \prod_{s=1}^{m}\widehat{p}_s$, as pointed out by Guyader (2011). This probability level p_0 governs how many intermediate failure domains $\mathcal{F}_{\mathbf{u},s}$ are required to reach the failure domain $\mathcal{F}_{\mathbf{u}}$. A small value for p_0 ensures a fast exploration but with the main disadvantage of poorly-estimated probabilities w.r.t. the intermediate levels y_s. A large value for p_0 enables good accuracy on the estimated probabilities but at the cost of a lengthy exploration (large m). According to Zuev et al. (2012), the optimal range for p_0 is 0.1-0.3. Optimality here means that we are searching for a value of p_0 that minimizes the variance of $\widehat{p}_{\mathrm{f}}^{\mathrm{SS}}$ for a given total number of samples $N_{\mathrm{t}} = mN$. It is assumed here that both $1/p_0$ and p_0N are positive integers. If not, we can work with slightly different values for p_0 and N, such that $p_0 = 1/k_0$ and $N = k_1k_0$, where $k_0 = \lfloor 1/p_0 \rceil$, $k_1 = \lfloor N/k_0 \rceil$ and $\lfloor x \rceil$ denotes the nearest integer to x.

The first intermediate level y_1 is straightforward to obtain. It is defined as the p_0-quantile of $\mathcal{Y}_1 = \{G(\mathbf{u}_1^{(j)}), 1 \le j \le N\}$, where $\mathcal{U}_1 = \{\mathbf{u}_1^{(j)}, 1 \le j \le N\}$ are the N i.i.d. samples drawn from φ_n, and we therefore have $\widehat{p}_1 = p_0$. At the following levels $s > 1$, we proceed similarly by defining y_s as the p_0-quantiles of $\mathcal{Y}_s = \{G(\mathbf{u}_s^{(j)}), 1 \le j \le N\}$, where $\mathcal{U}_s = \{\mathbf{u}_s^{(j)}, 1 \le j \le N\}$ are the i.i.d. samples drawn from $\varphi_n(\cdot|E_{s-1})$. The SS algorithm ends when the p_0-quantile of $\mathcal{Y}_s = \{G(\mathbf{u}_s^{(j)}), 1 \le j \le N\}$ becomes lower than zero. The last level y_m is set to zero, and the corresponding probability $\widehat{p}_m$ is given by $\widehat{p}_m = \#\mathcal{J}/N$, where $\mathcal{J} = \{j \in \{1, \ldots, N\} : G(\mathbf{u}_m^{(j)}) \le 0\}$ and $\#\mathcal{J}$ denotes the cardinality of the set $\mathcal{J}$. The probability $\widehat{p}_m$ estimated at the last level $y_m = 0$ is therefore greater than or equal to p_0, and the estimation of p_{f} by SS is simply given by:

$$\widehat{p}_{\mathrm{f}}^{\mathrm{SS}} = p_0^{m-1}\widehat{p}_m. \tag{I.60}$$

In SS, we need to generate independent samples from the n-dimensional standard normal PDF φ_n at the first level ($s = 1$), see Eq. (I.57), and from the conditional n-dimensional standard normal PDF $\varphi_n(\cdot|E_{s-1})$ at the next levels ($s > 1$), see Eq. (I.58). Sampling from φ_n is straightforward and corresponds to a crude MC simulation. Sampling from the conditional PDF $\varphi_n(\cdot|E_{s-1})$ for $s > 1$ is however not trivial. In SS, this is performed by means of *Markov chain Monte Carlo* (MCMC), which is a useful technique for approximate sampling from an arbitrary distribution (see, e.g., Robert and Casella, 2004; Kroese et al., 2011). The specific algorithm used in SS is detailed in the next section.

I–3.2.3 Approximate sampling from $\varphi_n(\cdot|E_{s-1})$ for $s = 2, \dots, m$

It should first be noticed that an acceptance-rejection method would be inefficient to generate samples from $\varphi_n(\cdot|E_{s-1})$ for $s = 2, \dots, m$ (draw samples from φ_n, accept those that belong to $\mathcal{F}_{\mathbf{u},s-1}$, reject otherwise). The acceptance probability is proportional to $\mathbb{P}(E_{s-1})$, which decreases with s to reach a value for $s = m$ in the order of the unknown and small probability p_f.

In order to simulate samples from $\varphi_n(\cdot|E_{s-1})$ for $s = 2, \dots, m$, SS resorts to Markov Chain Monte Carlo (MCMC). This technique was invented soon after crude Monte Carlo and dates back to 1953 with the original work of Metropolis et al. (1953) at Los Alamos. This section briefly presents the principle of Markov chains to generate samples from an arbitrary multivariate target distribution which cannot be directly sampled (e.g. known up to a scaling factor). The *Metropolis-Hastings algorithm*, one of the most popular MCMC techniques, is first described. This algorithm was adapted by Au and Beck (2001) for the specific needs of SS and this important variant is then detailed. Note that the presentation of Markov chains and the above-mentioned algorithms is made in the standard normal space $\mathbb{R}^n$, in coherence with the formulation of the SS method. A presentation in similar settings can be found in Papaioannou et al. (2015).

Let us introduce a time-homogeneous discrete-time *Markov chain* $\{\mathbf{U}^k, k \in \mathbb{N}\}$ in the continuous state space $\mathbb{R}^n$ (here the standard normal space). It is assumed that $\{\mathbf{U}^k, k \in \mathbb{N}\}$ is a first-order Markov chain:

$$\begin{aligned} \mathbb{P}\left(\mathbf{U}^{k+1} \in A \,|\, \textstyle\bigcap_{m=0}^{k} \{\mathbf{U}^m = \mathbf{u}^m\}\right) &= \mathbb{P}\left(\mathbf{U}^{k+1} \in A \,|\, \{\mathbf{U}^k = \mathbf{u}^k\}\right) \\ &\overset{\text{def}}{=} K\left(A|\mathbf{u}^k\right), \end{aligned} \tag{I.61}$$

for any $A \in \mathcal{B}$, $\mathcal{B}$ being the Borel σ-field of $\mathbb{R}^n$, and where K is the *transition kernel* of the Markov chain. $K\left(A|\mathbf{u}^k\right) = \int_A K\left(\mathrm{d}\mathbf{v}|\mathbf{u}^k\right)$ is a conditional distribution function that represents the probability of moving from $\mathbf{u}^k$ to a point in the set A. K is assumed to be independent of k, which makes the chain time-independent (or stationary). The marginal distribution of $\mathbf{U}^0$ is called the *initial distribution* of the chain.

At any given level $s > 1$ of the SS algorithm, the objective is to sample a Markov chain $\{\mathbf{U}^k, k \in \mathbb{N}\}$ whose invariant (or stationary) distribution is the *target distribution* $\varphi_n(\cdot|E_{s-1})$. MCMC algorithms start from a set of initial states of the chain which are in general not distributed according to the target distribution. The samples generated from the Markov chain are expected to follow the target distribution for sufficiently large k after a transient stage known as the *burn-in* period. It is important to point out that the generated samples are expected to be identically distributed according to the target density after this burn-in period but they are not independent. Some level of dependence in fact appears in the chain due to the use of a proposal PDF q, introduced later in this section. Convergence to a unique invariant distribution occurs under some regularity conditions of the constructed Markov chain, known as aperiodicity and irreducibility (see, e.g., Kroese et al., 2011). These conditions are met in usual MCMC samplers. They are in particular satisfied for proposal PDFs q with a restricted support, such as uniform PDFs centered at the current state of the chain with a finite width (Chib and Greenberg, 1995), as applied in SS.

The potential move in the standard normal space from a current state denoted $\mathbf{u}$ to a new state denoted $\mathbf{v}$ is characterized by a transition kernel K, generally expressed as follows:

$$K(\mathrm{d}\mathbf{v}|\mathbf{u}) = p(\mathbf{v}|\mathbf{u})\,\mathrm{d}\mathbf{v} + r(\mathbf{u})\,\delta_{\mathbf{u}}(\mathrm{d}\mathbf{v}) \;, \tag{I.62}$$

where $p : \mathbb{R}^n \times \mathbb{R}^n \to \mathbb{R}_{\geq 0}, (\mathbf{u},\mathbf{v}) \mapsto p(\mathbf{v}|\mathbf{u})$ is a given function, such that $p(\mathbf{u}|\mathbf{u}) = 0$, δ is the Dirac delta function, such that $\delta_{\mathbf{u}}(\mathrm{d}\mathbf{v}) = 1$ if $\mathbf{u} \in \mathrm{d}\mathbf{v}$ and 0 otherwise, and $r(\mathbf{u}) = 1 - \int_{\mathbb{R}^n} p(\mathbf{v}|\mathbf{u})\,\mathrm{d}\mathbf{v}$. The first continuous term of the sum defines the move from $\mathbf{u}$ to $\mathbf{v}$ according to $p(\mathbf{v}|\mathbf{u})$, and the second discrete term represents the stagnation at $\mathbf{u}$ with probability $r(\mathbf{u})$.

The invariant distribution of the Markov chain must satisfy the following condition, which states that if $\mathbf{U}^k$ is distributed according to the target distribution $\varphi_n(\cdot|E_{s-1})$, then $\mathbf{U}^{k+1}$ and all subsequent elements of the chain are also distributed according to $\varphi_n(\cdot|E_{s-1})$:

$$\varphi_n(\mathbf{v}|E_{s-1})\,\mathrm{d}\mathbf{v} = \int_{\mathbb{R}^n} K(\mathrm{d}\mathbf{v}\,|\,\mathbf{u})\,\varphi_n(\mathbf{u}|E_{s-1})\,\mathrm{d}\mathbf{u} \;. \tag{I.63}$$

A sufficient condition for the target distribution $\varphi_n(\cdot|E_{s-1})$ to be a stationary (or invariant) distribution for K is to satisfy the so-called *reversibility* condition a.k.a. *detailed balance*:

$$\varphi_n(\mathbf{u}|E_{s-1})\,p(\mathbf{v}|\mathbf{u}) = \varphi_n(\mathbf{v}|E_{s-1})\,p(\mathbf{u}|\mathbf{v}) \;. \tag{I.64}$$

It is easy to show that Eq. (I.64) implies Eq. (I.63) (see, e.g., Tierney, 1994; Chib and Greenberg, 1995).

We will be specifically interested here in the Metropolis-Hastings kernel (Hastings, 1970), defined such that:

$$p(\mathbf{v}|\mathbf{u}) = p_{\mathrm{MH}}(\mathbf{v}|\mathbf{u}) = \begin{cases} q(\mathbf{v}|\mathbf{u})\,\alpha(\mathbf{u},\mathbf{v}) & \text{if } \mathbf{u} \neq \mathbf{v} \,, \\ 0 & \text{if } \mathbf{u} = \mathbf{v} \,, \end{cases} \tag{I.65}$$

where $q(\mathbf{v}|\mathbf{u})$ is a *proposal* PDF (note that we have $\int_{\mathbb{R}^n} q(\mathbf{v}|\mathbf{u})\,\mathrm{d}\mathbf{v} = 1$), and $\alpha(\mathbf{u},\mathbf{v})$ is the probability of moving from $\mathbf{u}$ to $\mathbf{v}$. The reversibility of the transition kernel w.r.t. $\varphi_n(\cdot|E_{s-1})$ is imposed by construction, by defining $\alpha(\mathbf{u},\mathbf{v})$ as follows:

$$\alpha(\mathbf{u},\mathbf{v}) = \begin{cases} \min\left\{ \dfrac{\varphi_n(\mathbf{v}|E_{s-1})\,q(\mathbf{u}|\mathbf{v})}{\varphi_n(\mathbf{u}|E_{s-1})\,q(\mathbf{v}|\mathbf{u})} \,,\, 1 \right\} & \text{if } \varphi_n(\mathbf{u}|E_{s-1})\,q(\mathbf{v}|\mathbf{u}) > 0 \,, \\ 1 & \text{if } \varphi_n(\mathbf{u}|E_{s-1})\,q(\mathbf{v}|\mathbf{u}) = 0 \,. \end{cases} \tag{I.66}$$

The original Metropolis sampler (Metropolis et al., 1953) is obtained by assuming that the proposal PDF q is symmetric, i.e. such that $q(\mathbf{v}|\mathbf{u}) = q(\mathbf{u}|\mathbf{v})$. In such a case, the move probability (a.k.a. acceptance probability) is given by:

$$\alpha(\mathbf{u},\mathbf{v}) = \begin{cases} \min\left\{ \dfrac{\varphi_n(\mathbf{v}|E_{s-1})}{\varphi_n(\mathbf{u}|E_{s-1})} \,,\, 1 \right\} & \text{if } \varphi_n(\mathbf{u}|E_{s-1})\,q(\mathbf{v}|\mathbf{u}) > 0 \,, \\ 1 & \text{if } \varphi_n(\mathbf{u}|E_{s-1})\,q(\mathbf{v}|\mathbf{u}) = 0 \,. \end{cases} \tag{I.67}$$

If $\varphi_n(\mathbf{v}|E_{s-1}) > \varphi_n(\mathbf{u}|E_{s-1})$, the move from $\mathbf{u}$ to $\mathbf{v}$ is always accepted. Otherwise the move is accepted with a probability given by the ratio $\varphi_n(\mathbf{v}|E_{s-1})/\varphi_n(\mathbf{u}|E_{s-1})$. A straightforward choice to ensure symmetry in the proposal PDF q is to consider $\mathbf{v} = \mathbf{u} + \mathbf{z}$, where $\mathbf{z}$ is a realization of a random vector $\mathbf{Z}$ independent of $\mathbf{U}$ and whose n-variate PDF $f_{\mathbf{Z}}$ is symmetric about zero, i.e. such that $f_{\mathbf{Z}}(\mathbf{z}) = f_{\mathbf{Z}}(-\mathbf{z})$. The proposal PDF is then defined as $q(\mathbf{v}|\mathbf{u}) = f_{\mathbf{Z}}(\mathbf{v}-\mathbf{u})$. Straightforward choices for $f_{\mathbf{Z}}$ include the normal or uniform multivariate distributions. Because the candidate state is equal to the current state of the chain plus noise, samplers of this form are usually termed *random-walk* Metropolis samplers. Note that if q does not satisfy the symmetry property $q(\mathbf{v}|\mathbf{u}) = q(\mathbf{u}|\mathbf{v})$, the constructed sampler is usually referred to as a Metropolis-Hastings sampler.

Assuming that $\varphi_n(\mathbf{u}|E_{s-1})\,q(\mathbf{v}|\mathbf{u}) > 0$ (i.e. $\mathbf{u} \in \mathcal{F}_{\mathbf{u},s-1}$ and $q(\mathbf{v}|\mathbf{u}) > 0$), we can express the move probability $\alpha(\mathbf{u},\mathbf{v})$ as follows, using Eq. (I.59) (Papaioannou et al., 2015):

$$\begin{aligned}\alpha(\mathbf{u},\mathbf{v}) &= \min\left\{\frac{\varphi_n(\mathbf{v}|E_{s-1})\,q(\mathbf{u}|\mathbf{v})}{\varphi_n(\mathbf{u}|E_{s-1})\,q(\mathbf{v}|\mathbf{u})}\,,\,1\right\}\\ &= \min\left\{\frac{\varphi_n(\mathbf{v})\,q(\mathbf{u}|\mathbf{v})}{\varphi_n(\mathbf{u})\,q(\mathbf{v}|\mathbf{u})}\mathbb{1}_{\mathcal{F}_{\mathbf{u},s-1}}(\mathbf{v})\,,\,1\right\}\\ &= \min\left\{\frac{\varphi_n(\mathbf{v})\,q(\mathbf{u}|\mathbf{v})}{\varphi_n(\mathbf{u})\,q(\mathbf{v}|\mathbf{u})}\,,\,1\right\}\mathbb{1}_{\mathcal{F}_{\mathbf{u},s-1}}(\mathbf{v})\\ &= \alpha_{\varphi_n}(\mathbf{u},\mathbf{v})\,\mathbb{1}_{\mathcal{F}_{\mathbf{u},s-1}}(\mathbf{v})\ .\end{aligned} \tag{I.68}$$

From the above expression, it is found that the move probability $\alpha(\mathbf{u},\mathbf{v})$ of the Metropolis-Hastings kernel can be expressed as the product of the move probability $\alpha_{\varphi_n}(\mathbf{u},\mathbf{v})$ based on the unconditional n-dimensional standard normal PDF φ_n and the indicator function of the intermediate failure domain $\mathcal{F}_{\mathbf{u},s-1}$. This enables a two-step implementation of the Metropolis-Hastings algorithm for generating samples from the target distribution $\varphi_n(\cdot|E_{s-1})$:

1. First, a candidate sample $\mathbf{v}$ is drawn from the proposal PDF $q(\mathbf{v}|\mathbf{u})$ and the move from $\mathbf{u}$ to $\mathbf{v}$ is temporarily accepted with probability $\alpha_{\varphi_n}(\mathbf{u},\mathbf{v})$. This corresponds to a single application of a Metropolis-Hastings kernel where $p_{\mathrm{MH}}(\mathbf{v}|\mathbf{u}) = q(\mathbf{v}|\mathbf{u})\,\alpha_{\varphi_n}(\mathbf{u},\mathbf{v})$ for $\mathbf{u} \neq \mathbf{v}$, see Eq. (I.65).
2. Second, the move from $\mathbf{u}$ to $\mathbf{v}$ is finally accepted if $\mathbf{v} \in \mathcal{F}_{\mathbf{u},s-1}$. If not, the chain remains in its current state $\mathbf{u}$. This second step requires the evaluation of the LSF at $\mathbf{v}$ to know whether $\mathbf{v} \in \mathcal{F}_{\mathbf{u},s-1}$ or not.

An implementation of the standard Metropolis-Hastings sampler is given in Table I.1. For a given intermediate level with $s \in \{2,\ldots,m\}$, the objective is to construct the sample set $\mathcal{U}_s = \{\mathbf{u}_s^{(j)}, 1 \leq j \leq N\}$ such as defined in Section I–3.2.2. These samples are obtained from $K = 1/p_0$ successive draws of $N_c = p_0 N$ separate Markov chains, see lines 4-14 in Table I.1 (note that we do not consider any burn-in period as explained later in this section, all the draws are gathered in $\mathcal{U}_s$ starting from the first element of the chain and this for each chain [4]). The initial states of these N_c chains (called seeds of the chains) are taken as the samples of $\mathcal{U}_{s-1}$ whose LSF evaluations are lower than y_{s-1}, see lines 1-3 in Table I.1. The algorithm proposed in Table I.1 presents some deficiencies in high-dimensional spaces (large n) which make it inapplicable in such a context. The probability that a given Markov chain will remain in its current state $\mathbf{u}_s^{(j),k-1}$ approaches 1 when the dimension n increases (see Au and Beck, 2001, Appendix; Papaioannou et al., 2015, Section 3.1.2). The direct consequence is to obtain repeated samples in $\mathcal{U}_s$ sets and therefore a high level of correlation between samples in these sets. This results in a poor convergence of $\widehat{p}_s$ estimators given in Eq. (I.58) compared to the ideal case based on i.i.d. samples. A geometric interpretation of why the standard Metropolis-Hastings sampler fails in high dimensions can also be given (Katafygiotis and Zuev, 2008).

In order to address high-dimensional reliability problems, Au and Beck (2001) proposed a *componentwise* adaptation of the standard Metropolis sampler. This adaptation is known as the *modified Metropolis* (m-M) algorithm, which represents a key ingredient of SS. We assume again a two-step implementation of the m-M algorithm, as used for the standard Metropolis-Hastings sampler. The transition kernel applied in the first step is now expressed as a product of the transition kernels of each coordinate (Zuev and Katafygiotis, 2011b; Zuev et al., 2012):

$$K(\mathrm{d}\mathbf{v}|\mathbf{u}) = \prod_{i=1}^{n} K_i(\mathrm{d}v_i|u_i)\ , \tag{I.69}$$

[4] The notation $\mathbf{u}_s^{(j),k}$ will be used if an explicit mention of the k^{th} sample in the j^{th} chain is required. If not, the shorter notation $\mathbf{u}_s^{(j)}$ will be used for reference to the j^{th} sample in the set $\mathcal{U}_s$.

1	$\mathcal{J}_{\text{seeds}} = \{j \in \{1, \dots, N\} : G(\mathbf{u}_{s-1}^{(j)}) \leq y_{s-1}\}$ // index set of seeds in $\mathcal{U}_{s-1}$ (size $N_c = p_0 N$)
2	$\mathcal{J}_{\text{chains}} = \{1, \dots, N_c\}$ // index set of Markov chains in $\mathcal{U}_s$ (size $N_c = p_0 N$)
3	$\mathbf{u}_s^{(\mathcal{J}_{\text{chains}}),0} = \mathbf{u}_{s-1}^{(\mathcal{J}_{\text{seeds}})}$ // set initial state of N_c Markov chains
4	$K = 1/p_0$
5	**for** $k = 1$ **to** K
6	**for** $j = 1$ **to** N_c
7	// apply Metropolis-Hasting algorithm
8	Sample $\mathbf{v}$ from proposal PDF $q(\cdot\|\mathbf{u}_s^{(j),k-1})$
9	Compute acceptance ratio $\alpha_{\varphi_n}^k = \alpha_{\varphi_n}\left(\mathbf{u}_s^{(j),k-1}, \mathbf{v}\right) \dfrac{\varphi_n(\mathbf{v})\, q\left(\mathbf{u}_s^{(j),k-1}\|\mathbf{v}\right)}{\varphi_n\left(\mathbf{u}_s^{(j),k-1}\right) q\left(\mathbf{v}\|\mathbf{u}_s^{(j),k-1}\right)}$
10	Accept or reject $\mathbf{v}$: $\widetilde{\mathbf{v}} = \begin{cases} \mathbf{v} & \text{with probability } \min\{1, \alpha_{\varphi_n}^k\} \\ \mathbf{u}_s^{(j),k-1} & \text{with probability } 1 - \min\{1, \alpha_{\varphi_n}^k\} \end{cases}$
11	Accept or reject $\widetilde{\mathbf{v}}$: $\mathbf{u}_s^{(j),k} = \begin{cases} \widetilde{\mathbf{v}} & \text{if } \widetilde{\mathbf{v}} \in \mathcal{F}_{\mathbf{u},s-1} \\ \mathbf{u}_s^{(j),k-1} & \text{if } \widetilde{\mathbf{v}} \notin \mathcal{F}_{\mathbf{u},s-1} \end{cases}$
12	**end for**
13	**end for**
14	$\mathcal{U}_s = \{\mathbf{u}_s^{(j),k}, 1 \leq j \leq N_c, 1 \leq k \leq K\}$ // define new sample set $\mathcal{U}_s$

Note: $\lceil x \rceil$ stands for the smallest integer not lower than x.

Table I.1 – Application of the standard Metropolis-Hasting sampler, construction of the sample set $\mathcal{U}_s = \{\mathbf{u}_s^{(j)}, 1 \leq j \leq N\}$ for $s = 2, \dots, m$.

where $\mathrm{d}\mathbf{v} = (\mathrm{d}v_1, \dots, \mathrm{d}v_n)^{\mathrm{T}}$, $\mathbf{u} = (u_1, \dots, u_n)^{\mathrm{T}}$ and K_i represents the transition kernel of the i^{th} coordinate. For $i = 1, \dots, n$, K_i is taken as a standard Metropolis kernel defined as follows:

$$K_i(\mathrm{d}v_i|u_i) = p_i(v_i|u_i)\,\mathrm{d}v_i + r_i(u_i)\,\delta_{u_i}(\mathrm{d}v_i)\ , \tag{I.70}$$

$$\text{where } p_i: \quad \begin{array}{ccc} \mathbb{R}\times\mathbb{R} & \to & \mathbb{R}_{\geq 0} \\ (u_i, v_i) & \mapsto & p_i(v_i|u_i) = \begin{cases} q_i(v_i|u_i)\,\alpha_\varphi(u_i, v_i) & \text{if } u_i \neq v_i\ , \\ 0 & \text{if } u_i = v_i\ , \end{cases} \end{array}$$

in which q_i is a univariate proposal PDF (assumed symmetric in SS) and $\alpha_\varphi(u_i, v_i) = \dfrac{\varphi(v_i)}{\varphi(u_i)}$,

and where $r_i(u_i) = 1 - \int_{\mathbb{R}} p_i(v_i|u_i)\,\mathrm{d}v_i$.

The algorithm proposed in SS by Au and Beck (2001) is given in Table I.2. Note that this algorithm is similar to the one proposed in Table I.1, except lines 7-11 which are replaced by lines 7-13. The initial states of the $N_c = p_0 N$ chains are again defined as the samples of $\mathcal{U}_{s-1}$ whose LSF evaluations are lower than y_{s-1}, see the 2-dimensional example for $s = 2$ given in Figure I.8a. The n proposal PDFs q_i are chosen as uniform PDFs of width $2w_i = 2w$ centered at the i^{th} coordinate of the current state $\mathbf{u}_s^{(j),k-1}$, i.e. such that $q_i(v_i|u_i) = \frac{1}{2w}\mathbb{1}_{[u_i - w, u_i + w]}(v_i)$, see Figure I.8b for $k = 1$ (centering at the initial state of the chains). Note that the w_i parameters are identically set to a unique value denoted w, since we are working in the standard normal space, with the same "scale" along each axis u_i.

The m-M algorithm is characterized by the following important properties:

1. The m-M algorithm works componentwise with univariate proposal PDFs q_i, which allows independent moves along each axis. Such a technique reduces the number of repeated samples in $\mathcal{U}_s$ sets compared to the original Metropolis-Hastings algorithm, which makes SS well adapted to high-dimensional reliability problems (large n).

1 $\mathcal{J}_{\text{seeds}} = \{j \in \{1, \ldots, N\} : G(\mathbf{u}_{s-1}^{(j)}) \leq y_{s-1}\}$ // index set of seeds in $\mathcal{U}_{s-1}$ (size $N_c = p_0 N$)
2 $\mathcal{J}_{\text{chains}} = \{1, \ldots, N_c\}$ // index set of Markov chains in $\mathcal{U}_s$ (size $N_c = p_0 N$)
3 $\mathbf{u}_s^{(\mathcal{J}_{\text{chains}}),0} = \mathbf{u}_{s-1}^{(\mathcal{J}_{\text{seeds}})}$ // set initial state of N_c Markov chains
4 $K = 1/p_0$
5 **for** $k = 1$ **to** K
6 **for** $j = 1$ **to** N_c
7 // apply componentwise Metropolis algorithm from Au and Beck (2001)
8 **for** $i = 1$ **to** n
9 Sample v_i from proposal PDF $q_i(\cdot|u_{s,i}^{(j),k-1})$
10 Compute acceptance ratio $\alpha_{\varphi,i}^k = \alpha_\varphi\left(u_{s,i}^{(j),k-1}, v_i\right) = \dfrac{\varphi(v_i)}{\varphi\left(u_{s,i}^{(j),k-1}\right)}$
11 Accept or reject v_i : $\widetilde{v}_i = \begin{cases} v_i & \text{with probability } \min\{1, \alpha_{\varphi,i}^k\} \\ u_{s,i}^{(j),k-1} & \text{with probability } 1 - \min\{1, \alpha_{\varphi,i}^k\} \end{cases}$
12 **end for**
13 Accept or reject $\widetilde{\mathbf{v}} = (\widetilde{v}_1, \ldots, \widetilde{v}_n)^{\mathrm{T}}$: $\mathbf{u}_s^{(j),k} = \begin{cases} \widetilde{\mathbf{v}} & \text{if } \widetilde{\mathbf{v}} \in \mathcal{F}_{\mathbf{u},s-1} \\ \mathbf{u}_s^{(j),k-1} & \text{if } \widetilde{\mathbf{v}} \notin \mathcal{F}_{\mathbf{u},s-1} \end{cases}$
14 **end for**
15 **end for**
16 $\mathcal{U}_s = \{\mathbf{u}_s^{(j),k}, 1 \leq j \leq N_c, 1 \leq k \leq K\}$ // define new sample set $\mathcal{U}_s$

Note: $\lceil x \rceil$ stands for the smallest integer not lower than x.

Table I.2 – Application of the componentwise Metropolis sampler of Au and Beck (2001), construction of the sample set $\mathcal{U}_s = \{\mathbf{u}_s^{(j)}, 1 \leq j \leq N\}$ for $s = 2, \ldots, m$.

(a) Initial state of Markov chains $\mathbf{u}_s^{(j),0}$ for $s = 2$

(b) Sampling from univariate proposal PDFs $q_i(\cdot|u_{2,i}^{(j),0})$, $i = 1, 2$

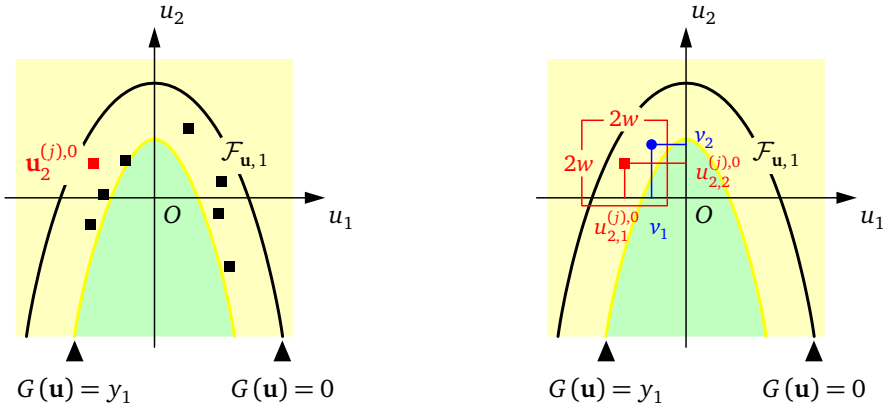

Figure I.8 – Modified Metropolis algorithm: seeds of Markov chains and proposal PDFs.

2. The target distribution of samples with MCMC is usually attained as the stationary distribution of the Markov chain, which generally imposes a burn-in period. In SS, the seeds already follow the target distribution $\varphi_n(\cdot|E_{s-1})$ which means that any further states of the chain are distributed according to this target distribution (see, e.g., Au and Beck, 2001; Zuev et al., 2012, for a demonstration). This property, known as *perfect sampling* in the MCMC literature, makes any burn-in period unnecessary. For this reason, the $\mathcal{U}_s$ sets are composed of all the states of the Markov chains from $k = 1$ to $K = 1/p_0$.
3. The samples generated with the m-M algorithm are not independent. The level of correlation in the chains (and therefore in the samples of the $\mathcal{U}_s$ sets) depends on the choice of the n proposal PDFs q_i. The idea of the m-M algorithm of SS is to use proposal PDFs q_i which are sufficiently local to ensure that the sample candidates $\widetilde{\mathbf{v}}$ mostly lie in $\mathcal{F}_{\mathbf{u},s-1}$. Practically, this is tuned by means of the unique parameter w of the uniform proposal PDFs q_i. If w is too small, the probability that $\widetilde{\mathbf{v}}$ lies in $\mathcal{F}_{\mathbf{u},s-1}$ is high, which thus avoids repeated samples in the $\mathcal{U}_s$ set. However, the candidate state $\widetilde{\mathbf{v}}$ is close to the current state $\mathbf{u}_s^{(j),k-1}$, which induces a high level of correlation in the chain due to the small moves and therefore reduces the efficiency of the conditional estimators $\widehat{p}_s$ for $s = 2, \ldots, m$. Moreover, proposal PDFs which are too local do not enable a sufficiently wide exploration of the intermediate failure domain $\mathcal{F}_{\mathbf{u},s-1}$, which may result in a biased estimate $\widehat{p}_\mathrm{f}^{\mathrm{SS}}$ if important failure zones are missed at intermediate levels. If w is too large, the proposal PDFs allow a sufficiently wide exploration of $\mathcal{F}_{\mathbf{u},s-1}$ but the probability that $\widetilde{\mathbf{v}}$ lies in $\mathcal{F}_{\mathbf{u},s-1}$ is low. The chain is expected to remain at the current state $\mathbf{u}_s^{(j),k-1}$, which results in an increase in the number of repeated samples in the $\mathcal{U}_s$ set. The consequence is again a high level of correlation in the chains, which therefore implies a drop in the efficiency of the conditional estimators $\widehat{p}_s$. According to Au and Beck (2001), the efficiency of the m-M algorithm is not sensitive to the type of proposal PDFs but to their spreads. A tradeoff is made in SS with a parameter w set to 2 (Au and Beck, 2001). It is worth pointing out that attempts to reduce the correlation in the chains have been made in a few works (Miao and Ghosn, 2011; Santoso et al., 2011; Zuev and Katafygiotis, 2011a; Zuev et al., 2012; Papaioannou et al., 2015). The reader may refer to the recent paper from Papaioannou et al. (2015) for a comparative review of these works.

I–3.2.4 Statistical properties of the SS failure probability estimator

(a) Coefficient of variation of $\widehat{p}_\mathrm{f}^{\mathrm{SS}}$

The coefficient of variation of $\widehat{p}_\mathrm{f}^{\mathrm{SS}}$ can be estimated from a single run of the SS method. This is important for assessing the accuracy of the probability estimate obtained by this method. Only the main expressions required to calculate this quantity are recalled here, and the reader may refer to Au and Beck (2001) for further details and proofs of the given expressions. The coefficient of variation of $\widehat{p}_\mathrm{f}^{\mathrm{SS}}$ denoted $\delta_{\widehat{p}_\mathrm{f}^{\mathrm{SS}}}$ can be bounded above according to the following expression:

$$\delta^2_{\widehat{p}_\mathrm{f}^{\mathrm{SS}}} = \mathbb{E}\left[\left(\frac{\widehat{p}_\mathrm{f}^{\mathrm{SS}} - p_\mathrm{f}}{p_\mathrm{f}}\right)^2\right] \leq \sum_{r,s=1}^{m} \delta_r \delta_s + o\left(\frac{1}{N}\right) = \mathcal{O}\left(\frac{1}{N}\right), \tag{I.71}$$

where δ_s represents the coefficient of variation of $\widehat{p}_s$ for $s = 1, \ldots, m$. This upper bound is established under the assumption of fully-correlated probability estimators $\widehat{p}_s$. It is worth pointing out that the coefficient of variation $\delta_{\widehat{p}_\mathrm{f}^{\mathrm{SS}}}$ is expressed in terms of a deviation w.r.t. the unknown probability p_f and not w.r.t. the expectation of the probability estimator such as defined in Eq. (I.52) for the MC estimator. For this reason, $\delta_{\widehat{p}_\mathrm{f}^{\mathrm{SS}}}$ accounts for the bias effect.

The coefficients of variation δ_s appearing in Eq. (I.71) for $s = 1, \dots, m$ are calculated as follows. The first level of SS is merely a crude MC simulation and the coefficient of variation of $\widehat{p}_1$ therefore reads:

$$\delta_1 = \sqrt{\frac{1-p_1}{Np_1}} \,. \tag{I.72}$$

At the next level $s = 2, \dots, m$, the coefficient of variation δ_s of the conditional estimators $\widehat{p}_s$ is given by the following expression (Au and Beck, 2001):

$$\delta_s = \sqrt{\frac{1-p_s}{Np_s}\left(1+\gamma_s\right)} \,, \tag{I.73}$$

where:

$$\gamma_s = 2\sum_{\ell=1}^{K-1}\left(1-\frac{\ell}{K}\right)\rho_s\left(\ell\right) \,, \tag{I.74}$$

in which $K = N/N_c = 1/p_0$ and $\rho_s\left(\ell\right) = R_s\left(\ell\right)/R_s\left(0\right)$,

and where $R_s\left(\ell\right)$ is the covariance between $\mathbb{1}_{\mathcal{F}_{\mathbf{u},s}}\left(\mathbf{u}_s^{(j),k}\right)$ and $\mathbb{1}_{\mathcal{F}_{\mathbf{u},s}}\left(\mathbf{u}_s^{(j),k+\ell}\right)$ for any lag $\ell = 0, \dots, (K-1)$ (note that this covariance should be independent of k due to stationarity, and independent of j since all chains are probabilistically equivalent):

$$R_s\left(\ell\right) = \mathbb{E}\left[\mathbb{1}_{\mathcal{F}_{\mathbf{u},s}}\left(\mathbf{u}_s^{(j),k}\right)\mathbb{1}_{\mathcal{F}_{\mathbf{u},s}}\left(\mathbf{u}_s^{(j),k+\ell}\right)\right] - p_s^2 \,. \tag{I.75}$$

The autocovariance sequence $\{R_s\left(\ell\right), \ell = 0, \dots, K-1\}$ is practically estimated from the samples of the set $\mathcal{U}_s$ by averaging on both the N_c chains and their elements according to the following expression:

$$\widehat{R}_s\left(\ell\right) = \left(\frac{1}{N_c\left(K-\ell\right)}\sum_{j=1}^{N_c}\sum_{k=1}^{K-\ell}\mathbb{1}_{\mathcal{F}_{\mathbf{u},s}}\left(\mathbf{u}_s^{(j),k}\right)\mathbb{1}_{\mathcal{F}_{\mathbf{u},s}}\left(\mathbf{u}_s^{(j),k+\ell}\right)\right) - \widehat{p}_s^2 \,. \tag{I.76}$$

The coefficient $\gamma_s > 0$ appearing in Eq. (I.73) makes the coefficient of variation δ_s of the conditional probabilities $\widehat{p}_s$ larger than that of the MC estimate with i.i.d. samples, which corresponds to the case $\gamma_s = 0$. Working with correlated MCMC samples therefore appears less efficient than a simulation with i.i.d. samples. For a better efficiency in the SS method, one could search for optimal values of the parameter w which controls the width of the n uniform proposal PDFs in order to minimize γ_s at each level $s = 2, \dots, m$. This problem investigated by Zuev et al. (2012) has unfortunately no practically implementable solution. An alternative proposed by these authors is to adapt w for an average number of accepted candidate states between 30 and 50%.

Another expression, less pessimistic than the upper bound given in Eq. (I.71), is often used to estimate the coefficient of variation of $\widehat{p}_f^{SS}$. This expression, based on the assumption of independent probability estimators $\widehat{p}_s$, writes (Au and Beck, 2001):

$$\delta^2_{\widehat{p}_f^{SS}} \approx \sum_{s=1}^{m}\delta_s^2 \,. \tag{I.77}$$

This second expression is reported to give fairly good approximations of the true coefficient of variation of $\widehat{p}_f^{SS}$ in Au and Beck (2001), although it underestimates it. From the author's experience neither of these two expressions is more accurate than the other. The upper bound sometimes appears closer to the true coefficient of variation in some problems.

(b) Bias of $\widehat{p}_{\mathrm{f}}^{\mathrm{SS}}$

The estimator $\widehat{p}_{\mathrm{f}}^{\mathrm{SS}} = \prod_{s=1}^{m} \widehat{p}_s$ is biased for any sample size N due to the correlation that exists between the estimators $\widehat{p}_s$ for $s = 1, \ldots, m$ (Au and Beck, 2001). This correlation is due to the way the seeds of the chains are selected: the seeds at level s are samples generated at the previous level $(s-1)$, see lines 1-3 of Table I.2. This therefore results in a correlation between $\widehat{p}_s$ and $\widehat{p}_{s-1}$ for $s = 2, \ldots, m$. The estimator $\widehat{p}_{\mathrm{f}}^{\mathrm{SS}}$ is asymptotically unbiased, and its relative bias can be bounded from above by the following expression (Au and Beck, 2001):

$$\left| \mathbb{E}\left[\frac{\widehat{p}_{\mathrm{f}}^{\mathrm{SS}} - p_{\mathrm{f}}}{p_{\mathrm{f}}} \right] \right| \leq \sum_{r>s} \delta_r \delta_s + o\left(\frac{1}{N}\right) = \mathcal{O}\left(\frac{1}{N}\right) . \tag{I.78}$$

This bias of order $1/N$ thus becomes negligible compared to the standard deviation when N is increased. Moreover, it can be shown that the bias is always positive (Guyader, 2011).

I–3.2.5 Remark about the computer implementation of SS

The SS method is available in FERUM 4.x as proposed by Au and Beck (2001). The implemented algorithm takes full advantage of the independence of:

- the first N calls to the LSF evaluated at the initial level $s = 1$ of SS (crude MC), which are sent as independent tasks,
- the N_{c} chains that are sampled in parallel for a given k, see lines 6-12 of Table I.2.

In SS, the LSF evaluation tasks are sent in the following sequence: N independent calls to the LSS for $s = 1$, then $p_0 N$ independent calls times K (length of the chains) times $(m-1)$ (for each intermediate level $s = 2, \ldots, m$). SS therefore appears less suited to distributed computations than crude MC. Improving the parallelization efficiency of the method may be of interest, as recently investigated by Walter (2015) in the framework of moving particles. Walter proposes a parallel multilevel splitting algorithm that allows the simultaneous and independent moves of several particles.

I–3.3 Importance sampling (IS) and cross-entropy (CE) methods

Importance sampling (IS) is one of the most well-known variance reduction techniques used for assessing small failure probabilities. The idea of IS is to draw samples following another distribution than the original one in order to populate the failure domain more frequently. The failure probability estimate assessed by IS is then obtained as a weighted average of these draws. The basic ideas of IS were outlined in the early fifties and this technique, used in conjunction with FORM, was later introduced in structural reliability (Schuëller and Stix, 1987; Melchers, 1989a). Several IS methods are available and the reader is invited to refer to general textbooks for an exhaustive list (see, e.g., Kroese et al., 2011). IS is also used in adaptive versions, one of which, known as the *cross-entropy* (CE) method, is presented in this report. The CE method has been used by the present author in different contexts: reliability assessment in time-invariant problems, see the examples given in Section I–3.4, reliability assessment in the context of uncertainty propagation with Markov chains considered as random inputs, see Section III–2.3.3, and stochastic optimization for hyperparameter selection of surrogate models, see Section II–2.4.

I–3.3.1 Importance sampling (IS)

Let us consider another PDF $h_{\mathbf{X}}$ in the problem formulated in Eq. (I.50), called *importance sampling PDF* or *instrumental PDF*, such that $f_{\mathbf{X}}$, from now on referred to as *nominal PDF*, is dominated by $h_{\mathbf{X}}$ in the absolutely continuous sense:

$$h_{\mathbf{X}}(\mathbf{x}) = 0 \Rightarrow \mathbb{1}_{\mathcal{F}_{\mathbf{x}}}(\mathbf{x})\, f_{\mathbf{X}}(\mathbf{x}) = 0 \quad \text{or equivalently} \quad \mathbb{1}_{\mathcal{F}_{\mathbf{x}}}(\mathbf{x})\, f_{\mathbf{X}}(\mathbf{x}) \neq 0 \Rightarrow h_{\mathbf{X}}(\mathbf{x}) \neq 0\,. \tag{I.79}$$

Note that this condition simply means that the support of $\mathbb{1}_{\mathcal{F}_{\mathbf{x}}}(\cdot)\, f_{\mathbf{X}}(\cdot)$ must be included in the support $\mathcal{D}_{h_{\mathbf{X}}}$ of $h_{\mathbf{X}}$.

Using the IS PDF $h_{\mathbf{X}}$, the unknown failure probability p_{f} is now rewritten as follows:

$$\begin{aligned} p_{\mathrm{f}} &= \int_{\mathcal{D}_{f_{\mathbf{X}}}} \mathbb{1}_{\mathcal{F}_{\mathbf{x}}}(\mathbf{x})\, f_{\mathbf{X}}(\mathbf{x})\, \mathrm{d}\mathbf{x} \\ &= \int_{\mathcal{D}_{h_{\mathbf{X}}}} \mathbb{1}_{\mathcal{F}_{\mathbf{x}}}(\mathbf{x})\, \frac{f_{\mathbf{X}}(\mathbf{x})}{h_{\mathbf{X}}(\mathbf{x})}\, h_{\mathbf{X}}(\mathbf{x})\, \mathrm{d}\mathbf{x} \\ &= \mathbb{E}_{h_{\mathbf{X}}}\left[\mathbb{1}_{\mathcal{F}_{\mathbf{x}}}(\mathbf{X})\, \frac{f_{\mathbf{X}}(\mathbf{X})}{h_{\mathbf{X}}(\mathbf{X})}\right] \\ &= \mathbb{E}_{h_{\mathbf{X}}}\left[\mathbb{1}_{\mathcal{F}_{\mathbf{x}}}(\mathbf{X})\, W(\mathbf{X})\right], \end{aligned} \tag{I.80}$$

where the ratio of densities $W(\mathbf{x}) = f_{\mathbf{X}}(\mathbf{x})/h_{\mathbf{X}}(\mathbf{x})$ is called the *likelihood ratio* or *importance sampling quotient*.

The IS estimator of p_{f} therefore reads:

$$\widehat{p}_{\mathrm{f}}^{\,\mathrm{IS}} = \frac{1}{N}\sum_{j=1}^{N} \mathbb{1}_{\mathcal{F}_{\mathbf{x}}}\left(\mathbf{X}^{(j)}\right) \frac{f_{\mathbf{X}}\left(\mathbf{X}^{(j)}\right)}{h_{\mathbf{X}}\left(\mathbf{X}^{(j)}\right)}\,, \tag{I.81}$$

where $\{\mathbf{X}^{(j)}, 1 \leq j \leq N\}$ are N independent copies of the random vector $\mathbf{X}$ following the IS PDF $h_{\mathbf{X}}$, i.e. $\mathbf{X}^{(1)}, \ldots, \mathbf{X}^{(N)} \overset{\text{i.i.d.}}{\sim} h_{\mathbf{X}}$, and N denotes the sample size.

The IS estimator is unbiased (i.e. $\mathbb{E}_{h_{\mathbf{X}}}\left[\widehat{p}_{\mathrm{f}}^{\,\mathrm{IS}}\right] = p_{\mathrm{f}}$) and its variance is given by:

$$\mathrm{Var}_{h_{\mathbf{X}}}\left[\widehat{p}_{\mathrm{f}}^{\,\mathrm{IS}}\right] = \frac{1}{N}\left(\mathbb{E}_{h_{\mathbf{X}}}\left[\left(\mathbb{1}_{\mathcal{F}_{\mathbf{x}}}(\mathbf{X})\, \frac{f_{\mathbf{X}}(\mathbf{X})}{h_{\mathbf{X}}(\mathbf{X})}\right)^2\right] - p_{\mathrm{f}}^2\right). \tag{I.82}$$

The accuracy of the approximation given by IS critically depends on the choice of the IS PDF $h_{\mathbf{X}}$. The optimal choice for this PDF is obtained by minimizing the variance of $\widehat{p}_{\mathrm{f}}^{\,\mathrm{IS}}$ defined in Eq. (I.82). The optimal solution $h_{\mathbf{X}}^*$ is given in Eq. (I.83) (see, e.g., Rubinstein and Kroese, 2007). It is easy to show that this choice leads to a zero variance of $\widehat{p}_{\mathrm{f}}^{\,\mathrm{IS}}$ from Eq. (I.82).

$$h_{\mathbf{X}}^*(\mathbf{x}) = \frac{\mathbb{1}_{\mathcal{F}_{\mathbf{x}}}(\mathbf{x})\, f_{\mathbf{X}}(\mathbf{x})}{p_{\mathrm{f}}}\,. \tag{I.83}$$

The use of this optimal PDF $h_{\mathbf{X}}^*$ is unfortunately not possible because it depends on the failure probability p_{f}, which is unknown. Nevertheless it is expected that the "good" candidates for IS sampling correspond to PDFs which are not too far from this optimal solution. One important condition that needs to be fulfilled is that the IS estimator $\mathrm{Var}_{h_{\mathbf{X}}}\left[\widehat{p}_{\mathrm{f}}^{\,\mathrm{IS}}\right]$ should have a finite variance, as expressed in Eq. (I.84).

Such a condition is met if $h_{\mathbf{X}}$ does not have lighter tails than $f_{\mathbf{X}}$ or if the likelihood ratio W is bounded (Kroese et al., 2011).

$$\mathbb{E}_{h_{\mathbf{X}}}\left[\mathbb{1}^2_{\mathcal{F}_{\mathbf{X}}}(\mathbf{X})\,\frac{f^2_{\mathbf{X}}(\mathbf{X})}{h^2_{\mathbf{X}}(\mathbf{X})}\right] = \mathbb{E}_{f_{\mathbf{X}}}\left[\mathbb{1}^2_{\mathcal{F}_{\mathbf{X}}}(\mathbf{X})\,\frac{f_{\mathbf{X}}(\mathbf{X})}{h_{\mathbf{X}}(\mathbf{X})}\right] < \infty\,. \tag{I.84}$$

In structural reliability, several types of IS PDF have been defined in the context of FORM (see a review of some of these strategies in Engelund and Rackwitz, 1993). The most common choice that has emerged is to perform IS in the standard normal space by means of a multivariate standard normal PDF centered on the supposedly unique MPFP identified by FORM (Schuëller and Stix, 1987; Melchers, 1989a):

$$h_{\mathbf{U}}(\mathbf{u}) = \varphi_n(\mathbf{u}-\mathbf{u}^*)\,. \tag{I.85}$$

In the case of multiple MPFPs, solutions based on mixtures of multivariate standard normal PDFs need to be considered. However such approaches assume that these MPFPs have been determined, which is often hardly possible. If some MPFPs corresponding to high probability content failure subdomains are missed, then the failure probability estimate may be seriously biased and therefore inaccurate.

In order to fit the optimal IS PDF, some works consider adaptively adjusting the IS PDF by iteratively using wisely-selected samples in order to populate the subdomains of higher probability density within the failure domain. Such methods are known as *adaptive importance sampling* and examples of such a strategy can be found in Bucher (1988), Karamchandani et al. (1989), Melchers (1989b), Melchers (1990), Au and Beck (1999), Zou et al. (2003), and Morio (2012). It is worth pointing out that these methods also relate to particle filters (Chopin, 2002) and sequential Monte Carlo methods (Doucet et al., 2001; Johansen et al., 2005; Del Moral et al., 2006; Cérou et al., 2012).

A convenient solution for the IS PDF is often to consider that it belongs to some *parametric family* of distributions, e.g. the same as that of the nominal PDF $f_{\mathbf{X}}$ as assumed later. Let us consider that $h_{\mathbf{X}}$ belongs to the following family:

$$h_{\mathbf{X}}(\cdot) \in \{h(\cdot;\mathbf{q})\,,\ \mathbf{q}\in\mathcal{Q}\}\,, \tag{I.86}$$

where $\mathbf{q} = (q_1, \ldots, q_{n_{\mathbf{q}}})$ is a finite-dimensional vector of $n_{\mathbf{q}}$ real parameters. The objective is therefore to select $\mathbf{q}$ such that $h(\cdot;\mathbf{q})$ is as "close" as possible to the optimal IS PDF $h^*_{\mathbf{X}}$.

A first and natural solution consists in finding the value of $\mathbf{q}$ that minimizes the variance of the IS estimator $\widehat{p}_{\mathrm{f}}^{\,\mathrm{IS}}$. The optimal solution $\mathbf{q}^*$ is given by:

$$\mathbf{q}^* = \arg\min_{\mathbf{q}} \int \mathbb{1}^2_{\mathcal{F}_{\mathbf{X}}}(\mathbf{x})\,\frac{f_{\mathbf{X}}(\mathbf{x})}{h(\mathbf{x};\mathbf{q})}\,f_{\mathbf{X}}(\mathbf{x})\,\mathrm{d}\mathbf{x}\,, \tag{I.87}$$

or equivalently by:

$$\mathbf{q}^* = \arg\min_{\mathbf{q}} \int \frac{h^{*2}_{\mathbf{X}}(\mathbf{x})}{h(\mathbf{x};\mathbf{q})}\,\mathrm{d}\mathbf{x}\,. \tag{I.88}$$

Solving this first type of optimization problem is known as the *variance minimization* (VM) *method* (Kroese et al., 2011).

A second solution is obtained by choosing the IS PDF $h(\cdot;\mathbf{q})$ that is the closest to $h^*_{\mathbf{X}}$ w.r.t. a given measure, here the *Kullback-Leibler* (KL) *divergence* or *Kullback-Leibler distance*[5] (Kullback and Leibler, 1951). The KL distance between $h^*_{\mathbf{X}}$ and $h(\cdot;\mathbf{q})$ is given by:

$$\begin{aligned}\mathcal{D}_{\mathrm{KL}}\left(h^*_{\mathbf{X}}, h(\cdot;\mathbf{q})\right) &= \int h^*_{\mathbf{X}}(\mathbf{x}) \ln\left(\frac{h^*_{\mathbf{X}}(\mathbf{x})}{h(\mathbf{x};\mathbf{q})}\right) \mathrm{d}\mathbf{x} \\ &= \int h^*_{\mathbf{X}}(\mathbf{x}) \ln\left(h^*_{\mathbf{X}}(\mathbf{x})\right) \mathrm{d}\mathbf{x} - \int h^*_{\mathbf{X}}(\mathbf{x}) \ln\left(h(\mathbf{x};\mathbf{q})\right) \mathrm{d}\mathbf{x}\,.\end{aligned} \tag{I.89}$$

The optimal solution $\mathbf{q}^*$ which leads to the minimal distance is therefore given by:

$$\mathbf{q}^* = \arg\min_{\mathbf{q}} \int h^*_{\mathbf{X}}(\mathbf{x}) \ln\left(\frac{h^*_{\mathbf{X}}(\mathbf{x})}{h(\mathbf{x};\mathbf{q})}\right) \mathrm{d}\mathbf{x}\,, \tag{I.90}$$

or equivalently by:

$$\mathbf{q}^* = \arg\max_{\mathbf{q}} \int h^*_{\mathbf{X}}(\mathbf{x}) \ln\left(h(\mathbf{x};\mathbf{q})\right) \mathrm{d}\mathbf{x}\,, \tag{I.91}$$

which can also be expressed as follows:

$$\mathbf{q}^* = \arg\max_{\mathbf{q}} \int \mathbb{1}_{\mathcal{F}_x}(\mathbf{x}) \ln\left(h(\mathbf{x};\mathbf{q})\right) f_{\mathbf{X}}(\mathbf{x}) \mathrm{d}\mathbf{x}\,. \tag{I.92}$$

Solving this second type of optimization problem is known as the *cross-entropy* (CE) *method* (Kroese et al., 2011).

Although the solutions of these two optimization problems are different, it is shown by Chan et al. (2011) that the CE and VM methods provide parameters $\mathbf{q}^*$ that are asymptotically identical from the treated examples. The optimization problem to solve using the VM method is known to be highly nonlinear and noisy (see, e.g., Botev and L'Ecuyer, 2011). In contrast, the optimization problem of the CE method appears easier to solve than its VM counterpart, especially when $h(\cdot;\mathbf{q})$ belongs to a natural exponential family, as detailed and used later in this chapter.

The CE method is often used with a parametric IS PDF $h_{\mathbf{X}}(\cdot) \in \{h(\cdot;\mathbf{q}), \mathbf{q} \in \mathcal{Q}\}$[6]. As described in the next section, the CE method consists of an adaptive scheme that updates the vector of parameters $\mathbf{q}$ iteratively until the IS PDF $h(\cdot;\mathbf{q})$ becomes sufficiently close to the optimal IS PDF $h^*_{\mathbf{X}}$. It is important to mention that the performances of both the CE and VM methods used with a parametric IS PDF are closely related to how well this parametric PDF can approximate the optimal IS PDF. For highly nonlinear LSS with possibly disconnected failure subdomains, such "rigid" parametric IS PDFs may not be able to approximate $h^*_{\mathbf{X}}$ sufficiently well. Such a problem was e.g. recently addressed by Kurtz and Song (2013), who used the CE method with a multimodal IS PDF based on a Gaussian mixture. Moreover, for high-dimensional problems, the number of parameters in the vector $\mathbf{q}$ necessarily becomes large and the CE and VM-optimization problems could become too hard and costly to solve.

As an alternative to IS based on parametric PDFs, the recourse to surrogate-based (and often adaptive) IS has been explored in several works. In such approaches, the first step consists in drawing samples that adaptively populate the subdomains of the failure domain with high probability content. This may be carried out by means of Markov chains (see, e.g., Au and Beck, 1999; Dai et al., 2012a).

[5] The KL divergence is in fact not a distance, since it is not symmetric: $\mathcal{D}_{\mathrm{KL}}(f,g) \neq \mathcal{D}_{\mathrm{KL}}(g,f)$. However, we have $\mathcal{D}_{\mathrm{KL}}(f,g) \geq 0$ with equality if and only if $f = g$.

[6] Note that the CE method can also be used in a non-parametric framework, i.e. without assuming any specific family of distributions. Examples of such approaches are found in Botev et al. (2007) in which a χ^2-divergence and kernel mixture densities are used, and in Homem-de-Mello (2007) in which a product form on the IS distribution is assumed.

From these samples, a nonparametric PDF is constructed as an approximation of the optimal IS PDF and then used for sampling. Several surrogate models are available to construct such approximate IS PDFs. A first type of surrogate model is known as *kernel density*, most often based on the choice of a Gaussian kernel. Such kernel PDFs were used by Au and Beck (1999), Morio (2011), and Dai et al. (2012a) among others. Kriging surrogate models constitute a second type of surrogate model, which was used for adaptive IS by Balesdent et al. (2013) and Echard et al. (2013). Kriging is also used by Dubourg et al. (2013) to define a kriging-based probabilistic classification function as a surrogate for the true failure indicator function that appears in the optimal IS PDF. A modification of the AK-IS algorithm of Echard et al. (2013), also based on kriging, is proposed in the work of Cadini et al. (2014), in which the assumption of a unique MPFP found by FORM is relaxed. This work makes use of the metamodel-based IS of Dubourg et al. (2013). A third and less common solution is to use support vector machines to build an approximate IS PDF, as in the work of Dai et al. (2012a).

As a final and important remark about IS, it is worth pointing out that finding a suitable IS PDF in high dimensions is a challenging task, especially for highly nonlinear LSS and possibly disconnected failure subdomains of similar probability weights. IS may yield erroneous failure probability estimates which are even worse than those obtained by crude MC, as pointed out by Au and Beck (2003) and Katafygiotis and Zuev (2008). Regarding surrogate-based IS, it is also hard to find an approximate PDF sufficiently close to the optimal one. If the surrogate-based IS PDF is too crude an approximation of the optimal IS PDF, then the surrogate-based IS method may require too many samples or, even worse, may fail to give a correct failure probability approximation even if a large number of samples is used, as pointed out by Dubourg et al. (2013).

I–3.3.2 Cross-entropy (CE) method

The CE method, whose basis was briefly introduced in Section I–3.3.1, is a generic approach which addresses a variety of problems, such as the probability estimation of rare events (Rubinstein, 1997) and the optimization of discrete or continuous problems (Rubinstein, 1999). The presentation will be limited here to rare-event probability estimation for the so-called static problems such as introduced in Section I–1. Another use of this method, still for rare-event probability estimation, is made in the context of Markov chains and hidden Markov model random inputs, which slightly differs from static problems, see Section III–2.3.3. An example of the application of the CE method to continuous optimization can also be found in Section II–2.4 for the purpose of hyperparameter selection of support vector machines. For a broader view and understanding of the CE method, the reader may refer to the general textbook of Kroese et al. (2011) and the tutorial of de Boer et al. (2005) in addition to the above cited seminal papers of Rubinstein.

(a) CE method for estimation

Let us now assume that the IS PDF $h_{\mathbf{X}}$ we use belongs to the same family as that of $f_{\mathbf{X}}$:

$$f_{\mathbf{X}}(\cdot), h_{\mathbf{X}}(\cdot) \in \{f(\cdot;\mathbf{q}), \mathbf{q} \in \mathcal{Q}\} \tag{I.93}$$

for some reference vector of parameters $\mathbf{q}$. Let us moreover consider that the nominal PDF $f_{\mathbf{X}}$ is parameterized by the vector of parameters $\mathbf{p}$ such that $f_{\mathbf{X}}(\cdot) = f(\cdot;\mathbf{p})$.

The optimization problem defined in Eq. (I.92) thus rewrites:

$$\mathbf{q}^* = \arg\max_{\mathbf{q}} \int \mathbb{1}_{\mathcal{F}_{\mathbf{x}}}(\mathbf{x}) \ln\left(f(\mathbf{x};\mathbf{q})\right) f(\mathbf{x};\mathbf{p}) \, \mathrm{d}\mathbf{x}\,, \tag{I.94}$$

or equivalently:

$$\mathbf{q}^* = \arg\max_{\mathbf{q}} \mathbb{E}_{f(\cdot;\mathbf{p})}\left[\mathbb{1}_{\mathcal{F}_{\mathbf{x}}}(\mathbf{X}) \ln\left(f(\mathbf{X};\mathbf{q})\right)\right]. \tag{I.95}$$

By IS with a change of measure $f(\cdot;\mathbf{r})$ corresponding to *any* vector of parameters $\mathbf{r}$ (we will define how to choose $\mathbf{r}$ in the following), we can write:

$$\mathbf{q}^* = \arg\max_{\mathbf{q}} \mathbb{E}_{f(\cdot;\mathbf{r})}\left[\mathbb{1}_{\mathcal{F}_\mathbf{x}}(\mathbf{X})\, W(\mathbf{X};\mathbf{p},\mathbf{r}) \ln\left(f(\mathbf{X};\mathbf{q})\right)\right], \tag{I.96}$$

where $W(\mathbf{x};\mathbf{p},\mathbf{r}) = f(\mathbf{x};\mathbf{p})/f(\mathbf{x};\mathbf{r})$ is the likelihood ratio at $\mathbf{x}$ between $f(\cdot;\mathbf{p})$ and $f(\cdot;\mathbf{r})$.

Practically, this problem is solved by simulation using the so-called *stochastic counterpart* of the CE program:

$$\max_{\mathbf{q}} \frac{1}{N}\sum_{j=1}^{N} \mathbb{1}_{\mathcal{F}_\mathbf{x}}\left(\mathbf{X}^{(j)}\right) W\left(\mathbf{X}^{(j)};\mathbf{p},\mathbf{r}\right) \ln\left(f\left(\mathbf{X}^{(j)};\mathbf{q}\right)\right), \tag{I.97}$$

where $\mathbf{X}^{(1)},\ldots,\mathbf{X}^{(N)} \overset{\text{i.i.d.}}{\sim} f(\cdot;\mathbf{r})$.

If we define $\mathcal{X}_{\text{el}} = \left\{\mathbf{X}^{(j)} : \mathbb{1}_{\mathcal{F}_\mathbf{x}}\left(\mathbf{X}^{(j)}\right) = 1\right\}$ as the set of samples that belongs to the failure domain $\mathcal{F}_\mathbf{x}$, known as the *elite* set of samples, Eq. (I.97) becomes:

$$\max_{\mathbf{q}} \widehat{D}(\mathbf{q}) = \max_{\mathbf{q}} \frac{1}{N} \sum_{\mathbf{X}^{(j)}\in\mathcal{X}_{\text{el}}} W\left(\mathbf{X}^{(j)};\mathbf{p},\mathbf{r}\right) \ln\left(f\left(\mathbf{X}^{(j)};\mathbf{q}\right)\right). \tag{I.98}$$

The above-defined function $\widehat{D}(\mathbf{q})$ is often convex and differentiable, and the solution of Eq. (I.98) can be obtained from the following system of equations:

$$\frac{1}{N} \sum_{\mathbf{X}^{(j)}\in\mathcal{X}_{\text{el}}} W\left(\mathbf{X}^{(j)};\mathbf{p},\mathbf{r}\right) \nabla_\mathbf{q} \ln\left(f\left(\mathbf{X}^{(j)};\mathbf{q}\right)\right) = \mathbf{0}. \tag{I.99}$$

For distributions that belong to a *natural exponential family* (NEF) (for a definition see, e.g., Kroese et al., 2011, Appendix D), the system of equations defined in Eq. (I.99) has an analytical solution, which is recognized as being a key advantage of the CE method. Such a type of distribution is used in Section I–3.4.

If we take $\mathbf{r} = \mathbf{p}$ in the case of rare events (i.e. $p_\text{f} \ll 1$), most of the evaluations of the indicator function $\mathbb{1}_{\mathcal{F}_\mathbf{x}}$ in Eq. (I.97) are equal to zero for a moderate sample size N. This results in an excessively small or even worse an empty elite set of samples and it is therefore difficult or impossible to solve Eq. (I.98) or Eq. (I.99). This motivates the introduction of the multilevel version of the CE method, which will be presented next.

(b) Multilevel CE method

In order to avoid too small an elite set of samples, and therefore too few terms in the sums appearing in Eq. (I.98) and Eq. (I.99), the idea is to build a sequence of reference parameters $\{\widehat{\mathbf{q}}_s, s\in\mathbb{N}\}$ with $\widehat{\mathbf{q}}_0 = \mathbf{p}$ and a sequence of LSF levels $\{\widehat{y}_s, s\in\mathbb{N}_{>0}\}$ and iterate on both $\widehat{y}_s$ and $\widehat{\mathbf{q}}_s$. The algorithm first proceeds with an update of $\widehat{y}_s$ before updating $\widehat{\mathbf{q}}_s$.

The algorithm of the *multilevel CE method* is given in Table I.3. It requires the specification of the so-called *rarity parameter* ρ (typically between 0.01 and 0.1), the sample size N used at each level s and the sample size N_1 used for the final estimation of the failure probability[7].

[7] N_1 is set equal to N in all the applications presented in this report.

Define ρ, N and N_1 // define the parameters of the multilevel CE algorithm
Set $s=0$, $\widehat{\mathbf{q}}_0=\mathbf{p}$ and $\widehat{y}_0=+\infty$ // initialize the algorithm
Do
  $s=s+1$
  Generate a sample $\mathbf{X}^{(1)},\dots,\mathbf{X}^{(N)} \overset{\text{i.i.d.}}{\sim} f\left(\cdot;\widehat{\mathbf{q}}_{s-1}\right)$
  Assess $g\left(\mathbf{X}^{(1)}\right),\dots,g\left(\mathbf{X}^{(N)}\right)$
  Define the sample ρ-quantile $\widehat{y}_s$ of $\mathcal{Y}=\left\{g(\mathbf{X}^{(j)}), 1\leq j\leq N\right\}$
  if $\widehat{y}_s<0$, **then** $\widehat{y}_s=0$, **end if** // reset $\widehat{y}_s$ if lower than zero
  Define the elite set of samples $\mathcal{X}_{\text{el}}=\left\{\mathbf{X}^{(j)} : g\left(\mathbf{X}^{(j)}\right)\leq\widehat{y}_s\right\}$
  Solve the stochastic program defined in Eq. (I.98) with $\mathbf{r}=\widehat{\mathbf{q}}_{s-1}$ and denote the solution by $\widetilde{\mathbf{q}}_s$:
  $\widetilde{\mathbf{q}}_s=\arg\max_{\mathbf{q}}\frac{1}{N}\sum_{\mathbf{X}^{(j)}\in\mathcal{X}_{\text{el}}} W\left(\mathbf{X}^{(j)};\mathbf{p},\widehat{\mathbf{q}}_{s-1}\right)\ln\left(f\left(\mathbf{X}^{(j)};\mathbf{q}\right)\right)$
  Update the reference parameter: $\widehat{\mathbf{q}}_s=\widetilde{\mathbf{q}}_s$
while $\widehat{y}_s>0$
Set $m=s$ // define the total number of levels used
Generate a sample $\mathbf{X}^{(1)},\dots,\mathbf{X}^{(N_1)} \overset{\text{i.i.d.}}{\sim} f\left(\cdot;\widehat{\mathbf{q}}_m\right)$
Estimate p_{f} by IS: $\widehat{p}_{\text{f}}^{\text{CE}}=\frac{1}{N_1}\sum_{j=1}^{N_1}\mathbb{1}_{\mathcal{F}_{\mathbf{x}}}\left(\mathbf{X}^{(j)}\right)W\left(\mathbf{X}^{(j)};\mathbf{p},\widehat{\mathbf{q}}_m\right)$

Table I.3 – Multilevel CE algorithm for rare-event probability estimation.

I–3.4 Reliability assessment with the CE method, comparison with SS

For illustration purposes, a multilevel CE algorithm applied in the standard normal space is proposed and the results are compared with those obtained by SS. The comparison is made by varying the sample size per level, denoted N for both the SS and CE methods. The bias and variance of the failure probability estimated by these two methods are empirically assessed via several independent runs. Some conclusions are drawn from the treated examples.

I–3.4.1 CE method in the standard normal space

The CE method is applied in the standard normal space in order to work with a NEF distribution and therefore have a stochastic counterpart program that has an analytical solution, see Eq. (I.99). The choice made here is to express the multivariate IS PDF in the following form:

$$f\left(\mathbf{u};\mathbf{q}\right)=\prod_{i=1}^{n}\frac{1}{\sigma_i\sqrt{2\pi}}\exp\left(-\frac{1}{2}\left(\frac{u_i-\mu_i}{\sigma_i}\right)^2\right), \tag{I.100}$$

where $\mathbf{q}=(\boldsymbol{\mu},\boldsymbol{\sigma})$ is vector of $2n$ parameters such that $\boldsymbol{\mu}=(\mu_1,\dots,\mu_n)$ and $\boldsymbol{\sigma}=(\sigma_1,\dots,\sigma_n)$. Note that only the variances are parameterized and not the full $n\times n$ covariance matrix, in order to maintain a number of parameters which does not grow too fast with the dimension n.

The nominal PDF φ_n here writes:

$$f\left(\mathbf{u};\mathbf{p}\right)=\varphi_n\left(\mathbf{u}\right), \tag{I.101}$$

where $\mathbf{p}=\widehat{\mathbf{q}}_0=(0,\dots,0,1,\dots,1)$.

The components of the gradient vector $\nabla_{\mathbf{q}} \ln\left(f\left(\mathbf{u};\mathbf{q}\right)\right)$ which appears in Eq. (I.99) write, for $i = 1, \ldots, n$:

$$\frac{\partial \ln\left(f\left(\mathbf{u};\mathbf{q}\right)\right)}{\partial \mu_i} = \frac{u_i - \mu_i}{\sigma_i^2} \,, \tag{I.102a}$$

$$\frac{\partial \ln\left(f\left(\mathbf{u};\mathbf{q}\right)\right)}{\partial \sigma_i} = \frac{(u_i - \mu_i)^2 - \sigma_i^2}{\sigma_i^3} \,. \tag{I.102b}$$

Let us now consider the multilevel CE method at a given iteration s.

From a given sample set $\mathbf{U}^{(1)}, \ldots, \mathbf{U}^{(N)} \overset{\text{i.i.d.}}{\sim} f\left(\cdot;\widehat{\mathbf{q}}_{s-1}\right)$ where $\widehat{\mathbf{q}}_{s-1} = (\widehat{\boldsymbol{\mu}}_{s-1}, \widehat{\boldsymbol{\sigma}}_{s-1})$ and the corresponding values of the LSF $\mathcal{Y} = \left\{G(\mathbf{U}^{(j)}), 1 \leq j \leq N\right\}$, we define the sample ρ-quantile $\widehat{y}_s$ of $\mathcal{Y}$ and the elite set of samples $\mathcal{U}_{\text{el}} = \left\{\mathbf{U}^{(j)} : G\left(\mathbf{U}^{(j)}\right) \leq \widehat{y}_s\right\}$. The solution $\widetilde{\mathbf{q}}_s = (\widetilde{\boldsymbol{\mu}}_s, \widetilde{\boldsymbol{\sigma}}_s)$ of the stochastic program of Eq. (I.98) is analytically defined, for $i = 1, \ldots, n$, by:

$$\widetilde{\mu}_{s,i} = \frac{\sum_{\mathbf{U}^{(j)} \in \mathcal{U}_{\text{el}}} W\left(\mathbf{U}^{(j)};\mathbf{p},\widehat{\mathbf{q}}_{s-1}\right) U_i^{(j)}}{\sum_{\mathbf{U}^{(j)} \in \mathcal{U}_{\text{el}}} W\left(\mathbf{U}^{(j)};\mathbf{p},\widehat{\mathbf{q}}_{s-1}\right)} \,, \tag{I.103}$$

where $U_i^{(j)}$ denotes the i^{th} component of $\mathbf{U}^{(j)}$ and $\widetilde{\mu}_{s,i}$ the i^{th} component of $\widetilde{\boldsymbol{\mu}}_s$,

and:

$$\widetilde{\sigma}_{s,i}^2 = \frac{\sum_{\mathbf{U}^{(j)} \in \mathcal{U}_{\text{el}}} W\left(\mathbf{U}^{(j)};\mathbf{p},\widehat{\mathbf{q}}_{s-1}\right) \left(U_i^{(j)} - \widetilde{\mu}_{i,s}\right)^2}{\sum_{\mathbf{U}^{(j)} \in \mathcal{U}_{\text{el}}} W\left(\mathbf{U}^{(j)};\mathbf{p},\widehat{\mathbf{q}}_{s-1}\right)} \,, \tag{I.104}$$

in which $\widetilde{\mu}_{s,i}$ is given by Eq. (I.103) and where $\widetilde{\sigma}_{s,i}$ denotes the i^{th} component of $\widetilde{\boldsymbol{\sigma}}_s$.

It is known by experience that updating the reference parameter $\widehat{\mathbf{q}}_s$ with the solution $\widetilde{\mathbf{q}}_s$ of the stochastic program defined in Eq. (I.98) may cause too fast a convergence to a degenerate distribution, which may result in large errors on the failure probability estimate obtained by the CE method. In practice it is often recommended to update $\widehat{\mathbf{q}}_s$ as a weighted-average between $\widetilde{\mathbf{q}}_s$ and the current parameter estimate $\widehat{\mathbf{q}}_{s-1}$ (see, e.g., de Boer et al., 2005; Kroese et al., 2006). Several strategies may be selected: smoothing is varied with each iteration (dynamic smoothing) or not (static smoothing), the smoothing parameters may be different for each component of the reference parameter $\mathbf{q}$, etc. In the following examples, we use basic static smoothing with a single smoothing parameter $\alpha \in [0,1]$ that applies to all the components of both $\boldsymbol{\mu}$ and $\boldsymbol{\sigma}$, see Eq. (I.105). If α is set to too small a value, the convergence of the CE algorithm is very slow. If too large a value is given, the convergence of the algorithm is faster but the IS PDF may converge to a suboptimal solution, which is not desirable.

$$\widehat{\boldsymbol{\mu}}_s = \alpha\widetilde{\boldsymbol{\mu}}_s + (1-\alpha)\widehat{\boldsymbol{\mu}}_{s-1} \quad \text{and} \quad \widehat{\boldsymbol{\sigma}}_s = \alpha\widetilde{\boldsymbol{\sigma}}_s + (1-\alpha)\widehat{\boldsymbol{\sigma}}_{s-1} \,. \tag{I.105}$$

I–3.4.2 Application examples

Three examples are considered for illustration purposes.

(a) Example 1.

This first example was initially proposed by De Stefano and Der Kiureghian (1990) and studied in several references published since 2010. The reliability assessment of a two-degree-of-freedom primary-secondary system under white noise base acceleration is considered. System failure is defined in terms of the exceedance of the peak response of the secondary spring during loading (see De Stefano and

Variable	m_p	m_s	k_p	k_s	ζ_p	ζ_s	F_s	S_0
Distribution	lognormal							
Mean	1.5	0.01	1	0.01	0.05	0.02	{15, 27.5}	100
C.o.V.	0.1	0.1	0.2	0.2	0.4	0.5	0.1	0.1

Table I.4 – Example 1 - Random variables.

Der Kiureghian, 1990, for details about how the LSF expression is derived). Uncertainty is modeled by 8 independent random variables whose distributions are given in Table I.4. The mean value of the force capacity of the secondary spring F_s is set to either 15 or 27.5. This problem is characterized by a single MPFP with a strongly curved LSS. The LSF expression writes as follows:

$$g(\mathbf{x}) = F_s - 3k_s \sqrt{\frac{\pi S_0}{4\zeta_s \omega_s^3} \left[\frac{\zeta_a \zeta_s}{\zeta_p \zeta_s \left(4\zeta_a^2 + \theta^2\right) + \gamma \zeta_a^2} \frac{\left(\zeta_p \omega_p^3 + \zeta_s \omega_s^3\right) \omega_p}{4\zeta_a \omega_a^4} \right]} \tag{I.106}$$

where $\mathbf{x} = (\, m_p,\, m_s,\, k_p,\, k_s,\, \zeta_p,\, \zeta_s,\, F_s,\, S_0 \,)^{\mathrm{T}}$,

and where $\omega_p = \sqrt{k_p/m_p}$, $\omega_s = \sqrt{k_s/m_s}$, $\omega_a = (\omega_p + \omega_s)/2$, $\zeta_a = (\zeta_p + \zeta_s)/2$, $\gamma = m_s/m_p$ and $\theta = (\omega_p - \omega_s)/\omega_a$.

(b) Example 2.

The second example is a reliability problem with a smooth LSS, a single MPFP and moderate (and equal) curvatures at the MPFP. The LSF is given by (Rackwitz, 2001):

$$g(\mathbf{x}) = \left(n + a\,\sigma\sqrt{n}\right) - \sum_{i=1}^{n} x_i \tag{I.107}$$

where $\{X_i, 1 \leq i \leq n\}$ are n i.i.d. lognormal random variables with unit means and the same standard deviation σ equal to 0.2. The dimension n is varied in order to investigate how the performances of the CE method scales with dimensionality, while keeping the same LSS shape. We take $n \in \{\,25\,;\,50\,;\,100\,;\,250\,;\,500\,;\,1000\,\}$ and $a = 3$ for a first analysis. In a second analysis and for the specific case of $n = 100$, we allow the failure probability to vary in the approximate range $\left[10^{-7}, 10^{-3}\right]$ by setting $a \in \{\,3\,;\,4\,;\,5\,\}$.

(c) Example 3.

The third and last example is a 16-dimensional series system reliability problem in which the failure domain $\mathcal{F}_{\mathbf{u}}$ in the standard normal space is defined as the union of four failure subdomains of almost equal probability contents and all four characterized by a linear LSS. This problem is derived from the FORM results of the reliability analysis of the Scordelis-Lo shell structure with random geometric imperfections and space-variant material properties and thickness, performed in Section III–1.4. The initial 93-dimensional problem is replaced by an equivalent series system reliability problem with four linear LSSs. Only the 16 most influential variables are kept for the analysis, based on the importance factors of the four FORM solutions of the initial problem. The LSF of the simplified problem considered here is defined as follows:

$$G(\mathbf{u}) = \min_{k \in \{1,\ldots,4\}} G_k(\mathbf{u})\,, \tag{I.108}$$

where $G_k(\mathbf{u}) = \beta_k - \boldsymbol{\alpha}_k^{\mathrm{T}}\mathbf{u}$ for $k = 1, \ldots, 4$.

The LSFs of each component are defined by:

$$\beta_1 = 4.0118 \qquad \beta_2 = 4.0109 \qquad \beta_3 = 4.0108 \qquad \beta_4 = 4.0051\,,$$

and

$$\boldsymbol{\alpha}_1 = \begin{Bmatrix} 0.3040 \\ -0.4013 \\ 0.2131 \\ 0.3218 \\ -0.3253 \\ 0.2534 \\ 0.1582 \\ 0.1067 \\ 0.2065 \\ -0.3173 \\ 0.1614 \\ 0.2842 \\ -0.2397 \\ 0.2022 \\ 0.1601 \\ 0.1306 \end{Bmatrix} \quad \boldsymbol{\alpha}_2 = \begin{Bmatrix} 0.3061 \\ 0.4007 \\ 0.2131 \\ 0.3219 \\ 0.3253 \\ 0.2534 \\ -0.1582 \\ -0.1060 \\ 0.2064 \\ 0.3164 \\ 0.1614 \\ 0.2838 \\ 0.2394 \\ 0.2020 \\ -0.1600 \\ -0.1319 \end{Bmatrix} \quad \boldsymbol{\alpha}_3 = \begin{Bmatrix} 0.3038 \\ 0.4006 \\ -0.2133 \\ 0.3217 \\ -0.3262 \\ -0.2535 \\ -0.1582 \\ 0.1065 \\ 0.2065 \\ 0.3166 \\ -0.1615 \\ 0.2841 \\ -0.2396 \\ -0.2023 \\ -0.1603 \\ -0.1319 \end{Bmatrix} \quad \boldsymbol{\alpha}_4 = \begin{Bmatrix} 0.3004 \\ -0.4077 \\ -0.2181 \\ 0.3262 \\ 0.2787 \\ -0.2586 \\ 0.1605 \\ -0.1120 \\ 0.2102 \\ -0.3231 \\ -0.1649 \\ 0.2894 \\ 0.2445 \\ -0.2067 \\ 0.1632 \\ 0.1346 \end{Bmatrix}.$$

As an additional element of information, the pairwise distances between the four MPFPs are given in the following matrix $\mathbf{D} = [d_{ij}]_{1\le i,j\le 4}$ where $d_{ij} = \mathrm{dist}(P_i^*, P_j^*)$:

$$\mathbf{D} = \begin{bmatrix} 0 & 5.6929 & 5.7056 & 4.6901 \\ 5.6929 & 0 & 4.7552 & 5.7572 \\ 5.7056 & 4.7552 & 0 & 5.6509 \\ 4.6901 & 5.7572 & 5.6509 & 0 \end{bmatrix}. \tag{I.109}$$

I–3.4.3 Results and comments

The reference failure probabilities obtained by the SS and CE methods are given in Table I.5. These failure probabilities are computed with $N = 2^{20} \approx 1.05 \times 10^6$ samples per level with both methods. The probability level p_0 is set equal to 0.1 in the SS analysis. For the CE method, the rarity parameter ρ is set to 0.05 and the static smoothing parameter α to 1 (i.e. no smoothing). By experience it appears that results obtained for large values of N without smoothing are better in terms of variance of the failure probability estimate than those obtained with smoothing. The failure probabilities reported in Table I.5 are obtained by averaging over the results of 500 independent runs of each method. The coefficients of variation listed in this table are those empirically assessed from these 500 runs. In this table, $\overline{N_{\mathrm{t}}}$ represents the averaged total numbers of samples used in each analysis, i.e. $\overline{N_{\mathrm{t}}} = \overline{m}N$ for a SS analysis and $\overline{N_{\mathrm{t}}} = \overline{m}N + N_1 = (\overline{m}+1)N$ for a CE analysis[7], where $\overline{m}$ denotes the averaged number of levels necessary for each method to converge and N is the number of samples used in each level.

The averaged failure probability estimates obtained by both methods are in excellent agreement for each example up to a 3-digit accuracy. The c.o.v. of p_{f} is always lower with the CE method than with the SS method, except in example 3 for which it is slightly greater. The relative gain on the c.o.v. in the first two examples is in the range 2 to 5, with a similar cost in terms of number of calls to the LSF for

	$p_{\text{fref}}^{\text{CE}} = \overline{\widehat{p}_{\text{f}}^{\text{CE}}}$	$\delta_{\widehat{p}_{\text{f}}^{\text{CE}}}$ $\times 10^{-2}$	$\overline{N_{\text{t}}^{\text{CE}}}$ $\times 10^{6}$	$p_{\text{fref}}^{\text{SS}} = \overline{\widehat{p}_{\text{f}}^{\text{SS}}}$	$\delta_{\widehat{p}_{\text{f}}^{\text{SS}}}$ $\times 10^{-2}$	$\overline{N_{\text{t}}^{\text{SS}}}$ $\times 10^{6}$
Example 1 - $\mu_{F_{\text{s}}} = 15$	4.774×10^{-3}	0.30	3.15	4.775×10^{-3}	0.64	3.16
Example 1 - $\mu_{F_{\text{s}}} = 27.5$	3.783×10^{-7}	0.54	5.24	3.784×10^{-7}	2.27	7.67
Example 2 - $n = 25$ - $a = 3$	2.169×10^{-3}	0.18	3.15	2.169×10^{-3}	0.70	3.15
Example 2 - $n = 50$ - $a = 3$	1.909×10^{-3}	0.18	3.15	1.909×10^{-3}	0.71	3.15
Example 2 - $n = 100$ - $a = 3$	1.735×10^{-3}	0.18	3.15	1.734×10^{-3}	0.74	3.15
Example 2 - $n = 250$ - $a = 3$	1.587×10^{-3}	0.18	3.15	1.588×10^{-3}	0.70	3.15
Example 2 - $n = 500$ - $a = 3$	1.516×10^{-3}	0.17	3.15	1.516×10^{-3}	0.74	3.15
Example 2 - $n = 1000$ - $a = 3$						
Example 2 - $n = 100$, $a = 4$	5.750×10^{-5}	0.21	4.19	5.751×10^{-5}	1.01	5.31
Example 2 - $n = 100$, $a = 5$	9.078×10^{-7}	0.24	4.19	9.068×10^{-7}	1.26	7.56
Example 3	1.215×10^{-4}	1.25	4.19	1.214×10^{-4}	0.96	4.24

Table I.5 – Reference failure probabilities obtained with the CE and SS methods ($N = 2^{20}$ samples per level, results averaged over 500 independent runs).

probabilities close to 10^{-3}, with a lower cost for probabilities lower that 10^{-3} (i.e. in example 1 with $\mu_{F_{\text{s}}} = 27.5$ and in example 2 with $n = 100$ and $a = 4$ or $a = 5$). The c.o.v. of p_{f} with the CE method is 25% larger than that of the SS method for example 3.

In order to compare the accuracy and efficiency of the two methods, it is proposed to vary the number of samples per level N in the SS and CE analyses such that $N = 2^m$ where $m = 6, \ldots, 15$ for the SS analysis and $m = 7, \ldots, 15$ for the CE analysis. The settings are $p_0 = 0.1$ for the SS method and $\rho = 0.05$, $\alpha = 0.4$ for the CE method[8]. Smoothing is applied here in order to improve the quality of the failure probability estimates for the lowest selected values of N. It is found that some unreliable estimates of p_{f} are obtained for small N if α is too large. Smoothing, however, slightly increases the variance of the failure probability estimates and the number of levels required for convergence of the CE method (and therefore the number of calls to the LSF). The absolute relative bias of the averaged failure probability estimates w.r.t. the reference solutions ($p_{\text{fref}}^{\text{CE}}$ and $p_{\text{fref}}^{\text{SS}}$ respectively for the CE and SS analyses) and the coefficient of variation of the failure probability estimates empirically assessed from 500 independent runs of each method[9] are represented in Figure I.9 for example 1, in Figures I.10 and I.11 for example 2, and in Figure I.12 for example 3. The absolute relative bias and the coefficient of variation are represented as a function of $\overline{N_{\text{t}}}$ which denotes the averaged total numbers of samples used in each analysis.

As expected it is found that the c.o.v. of the SS analysis is inversely proportional to $\sqrt{N}$ and that the bias is always positive except when it becomes quite low (i.e. for absolute bias lower than 10^{-2}), see the bias plots in Figures I.9–I.12 in which a positive bias is marked by a triangle-up. We can also notice that the performance of the SS method is insensitive to the dimension n of the problem: the plots representing the c.o.v. of p_{f} vs. $\overline{N_{\text{t}}}$ for example 2 with $n \in \{25\,;\,50\,;\,100\,;\,250\}$ are all much the same.

Regarding the results obtained with the CE method, the following comments can be made:

[8] The following values were used as candidates for the CE parameters: $\rho \in \{0.05\,;\,0.075\,;\,0.1\,;\,0.15\,;\,0.2\}$ and $\alpha \in \{0.4\,;\,0.6\,;\,0.8\,;\,1\}$. Only the results with $\rho = 0.05$ and $\alpha = 0.4$ are presented here.

[9] The coefficients of variation plotted in Figures I.9–I.12 are empirically estimated from 500 independent runs of each method. For SS, it is important to point out that the empirical c.o.v. may be substantially larger than the value given by Eq. (I.77), such as in example 1 with $\mu_{F_{\text{s}}} = 27.5$ (Bourinet et al., 2011, Fig. 4.c).

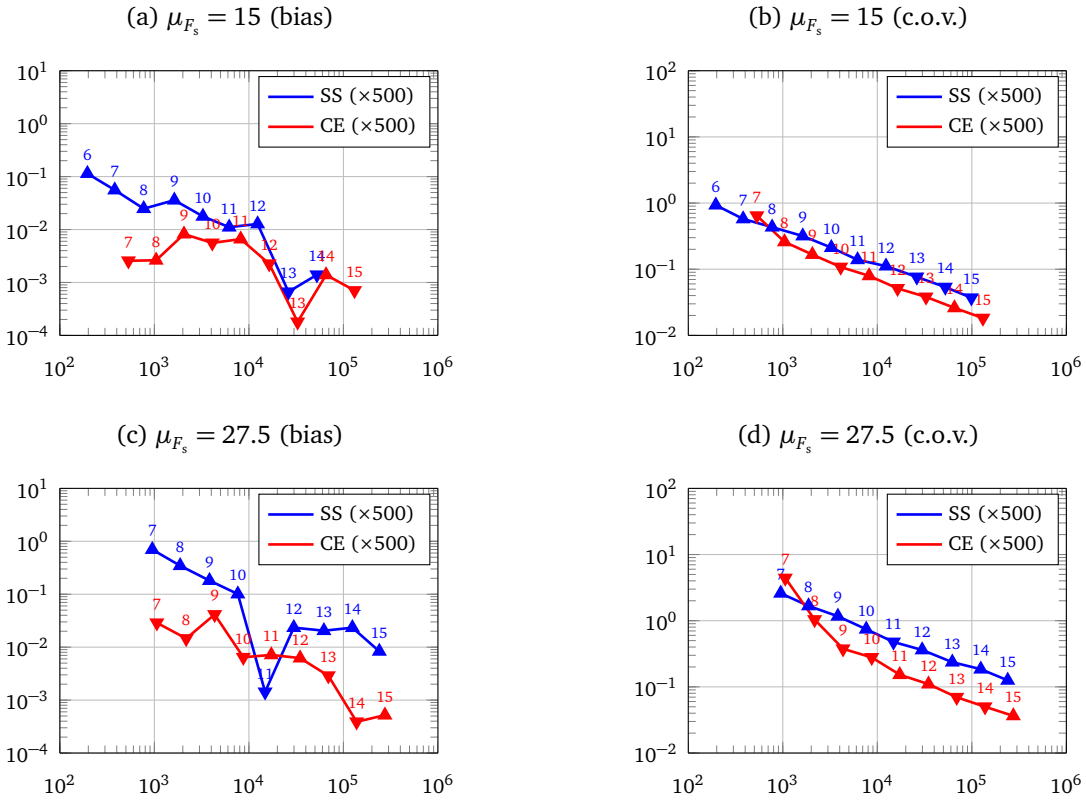

Figure I.9 – Example 1. Absolute relative bias $|\widehat{\overline{p}}_f - p_{f\,ref}|/p_{f\,ref}$ (left) and coefficient of variation $\delta_{\widehat{p}_f}$ (right) vs. averaged total number of samples $\overline{N}_t$. The indices $m = 6, \ldots, 15$ refer to the 2^m number of samples per level used in the analyses. The results are based on 500 independent runs of each method: $\widehat{\overline{p}}_f$ denotes the average of the 500 failure probability estimates and $\delta_{\widehat{p}_f}$ its empirical c.o.v.. A triangle-up (resp. down) marker denotes a positive (resp. negative) bias. Biases lower than 10^{-4} are not plotted.

- *Influence of the dimension n*: From the results obtained, it is found that the performances of CE method decrease with n. For the 8-dimensional problem of example 1, the CE method outperforms the SS method both in terms of bias and variance for $N \geq 2^8$, see Figure I.9. From the results obtained for example 2, in which the dimension is varied, it appears that the CE method outperforms the SS method in terms of variance for a sample size N which increases with the dimension n. For $p_f \approx 10^{-3}$ (case $a = 3$), the failure probability is better estimated for $N \geq 2^8$ for $n = 25$, 2^9 for $n = 50$, 2^{10} for $n = 100$ and 2^{12} for $n = 250$. The c.o.v. of p_f is inversely proportional to $\sqrt{N}$ as in a SS analysis, but is appears about three times lower than its SS counterpart for sufficiently large values of N.

- *Influence of the failure probability level p_f*: The influence of the failure probability level can be analyzed from the results obtained for example 1 ($\mu_{F_s} = 15$ vs. 27.5) and example 2 with $n = 100$ ($a = 3$, 4 or 5). It appears that the efficiency of the CE method increases when the probability level decreases. For example 1, the gain in terms of c.o.v. is larger for $\mu_{F_s} = 27.5$ than for $\mu_{F_s} = 15$, see Figure I.9 (b) and (d). For example 2, the gain in terms of c.o.v. becomes larger when a is increased, see Figure I.11 (b), (d) and (f).

- *Bias of the failure probability estimate obtained with the CE Method*: The bias on p_f with the CE method always appears lower than that of the SS estimates, if a sufficiently large value of N is selected. For very small values of N, the CE estimate is unreliable (usually too low values for p_f, which results in an absolute relative bias close to 100%), which clearly shows that the CE method is inefficient for small sample sizes.

(a) $n = 25$ - $a = 3$ (bias)

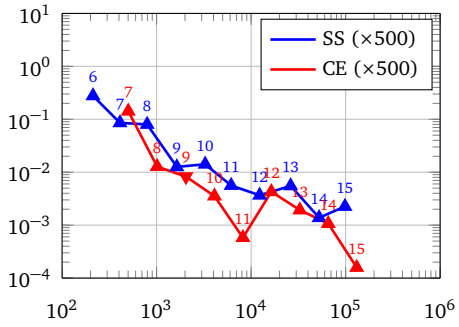

(b) $n = 25$ - $a = 3$ (c.o.v.)

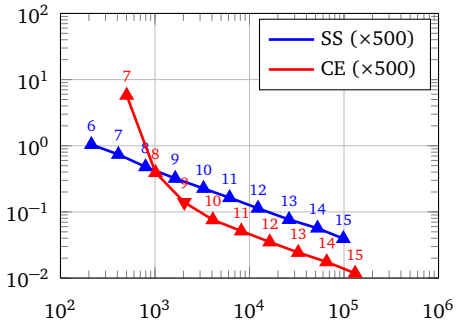

(c) $n = 50$ - $a = 3$ (bias)

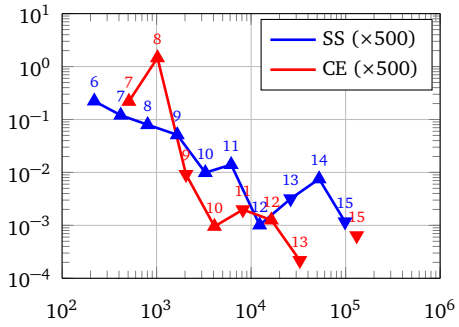

(d) $n = 50$ - $a = 3$ (c.o.v.)

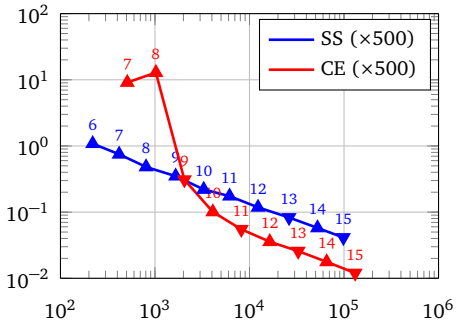

(e) $n = 100$ - $a = 3$ (bias)

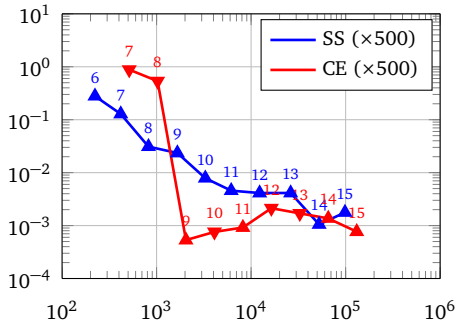

(f) $n = 100$ - $a = 3$ (c.o.v.)

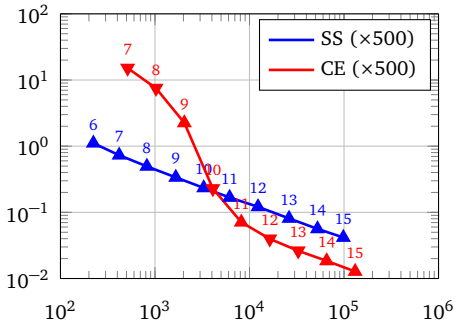

(g) $n = 250$ - $a = 3$ (bias)

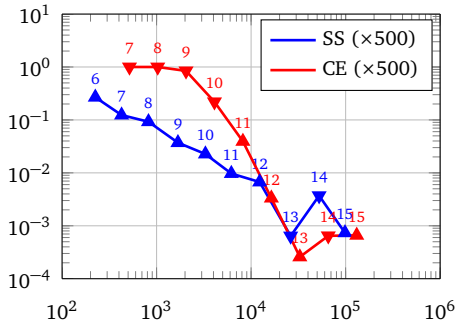

(h) $n = 250$ - $a = 3$ (c.o.v.)

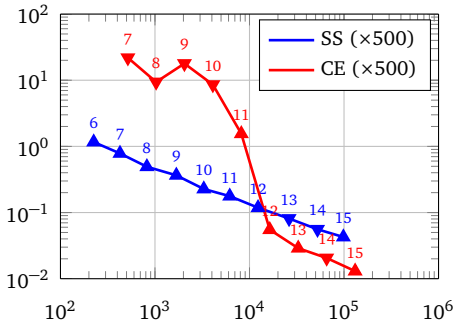

Figure I.10 – Example 2, $n \in \{25; 50; 100; 250\}$, $a = 3$. Absolute relative bias $|\overline{\widehat{p}_f} - p_{f\,\mathrm{ref}}|/p_{f\,\mathrm{ref}}$ (left) and coefficient of variation $\delta_{\widehat{p}_f}$ (right) vs. averaged total number of samples $\overline{N_t}$. See plotting details in Figure I.9.

(a) $n = 100$ - $a = 3$ (bias)

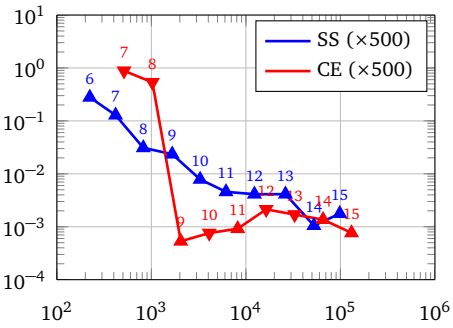

(b) $n = 100$ - $a = 3$ (c.o.v.)

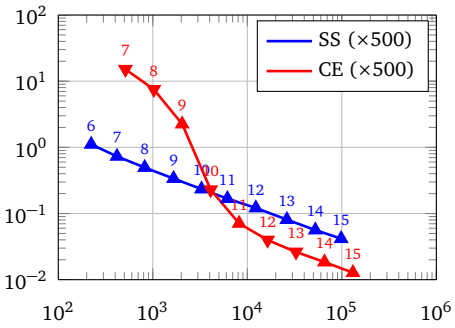

(c) $n = 100$ - $a = 4$ (bias)

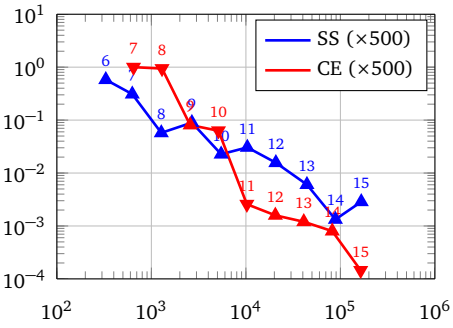

(d) $n = 100$ - $a = 4$ (c.o.v.)

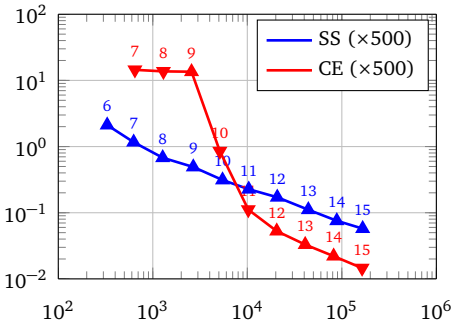

(e) $n = 100$ - $a = 5$ (bias)

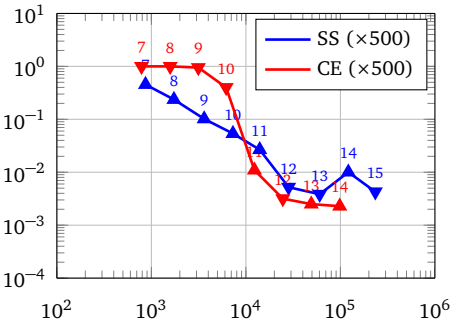

(f) $n = 100$ - $a = 5$ (c.o.v.)

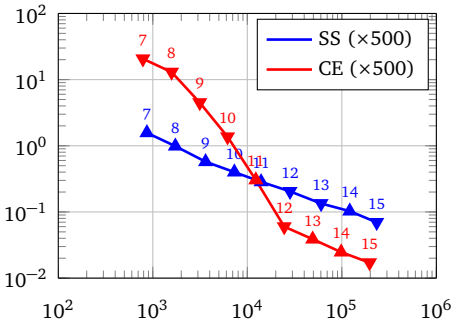

Figure I.11 – Example 2, $n = 100$, $a \in \{3; 4; 5\}$. Absolute relative bias $|\overline{\widehat{p}_f} - p_{f\,ref}|/p_{f\,ref}$ (left) and coefficient of variation $\delta_{\widehat{p}_f}$ (right) vs. averaged total number of samples $\overline{N}_t$. See plotting details in Figure I.9.

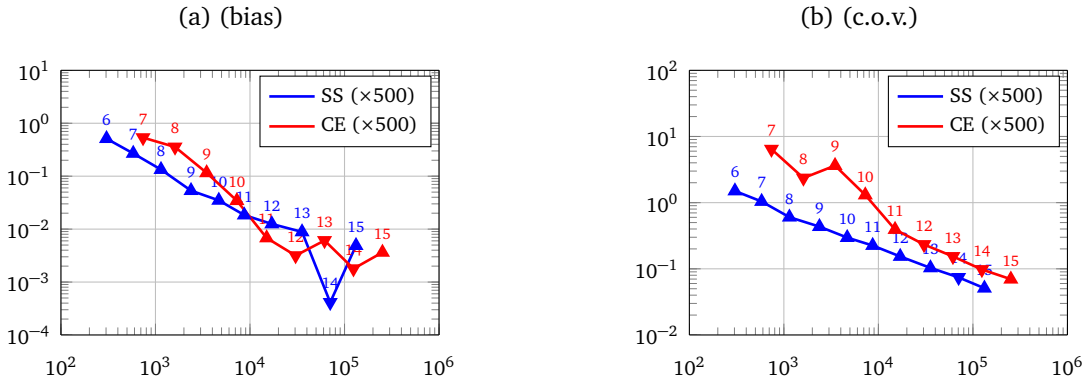

Figure I.12 – Example 3. Absolute relative bias $|\widehat{\overline{p_f}} - p_{f\,ref}|/p_{f\,ref}$ (left) and coefficient of variation $\delta_{\widehat{p}_f}$ (right) vs. averaged total number of samples $\overline{N_t}$. See plotting details in Figure I.9.

- *Specific case of multiple MPFPs*: The CE method appears less efficient than the SS method in example 3. The CE c.o.v. of p_f never gets lower than that obtained by the SS method when the sample size is increased. This is not surprising, since the parametric IS PDF used by the CE method is far from the optimal one. Nevertheless, the CE method is still able to give an estimate of p_f with an acceptable accuracy compared to SS for $N \geq 2^{11}$.

As a final comment, it can be said that the CE method represents an interesting alternative to SS if the number of samples per level N is set sufficiently high, and under the assumption that the LSS is not too "exotic" (in other words, one needs to be cautious if the LSS features several MPFPs of similar importances). If an accurate solution needs to be found, say p_f estimated with a c.o.v. of less than 10%, then the CE method is a good candidate. Moreover, the gain in terms of accuracy increases for small failure probabilities. It is worth pointing out that the CE method is also applicable to reliability problems with Markov chains and hidden Markov models considered as random inputs, as later presented in Section III–2.3.3.

I–4 Sensitivity measures

I–4.1 Introduction

In uncertainty propagation, it is of interest to quantify, in a probabilistic sense, how each random input contributes to a given output of interest. A first type of approach, known as global sensitivity analysis (Saltelli et al., 2008), consists in assessing the sensitivity to inputs over the entire support of the joint PDF $f_{\mathbf{X}}$. Several methods are available to perform such a global analysis, among which are screening methods, variance-based methods such as those based on Sobol' indices (Sobol', 1993), nonparametric methods and density-based methods. Note that global sensitivity analysis is not considered within the scope of this report.

If reliability assessment is the objective pursued, then the analyst is usually interested in the sensitivities to random inputs at failure. These sensitivities are therefore of a local nature and they need to be evaluated at failure, e.g. at the MPFP in a FORM analysis. Such local importance measures introduced in the context of FORM are briefly reviewed in Section I–4.2.1, either with independent or Nataf-correlated random inputs.

In engineering problems of practical interest, the statistical data available is often limited, and assessing how the results of an uncertainty propagation analysis are sensitive to the statistical model used as an input turns out to be of paramount importance. Several uncertainties may be considered, such as the types of marginal distributions, the dependence structure between the random components or any related model parameters that are used in the analysis. In this report, the scope will be limited to the sensitivity of the failure probability p_f w.r.t. distribution parameters, assuming that choices have been made regarding the types of marginal distributions and the dependence structure that are used (here linear correlation, accounted for by means of the Nataf model). We assume that all the distribution parameters are gathered in a vector denoted $\boldsymbol{\theta} = (\theta_1, \ldots, \theta_{n_\theta})$ in which θ_k designates any given parameter of this vector. These parameters include the statistical moments of the components X_i of the random vector $\mathbf{X}$ for $i = 1, \ldots, n$, but also and more generally any parameters used to define the corresponding marginal distributions. The appropriate notation for the joint PDF of $\mathbf{X}$ would be $f_{\mathbf{X}}(\cdot; \boldsymbol{\theta})$ but we will simply use $f_{\mathbf{X}}(\cdot)$ in the following without making explicit the dependence on $\boldsymbol{\theta}$ for shorter notations.

The sensitivities of p_f w.r.t. distribution parameters in the FORM context and under the assumption of a Nataf model are presented first. Section I–4.2 addresses FORM sensitivities w.r.t. parameters of the marginal distributions of $\mathbf{X}$ and also those w.r.t. correlations between the components of $\mathbf{X}$. Note that these sensitivity measures are available in FERUM 4.x (Bourinet et al., 2009).

Sensitivity w.r.t. distribution parameters is then placed in the broader context of MC methods. The sensitivities of p_f w.r.t. distribution parameters can be obtained from a crude MC analysis by means of the score function introduced by Rubinstein (1976), as described in Section I–4.3.1. Such sensitivities were later derived in the SS framework by Song et al. (2009), as presented in Section I–4.3.2. An interpretation of these sensitivities in the standard normal space is proposed in Section I–4.3.3, allowing the components of $\mathbf{X}$ to be ranked by importance in the specific case of independent inputs. Note that it is also possible to assess such sensitivities by means of surrogate models, as recently proposed by Dubourg and Sudret (2014), in which the sensitivities of p_f w.r.t. distribution parameters are assessed by means of the meta-IS adaptive refinement technique initially proposed for reliability assessment (Dubourg et al., 2013) .

I–4.2 FORM

I–4.2.1 Importance factors

In a FORM analysis, the variance of $G_1(\mathbf{U})$ defined in Eq. (I.36) can be expressed as follows (see, e.g., Der Kiureghian, 1999; Ditlevsen and Madsen, 2007):

$$\begin{aligned} \mathrm{Var}\left[G_1(\mathbf{U})\right] &= \mathrm{Var}\left[-\|\nabla G(\mathbf{u}^*)\|\left(\boldsymbol{\alpha}^{\mathrm{T}}\mathbf{U} - \beta\right)\right] \\ &= \|\nabla G(\mathbf{u}^*)\|^2 \,\mathrm{Var}\left[\boldsymbol{\alpha}^{\mathrm{T}}\mathbf{U}\right] \\ &= \|\nabla G(\mathbf{u}^*)\|^2 \left(\alpha_1^2 + \alpha_2^2 + \ldots + \alpha_n^2\right), \end{aligned} \tag{I.110}$$

where α_i for $i = 1, \ldots, n$ are the components of the unit vector $\boldsymbol{\alpha}$.

From this expression, it appears that the squared values of the components of the $\boldsymbol{\alpha}$-vector are indicative of the relative importance of the corresponding random inputs in the standard normal space in the neighborhood of the MPFP. These α_i^2-values are known as *importance factors*. If the random inputs are independent, these importance factors clearly express the relative importance of each random component X_i. This is no longer true when correlated inputs are used in reliability analysis. In such a context, Der Kiureghian introduced a new vector $\boldsymbol{\gamma}$ of importance factors by considering an "equivalent" normal vector in the $\mathbf{x}$-space at the MPFP $\mathbf{x}^*$, denoted $\widehat{\mathbf{X}}$, such that $\mathbf{u} = \mathbf{u}^* + \mathbf{J}_T(\widehat{\mathbf{x}} - \mathbf{x}^*)$ where $\mathbf{J}_T = \mathbf{J}_{\mathbf{u},\mathbf{x}}$

is the Jacobian matrix of the diffeomorphism T evaluated at $\mathbf{x}^*$. This vector of importance factors is expressed as follows (Der Kiureghian, 1999):

$$\boldsymbol{\gamma}^{\mathrm{T}} = \frac{\boldsymbol{\alpha}^{\mathrm{T}} \mathbf{J}_T \widehat{\mathbf{D}}}{\|\boldsymbol{\alpha}^{\mathrm{T}} \mathbf{J}_T \widehat{\mathbf{D}}\|} , \tag{I.111}$$

where $\widehat{\mathbf{D}} = [\widehat{D}_{ii}]_{1\leq i\leq n}$ is a $(n \times n)$-diagonal matrix such that $\widehat{D}_{ii} = \sqrt{J_{2,ii}}$ for $i = 1, \dots, n$ and $J_{2,ii}$ is the i^{th} diagonal term of the $(n \times n)$-matrix $\mathbf{J}_2 = [J_{2,ij}]_{1\leq i,j\leq n} = \mathbf{J}_{T^{-1}} \mathbf{J}_{T^{-1}}^{\mathrm{T}}$ where $\mathbf{J}_{T^{-1}} = \mathbf{J}_{\mathbf{x},\mathbf{u}}$ is the Jacobian matrix of the inverse T^{-1} of T evaluated at $\mathbf{u}^*$. It should be noted that $\boldsymbol{\gamma} = \boldsymbol{\alpha}$ for the specific case of independent components X_i.

I–4.2.2 Sensitivities of p_{f} w.r.t. distribution parameters

In the context of a FORM analysis, the gradient of the failure probability approximation $p_{\mathrm{f}}^{\mathrm{FORM}}$ w.r.t. the distribution parameters $\boldsymbol{\theta}$ is given by:

$$\nabla_{\boldsymbol{\theta}} p_{\mathrm{f}}^{\mathrm{FORM}} = -\varphi(\beta) \nabla_{\boldsymbol{\theta}} \beta . \tag{I.112}$$

The gradient of the reliability index β w.r.t. $\boldsymbol{\theta}$ reads as follows, as shown by Hohenbichler and Rackwitz (1986):

$$\nabla_{\boldsymbol{\theta}} \beta = \mathbf{J}_{\mathbf{u},\boldsymbol{\theta}}(\mathbf{u}^*; \boldsymbol{\theta})^{\mathrm{T}} \boldsymbol{\alpha} , \tag{I.113}$$

where $\mathbf{J}_{\mathbf{u},\boldsymbol{\theta}}(\mathbf{u}; \boldsymbol{\theta}) = [\partial u_i / \partial \theta_j]_{1\leq i\leq n,\, 1\leq j\leq n_{\boldsymbol{\theta}}}$ represents the Jacobian of the transformation T w.r.t. the distribution parameters $\boldsymbol{\theta}$. Note that this Jacobian is expressed at the MPFP $\mathbf{u}^*$.

The k^{th} column of this Jacobian matrix for $k = 1, \dots, n_{\boldsymbol{\theta}}$ can be obtained by differentiating $\mathbf{u}$ defined in Eq. (I.25) w.r.t. the k^{th} element θ_k of the vector of distribution parameters $\boldsymbol{\theta}$:

$$\frac{\partial \mathbf{u}}{\partial \theta_k} = \mathbf{L}_0^{-1} \frac{\partial \mathbf{z}}{\partial \theta_k} + \frac{\partial \mathbf{L}_0^{-1}}{\partial \theta_k} \mathbf{z} . \tag{I.114}$$

Two main cases deserve attention, as respectively detailed in Section I–4.2.2 (a) and (b):

(a) The first case appears when θ_k is a correlation coefficient of $\mathbf{R}$. The components $z_i = \Phi^{-1}\left(F_{X_i}(x_i)\right)$ of $\mathbf{z}$ for $i = 1, \dots, n$ are expressed in terms of the parameters of the marginal distributions of $\mathbf{X}$ and therefore do not depend on θ_k. For this reason the first term of Eq. (I.114) vanishes.

(b) The second case appears when θ_k is a parameter of a given marginal distribution (e.g. its mean or standard deviation or, more generally, any parameter of this marginal distribution). The dependence of $\mathbf{z}$ on θ_k is clear from the transformation $(T_{vz} \circ T_{xv})$ defined in Eq. (I.114). The calculation of the first term of Eq. (I.114) is therefore required to assess the sensitivity to θ_k. The contribution of the second term is less clear and often neglected. It is however non-zero, due to μ_i, σ_i, μ_j and σ_j that appear in Eq. (I.30), which may imply a dependence of $\mathbf{R}_0$, and therefore of $\mathbf{L}_0^{-1}$, on θ_k.

(a) Sensitivities to correlation

Sensitivity to correlation in the framework of the Nataf transformation has been studied in very few works (Žanić and Žiha, 1998; Žanić and Žiha, 2001; Bourinet and Lemaire, 2008; Bourinet, 2017a). The methods proposed by Žanić and Žiha are based on the approximate formulas $F = \rho_{0,ij}/\rho_{ij}$ of Liu and Der Kiureghian (1986) derived for pairs of commonly-used marginal distributions. Two methods are proposed in this work, one based on the Cholesky decomposition, as later used by Bourinet and Lemaire (2008) and presented in the following, the other based on a spectral decomposition of $\mathbf{R}_0$. The objective here is to assess these sensitivities by numerical integration from the integral problem defined in Eq. (I.30) in order to obtain highly accurate sensitivities.

The sensitivity to a given correlation coefficient ρ_{ij} of $\mathbf{R}$ requires evaluating the following expression at $\mathbf{u}^*$:

$$\frac{\partial \mathbf{u}}{\partial \rho_{ij}} = \frac{\partial \mathbf{L}_0^{-1}}{\partial \rho_{ij}} \mathbf{z} \,. \tag{I.115}$$

From $\mathbf{L}_0^{-1}\mathbf{L}_0 = \mathbf{I}$, where $\mathbf{I}$ is the $n \times n$ identity matrix, we can straightforwardly obtain:

$$\frac{\partial \mathbf{L}_0^{-1}}{\partial \rho_{ij}} = -\mathbf{L}_0^{-1} \frac{\partial \mathbf{L}_0}{\partial \rho_{ij}} \mathbf{L}_0^{-1} \,. \tag{I.116}$$

This expression shows that the sensitivity of $\mathbf{L}_0^{-1}$ w.r.t. ρ_{ij} can be obtained from that of $\mathbf{L}_0$. The evaluation of $\partial \mathbf{L}_0 / \partial \rho_{ij}$ is carried out in two steps, as described in the following.

In the first step, the sensitivity of $\mathbf{R}_0$ is derived from Eq. (I.30). All the elements of the matrix $\partial \mathbf{R}_0 / \partial \rho_{ij}$ are zeros except the one in the i^{th} row and j^{th} column, which can be expressed as follows:

$$\frac{\partial \rho_{0,ij}}{\partial \rho_{ij}} = \left(\frac{\partial \rho_{ij}}{\partial \rho_{0,ij}} \right)^{-1} \,. \tag{I.117}$$

The sensitivity $\partial \rho_{ij} / \partial \rho_{0,ij}$ is assessed from the following equation by numerical integration with the same rule as the one used to solve Eq. (I.30), see Eq. (I.31):

$$\frac{\partial \rho_{ij}}{\partial \rho_{0,ij}} = \int_{\mathbb{R}} \int_{\mathbb{R}} h\left(z_i, z_j, \mu_i, \mu_j, \sigma_i, \sigma_j\right) \frac{\partial \varphi_2\left(z_i, z_j, \rho_{0,ij}\right)}{\partial \rho_{0,ij}} \mathrm{d}z_i \mathrm{d}z_j \,. \tag{I.118}$$

In the second step, the sensitivity of $\mathbf{L}_0$ w.r.t. ρ_{ij} is obtained from that of $\mathbf{R}_0$ through a step-by-step differentiation of the Cholesky algorithm. The algorithm used to calculate both $\mathbf{L}_0$ and $\partial \mathbf{L}_0 / \partial \rho_{ij}$ can be found in Bourinet (2017a).

(b) Sensitivities to other distribution parameters

For $k = 1, \ldots, n_{\boldsymbol{\theta}}$, we want to assess $\partial \mathbf{u} / \partial \theta_k$ in Eq. (I.114), where θ_k represents any given marginal distribution parameter. Evaluating the first term $\mathbf{L}_0^{-1} \partial \mathbf{z} / \partial \theta_k$ is quite standard from the following expression obtained from Eq. (I.22), for $i = 1, \ldots, n$:

$$\frac{\partial z_i}{\partial \theta_k} = \frac{1}{\varphi\left(F_{X_i}(x_i)\right)} \frac{\partial F_{X_i}(x_i)}{\partial \theta_k} \,, \tag{I.119}$$

in which $\partial F_{X_i} / \partial \theta_k$ has to be derived for any usual statistical distribution.

Evaluating the second term $(\partial \mathbf{L}_0^{-1} / \partial \theta_k)\mathbf{z}$ is less easy. The sensitivity of $\mathbf{L}_0^{-1}$ to θ_k is obtained in three steps, similarly to the process for the sensitivity of $\mathbf{L}_0^{-1}$ to correlation in the previous section:

(1) We first express the sensitivity $\dfrac{\partial \mathbf{R}_0}{\partial \theta_k}$, as described in the following.

(2) $\dfrac{\partial \mathbf{L}_0}{\partial \theta_k}$ is obtained from $\mathbf{R}_0$ and $\dfrac{\partial \mathbf{R}_0}{\partial \theta_k}$ by means of the algorithm given in Bourinet (2017a).

(3) $\dfrac{\partial \mathbf{L}_0^{-1}}{\partial \theta_k}$ is obtained from $\dfrac{\partial \mathbf{L}_0}{\partial \theta_k}$, see Eq. (I.116).

The sensitivity of $\mathbf{R}_0$ to θ_k is obtained from the following equation. For any $i, j = 1, \ldots, n$, we have:

$$\frac{\partial \rho_{ij}}{\partial \theta_k} = \int_{\mathbb{R}} \int_{\mathbb{R}} \left[\frac{\partial h\left(z_i, z_j, \mu_i, \mu_j, \sigma_i, \sigma_j\right)}{\partial \theta_k} \varphi_2\left(z_i, z_j, \rho_{0,ij}\right) + h\left(z_i, z_j, \mu_i, \mu_j, \sigma_i, \sigma_j\right) \frac{\partial \varphi_2\left(z_i, z_j, \rho_{0,ij}\right)}{\partial \theta_k} \right] \mathrm{d}z_i \mathrm{d}z_j \,, \tag{I.120}$$

where:

$$\frac{\partial h}{\partial \theta_k} = \frac{\partial h}{\partial z_i}\frac{\partial z_i}{\partial \theta_k} + \frac{\partial h}{\partial z_j}\frac{\partial z_j}{\partial \theta_k} + \frac{\partial h}{\partial \mu_i}\frac{\partial \mu_i}{\partial \theta_k} + \frac{\partial h}{\partial \mu_j}\frac{\partial \mu_j}{\partial \theta_k} + \frac{\partial h}{\partial \sigma_i}\frac{\partial \sigma_i}{\partial \theta_k} + \frac{\partial h}{\partial \sigma_j}\frac{\partial \sigma_j}{\partial \theta_k} \,, \tag{I.121}$$

and:

$$\frac{\partial \varphi_2}{\partial \theta_k} = \frac{\partial \varphi_2}{\partial z_i}\frac{\partial z_i}{\partial \theta_k} + \frac{\partial \varphi_2}{\partial z_j}\frac{\partial z_j}{\partial \theta_k} + \frac{\partial \varphi_2}{\partial \rho_{0,ij}}\frac{\partial \rho_{0,ij}}{\partial \theta_k} \,. \tag{I.122}$$

It is important to notice that the unknown sensitivity $\partial \rho_{0,ij}/\partial \theta_k$ (i.e. the element of $\partial \mathbf{R}_0/\partial \theta_k$ in the i^{th} row and j^{th} column) appears in the integrand of Eq. (I.120), see last term of Eq. (I.122). This sensitivity is obtained by solving Eq. (I.120) by numerical integration, in which we have $\partial \rho_{ij}/\partial \theta_k = 0$. We use again the same rule for numerical integration as the one defined for the calculation of $\mathbf{R}_0$. Note that the partial derivatives of μ_i, μ_j, σ_i and σ_j w.r.t. θ_k in Eq. (I.121) are all zeros if θ_k is a distribution parameter of a component of $\mathbf{X}$ other than X_i or X_j.

From the examples investigated in Bourinet (2017a), it is found that the contribution of the second term of Eq. (I.114) is important only when correlated components with sufficiently large variances are present in $\mathbf{X}$. Accounting for this second term is moreover only required when at least one component of $\mathbf{X}$ has a distribution belonging to Group 2 as defined by Liu and Der Kiureghian (1986). As a reminder, this group includes the lognormal, gamma, type-II largest value and type-III smallest value distributions. When X_i belongs to Group 2, $\rho_{0,ij}$ (therefore $\mathbf{R}_0$) depends on the coefficient of variation δ_i of X_i, see approximate expressions of $F = \rho_{0,ij}/\rho_{ij}$ given by Liu and Der Kiureghian. This implies a dependence of $\mathbf{L}_0^{-1}$ on the marginal distribution parameters of X_i and, as a consequence, a non-zero sensitivity of $\mathbf{L}_0^{-1}$ w.r.t. those parameters.

I–4.3 Crude MC simulation and subset simulation

I–4.3.1 Crude MC sensitivities of p_f w.r.t. distribution parameters: the score function

The sensitivities of p_f w.r.t. distribution parameters can be assessed as a simple post-processing of a crude MC simulation by means of the score function introduced by Rubinstein (Rubinstein, 1976; Rubinstein, 1986). Such an approach was later brought to the structural reliability community by Wu (1994).

We wish to assess the sensitivity of p_f w.r.t. a given distribution parameter θ_k of $\boldsymbol{\theta}$:

$$\frac{\partial p_\mathrm{f}}{\partial \theta_k} = \frac{\partial}{\partial \theta_k} \int_{\mathcal{X}} \mathbb{1}_{\mathcal{F}_\mathbf{x}}(\mathbf{x})\, f_\mathbf{X}(\mathbf{x})\, \mathrm{d}\mathbf{x} \,. \tag{I.123}$$

Assuming that (i) the joint PDF of $\mathbf{X}$ is continuously differentiable w.r.t. θ_k, and that (ii) the integration domain $\mathcal{X}$ does not depend on θ_k, we can write:

$$\frac{\partial p_\mathrm{f}}{\partial \theta_k} = \int_{\mathcal{X}} \mathbb{1}_{\mathcal{F}_\mathbf{x}}(\mathbf{x}) \frac{\partial f_\mathbf{X}(\mathbf{x})}{\partial \theta_k} \mathrm{d}\mathbf{x} \,. \tag{I.124}$$

It is important to point out that assumption (ii) is not met for truncated distributions. An example of such distributions is the uniform distribution for which the bounds of the integration domain depend on its statistical moments (see, e.g., Lee et al., 2011a; Lee et al., 2011b).

This integral can be assessed by IS with the joint PDF $f_{\mathbf{X}}$, as detailed in the first line of Eq. (I.125). It is worth pointing out that this IS PDF is the same as the one used in a crude MC simulation, which therefore implies that the sample drawn for the estimation of p_f by crude MC can also be used to estimate the sensitivity of p_f w.r.t. any $\theta_k \in \boldsymbol{\theta}$. The function $\kappa_{\theta_k}(\mathbf{x}) = \partial \ln(f_{\mathbf{X}}(\mathbf{x}))/\partial\theta_k$ which is introduced line 3 of this equation is known as the *score function*.

$$\begin{aligned}\frac{\partial p_\mathrm{f}}{\partial \theta_k} &= \int_{\mathcal{X}} \mathbb{1}_{\mathcal{F}_\mathbf{x}}(\mathbf{x}) \, \frac{\dfrac{\partial f_{\mathbf{X}}(\mathbf{x})}{\partial \theta_k}}{f_{\mathbf{X}}(\mathbf{x})} \, f_{\mathbf{X}}(\mathbf{x}) \, \mathrm{d}\mathbf{x} \\ &= \int_{\mathcal{X}} \mathbb{1}_{\mathcal{F}_\mathbf{x}}(\mathbf{x}) \, \frac{\partial \ln(f_{\mathbf{X}}(\mathbf{x}))}{\partial \theta_k} \, f_{\mathbf{X}}(\mathbf{x}) \, \mathrm{d}\mathbf{x} \\ &= \mathbb{E}_{f_{\mathbf{X}}}\left[\mathbb{1}_{\mathcal{F}_\mathbf{x}}(\mathbf{X}) \, \kappa_{\theta_k}(\mathbf{X})\right] .\end{aligned} \tag{I.125}$$

The corresponding MC estimator of $\partial p_\mathrm{f}/\partial\theta_k$ is given by:

$$\widehat{\frac{\partial p_\mathrm{f}}{\partial \theta_k}} = \frac{1}{N}\sum_{j=1}^{N} \mathbb{1}_{\mathcal{F}_\mathbf{x}}\left(\mathbf{X}^{(j)}\right) \kappa_{\theta_k}\left(\mathbf{X}^{(j)}\right), \tag{I.126}$$

where $\{\mathbf{X}^{(j)}, 1 \le j \le N\}$ are N independent copies of the random vector $\mathbf{X}$, i.e. $\mathbf{X}^{(1)}, \ldots, \mathbf{X}^{(N)} \overset{\text{i.i.d.}}{\sim} f_{\mathbf{X}}$, and N denotes the sample size.

I–4.3.2 SS sensitivities of p_f w.r.t. distribution parameters

A similar approach can be applied to SS to derive the sensitivities of p_f w.r.t. distribution parameters, as proposed by Song et al. (2009), see also the presentation by Dubourg (2011, pp. 161–163). From Eq. (I.53), the sensitivity of the failure probability p_f w.r.t. a given distribution parameter $\theta_k \in \boldsymbol{\theta}$ can be expressed as follows:

$$\frac{\partial p_\mathrm{f}}{\partial \theta_k} = \sum_{s=1}^{m} \frac{p_\mathrm{f}}{p_s} \frac{\partial p_s}{\partial \theta_k}, \tag{I.127}$$

where $p_1 = \mathbb{P}(E_1)$ and $p_s = \mathbb{P}(E_s|E_{s-1})$ for $s = 2, \ldots, m$,
and where the partial derivatives of the intermediate probabilities p_s for $s = 1, \ldots, m$ are defined by recurrence (Song et al., 2009):

$$\frac{\partial p_1}{\partial \theta_k} = \mathbb{E}_{\varphi_n}\left[\mathbb{1}_{\mathcal{F}_{\mathbf{u},1}}(\mathbf{U}) \, K_{\theta_k}(\mathbf{U})\right], \tag{I.128}$$

and, for $s = 2, \ldots, m$:

$$\frac{\partial p_s}{\partial \theta_k} = \mathbb{E}_{\varphi_n(\cdot|E_{s-1})}\left[\mathbb{1}_{\mathcal{F}_{\mathbf{u},s}}(\mathbf{U})\left(K_{\theta_k}(\mathbf{U}) - \sum_{r=1}^{s-1} \frac{1}{p_r} \frac{\partial p_r}{\partial \theta_k}\right)\right], \tag{I.129}$$

where $K_{\theta_k}(\mathbf{u}) = (\kappa_{\theta_k} \circ T^{-1})(\mathbf{u})$ denotes the score function expressed in the standard normal space.

The corresponding sensitivity estimator at the first level of SS is:

$$\widehat{\frac{\partial p_1}{\partial \theta_k}} = \frac{1}{N}\sum_{j=1}^{N}\left[\mathbb{1}_{\mathcal{F}_\mathbf{u}}\left(\mathbf{U}^{(j)}\right) K_{\theta_k}\left(\mathbf{U}^{(j)}\right)\right], \tag{I.130}$$

where $\{\mathbf{U}^{(j)}, 1 \leq j \leq N\}$ are N independent copies of the random vector $\mathbf{U}$ at the first SS level, i.e. such that $\mathbf{U}^{(1)}, \ldots, \mathbf{U}^{(N)} \overset{\text{i.i.d.}}{\sim} \varphi_n$, and N denotes the sample size of the SS levels.

At the next levels $s = 2, \ldots, m$, the sensitivity estimator writes:

$$\widehat{\frac{\partial p_s}{\partial \theta_k}} = \frac{1}{N} \sum_{j=1}^{N} \left[\mathbb{1}_{\mathcal{F}_{\mathbf{u},s}}\left(\mathbf{U}^{(j)}\right) \left(K_{\theta_k}\left(\mathbf{U}^{(j)}\right) - \sum_{r=1}^{s-1} \frac{1}{p_r} \widehat{\frac{\partial p_r}{\partial \theta_k}} \right) \right], \tag{I.131}$$

where $\{\mathbf{U}^{(j)}, 1 \leq j \leq N\}$ are N independent copies of the random vector $\mathbf{U}$ at level s, i.e. such that $\mathbf{U}^{(1)}, \ldots, \mathbf{U}^{(N)} \overset{\text{i.i.d.}}{\sim} \varphi_n(\cdot|E_{s-1})$.

I–4.3.3 Normalized sensitivities in the standard normal space

The sensitivities defined in Sections I–4.3.1 and I–4.3.2 are defined w.r.t. distribution parameters of the joint PDF $f_{\mathbf{X}}$. These sensitivities are often useful for optimal design under uncertainty in a gradient-based algorithm, such as presented in Section II–5.2 where the design parameters are the means of some components of the random vector $\mathbf{X}$. It is now proposed to assess the sensitivity of the failure probability w.r.t. distribution parameters of the standard normal space PDF, i.e. φ_n. Such an approach presents the major advantage of obtaining normalized sensitivities, since each component of $\mathbf{U}$ follows a univariate standard normal PDF. The disadvantage is that the correlation structure is lost, which makes it difficult to interpret such sensitivities in the case of correlated random inputs.

The n-dimensional standard normal PDF is written as follows, as already introduced in Section I–3.4.1, see Eq. (I.100):

$$\varphi_n(\mathbf{u}) = \varphi_n(\mathbf{u}; \boldsymbol{\theta}) = \prod_{i=1}^{n} \frac{1}{\sigma_i \sqrt{2\pi}} \exp\left(-\frac{1}{2} \left(\frac{u_i - \mu_i}{\sigma_i} \right)^2 \right), \tag{I.132}$$

where $\boldsymbol{\theta} = (\mu_1, \ldots, \mu_n, \sigma_1, \ldots, \sigma_n) = (0, \ldots, 0, 1, \ldots, 1)$.

The score function of φ_n, denoted $\kappa_{\theta_k}(\mathbf{u})$, is given, for $k = 1, \ldots, 2n$ [10], by:

$$\begin{aligned} \kappa_{\theta_k}(\mathbf{u}) &= \frac{\partial \ln(\varphi_n(\mathbf{u}))}{\partial \theta_k} \\ &= \begin{cases} \dfrac{u_i - \mu_i}{\sigma_i^2} & = u_i \quad \text{if} \quad \theta_k = \mu_i, \quad i = 1, \ldots, n, \\ \dfrac{(u_i - \mu_i)^2 - \sigma_i^2}{\sigma_i^3} & = u_i^2 - 1 \quad \text{if} \quad \theta_k = \sigma_i, \quad i = 1, \ldots, n. \end{cases} \end{aligned} \tag{I.133}$$

The SS sensitivity estimators defined in Eqs. I.130-I.131 now rewrite:

$$\widehat{\frac{\partial p_1}{\partial \theta_k}} = \begin{cases} \dfrac{1}{N} \displaystyle\sum_{j=1}^{N} \left[\mathbb{1}_{\mathcal{F}_{\mathbf{u}}}\left(\mathbf{U}^{(j)}\right) \mathbf{U}^{(j)} \right] & \text{if} \quad \theta_k = \mu_i, \quad i = 1, \ldots, n, \\ \dfrac{1}{N} \displaystyle\sum_{j=1}^{N} \left[\mathbb{1}_{\mathcal{F}_{\mathbf{u}}}\left(\mathbf{U}^{(j)}\right) \left(\mathbf{U}^{(j)^2} - 1 \right) \right] & \text{if} \quad \theta_k = \sigma_i, \quad i = 1, \ldots, n. \end{cases} \tag{I.134}$$

[10] Note that the score function of φ_n was already given in Eqs. I.102a-I.102b for the application of the CE method in the standard normal space.

and, for $s = 2, \dots, m$:

$$\widehat{\frac{\partial p_s}{\partial \theta_k}} = \begin{cases} \dfrac{1}{N}\displaystyle\sum_{j=1}^{N}\left[\mathbb{1}_{\mathcal{F}_{\mathbf{u},s}}\left(\mathbf{U}^{(j)}\right)\left(\mathbf{U}^{(j)} - \sum_{r=1}^{s-1}\frac{1}{p_r}\widehat{\frac{\partial p_r}{\partial \theta_k}}\right)\right] & \text{if} \quad \theta_k = \mu_i, \quad i = 1, \dots, n\,, \\ \dfrac{1}{N}\displaystyle\sum_{j=1}^{N}\left[\mathbb{1}_{\mathcal{F}_{\mathbf{u},s}}\left(\mathbf{U}^{(j)}\right)\left(\left(\mathbf{U}^{(j)2} - 1\right) - \sum_{r=1}^{s-1}\frac{1}{p_r}\widehat{\frac{\partial p_r}{\partial \theta_k}}\right)\right] & \text{if} \quad \theta_k = \sigma_i, \quad i = 1, \dots, n\,. \end{cases} \tag{I.135}$$

The sensitivities of p_f to distribution parameters in the standard normal space as proposed above are assessed for example 1 introduced in Section I–3.4.2 with $\mu_{F_s} = 27.5$. These sensitivities are obtained by means of a simple post-processing of a SS simulation run, from the samples used at each level of SS and the corresponding LSF values. Let us introduce the following probabilities π_s for $s = 1, \dots, m$:

$$\pi_s = \prod_{k=1}^{s} p_k\,. \tag{I.136}$$

Note that we have $p_\mathrm{f}^{\mathrm{SS}} = \pi_m$.

The choice made here is to represent the sensitivity of π_s w.r.t. any $\theta_k \in \boldsymbol{\theta}$ normalized by π_s for $s = 1, \dots, m$, which enables us to investigate how this sensitivity evolves with the SS levels:

$$\begin{aligned} \frac{1}{\pi_s}\frac{\partial \pi_s}{\partial \theta_k} &= \frac{1}{\pi_s}\sum_{r=1}^{s}\frac{\pi_s}{p_r}\frac{\partial p_r}{\partial \theta_k} \\ &= \sum_{r=1}^{s}\frac{1}{p_r}\frac{\partial p_r}{\partial \theta_k}\,. \end{aligned} \tag{I.137}$$

The corresponding estimator of these sensitivities is given by the following expression:

$$\widehat{\frac{1}{\pi_s}\frac{\partial \pi_s}{\partial \theta_k}} = \sum_{r=1}^{s}\frac{1}{\widehat{p}_r}\widehat{\frac{\partial p_r}{\partial \theta_k}}\,, \tag{I.138}$$

where $\widehat{p}_r$ is given in Eqs. I.57-I.58, and $\widehat{\partial p_r/\partial \theta_k}$ is given in Eqs. I.134-I.135.

These normalized sensitivities, estimated from a single application of the SS method with $N = 10^6$ samples per level and $p_0 = 0.5$, are represented in Figure I.13. Note that a large number of samples N is taken here for the sake of accurate sensitivities. The unusual choice of $p_0 = 0.5$ is made in order to obtain an increased number of SS levels compared to the case $p_0 = 0.1$ (here $m = 22$ instead of $m = 7$) and therefore a finer representation of the normalized sensitivities of $p_\mathrm{f}^{\mathrm{SS}}$ w.r.t. μ_i and σ_i in the plots for $i = 1, \dots, 8$. For example 1, all the random components X_i for $i = 1, \dots, 8$ are statistically independent, which allows a straightforward interpretation of the obtained sensitivities. A single random component X_i is important if its normalized sensitivity to mean $(\partial \pi_s/\partial \mu_i)/\pi_s$ and/or its normalized sensitivity to standard deviation $(\partial \pi_s/\partial \sigma_i)/\pi_s$ is/are important, i.e. if their values noticeably differ from zero. As observed in this example, the three most important variables are ζ_p, F_s and ζ_s, in decreasing order of importance. It is also worth pointing out that the most important variables may change with the SS level, indicating that some variables are more important in the central tendency than at failure, or vice versa. This therefore shows that a dimension reduction of the reliability problem based on a selection of the most important variables in the central tendency could result in an incorrectly set-up problem and therefore an incorrect failure probability estimation. These normalized sensitivities have not yet been extended to Nataf-correlated random inputs. One direction to explore would be to derive sensitivities similar to those proposed, but in the **z**-space, in which all the inputs are scaled to standard normal but still correlated random variates.

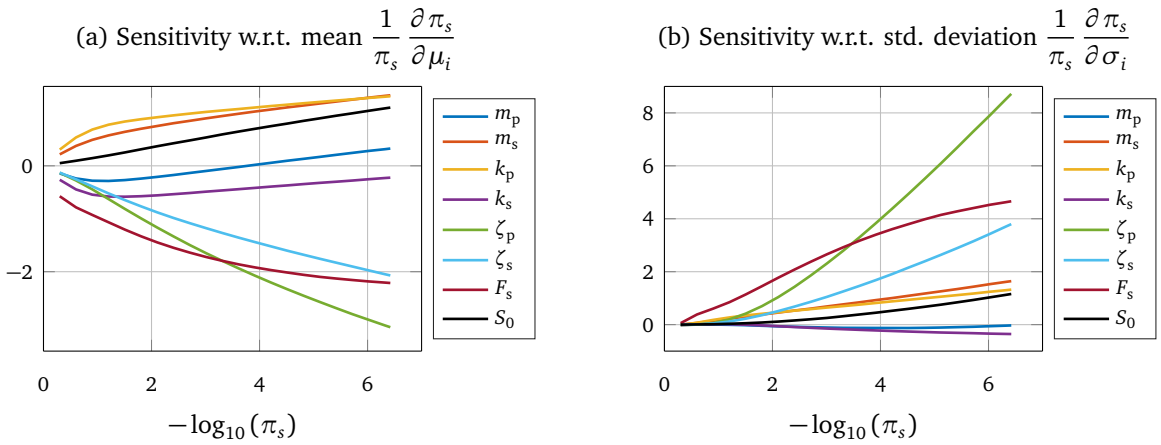

Figure I.13 – Example 1, $\mu_{F_s} = 27.5$. Normalized sensitivities of π_s w.r.t. mean μ_i and standard deviation σ_i in the standard normal space for $i = 1, \ldots, 8$. The normalized sensitivities of p_f w.r.t. μ_i and σ_i correspond to the right-hand points of these plots, i.e. when $\widehat{p}_f^{SS} = \widehat{\pi}_m = \prod_{k=1}^{m} \widehat{p}_k$. The results are obtained from a single SS analysis with $N = 10^6$ samples per level and a prescribed probability level $p_0 = 0.5$.

II

Surrogate models & adaptive strategies for uncertainty propagation

Overview: *The estimation of low failure probabilities in reliability is often confronted with the limits imposed by the available computational resources. This burden is alleviated by using surrogates for the costly-to-evaluate models involved in the analysis, under some assumptions about the dimensionality and complexity of the model we want to approximate. This chapter gives an overview of the main surrogate models and their use in adaptive approaches,* i.e. *methods that sequentially select a few points to evaluate in the input space and update the surrogate model until sufficient accuracy is attained. The focus in this report is on kernel-based techniques, mainly support vector machines (SVMs) but also kriging to a lesser extent. This chapter recalls the main principles of these two techniques, with technical details about their construction and the tuning of their parameters. SVMs in classification were used in the PhD work of Deheeger (2008) for the purpose of reliability assessment. I recently extended this work to support vector regression based on the ϵ-insensitive loss function. Kriging was used in surrogate-based approaches for the purpose of reliability-based design optimization (RBDO) in the PhD works of Dubourg (2011) and Moustapha (2016).*

Contributions: *This chapter presents linear SVMs in their two main forms, classification and regression, with their extension to the nonlinear case by means of kernels. Emphasis is placed on the tradeoff to be made between a model which is simple to learn and its closeness to the data, by placing the problem to solve in a regularization framework, see Section II–2.3. The two proposed adaptive methods for reliability assessment are recalled in Section II–3. The first, called ^{2}SMART, is based on SVMs used in classification (Bourinet et al., 2011). The second and more recent one, called ASVR, is based on support vector regression (Bourinet, 2016). A key ingredient of this latter method is the accuracy of the constructed approximate models, which are obtained by minimizing an approximation of the leave-one-out error, see Section II–2.4. The most important aspects of kriging are given in Section II–4, which also clearly identifies the relationship between kriging and least squares support vector regression, one of the forms of SVMs in regression. The two proposed adaptive methods for RBDO based on kriging are detailed in Section II–5.3 (Dubourg et al., 2011; Moustapha et al., 2016). These methods are expressed in an augmented space and take advantage of the kriging variance.*

Credits: *This chapter has excerpts from:*
- *papers of Bourinet et al. (2011) and Bourinet (2016) in Section II–3,*
- *PhD manuscripts of Dubourg (2011) and Moustapha (2016), papers of Dubourg et al. (2011) and Moustapha et al. (2016) in Section II–5.*

II–1 Introduction

The propagation of uncertainties in costly-to-evaluate numerical models used in several fields of engineering physics is often a challenging task. In practice, the analyst is almost always confronted with insufficient computational resources to analyze the many situations he(she) wishes to solve in order to identify the most influential variables, allowing him(her) to find a better design of the studied system in subsequent steps. We will here focus on the situations that arise in uncertainty propagation, but similar challenges are also found e.g. in deterministic optimization (Jones, 2001; Forrester and Keane, 2009). More explicitly, we will consider the specific cases of reliability assessment characterized by low failure probabilities such as addressed in Section I, but also uncertainty propagation for optimal design (also termed as *optimization under uncertainty*), such as the reliability-based design optimization introduced in Section II–5. For engineering problems of practical interest, assessing small failure probabilities by the methods presented in Section I requires a number of calls to a numerical model that may exceed the maximum number authorized. Such a situation is often met in high-dimensional problems with inputs modeled by random processes or random fields, for which the SS method still requires thousands to tens of thousands calls to the LSF for a failure probability estimate of an acceptable accuracy (say with a c.o.v. of p_f close to 10-20%).

To alleviate the computational burden, interesting alternative methods have emerged in the past few decades. Their basic principle consists in substituting the true and costly-to-evaluate model which we cannot afford to call too often with a cheap-to-evaluate model that should be sufficiently "close" to the true one (note that we therefore assume that this model is an approximation of the true one). Practically, the construction of this cheap-to-evaluate model necessitates few calls to the costly-to-evaluate one and the main objective is to keep this number minimal for the sake of computational efficiency. This field is often known as *computer simulation experiments* (Sacks et al., 1989; Santner et al., 2003; Kleijnen, 2007).

Such approximate models have been proposed in various contexts over the years and several terms can be found to designate such models: response surfaces (most often assumed in a polynomial form), *surrogate models*[1], meta-models, proxy models, emulators and machines (in machine learning), to cite the most common terms. From our perspective, a natural approach is to consider a surrogate model that replaces the costly-to-evaluate LSF in reliability assessment or the cost function and/or probabilistic constraints in optimization under uncertainty. Let us assume that the true model is defined by means of a scalar function $y : \mathcal{X} \to \mathcal{Y}, \mathbf{x} \mapsto y = y(\mathbf{x})$ where $\mathcal{X} \subseteq \mathbb{R}^n$ denotes the *input space* and $\mathcal{Y} \subseteq \mathbb{R}$ the *output space*. Unless otherwise stated, the surrogate of y is denoted $\widetilde{y} : \mathbf{x} \mapsto \widetilde{y} = \widetilde{y}(\mathbf{x}) = \widetilde{y}(\mathbf{x}; \mathcal{T})$ in this report, where $\mathcal{T}$ is the set of data on which $\widetilde{y}$ is trained, see Section II–1.1. The notation $\widetilde{y}_{\mathcal{T}}$ is sometimes used for making explicit the dependence of the surrogate model on the training data $\mathcal{T}$. The approximation $\widetilde{y}$ depends on the type of surrogate model that is selected, see the short overview of existing techniques given in Section II–1.3. Some types of surrogate models may require some additional parameters which, as seen later in this report, need to be tuned from the available data $\mathcal{T}$ for accurate predictions of the model $\widetilde{y}$. It is also important to stress that *any* type of surrogate model is characterized by its own underlying assumptions due to the specific form of the approximation. It is worth pointing out that these assumptions are expected to be "compatible" with the properties of the true function y (e.g. continuity, differentiability, smoothness of y). If this is not the case, the constructed approximate model $\widetilde{y}$ could be severely biased and therefore inappropriate to surrogate y.

II–1.1 Construction of surrogate models

It is assumed that we are given a set of N data pairs $\mathcal{D} = \{(\mathbf{x}_i, y_i) \in \mathcal{X} \times \mathcal{Y}, 1 \leq i \leq N\}$. We will restrict the presentation to a scalar output for simplicity. Let us also assume that the y_i's are the respective evaluations of the true function y we want to surrogate at the given $\mathbf{x}_i$'s: $y_i = y(\mathbf{x}_i)$ for $i = 1, \ldots, N$. We consider that the surrogate model $\widetilde{y}$ is constructed from a set of data pairs $\mathcal{T}$ called the *training set* (called *design of experiments* [2] or *experimental design* in the context of surrogate models applied to deterministic functions y). It should be indicated that $\mathcal{T}$ is often (but not necessarily[3]) equal to the set of known data pairs $\mathcal{D}$. If the set of outputs $\mathcal{Y}$ is continuous, the construction of the surrogate model is known as *regression* and $\widetilde{y}$ is termed a regressor. In the case of a discrete set $\mathcal{Y}$ the approach is known as *classification* and $\widetilde{y}$ is a classifier. Both cases are considered in this chapter, see Sections II–2.2 and II–4 for regression with support vector machines and Gaussian process emulators respectively, and Section II–2.1 for binary classification with support vector machines.

[1] This term *surrogate model* is the one that is most often used in this report. The costly-to-evaluate model is often referred to as the *true model*.

[2] Experimental designs are also widely used for real physical experiments (see, e.g., Box and Draper, 1987). For a discussion of the differences between the two types of practice, the reader may refer to Sacks et al. (1989, p. 411).

[3] Some algorithms can be devised to learn over a subset of the known data pairs. In the case of regression, this means that a local regression is made.

For a broader perspective, the construction of surrogate models should be placed in the context of *machine learning* (Rasmussen and Williams, 2006) or *statistical learning* (Hastie et al., 2009). Constructing regressors or classifiers from data is known as *supervised learning* in such contexts. It is also worth mentioning that machine learning methods were not developed for the specific case of deterministic function approximation of interest in this chapter. These methods are able to *learn from data* in a general sense, without requiring that the data comes from a physical model (here the costly-to-evaluate model defined through the function y). This could be real (and most often noisy) data gathered from any observed phenomenon.

Assuming that a set of training data has been defined and that a type of surrogate model has been selected, it is then necessary to tune the unknown parameters of the surrogate model $\widetilde{y}$. Selecting optimal parameters of $\widetilde{y}$ from a training set $\mathcal{T}$ is often specific to each type of surrogate model. In order to clarify what optimality means, it is useful to introduce some definitions from statistical learning theory.

In the classical framework of statistical learning, it is assumed that the training set $\mathcal{T} = \{(\mathbf{x}_i, y_i) \in \mathcal{X} \times \mathcal{Y}, 1 \leq i \leq N\}$ is composed of i.i.d. samples drawn from an unknown distribution denoted $p(\mathbf{x}, y)$[4].

The accuracy of a given surrogate model $\widetilde{y}$ can be defined in terms of its ability to make good predictions on new points. This performance is measured by the so-called *expected risk* $R(\widetilde{y})$ that defines the *generalization error*:

$$R(\widetilde{y}) = \mathbb{E}_{p(\mathbf{x},y)}[\ell(Y, \widetilde{y}(\mathbf{X}))] = \int_{\mathcal{X}\times\mathcal{Y}} \ell(y, \widetilde{y}(\mathbf{x}))\, p(\mathbf{x}, y)\, \mathrm{d}\mathbf{x}\mathrm{d}y\ , \tag{II.1}$$

where $\ell : \mathcal{Y} \times \mathbb{R} \to \mathbb{R}_{\geq 0}$ is a chosen *loss function* (or cost function) which specifies the cost incurred by replacing y by $\widetilde{y}(\mathbf{x})$ (this loss measures how "different" y and $\widetilde{y}(\mathbf{x})$ are).

The distribution $p(\mathbf{x}, y)$ is in general unknown. We therefore introduce the *empirical risk* $R_{\text{emp}}(\widetilde{y})$ that can be directly assessed from the training data $\mathcal{T}$:

$$R_{\text{emp}}(\widetilde{y}) = \frac{1}{N}\sum_{i=1}^{N} \ell(y_i, \widetilde{y}(\mathbf{x}_i))\ . \tag{II.2}$$

Let us assume that we are searching for a surrogate model in a space of functions denoted $\mathcal{H}$ (called *hypothesis space* in machine learning) from a given training set $\mathcal{T}$. If we denote $\widetilde{y}^*_{\mathcal{H}}$ the minimizer of the expected risk R in the hypothesis space $\mathcal{H}$:

$$\widetilde{y}^*_{\mathcal{H}} = \arg\min_{f\in\mathcal{H}} R(f)\,, \tag{II.3}$$

and by $\widetilde{y}^*_{\mathcal{H}\,\text{emp}}$ the minimizer of the empirical risk R_{emp}:

$$\widetilde{y}^*_{\mathcal{H}\,\text{emp}} = \arg\min_{f\in\mathcal{H}} R_{\text{emp}}(f)\,, \tag{II.4}$$

a central question of statistical learning is whether the expected risk of $\widetilde{y}^*_{\mathcal{H}\,\text{emp}}$ is sufficiently close to that of $\widetilde{y}^*_{\mathcal{H}}$, i.e. $R(\widetilde{y}^*_{\mathcal{H}\,\text{emp}}) \approx R(\widetilde{y}^*_{\mathcal{H}})$ (see, e.g., Evgeniou et al., 2000). It is important here to stress out that minimizing the expected risk R is out of reach, since the distribution $p(\mathbf{x}, y)$ is unknown. Hence minimizing the empirical risk R_{emp} appears as a natural solution to resort to, since it is defined from the

[4] In statistical learning, a probabilistic relationship between $\mathbf{x}$ and y is assumed in order to account for noise. Two different values of y could be obtained for the same $\mathbf{x}$.

training data. This approach, known as *empirical risk minimization* (ERM), is unfortunately ill-posed, as illustrated by the following example taken in the context of binary classification (Smola et al., 2000, Chapter "Introduction to large margin classifiers", p. 9).

In binary classification, the 0-1 loss function $\ell(y,u) = \mathbb{1}_{\{u \neq y\}}$ is often used as a measure of the classification error. The expected risk in such a context represents the probability of misclassification:

$$R(\widetilde{y}) = \mathbb{P}\left(\widetilde{y}(\mathbf{X}) \neq y(\mathbf{X})\right) , \tag{II.5}$$

and the empirical risk is given by:

$$R_{\text{emp}}(\widetilde{y}) = \frac{1}{N}\sum_{i=1}^{N} \mathbb{1}_{\{\widetilde{y}(\mathbf{x}_i) \neq y_i\}} , \tag{II.6}$$

which is simply the training error.

If ERM is applied to a binary classification problem in which $\mathcal{Y} = \{-1, +1\}$, we can choose $\widetilde{y}^*_{\mathcal{H}\,\text{emp}}$ such that all the training pairs of $\mathcal{T}$ are memorized, and a random output in $\mathcal{Y}$ is given at points other that those belonging to $\mathcal{T}$. With such a model, the empirical risk is $R_{\text{emp}}(\widetilde{y}^*_{\mathcal{H}\,\text{emp}}) = 0$ but the expected (and therefore true) risk is $R(\widetilde{y}^*_{\mathcal{H}\,\text{emp}}) = 0.5$ provided that the finite training sample $\mathcal{T}$ has a zero probability measure. This clearly indicates that a model characterized by a zero training error on the training data may be unable to predict well on new data. Such a phenomenon is known as *overfitting*, and of course it should be avoided.

In order to assess the performance of a surrogate model, it is usual to express the difference between the expected risk of the constructed surrogate model $\widetilde{y} = \widetilde{y}_{\mathcal{T}}$ averaged over all possible training sets $\mathcal{T}$ (expectation on $\mathcal{T}$) and the so-called Bayes' risk $R^* = R(\widetilde{y}^*)$:

$$\mathbb{E}_{\mathcal{T}}\left[R(\widetilde{y}_{\mathcal{T}})\right] - R(\widetilde{y}^*) = \left[\mathbb{E}_{\mathcal{T}}\left[R(\widetilde{y}_{\mathcal{T}})\right] - R\left(\widetilde{y}^*_{\mathcal{H}}\right)\right] + \left[R\left(\widetilde{y}^*_{\mathcal{H}}\right) - R(\widetilde{y}^*)\right] , \tag{II.7}$$

where

$$\widetilde{y}^* = \arg\min_{f} R(f) \tag{II.8}$$

denotes the best possible model that can be obtained by minimizing the expected risk over all measurable functions, and where $\widetilde{y}^*_{\mathcal{H}}$ denotes the best model that can be obtained within the class of models defined by $\mathcal{H}$, see Eq. (II.3).

In Eq. (II.7), the first term of the sum is called the *estimation error* (this error, due to the random choice of the training set $\mathcal{T}$, quantifies how well it is possible to identify the best model from data within the class $\mathcal{H}$), and the second term is called the *approximation error* (this error does not involve the data set $\mathcal{T}$ on which $\widetilde{y}_{\mathcal{T}}$ is trained; it quantifies how well it is possible to approximate y under the restrictive assumption that the surrogate model belongs to $\mathcal{H}$). In regression based on the square loss $\ell(y,u) = (y-u)^2$, this decomposition into two terms is known as the bias/variance decomposition (see, e.g., Geman et al., 1992, p. 10), in which the first term (estimation error) represents the variance and the second term (approximation error) the squared bias.

From a practical viewpoint, the construction of an accurate surrogate model $\widetilde{y}$ requires choosing both a type of model through $\mathcal{H}$ and a training set through $\mathcal{T}$. If $\mathcal{H}$ is chosen sufficiently large (high complexity of the approximation $\widetilde{y}$), we quite naturally expect that the approximation error will be small, but the adverse effect is that the estimation error will grow, thus imposing the use of prohibitively large training sets $\mathcal{T}$ (case of overfitting). Conversely, if $\mathcal{H}$ is small (low complexity of $\widetilde{y}$), the estimation error will be small (we do not need a large set of data to train $\widetilde{y}$ with good accuracy) but the approximation error will become large (case of underfitting). A tradeoff therefore needs to be found in order to avoid the two above-mentioned issues. It is desirable to find the right balance between the level of complexity of the approximation $\widetilde{y}$ and the amount of data that is required to train the surrogate model.

This is usually achieved by restricting the "size" of the space of functions $\mathcal{H}$ in which the surrogate is sought (the complexity of the surrogate model is controlled by the type of approximation that is used, e.g. polynomials of a given maximum degree) and/or by working with a regularized risk instead of the empirical risk, such as presented in Section II–2.3.2 in the context of support vector machines.

II–1.2 Data-adaptive strategies

So far it has been assumed that we were given a training set $\mathcal{T}$ and the objective was to construct the "best" surrogate model from it. The points $\mathbf{x}_i$ for $i = 1, \ldots, N$ were supposedly drawn *passively* from some given probability distribution $p(\mathbf{x})$. With no prior information about the distribution $p(\mathbf{x})$ and the true response $y(\mathbf{x})$, these points are expected to uniformly cover the entire space $\mathcal{X}$ in order to construct a surrogate model that is able to predict equally well at any point $\mathbf{x}$ in $\mathcal{X}$. In computer experiments, samplings that achieve such a purpose are known as *space filling* designs (see, e.g., Pronzato and Müller, 2012). They include Latin hypercube sampling (LHS) (McKay et al., 1979) and distance-based samplings such as the maximin- and minimax-distance designs (Johnson et al., 1990), among others.

In many applications including those addressed in this chapter, it is unnecessary for the surrogate model to be equally accurate in the entire space $\mathcal{X}$. It appears intuitive that more training samples should be placed in those sub-domains of the input space $\mathcal{X}$ which are the most influential on the accuracy of the output response y or any post-processed quantity(ies) derived from y. A greater accuracy of the surrogate model is expected to be achieved, e.g., near the optimal solution $\mathbf{x}^*$ in deterministic optimization, or within failure subdomains with high probability contents in reliability assessment. With this objective the idea is to move from passive to active sampling. Such active sampling strategies have emerged in various contexts with very similar purposes. They are referred to as *active learning*[5] or *query learning* in machine learning (MacKay, 1992; Cohn, 1996), see also the review by Settles (2009) for a smooth introduction, and *adaptive designs* or *sequential designs* in computer experiments and statistics (Santner et al., 2003).

Such strategies often adopt the following scheme:

(1) First step $s = 1$. A first surrogate model $\widetilde{y}_1$ is constructed from an initial training set denoted $\mathcal{T}_1 = \mathcal{D}_1 = \{(\mathbf{x}_i, y_i) \in \mathcal{X} \times \mathcal{Y}, i \in \mathcal{I}_1\}$ where $y_i = y(\mathbf{x}_i)$ for $i \in \mathcal{I}_1$ and $\#\mathcal{I}_1 = N_1$.

(2) Proceed to the next step: $s = s + 1$.

(3) A set of N_s new input points $\{\mathbf{x}_i \in \mathcal{X}, i \in \mathcal{I}_s\}$ is chosen at each subsequent step $s > 1$, where $\#\mathcal{I}_s = N_s$. The locations in $\mathcal{X}$ of these N_s new points are selected based on the information obtained from the surrogate models constructed up to step $(s-1)$. Most often this information comes from the last constructed surrogate only, i.e. $\widetilde{y}_{s-1}$. In machine learning, these new points may be required to belong to a large pool of input points with predefined locations in $\mathcal{X}$ and unknown outputs (so called unlabeled pool of examples). Strategies with only one point added at a time are often proposed, i.e. $N_s = 1$ for any $s > 1$, but it is of interest to explore the case $N_s > 1$ with currently available multi-cpu and multi-core computer systems.

(4) The true model y is evaluated at these N_s new points $\{\mathbf{x}_i \in \mathcal{X}, i \in \mathcal{I}_s\}$. Let us denote $\mathcal{D}_s = \{(\mathbf{x}_i, y_i) \in \mathcal{X} \times \mathcal{Y}, i \in \mathcal{I}_s\}$ where $y_i = y(\mathbf{x}_i)$ for $i \in \mathcal{I}_s$.

(5) A new training set $\mathcal{T}_s$ is defined, e.g. $\mathcal{T}_s = \bigcup_{k=1}^{s} \mathcal{D}_k$, but this could also be only a subset of this union of $\mathcal{D}_k$ sets.

(6) A new surrogate model $\widetilde{y}_s$ is trained on $\mathcal{T}_s$.

[5] Active learning is defined by Cohn et al. (1994) as "any form of learning in which the learning program has some control over the inputs on which it trains".

(7) A sequence $\{\widetilde{y}_s, 1 \leq s \leq s_{\text{final}}\}$ of surrogate models is constructed by repeating the adaptive construction from (2) until the final model $\widetilde{y} = \widetilde{y}_{s_{\text{final}}}$ meets some prescribed accuracy criterion. The total number of calls to the true model y therefore is $N_{\text{t}} = \sum_{s=1}^{s_{\text{final}}} N_s$.

Finding the most computationally efficient surrogate-based adaptive strategy with controlled accuracy can therefore be formalized through the following optimization problem:

$$\min N_{\text{t}} \quad \text{s.t.} \quad \epsilon\left(\psi\left(y\right), \psi\left(\widetilde{y}\right)\right) \leq \epsilon_{\text{tol}}\,, \tag{II.9}$$

where ψ denotes a real-valued scalar or vector function applied to the true or surrogated output response (e.g., $\psi(y)$ may represent a failure probability if y is a given LSF in reliability assessment, a set of Sobol' indices in a global sensitivity analysis w.r.t. a given output y or the global minimum/maximum of the function y in the domain $\mathcal{X}$ in a deterministic optimization analysis), ϵ defines an error measure between $\psi\left(y\right)$ and $\psi\left(\widetilde{y}\right)$ and ϵ_{tol} is a prescribed accuracy level. The minimization in Eq. (II.9) should be viewed as one carried out over all the strategies that can be devised, i.e. all possible numbers of new points and their locations in space $\mathcal{X}$ for $s = 1, \ldots, s_{\text{final}}$. Additional constraints may also be added to this optimization problem, e.g. $N_s \geq N_{\text{core}}$ for any s where N_{core} is the minimum number of cores that need to be used simultaneously in case of computations run on multi-core systems. In practice, this optimization problem is never solved in such formal settings. Strategies are proposed based on a selected type of surrogate model, and their efficiency/accuracy are assessed on a set of examples.

A central question should now be asked: can we make sure that active learning always performs better than passive learning for a given type of surrogate model? This question is asked in a few works (see, e.g., Niyogi, 1995, Chap. 3), but no general answer can be given and this remains quite an open problem in the author's opinion, despite the evidence of successful approaches reported in the literature. Surrogate-model-driven sampling used to select new training points in active learning departs from the uniform distribution, which has the best exploration ability. A tradeoff therefore needs to be found for such adaptive learning strategies: sampling should focus on the domains which are important for the problem of interest while remaining sufficiently explorative. This is also known as the compromise between *exploration* (searching in the unexplored space $\mathcal{X}$) and *exploitation* (using available information provided by the previously constructed surrogate models) in the context of Kriging surrogate models (Forrester and Keane, 2009). In the case of insufficiently explorative sampling (too much exploitation), the risk is to miss important zones of the input space $\mathcal{X}$, which results in an inaccurate final surrogate and therefore a biased solution. Conversely if the sampling is too explorative (case of insufficient exploitation), the risk is to generate too many samples in order to construct a surrogate model that is accurate everywhere in $\mathcal{X}$, therefore also in unimportant zones (i.e. strategy not optimal in terms of computational efficiency).

Examples of such surrogate-based adaptive strategies will be given in the context of the estimation of rare event probabilities in Section II–3 and reliability-based design optimization in Section II–5.

II–1.3 Main types of surrogate models

The aim of this section is to briefly recall the main types of surrogate models that are often used for uncertainty propagation. The support vector machines (SVM) and kriging specifically applied in the works presented in this report are respectively detailed in Sections II–2 and II–4. For details about the theoretical basis and practical implementation of the other models, the reader is invited to refer to specialized textbooks or papers, some of which cited here.

(a) Polynomial response surface

The construction of surrogate models for real-valued functions has been often performed by regression based on polynomial *response surfaces* (RS). The RS methodology (Box and Draper, 1987; Myers et al., 2009) finds its roots in the seminal work by Fisher in the early 1930s. The expression of the surrogate model $\widetilde{y}$ used in a polynomial RS regression can be written as follows:

$$\widetilde{y}(\mathbf{x}) = \phi(\mathbf{x})^{\mathrm{T}}\,\mathbf{w}\,, \tag{II.10}$$

where the map $\phi : \mathcal{X} \subseteq \mathbb{R}^n \to \mathbb{R}^p, \mathbf{x} \mapsto \phi(\mathbf{x}) = (\phi_1(\mathbf{x}), \ldots, \phi_p(\mathbf{x}))^{\mathrm{T}}$ is known as the basis expansion and where $\mathbf{w} \in \mathbb{R}^p$ is a vector of weights to be determined from the training set $\mathcal{T} = \{(\mathbf{x}_i, y_i) \in \mathcal{X} \times \mathcal{Y}, 1 \leq i \leq N\}$. A quadratic basis expansion is often considered in structural reliability approaches based on polynomial RS, see Section II–3. For $n = 2$, such a quadratic basis, including cross-terms, writes $\phi(\mathbf{x}) = (1, x_1, x_2, x_1^2, x_1x_2, x_2^2)^{\mathrm{T}}$ where $\mathbf{x} = (x_1, x_2)^{\mathrm{T}}$. It is assumed that the number N of data pairs in the training set $\mathcal{T}$ is greater than the number p of regression functions in $\phi(\mathbf{x})$, so that the problem is not under-determined.

The unknown weights are obtained from the training data set by minimizing the empirical risk w.r.t. the square loss function $\ell(y,u) = (y-u)^2$:

$$\mathbf{w}^* = \underset{\mathbf{w}\in\mathbb{R}^p}{\arg\min}\ \frac{1}{N}\sum_{i=1}^{N}(y_i - \widetilde{y}(\mathbf{x}_i))^2\,. \tag{II.11}$$

This minimization problem has an exact closed-form solution:

$$\mathbf{w}^* = \left(\mathbf{\Phi}^{\mathrm{T}}\mathbf{\Phi}\right)^{-1}\mathbf{\Phi}^{\mathrm{T}}\mathbf{y}\,, \tag{II.12}$$

where $\mathbf{\Phi} = [\phi_j(\mathbf{x}_i)]_{1\leq i\leq N\,,\,1\leq j\leq p}$ and $\mathbf{y} = (y_1, \ldots, y_N)^{\mathrm{T}}$.

The expression of the approximate model $\widetilde{y}$ therefore writes:

$$\widetilde{y}(\mathbf{x}) = \phi(\mathbf{x})^{\mathrm{T}}\left(\mathbf{\Phi}^{\mathrm{T}}\mathbf{\Phi}\right)^{-1}\mathbf{\Phi}^{\mathrm{T}}\mathbf{y}\,. \tag{II.13}$$

This approach is also known as *ordinary least squares* regression, where it is assumed that the magnitudes of the residuals $y_i - \widetilde{y}(\mathbf{x}_i)$ for $i = 1, \ldots, N$ are all independent from each other.

The main drawback of polynomial RS is the rigid structure of the low-degree polynomial approximations that are commonly used (most often either a full or incomplete quadratic basis), which may be not flexible enough to accurately fit the true function y we want to surrogate (see, e.g., Hurtado, 2004). This drawback is avoided by kernel-based surrogate models (e.g. kriging and support vector machines) whose unknown parameters are identified from locally-controlled errors over the training set. Another drawback of polynomial RS is the number N of training pairs needed for the regression, which is in the order of n^d for a complete d-order polynomial basis. This may require too large a training set for not particularly high dimensions n of the input space $\mathcal{X}$.

(b) Moving least squares polynomial regression

An alternative technique consists in constructing a *local* approximation based on *moving least squares* (MLS) (Lancaster and Salkauskas, 1981; Levin, 1998). The term "moving" is used because the weight function θ appearing in Eq. (II.15) (and therefore the weight coefficients $\mathbf{w}$) depends on the location of any new point $\mathbf{x}$ where we want to predict y, and therefore "moves" with $\mathbf{x}$. This method is presented here in conjunction with a polynomial approximation, but it can also be used with other types of basis,

e.g. splines or radial basis functions. The surrogate model $\widetilde{y}$ used in a MLS polynomial regression is given by:

$$\widetilde{y}(\mathbf{x}) = \phi(\mathbf{x})^{\mathrm{T}} \mathbf{w}(\mathbf{x}) \,, \tag{II.14}$$

where, for any given point $\mathbf{x} \in \mathcal{X}$, the unknown weight vector $\mathbf{w} = \mathbf{w}(\mathbf{x})$ is now obtained by minimizing the following weighted least squares error:

$$\mathbf{w}^* = \mathbf{w}^*(\mathbf{x}) = \underset{\mathbf{w}\in\mathbb{R}^p}{\arg\min} \sum_{i=1}^{N} \left(y_i - \phi(\mathbf{x}_i)^{\mathrm{T}} \mathbf{w}\right)^2 \theta(\|\mathbf{x}_i - \mathbf{x}\|) \,, \tag{II.15}$$

where θ is a non-negative *weight function* and $\|\cdot\|$ denotes the Euclidean distance in $\mathbb{R}^n$ (usual choices are Gaussian or spline weight functions).

This optimization problem again has a closed-form solution, which writes:

$$\mathbf{w}^*(\mathbf{x}) = \mathbf{A}(\mathbf{x})^{-1} \mathbf{B}(\mathbf{x}) \, \mathbf{y} \,, \tag{II.16}$$

where $\mathbf{A}(\mathbf{x}) = \mathbf{\Phi}^{\mathrm{T}} \mathbf{W}(\mathbf{x}) \mathbf{\Phi}$, $\mathbf{B}(\mathbf{x}) = \mathbf{\Phi}^{\mathrm{T}} \mathbf{W}(\mathbf{x})$ and $\mathbf{W}(\mathbf{x}) = [w_{ii}(\mathbf{x})]_{1\leq i\leq N}$ is a $(N \times N)$-diagonal matrix such that $w_{ii}(\mathbf{x}) = \theta(\|\mathbf{x}_i - \mathbf{x}\|)$ for $i = 1, \ldots, N$ (we again assume that the number N of training pairs is greater than the number p of regression functions), and the approximate model $\widetilde{y}$ therefore writes:

$$\widetilde{y}(\mathbf{x}) = \phi(\mathbf{x})^{\mathrm{T}} \mathbf{A}(\mathbf{x})^{-1} \mathbf{B}(\mathbf{x}) \, \mathbf{y} \,. \tag{II.17}$$

The MLS polynomial regression is often used for responses with improved accuracy close to a point of interest by putting more weight on the points of the training set that are in the neighborhood of this given point. The lack of flexibility of low-order polynomials mentioned for RS is still present to some degree with the MLS polynomial regression technique. Another disadvantage of MLS surrogate models is due to the parameter(s) of the weight function θ governing the locality of the approximation which is(are) often hard to tune, such as the parameter controlling the bandwidth of the Gaussian weight function.

(c) Polynomial chaos expansion

In the specific context of uncertainty propagation, a common practice consists in expanding the random output $Y = y(\mathbf{X})$ onto an appropriate orthogonal polynomial basis. For such an expansion, we will assume that Y has finite variance and that the components of $\mathbf{X} = (X_1, \ldots, X_n)^{\mathrm{T}}$ are independent (if not, a suitable transformation may be applied, such as described in Section I–1.3). The exact representation of Y requires an infinite number of basis terms and is usually referred to as *polynomial chaos expansion* (PCE) (Soize and Ghanem, 2004). For computational purposes, an approximation limited to a finite number of terms is considered:

$$\widetilde{Y} = \widetilde{y}(\mathbf{X}) = \sum_{\boldsymbol{\alpha}\in\mathcal{A}} w_{\boldsymbol{\alpha}} \Phi_{\boldsymbol{\alpha}}(\mathbf{X}) \,, \tag{II.18}$$

where $\Phi_{\boldsymbol{\alpha}}$ are multivariate polynomials and $w_{\boldsymbol{\alpha}}$ are unknown deterministic coefficients for any multi-indice $\boldsymbol{\alpha} = (\alpha_1, \ldots, \alpha_n)$ belonging to a finite-size set $\mathcal{A} \subset \mathbb{N}^n$, e.g. $\mathcal{A} = \{\boldsymbol{\alpha} \in \mathbb{N}^n : \sum_{i=1}^n \alpha_i \leq p\}$ for polynomials with a total degree not greater than a maximum degree p.

Under the assumption that the components of $\mathbf{X}$ are independent, the multivariate polynomials $\Phi_{\boldsymbol{\alpha}}$ can be obtained as tensor products of univariate polynomials and expressed as follows:

$$\Phi_{\boldsymbol{\alpha}}(\mathbf{x}) = \prod_{i=1}^{n} \phi_{\alpha_i}^{(i)}(x_i) \,, \tag{II.19}$$

where $\phi_{\alpha_i}^{(i)}$ is the univariate polynomial of degree α_i from the orthonormal family associated with X_i for $i = 1, \ldots, n$, i.e. such that:

$$\mathbb{E}\left[\phi_j^{(i)}(X_i), \phi_k^{(i)}(X_i)\right] = \delta_{jk} \,, \tag{II.20}$$

and where $\delta_{jk} = 1$ if $j = k$, $\delta_{jk} = 0$ otherwise.

Hermite polynomials are selected for standard normal inputs, as proposed by Wiener in the homogeneous chaos expansion (see, e.g., Ghanem and Spanos, 1991). Polynomials are also available for a few other types of random input distributions from the Wiener-Askey PCE (Xiu and Karniadakis, 2002). With non-normal distributions, the expansion in Eq. (II.18) is referred to as *generalized* PCE. For distributions for which these polynomials are not known, recourse to isoprobabilistic mapping is made, so that the generalized PCE can be applied. We can e.g. define the generalized PCE in the standard normal space by expressing it in terms of the n-dimensional standard normal random vector $\mathbf{U} = T(\mathbf{X})$, see Section I–1.

The unknown coefficients $\mathbf{w}_{\boldsymbol{\alpha}} = \{w_{\boldsymbol{\alpha}}, \boldsymbol{\alpha} \in \mathcal{A}\}$ can be obtained by regression from a given training set $\mathcal{T} = \{(\mathbf{x}_i, y_i) \in \mathcal{X} \times \mathcal{Y}, 1 \leq i \leq N\}$, by minimizing the empirical risk w.r.t. the square loss function (ordinary least squares regression) (Berveiller et al., 2006), similarly to the approach applied for polynomial RS. The solution writes:

$$\mathbf{w}^*_{\boldsymbol{\alpha}} = \left(\boldsymbol{\Phi}^{\mathrm{T}}\boldsymbol{\Phi}\right)^{-1}\boldsymbol{\Phi}^{\mathrm{T}}\mathbf{y}\,, \tag{II.21}$$

where $\boldsymbol{\Phi} = [\Phi_{\boldsymbol{\alpha}_j}(\mathbf{x}_i)]_{1\leq i\leq N\,,\,1\leq j\leq \#\mathcal{A}}$ and $\mathbf{y} = (y_1, \ldots, y_N)^{\mathrm{T}}$, in which $\boldsymbol{\alpha}_j$ denotes the j^{th} multi-index in the set $\mathcal{A}$ and $\#\mathcal{A}$ the cardinality of $\mathcal{A}$.

The number of coefficients to be evaluated depends both on the dimension n of the problem of interest and the selected maximum total order p of the expansion. For a complete basis of polynomials with a total degree not greater than a given maximum degree p, we have:

$$\#\mathcal{A} = \binom{n+p}{p}\,. \tag{II.22}$$

The number of polynomials in $\mathcal{A}$ (and consequently the number of data pairs required in the training set $\mathcal{T}$) rapidly increases with the dimension n. Several strategies have been proposed to limit the number of polynomials for large n and therefore alleviate the curse of dimensionality. A first approach proposed by Blatman and Sudret (2009) consists in choosing a hyperbolic truncation scheme that only retains the interaction terms of low orders:

$$\mathcal{A} = \left\{\boldsymbol{\alpha} \in \mathbb{N}^n : \|\boldsymbol{\alpha}\|_q \leq p\right\}\,, \tag{II.23}$$

where:

$$\|\boldsymbol{\alpha}\|_q = \left(\sum_{i=1}^{n} \alpha_i^q\right)^{1/q}\,, \tag{II.24}$$

and q is an arbitrary selected parameter in $]0,1]$. Another approach consists in using the hybrid least angle regression method for the construction of sparse PCE (Blatman and Sudret, 2011). The selection of the best set of predictors is based on the LAR algorithm of Efron et al. (2004) and the unknown coefficients are obtained by ordinary least squares regression.

(d) Artificial neural networks

Artificial neural networks (ANN) or simply *neural networks* (NN) are another type of surrogate model often used in uncertainty propagation, and are part of machine learning. Several models can be used for supervised or unsupervised learning. Among the supervised techniques, the multilayer perceptron (MLP) and the radial basis function (RBF) networks are the most common models. An ANN is composed of neurons (a.k.a. nodes) assembled into an architecture that connects these neurons together. In each neuron (let us denote a given neuron by the subscript m), a transfer or activation function $f : \mathbb{R} \to [0,1]$ is built in:

$$y_m = f\left(b_m + \mathbf{w}_m^{\mathrm{T}}\mathbf{x}_m\right)\,, \tag{II.25}$$

where $\mathbf{x}_m = (x_{m,1}, \ldots, x_{m,n_m})^{\mathrm{T}}$ denotes the vector of inputs of the neuron (n_m scalar inputs), y_m its scalar output, $\mathbf{w}_m = (w_{m,1}, \ldots, w_{m,n_m})^{\mathrm{T}}$ its weights and b_m its bias.

Among all these architectures, the *feedforward multilayer perceptron* (FFMLP) network is the most widely used. It is composed of three or more layers, the first one being composed of the inputs and the last one of the output(s). The intermediate layers (also called hidden layers) are fully connected, meaning that each neuron belonging to an intermediate layer is connected to those of the previous layer and to those of the next one. Several types of transfer functions can be chosen in the hidden layers, among which the sigmoid function $f : a \mapsto f(a) = 1/(1+\exp(-\alpha a))$ is a common choice, where α is a parameter that defines the slope of the function.

The construction of an ANN surrogate model requires first that we choose an architecture and then train the model on the data in order to find the biases and weights of all the neurons of the network. Choosing an architecture for a network is something of an art. It is argued in Hornik et al. (1989) that a single hidden layer with well-chosen activation functions (so-called squashing functions) is sufficient for an ANN to surrogate continuous functions to any desired accuracy. However, it sometimes appears more efficient to increase the number of hidden layers for complex functions. Practically, the choice of the number of hidden layers and number of neurons is often made empirically by expert judgment. Regarding the training of ANNs, the objective consists in minimizing some cost function defined over the training set $\mathcal{T}$ (often the empirical risk expressed by means of the square loss function) and finding the optimal combination of weights and biases for the ANN. Note that several techniques are also available to improve the generalization ability of ANNs (e.g. early stopping and regularization) (see, e.g., Orr and Müller, 1998, Chapters 2–6). One popular approach to train an ANN is the so-called *backpropagation* algorithm (Haykin, 1998). This algorithm seeks a local minimum of the selected cost function over $\mathcal{T}$ by using a steepest descent method based on the gradients of this cost function (note that this imposes a differentiability property for the activation functions, which is verified for the sigmoid function). The algorithm is said to be recursive, since it first adjusts the weights in the output layer based on the cost function, and then propagates recursively in the hidden layers to adjust the weights of their neurons.

(e) Radial basis function networks

Among all types of ANNs, *radial basis function* (RBF) networks are a very popular model. RBFs were developed for data interpolation by Hardy (1971) and later introduced to ANN by Broomhead and Lowe (1988). An RBF network is expressed as a linear combination of radially symmetric activation functions:

$$\widetilde{y}(\mathbf{x}) = \sum_{j=1}^{M} w_j \, \phi\left(\|\mathbf{x} - \mathbf{c}_j\|\right) , \tag{II.26}$$

where M denotes the number of neurons, $\mathbf{c}_j \in \mathbb{R}^n$ for $j = 1, \ldots, M$ are their respective centers and $w_j \in \mathbb{R}$ for $j = 1, \ldots, M$ are the corresponding weights. An RBF network is therefore composed of three layers: an input layer, a hidden layer with the same radially symmetric activation function ϕ for the M neurons, and a linear output layer.

If the RBF network surrogate model is used for interpolation on the training set $\mathcal{T} = \{(\mathbf{x}_i, y_i) \in \mathcal{X} \times \mathcal{Y}, 1 \leq i \leq N\}$, the neuron centers are naturally taken as the training points ($\mathbf{c}_i = \mathbf{x}_i$ for $i = 1, \ldots, N$) and we must satisfy:

$$\mathbf{y} = \mathbf{\Phi}\mathbf{w} , \tag{II.27}$$

where $\mathbf{y} = (y_1, \ldots, y_N)^{\mathrm{T}}$, $\mathbf{\Phi} = [\phi(\|\mathbf{x}_i - \mathbf{x}_j\|)]_{1 \leq i,j \leq N}$ and $\mathbf{w} = (w_1, \ldots, w_N)^{\mathrm{T}}$. For commonly-used basis functions ϕ (e.g. Gaussian and inverse multiquadric), $\mathbf{\Phi}$ is symmetric positive definite and the linear system in Eq. (II.27) can be solved by standard techniques in order to obtain the unknown weight vector $\mathbf{w}^* = \mathbf{\Phi}^{-1}\mathbf{y}$. Special iterative methods have also been proposed in the case of an ill-conditioned matrix $\mathbf{\Phi}$ (see, e.g., Dyn et al., 1986).

When the number of neuron centers M is lower than the size of the training set N, the RBF network surrogate model is a regressor and the weights can be obtained by ordinary least squares, similarly to the polynomial RS:

$$\mathbf{w}^* = \left(\mathbf{\Phi}^{\mathrm{T}}\mathbf{\Phi}\right)^{-1}\mathbf{\Phi}^{\mathrm{T}}\mathbf{y}\,, \tag{II.28}$$

where $\mathbf{\Phi} = [\phi(\|\mathbf{x}_i - \mathbf{c}_j\|)]_{1\leq i\leq N\,,\,1\leq j\leq M}$ and $\mathbf{y} = (y_1, \ldots, y_N)^{\mathrm{T}}$.

The choice of the number of neurons M and their respective centers is a key aspect for the accuracy of the RBF network (note that additional parameters such as the M radii appearing in the activation function also need to be tuned). If too many centers are used, the surrogate model has a large number of parameters to calibrate (high complexity). In such a case it is prone to overfitting, and has therefore poor generalization performances. Again two strategies previously mentioned can be followed, which consist either in introducing some regularization into the model or in limiting its complexity, i.e. by limiting the number of neuron centers (see, e.g., Orr, 1995). For a review of some techniques used for the optimal determination of neuron centers, the reader may also refer to (Cohen and Intrator, 2000).

(f) Other models

In addition to the methods briefly described in this section, it is worth mentioning a few others, which are not presented in this report for the sake of brevity. The following two techniques, *high-dimensional model representation* (HDMR) (Rabitz et al., 1999) and *multivariate adaptive regression splines* (MARS) Friedman (1991), have also been found to be useful in uncertainty propagation for the construction of surrogate models.

(g) Comparisons

The techniques presented in this section have been compared by several authors and a non-exhaustive list of such works is given hereafter. It is important to point out that the performances of these models are often problem-dependent and it is hard to draw general conclusions in light of the results obtained from a very few examples. Note also that a number of these comparative studies were made in the specific context of reliability assessment. For an overview, the reader may refer to the following works, listed in chronological order, for a review and/or comparative results concerning surrogate models:

- MLP and RBF networks used in a MC analysis (Hurtado and Alvarez, 2001),
- Polynomial RS, MARS, RBF networks and kriging for the optimization of deterministic nonlinear functions (Jin et al., 2001),
- Polynomial RS, ANN and kriging and other techniques for the approximation of deterministic functions (Simpson et al., 2001),
- SVR, polynomial RS, kriging, RBF networks and MARS for the approximation of deterministic functions (Clarke et al., 2004),
- RSM and ANN used with FORM, crude MC simulation and IS (Gomes and Awruch, 2004),
- Polynomial RS, ANN, MARS and other techniques for the optimization of deterministic and stochastic nonlinear functions (Chen et al., 2006),
- MLS, ANN and RBF networks for structural reliability analysis (Bucher and Most, 2008),
- Kriging, SVR and RBF networks for the optimization of deterministic nonlinear functions (Bompard, 2011),
- RSM, PCE and kriging for structural reliability analysis (Sudret, 2012),
- SVR and kriging for the approximation of nonlinear deterministic functions (Moustapha et al., 2018).

II–1.4 Challenges

The objective of surrogate-model-based approaches is to make accurate predictions (low bias between $\widetilde{y}$ and y *and* low variance of $\widetilde{y}$ w.r.t. the choice of the training set $\mathcal{T}$) based on limited information (small training sets $\mathcal{T}$) and under the assumptions of a selected type of approximation (corresponding to a given class of surrogate model).

The time spent in the evaluation of the true function y should be kept to a minimum, which usually implies limiting the size of the training sets $\mathcal{T}$ as much as possible.

A surrogate model which is fast to train is also often of interest. Note that the training time should be compared with that spent in the evaluation of the true function y. Since these two tasks alternate, the computational resources used for the true function evaluations may also be used for training if the algorithm chosen for training can take advantage of the available computer resources (e.g. independent tasks that can be parallelized).

Additionally, the selected surrogate model needs to be fast to evaluate, in general. In the context of uncertainty propagation, simulation methods often require thousands to millions of calls to the surrogate model. A fast-to-evaluate surrogate model is therefore of practical interest for reliability assessment and optimal design under uncertainty.

A critical step in any surrogate-based approach is to first choose a type of surrogate model and therefore the associated approximation that is applied to the problem. Most often a given type is arbitrarily selected in accordance with the practitioner's experience. An alternative strategy consists in considering a set of surrogate candidates and then defining the approximation as a weighted sum of these models, where the weights are obtained by optimization from the training data (see, e.g., Goel et al., 2007; Viana et al., 2009) and the references therein. Note that similar approaches were developed for SVMs, where the idea is to consider models based on a combination of kernels (Lanckriet et al., 2004; Sonnenburg et al., 2006; Rakotomamonjy et al., 2007). As already pointed out in the introduction to Section II–1, the choice of a given type of surrogate model is critical in the sense that the associated approximation needs to be compatible with the characteristics of the true function y, which are *unknown* in general. If the assumptions of the selected approximation are not met, the surrogate construction approach is flawed and this often results in an incorrect approximate model.

Several obstacles are encountered in the construction of accurate surrogate models and it is proposed to give an overview of the main challenges that need to be addressed. The main difficulties experienced in surrogate-based approaches are closely related to the dimensionality n of the input space $\mathcal{X}$ and the smoothness of the function y to learn. Other critical issues may also come from the adaptive strategies used for the construction of approximate models.

(a) Input space dimensionality

The dimensionality of the input space is critical for any surrogate model, which often restricts the analysis to relatively low-dimensional problems or problems of a larger dimension addressed by simple models. This phenomenon is commonly referred to as the *curse of dimensionality* coined by Bellman (1961). In simple terms, the learning cost defined in terms of the number of data pairs required to train a sufficiently accurate surrogate model rapidly grows with the dimension of the input space, making intractable any approach in high-dimensional spaces with a reasonable amount of training data. If the function y is simple to learn (the case e.g. of a linear or an almost linear function), then it may be possible to select models that perform well at a moderate cost. Making the assumption of a very simple approximate model is e.g. often made in genomics and other areas of computational biology, where we have more inputs that the number of available data pairs, i.e. $n \gg N$ (see, e.g., Hastie et al., 2009,

Chapter 18, for a presentation of the techniques used in such areas). For more complex functions y, the performances of all surrogate models worsen with n and building a surrogate to the true function is often out of reach when y is costly to evaluate.

(b) Smoothness of the true function y

In order to choose one approximate model rather than another, some a priori knowledge about the true function y we want to approximate would be useful. Unfortunately, the form of the functional relation between the input vector $\mathbf{x}$ and the output $y = y(\mathbf{x})$ is often unknown and the only source of knowledge comes from the pointwise evaluations of y at the selected points $\mathbf{x}_i$'s of the training set. Nevertheless, assumptions need to be made to approximate y and quite a usual choice (common to all types of surrogate models) is to assume that the unknown function y is *smooth*. A natural interpretation of smoothness is that two similar inputs $\mathbf{x}$ and $\mathbf{x}'$ are expected to have similar outputs. Within a class of differentiable functions, a function which is smoother than another means that it oscillates less. In more formal settings, smoothness functionals can be defined in terms of the Fourier transform of y (see, e.g., Girosi et al., 1995). With such a definition, a smooth function is characterized by a low frequency content. In the framework of SVM regularization, see Section II–2.3.2, the degree of smoothness of the approximation is equivalently controlled by means of the norm of the approximate function in a reproducing kernel Hilbert space $\mathcal{H}$. The less prominent the high-frequency content of the approximate function, the lower its norm in $\mathcal{H}$. When y is nonsmooth everywhere in $\mathcal{X}$, or worse when it is characterized by nonstationary smoothness, it becomes less easy to learn a surrogate to y. For globally nonsmooth functions, one solution is a recourse to kernel methods with controlled smoothness, e.g. the Matérn kernel, see Section II–2.3.1. For functions with nonstationary smoothness, it is harder to find an approximate solution. If the lack of smoothness is limited to subdomains of $\mathcal{X}$ that are unimportant w.r.t. the quantity of interest assessed from the surrogate model, the problem is expected to be satisfactorily learned with the techniques available for smooth functions. If not, learning the true function y is a great challenge. Examples of functions with nonstationary smoothness may appear in reliability assessment (see, e.g., Kouassi et al., 2016, application example 1) where the nonsmoothness due to one of the most influential inputs is unfortunately located at the MPFP. This example is recalled in Appendix A–1.

(c) Adaptive surrogate models

Choosing an adaptive strategy in any surrogate model-based analysis is quite a critical exercise. As already pointed out in Section II–1.2, a good tradeoff should be found between a fully explorative strategy independent of the data pairs $(\mathbf{x}_i, y_i)$ evaluated so far and a strategy exploiting such data that is driven too much by the objective aimed at. In deterministic optimization, the risk is to focus too early on subdomains of $\mathcal{X}$ that are unimportant and to finally miss the subdomain where the global optimum is located. In reliability assessment, the risk is to converge too early to some subdomains of the failure domain $\mathcal{F}_\mathbf{x}$ that are not the most important ones. As reviewed in Section II–3, several adaptive methods have been devised in the specific context of reliability assessment and have been successfully applied, with various results, to a few selected examples (most often of low dimension). It should however be emphasized that such adaptive strategies are less robust than a crude MC analysis, which naively but exhaustively explores the outcome space $\mathcal{X}$ according to the joint PDF of the random inputs. What we gain in efficiency is lost in robustness. Note that robustness is also diminished in other simulation methods, such as the SS method. In SS, adaptive exploration may be triggered to unimportant zones if an insufficient number of samples per level is used (remember that SS is only asymptotically unbiased). Such a failure of the SS method is exemplified in Appendix A–2, in which the gradient of the LSF is highly nonstationary. It should moreover be noted that adaptive approaches based on surrogate models

are more prone to such failures than simulation methods, due to the low sample sizes that are used for training. The less information we get from the problem, the more risk we have of missing important zones of $\mathcal{X}$.

To conclude this section, it should be emphasized that the choice of a hypothesis space (which defines the type of approximation of the surrogate model) which is compatible with the properties of the unknown true function is a key ingredient for the success of any surrogate-based analysis. Quoting MacKay (1992) about criteria for selecting data in active learning: "All these criteria depend on the assumption that the hypothesis space is correct, which may prove to be their main weakness". Function approximation is highly challenging, since it is hard to infer the main properties of the true function from very little data (e.g. degree of smoothness, level of noise, ..., all properties that may be spatially dependent in $\mathcal{X}$) and this task becomes harder in high-dimensional spaces.

II–2 Support vector machines (SVM)

Support vector machines (SVMs) are supervised learning models proposed by Vapnik and Chervonenkis as early as the 1960s. They are based on structural risk minimization (Vapnik, 1995; Vapnik et al., 1997), whose objective is to construct a parsimonious model in the sense of the Vapnik-Chervonenkis dimension (VC dimension). SVMs were first introduced in the context of binary classification with the concept of optimal separating hyperplanes. Their extension to nonlinear problems is due to Boser et al. (1992). The principle is to apply a nonlinear transformation of the input space $\mathcal{X}$ into a space of a larger dimension (possibly infinite) known as the *feature space*. In a nutshell, this nonlinear mapping only requires the use of a *kernel* which represents the dot product in the kernel-induced feature space. For non-separable data (e.g. due to noise in the data) it is necessary to make some adaptations of the method, and this is achieved by means the so-called *soft margin* technique proposed by Cortes and Vapnik (1995). SVMs were later extended to regression by Vapnik and coauthors using the ϵ-insensitive loss function (Vapnik, 1995; Drucker et al., 1997; Vapnik et al., 1997).

The organization of this section is quite conventional in its first part and follows the introduction made above. Binary classification is addressed first in Section II–2.1. The specific case of linearly separable data is considered in Section II–2.1.1 and the corresponding quadratic program to solve is given in Section II–2.1.2. In Section II–2.1.3, the hypothesis of perfectly linearly separable data is relaxed with the introduction of soft margin linear classifiers. Section II–2.2 is then devoted to linear regression by means of SVMs. *Support vector regression* (SVR) based on ϵ-insensitive loss function is detailed first, see Section II–2.2.1. Another quite popular technique, known as *least squares support vector machines* (LS-SVM), is then described in the context of regression, see Section II–2.2.2. Moving from linear to nonlinear SVMs is exposed in Section II–2.3.1, where the central concept of kernels is introduced. In Section II–2.3.2, SVMs are presented from the viewpoint of regularization theory (Girosi et al., 1995; Evgeniou et al., 2000), which gives a broader perspective to function approximation using SVMs. Another approach to the SVM optimization problem based on Fenchel duality (as opposed to the Lagrange duality conventionally used in SVMs) is also given for a unified framework of both SVM classification and regression. Section II–2.4 finally addresses the optimal tuning of SVM models by taking the leave-one-out error (LOO) as an estimate of the generalization error. After a short review of the approximations and bounds of the LOO error available for SVMs in classification and regression, a stochastic algorithm is proposed for the selection of optimal hyperparameters based on the *span bound* approximation of the LOO error (Vapnik and Chapelle, 2000; Chang and Lin, 2005).

The theoretical concepts of SVMs will be left aside and we will focus on the construction of SVM surrogates and the technical details of their optimal tuning. The reader may refer to general textbooks for the SVM theoretical basis (see, e.g., Vapnik, 1995; Schölkopf and Smola, 2001). Other useful ref-

erences concerning SVMs are Cristianini and Shawe-Taylor (2000) and Smola et al. (2000). We will moreover assume that the reader has the necessary background on the convex programming behind SVMs (see, e.g., López, 2011, Chapter 2, for a list of minimal recalls).

II–2.1 Linear models for binary classification

We want to predict a response of interest $y \in \mathcal{Y}$ at a given point $\mathbf{x} \in \mathcal{X} \subseteq \mathbb{R}^n$ knowing a set of training data pairs $\mathcal{T} = \{(\mathbf{x}_i, y_i) \in \mathcal{X} \times \mathcal{Y}, 1 \leq i \leq N\}$. We here restrict the approach to *binary classification*, where $\mathcal{Y} = \{-1, +1\}$ is discrete, see Figure II.1a. Such a binary classification appears e.g. in the context of reliability assessment, where the input space $\mathcal{X}$ (or $\mathbb{R}^n$ if the problem is expressed in the standard normal space) is split into two classes: the failure domain and the safe domain. In such a context, the class y of a point $\mathbf{x}$ is given by $y = \operatorname{sgn} g(\mathbf{x})$.

(a) Binary classification

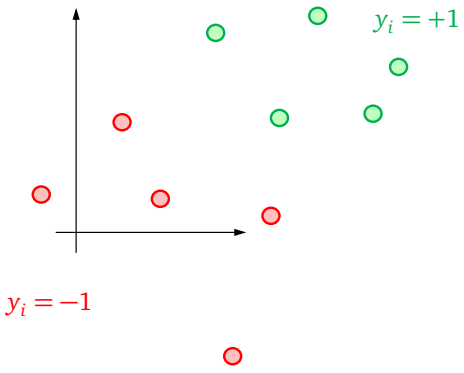

(b) Several candidate linear classifiers

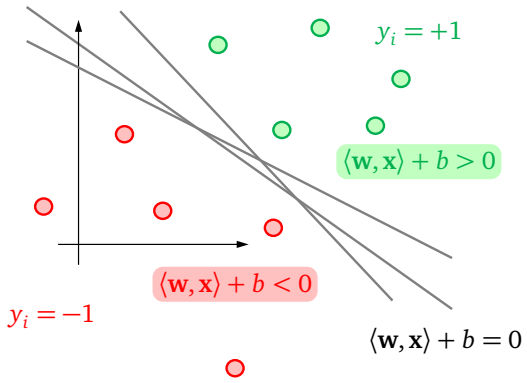

(c) Canonical form of the decision function

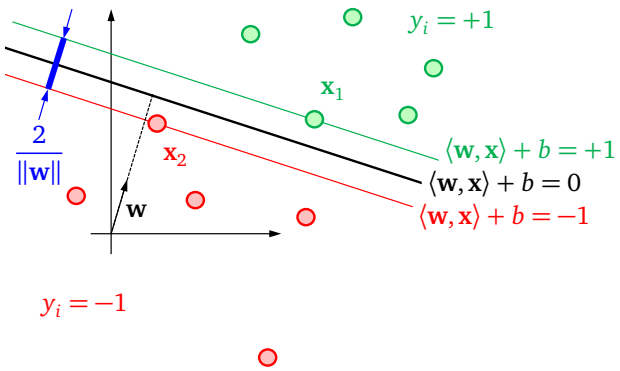

(d) Optimal linear classifier

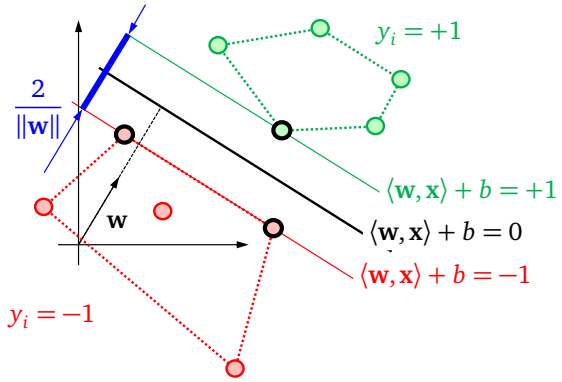

Figure II.1 – Classification of linearly separable data and optimal linear classifier.

II–2.1.1 Linearly separable data

It is first assumed that the two classes can be *perfectly* separated by a *linear* classifier, i.e. a $(n-1)$-dimensional hyperplane. In the context of binary classification, such models are known as *hard-margin* SVMs, as opposed to *soft-margin* SVMs presented in Section II–2.1.3, for which the strict assumption of linear separation is relaxed. The principles of hard-margin SVMs for binary classification are detailed in the seminal paper of Boser et al. (1992). Training a linear SVM classifier on the known set of data $\mathcal{T}$

consists in learning the following *decision function* $\widetilde{f} : \mathcal{X} \to \mathbb{R}$:

$$\widetilde{f}(\mathbf{x}) = \langle \mathbf{w}, \mathbf{x} \rangle + b \,, \tag{II.29}$$

where the *weight vector* $\mathbf{w} \in \mathbb{R}^n$ and the scalar *bias term* $b \in \mathbb{R}$ are the unknown parameters of the SVM model, and where $\langle \cdot, \cdot \rangle$ denotes the dot product.

The predicted class $\widetilde{y}$ of any point $\mathbf{x} \in \mathcal{X}$ is given by the following *decision rule*:

$$\widetilde{y} = \widetilde{y}(\mathbf{x}) = \operatorname{sgn} \widetilde{f}(\mathbf{x}) \,. \tag{II.30}$$

As represented in Figure II.1b, several candidate classifiers exist which all separate the data without error. The solution of this classification problem is uniquely defined by selecting the SVM classifier that is the farthest from the training data points $\mathbf{x}_i$ for $i = 1, \dots, N$. A rescaling of the problem is applied, such that the closest points to the separating classifier satisfy the following normalizing condition:

$$\min_{i \in \{1, \dots, N\}} |\langle \mathbf{w}, \mathbf{x}_i \rangle + b| = 1 \,. \tag{II.31}$$

The *canonical* form of the decision function $\langle \mathbf{w}, \mathbf{x} \rangle + b$ which results from this rescaling satisfies $(\langle \mathbf{w}, \mathbf{x}_i \rangle + b) \geq 1$ for $i = 1, \dots, N$. Starting from two points $\mathbf{x}_1$ and $\mathbf{x}_2$ respectively belonging to the two linear classifiers $\widetilde{\mathcal{F}}^{+1} = \{\mathbf{x} \in \mathcal{X} : \langle \mathbf{w}, \mathbf{x} \rangle + b = +1\}$ and $\widetilde{\mathcal{F}}^{-1} = \{\mathbf{x} \in \mathcal{X} : \langle \mathbf{w}, \mathbf{x} \rangle + b = -1\}$, see Figure II.1c, the Euclidean distance between $\widetilde{\mathcal{F}}^{+1}$ and $\widetilde{\mathcal{F}}^{-1}$ writes:

$$\begin{aligned} \mathcal{D}\left(\widetilde{\mathcal{F}}^{-1}, \widetilde{\mathcal{F}}^{+1}\right) &= \langle \frac{\mathbf{w}}{\|\mathbf{w}\|}, \mathbf{x}_1 - \mathbf{x}_2 \rangle \\ &= \frac{(\langle \mathbf{w}, \mathbf{x}_1 \rangle + b) - (\langle \mathbf{w}, \mathbf{x}_2 \rangle + b)}{\|\mathbf{w}\|} \\ &= \frac{+1 - (-1)}{\|\mathbf{w}\|} \\ &= \frac{2}{\|\mathbf{w}\|} \,, \end{aligned} \tag{II.32}$$

where $1/\|\mathbf{w}\|$ is known as the *margin* of the SVM classifier.

The optimal linear classifier is obtained by maximizing the margin under the constraint of a correct classification of the training data[6], see Figure II.1d. We therefore need to solve the following optimization problem:

$$\max_{\mathbf{w}, b} \frac{2}{\|\mathbf{w}\|} \quad \text{s.t.} \quad \begin{cases} \langle \mathbf{w}, \mathbf{x}_i \rangle + b \geq 1 & \text{if } y_i = +1 \quad \text{for } i = 1, \dots, N \\ \langle \mathbf{w}, \mathbf{x}_i \rangle + b \leq 1 & \text{if } y_i = -1 \quad \text{for } i = 1, \dots, N \end{cases} , \tag{II.33}$$

which in turn is equivalent to minimizing $\|\mathbf{w}\|$ or $\|\mathbf{w}\|^2$:

$$\min_{\mathbf{w}, b} \frac{\|\mathbf{w}\|^2}{2} \quad \text{s.t.} \quad y_i (\langle \mathbf{w}, \mathbf{x}_i \rangle + b) \geq 1 \quad \text{for } i = 1, \dots, N \,. \tag{II.34}$$

This latter formulation is the *primal* optimization problem of hard-margin binary classification with SVMs. For a given i, it is important to note that the two constraints of Eq. (II.33) are grouped into the following single constraint in Eq. (II.34):

$$y_i \widetilde{f}(\mathbf{x}_i) \geq 1 \,. \tag{II.35}$$

[6] From geometric considerations, the optimal hyperplane is orthogonal to the shortest line which connects the convex hulls of the two classes, and it intersects this line at its half-way point, see Figure II.1d.

II–2.1.2 Solving the optimization problem

The primal formulation defined in Eq. (II.34) is in the form of a quadratic program (QP) with N linear constraints. A convenient approach to solving it is to derive the *Wolfe dual* QP using Lagrange multipliers[7]. The *Lagrangian* takes the following expression:

$$\mathcal{L}(\mathbf{w}, b, \boldsymbol{\alpha}) = \frac{\|\mathbf{w}\|^2}{2} - \sum_{i=1}^{N} \alpha_i \left[y_i \left(\langle \mathbf{w}, \mathbf{x}_i \rangle + b \right) - 1 \right] , \tag{II.36}$$

where $\boldsymbol{\alpha} = (\alpha_1, \ldots, \alpha_N)^{\mathrm{T}}$ contains the N Lagrange multipliers and $\alpha_i \geq 0$ for $i = 1, \ldots, N$.

The Lagrangian $\mathcal{L}$ has to be minimized w.r.t. the primal variables $\mathbf{w}$ and b, and maximized w.r.t. the dual variables α_i with nonnegativity constraints on the α_i's (saddle point solution). The Karush-Kuhn-Tucker (KKT) conditions give:

$$\begin{aligned} \nabla_{\mathbf{w}} \mathcal{L}(\mathbf{w}, b, \boldsymbol{\alpha}) = 0 \quad &\rightarrow \quad \mathbf{w} = \sum_{i=1}^{N} \alpha_i y_i \mathbf{x}_i \, , \\ \frac{\partial \mathcal{L}(\mathbf{w}, b, \boldsymbol{\alpha})}{\partial b} = 0 \quad &\rightarrow \quad \sum_{i=1}^{N} \alpha_i y_i = 0 \, , \end{aligned} \tag{II.37}$$

and the Lagrangian, reduced in terms of the remaining variables, rewrites:

$$\mathcal{W}(\boldsymbol{\alpha}) = -\frac{1}{2} \sum_{i=1}^{N} \sum_{j=1}^{N} \alpha_i \alpha_j q_{ij} + \sum_{i=1}^{N} \alpha_i \, , \tag{II.38}$$

where, for $i, j = 1, \ldots, N$:

$$q_{ij} = y_i y_j \langle \mathbf{x}_i, \mathbf{x}_j \rangle \, . \tag{II.39}$$

The Wolfe dual of the optimization problem defined in Eq. (II.34) therefore writes[8]:

$$\max_{\boldsymbol{\alpha}} \mathcal{W}(\boldsymbol{\alpha}) = -\frac{1}{2} \sum_{i=1}^{N} \sum_{j=1}^{N} \alpha_i \alpha_j q_{ij} + \sum_{i=1}^{N} \alpha_i \quad \text{s.t.} \quad \begin{cases} \displaystyle\sum_{i=1}^{N} \alpha_i y_i = 0 \\ \alpha_i \geq 0 \quad \text{for } i = 1, \ldots, N \end{cases} , \tag{II.40}$$

with the following additional KKT complementary slackness conditions (i.e. the relations between the inequality constraints of the primal problem and their associated Lagrange multipliers):

$$\alpha_i \left[y_i \left(\langle \mathbf{w}, \mathbf{x}_i \rangle + b \right) - 1 \right] = 0 \quad \text{for } i = 1, \ldots, N \, . \tag{II.41}$$

From these conditions, two cases need to be considered:

- The first case corresponds to an $\mathbf{x}_i$ irrelevant to the construction of the decision function, for which we have $\alpha_i = 0$ and $y_i(\langle \mathbf{w}, \mathbf{x}_i \rangle + b) > 1$. The corresponding set of indices is denoted $\overline{\mathcal{I}}_{\text{sv}} = \{i \in \{1, \ldots, N\} : \alpha_i = 0\}$.

[7] The dual formulation presents the following advantages (Chapelle, 2007): 1) the constraints of the dual are easier to handle than those of the primal formulation (the dual no longer features the complicated constraints expressed by the Lagrange multipliers), 2) the dual optimization problem can be written in terms of dot products, which enables the use of kernels for the construction of nonlinear SVMs, see Section II–2.3.1.

[8] It is important to note that the constraint $\sum_{i=1}^{N} \alpha_i y_i = 0$ in the dual optimization problem is due to the presence of the bias term b in the decision function.

- The second case corresponds to the so-called *support vectors* (SV) $\mathbf{x}_i$ for which we have $\alpha_i > 0$ and $y_i(\langle \mathbf{w}, \mathbf{x}_i \rangle + b) = 1$ (points belonging to either $\widetilde{\mathcal{F}}^{+1}$ or $\widetilde{\mathcal{F}}^{-1}$, see points circled in black in Figure II.1d). The corresponding set of indices is denoted $\mathcal{I}_{\text{sv}} = \{i \in \{1, \dots, N\} : \alpha_i > 0\}$.

The bias term b can be obtained from the KKT complementary slackness condition of any SV:

$$b = y_i - \langle \mathbf{w}, \mathbf{x}_i \rangle \quad \text{for any } i \in \mathcal{I}_{\text{sv}} \,, \tag{II.42}$$

where $\mathbf{w}$ is defined in Eq. (II.37). For better numerical stability, the bias term is preferably obtained by averaging the expression given in Eq. (II.42) over the whole set of SVs:

$$b = \frac{1}{\#\mathcal{I}_{\text{sv}}} \sum_{i \in \mathcal{I}_{\text{sv}}} (y_i - \langle \mathbf{w}, \mathbf{x}_i \rangle) \,. \tag{II.43}$$

As an alternative, b can be obtained as a by-product of the interior-point optimization algorithm used to solve Eq. (II.40) if such a type of algorithm is applied.

The decision function $\widetilde{f}$ can then be expressed in terms of the SVs as follows:

$$\begin{aligned} \widetilde{f}(\mathbf{x}) &= \langle \mathbf{w}, \mathbf{x} \rangle + b \\ &= \sum_{i=1}^{N} \alpha_i y_i \langle \mathbf{x}_i, \mathbf{x} \rangle + b \\ &= \sum_{i \in \mathcal{I}_{\text{sv}}} \alpha_i y_i \langle \mathbf{x}_i, \mathbf{x} \rangle + b \,. \end{aligned} \tag{II.44}$$

A few but important remarks should be made regarding the type of optimization problem we need to solve to define $\widetilde{f}$ and the best algorithms we can use for a numerical solution.

The primal formulation defined in Eq. (II.34) is a convex program[9] because of the convexity of both the objective function and the inequality constraints. If the objective function of the primal has a minimum, it is a *global* one. This therefore implies that there are no local minima. It is important to point out that the convexity of the optimization problem will appear in all the other SVM formulations presented in the following (soft-margin classification and regression), which is a key advantage of SVMs compared with e.g. neural networks, where local minimum solutions may be found by training. The dual formulation defined in Eq. (II.40) is not only a convex but also a quadratic program (QP)[9], which can therefore be solved (more or less efficiently) by several available techniques. Note that the primal defined in Eq. (II.34) is also a QP in the specific case of linear classification, but this is not true with more general formulations involving kernels other than the linear one, see Section II–2.3.1.

In practice the most common approach consists in solving the dual. Solving the primal is often considered of interest in the case of linear SVMs, although a few attempts have been made to investigate the nonlinear case (see, e.g., Chapelle, 2007). The dual QP of hard-margin classification with SVMs is expressed in terms of the N variables of the input vector $\boldsymbol{\alpha}$ under a single affine equality constraint and N affine inequality constraints:

$$\min_{\boldsymbol{\alpha}} \frac{1}{2} \boldsymbol{\alpha}^{\mathrm{T}} \mathbf{Q} \boldsymbol{\alpha} - \mathbf{1}^{\mathrm{T}} \boldsymbol{\alpha} \quad \text{s.t.} \quad \begin{cases} \mathbf{y}^{\mathrm{T}} \boldsymbol{\alpha} = 0 \\ \boldsymbol{\alpha} \geq \mathbf{0} \end{cases} , \tag{II.45}$$

[9] We here recall a few definitions (see, e.g., López, 2011, Chapter 2). 1) A convex program is a constrained optimization problem where the objective function and the inequality constraint functions are convex and the equality constraint functions are affine. 2) A quadratic program is a constrained optimization problem where the objective function is quadratic and all the constraint functions (inequalities or equalities) are affine.

where $\mathbf{y} = (y_1, \ldots, y_N)^{\mathrm{T}}$, $\mathbf{Q} = [q_{ij}]_{1 \leq i,j \leq N}$ and $q_{ij} = y_i y_j \langle \mathbf{x}_i, \mathbf{x}_j \rangle$ for $i, j = 1, \ldots, N$. This clearly shows that problem-solving complexity is closely related to the size N of the training set $\mathcal{T}$. For this reason, the choice of an algorithm to solve Eq. (II.45) is highly dependent on N (see, e.g., Vogt and Kecman, 2005; Bottou and Lin, 2007; Shawe-Taylor and Sun, 2011, for a review of the main types of algorithms with their advantages and limitations).

For low N (say N in the order of 1000 to 10,000 or less), *interior-point* methods (see, e.g., Boyd and Vandenberghe, 2004), are considered a good choice (Schölkopf and Smola, 2001, p. 297). These methods are expected to give reliable and accurate solutions at the expense of a Cholesky decomposition of a matrix whose dimension scales with N. The size of the KKT gap is found to be several orders of magnitude lower than that achieved by means of the SMO type of algorithm described next. Interior-point algorithms for convex optimization are available in a number of software packages such as LOQO (Vanderbei, 2006), MATLAB Optimization Toolbox (The MathWorks, 2012), MOSEK (MOSEK ApS, 2014) and QPC (Wills, 2009) among others. Due to the above-cited advantages (accuracy of the solution and reliability of the algorithms), a recourse to interior-point methods was preferred in the most recent works of the author (Bourinet, 2014; Bourinet, 2015; Bourinet, 2016).

For very large data sets, as often encountered in SVM applications (N in the range of several thousands to millions), solving the QP often becomes intractable in memory and time requirements. The matrix $\mathbf{Q}$ in Eq. (II.45) is fully dense and is too large to be stored (the required memory increases with N^2). In such a context the main idea is to devise algorithms that solve smaller QP subproblems by working with only one subset of the vector $\boldsymbol{\alpha}$ per iteration. The corresponding methods are known as *decomposition* methods or *working-set* methods (see, e.g., Osuna et al., 1997; Platt, 1998; Joachims, 1999). The most extreme case is the *Sequential Minimal Optimization* (SMO) algorithm of Platt (1998), which takes only two elements α_i and α_j in the working set at each iteration. This allows the QP subproblem to be solved exactly by means of a simple analytical update (Platt, 1998, Appendix). Several strategies have been tested to select the working set i, j at each iteration. One of the fastest implementations of SMO is based on the working set selection of Fan et al. (2005). The corresponding strategy is implemented in the most recent version of LIBSVM software (Chang and Lin, 2011). It should be noted that SMO may be slow to converge if high accuracy is required for the solution (Platt, 1998). Moreover the accuracy that can be reached by SMO is lower than that achieved by interior-point algorithms. As pointed out by Bottou and Lin (2007, Section 1.1.1), too high an accuracy is not especially required in *most usual* SVM applications. Some errors on the SVM models due to the optimization algorithm may be tolerated w.r.t. other sources of error, i.e. approximation and estimation errors. In the specific context of function approximation, as investigated in the scope of this report, it is the author's belief that accuracy is a key point for high-quality surrogate models. As described in Section II–2.4.3, the strategy proposed to select optimal values of the parameters of the SVM models is based on the computed vector $\boldsymbol{\alpha}$. Inaccuracies on $\boldsymbol{\alpha}$ therefore induce non-optimal parameters of SVM models, which themselves induce inaccurate SVM models. This motivates the exclusion of SMO techniques from the candidate strategies applicable to SVM training.

II–2.1.3 From hard- to soft-margin classifiers

For hard-margin SVMs, we assumed that the training data were perfectly separable. If the data are not separable (e.g. in the case of noisy data), see Figure II.2, there is no feasible solution and the hard-margin problem is unsolvable. We need to allow some training errors, and this is achieved by using the so-called *soft-margin* formulation of SVMs proposed by Cortes and Vapnik (1995). The following soft constraints are imposed:

$$y_i \widetilde{f}(\mathbf{x}_i) \geq 1 - \xi_i \,, \tag{II.46}$$

where $\boldsymbol{\xi} = (\xi_1, \ldots, \xi_N)^{\mathrm{T}}$ is set of nonnegative *slack variables* which define the amount by which the constraints of the hard-margin binary classification problem defined in Eq. (II.35) are violated, see Figure II.2. The corresponding deviations are cumulated in the objective function of the primal (summation or summation of squared values) and penalized by means of a strictly positive tradeoff parameter denoted C. The formulation is known as Lp or p-norm soft-margin SVM, where $p \in \{1, 2\}$ denotes the power these slack variables are raised to in the objective function, see Eq. (II.47) corresponding to $p = 1$. In the following we will use the acronym L1-SVC for L1 soft-margin SVM used in classification. The presentation is restricted to L1-SVC since it is the only formulation that is used in the subsequent applications of Section II–3. The reader may refer to López (2011) for a detailed description of L2-SVC.

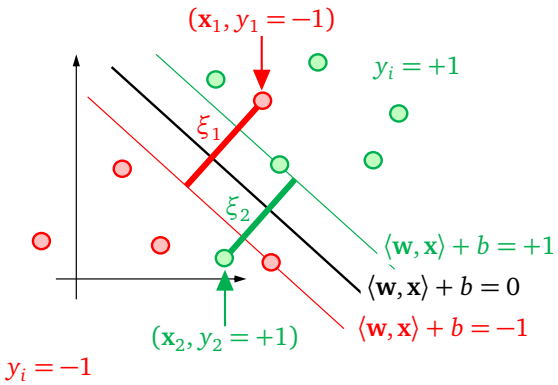

Figure II.2 – Soft-margin linear classifier.

The primal optimization problem for L1-SVC is written as follows:

$$\min_{\mathbf{w},b,\boldsymbol{\xi}} \frac{\|\mathbf{w}\|^2}{2} + C \sum_{i=1}^{N} \xi_i \quad \text{s.t.} \quad \begin{cases} y_i \left(\langle \mathbf{w}, \mathbf{x}_i \rangle + b \right) \geq 1 - \xi_i \\ \xi_i \geq 0 \end{cases} \quad \text{for } i = 1, \ldots, N \,. \tag{II.47}$$

Based on the Lagrangian, the Wolfe dual optimization problem is derived similarly to the hard-margin SVM case by introducing the Lagrange multipliers of the $2N$ primal inequality constraints (see, e.g., López, 2011, Chapter 3) for further details. The following Wolfe dual is obtained for L1-SVC:

$$\max_{\boldsymbol{\alpha}} W(\boldsymbol{\alpha}) = -\frac{1}{2} \sum_{i=1}^{N} \sum_{j=1}^{N} \alpha_i \alpha_j q_{ij} + \sum_{i=1}^{N} \alpha_i \quad \text{s.t.} \quad \begin{cases} \displaystyle\sum_{i=1}^{N} \alpha_i y_i = 0 \\ 0 \leq \alpha_i \leq C \quad \text{for } i = 1, \ldots, N \end{cases} , \tag{II.48}$$

where $\boldsymbol{\alpha} = (\alpha_1, \ldots, \alpha_N)^{\mathrm{T}}$ in which, for $i = 1, \ldots, N$, the Lagrange multiplier α_i corresponds to the inequality constraint $y_i \left(\langle \mathbf{w}, \mathbf{x}_i \rangle + b \right) \geq 1 - \xi_i$ of the primal, see Eq. (II.47), and where, for $i, j = 1, \ldots, N$:

$$q_{ij} = y_i y_j \langle \mathbf{x}_i, \mathbf{x}_j \rangle \,. \tag{II.49}$$

It should be noted that this dual is identical to the one obtained for hard-margin SVMs except that the N multipliers α_i are upper-bounded by C, see Eq. (II.40):

$$\min_{\boldsymbol{\alpha}} \frac{1}{2} \boldsymbol{\alpha}^{\mathrm{T}} \mathbf{Q} \boldsymbol{\alpha} - \mathbf{1}^{\mathrm{T}} \boldsymbol{\alpha} \quad \text{s.t.} \quad \begin{cases} \mathbf{y}^{\mathrm{T}} \boldsymbol{\alpha} = 0 \\ \mathbf{0} \leq \boldsymbol{\alpha} \leq C \mathbf{1} \end{cases} . \tag{II.50}$$

If $C = +\infty$, the hard-margin case is recovered. It is also worth pointing out that the L1-SVC optimization problem is again a convex and quadratic program.

The following three cases are obtained for L1-SVC (see the corresponding justifications e.g. in Abe, 2010; López, 2011):

- The first case corresponds to $\alpha_i = 0$. Then $\xi_i = 0$ and therefore $y_i(\langle \mathbf{w}, \mathbf{x}_i \rangle + b) \geq 1$. Point $\mathbf{x}_i$ is not a SV and it is correctly classified. The corresponding set of indices is denoted $\mathcal{I}_{\text{sv}} = \{i \in \{1, \dots, N\} : \alpha_i = 0\}$.
- The second case corresponds to $0 < \alpha_i < C$. Then $\xi_i = 0$ and $y_i(\langle \mathbf{w}, \mathbf{x}_i \rangle + b) = 1$. Point $\mathbf{x}_i$ is called an *unbounded* SV. It belongs to either $\widetilde{\mathcal{F}}^{+1}$ or $\widetilde{\mathcal{F}}^{-1}$ and it is therefore correctly classified. The corresponding set of indices is denoted $\mathcal{I}_{\text{usv}} = \{i \in \{1, \dots, N\} : 0 < \alpha_i < C\}$.
- The third and last case corresponds to $\alpha_i = C$. Then $\xi_i \geq 0$ and $y_i(\langle \mathbf{w}, \mathbf{x}_i \rangle + b) = 1 - \xi_i \leq 1$. Point $\mathbf{x}_i$ is called a *bounded* SV. If $0 \leq \xi_i < 1$, point $\mathbf{x}_i$ is correctly classified. If $\xi_i \geq 1$, point $\mathbf{x}_i$ is misclassified. The corresponding set of indices is denoted $\mathcal{I}_{\text{bsv}} = \{i \in \{1, \dots, N\} : \alpha_i = C\}$.

The decision function is expressed in terms of all the SVs (i.e. bounded or unbounded SVs):

$$\widetilde{f}(\mathbf{x}) = \sum_{i \in \mathcal{I}_{\text{usv}} \cup \mathcal{I}_{\text{bsv}}} \alpha_i y_i \langle \mathbf{x}_i, \mathbf{x} \rangle + b \,. \tag{II.51}$$

II–2.2 Linear models for regression

The objective now is to predict a response of interest $y \in \mathcal{Y} = \mathbb{R}$ at a given point $\mathbf{x} \in \mathcal{X} \subseteq \mathbb{R}^n$ knowing a set of training data pairs $\mathcal{T} = \{(\mathbf{x}_i, y_i) \in \mathcal{X} \times \mathcal{Y}, 1 \leq i \leq N\}$. It should be noted that $\mathcal{Y}$ is now *continuous* as opposed to the case of binary classification in which $\mathcal{Y}$ was discrete. As in classification, we start from the linear problem and the formulation will be extended to nonlinear regression in Section II–2.3.1 by means of kernels. Training a linear SVM *regressor* on the known set of data $\mathcal{T}$ consists in learning the following function $\widetilde{f} : \mathcal{X} \to \mathbb{R}$:

$$\widetilde{f}(\mathbf{x}) = \langle \mathbf{w}, \mathbf{x} \rangle + b \,, \tag{II.52}$$

where the *weight vector* $\mathbf{w} \in \mathbb{R}^n$ and the scalar *bias term* $b \in \mathbb{R}$ are the unknown parameters of the SVM model.

The predicted value $\widetilde{y}$ at any point $\mathbf{x} \in \mathcal{X}$ is given by:

$$\widetilde{y} = \widetilde{y}(\mathbf{x}) = \widetilde{f}(\mathbf{x}) \,. \tag{II.53}$$

II–2.2.1 Support vector regression based on the ϵ-insensitive loss function

The most current form of SVM regression is based on the ϵ-insensitive loss function introduced by Vapnik (1995), see right plot in Figure II.3:

$$\ell(y, u) = (|y - u| - \epsilon)_+ = \begin{cases} 0 & \text{if } |y - u| < \epsilon \,, \\ |y - u| - \epsilon & \text{otherwise} \,, \end{cases} \tag{II.54}$$

where $\epsilon \in \mathbb{R}_{\geq 0}$ is a given parameter and $(x)_+ = \max(x, 0)$. If the magnitude of the difference between the predicted value $\widetilde{f}(\mathbf{x}_i)$ and the true value y_i is lower than ϵ, it is assigned a zero loss. The points $\mathbf{x}_i$ with such an error level are said to belong to the *ϵ-insensitive zone* or *ϵ-insensitive tube* (see shaded area in blue in the left plot of Figure II.3). Outside of this zone, the loss is set equal to the difference between the magnitude of $y_i - \widetilde{f}(\mathbf{x}_i)$ and ϵ. The approach used for regression based on the ϵ-insensitive loss function shares some similarities with that used for classification. Instead of requiring that $y_i \widetilde{f}(\mathbf{x}_i)$ exceed the value of one for a perfect linear classification, see Eq. (II.35), it is now required that $y_i - \widetilde{f}(\mathbf{x}_i)$ be bounded by a margin of width ϵ on both sides for a perfect linear regression, see left plot in Figure II.3. In order to handle potentially nonfeasible solutions (some points outside of the ϵ-insensitive zone), we use again the concept of soft margins. The following soft constraints are imposed, for $i = 1, \dots, N$:

$$y_i - \widetilde{f}(\mathbf{x}_i) \leq \epsilon + \xi_i \quad \text{and} \quad \widetilde{f}(\mathbf{x}_i) - y_i \leq \epsilon + \xi_i^* \,, \tag{II.55}$$

where the two sets of slack variables $\boldsymbol{\xi} = (\xi_1, \ldots, \xi_N)^{\mathrm{T}}$ and $\boldsymbol{\xi}^* = (\xi_1^*, \ldots, \xi_N^*)^{\mathrm{T}}$ are introduced to measure the deviation above and below the ϵ-insensitive zone, respectively, see left plot in Figure II.3.

This constructed surrogate model based on the ϵ-insensitive loss function will be denoted by the acronym L1-ϵ-SVR for L1 soft-margin SVM used in regression. As for classification, a 2-norm formulation (L2-ϵ-SVR) also exists, based on the squared ϵ-insensitive loss function $\ell(y,u) = (|y-u| - \epsilon)_+^2$ (see, e.g., López, 2011).

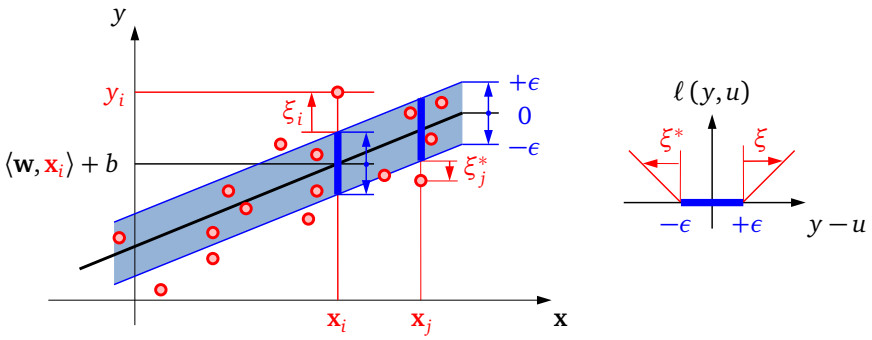

Figure II.3 – Linear regression based on the ϵ-insensitive loss function.

For L1-ϵ-SVR, the primal optimization problem writes (Vapnik, 1995; Smola and Schölkopf, 2004):

$$\min_{\mathbf{w},b,\boldsymbol{\xi},\boldsymbol{\xi}^*} \frac{\|\mathbf{w}\|^2}{2} + C\sum_{i=1}^{N}(\xi_i + \xi_i^*) \quad \text{s.t.} \quad \begin{cases} y_i - \langle \mathbf{w}, \mathbf{x}_i \rangle - b \le \epsilon + \xi_i \\ \langle \mathbf{w}, \mathbf{x}_i \rangle + b - y_i \le \epsilon + \xi_i^* \\ \xi_i,\ \xi_i^* \ge 0 \end{cases} \text{for } i = 1, \ldots, N\,, \tag{II.56}$$

where C is a strictly positive tradeoff parameter.

The Wolfe dual is expressed as follows:

$$\max_{\boldsymbol{\alpha},\boldsymbol{\alpha}^*} W(\boldsymbol{\alpha}, \boldsymbol{\alpha}^*) = -\frac{1}{2}\sum_{i=1}^{N}\sum_{j=1}^{N}(\alpha_i - \alpha_i^*)(\alpha_j - \alpha_j^*)k_{ij} + \sum_{i=1}^{N} y_i(\alpha_i - \alpha_i^*) - \epsilon\sum_{i=1}^{N}(\alpha_i + \alpha_i^*)$$
$$\text{s.t.} \quad \begin{cases} \displaystyle\sum_{i=1}^{N}(\alpha_i - \alpha_i^*) = 0 \\ 0 \le \alpha_i \le C \quad \text{for } i = 1, \ldots, N \\ 0 \le \alpha_i^* \le C \quad \text{for } i = 1, \ldots, N \end{cases}, \tag{II.57}$$

where $\boldsymbol{\alpha} = (\alpha_1, \ldots, \alpha_N)^{\mathrm{T}}$ (resp. $\boldsymbol{\alpha}^* = (\alpha_1^*, \ldots, \alpha_N^*)^{\mathrm{T}}$) contains the Lagrange multipliers corresponding to the N inequality constraint $y_i - \langle \mathbf{w}, \mathbf{x}_i \rangle - b \le \epsilon + \xi_i$ (resp. $\langle \mathbf{w}, \mathbf{x}_i \rangle + b - y_i \le \epsilon + \xi_i^*$) of the primal formulation defined in Eq. (II.56), and where, for $i, j = 1, \ldots, N$:

$$k_{ij} = \langle \mathbf{x}_i, \mathbf{x}_j \rangle\,. \tag{II.58}$$

The dual of the QP is reformulated in the following matrix form:

$$\min_{\boldsymbol{\alpha},\boldsymbol{\alpha}^*} \frac{1}{2}\begin{pmatrix}\boldsymbol{\alpha}\\ \boldsymbol{\alpha}^*\end{pmatrix}^{\mathrm{T}}\begin{bmatrix}\mathbf{K} & -\mathbf{K}\\ -\mathbf{K} & \mathbf{K}\end{bmatrix}\begin{pmatrix}\boldsymbol{\alpha}\\ \boldsymbol{\alpha}^*\end{pmatrix} + \begin{pmatrix}\epsilon\mathbf{1} - \mathbf{y}\\ \epsilon\mathbf{1} + \mathbf{y}\end{pmatrix}^{\mathrm{T}}\begin{pmatrix}\boldsymbol{\alpha}\\ \boldsymbol{\alpha}^*\end{pmatrix}$$
$$\text{s.t.} \quad \begin{pmatrix}\mathbf{1}\\ -\mathbf{1}\end{pmatrix}^{\mathrm{T}}\begin{pmatrix}\boldsymbol{\alpha}\\ \boldsymbol{\alpha}^*\end{pmatrix} = 0 \quad , \quad \begin{pmatrix}\mathbf{0}\\ \mathbf{0}\end{pmatrix} \le \begin{pmatrix}\boldsymbol{\alpha}\\ \boldsymbol{\alpha}^*\end{pmatrix} \le C\begin{pmatrix}\mathbf{1}\\ \mathbf{1}\end{pmatrix}, \tag{II.59}$$

where $\mathbf{y} = (y_1, \dots, y_N)^{\mathrm{T}}$, $\mathbf{K} = [k_{ij}]_{1 \leq i,j \leq N}$ is the Gram matrix and $k_{ij} = \langle \mathbf{x}_i, \mathbf{x}_j \rangle$ for $i, j = 1, \dots, N$.

It is important to note that this new formulation of the QP to solve is expressed in terms of the $2N$ variables of $(\boldsymbol{\alpha}^{\mathrm{T}}, \boldsymbol{\alpha}^{*\mathrm{T}})^{\mathrm{T}}$. This dual is again a convex QP, since $\mathbf{K}$ (and therefore $\begin{bmatrix} \mathbf{K} & -\mathbf{K} \\ -\mathbf{K} & \mathbf{K} \end{bmatrix}$) are positive semi-definite matrices.

Several comments can be made regarding the different cases resulting from the resolution of the QP defined in Eq. (II.59). First of all, α_i and α_i^* cannot be simultaneously nonzero for a given i, since the corresponding point $\mathbf{x}_i$ cannot belong to both sides of the ϵ-insensitive zone (it is easy to prove that $\alpha_i \alpha_i^* = 0$). The following six cases may occur (López, 2011):

- Case $\alpha_i = 0$. Then $\xi_i = 0$ and $y_i - \langle \mathbf{w}, \mathbf{x}_i \rangle - b \leq \epsilon$. Point $\mathbf{x}_i$ is not a SV and it belongs to the ϵ-insensitive zone.
- Case $\alpha_i^* = 0$. Then $\xi_i^* = 0$ and $\langle \mathbf{w}, \mathbf{x}_i \rangle + b - y_i \leq \epsilon$. Point $\mathbf{x}_i$ is not a SV and it belongs to the ϵ-insensitive zone.
- Case $0 < \alpha_i < C$. Then $\xi_i = 0$ and $y_i - \langle \mathbf{w}, \mathbf{x}_i \rangle - b = \epsilon$. Point $\mathbf{x}_i$ is an *unbounded* SV and it is on the "upper" bound of the ϵ-insensitive zone.
- Case $0 < \alpha_i^* < C$. Then $\xi_i^* = 0$ and $\langle \mathbf{w}, \mathbf{x}_i \rangle + b - y_i = \epsilon$. Point $\mathbf{x}_i$ is an *unbounded* SV and it is on the "lower" bound of the ϵ-insensitive zone.
- Case $\alpha_i = C$. Then $y_i - \langle \mathbf{w}, \mathbf{x}_i \rangle - b \geq \epsilon$. Point $\mathbf{x}_i$ is a *bounded* SV and it is "above" the ϵ-insensitive zone.
- Case $\alpha_i^* = C$. Then $\langle \mathbf{w}, \mathbf{x}_i \rangle + b - y_i \geq \epsilon$. Point $\mathbf{x}_i$ is a *bounded* SV and it is "below" the ϵ-insensitive zone.

Let us denote $\mathcal{I}_{\mathrm{usv}} = \{i \in \{1, \dots, N\} : 0 < \alpha_i < C \vee 0 < \alpha_i^* < C\}$ the set of *unbounded* SVs, and $\mathcal{I}_{\mathrm{bsv}} = \{i \in \{1, \dots, N\} : \alpha_i = C \vee \alpha_i^* = C\}$ the set of bounded SVs, where $\vee$ denotes the inclusive OR operator.

As for binary classification, the bias parameter b can be obtained in theory from any unbounded SV for which the inequality constraints become equalities (Smola and Schölkopf, 1998):

$$b = y_i - \langle \mathbf{w}, \mathbf{x}_i \rangle - \epsilon \quad \text{for } 0 < \alpha_i < C \quad \text{or} \quad b = y_i - \langle \mathbf{w}, \mathbf{x}_i \rangle + \epsilon \quad \text{for } 0 < \alpha_i^* < C \,. \tag{II.60}$$

An alternative is to obtain b as an output of interior-point algorithms (Smola, 1998; Bompard, 2011). This latter approach is applied in the ASVR method presented in Section II–3.3.

The regressor $\widetilde{f}$ can be expressed in terms of all the SVs (i.e. bounded or unbounded SVs):

$$\widetilde{f}(\mathbf{x}) = \sum_{i \in \mathcal{I}_{\mathrm{usv}} \cup \mathcal{I}_{\mathrm{bsv}}} \left(\alpha_i - \alpha_i^*\right) \langle \mathbf{x}_i, \mathbf{x} \rangle + b \,. \tag{II.61}$$

II–2.2.2 Least squares SVM for regression

This section presents another form of SVM regression known as *least squares support vector machines* (LS-SVM), initially proposed by Suykens and Vandewalle (1999) for the purpose of binary classification. The version of this method adapted to regression is the one we focus on here (see, e.g., Suykens et al., 2002). It will be denoted LS-SVR in the following. The optimization problem to solve is set up as follows:

$$\min_{\mathbf{w}, b, \boldsymbol{\xi}} \frac{\|\mathbf{w}\|^2}{2} + \frac{C}{2} \sum_{i=1}^{N} \xi_i^2 \quad \text{s.t.} \quad y_i - \langle \mathbf{w}, \mathbf{x}_i \rangle - b = \xi_i \quad \text{for } i = 1, \dots, N \,, \tag{II.62}$$

where $\boldsymbol{\xi} = (\xi_1, \dots, \xi_N)^{\mathrm{T}} \in \mathbb{R}^N$ and C is a strictly positive tradeoff parameter.

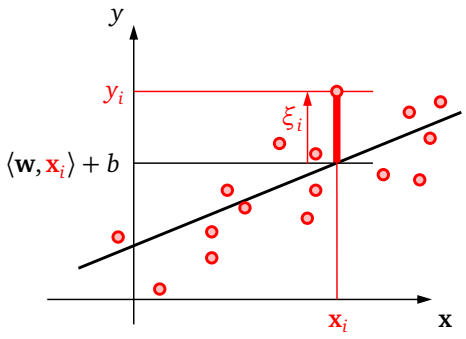

Figure II.4 – LS-SVM linear regression.

Several comments can be made about this formulation. All the errors $\xi_i = y_i - \widetilde{f}(\mathbf{x}_i)$ are penalized by means of the parameter C, which is applied to the sum of squares of these errors, see Eq. (II.4). The LS-SVR optimization problem defined in Eq. (II.62) is shown to correspond to the primal optimization problem of Vapnik's L2-ϵ-SVR with $\epsilon = 0$ (see, e.g., Saunders et al., 1998). LS-SVR is in this sense less general than L2-ϵ-SVR, which has a suitable parameter $\epsilon > 0$ to tune, but it appears to be less computationally expensive than L2-ϵ-SVR, as detailed in the following. In the context of linear regression, the LS-SVR formulation without the bias term b is equivalent to the so-called *ridge regression* (Hoerl and Kennard, 1970). Note, however, that ridge regression is sometimes presented with a bias term, such as in Hastie et al. (2009, Section 3.4.1). In the more general context of nonlinear models based on kernels, LS-SVR is also known as *kernel ridge regression* (see, e.g., Cristianini and Shawe-Taylor, 2000, Section 6.2.2; Saunders et al., 1998). The LS-SVR formulation also encompasses ordinary least squares regression (see Section II–1.3) by setting $C = +\infty$. It is easy to see that, in this case, Eq. (II.62) is equivalent to minimizing the empirical risk w.r.t. the square loss function.

The Lagrangian $\mathcal{L}$ is given by:

$$\mathcal{L}\left(\mathbf{w}, b, \boldsymbol{\xi}, \boldsymbol{\alpha}\right) = \frac{\|\mathbf{w}\|^2}{2} + \frac{C}{2}\sum_{i=1}^{N}\xi_i^2 - \sum_{i=1}^{N}\alpha_i\left[\langle \mathbf{w}, \mathbf{x}_i\rangle + b + \xi_i - y_i\right], \tag{II.63}$$

where $\boldsymbol{\alpha} = (\alpha_1, \ldots, \alpha_N)^{\mathrm{T}}$ contains the N Lagrange multipliers and $\alpha_i \in \mathbb{R}$ for $i = 1, \ldots, N$.

The Lagrangian $\mathcal{L}$ has to be minimized w.r.t. the primal variables $\mathbf{w}$, b and $\boldsymbol{\xi}$, and maximized w.r.t. the dual variables α_i (saddle point solution). The KKT conditions for optimality are:

$$\nabla_{\mathbf{w}}\mathcal{L}\left(\mathbf{w}, b, \boldsymbol{\xi}, \boldsymbol{\alpha}\right) = 0 \quad \rightarrow \quad \mathbf{w} = \sum_{i=1}^{N}\alpha_i\mathbf{x}_i\,, \tag{II.64a}$$

$$\frac{\partial\mathcal{L}\left(\mathbf{w}, b, \boldsymbol{\xi}, \boldsymbol{\alpha}\right)}{\partial b} = 0 \quad \rightarrow \quad \sum_{i=1}^{N}\alpha_i = 0\,, \tag{II.64b}$$

$$\nabla_{\boldsymbol{\xi}}\mathcal{L}\left(\mathbf{w}, b, \boldsymbol{\xi}, \boldsymbol{\alpha}\right) = 0 \quad \rightarrow \quad \alpha_i = C\xi_i \quad \text{for } i = 1, \ldots, N\,, \tag{II.64c}$$

$$\nabla_{\boldsymbol{\alpha}}\mathcal{L}\left(\mathbf{w}, b, \boldsymbol{\xi}, \boldsymbol{\alpha}\right) = 0 \quad \rightarrow \quad \langle \mathbf{w}, \mathbf{x}_i\rangle + b + \xi_i - y_i = 0 \quad \text{for } i = 1, \ldots, N\,. \tag{II.64d}$$

By plugging Eqs (II.64a–II.64c) into Eq. (II.64d), we obtain the dual optimization problem to be solved, which writes as follows:

$$\begin{bmatrix} \mathbf{K} + C^{-1}\mathbf{I} & \mathbf{1} \\ \mathbf{1}^{\mathrm{T}} & 0 \end{bmatrix}\begin{pmatrix} \boldsymbol{\alpha} \\ b \end{pmatrix} = \begin{pmatrix} \mathbf{y} \\ 0 \end{pmatrix}, \tag{II.65}$$

where $\mathbf{y} = (y_1, \dots, y_N)^{\mathrm{T}}$, $\mathbf{I}$ is the $N \times N$ identity matrix, $\mathbf{K} = [k_{ij}]_{1 \leq i,j \leq N}$ is the Gram matrix and where, for $i, j = 1, \dots, N$:

$$k_{ij} = \langle \mathbf{x}_i, \mathbf{x}_j \rangle \,. \tag{II.66}$$

The regressor $\widetilde{f}$ can be expressed in terms of *all* the points $\mathbf{x}_i$ of the training set $\mathcal{T}$:

$$\widetilde{f}(\mathbf{x}) = \sum_{i=1}^{N} \alpha_i \langle \mathbf{x}_i, \mathbf{x} \rangle + b \,. \tag{II.67}$$

From Eq. (II.65), we can notice that the LS-SVR formulation requires the solving of a linear set of equations, instead of the convex QP problem appearing in L2-SVR (and in the other SVM formulations addressed so far, i.e. hard-margin SVC, L1-SVC and L1-ϵ-SVR). LS-SVR therefore enables the use of less computationally involved methods and the solution can be obtained faster. However, the sparseness of the $\boldsymbol{\alpha}$ vector found in other SVM formulations is lost, due the choice of the square loss function for error penalization. The prediction writes in terms of *all* the points of the training set, see Eq. (II.67). The entire set of training data points could therefore be viewed as SVs, although there is no strict concept of support vectors in LS-SVMs. The lack of sparseness of the LS-SVR solution is often considered as a serious disadvantage with regard to classical SVMs, but this is not really troublesome in the context of function approximations since we work with small sets of training data.

II–2.3 Kernels for nonlinear models and regularization theory framework

II–2.3.1 From linear to nonlinear models, kernels and RKHS

The main concepts of SVMs and the details about the derivation of the corresponding models have been given in a *linear* context for binary classification in Section II–2.1 and for regression in Section II–2.2. In most general situations the binary classifiers or regressors are *nonlinear* and such an assumption in SVMs can be accounted for by means of kernels. The main idea is to map the input data into a high-dimensional *feature space* denoted $\mathcal{F}$ (whose dimension may be infinite) so as to enable the construction of a linear SVM model in this space $\mathcal{F}$. The power of SVMs (and other kernel-based methods) is that it is unnecessary to explicitly define this mapping, denoted $\phi : \mathcal{X} \to \mathcal{F}$, it is sufficient to choose a given *kernel* k which corresponds to a dot product of the input data mapped into $\mathcal{F}$ (Aizerman et al., 1964; Boser et al., 1992):

$$\begin{array}{rccl} k: & \mathcal{X} \times \mathcal{X} & \to & \mathbb{R} \\ & (\mathbf{x}, \mathbf{x}') & \mapsto & k(\mathbf{x}, \mathbf{x}') = \langle \phi(\mathbf{x}), \phi(\mathbf{x}') \rangle \end{array} \tag{II.68}$$

Before defining the main requirements that the function k must fulfill to be a valid kernel verifying Eq. (II.68), let us see how the hard-margin SVC problem reformulates by working in the feature space $\mathcal{F}$. Eqs. (II.29), (II.34), (II.40), (II.39) and (II.44) respectively rewrite:

Decision function:

$$\widetilde{f}(\mathbf{x}) = \langle \mathbf{w}, \phi(\mathbf{x}) \rangle + b \tag{II.69a}$$

Primal:

$$\min_{\mathbf{w}, b} \frac{\|\mathbf{w}\|^2}{2} \quad \text{s.t.} \quad y_i \left(\langle \mathbf{w}, \phi(\mathbf{x}_i) \rangle + b \right) \geq 1 \quad \text{for } i = 1, \dots, N \tag{II.69b}$$

Dual:

$$\max_{\boldsymbol{\alpha}} -\frac{1}{2} \sum_{i=1}^{N} \sum_{j=1}^{N} \alpha_i \alpha_j q_{ij} + \sum_{i=1}^{N} \alpha_i \quad \text{s.t.} \quad \begin{cases} \displaystyle\sum_{i=1}^{N} \alpha_i y_i = 0 \\ \alpha_i \geq 0 \quad \text{for } i = 1, \dots, N \end{cases} \tag{II.69c}$$

where, for $i, j = 1, \dots, N$:

$$\begin{aligned} q_{ij} &= y_i y_j \langle \phi(\mathbf{x}_i), \phi(\mathbf{x}_j) \rangle \\ &= y_i y_j \, k(\mathbf{x}_i, \mathbf{x}_j) \end{aligned} \tag{II.69d}$$

Decision function (solution):

$$\begin{aligned} \widetilde{f}(\mathbf{x}) &= \sum_{i \in \mathcal{S}} \alpha_i y_i \langle \phi(\mathbf{x}_i), \phi(\mathbf{x}) \rangle + b \\ &= \sum_{i \in \mathcal{S}} \alpha_i y_i k(\mathbf{x}_i, \mathbf{x}) + b \end{aligned} \tag{II.69e}$$

Several important comments can be made in light of these newly-obtained equations. First of all, the norm $\|\mathbf{w}\|$ which appears in the primal formulation of Eq. (II.69b) now corresponds to the weight vector $\mathbf{w}$ of the linear representation of $\widetilde{f}$ *in the feature space* $\mathcal{F}$. Secondly, it is noticed that the optimization problem to solve (dual formulation) can be expressed in terms of the kernel k only, without explicitly needing the map ϕ, see Eq. (II.69d). The same remark also applies to the decision function, which is also expressed in terms of k, see Eq. (II.69e). We therefore need the dot product in the feature space (i.e. the kernel k) without requiring an explicit definition of ϕ, and this is known as the *kernel trick* in the SVM literature. The introduction of kernels is a key ingredient of all SVM formulations, including those mentioned so far (soft-margin SVC, soft-margin SVR based on the ϵ-insensitive loss function and LS-SVR). Practically, to construct nonlinear SVM models, it is sufficient to replace the dot product in the input space $\mathcal{X}$ by the dot product in $\mathcal{F}$, i.e. replacing $\langle \mathbf{x}_i, \mathbf{x}_j \rangle$ by $k(\mathbf{x}_i, \mathbf{x}_j)$ in Eqs. (II.39), (II.49), (II.58) and (II.66).

Let us now recall a few definitions concerning some important properties of kernels. For a clear introduction to kernels, along with more details, the reader may refer to (Genton, 2001; Hofmann et al., 2008).

By definition, the *Gram matrix* $\mathbf{K} = [k_{ij}]_{1 \leq i,j \leq N}$ associated with a given kernel $k : \mathcal{X} \times \mathcal{X} \to \mathbb{R}$ and with the data $\mathbf{x}_1, \ldots, \mathbf{x}_N \in \mathcal{X}$ is defined by:

$$k_{ij} = k(\mathbf{x}_i, \mathbf{x}_j) \,. \tag{II.70}$$

A symmetric function $k : \mathcal{X} \times \mathcal{X} \to \mathbb{R}$ is called a *positive definite* (p.d.) kernel[10] if its $N \times N$ Gram matrix $\mathbf{K} = [k(\mathbf{x}_i, \mathbf{x}_j)]_{1 \leq i,j \leq N}$ verifies:

$$\boldsymbol{\alpha}^{\mathrm{T}} \mathbf{K} \boldsymbol{\alpha} \geq 0 \,, \tag{II.71}$$

for all $N \in \mathbb{N}$, for all $(\mathbf{x}_1, \ldots, \mathbf{x}_N) \in \mathcal{X}^N$ and for all $\boldsymbol{\alpha} = (\alpha_1, \ldots, \alpha_N)^{\mathrm{T}} \in \mathbb{R}^N$. A positive definite kernel is therefore a kernel whose $N \times N$ Gram matrix is positive semidefinite for all $N \in \mathbb{N}$ and all $\mathbf{x}_1, \ldots, \mathbf{x}_N \in \mathcal{X}$. The use of p.d. kernels k ensures that dual optimization problems are convex w.r.t. $\boldsymbol{\alpha}$ in Eq. (II.45) and Eq. (II.50), or w.r.t. $(\boldsymbol{\alpha}^{\mathrm{T}}, \boldsymbol{\alpha}^{*\mathrm{T}})^{\mathrm{T}}$ in Eq. (II.59), and thus that they feature a unique minimum. A p.d. kernel is *strictly* positive definite (strictly p.d.) if for any distinct vectors $\mathbf{x}_1, \ldots, \mathbf{x}_N \in \mathcal{X}$ the above-defined inequality holds strictly when at least one of the α_i's is not zero (case of a positive definite Gram matrix $\mathbf{K}$).

Let us also introduce the less common conditionally positive definite (c.p.d.) kernels w.r.t. an arbitrary finite dimensional vector space of functions $\mathcal{P}$ (see, e.g., Walder and Chapelle, 2008; Auffray and Barbillon, 2009). Such c.p.d. kernels will be useful to broaden the presentation of some specific points, such as the use of a bias term in SVM formulations and the relation between SVM and kriging surrogates later addressed in this report. A function $k : \mathcal{X} \times \mathcal{X} \to \mathbb{R}$ is called a *conditionally positive definite* (c.p.d.) kernel w.r.t. the linear space of functions $\mathcal{P}$ if its $N \times N$ Gram matrix $\mathbf{K} = [k(\mathbf{x}_i, \mathbf{x}_j)]_{1 \leq i,j \leq N}$ verifies:

$$\boldsymbol{\alpha}^{\mathrm{T}} \mathbf{K} \boldsymbol{\alpha} \geq 0 \,, \tag{II.72}$$

[10] Symmetric positive definite kernels are called covariances in the statistics literature.

for all $N \in \mathbb{N}$, for all $(\mathbf{x}_1, \dots, \mathbf{x}_N) \in \mathcal{X}^N$ and for all $\boldsymbol{\alpha} = (\alpha_1, \dots, \alpha_N)^{\mathrm{T}} \in \mathbb{R}^N$ such that, for all $p \in \mathcal{P}$:

$$\boldsymbol{\alpha}^{\mathrm{T}} \mathbf{p} = 0 \,, \tag{II.73}$$

where $\mathbf{p} = (p(\mathbf{x}_1), \dots, p(\mathbf{x}_N))^{\mathrm{T}}$.

Note that c.p.d. kernels may be defined in slightly different settings in the literature, as pointed out by Walder and Chapelle (2008). The c.p.d. kernels of order m on $\mathbb{R}^n$ considered in Poggio and Girosi (1989) and Smola et al. (1998) are defined such that $\mathcal{P}$ denotes the set of all polynomials p on $\mathbb{R}^n$ of degree $m-1$ at most. C.p.d. kernels may specifically designate the only c.p.d. kernels of order $m = 1$ as default notation (Schölkopf and Smola, 2001; Hofmann et al., 2008). In this latter case we have $\mathcal{P} = \{1\}$, and Eq. (II.73) rewrites:

$$\sum_{i=1}^{N} \alpha_i = 0 \,. \tag{II.74}$$

We recall here a few classes of kernels (see, e.g., Genton, 2001, for a useful review on the subject). *Stationary* (or *translation-invariant* or *shift-invariant*) kernels are defined by $k(\mathbf{x}, \mathbf{x}') = f(\mathbf{x} - \mathbf{x}')$ and therefore depend only on the lag $\mathbf{x} - \mathbf{x}'$. The class of stationary kernels encompasses that of *isotropic* (or *radial*) kernels $k(\mathbf{x}, \mathbf{x}') = f(\|\mathbf{x} - \mathbf{x}'\|)$, which depends only on the norm of $\mathbf{x} - \mathbf{x}'$ and not on its direction (it is assumed that $\|\cdot\| = \|\cdot\|_2$). When a kernel is not isotropic it is said to be *anisotropic*. For anisotropic stationary multivariate kernels, a tensor product of stationary univariate kernels is often assumed in the form $k(\mathbf{x}, \mathbf{x}') = \prod_{i=1}^{n} k_i(x_i - x_i')$. Examples of such kernels (often called *separable* kernels) are commonly used in the construction of kriging surrogate models, where k_i for $i = 1, \dots, n$ are e.g. Gaussian or Matérn univariate kernels.

A list of popular kernels in SVMs is given below (see, e.g., Smola et al., 2000; Schölkopf and Smola, 2001). The Matérn kernel is also introduced, although it is rarely used in SVMs (see, e.g., Vazquez and Walter, 2003; Moustapha et al., 2014; Bourinet, 2016).

- Gaussian radial basis function kernel (Gaussian RBF kernel):

$$k(\mathbf{x}, \mathbf{x}') = \exp\left(-\gamma \|\mathbf{x} - \mathbf{x}'\|^2\right) \,, \tag{II.75}$$

  where $\gamma \in \mathbb{R}_{>0}$. This kernel is p.d. and the corresponding feature space is infinite dimensional. The γ parameter determines the locality of the basis functions. This kernel is often parameterized with a parameter, denoted σ, which represents the bandwidth of the kernel such that $\gamma = 1/2\sigma^2$. The Gaussian RBF Kernel is the most common kernel used by SVM practitioners. It is an excellent choice for approximating smooth functions and it is defined in terms of one single parameter γ, which makes it easy to tune, see Section II–2.4. Its anisotropic version writes:

$$k(\mathbf{x}, \mathbf{x}') = \exp\left(-\sum_{i=1}^{n} \gamma_i (x_i - x_i')^2\right) \,, \tag{II.76}$$

  where $\gamma_1, \dots, \gamma_n \in \mathbb{R}_{>0}$.

- Polynomial kernel (inhomogeneous form here):

$$k(\mathbf{x}, \mathbf{x}') = \left(c + \langle \mathbf{x}, \mathbf{x}' \rangle\right)^d \,, \tag{II.77}$$

  where $d \in \mathbb{N}_{>0}$ and $c \in \mathbb{R}_{>0}$. With such a kernel, $\mathcal{F}$ is the space spanned by all monomials *up* to degree d, and the dimension of the corresponding feature space is:

$$\#\mathcal{F} = \binom{n+d}{d} \,. \tag{II.78}$$

- Sigmoid kernel:

$$k(\mathbf{x},\mathbf{x}') = \tanh\left(\kappa\langle\mathbf{x},\mathbf{x}'\rangle + \theta\right), \tag{II.79}$$

  where $\kappa \in \mathbb{R}_{>0}$ and $\theta \in \mathbb{R}_{<0}$. Though this kernel is not p.d., it has found useful applications in the SVM literature.

- $C^{2\nu}$-Matérn kernel:

$$k(\mathbf{x},\mathbf{x}') = \frac{1}{2^{\nu-1}\Gamma(\nu)}\left(\gamma\sqrt{2\nu}\|\mathbf{x}-\mathbf{x}'\|\right)^{\nu} K_{\nu}\left(\gamma\sqrt{2\nu}\|\mathbf{x}-\mathbf{x}'\|\right), \tag{II.80}$$

  where $\nu \geq 1/2$ is a regularity parameter which controls the smoothness of the approximation, $\gamma \in \mathbb{R}_{\geq 0}$ is again a parameter that determines the locality of the kernel, Γ is the Gamma function and K_{ν} is the modified Bessel function of second kind of order ν (a.k.a. modified Bessel function of third kind or MacDonald's function). This kernel has been used in spatial interpolation (see, e.g., Stein, 1999). The $C^{2\nu}$-Matérn kernel includes the Gaussian RBF kernel as the limiting case $\nu \to \infty$. This kernel is p.d. and it has a closed form expression for $\nu = m + 1/2$ where $m \in \mathbb{N}$. The kernels with $\nu = 3/2$ and $\nu = 5/2$ are most often used in their isotropic or anisotropic versions.

Several other types of kernels are available and there is no intention here to establish a complete list. It is nevertheless of interest to cite a few other kernels which are mainly used in regularized networks (Girosi et al., 1995): multiquadratic kernel (c.p.d., $m = 1$), inverse multiquadratic kernel (p.d.), m-th order thin-plate splines kernel (c.p.d w.r.t. the set of n-variate polynomials of degree $m-1$ at most) (Wahba, 1990; Walder and Chapelle, 2008).

At the beginning of this section, it was mentioned that the kernel k introduced in the SVM formulation should correspond to a dot product in the feature space $\mathcal{F}$, see Eq. (II.68). We will now look at the different ways of constructing feature spaces for a given kernel k. Two main types of approaches are found in the SVM literature, one based on Mercer kernels and another based on *reproducing kernel Hilbert spaces* (RKHS) associated with k. We will provide the reader with a short description of the latter approach (see Schölkopf and Smola, 2001; Shawe-Taylor and Cristianini, 2004; Hofmann et al., 2008, for further details).

For the construction of the RKHS associated with a given kernel k, we consider a map from $\mathcal{X}$ in the space of functions, mapping $\mathcal{X}$ into $\mathbb{R}$, denoted $\mathbb{R}^{\mathcal{X}}$, such that:

$$\begin{array}{rccc} \phi: & \mathcal{X} & \to & \mathbb{R}^{\mathcal{X}} \\ & \mathbf{x} & \mapsto & \phi(\mathbf{x}) = k(\mathbf{x},\cdot) \end{array} \tag{II.81}$$

It is worth noting that $\phi(\mathbf{x}) : \mathbf{x}' \mapsto k(\mathbf{x},\mathbf{x}')$ is a function of $\mathbf{x}'$, for any $\mathbf{x} \in \mathcal{X}$.

We want to construct a dot product space containing the images of $\mathcal{X}$ under ϕ.

The image of ϕ is first turned into a vector space. This is done by taking all linear combinations of the functions $k(\mathbf{x}_i,\cdot)$ for $i = 1,\ldots,N$, for any $N \in \mathbb{N}$ and for any $\mathbf{x}_i \in \mathcal{X}$:

$$\left\{ f(\cdot) = \sum_{i=1}^{N} \alpha_i k(\mathbf{x}_i,\cdot),\, N \in \mathbb{N},\, (\mathbf{x}_1,\ldots,\mathbf{x}_N) \in \mathcal{X}^N,\, (\alpha_1,\ldots,\alpha_N) \in \mathbb{R}^N \right\}. \tag{II.82}$$

The second step consists in equipping this vector space of functions with a suitable dot product. The dot product between two functions $f(\cdot) = \sum_{i=1}^{N} \alpha_i k(\mathbf{x}_i,\cdot)$ and $g(\cdot) = \sum_{j=1}^{M} \beta_j k(\mathbf{x}'_j,\cdot)$ is defined by:

$$\langle f, g\rangle = \sum_{i=1}^{N}\sum_{j=1}^{M} \alpha_i \beta_j k(\mathbf{x}_i,\mathbf{x}'_j), \tag{II.83}$$

where $N, M \in \mathbb{N}$, where $\mathbf{x}_i \in \mathcal{X}$ and $\alpha_i \in \mathbb{R}$ for $i = 1, \ldots, N$, and where $\mathbf{x}'_j \in \mathcal{X}$ and $\beta_j \in \mathbb{R}$ for $j = 1, \ldots, M$. This dot product is well defined. It is shown to be bilinear and symmetric. It is additionally positive definite, since we assume that k is also positive definite:

$$\langle f, f \rangle = \sum_{i=1}^{N} \sum_{j=1}^{N} \alpha_i \alpha_j k(\mathbf{x}_i, \mathbf{x}_j) = \boldsymbol{\alpha}^{\mathrm{T}} \mathbf{K} \boldsymbol{\alpha} \geq 0 \,, \tag{II.84}$$

where $\boldsymbol{\alpha} = (\alpha_1, \ldots, \alpha_N)^{\mathrm{T}} \in \mathbb{R}^N$ and $\mathbf{K}$ is the $N \times N$ Gram matrix defined in Eq. (II.70). We can also show that $\langle f, f \rangle = 0 \Rightarrow f = 0$.

From these definitions, the so-called reproducing property of the kernel k can be found:

$$\langle k(\mathbf{x}, \cdot), f \rangle = f(\mathbf{x}) \,, \tag{II.85}$$

and, in particular, it also holds that:

$$\langle k(\mathbf{x}, \cdot), k(\mathbf{x}', \cdot) \rangle = k(\mathbf{x}, \mathbf{x}') \quad \equiv \quad \langle \phi(\mathbf{x}), \phi(\mathbf{x}') \rangle = k(\mathbf{x}, \mathbf{x}') \,, \tag{II.86}$$

which makes it clear that the reproducing kernel k can be seen as the dot in the feature space, as required from Eq. (II.68).

With the above-defined properties the kernel k is called a *reproducing kernel* (Aronszajn, 1950). The vector space of functions defined in Eq. (II.82) endowed with the dot product defined in Eq. (II.83) is a dot product space a.k.a. a pre-Hilbert space. It is turned into a Hilbert space over $\mathbb{R}$ by completing it by the norm corresponding to the dot product, i.e. $\|\cdot\| = \sqrt{\langle \cdot, \cdot \rangle}$ (see, e.g., Schölkopf and Smola, 2001, Appendix B). A Hilbert space of functions that possesses a reproducing kernel is called a *reproducing kernel Hilbert space* (RKHS). We will denote $\mathcal{H}_k$ the RKHS of functions generated by k, $\langle \cdot, \cdot \rangle_{\mathcal{H}_k}$ the dot product of $\mathcal{H}_k$ and $\|\cdot\|_{\mathcal{H}_k}$ the corresponding norm. It is important to note that there is a perfect equivalence between RKHS and p.d. kernels. To every RKHS there corresponds a p.d. reproducing kernel, and conversely, given a p.d. kernel $k : \mathcal{X} \times \mathcal{X} \to \mathbb{R}$, we can construct a unique RKHS of real-valued functions on $\mathcal{X}$ with k as its reproducing kernel (Aronszajn, 1950). If instead of assuming k to be p.d., it is assumed to be c.p.d. w.r.t. an arbitrary finite dimensional vector space of functions $\mathcal{P}$, then $\mathcal{H}_k$ is a *semi*-reproducing kernel Hilbert space (Wahba, 1990). The theory behind semi-RKHS is more complicated than that of RKHS, due to the null space of the semi-norm.

II–2.3.2 SVMs in the framework of regularization theory

Learning an approximate model $\widetilde{f} : \mathcal{X} \to \mathcal{Y}, \mathbf{x} \mapsto \widetilde{y} = \widetilde{f}(\mathbf{x})$ from a finite set of training data $\mathcal{T} = \{(\mathbf{x}_i, y_i) \in \mathcal{X} \times \mathcal{Y}, 1 \leq i \leq N\}$ is known to be an ill-posed problem. In simple terms, this means that the amount of information in the (possibly noisy) training data is insufficient to construct a uniquely-defined approximate model. In order to make the learning problem well-posed, it is necessary to impose some a priori assumptions about the form of the approximation. The most common strategy consists in imposing some degree of smoothness on the approximate function that constrains the hypothesis space in which a solution is sought. The techniques that exploit such smoothness constraints are known under the term of *standard regularization* (Tikhonov and Arsenin, 1977; Wahba, 1990), and SVM falls into this category of techniques. The reader may refer to the following useful references from which this text is inspired for a deeper insight on the subject (Girosi, 1998; Smola et al., 1998; Evgeniou et al., 2000). The central idea in regularization is to minimize the following objective function, called the *regularized risk functional* (Schölkopf and Smola, 2001):

$$R_{\mathrm{reg}}[\widetilde{f}] = R_{\mathrm{emp}}[\widetilde{f}] + \lambda \, \Omega[\widetilde{f}] \,, \tag{II.87}$$

where $R_{\text{emp}}[\widetilde{f}]$ is the empirical risk, see Eq. (II.2), $\Omega[\widetilde{f}]$ is a selected regularizer and $\lambda \in \mathbb{R}_{>0}$ a regularization parameter.

The regularization problem is now expressed in the context of kernels and associated RKHS. By application of the representer theorem, see Eq. (II.89), we will see that the functions h solutions of this problem are expressed without a bias term, i.e. in the general form $\widetilde{f}(\mathbf{x}) = h(\mathbf{x}) = \sum_{i=1}^{N} \alpha_i k(\mathbf{x}_i, \mathbf{x})$. Accounting for a bias term b in the solution (as considered in all the SVM models presented so far) makes the problem harder to tackle, and this will be addressed later in this section. The minimization of the regularized risk functional defined in Eq. (II.87) is reformulated as follows:

$$\min_{h \in \mathcal{H}_k} \sum_{i=1}^{N} \ell\left(y_i, h(\mathbf{x}_i)\right) + \lambda\, \Omega\left(\|h\|_{\mathcal{H}_k}\right), \tag{II.88}$$

where $\ell : \mathcal{Y} \times \mathbb{R} \to \mathbb{R} \cup \{+\infty\}$ is an arbitrary loss function and $\Omega : \mathbb{R}_{\geq 0} \to \mathbb{R}$ is strictly monotonic increasing function. The first term enforces the closeness to the data. It corresponds to the empirical risk from which the factor $1/N$ has been dropped, see Eq. (II.2). The second term, expressed in terms of the norm of h in the RKHS, embeds the a priori information on the smoothness of h (see, e.g., Girosi et al., 1995). Relations between the norm of the RKHS and the smoothness of the function can be established, depending on the chosen kernel k (a clear understanding of this relation can be given by means of the so-called *regularization operators*, which go beyond the scope of this report). If we additionally assume the convexity of ℓ and Ω, then the dual optimization problem is also convex (therefore featuring a unique global minimum) and we can solve it by means of convex optimization methods.

By virtue of the *representer theorem* (Kimeldorf and Wahba, 1970; Schölkopf and Smola, 2001), the minimizer of Eq. (II.88) admits a representation in the form:

$$h(\mathbf{x}) = \sum_{i=1}^{N} c_i k(\mathbf{x}_i, \mathbf{x}), \tag{II.89}$$

where $\mathbf{c} = (c_1, \ldots, c_N)^{\mathrm{T}} \in \mathbb{R}^N$ is the vector of unknown expansion coefficients.

The representer theorem initially proven in the context of the square loss is of prime importance. It clearly states that the solution of an optimization problem in a potentially *infinite* dimensional space $\mathcal{H}_k$ can be expressed in terms of a linear combination of the kernel evaluated at the points of a *finite* dimensional set $(\mathbf{x}_1, \ldots, \mathbf{x}_N)$. The optimization problem defined in Eq. (II.88) therefore boils down to one over $\mathbb{R}^N$.

For an equivalence between the solution of the regularized problem and those obtained for classification in Section II–2.1 and regression in Section II–2.2, Eq. (II.88) is rewritten as follows:

$$\min_{h \in \mathcal{H}_k} C \sum_{i=1}^{N} \ell\left(y_i, h(\mathbf{x}_i)\right) + \frac{1}{2}\|h\|_{\mathcal{H}_k}^2. \tag{II.90}$$

The regularization parameter is now C (such as introduced in Sections II–2.1 and II–2.2), where $C = 1/\lambda$ and we take $\Omega\left(\|h\|_{\mathcal{H}_k}\right) = \frac{1}{2}\|h\|_{\mathcal{H}_k}^2$, which is quite a standard choice in regularization (note that such a choice leads to a convex QP). The parameter C controls the tradeoff between finding a function h of low complexity (i.e. small norm of h in the RKHS) and fitting the training data well (i.e. small empirical risk over the training set w.r.t. the loss function ℓ), which thus avoids overfitting.

As can be seen in Eq. (II.89), the kernel expansion obtained by the representer theorem does not include any bias term b, which was considered in all the SVM models defined in Sections II–2.1 and II–2.2. The role of this bias term, which appears in the SVM formulations due to Vapnik, is not so clear in the literature (Poggio et al., 2002) and we will see that b is introduced in the formulation as

an unregularized term. In a few specific contexts, we may search for solutions $\widetilde{f}$ of the regularization problem in the following form, which is more general than the one obtained in Eq. (II.89):

$$\begin{aligned}\widetilde{f}(\mathbf{x}) &= h(\mathbf{x}) + p(\mathbf{x}) \\ &= \sum_{i=1}^{N} c_i k(\mathbf{x}_i, \mathbf{x}) + \sum_{j=1}^{M} d_j p_j(\mathbf{x}) ,\end{aligned} \tag{II.91}$$

where $p_j : \mathcal{X} \to \mathbb{R}$ for $1, \ldots, M$ is a set of M real-valued functions, $M \in \mathbb{N}$, and $d_1, \ldots, d_M \in \mathbb{R}$. Note that a kernel expansion with a bias term corresponds to the particular case $M = 1$ and $p_1 : \mathcal{X} \to \mathbb{R}, \mathbf{x} \mapsto 1$.

Such a representation is found to be the solution of the following minimization problem:

$$\min_{h \in \mathcal{H}_k,\, p \in \operatorname{span}(p_j)} \sum_{i=1}^{N} \ell\left(y_i, \widetilde{f}(\mathbf{x}_i)\right) + \lambda\, \Omega\left(\|h\|_{\mathcal{H}_k}\right) , \tag{II.92}$$

where $\widetilde{f} = h + p$, Ω is again assumed to be a strictly monotonic increasing function and where the $N \times M$ matrix $\mathbf{P} = [p_j(\mathbf{x}_i)]_{1 \le i \le N, 1 \le j \le M}$ has rank M. This extension of the representer theorem is due to Schölkopf et al. (2001) and it is called the *semiparametric* representer theorem. It is important to note that the contributions of the functions $p_1, \ldots, p_M$ are not regularized. Examples of application include the so-called *semi-parametric* approaches, where we have some a priori knowledge about the approximate solution we expect to obtain. In such a context the parametric part of the solutions comes from the linear combination over the function basis $p_1, \ldots, p_M$, and the nonparametric part is accounted for by means of the kernel expansion over the training data. The solution of Eq. (II.92), i.e. both $\mathbf{c} = (c_1, \ldots, c_N)^{\mathrm{T}}$ and $\mathbf{d} = (d_1, \ldots, d_M)^{\mathrm{T}}$, can be found by solving an optimization problem similar to that of classical SVMs (see Smola et al., 1999, where a solution is obtained with the ϵ-insensitive loss function). In comparison with Eq. (II.57), the dual optimization problem has the following M additional equality constraints:

$$\sum_{i=1}^{N} c_i p_j(\mathbf{x}_i) = 0 \quad \text{for } j = 1, \ldots, M , \tag{II.93}$$

and the coefficients $d_1, \ldots, d_M$ can be found from the KKT conditions or directly as by-products of interior-point methods. It is worth noting that Eq. (II.93) corresponds to the unique equality constraint found in all SVC and ϵ-SVR formulations (case $M = 1$ and $p_1(\cdot) = 1$), see Eq. (II.48) and Eq. (II.57).

The representation of $\widetilde{f}$ given in Eq. (II.91) is also the form of the solution obtained in the context of regularization based on c.p.d kernels. For c.p.d. kernels, the regularization operator has a null space which is spanned by a set of functions $p_1, \ldots, p_M$ which are not regularized. An analog of the representer theorem can be derived for c.p.d. kernels w.r.t. an arbitrary finite dimensional vector space of functions $\mathcal{P}$ (see Walder and Chapelle, 2008, Theorem 4.6; Auffray and Barbillon, 2009, Theorem 6.1). For c.p.d. kernels of order m, $\mathcal{P} = \Pi_n^{m-1}$ denotes the set of all polynomials p on $\mathbb{R}^n$ of degree $m-1$ at most, whose dimension is:

$$M = \dim\left(\Pi_n^{m-1}\right) = \binom{n+m-1}{m-1} . \tag{II.94}$$

An application example is the m-th order thin-plate kernel, which is c.p.d. w.r.t. Π_n^{m-1} (Walder and Chapelle, 2008).

In Lp-SVC and Lp-ϵ-SVR, $p \in \{1, 2\}$, we are searching for a solution $\widetilde{f}$ in the form:

$$\widetilde{f}(\mathbf{x}) = h(\mathbf{x}) + b \quad \text{where} \quad h(\mathbf{x}) = \sum_{i=1}^{N} c_i k(\mathbf{x}_i, \mathbf{x}) , \tag{II.95}$$

where $\mathbf{c} = (c_1, \ldots, c_N)^{\mathrm{T}}$ is the vector of unknown expansion coefficients and where b is an unregularized bias term.

The norm of h in the RKHS $\mathcal{H}_k$ writes:

$$\|h\|_{\mathcal{H}_k} = \sqrt{\langle h, h \rangle_{\mathcal{H}_k}} = \sqrt{\mathbf{c}^{\mathrm{T}} \mathbf{K} \mathbf{c}}\,, \tag{II.96}$$

where $\mathbf{K} = [k_{ij}]_{1 \leq i,j \leq N}$ is the Gram matrix such that $k_{ij} = k(\mathbf{x}_i, \mathbf{x}_j)$.

The evaluation of $\widetilde{f}$ at points $\mathbf{x}_i$ of the training set can be expressed as follows:

$$\widetilde{f}\,(\mathbf{x}_i) = \sum_{j=1}^{N} c_j k(\mathbf{x}_j, \mathbf{x}_i) + b = (\mathbf{K}\mathbf{c})_i + b\,. \tag{II.97}$$

The regularization problem to solve can therefore be expressed as follows:

$$\min_{\mathbf{c}, b} C \sum_{i=1}^{N} \ell\,(y_i, (\mathbf{K}\mathbf{c})_i + b) + \widetilde{g}\left(\sqrt{\mathbf{c}^{\mathrm{T}} \mathbf{K} \mathbf{c}}\right), \tag{II.98}$$

where $\mathbf{c} = (c_1, \ldots, c_N)^{\mathrm{T}} \in \mathbb{R}^N$, $b \in \mathbb{R}$ and $\widetilde{g} : \mathbb{R} \to \mathbb{R} \cup \{+\infty\}, t \mapsto \frac{1}{2}t^2$ if $t \geq 0$, $+\infty$ otherwise. The second term of the objective function is slightly modified to allow the derivation of its conjugate by Fenchel duality in the following (introduction of the function $\widetilde{g}$ (Heinrich, 2012)). The loss function $\ell\,(y_i, u)$ is assumed to be convex w.r.t. its second argument, but not necessarily differentiable. This assumption is verified for the loss functions used in Lp-SVC and Lp-ϵ-SVR, which are given in Table II.1 and represented in Figure II.5.

A dual formulation of Eq. (II.98) can be obtained by means of the theory of Fenchel duality (Borwein and Lewis, 2000) instead of the more common Lagrangian duality used so far. The use of Fenchel duality in SVMs was investigated by Bach et al. (2005), Rifkin and Lippert (2007), Bach (2009), and Heinrich (2012), and the reader may refer to these references for details. We simply recall here the dual formulation of the regularization problem obtained by Fenchel duality, which can be written nicely in terms of the Fenchel conjugate of the loss function:

$$\max_{\mathbf{p}} -C \sum_{i=1}^{N} \ell(y_i, \cdot)^*\left(-\frac{p_i}{C}\right) - \frac{1}{2}\mathbf{p}^{\mathrm{T}} \mathbf{K} \mathbf{p} \quad \text{s.t.} \quad \mathbf{1}^{\mathrm{T}} \mathbf{p} = 0\,, \tag{II.99}$$

where $\mathbf{p} = (p_1, \ldots, p_N)^{\mathrm{T}} \in \mathbb{R}^N$ and $\ell(y_i, \cdot)^* : \mathbb{R} \to \mathbb{R}$ is the Fenchel conjugate of the convex function $\ell(y_i, \cdot)$:

$$\ell(y_i, \cdot)^*(v) = \max_{u \in \mathbb{R}} uv - \ell\,(y_i, u)\,. \tag{II.100}$$

Method	Loss function name	Loss function $\ell(y,u)$	Fenchel conjugate $\ell(y,\cdot)^*(v)$		
LS-SVM, RN*	square	$\frac{1}{2}(y-u)^2$	$\frac{1}{2}v^2 + vy$		
L1-SVC	hinge	$(1-yu)_+$	vy	if $vy \in [-1,0]$,	$+\infty$ otherwise
L2-SVC	squared hinge	$\frac{1}{2}(1-yu)_+^2$	$\frac{1}{2}v^2 + vy$	if $vy \leq 0$,	$+\infty$ otherwise
L1-ϵ-SVR	ϵ-insensitive	$(\lvert y-u\rvert - \epsilon)_+$	$vy + \lvert v\rvert\,\epsilon$	if $\lvert v\rvert \leq 1$,	$+\infty$ otherwise
L2-ϵ-SVR	squared ϵ-insensitive	$\frac{1}{2}(\lvert y-u\rvert - \epsilon)_+^2$	$\frac{1}{2}v^2 + vy + \lvert v\rvert\,\epsilon$		

*: regularized networks (see, e.g., Girosi et al., 1995).

N.B.: $(x)_+ = \max(x, 0)$.

Table II.1 – Methods, loss functions and Fenchel conjugates (from Bach, 2009).

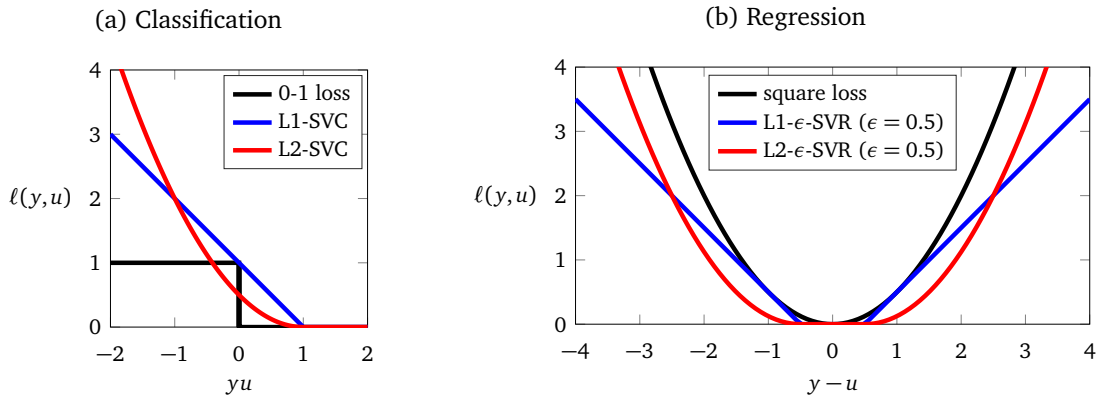

Figure II.5 – Loss functions in classification and regression.

The Fenchel conjugates of Lp-SVC and Lp-ϵ-SVR loss functions are given in Table II.1 for $p \in \{1,2\}$ (Rifkin and Lippert, 2007; Bach, 2009). The Lagrangian dual problems defined in Eq. (II.48) for L1-SVC and Eq. (II.57) for L1-ϵ-SVR are equivalent to the Fenchel dual defined in Eq. (II.99), where $\ell(y_i,u) = (1-y_iu)_+$ and $(|y_i-u|-\epsilon)_+$, respectively. It is worth emphasizing that the unique equality constraint $\mathbf{1}^{\mathrm{T}}\mathbf{p} = 0$ appearing in Eq. (II.99) is due to the presence of the unregularized bias term b in the expression of $\widetilde{f}$.

II–2.4 Hyperparameter selection

So far we have focused on finding the solution of a regularization problem for a given type of kernel and assuming some values for its parameters. Moreover, the level of regularization introduced in the problem was also assumed given through the parameter C. In regression based on the ϵ-insensitive loss function, the parameter ϵ was also assumed fixed to some arbitrary value.

Based on given data $\mathcal{T} = \{(\mathbf{x}_i, y_i) \in \mathcal{X} \times \mathcal{Y}, 1 \leq i \leq N\}$, solving the learning problem requires:

1. finding the most appropriate kernel or combination of kernels,
2. choosing the most suitable parameterization of the selected kernel(s),
3. choosing a regularization level which avoids both overfitting and underfitting.

This general problem, which is not specific to SVMs, is a great challenge and it is referred to as *model selection*. In the scope of this report we will assume that the kernel type is given, which leaves us to tackle only points 2 and 3 (if we have no prior knowledge about the function f to surrogate, the choice of an isotropic Gaussian RBF kernel is often assumed by SVM practitioners, even though this choice may be questionable). The problem therefore reduces to the selection of a finite number of parameter values, and this parametric form of model selection is known as *hyperparameter selection*. *Hyperparameters* include the parameters of the selected kernel, e.g. the unique parameter γ of a Gaussian RBF kernel, see Eq. (II.75), and the other SVM formulation parameters such as the regularization parameter C and additional parameters like the ϵ parameter of the ϵ-insensitive loss function in regression. These hyperparameters are assumed to be gathered in a vector denoted $\boldsymbol{\theta} = (\theta_1, \ldots, \theta_{n_\theta}) \in \Theta$ in the following. The number of kernel parameters is usually low unless an anisotropic form is selected for the kernel, in which case $n_{\boldsymbol{\theta}} \propto n = \dim(\mathcal{X})$.

The objective pursued in hyperparameter selection (or more generally in model selection) is to minimize the generalization error, defined in terms of the expected risk, see Eq. (II.1). As pointed out in Section II–1.1, the expected risk is *unknown* and, as a consequence, we must consider an estimate of the

generalization error based on the given data $\mathcal{T}$. Two questions then arise: 1) what is the best estimate we can take to quantify the generalization error and how can we assess its value from the known data $\mathcal{T}$, 2) how can we efficiently minimize this estimate in the search domain of hyperparameters Θ.

Regarding question 1, we will focus first on *cross-validation* (CV), which is a standard technique used in model selection. The principle of K-fold cross-validation (K-fold CV) and one of its variants known as *leave-one-out* cross validation (LOO-CV) are briefly recalled in Section II–2.4.1. The set of hyperparameter values that minimize the errors assessed by either K-fold CV or LOO-CV are considered as optimal values, i.e. they are assumed to ensure the lowest generalization error of the constructed model.

In a practical situation, K-fold CV and especially LOO-CV are often computationally expensive. For LOO-CV, N model trainings are required to assess the LOO error for a given set of hyperparameters, which precludes the use of this technique for sizes N of practical interest. As an alternative to true LOO-CV, it is possible to consider using approximations (or bounds) of the LOO error which have been derived in the SVM context. Such approximations are briefly reviewed in Section II–2.4.2, and we will focus on one of the most accurate ones, known as LOO span bounds. A description of these LOO span bounds is given, based on the work of Vapnik and Chapelle (2000) for classification and that of Chang and Lin (2005) for ϵ-insensitive regression.

In Section II–2.4.3, we give a brief outline of some techniques used to minimize the generalization error and thus tune the SVM hyperparameters (answer to question 2). Minimizing the approximate LOO error given by the span bounds is investigated and an algorithm based on the cross-entropy method is proposed in order to solving the optimization problem in classification and regression.

Before moving on to the technical details of hyperparameter selection, it is worth making some important comments. A proper tuning of SVM model hyperparameters is of paramount importance in the case of training on small sample sets. Inadequate choices for these hyperparameters could result in a poor predictive capacity of the SVM models, with either severe underfitting or overfitting. Finding optimal values for these hyperparameters therefore requires 1) using an estimate of the generalization error which is a good proxy of the true and unknown expected risk (accuracy of the selected generalization error estimate), 2) finding a set of hyperparameter values that truly minimizes this estimate (use of a robust optimization technique to find a reliable solution).

II–2.4.1 Cross-validation (CV), leave-one-out (LOO)

For hyperparameter selection, the ideal situation would be to train on the given data $\mathcal{T} = \mathcal{T}_{\text{train}}$, then use another set of independent data $\mathcal{T}_{\text{test}}$ to test the accuracy of the constructed model, and thus find the best values of $\boldsymbol{\theta}$ leading to the lowest level of errors on $\mathcal{T}_{\text{test}}$. Since the only information at our disposal is given by $\mathcal{T}$, the main idea of *cross-validation* (CV), independently introduced by Allen (1974), Stone (1974), and Geisser (1975) is to split the set of available data $\mathcal{T}$ into *training sets* and corresponding *testing sets* in order to find hyperparameter values that minimize the errors averaged over the testing sets. Practically, *K-fold cross validation* (Geisser, 1975) consists in splitting the training set $\mathcal{T} = \{(\mathbf{x}_i, y_i) \in \mathcal{X} \times \mathcal{Y}, 1 \leq i \leq N\}$ into K randomly selected and mutually exclusive subsets $\mathcal{T}^{(1)}, \ldots, \mathcal{T}^{(K)}$ (called folds) of equal or nearly equal size $\lfloor N/K \rceil$ ($\lfloor x \rceil$ denoting the nearest integer to x) where $\mathcal{T}^{(k)} = \{(\mathbf{x}_i, y_i), i \in \mathcal{I}^{(k)}\}$ and the set of indices $\mathcal{I}^{(1)}, \ldots, \mathcal{I}^{(K)}$ are defined such that:

$$\bigcup_{k=1}^{K} \mathcal{I}^{(k)} = \{1, \ldots, N\} \quad \text{and} \quad \mathcal{I}^{(i)} \cap \mathcal{I}^{(j)} \text{ for } i \neq j \,. \tag{II.101}$$

For each subset $\mathcal{T}^{(k)}$, a SVM model denoted $\widetilde{f}^{(-k)}$ is trained on the data of the $(K-1)$ remaining subsets, denoted $\mathcal{T}^{(-k)} = \{(\mathbf{x}_i, y_i), i \in \mathcal{I}^{(-k)}\}$, where $\mathcal{I}^{(-k)}$ denotes the complementary set of $\mathcal{I}^{(k)}$ in $\{1, \dots, N\}$, see Eq. (II.102), and the constructed model is tested on the data set $\mathcal{T}^{(k)}$ considered as validation data.

$$\mathcal{I}^{(-k)} = \{1, \dots, N\} \setminus \mathcal{I}^{(k)} . \tag{II.102}$$

The SVM model trained on $\mathcal{T}^{(-k)}$ writes:

$$\widetilde{f}^{(-k)}(\mathbf{x}; \boldsymbol{\theta}) = \sum_{i \in \mathcal{I}^{(-k)}} c_i^{(-k)}(\boldsymbol{\theta}) k(\mathbf{x}_i, \mathbf{x}; \boldsymbol{\theta}) + b^{(-k)}(\boldsymbol{\theta}) , \tag{II.103}$$

where $\boldsymbol{\theta}$ are given hyperparameter values (same values for $k = 1, \dots, K$), and where $c_i^{(-k)}(\boldsymbol{\theta})$ and $b^{(-k)}(\boldsymbol{\theta})$ are the coefficient solutions of the corresponding dual optimization problem.

K trainings are performed and the CV error is given by averaging the errors committed on $\mathcal{T}^{(k)}$ for $k = 1, \dots, K$:

$$\widehat{\mathrm{Err}}_{K\text{-CV},\ell}(\boldsymbol{\theta}) = \frac{1}{K} \sum_{k=1}^{K} \frac{1}{\#\mathcal{I}^{(k)}} \sum_{i \in \mathcal{I}^{(k)}} \ell\left(y_i, \widetilde{f}^{(-k)}(\mathbf{x}_i; \boldsymbol{\theta})\right) , \tag{II.104}$$

where ℓ is a given loss function. This loss function is chosen as a measure of errors, and has no connection with the loss function used in the SVM formulation. In practice, it is often taken as the square loss $\ell(y,u) = (y-u)^2$ or the absolute loss $\ell(y,u) = |y-u|$ for regression, and the 0-1 loss for classification. It worth pointing out that the CV error is an estimate (hat notation) since there are many choices when selecting the K folds.

In order to reduce the variance of the CV error, we may consider repeating the CV M times using different random subsets $\{\mathcal{T}^{(1,m)}, \dots, \mathcal{T}^{(K,m)}\}$, $m = 1, \dots, M$, and averaging the errors of the M CVs. Let us therefore consider M random sets of indices $\{\mathcal{I}^{(1,m)}, \dots, \mathcal{I}^{(K,m)}\}$ verifying Eq. (II.101) for $m = 1, \dots, M$ with the associated complementary sets $\{\mathcal{I}^{(-1,m)}, \dots, \mathcal{I}^{(-K,m)}\}$ and such that $\#\mathcal{I}^{(k,m)} \approx \lfloor N/K \rceil$ for all m and k. The M-averaged K-fold CV error is expressed as follows:

$$\widehat{\mathrm{Err}}_{M,K\text{-CV},\ell}(\boldsymbol{\theta}) = \frac{1}{M} \sum_{m=1}^{M} \left\{ \frac{1}{K} \sum_{k=1}^{K} \frac{1}{\#\mathcal{I}^{(k,m)}} \sum_{i \in \mathcal{I}^{(k,m)}} \ell\left(y_i, \widetilde{f}^{(-k,m)}(\mathbf{x}_i; \boldsymbol{\theta})\right) \right\} . \tag{II.105}$$

Such a CV requires $M \times K$ SVM trainings for a given set of hyperparameter values $\boldsymbol{\theta}$.

The choice of K for CV is subject to debate and there are unfortunately no general rules for an "optimal" choice. For an in-depth analysis of CV, the reader may refer to Arlot and Celisse (2010), where the performances of CV are analyzed in various contexts, including classification and regression. Some asymptotic results can be obtained under certain restrictive assumptions, but they are unfortunately of little help since we are working with finite sets of training data. Among SVM practitioners, $K = 5$ or 10 is often assumed for model selection and only one CV is performed in order to keep CV runtime reasonable (i.e. $M = 1$).

Leave-one-out cross-validation (LOO-CV) is obtained in the limiting case $K = N$, for which we have $\mathcal{I}^{(k)} = \{k\}$ (and therefore $\#\mathcal{I}^{(k)} = 1$) and $\mathcal{I}^{(-k)} = \{1, \dots, N\} \setminus \{k\}$. For each $k = 1, \dots, N$, a SVM model is trained on the $(N-1)$ data pairs of the set $\mathcal{T}^{(-k)}$ and is tested on the left-out pair $(\mathbf{x}_k, y_k)$. The LOO-CV error (simply termed LOO error in the sequel) thus writes:

$$\mathrm{Err}_{\mathrm{LOO},\ell}(\boldsymbol{\theta}) = \frac{1}{N} \sum_{i=1}^{N} \ell\left(y_i, \widetilde{f}^{(-i)}(\mathbf{x}_i; \boldsymbol{\theta})\right) . \tag{II.106}$$

In this specific case, the CV error is not an estimate since there is a single possible choice. LOO-CV is known to give an *almost* unbiased estimate of the generalization error (see, e.g., Chapelle et al., 2002). The bias is due to the training on $N-1$ data pairs instead of the full set of N pairs. Intuitively, LOO-CV is

expected to give a better estimate than K-fold CV in the case of low-sample training sets[11] since almost of the information of $\mathcal{T}$ is used to train each of the N SVM models. However the variance of the CV error also needs to be considered, due to the limited amount of known data and the way the training samples are selected. According to Efron (1983), LOO-CV is characterized by a large variance in the context of small training sets. In practical situations LOO-CV is often too demanding in terms of computational resources, since it requires N model trainings. Approximations or bounds of the LOO error are often preferred, as presented in the following section.

II–2.4.2 Approximations of the LOO error

For shorter and clearer notations, the hyperparameter vector $\boldsymbol{\theta}$ is dropped in all the expressions of this section. All quantities have therefore to be understood for a given $\boldsymbol{\theta}$.

(a) Classification (L1-SVC)

In classification, the LOO error is expressed in terms of the number of misclassified points:

$$\begin{aligned} \mathrm{Err}_{\mathrm{LOO},\ell_{0\text{-}1}} &= \frac{1}{N} \#\left\{i \in \{1,\dots,N\} : y_i \neq \operatorname{sgn} \widetilde{f}^{(-i)}(\mathbf{x}_i)\right\} \\ &= \frac{1}{N}\sum_{i=1}^{N} \ell_{0\text{-}1}\left(y_i, \widetilde{f}^{(-i)}(\mathbf{x}_i)\right) \\ &= \frac{1}{N}\sum_{i=1}^{N} \Psi\left(-y_i\, \widetilde{f}^{(-i)}(\mathbf{x}_i)\right) , \end{aligned} \tag{II.107}$$

where $\ell_{0\text{-}1}(y,u) = \Psi(-yu)$ is the 0-1 loss function, see Figure II.5a, and Ψ is the unit step function: $\Psi(x) = 1$ if $x > 0$, 0 otherwise.

The LOO error can also be equivalently rewritten in the following form:

$$\mathrm{Err}_{\mathrm{LOO},\ell_{0\text{-}1}} = \frac{1}{N}\sum_{i=1}^{N} \Psi\left(-y_i\, \widetilde{f}(\mathbf{x}_i) + y_i\left[\widetilde{f}(\mathbf{x}_i) - \widetilde{f}^{(-i)}(\mathbf{x}_i)\right]\right) . \tag{II.108}$$

Several expressions have been proposed to upper-bound the LOO error in classification (see, e.g., Chapelle et al., 2002). The simplest one is obtained as the ratio of the number of SVs over N in the case of hard-margin SVCs. Other bounds have been derived, such as the Jaakkola-Haussler, the Opper-Winter and the radius-margin bounds. These bounds are derived for SVCs without a bias term and the last two bounds are only valid for the hard-margin case. Another more accurate estimate of the LOO error, known as the *span bound*, was proposed by Vapnik and Chapelle (2000) (see also Chapelle, 2004, for a more detailed description). This estimate is based on the geometrical concept of *span* of the SV $\mathbf{x}_i$, denoted S_i for $i = 1,\dots,N$ and given by the following distance in the feature space:

$$S_i = \operatorname{dist}(\phi(\mathbf{x}_i), \Lambda_i) = \min_{\mathbf{z}\in\Lambda_i} \|\phi(\mathbf{x}_i) - \mathbf{z}\| , \tag{II.109}$$

where the set Λ_i is a constrained linear combination of the points $\{\phi(\mathbf{x}_j) : j \neq i\}$, defined as follows for L1-SVC:

$$\Lambda_i = \left\{ \sum_{j\in\mathcal{I}_{\mathrm{usv}}, j\neq i} \lambda_j \phi(\mathbf{x}_j) \,:\, \lambda_j \in \mathbb{R} \,,\, \sum_{j\in\mathcal{I}_{\mathrm{usv}}, j\neq i} \lambda_j = 1 \,,\, \forall j \neq i,\ 0 \leq \alpha_j + y_j y_i \alpha_i \lambda_j \leq C \right\} . \tag{II.110}$$

[11] Note that this corresponds to the context of surrogate models of costly-to-evaluate functions.

Under the assumption that the set of both unbounded and bounded SVs remains unchanged during the LOO-CV, i.e. $\mathcal{I}_{\text{usv}}^{(-i)} = \mathcal{I}_{\text{usv}}$ and $\mathcal{I}_{\text{bsv}}^{(-i)} = \mathcal{I}_{\text{bsv}}$ for $i = 1, \dots, N$, Vapnik and Chapelle (2000) demonstrate that the following equality holds true, for $i = 1, \dots, N$:

$$y_i \left[\widetilde{f}(\mathbf{x}_i) - \widetilde{f}^{(-i)}(\mathbf{x}_i) \right] = \alpha_i S_i^2 \,. \tag{II.111}$$

Under this assumption, the expression of Λ_i can be simplified to:

$$\Lambda_i = \left\{ \sum_{j \in \mathcal{I}_{\text{usv}}, j \neq i} \lambda_j \phi(\mathbf{x}_j) \,:\, \lambda_j \in \mathbb{R} \,,\, \sum_{j \in \mathcal{I}_{\text{usv}}, j \neq i} \lambda_j = 1 \right\} , \tag{II.112}$$

and the LOO error rewrites:

$$\begin{aligned} \text{Err}_{\text{LOO},\ell_{0\text{-}1}} \approx \text{Err}_{\text{LOO},\ell_{0\text{-}1}}^{\text{span}} &= \frac{1}{N} \sum_{i=1}^{N} \Psi\left(-y_i \widetilde{f}(\mathbf{x}_i) + \alpha_i S_i^2 \right) \\ &= \frac{1}{N} \, \# \left\{ i \in \{1, \dots, N\} : \alpha_i S_i^2 \geq y_i \widetilde{f}(\mathbf{x}_i) \right\} \,. \end{aligned} \tag{II.113}$$

$\text{Err}_{\text{LOO},\ell_{0\text{-}1}}^{\text{span}}$ will be used as an *approximation* of the true LOO error. This is not an upper bound, as pointed out by Schölkopf and Smola (2001), since the main assumption (the sets of SVs do not change in LOO-CV) has no chance of being verified in general.

Another important point is that $\text{Err}_{\text{LOO},\ell_{0\text{-}1}}^{\text{span}}$ is not a continuous function. The spans S_i are not continuous (Chapelle et al., 2002), and discontinuities also appear due the use of the step function Ψ in the definition of the span approximation of the LOO error. This makes the minimization of the estimate of the LOO error harder to solve, as later addressed in Section II–2.4.3.

Practically, the span bound S_i can be computed as follows (Chapelle, 2004):

- $\mathbf{x}_i$ is an unbounded SV:

$$S_i^2 = \frac{1}{(\widetilde{\mathbf{K}}_{\text{SV}}^{-1})_{ii}} \quad \text{for } i \in \mathcal{I}_{\text{usv}} \,, \tag{II.114a}$$

  where $\widetilde{\mathbf{K}}_{\text{SV}} = \begin{bmatrix} \mathbf{K}_{\text{u}} & \mathbf{1} \\ \mathbf{1}^{\text{T}} & 0 \end{bmatrix}$, $\mathbf{K}_{\text{u}} = [k_{\text{u},ij}]_{1 \leq i,j \leq \#\mathcal{I}_{\text{usv}}}$ and $k_{\text{u},ij} = k(\mathbf{x}_i, \mathbf{x}_j)$ for $i, j \in \mathcal{I}_{\text{usv}}$.

- $\mathbf{x}_i$ is a bounded SV:

$$S_i^2 = k(\mathbf{x}_i, \mathbf{x}_i) - \mathbf{v}_i^{\text{T}} \widetilde{\mathbf{K}}_{\text{SV}}^{-1} \mathbf{v}_i \quad \text{for } i \in \mathcal{I}_{\text{bsv}} \,, \tag{II.114b}$$

  where $\mathbf{v}_i$ is a $(\#\mathcal{I}_{\text{usv}} + 1)$-dimensional column vector whose j^{th} element is $k(\mathbf{x}_i, \mathbf{x}_j)$ for $j \in \mathcal{I}_{\text{usv}}$ and whose last element is 1.

- $\mathbf{x}_i$ is not a SV:

$$S_i^2 = 0 \quad \text{for } i \in \overline{\mathcal{I}}_{\text{sv}} \,, \tag{II.114c}$$

  since $\widetilde{f}^{(-i)} = \widetilde{f}$.

(b) Regression (L1-ϵ-SVR)

Similarly to classification, span approximations of the LOO error were derived by Chang and Lin (2005) for regression, based on the ϵ-insensitive loss function. The LOO error considered by Chang and Lin is based on the absolute loss function $\ell_1(y,u) = |y-u|$:

$$\begin{aligned} \mathrm{Err}_{\mathrm{LOO},\ell_1} &= \frac{1}{N}\sum_{i=1}^{N} \ell_1\left(y_i, \widetilde{f}^{(-i)}(\mathbf{x}_i)\right) \\ &= \frac{1}{N}\sum_{i=1}^{N} |y_i - \widetilde{f}^{(-i)}(\mathbf{x}_i)| \,. \end{aligned} \tag{II.115}$$

Under the assumption that the set of SVs remains the same during LOO-CV, the following approximations of the LOO error are obtained for L1-ϵ-SVR[12]:

$$\mathrm{Err}_{\mathrm{LOO},\ell_1} \approx \mathrm{Err}^{\mathrm{span}}_{\mathrm{LOO},\ell_1} = \frac{1}{N}\sum_{i=1}^{N}(\alpha_i + \alpha_i^*)S_i^2 + \frac{1}{N}\sum_{i=1}^{N}(\xi_i + \xi_i^*) + \epsilon \,, \tag{II.116}$$

where the span S_i is given by Eqs (II.114a-II.114b-II.114c) and where:

$$\begin{aligned} \mathcal{I}_{\mathrm{usv}} &= \{i \in \{1,\ldots,N\} : 0 < \alpha_i < C \vee 0 < \alpha_i^* < C\} \equiv \{i \in \{1,\ldots,N\} : 0 < \alpha_i + \alpha_i^* < C\} \,, \\ \mathcal{I}_{\mathrm{bsv}} &= \{i \in \{1,\ldots,N\} : \alpha_i = C \vee \alpha_i^* = C\} \,, \\ \overline{\mathcal{I}}_{\mathrm{sv}} &= \{i \in \{1,\ldots,N\} : \alpha_i = 0 \wedge \alpha_i^* = 0\} \,, \end{aligned} \tag{II.117}$$

in which $\vee$ denotes the OR operator and $\wedge$ denotes the AND operator.

As for soft margin classification, it is shown that the spans S_i of ϵ-SVR are not continuous (Chang and Lin, 2005).

(c) Regression (LS-SVR)

For LS-SVR, an exact expression of LOO error can be obtained. Let us define the LOO error in terms of the square loss $\ell_2(y,u) = (y-u)^2$:

$$\begin{aligned} \mathrm{Err}_{\mathrm{LOO},\ell_2} &= \frac{1}{N}\sum_{i=1}^{N} \ell_2\left(y_i, \widetilde{f}^{(-i)}(\mathbf{x}_i)\right) \\ &= \frac{1}{N}\sum_{i=1}^{N} \left(y_i - \widetilde{f}^{(-i)}(\mathbf{x}_i)\right)^2 \\ &= \frac{1}{N}\mathrm{PRESS} \,, \end{aligned} \tag{II.118}$$

where PRESS is Allen's predicted residual sum of squares statistic (Allen, 1974).

For $i = 1,\ldots,N$, the loss between y_i and $\widetilde{f}^{(-i)}(\mathbf{x}_i)$ is given by (see, e.g., Cawley et al., 2006, Appendix A):

$$y_i - \widetilde{f}^{(-i)}(\mathbf{x}_i) = \frac{\alpha_i}{\left(\widetilde{\mathbf{K}}^{-1}\right)_{ii}} \,, \tag{II.119}$$

[12] An approximation of the LOO error is also available for L2-ϵ-SVR (Chang and Lin, 2005). It is given by the sum of the first and last terms of Eq. (II.116).

where $\boldsymbol{\alpha} = (\alpha_1, \ldots, \alpha_N)^{\mathrm{T}}$ is the solution of Eq. (II.65),
and where $\left(\widetilde{\mathbf{K}}^{-1}\right)_{ii}$ is the i^{th} diagonal element of the inverse of $\widetilde{\mathbf{K}} = \begin{bmatrix} \mathbf{K} + C^{-1}\mathbf{I} & \mathbf{1} \\ \mathbf{1}^{\mathrm{T}} & 0 \end{bmatrix}$.

The *exact* LOO error for LS-SVR therefore writes:

$$\mathrm{Err}_{\mathrm{LOO},\ell_2} = \frac{1}{N}\sum_{i=1}^{N} \frac{\alpha_i^2}{\left(\widetilde{\mathbf{K}}^{-1}\right)_{ii}^2} \,. \tag{II.120}$$

II–2.4.3 Strategies for optimal hyperparameter selection

Several strategies have been proposed for the selection of optimal (or nearly optimal) values of SVM model hyperparameters. The most popular strategies, sorted by increasing complexity, are briefly outlined in this section. Due to the popularity of the isotropic Gaussian RBF kernel in SVMs, most of the techniques found in the literature aim at finding suitable values for C and γ (or σ) in soft-margin classification, and additionally for ϵ in regression based on the ϵ-insensitive loss function. Tackling problems with a large number of hyperparameters is less common in SVMs (see, e.g., Chapelle et al., 2002) for the tuning of the anisotropic Gaussian RBF kernel given in Eq. (II.76). For such problems, model selection becomes much more complex.

If the runtime for model selection is a concern, heuristic choices for the hyperparameter values may be considered, see the following examples suggested for a Gaussian RBF kernel:

- Selection of σ: For SVC classification, Jaakkola et al. (1999) propose to take σ as the median distance in the input space $\mathcal{X}$ between all pairs composed of one point from the positive class and another from the negative class.
- Selection of C: Following the work of Mattera and Haykin (1999), which suggests taking a value for C in the range of the output response, Cherkassky and Ma (2004) propose to take C equal to $\max(|\overline{y} - 3s_y^*|, |\overline{y} + 3s_y^*|)$, where $\overline{y}$ and s_y^* are respectively the mean and standard deviation of the y-values of the training data.
- Selection of ϵ: In Cherkassky and Ma (2004), it is proposed to take $\epsilon = 3\sigma\sqrt{\ln N / N}$ where σ is an estimated noise level and N is the number of training data elements.

From the author's experience, such heuristics as those defined above are not able to give SVM models of suitable accuracy in the context of function approximation based on few training data elements.

Among SVM practitioners, the most common technique for tuning the hyperparameters of a SVM model is called *grid search* (see, e.g., Hsu et al., 2016). This simple yet efficient technique consists in estimating the generalization error (usually by means of a K-fold CV) over a grid $\mathcal{G}$ composed of all combinations of exponentially growing sequences of values of the SVM hyperparameters:

$$\mathcal{G} = \mathcal{G}_1 \times \ldots \times \mathcal{G}_{n_{\boldsymbol{\theta}}} \quad \text{where} \quad \mathcal{G}_i = \{b^{a_i + j(b_i - a_i)/N_i}, 0 \leq j \leq N_i\} \quad \text{for } i = 1, \ldots, n_{\boldsymbol{\theta}} \,, \tag{II.121}$$

where b defines the basis of the log-scale used for the grid (a usual choice is $b = 2$), $[a_i, b_i]$ defines the $\log_b$-range over which the hyperparameter θ_i is sought, and N_i defines the associated grid resolution.

The best model is then the one which achieves the minimal generalization error over the grid:

$$\boldsymbol{\theta}^* = \underset{\boldsymbol{\theta} \in \mathcal{G}}{\arg\min}\, \widehat{\mathrm{Err}}_{K\text{-CV},\ell}(\boldsymbol{\theta}) \,, \tag{II.122}$$

where $\boldsymbol{\theta} = (\theta_1, \ldots, \theta_{n_{\boldsymbol{\theta}}})$.

Grid search, however, presents two main drawbacks. First the exploration of the hyperparameter space $\Theta = [b^{a_1}, b^{b_1}] \times \ldots \times [b^{a_{n_{\boldsymbol{\theta}}}}, b^{b_{n_{\boldsymbol{\theta}}}}]$ is discrete. If the solution $\boldsymbol{\theta}^*$ is required to be found with high accuracy, we need to define a very fine grid, which may result in too expensive a hyperparameter

selection procedure. The second drawback is that grid search cannot be used for the tuning of many hyperpameters, since the number of combinations grows too fast with $n_{\boldsymbol{\theta}}$. As an example, if we consider L1-ϵ-SVR with a Gaussian RBF kernel, we need to find an optimal triple (C, ϵ, γ). If we take a $20\times20\times20$ grid (which is a rather coarse grid) and a 5-fold cross validation, we need to solve $20 \times 20 \times 20 \times 5 = 40,000$ QP problems in order to tune C, ϵ and γ.

As an alternative, robust optimization algorithms can be used to solve the hyperparameter selection problem. Two main types of methods have been investigated in the SVM context. A first solution is a recourse to stochastic optimization algorithms. Several techniques have been applied for the tuning of SVM hyperparameters, such as simulated annealing (Pai and Hong, 2006; Lin et al., 2008a), the particle swarm optimization method (Lin et al., 2008b; Fei et al., 2009), the cross-entropy method (Bourinet, 2014; Bourinet, 2015; Bourinet, 2016) and the covariance matrix adaptation evolution strategy (Bourinet, 2017b) among others. The second solution consists in using gradient-descent algorithms under the assumption that the gradient can be derived for the estimate of the generalization error chosen for the analysis. With span approximations, it is first necessary to adapt the formulation for a smooth estimate, since these approximations are not continuous. Such smooth estimates are usually obtained by introducing an additional regularization term in the definition of the span of SVs (see, e.g., Chapelle, 2004, pp. 71–73, for classification, and Chang and Lin, 2005, for regression). Such a gradient-based approach can also be applied with other approximations than the span estimate (see, e.g., Keerthi, 2002; Chung et al., 2003, where a BFGS optimization algorithm is used to minimize the radius/margin bound).

We give hereafter some details about hyperparameter selection based on the LOO error approximations introduced in Section II–2.4.2. Assuming that these LOO error estimates are good proxies of the true and unknown generalization error, finding optimal hyperparameter values consists in solving the following optimization problem:

$$\boldsymbol{\theta}^* = \arg\min_{\boldsymbol{\theta}\in\Theta} \widetilde{\mathrm{Err}}_{\mathrm{LOO}}(\boldsymbol{\theta}) \,, \tag{II.123}$$

where:

- $\widetilde{\mathrm{Err}}_{\mathrm{LOO}} = \mathrm{Err}^{\mathrm{span}}_{\mathrm{LOO},\ell_{0\text{-}1}}$ (approximation) for Lp-SVC, $p \in \{1,2\}$,
- $\widetilde{\mathrm{Err}}_{\mathrm{LOO}} = \mathrm{Err}^{\mathrm{span}}_{\mathrm{LOO},\ell_1}$ (approximation) for Lp-ϵ-SVR, $p \in \{1,2\}$,
- and $\widetilde{\mathrm{Err}}_{\mathrm{LOO}} = \mathrm{Err}_{\mathrm{LOO},\ell_2}$ (exact) for LS-SVR.

First, we need to make some important comments, which justify the favored solving strategy w.r.t. those commonly applied in other works in the literature:

- The accuracy of the LOO error estimates is closely related to that achieved in the solution of the dual optimization problem, i.e. on the coefficients α_i of the kernel expansion (and α_i^* in the case of ϵ-SVR) and on the bias term b. For accurate estimates of the LOO error, the QP problems of soft margin SVC and ϵ-SVR need to be solved by interior point algorithms instead of usually-preferred SMO algorithms.
- In the optimization problem defined in Eq. (II.123), the domain Θ in which the solution is sought needs to be defined. In the case of a Gaussian RBF kernel, the searches are usually carried out within the following bounds: $\log_{10} C \in [-5,4]$, $\log_{10}\epsilon \in [-4,0]$ and $\log_{10}\gamma \in [-9,4]$. In the proposed approach, the search is allowed beyond these bounds, and this is where the optimal hyperparameter values often lie. In particular, the optimal C parameter is found to take large values, e.g. 10^7-10^8 (this results in longer QP solving times), and the optimal ϵ parameter takes small values, e.g. 10^{-7}-10^{-6}, see Figure II.6.

- In the author's experience, the slight regularization of the span approximation of the LOO error proposed by Chapelle (2004) for SVC and by Chang and Lin (2005) for ϵ-SVR induces unacceptably large variations of the LOO error estimate, resulting in non-optimal values for the hyperparameters. For this reason, a stochastic search directly applied to the span estimate without any regularization is preferred.
- The optimization problem defined in Eq. (II.123) appears rather noisy, with many local minima, which precludes the use of gradient-descent algorithms. The choice made here is to apply a robust stochastic optimization algorithm in order to find the lowest minimum in Θ. The direction followed here goes against the common practice, which assumes that it is not necessary to find the true minimizer of the generalization error estimate in order to obtain good hyperparameter values, as recommended e.g. by Keerthi (2002) and Chung et al. (2003).

The cross-entropy (CE) method presented in Section I–3.3.2 in the context of the estimation of rare event probabilities can also be used for continuous optimization, as described in Botev et al. (2013). The CE method has been applied to hyperparameter selection of soft margin classification with L1-SVC (Bourinet, 2014) and regression with L1-ϵ-SVR (Bourinet, 2015; Bourinet, 2016). In these works it was used in the specific context of an isotropic Gaussian kernel, which involves a small number of hyperparameters to tune (2 for classification and 3 for regression based on the ϵ-insensitive loss function). With kernels involving many parameters to tune, such as the anisotropic Gaussian kernel, the covariance matrix adaptation evolution strategy (CMA-ES) algorithm proposed by Hansen (2016) appears more appropriate than its CE counterpart, as reported by Bourinet (2017b) and Moustapha et al. (2018).

For the sake of illustration, we describe hereafter the CE-algorithm applied to hyperparameter selection of L1-ϵ-SVR based on a Gaussian RBF kernel (Bourinet, 2016):

1. The hyperparameter space Θ is explored in base-10 logarithmic scale. Formulating the optimization problem in log-scale is a common practice that brings stability to optimization algorithms (see, e.g., Chapelle et al., 2002). Let us denote $\log_{10}\boldsymbol{\theta} = (\log_{10} C, \log_{10}\epsilon, \log_{10}\gamma)$ a given point in Θ. Let us define the following base-10 logarithmic ranges for $\log_{10}\boldsymbol{\theta}$: $\log_{10} C \in [a_C, b_C]$, $\log_{10}\epsilon \in [a_\epsilon, b_\epsilon]$, $\log_{10}\gamma \in [a_\gamma, b_\gamma]$ (line 2 of Table II.2).
2. At each iteration $s > 0$, the following sample $\{\log_{10}\boldsymbol{\theta}^{(k)}, 1 \leq k \leq K\}$ is composed of realizations of 3 independent and truncated normal PDFs (line 8). $\widehat{\boldsymbol{\mu}}_{t-1}$ and $\widehat{\boldsymbol{\sigma}}_{t-1}$ respectively denote the mean and standard deviation vectors of the corresponding untruncated normal PDFs. $[\mathbf{a}, \mathbf{b}] = [a_C, b_C] \times [a_\epsilon, b_\epsilon] \times [a_\gamma, b_\gamma]$ defines the supports of the truncated normal PDFs.
3. K SVR models are trained (lines 9–11) and the respective span approximations of the LOO error are assessed from Eq. (II.116). These K SVR trainings are independent and can be run in parallel to reduce the time spent in hyperparameter selection.
4. The so-called elite set of samples $\{\log_{10}\boldsymbol{\theta}^{(k)}, k \in \mathcal{I}_{\text{el}}\}$ is composed of the $N_{\text{el}} = \#\mathcal{I}_{\text{el}} = \lceil \rho K \rceil$ samples whose approximations of the LOO error are lower than the sample ρ-quantile of $\{\widetilde{\text{Err}}^{(k)}_{\text{LOO}}, 1 \leq k \leq K\}$ (lines 12–13).
5. From the elite set of samples, new values $\widetilde{\boldsymbol{\mu}}_s$ and $\widetilde{\boldsymbol{\sigma}}_s$ are respectively proposed for means and standard deviations of the untruncated normal PDFs (lines 19–20). These values are smoothed using a parameter α in order to define the distribution parameters used at the next iteration. The best candidate obtained so far, denoted $\boldsymbol{\theta}_{\text{best}}$, is used for the updated mean vector $\widehat{\boldsymbol{\mu}}_s$, and the current standard deviation vector $\widehat{\boldsymbol{\sigma}}_{s-1}$ is used for the updated standard deviation vector $\widehat{\boldsymbol{\sigma}}_s$ (lines 21–22).
6. The algorithm iterates until the standard deviation components $\widehat{\sigma}_{s;j}$, $j = 1, \ldots, 3$, all fall below a prescribed accuracy level (line 23).

The following settings have been found to ensure a sufficient level of accuracy of the SVR models. Such settings are used in the ASVR method presented later in Section II–3.3.

- sample size $K = 300$, parameter $\rho = 0.05$,

- base-10 log-range for parameter C: $[a_C, b_C] = [0, 16]$,
- base-10 log-range for parameter ϵ: $[a_\epsilon, b_\epsilon] = [-13 + \log_{10}(y_{\max} - y_{\min}), \log_{10}(y_{\max} - y_{\min})]$, where $y_{\min} = \min\{y_i, 1 \leq i \leq N\}$ and $y_{\max} = \max\{y_i, 1 \leq i \leq N\}$,
- base-10 log-range for parameter γ: $[a_\gamma, b_\gamma] = [-16, \log_{10}(1/(2d_{\min}^2))]$, where $d_{\min}$ represents the minimal pairwise-distance between $\{\mathbf{x}_i, 1 \leq i \leq N\}$,
- constant static smoothing parameter: $\alpha = 0.4$,
- standard deviation threshold values for convergence of the CE algorithm: $\sigma_{\text{th};C} = 0.1$, $\sigma_{\text{th};\epsilon} = 0.5$, $\sigma_{\text{th};\gamma} = 0.1$.

1	// **initialization**	
2	$\mathbf{a} = (a_C, a_\epsilon, a_\gamma)$, $\mathbf{b} = (b_C, b_\epsilon, b_\gamma)$	// lower and upper bounds for $\log_{10} C$, $\log_{10} \epsilon$ and $\log_{10} \gamma$
3	$\widehat{\boldsymbol{\mu}}_0 = (\mathbf{a} + \mathbf{b})/2$, $\widehat{\boldsymbol{\sigma}}_0 = 100\,(\mathbf{b} - \mathbf{a})$	// initial means and standard deviations
4	$\widetilde{\text{err}}_{\text{loo,min}} = +\infty$	// minimal value of LOO error span approximation
5	$s = 0$	// iteration counter
6	**do**	
7	$s = s + 1$	
8	Draw $\log_{10} \boldsymbol{\theta}^{(1)}, \ldots, \log_{10} \boldsymbol{\theta}^{(K)} \overset{\text{i.i.d.}}{\sim} \mathcal{N}_{[\mathbf{a},\mathbf{b}]}(\widehat{\boldsymbol{\mu}}_{s-1}, \widehat{\boldsymbol{\sigma}}_{s-1})$ where $\widehat{\boldsymbol{\mu}}_{s-1}$ and $\widehat{\boldsymbol{\sigma}}_{s-1}$ denote the vectors of means and standard deviations of the untruncated normal PDFs	
9	**for** $k = 1$ **to** K	
10	$(\widetilde{f}^{(k)}, \widetilde{\text{Err}}_{\text{LOO}}^{(k)}) = \textbf{train}(\mathcal{T}, \boldsymbol{\theta}^{(k)})$ where $\mathcal{T} = \{(\mathbf{x}_i, y_i) \in \mathcal{X} \times \mathbb{R}, 1 \leq i \leq N\}$	
11	**end for**	
12	Define the sample ρ-quantile $\widetilde{\text{err}}_{\text{loo},s}$ of $\{\widetilde{\text{Err}}_{\text{LOO}}^{(k)}, 1 \leq k \leq K\}$	
13	Define the elite set of indices $\mathcal{I}_{\text{el}} = \{k \in \{1, \ldots, K\} : \widetilde{\text{Err}}_{\text{LOO}}^{(k)} \leq \widetilde{\text{err}}_{\text{loo},s}\}$	
14	Define the indice of the sample with lowest LOO error $k_{\text{best}} = \arg\min_k \{\widetilde{\text{Err}}_{\text{LOO}}^{(k)}, 1 \leq k \leq K\}$	
15	**if** $\widetilde{\text{Err}}_{\text{LOO}}^{(k_{\text{best}})} < \widetilde{\text{err}}_{\text{loo,min}}$ **then**	
16	$\widetilde{\text{err}}_{\text{loo,min}} = \widetilde{\text{Err}}_{\text{LOO}}^{(k_{\text{best}})}$	// minimal LOO error obtained so far
17	$\boldsymbol{\theta}_{\text{best}} = \boldsymbol{\theta}^{(k_{\text{best}})}$, $\widetilde{f}_{\text{best}} = \widetilde{f}^{(k_{\text{best}})}$	// best solution obtained so far
18	**end if**	
19	$\widetilde{\mu}_{s;j} = \dfrac{1}{\#\mathcal{I}_{\text{el}}} \displaystyle\sum_{k \in \mathcal{I}_{\text{el}}} \theta_j^{(k)}$ for $j = 1, 2, 3$	// mean update
20	$\widetilde{\sigma}_{s;j}^2 = \dfrac{1}{\#\mathcal{I}_{\text{el}}} \displaystyle\sum_{k \in \mathcal{I}_{\text{el}}} (\theta_j^{(k)} - \widetilde{\mu}_{s;j})^2$ for $j = 1, 2, 3$	// variance update
21	$\widehat{\boldsymbol{\mu}}_s = \alpha \widetilde{\boldsymbol{\mu}}_s + (1 - \alpha) \log_{10} \boldsymbol{\theta}_{\text{best}}$	// static smoothing of means
22	$\widehat{\boldsymbol{\sigma}}_s = \alpha \widetilde{\boldsymbol{\sigma}}_s + (1 - \alpha) \widehat{\boldsymbol{\sigma}}_{s-1}$	// static smoothing of standard deviations
23	**while** $(\widehat{\sigma}_{s;1} > \sigma_{\text{th};C})$ **or** $(\widehat{\sigma}_{s;2} > \sigma_{\text{th};\epsilon})$ **or** $(\widehat{\sigma}_{s;3} > \sigma_{\text{th};\gamma})$	
24	$\boldsymbol{\theta}^* = \boldsymbol{\theta}_{\text{best}}$, $\widetilde{f}^* = \widetilde{f}_{\text{best}}$	// optimal hyperparameter values, optimal SVR model

Table II.2 – Pseudo-code of the proposed CE algorithm for hyperparameter selection.

In Figure II.6, a representation of the LOO error estimate is given at the optimal triple (C, ϵ, γ) found by the CE method. This representation is made through the three pairwise cross-cuts $(\log_{10} \gamma, \log_{10} C)$, $(\log_{10} \gamma, \log_{10} \epsilon)$ and $(\log_{10} \epsilon, \log_{10} C)$, the third parameter being set equal to its optimal value. The training set $\mathcal{T} = \{(\mathbf{x}_i, y_i) \in \mathcal{X} \times \mathbb{R}, 1 \leq i \leq N\}$ is the one used to construct the final LSF surrogate with the ASVR method, see Section II–3.3. These representations are given for example 1 with $\mu_{F_s} = 27.5$ where $N = 250$ (top plots) and example 2 with $n = 100$ where $N = 480$ (bottom plots).

A first comment is that the optimal triple (C, ϵ, γ) is found in a very flat basin and at the limits of the solutions that can be obtained by the interior point method. The white areas correspond to solutions that are either not feasible or not converged. A second comment is that the shapes of the iso-LOO-error

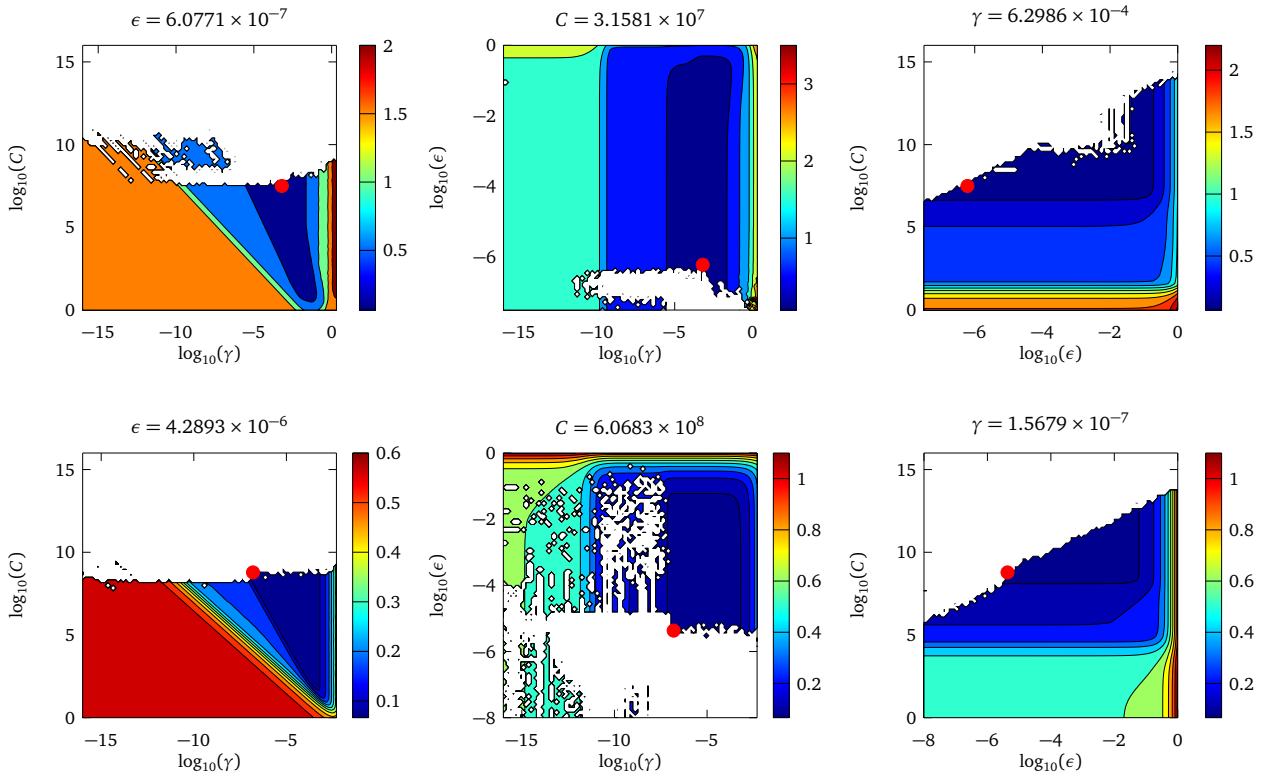

Figure II.6 – Span approximation of the LOO error. Example 1, $\mu_{F_s} = 27.5$, $N = 250$ (top plots). Example 2, $n = 100$, $N = 480$ (bottom plots). Cross-cut $(\log_{10}\gamma, \log_{10} C)$ for optimal ϵ (left), cross-cut $(\log_{10}\gamma, \log_{10}\epsilon)$ for optimal C (middle), cross-cut $(\log_{10}\epsilon, \log_{10} C)$ for optimal γ (right).

contours of the $(\log_{10}\gamma, \log_{10} C)$-plot are quite independent of the considered example (similar shapes are also observed for other examples than the two presented ones). These iso-contours are in close agreement with the generic shape reported by Keerthi and Lin (2003), whose proposal is to select an optimal pair $(\log_{10} C, \log_{10}\gamma)$ (in a classification context) along a given line going through the flat basin.

The CE algorithm used in classification and applied in Bourinet (2014) is not given for the sake of brevity. It is important to point out that the definition of the elite set of samples in such a context cannot be made based on the sole consideration of the span estimate of the LOO error. Several pairs $(\log_{10} C, \log_{10}\gamma)$ may in fact ensure a zero LOO error estimate and we need to add extra criteria to define the elite set of samples. It is proposed to select the samples with the lowest training errors among those ensuring a zero LOO error. If the size of this set is still greater than $\lceil \rho K \rceil$, then we suggest keeping the samples achieving the lowest level of regularization on the SVC solution, i.e. corresponding to the lowest parameter C. It is worth noting that this approach differs from the one proposed by Basudhar (2011), which consists in selecting the lowest γ parameter under the assumption of no training errors ensured by a sufficiently large value of C.

II–3 Surrogate-based reliability assessment

II–3.1 Short review of existing methods

This section gives a short overview of the works based on surrogate models in the specific context of small failure probability estimation. These works are mainly applied to structural mechanics problems, and are therefore referred to as structural reliability problems in the literature. The reader may find ad-

ditional details in the following references focusing on uncertainty propagation (Hurtado and Alvarez, 2001; Gomes and Awruch, 2004; Bucher and Most, 2008; Sudret, 2012). The constructed approximate models are most often used as surrogate models, i.e. in replacement of a true and costly-to-evaluate function. Some other methods use these approximate models in conjunction with sampling methods, either to improve the performances of the sampling method or to correct the potential bias of the constructed approximate model.

(a) Polynomial response surfaces (RS), polynomial moving least-squares (MLS) regression

The first occurrence of *polynomial response surfaces* (RS) used as surrogates of limit-state functions (LSF) in structural mechanics is due to Faravelli (1989). This seminal work then inspired many other researchers in the nineties (Bucher and Bourgund, 1990; Enevoldsen et al., 1993; Rajashekhar and Ellingwood, 1993; Kim and Na, 1997; Das and Zheng, 2000), with variants of the method based on the choice of the polynomial approximation and the way the training points were selected to construct the RS. In all these works, a quadratic multivariate polynomial representation is assumed, with or without cross-terms, and the approximation is constructed in the neighborhood of a supposedly unique MPFP. A weighted quadratic polynomial regression was preferred by Bourinet et al. (2000), Kaymaz and McMahon (2005), and Nguyen et al. (2009). In Gayton et al. (2003), a complete quadratic polynomial approximation is used with a LOO procedure in order to derive confidence intervals on the MPFP. In order to limit the number of terms in the polynomial basis, Roussouly et al. (2013) used a forward regression method to select the most important terms. They also provide a bootstrap-based confidence interval on the failure probability. In all RS approaches, the quality of the approximate model and therefore of the failure probability estimate is highly dependent on the shape of the true LSS, as pointed out in some of these works. The failure probability estimate may be severely biased if the single MPFP assumption does not hold or if the polynomial approximation is too "rigid" for the true LSF. For a more flexible polynomial model, a local approximation of the true function may be preferred. This can be achieved by means of moving least-squares polynomial regression, as addressed by Bucher and Most (2008), Proppe (2008), and Kang et al. (2010) in the context of reliability assessment.

(b) Polynomial chaos expansions (PCE)

Polynomial chaos expansions (PCE) are rooted in the fundamental work of Ghanem and Spanos (1991) on stochastic finite elements, and the generalized version of PCEs is based on the Wiener-Askey extension of Xiu and Karniadakis (2002). Their non-intrusive use as LSF surrogates in reliability analysis was originally explored by Sudret (2000). The application of PCE surrogate models to structural reliability was further investigated in the works of Sudret and Der Kiureghian (2002) and Choi et al. (2004). For the estimation of rare failure events the accuracy of the PCE, usually achieved around mean values, must occur in the tail of the joint distribution of $\mathbf{X}$, more precisely in the most important subregions of the failure domain $\mathcal{F}_{\mathbf{x}}$. For this purpose, the idea of Paffrath and Wever (2007) is to use a shifted and windowed Hermite PCE to enhance the accuracy of the approximate model in the failure domain. The shift is selected based on a known FORM MPFP P^* and the windowed PCE corresponds to a local approximation around this MPFP. When the number of random inputs n is large, the number of terms in the PCE basis blows up and it is necessary to consider the construction of sparse PCE models. The most significant terms of the PCE are selected with adaptive algorithms in Blatman and Sudret (2010) and Hu and Youn (2011) and the proposed algorithms are applied to structural reliability problems. Sparse PCEs, based on least angle regression, are also proposed by Blatman and Sudret (2011), see the PhD manuscript of Blatman (2009) for further details.

(c) Artificial neural networks (ANN), radial basis function (RBF) networks

The first application of *artificial neural networks* (ANN) to structural reliability is due to Papadrakakis et al. (1996), based on the training of a feedforward multilayer perceptron (MLP). The authors' interest is in the collapse of elasto-plastic structures, and failure probabilities are assessed by means of crude MC and IS. The use of ANNs as surrogate models for reliability assessment was later investigated by several researchers, among whom Hurtado and Alvarez (2000), Deng et al. (2005), Hosni Elhewy et al. (2006), Most and Bucher (2006), Cardoso et al. (2008), and Cheng and Li (2008). In these works, the feedforward multilayer perceptron with three layers (i.e. with only one hidden layer) and a sigmoid transfer function is a common choice. In most cases, a crude MC simulation is applied to estimate the failure probability based on the ANN model. ANNs have also been used in conjunction with subset simulation (SS) to increase the number of samples per subset level and improve SS efficiency (Papadopoulos et al., 2012). Selecting an optimal ANN architecture with no prior information about the function to approximate is known to be a difficult task. The choices that are made have consequences on the quality of the ANN predictions. If too large a number of nodes is e.g. chosen in the hidden layers, the network can fit the data well (small empirical risk), but it is also well known that it will have poor prediction performances (large expected risk). Some simple heuristics or tricks are available to choose a "good" ANN architecture (see, e.g., LeCun et al., 1998), but these recommendations are rather general ones and the best architecture is often problem-dependent. Among ANNs, the use of *radial basis function* (RBF) networks is less common for reliability assessment (see, e.g., Deng, 2006, where three RBF networks are used with crude MC, FORM and SORM). The reader may also refer to Hurtado and Alvarez (2001) for an overview of MLP and RBF networks in the specific context of structural reliability, with details about their training.

(d) Support vector machines (SVM)

Support vector machines (SVM) were introduced to structural reliability by the seminal works of Rocco and Moreno (2002) and Hurtado and Alvarez (2003). In these works, the estimation of a failure probability is considered as a binary classification problem, where the two classes correspond to the failure and safe domains. In line with these original approaches, the use of SVC as surrogate models was also investigated by Deheeger and Lemaire (2006), Li et al. (2006), Most (2007), Basudhar et al. (2008), Basudhar and Missoum (2010), Bourinet et al. (2011), and Bourinet (2014). An alternative approach consists in approximating the LSF from a regression viewpoint. In such a case, the constructed approximation uses the full information provided by the evaluation of the LSF at the points of the training set (i.e. the values in $\mathbb{R}$), and not just the binary information given by the signs of these evaluations. This type of approach was followed by Pai and Hong (2006), Chen (2007), Yuan et al. (2009), Dai et al. (2012b), Bourinet (2015), Bourinet (2016), and Bourinet (2017b), by means of SVR based on the ϵ-insensitive loss function. The use of LS-SVM has remained rather marginal for reliability analysis (see, e.g., Guo and Bai, 2009b; Guo and Bai, 2009a; Wang et al., 2013, for application examples in classification and regression).

The training data set $\mathcal{T}$ is selected adaptively in general. In classification-based approaches, it has mainly been assumed that at least one data point was needed in the failure domain to start the adaptive training. One solution was often to consider sufficiently widespread initial samples to meet such a condition (see, e.g., Li et al., 2006). Note that it is not mandatory to have data points in the two classes to start the training process, see e.g. the adaptive method proposed by Bourinet (2014) which consists in selecting SVM classifiers associated with a decreasing sequence of positive LSF values, the final one being equal to zero and therefore corresponding to the LSS. In SVM classification, several strategies have been developed to generate new points which are sequentially added to the training set. In Deheeger and Lemaire (2006), it is suggested to take samples belonging to the SVC margin. In Most (2007), the idea is to select the point of a given MC sample set that minimizes both the distance to the

SVC classifier $\widetilde{\mathcal{F}}^0_{\mathbf{u}} = \{\mathbf{u} \in \mathbb{R}^n : \widetilde{f}(\mathbf{u}) = 0\}$ in the standard normal space and an inter-point potential energy. In Basudhar and Missoum (2010), it is proposed to include points on the SVC classifier $\widetilde{\mathcal{F}}^0_{\mathbf{u}}$ that maximize the distance to the closest training point. Alternative strategies have been applied to SVR-based approaches. A common idea shared in a few works has been to elaborate training sets from Markov chain samples or sample candidates (Yuan et al., 2009; Dai et al., 2012b; Bourinet, 2014; Bourinet, 2016; Bourinet, 2017b).

In SVM-based reliability assessment, the isotropic Gaussian RBF kernel has often been preferred, despite a few works based on the polynomial kernel (Rocco and Moreno, 2002; Li et al., 2006; Basudhar and Missoum, 2010). As already pointed out by Li et al. (2006) and Chen (2007), the selection of optimal hyperparameters is a key issue for the accuracy of the SVM model. The method used to select these hyperparameters is not always clear in the above cited works, and it is sometimes not even mentioned. A simulated annealing algorithm based on a sum of square errors and normalized root mean square error measure is used by Pai and Hong (2006). A genetic algorithm, again based on this same error measure, is preferred in Pai (2006). A genetic algorithm is also applied for hyperparameter selection by Chen (2007), but here based on a 5-fold CV error. In the works of Basudhar (2011), it is proposed to take the lowest parameter γ for an isotropic Gaussian RBF kernel or the lowest degree d for a polynomial kernel, under the assumption of no training errors of the SVC classifier (C being set to an "infinite" value). In the ^{2}SMART method of Bourinet et al. (2011), a grid search based on a 3-fold CV error is used to select an optimal pair (C, γ). Regarding the solver of the SVM QP problem, there are often no details reported in the papers. A SMO algorithm is e.g. used in Most (2007) and Bourinet et al. (2011) and a SQP algorithm in Basudhar and Missoum (2010).

The reliability problems addressed by SVM surrogates are most often low-dimensional, i.e. $n \leq 10$. A three-span five-story frame structure with 21 random inputs is solved by Most (2007) but it can be shown that the corresponding LSS in the standard normal space is almost linear. High-dimensional problems with weakly nonlinear LSS are also studied by Most (2007) (example 2 with $a = 3$ and n up to 100) and by Bourinet (2011; 2016) (same example with n up to 250). Problems featuring disjoint failure domains or multiple MPFPs have also been reported in the literature. These problems are often limited to a very few random inputs, bidimensional cases in general except in Most (2007), and to a very few disjoint domains or multiple MPFPs.

(e) Kriging (or Gaussian process prediction)

Kriging (or Gaussian process emulators) described in Section II–4 are also used as surrogate models for rare event probability estimation. The first occurrences of kriging surrogates in structural reliability date back to 2005 and are due to Kaymaz (2005) and Schueremans and Van Gemert (2005).

The training set, often called design of experiments (DoE) in the kriging literature, is, as with SVMs, constructed adaptively. In Kaymaz (2005), a simple two-step procedure was proposed: construction of an initial training set centered on mean values, followed by the construction of a second set shifted toward the MPFP found by FORM run on the kriging surrogate trained on the initial training set. Several criteria were later proposed for the enrichment of an initial training set. These criteria define the optimal location(s) of the next point(s) to add to the training set. The central idea of these criteria used in kriging-based adaptive strategies is to make a controlled tradeoff between the exploration of the regions of interest (subdomains of $\mathcal{F}_{\mathbf{x}}$ with high probability content in reliability assessment) and the reduction of the global uncertainty of the surrogate model (unexplored regions of $\mathcal{X}$ due to the limited information available through the current training set $\mathcal{T}$). These criteria are defined in terms of the kriging predictor and the kriging variance, which are directly provided by the kriging model that is trained, see Section II–4. The most popular criteria are due to Ranjan et al. (2008), Bichon et al. (2008), Picheny et al. (2010), Echard et al. (2011), and Bect et al. (2012). The criteria defined by Ranjan et al. (2008), Bichon et al. (2008), and Echard et al. (2011) are heuristic extensions of the expected improvement criterion

of Jones et al. (1998). Their corresponding functions are respectively called improvement function, expected feasibility function and learning function U. These criteria directly depend on the marginal posterior distribution at a given point $\mathbf{x} \in \mathcal{X}$ (Gaussian distribution). For this reason these simple functions are fast to evaluate. Conversely, the stepwise uncertainty reduction (SUR) criterion of Bect et al. (2012) and the integrated mean square error of Picheny et al. (2010) are integral criteria, which are therefore more costly to evaluate. The SUR strategy can be generalized to more than one point added at a time, as proposed by Chevalier et al. (2014). For complete descriptions and a numerical comparison of these criteria (including their respective costs), the reader may refer to Bect et al. (2012) and Chevalier (2013, Appendix E).

In reliability assessment, ordinary kriging is most often applied for the training of surrogate models. It is argued in Bichon et al. (2011) that universal kriging does not make the adaptive strategy more efficient. Since it requires additional parameters to be tuned, these authors' preference is ordinary kriging. A recent alternative approach was proposed by Schöbi et al. (2017), which consists in using a finite set of multivariate orthogonal polynomials as the trend of a universal kriging model (the most common practice in universal kriging is to consider a multivariate linear trend). The optimal sparse set of polynomials is obtained by least-angle regression. Such an approach seems to improve the results in terms of the total number of LSF evaluations compared with ordinary kriging.

In most of the reliability analyses based on kriging surrogates, the covariance function is taken as a translation-invariant function. The correlation function is often assumed to be componentwise anisotropic with Gaussian or Matérn univariate correlation functions. For the Gaussian case, the expression of the correlation function is identical to that of the kernel given in Eq. (II.76). It is worth pointing out that the reliability problems addressed by kriging are low-dimensional in general ($n \leq 10$), which results in a small set of parameters to tune with componentwise anisotropic functions. High-dimensional examples are addressed by Echard et al. (2011) and Huang et al. (2016), where example 2 is taken with $n \in \{40, 100\}$ and $a = 3$.

In kriging-based reliability approaches, a space-filling initial training set is first constructed (usually based on a LHS). Its size is arbitrarily chosen, most often proportionally to the dimension n of the problem (and therefore irrespective of the complexity of the true function to surrogate). One of the above-cited adaptive strategies for the optimal placement of new points is then applied. In the AK-MCS method (Echard et al., 2011), the new points are chosen among a MC sample set of a given size, which needs to be chosen according the targeted failure probability level. In the case of low failure probabilities this sample set becomes too large, and more efficient techniques may be used, such as FORM-based importance sampling (Echard et al., 2013) or subset simulation (Huang et al., 2016).

(f) Other types of surrogate models, other uses of approximate models

A few other methods have been derived for surrogate-based reliability assessment, whose review is omitted in this report for the sake of brevity. Among these other methods, high dimensional model representation (HDMR) techniques (Rabitz et al., 1999) are worth noting and were found useful for the estimation of small failure probabilities by Chowdhury et al. (2009a; 2009). Another version of HDMR, used in conjunction with moving least squares, is also proposed by Chowdhury and Rao (2009b). The main idea of HDMR is to capture the high-dimensional input-output relationships by neglecting higher-order input correlations. In the methods developed by Chowdhury and his coauthors, the sampling scheme is adapted according to the order of the HDMR representation (first or second-order).

In all the methods reviewed so far, the approximate model was used as a *substitute* for the true and costly-to-evaluate response function (which justifies the use of a *surrogate model*). It is in fact never sure that the approximation error between the surrogate and true models is acceptable. *Whatever the complexity of the approximate model, we may find an even more complex true function that will not be fitted with sufficient accuracy*. This issue is considered as the main drawback of surrogate-based approaches.

In order to address this main issue, it is worth devising methods that are able to either 1) reduce or better cancel the approximation error that may appear in the surrogate-based approach, or 2) take advantage of the approximate model to obtain a failure probability estimate more efficiently, and possibly with no bias.

The first objective has been pursued in a few works. A method is proposed by Au (2007) for a consistent failure probability estimate based on an approximation of the true LSF. With this sampling method, an unbiased failure probability estimate is obtained based on the theorem of total probability. The approximate model may be a surrogate model or a simplified model, e.g. an elastic model instead of an elasto-plastic one. Another method is proposed by Li and Xiu (2010) to correct a potentially biased failure probability estimate induced by an inaccurate surrogate model (the method is applied to generalized PCE models of insufficient accuracy in the paper). The main idea of this hybrid method is to generate a small set of samples from the true and expensive model close to the LSS and many other samples from the cheap-to-evaluate surrogate model elsewhere. Li et al. (2011) use this hybrid approach in conjunction with the CE method for enhanced efficiency in the case of rare event probability estimation. The meta-IS method of Dubourg et al. (2013), based on kriging, achieves the same purpose in its second stage, through the computation of a correction factor based on samples of the true model. How the efficiency of these methods varies with the approximation error of the surrogate model and the complexity/dimension of the true function has not been quantified, to the author's knowledge. Efficiency is expected to be altered, as pointed out by Dubourg et al. (2013) in the specific case of the meta-IS method (see example 1 with $\mu_{F_s} = 27.5$ for which a crude kriging surrogate is obtained).

The second objective is pursued e.g. in adaptive importance sampling methods based on approximate models, such as those introduced in Section I–3.3.1 (see, e.g., Balesdent et al., 2013; Dubourg et al., 2013; Cadini et al., 2014, for kriging-based IS, and Dai et al., 2012a, for ϵ-SVR-based IS). Another recent method proposed by Li and Der Kiureghian (2016) also aims to reach such an objective. The proposed method, based on subset simulation, avoids too many calls to the true LSF and uses a kriging surrogate trained on the fly instead. This is in practice based on a modification of the acceptance ratio of SS (delayed acceptance strategy), which is explicitly expressed in terms of the probability of belonging to the kriging-based intermediate failure domain. According to Li and Der Kiureghian, this method yields unbiased failure probability estimates but its efficiency depends on the quality of the approximate model (i.e. on the approximation error w.r.t. the true LSF).

II–3.2 ^{2}SMART method

This section gives a short description and the main ideas of the ^{2}*SMART method* (see Bourinet et al., 2011, for more details including a pseudo-code for the implementation of the method). Its performances, assessed on a few selected examples, are commented in Section II–3.4 compared with those of the ASVR method more recently proposed by Bourinet (2016) and described in Section II–3.3.

This adaptive surrogate-based reliability method was elaborated for the estimation of small failure probabilities of time-invariant problems. The method hinges on SVMs used for classification. The main objective was to bring improvements to the method proposed by Hurtado and Alvarez (2003) based on the prospective work of Deheeger and Lemaire (2006).

The proposed SVM settings used in the ^{2}SMART method are:

- The method is based on L1-SVC models and an isotropic Gaussian RBF kernel.
- The QP solver is libsvm embedded in the *Spider Toolbox for Matlab, Version 1.71* (2006). It is therefore based on an SMO algorithm.
- Hyperparameter selection is made via a grid search technique over γ only. C is set to infinite.

$s = 0$, $y_0 = +\infty$, $\mathcal{T}_0 = \varnothing$ // initialization of algorithm

while $y_s > 0$ // loop on each intermediate threshold value y_s

$s = s + 1$

Define set of N_u data pairs $\{ (\mathbf{u}^{(j)}, y^{(j)}) , j \in \mathcal{I}_\mathrm{u} \}$ where $y^{(j)} = G(\mathbf{u}^{(j)})$ and $\#\mathcal{I}_\mathrm{u} = N_\mathrm{u}$

Define set of N_n data pairs $\{ (\mathbf{u}^{(j)}, y^{(j)}) , j \in \mathcal{I}_\mathrm{n} \}$ where $y^{(j)} = G(\mathbf{u}^{(j)})$ and $\#\mathcal{I}_\mathrm{n} = N_\mathrm{n}$

Define y_s as the p_0-quantile of $\{ y^{(j)} , j \in \mathcal{I}_\mathrm{n} \}$ where $p_0 = 0.1$. Set $y_s = 0$ if $y_s < 0$

Define initial training set at level s: $\mathcal{T}_s = \mathcal{T}_{s-1} \cup \{ (\mathbf{u}^{(j)}, \mathrm{sgn}(y^{(j)} - y_s)) , j \in \mathcal{I}_\mathrm{u} \cup \mathcal{I}_\mathrm{n} \}$

Train initial SVC classifier $\widetilde{f}_s$ at level s on $\mathcal{T}_s$

for $m = 1$ **to** M // update of SVC classifier $\widetilde{f}_s$ at each iteration m

Define sample set $\mathcal{W} = \{ \mathbf{u}^{(j)} , j \in \mathcal{I}_\mathrm{w} \}$ where $\#\mathcal{I}_\mathrm{w} = \begin{cases} N_1 & \text{if } m < m_1 \quad \text{(localization stage)} \\ N_2 & \text{if } m_1 \leq m < m_2 \quad \text{(stabilization stage)} \\ N_3 & \text{if } m_2 \leq m \leq M \quad \text{(convergence stage)} \end{cases}$

and where $\begin{cases} \mathcal{I}_\mathrm{margin} \in \mathcal{I}_\mathrm{w} & : \text{points in the margin} \\ \mathcal{I}_\mathrm{switch} \in \mathcal{I}_\mathrm{w} & : \text{points switching from one side of the classifier to the other} \\ \mathcal{I}_\mathrm{close} \in \mathcal{I}_\mathrm{w} & : \text{closest points to the classifier } \widetilde{f}_s(\mathbf{u}) = 0 \end{cases}$

Select $N_\mathrm{a} = N_{\mathrm{a\ margin}} + N_{\mathrm{a\ switch}} + N_{\mathrm{a\ close}}$ additional training points whose indices j belongs to:

$\begin{cases} \mathcal{I}_{\mathrm{a\ margin}} \subset \mathcal{I}_\mathrm{margin} & \text{where } \#\mathcal{I}_{\mathrm{a\ margin}} = N_{\mathrm{a\ margin}} \\ \mathcal{I}_{\mathrm{a\ switch}} \subset \mathcal{I}_\mathrm{switch} & \text{where } \#\mathcal{I}_{\mathrm{a\ switch}} = N_{\mathrm{a\ switch}} \\ \mathcal{I}_{\mathrm{a\ close}} \subset \mathcal{I}_\mathrm{close} & \text{where } \#\mathcal{I}_{\mathrm{a\ close}} = N_{\mathrm{a\ close}} \end{cases}$

Evaluate LSF at new training points $\{ y^{(j)} : j \in \mathcal{I}_{\mathrm{a\ margin}} \cup \mathcal{I}_{\mathrm{a\ switch}} \cup \mathcal{I}_{\mathrm{a\ close}} \}$ where $y^{(j)} = G(\mathbf{u}^{(j)})$

Update training set: $\mathcal{T}_s = \mathcal{T}_s \cup \{ (\mathbf{u}^{(j)}, \mathrm{sgn}(y^{(j)} - y_s)) , j \in \mathcal{I}_{\mathrm{a\ margin}} \cup \mathcal{I}_{\mathrm{a\ switch}} \cup \mathcal{I}_{\mathrm{a\ close}} \}$

Update SVC classifier $\widetilde{f}_s$ by a new training on $\mathcal{T}_s$

end for

Assess estimate $\widehat{\widetilde{p}}_s$ of $\widetilde{p}_s = \mathbb{P}\left(\widetilde{E}_s\right)$ if $s = 1$ or $\widetilde{p}_s = \mathbb{P}\left(\widetilde{E}_s | \widetilde{E}_{s-1}\right)$ if $s > 1$ where $\widetilde{E}_s = \{ \widetilde{f}_s(\mathbf{U}) \leq 0 \}$

Define $p_0 N_1$, $p_0 N_2$ and $p_0 N_3$ seeds to be used at next level s if $y_s > 0$

end while

Set $m = s$, compute failure probability estimate as $\widehat{p}_\mathrm{f}^{\,^2\mathrm{SMART}} = \prod_{s=1}^{m} \widehat{\widetilde{p}}_s$

Table II.3 – General flowchart of the ^{2}SMART method.

A general flowchart of the method is given in Table II.3 (for a detailed pseudo-code, see Bourinet et al., 2011). The ^{2}SMART method proceeds similarly to the subset simulation method. Intermediate threshold values y_s of the LSF are selected until y_s becomes lower than zero. At each intermediate level s, a SVC surrogate model $\widetilde{f}_s$ is constructed iteratively. At each iteration $m = 1, \ldots, M$, N_a new data pairs are defined and added to the training set $\mathcal{T}$. For each m, the updated SVC model $\widetilde{f}_s$ is obtained by training on the newly-defined set $\mathcal{T}$. Let us denote $\widetilde{\mathcal{F}}_{\mathbf{u},s}$ the obtained approximation of the true failure domain $\mathcal{F}_{\mathbf{u},s}$:

$$\widetilde{\mathcal{F}}_{\mathbf{u},s} = \left\{ \mathbf{u} \in \mathbb{R}^n : \widetilde{f}_s(\mathbf{u}) \leq 0 \right\} \approx \mathcal{F}_{\mathbf{u},s} = \{ \mathbf{u} \in \mathbb{R}^n : G(\mathbf{u}) \leq y_s \} . \tag{II.124}$$

The approximate failure probability of the ^{2}SMART method is given by:

$$p_\mathrm{f}^{\,^2\mathrm{SMART}} = \prod_{s=1}^{m} \widetilde{p}_s , \tag{II.125}$$

where:

$$\widetilde{p}_1 = \mathbb{P}\left(\widetilde{E}_1\right) = \mathbb{E}_{\varphi_n}\left[\mathbb{1}_{\widetilde{\mathcal{F}}_{\mathbf{u},1}}(\mathbf{U}) \right] , \tag{II.126}$$

and, for $s = 2, \ldots, m$:

$$\widetilde{p}_s = \mathbb{P}\left(\widetilde{E}_s | \widetilde{E}_{s-1}\right) = \mathbb{E}_{\varphi_n(\cdot | \widetilde{E}_{s-1})}\left[\mathbb{1}_{\widetilde{\mathcal{F}}_{\mathbf{u},s}}(\mathbf{U}) \right] . \tag{II.127}$$

Practically, these probabilities are estimated by the SS method applied to the constructed SVC surrogate models $\widetilde{f}_s$ for $s = 1, \ldots, m$.

At each level s, the training set $\mathcal{T}$ is composed of the following points, see Table II.3:

- Initially, N_u points $\{\,\mathbf{u}^{(j)}\,,\, j\in\mathcal{I}_\mathrm{u}\,\}$ (see lines 4) and N_n points $\{\,\mathbf{u}^{(j)}\,,\, j\in\mathcal{I}_\mathrm{n}\,\}$ (see line 5),
- at each iteration m, N_a points $\{\,\mathbf{u}^{(j)}\,,\, j\in\mathcal{I}_{\text{a margin}}\cup\mathcal{I}_{\text{a switch}}\cup\mathcal{I}_{\text{a close}}\,\}$ (see line 11).

During the iterative construction of the SVC surrogate, the selection of the N_a new points is made from a set of samples denoted $\mathcal{W}$ (see Table II.3, line 10). The way in which this set is composed depends on m, and the number of additional training N_a also varies with m (see Bourinet et al., 2011, Table A.1, for a full description of the parameter settings of the ^{2}SMART method). The cardinality of $\mathcal{W}$ is increased in three steps, from a coarse sample set taken initially ($\#\mathcal{W}=N_1=10,000$ for $1\le m<m_1$), to a finer set ($\#\mathcal{W}=N_2=50,000$ for $m_1\le m<m_2$) and finally to a more refined set ($\#\mathcal{W}=N_3=200,000$ for $m_2\le m\le M$). The number of iterations varies with the input dimension n of the reliability problem: $m_1=\lfloor 6(n/2)^{0.2}\rceil$, $m_2=\lfloor 12(n/2)^{0.2}\rceil$ and $M=m_2+16$.

For the first level ($s=1$), $\mathcal{W}$ is composed of uniform samples in the n-dimensional hypersphere $\mathcal{S}_n(r_\mathrm{u})$ of radius $r_\mathrm{u}=\max\{\,\|\mathbf{u}^{(j)}\|\;:\;\mathbf{u}^{(j)}\overset{\text{i.i.d.}}{\sim}\varphi_n\,,\,j=1,\ldots,N_3\,\}$ for $m<m_2$, see the left column of Figure II.7, top and middle plots. For $s=1$ and $m_2\le m\le M$, $\mathcal{W}$ is composed of N_3 n-dimensional standard normal samples.

For the next levels ($s>1$), the sample set $\mathcal{W}$ is generated by means of the componentwise Metropolis sampler of Au and Beck (2001) for $m_2\le m\le M$ (m-M algorithm). For $m<m_2$, the spread of the sample candidates is widened by increasing the acceptance ratio $\alpha^k_{\varphi,i}$ by a factor $\lambda>1$ in the m-M algorithm. In practice, $\alpha^k_{\varphi,i}$ is replaced by $\lambda\alpha^k_{\varphi,i}$ in line 11 of the algorithm, see Table I.2. The corresponding algorithm is referred to as the $\lambda\alpha$-m-M algorithm in the following. We choose $\lambda=\lambda_1=7$ for $1\le m<m_1$ and $\lambda=\lambda_2=3.5$ for $m_1\le m<m_2$, see the corresponding samples in the right column of Figure II.7, top and middle plots.

From the SVC model constructed at each iteration m, it is possible to identify three subsets of samples in $\mathcal{W}$: those that are in the margin of the SVC (set of indices denoted $\mathcal{I}_{\text{margin}}$), those that are switching from one class to another during two successive iterations (set of indices denoted $\mathcal{I}_{\text{switch}}$) and those that are the closest to the classifier $\widetilde{f}_s(\mathbf{u})=0$ (ordered set of indices denoted $\mathcal{I}_{\text{switch}}$). The N_a additional training points are selected within these sample subsets: $N_{\text{a margin}}$ cluster centers of $\{\,\mathbf{u}^{(j)}\,,\,j\in\mathcal{I}_{\text{margin}}\,\}$, $N_{\text{a switch}}$ cluster centers of $\{\,\mathbf{u}^{(j)}\,,\,j\in\mathcal{I}_{\text{switch}}\,\}$, and $N_{\text{a close}}$ points of $\{\,\mathbf{u}^{(j)}\,,\,j\in\mathcal{I}_{\text{close}}\,\}$ that are the closest to the SVC classifier. The ratios $N_{\text{a margin}}/N_\mathrm{a}$, $N_{\text{a switch}}/N_\mathrm{a}$ and $N_{\text{a close}}/N_\mathrm{a}$ vary with each iteration (see Bourinet et al., 2011, Table A.1, for details). The number of additional training points N_a varies with iterations m from $3\sqrt{n}$ to $5\sqrt{n}$.

For $s=1$, the set of points $\{\,\mathbf{u}^{(j)}\,,\,j\in\mathcal{I}_\mathrm{u}\,\}$ is composed of N_u samples uniformly distributed in $\mathcal{S}_n(r_\mathrm{u})$ (see Table II.3, line 4). For $s>1$, these N_u points are cluster centers of N_1 samples generated by the $\lambda_1\alpha$-m-M algorithm and belonging to $\widetilde{\mathcal{F}}_{\mathbf{u},s-1}$.

For $s=1$, points $\{\,\mathbf{u}^{(j)}\,,\,j\in\mathcal{I}_\mathrm{n}\,\}$ are N_n standard normal samples (see Table II.3, line 5). For $s>1$, these points are samples generated by the m-M algorithm and belonging to $\widetilde{\mathcal{F}}_{\mathbf{u},s-1}$. Note that the determination of the threshold values y_s of the intermediate level s is based on these N_n samples. In the proposed implementation of the ^{2}SMART method, N_n is set to 100.

II–3.3 ASVR method

This section presents the adaptive surrogate-based reliability method proposed by Bourinet (2016). Early developments of this method can also be found in Bourinet (2015). Its performances are commented in Section II–3.4. This method referred to as *ASVR method* is characterized by the following properties:

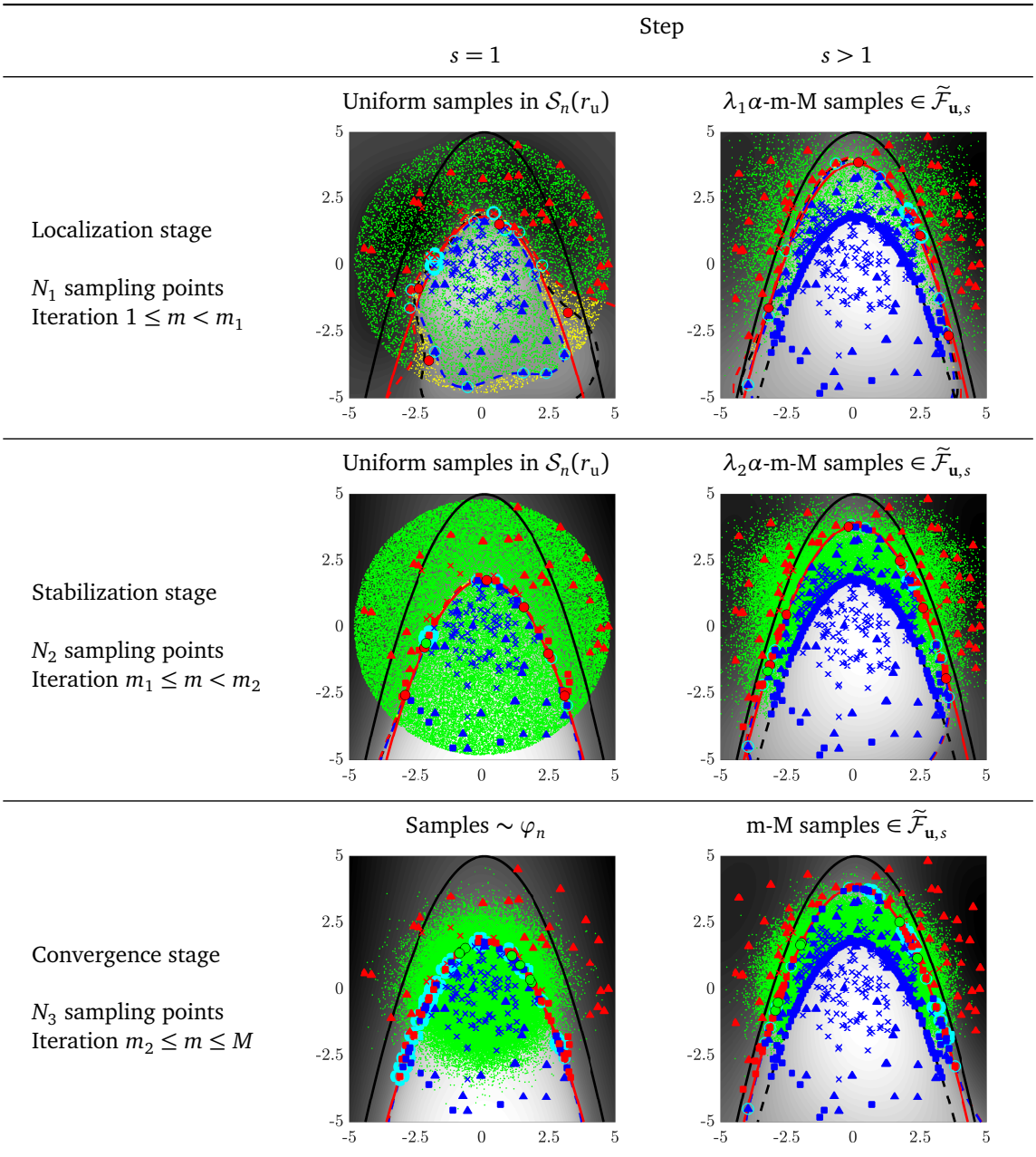

Figure II.7 – Generation of sample set $\mathcal{W}$ (coarse to fine sampling process).

- *Adaptive surrogate models*. An iterative sequence of surrogate models $\{\widetilde{G}_s : \mathbf{u} \mapsto \widetilde{G}_s(\mathbf{u}), s = 1, \ldots, s_{\text{final}}\}$ is constructed in the standard normal space. A key idea of the method is to first explore the safe domain as fast as possible with surrogate models of moderate accuracy. The accuracy of the surrogate models is only increased in the final iterations s, when the failure domain $\mathcal{F}_{\mathbf{u}}$ is reached by the generated training samples. This is in contrast with the conceptual idea of the ^{2}SMART method (Bourinet et al., 2011) which constructs accurate surrogate models at each SS-like intermediate threshold value y_s of the LSF.

- *Surrogate regression models*. The ASVR method uses SVM surrogate models in *regression*, as also proposed by Pai and Hong (2006), Chen (2007), Yuan et al. (2009), and Dai et al. (2012b). More specifically, it uses L1-ϵ-SVR models based on the ϵ-insensitive loss function, see Section II–2.2.1. Although reliability assessment can be viewed as a binary classification problem, the author's opinion is that exploiting the $\mathbb{R}$-value of the LSF is more informative than its sign alone is. Based on the same adaptive strategy, it has been noticed that SVR are superior to SVC in terms of the accuracy of their failure probability estimates (see Bourinet, 2014, for preliminary results based on L1-SVC).

- *Enrichment of the training set $\mathcal{T}$*. Additional training points are defined at each iteration s of the method. These points are taken as a random subset of *MCMC samples* generated based on the currently constructed SVR surrogate $\widetilde{G}_s$. As for the ^{2}SMART method, this is specifically achieved by means of the componentwise Metropolis sampler of Au and Beck (2001) (m-M algorithm), see Table I.2. MCMC samples were also used in prior works to adaptively populate important regions of the failure domain (see, e.g., Proppe, 2008, for their use with polynomial moving least squares, and Yuan et al., 2009; Dai et al., 2012b, with SVR). Distance-based and other space-filling driven criteria often used in the literature may be quite efficient in low-dimensional spaces, but it is the author's belief that such criteria do not scale well with the dimensionality n of the reliability problem.

- *Local regression, left-out data for testing*. The cost of SVR training increases with the size of the training set $\mathcal{T}$. In order to keep the training runtime reasonable[13], the surrogate models are trained on a subset of the currently available data. Only the data pairs with the lowest LSF values are selected, and the left-out data pairs are used for testing. We therefore make a *local regression* on the closest data to the failure domain $\mathcal{F}_{\mathbf{u}}$. The left-out data constitutes the so-called *trailing set*. If some errors occur in this set (points incorrectly classified w.r.t. the currently-selected intermediate threshold value y_s), the corresponding data pairs are transferred to the training set $\mathcal{T}$ and a new SVR surrogate $\widetilde{G}_s$ is trained.

- *Highly accurate SVR surrogate models*. The use of highly accurate SVR surrogate models at each iteration s is of paramount importance for the efficiency and robustness of the adaptive strategy. In the ASVR method, this is achieved thanks to 1) the use of an interior point algorithm to solve the SVR QP problems, and 2) the selection of optimal hyperparameter values by minimizing the span bound approximation of the LOO error with the CE method, see Section II–2.4.3.

The main conceptual ideas of the ASVR method are depicted in Figure II.8 and a pseudo-code is given in Table II.4. The algorithm is composed of three main phases (1, 2 and 3) which are iterated with s. These phases differ in the way the training set is composed and how the additional training points are defined. The transition from phase 1 to 2 occurs when the intermediate threshold level y_s becomes lower than zero. The transition from phase 2 to 3 occurs when the mean ratio of switching points $\overline{r}_{\text{SS switch}}$ drops below the given value of 0.1, see Table II.4, lines 34–39. This criterion quantifies the accuracy of the constructed SVR surrogate.

[13] From a general perspective, the training time should not be an issue in surrogate modeling. In several problems, the computational burden may be alleviated by an efficient computer implementation of the algorithms (e.g. parallel training). However it often becomes an issue in practical situations, which justifies some efforts to lower this time as much as possible.

(a) Initial training set, SVR surrogate $\widetilde{G}_1$

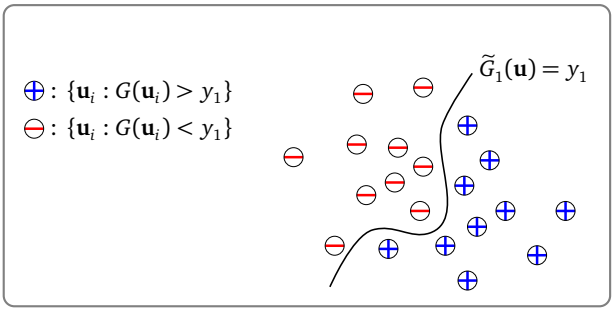

(b) $\mathbf{u}_{\text{SS}}$ samples, new training points

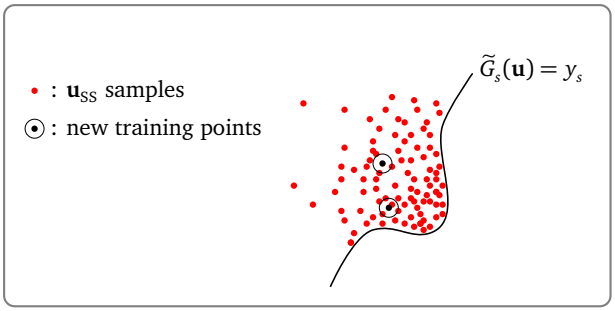

(c) Current training set, new training points

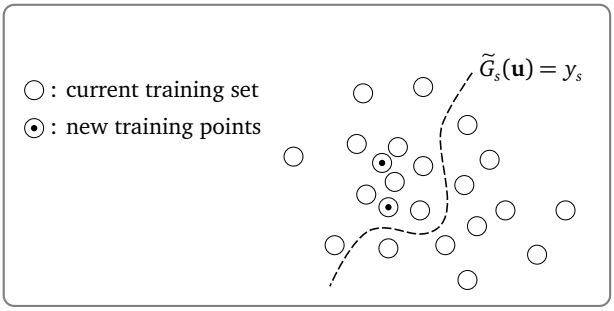

(d) Trailing points, new training set

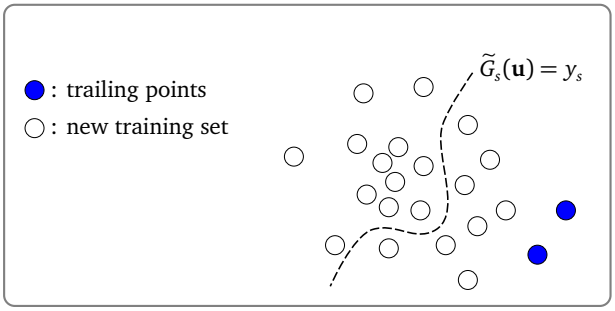

(e) New threshold value y_{s+1}

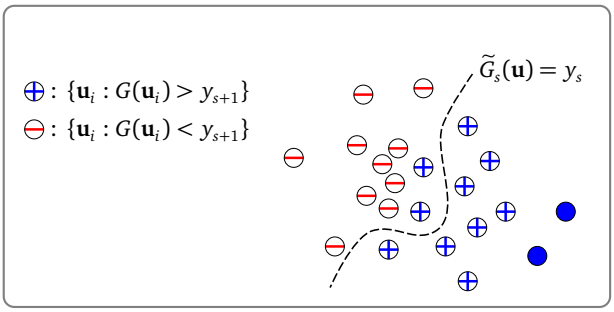

(f) Updated SVR surrogate $\widetilde{G}_{s+1}$

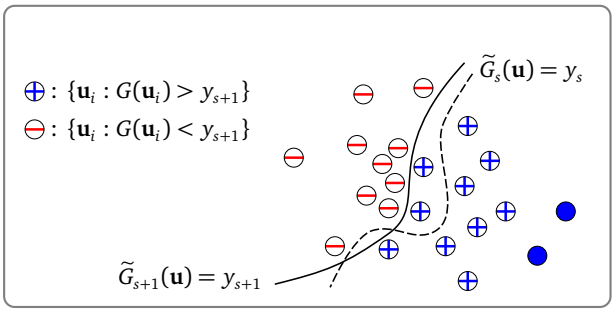

(g) $\mathbf{u}_{\text{SS}}$ samples at current iteration s

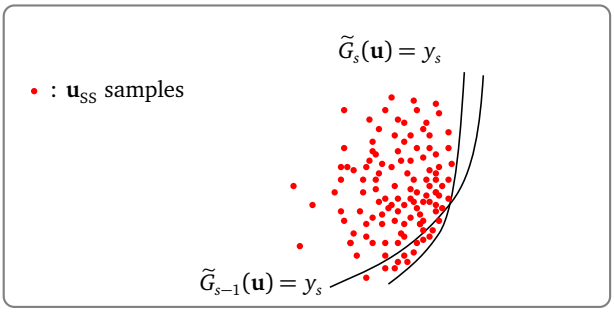

(h) $\mathbf{u}_{\text{SS switch}}$ samples, new training points

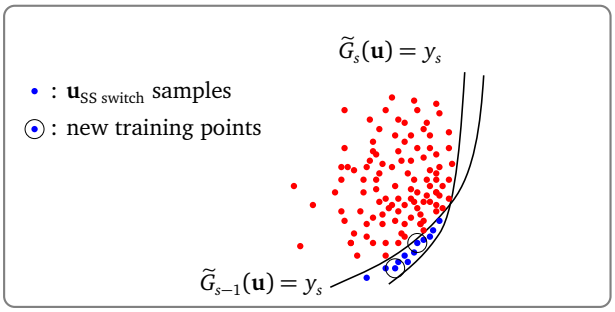

Figure II.8 – Main conceptual ideas of the ASVR method.

The parameters of the ASVR method are: initial and minimal numbers of data pairs in $\mathcal{T}$, resp. N and $N_{\min}$, and ratio p_{a} over N of additional training points at each iteration s (this ratio is considered specific to each phase, i.e. $p_{\text{a}} = p_{\text{a1}}$, p_{a2} or p_{a3}). The default settings of these parameters can be found in Table II.5.

// **initialization**
phase $= 1$, $p_\mathrm{a} = p_{\mathrm{a}1}$ // type of training phase, current ratio p_a to use
$s = 0$, $s_\mathrm{final} = +\infty$ // current iteration, maximal number of iterations
$N_s = 0$ // total number of calls to LSF
$\mathbf{u} = \varnothing$, $\mathbf{g} = \varnothing$ // recorded sets of $\mathbf{u}$-vectors and corresponding g-values
$\mathcal{I}_\mathrm{train} = \varnothing$, $\mathcal{I}_\mathrm{trail} = \varnothing$ // sets of indices corresponding to training and trailing points

// **main algorithm**
$N_\mathrm{a} = N$, $\mathbf{u}_\mathrm{a} = \{ \mathbf{u}_i \, : \, i = 1, \ldots, N_\mathrm{a} \}$ where $\mathbf{u}_i$ are realizations of i.i.d. $\mathbf{U}_i \sim \varphi_n$
do
  $\mathbf{g}_\mathrm{a} = G(\mathbf{u}_\mathrm{a})$ // evaluate N_a new training points $\mathbf{u}_\mathrm{a}$
  $\mathbf{u} = \{ \mathbf{u} \, , \, \mathbf{u}_\mathrm{a} \}$, $\mathbf{g} = \{ \mathbf{g} \, , \, \mathbf{g}_\mathrm{a} \}$ // update recorded sets of $\mathbf{u}$-vectors and corresponding LSF values
  // define sets of indices of training and trailing points
  $\mathcal{I}_\mathrm{train} = \mathcal{I}_\mathrm{train} \cup \{ (N_s + 1), \ldots, (N_s + N_\mathrm{a}) \}$, $N_\mathrm{train} = \#\mathcal{I}_\mathrm{train}$
  $\mathcal{I} = \mathrm{sort}(\mathbf{g}_{\mathcal{I}_\mathrm{train}} \, , \, \text{'ascend'})$, $\mathcal{I}_\mathrm{train} = \mathcal{I}_\mathrm{train}(\mathcal{I})$
  if (phase $= 1$) **and** ($N_\mathrm{train} > N_\mathrm{min}$) **then**
    $\mathcal{I}_\mathrm{train} = \mathcal{I}_{\mathrm{train};\, 1,\ldots,N_\mathrm{min}}$, $N_\mathrm{train} = N_\mathrm{min}$
    $\mathcal{I}_\mathrm{trail} = \mathcal{I}_\mathrm{trail} \cup \mathcal{I}_{\mathrm{train};\,(N_\mathrm{min}+1),\ldots,N_\mathrm{train}}$
  end if
  $N_{s+1} = N_s + N_\mathrm{a}$, $s = s + 1$ // update number of calls to LSF, increment s
  if (phase $= 1$) **then**
    $y_s = \mathrm{median}(\mathbf{g}_{\mathcal{I}_{\mathrm{train};\,1,\ldots,N}})$ // select current threshold value of the LSF
    if $y_s < 0$ **then** , $y_s = 0$, phase $= 2$, $p_\mathrm{a} = p_{\mathrm{a}2}$, **end if**
  else
    $y_s = 0$
  end if
  do // train SVR until no error is made in trailing points
    $\widetilde{G}_s = \mathrm{train}(\mathbf{u}_{\mathcal{I}_\mathrm{train}} \, , \, \mathbf{g}_{\mathcal{I}_\mathrm{train}})$
    $\mathcal{I}_\mathrm{atrail} = \{ i \in \mathcal{I}_\mathrm{trail} \, : \, \widetilde{G}_s(\mathbf{u}_i) \leq y_s \}$
    $\mathcal{I}_\mathrm{train} = \mathcal{I}_\mathrm{train} \cup \mathcal{I}_\mathrm{atrail}$, $N_\mathrm{train} = \#\mathcal{I}_\mathrm{train}$
    $\mathcal{I}_\mathrm{trail} = \mathcal{I}_\mathrm{trail} \backslash \mathcal{I}_\mathrm{atrail}$
  while $\mathcal{I}_\mathrm{atrail} \neq \varnothing$
  // assess probability estimate $\widehat{p}_s$ and generate training point candidates by subset simulation
  $(\widehat{p}_s \, , \, \mathbf{u}_\mathrm{SS}) = \mathrm{SubSim}(N_\mathrm{SS} \, , \, p_\mathrm{SS} \, , \, \widetilde{G}_s - y_s)$
  // assess ratios of switching samples in $\mathbf{u}_\mathrm{SS}$ set
  for $k = \max\{ 1 \, , \, (s - \max\{3, \lfloor 1/p_\mathrm{a} \rceil\}) \}$ **to** $(s-1)$
    $\mathcal{I}_{\mathrm{SS\ switch};\,k} = \{ i \in \{1, \ldots, \#\mathbf{u}_\mathrm{SS}\} \, : \, \widetilde{G}_k(\mathbf{u}_{\mathrm{SS};\,i}) > y_s \}$
    $\mathbf{r}_{\mathrm{SS\ switch};\,k} = \#\mathcal{I}_{\mathrm{SS\ switch};\,k} / \#\mathbf{u}_\mathrm{SS}$
  end for
  $\overline{r}_\mathrm{SS\ switch} = \mathrm{mean}(\mathbf{r}_\mathrm{SS\ switch})$, $\mathbf{u}_\mathrm{SS\ switch} = \mathbf{u}_{\mathrm{SS};\,\mathcal{I}_{\mathrm{SS\ switch};\,s-1}}$
  if (phase $= 2$) **and** ($\overline{r}_\mathrm{SS\ switch} < 0.1$) **then** , phase $= 3$, $p_\mathrm{a} = p_{\mathrm{a}3}$, $s_\mathrm{final} = s + \lfloor 3/p_\mathrm{a} \rceil$, **end if**
  // select N_a new training points
  $N_\mathrm{a} = p_\mathrm{a} N$
  switch phase
    case $\{1, 2\}$, $\mathbf{u}_\mathrm{a} = \mathbf{u}_{\mathrm{SS};\,1,\ldots,N_\mathrm{a}}$
    case 3, $\mathbf{u}_\mathrm{a} = \mathbf{u}_{\mathrm{SS\ switch};\,1,\ldots,N_\mathrm{a}}$
  end switch
while $(s < s_\mathrm{final})$
$N_\mathrm{t} = N_s$ // total number of calls to LSF
$\widehat{p}_\mathrm{f}^{\,\mathrm{ASVR}} = \widehat{p}_s$ // failure probability estimate

Table II.4 – Pseudo-code of ASVR method.

General parameters	
$N = 50$, $N_{\min} = 100$	initial, minimal number of data pairs in $\mathcal{T}$
$p_{a1} = 1/10$, $p_{a2} = 1/2$, $p_{a3} = 1/2$	ratios (over N) of new data pairs added at each iteration
Parameters of the m-M algorithm	
$p_{SS} = 0.5$	prescribed probability level p_0 of SS
$N_{SS} = 10,000/p_{SS} = 20,000$	sample size at each subset level

Table II.5 – Settings of the ASVR method.

The algorithm proceeds as follows:

1. A first SVR surrogate $\widetilde{G}_1$ is trained from an initial training set $\mathcal{T}$ composed of N data pairs $\{(\mathbf{u}_i, G(\mathbf{u}_i)), i = 1, \dots, N)\}$ where $\mathbf{u}_i$ are sampled from the n-dimensional standard normal PDF φ_n. The first intermediate threshold level y_1 is defined as the median of the sample $\{G(\mathbf{u}_i), i = 1, \dots, N\}$ (Table II.4, line 21) and a first intermediate LSS $\widetilde{\mathcal{F}}^0_{\mathbf{u},1} = \{\mathbf{u} \in \mathbb{R}^n : \widetilde{G}_1(\mathbf{u}) = y_1\}$ is obtained (Figure II.8a).

2. From this first SVR surrogate $\widetilde{G}_1$ and more generally from those constructed at any iteration s and denoted $\widetilde{G}_s$, subset simulation (SS) is applied to the LSF $\mathbf{u} \mapsto \widetilde{G}_s(\mathbf{u}) - y_s$. The prescribed probability level of SS is set to $p_{SS} = 0.5$ and the sample size at each level to $N_{SS} = 20,000$, see Table II.5. The objective is twofold: 1) find an estimate of the probability $p_s = \mathbb{P}(\widetilde{G}_s(\mathbf{u}) \leq y_s)$, and 2) define a set of samples $\mathbf{u}_{SS} = \{\mathbf{u}_{SS;i} : i = 1, \dots, N_{\mathbf{u}_{SS}}\} \sim \varphi_n(\cdot|\widetilde{E}_s)$ where $\widetilde{E}_s = \{\widetilde{G}_s(\mathbf{U}) \leq y_s\}$ and $N_{\mathbf{u}_{SS}}$ is set to $p_{SS}N_{SS} = 10,000$. This set $\mathbf{u}_{SS}$ is composed of MCMC samples of the last level of SS verifying $\widetilde{G}_s(\mathbf{u}_{SS;i}) \leq y_s$ for $i = 1, \dots, N_{\mathbf{u}_{SS}}$ (Figure II.8b and Table II.4, line 33). Note that we have at least $p_{SS}N_{SS}$ samples verifying such a condition in the final level of SS. $N_a = p_a N$ samples are then randomly selected in the set $\mathbf{u}_{SS}$ (Figure II.8b and Table II.4, line 44) and used as additional training points at the next iteration (Figure II.8c, Table II.4, lines 10–11).

3. At each iteration s, the intermediate threshold level y_s is defined as the median of the N smallest LSF values of the training data pairs $\mathcal{T} = \{(\mathbf{u}_i, G(\mathbf{u}_i)), i \in \mathcal{I}_{\text{train}}\}$ where $\mathcal{I}_{\text{train}}$ denotes the set of indices of the training data (Table II.4, lines 14 and 21) and a new SVR surrogate $\widetilde{G}_s$ is trained (Table II.4, line 27).

4. The algorithm iterates with the above-defined steps until the size of the training set $\mathcal{T}$ reaches $N_{\min}$. Then, at each next iteration, the N_a data pairs with the largest LSF values are withdrawn from the training set $\mathcal{T}$ and transferred to so-called trailing set (Figure II.8d, Table II.4, lines 15–18) prior to the training of a new SVR surrogate.

5. A new intermediate threshold level y_{s+1} is defined as the median of the N smallest LSF values of the training data pairs $\mathcal{T} = \{(\mathbf{u}_i, G(\mathbf{u}_i)), i \in \mathcal{I}_{\text{train}}\}$ (Figure II.8e, Table II.4, lines 14 and 21) and a new SVR surrogate $\widetilde{G}_{s+1}$ is trained (Figure II.8f and Table II.4, line 27).

6. The points belonging to the trailing set must verify $\widetilde{G}_{s+1}(\mathbf{u}_i) > y_{s+1}$ for $i \in \mathcal{I}_{\text{trail}}$. If this condition is not met, the corresponding data pairs are withdrawn from the trailing set and transferred to the training set $\mathcal{T}$, and the SVR surrogate $\widetilde{G}_{s+1}$ is updated by a new training (Table II.4, lines 26–31). This testing/training process is repeated until no error is made in the trailing set.

7. The algorithm iterates with the above-defined steps until $y_s < 0$. Reaching this condition corresponds to the end of phase 1. y_s is set to zero for subsequent iterations (Table II.4, line 22).

8. The above-defined steps are repeated during phase 2, with the main difference that no data pairs are excluded from the training set $\mathcal{T}$. The ratio of additional training points p_a is then set to p_{a2}.

9. Based on the set of samples $\mathbf{u}_{SS}$ generated at iteration s, we investigate the ratio of such samples that verify $\widetilde{G}_k(\mathbf{u}_{SS;i}) > y_s$ where $k < s$ is a given previous iteration and $y_s = 0$. Let us denote $\mathcal{I}_{SS\ switch;k}$ the set of indices of such samples (represented by blue dots in Figure II.8h for the specific case $k = s-1$). We therefore consider the following ratios $\mathbf{r}_{SS\ switch;k} = \#\mathcal{I}_{SS\ switch;k}/N_{\mathbf{u}_{SS}}$ for $k < s$. These ratios, averaged over a given number of iterations k (3 for phase 2), are representative of the stability of the constructed SVR surrogate models (Table II.4, lines 35–39). Phase 2 ends when the averaged ratio $\overline{r}_{SS\ switch}$ falls below a prescribed threshold value set to 0.1 (Table II.4, line 40).

10. During phase 3, the additional training points are N_a samples randomly selected from the set $\mathbf{u}_{SS\ switch} = \mathbf{u}_{SS;\mathcal{I}_{SS\ switch;s-1}}$, which gathers the samples $\mathbf{u}_{SS,i}$ of the set $\mathbf{u}_{SS}$ that switch from $\widetilde{G}_k(\mathbf{u}_{SS,i}) > 0$ at iteration $s-1$ to $\widetilde{G}_k(\mathbf{u}_{SS,i}) \leq 0$ at iteration s (Table II.4, line 45). As in phase 2, no points are excluded from the training set and y_s is still set to zero. The ratio of additional training points p_a is set to p_{a3} and $\lfloor 3/p_a \rceil = 6$ iterations are performed in phase 3.

11. The failure probability is estimated from the SVR surrogate $\widetilde{G}_{s_{final}}$ trained at the final iteration: $\widehat{p}_f^{ASVR} = \widehat{p}_{s_{final}}$ (Table II.4, line 49). $N_t = N_{s_{final}}$ stands for the total number of calls to the LSF (Table II.4, line 48).

II–3.4 Results and comparison

Some results obtained with the ^{2}SMART and ASVR methods are presented in this section. These results are compared with reference failure probabilities obtained by SS. The focus is put on example 1 with $\mu_{F_s} = 27.5$ and example 2 with $a = 3$, $n \in \{100, 250\}$ (see Bourinet et al., 2011; Bourinet, 2016, for more detailed results and additional examples).

It is first worth noting that the failure probabilities obtained by the ^{2}SMART and ASVR methods are estimates (i.e. random quantities). The random nature of the results has two sources. First, the adaptive strategy applied for reliability assessment is based on training sets composed of samples generated by the componentwise Metropolis algorithm of Au and Beck. Second, the failure probability approximations are obtained from the constructed surrogate models by means of the SS method, which therefore gives estimates of such probabilities. As a consequence, independent applications of the ^{2}SMART or ASVR methods give different failure probability estimates. For illustration, the plots of $\widehat{p}_s$ expressed in terms of the cumulative number of calls to the LSF N_s and obtained from 3 independent runs of the ASVR method are presented in Figure II.9 for example 1.

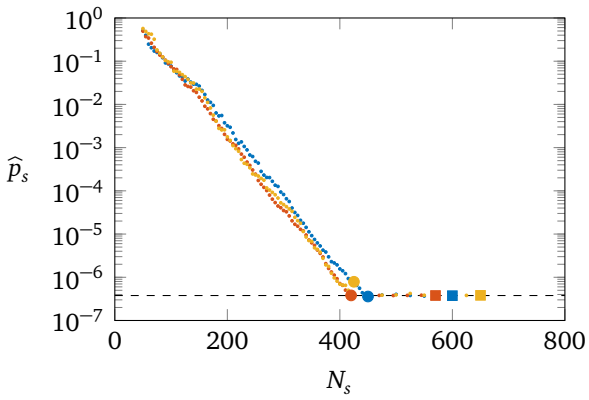

Figure II.9 – Example 1, $\mu_{F_s} = 27.5$. ASVR results with $(N, N_{min}) = (50, 100)$. Plots of $\widehat{p}_s$ vs. N_s from 3 independent runs. Dots are used for each pair $(N_s, \widehat{p}_s)$, a solid circle indicates the iteration at which y_s becomes negative (end of phase 1) and a solid square the final iteration s_{final} (end of phase 3).

The accuracy of the ^{2}SMART and ASVR methods needs to be assessed in the light of the statistical properties of the failure probability estimates obtained from independent runs of these methods. These properties are expressed in terms of sample variance and bias w.r.t. the reference probabilities obtained by SS. The presented results are averaged over 50 (resp. 20) independent runs of the ^{2}SMART (resp. ASVR) method. These results are compared with those averaged from 500 independent runs of the SS method. The averaged relative bias and coefficient of variation obtained by these methods are presented in Figure II.10 for example 1 with $\mu_{F_s} = 27.5$ and in Figure II.11 for example 2 with $a = 3$, $n \in \{100, 250\}$.

In the case of example 1 with $\mu_{F_s} = 27.5$, both the ^{2}SMART and ASVR methods give almost unbiased estimates. The bias, respectively averaged over 50 and 20 independent runs, is close to 3% with the ^{2}SMART method and 1% with ASVR, see left plot in Figure II.10. Note also that the coefficient of variation from these runs is very low, less than 10% and 2% respectively, see right plot in Figure II.10. A solution using SS of similar accuracy as that obtained with the ASVR method would require about 10 millions calls to the LSF. The ASVR method yields more accurate failure probability estimates than ^{2}SMART, with a lower number of calls to the LSF (648 w.r.t. 4011 in average). This computational cost is similar to that of the metamodel-based importance sampling of Dubourg et al. (2013), based on a kriging surrogate: 480 plus an additional $N_{\text{corr}} = 200$ samples for the estimation of the correction factor of this method.

The LSS surface geometry of example 1 with $\mu_{F_s} = 27.5$ has been explored. Figure II.12 gives (u_i, u_j) pairwise cross-cuts passing through the MPFP P^* in the standard normal space for $i, j \in \{1, \ldots, 8\}$. The approximate LSS obtained by the ASVR method is nearly coincident with the true one. The Gaussian RBF kernel with a single parameter γ to tune appears appropriate in this problem. This type of kernel is often a good candidate for smooth LSS. However, it is of importance to point out that it may lack flexibility in problems with a more intricate geometry. In such situations an anisotropic Gaussian kernel can be more appropriate, as found in example 2 addressed by Bourinet (2017b). It is however important to mention that this latter kernel is more difficult to tune in high dimensions, its number of parameters γ_i being equal to the dimension n of the input space, see Eq. (II.76).

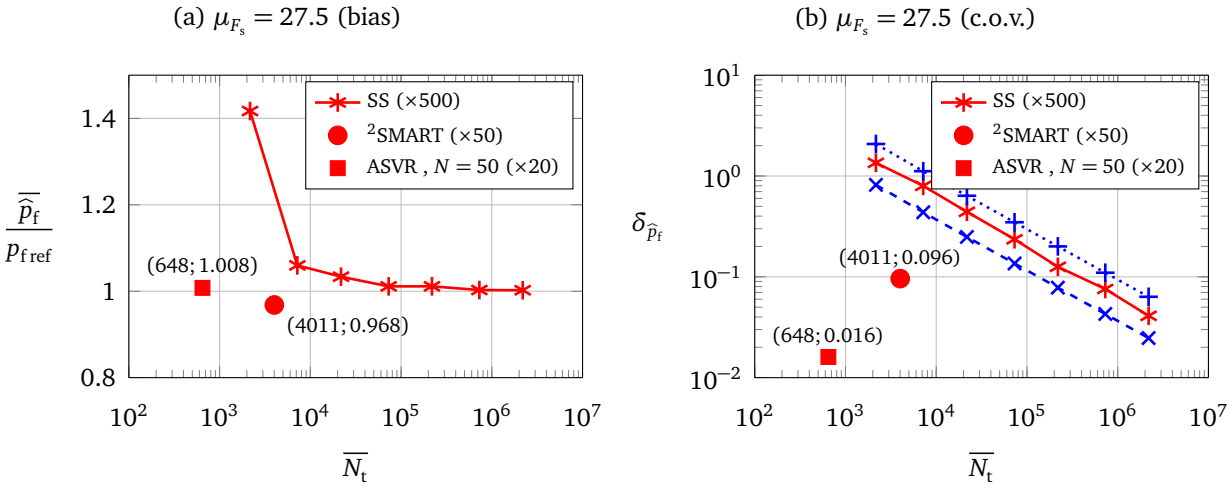

Figure II.10 – Example 1, $\mu_{F_s} = 27.5$. ^{2}SMART, ASVR and SS results.

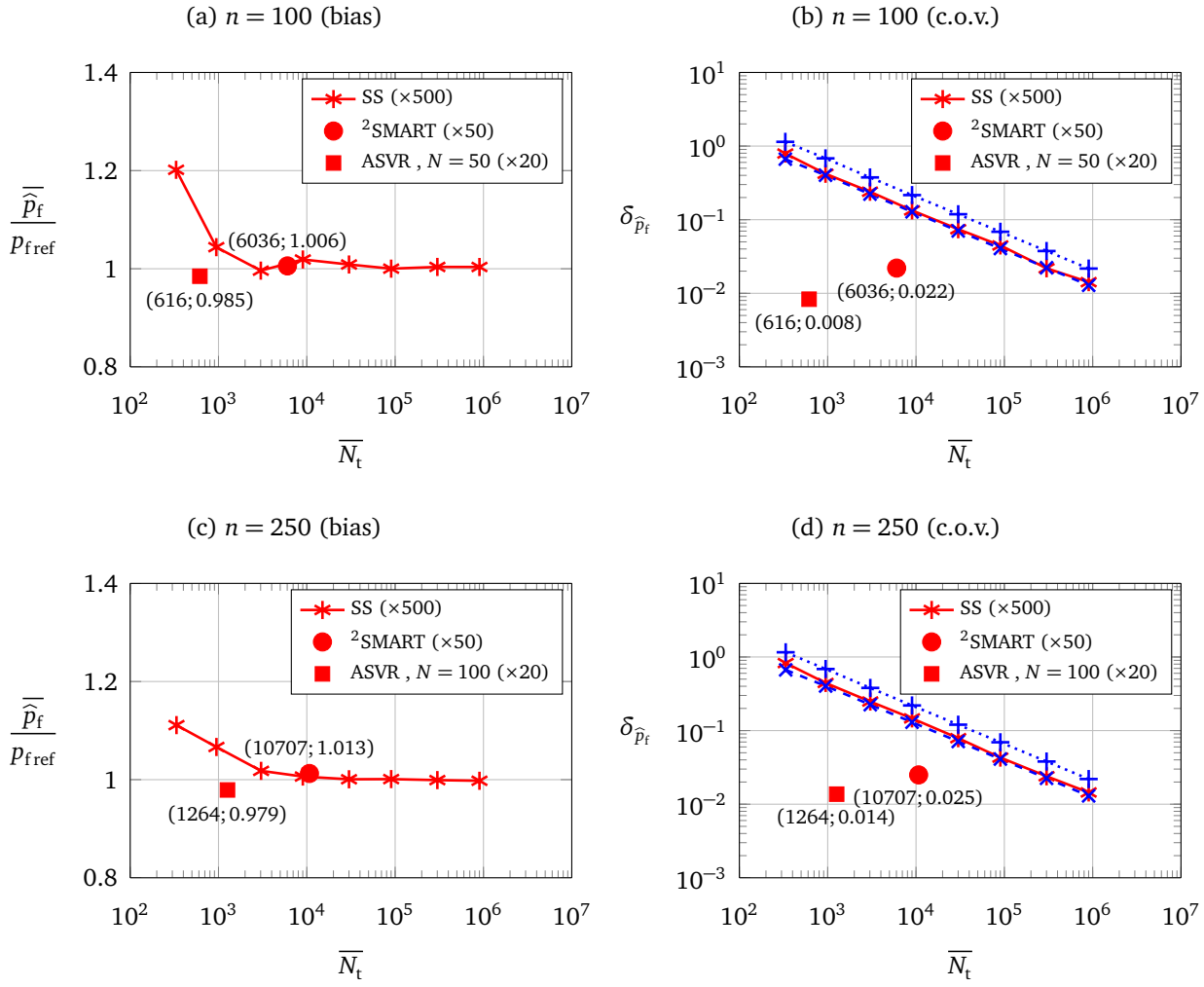

Figure II.11 – Example 2, $a = 3$, $n \in \{100; 250\}$. ²SMART, ASVR and SS results.

II–4 Kriging

This section gives a description of a surrogate modeling technique known as kriging. This method was originally developed in the 1950s by Krige (1951) in the context of geostatistics and later formalized by Matheron (1963) with the name of kriging. In this context the unknown function to approximate is a 2D or 3D spatial field observed only at a few points. The application of kriging to computer experiments is due to Sacks et al. (1989), where the number of inputs n could be larger than 2 or 3. Kriging in the context of SVMs uses kernels, and its relation to RKHS and regularization theory is well established through early studies on splines, see e.g. the synthesis made by Vazquez (2005). Due to its formulation based on Gaussian processes, kriging differs from SVMs by its probabilistic formulation. In this framework, the approximation model obtained by kriging makes use of the conditional process knowing the training data.

Section II–4.1 establishes the main equations of kriging in the case of a process of zero or known mean. Section II–4.2 extends the formulation to kriging with a trend in the case of an unknown mean of the process, with an introduction to universal kriging. Lastly, kriging in the context of noisy data is addressed in Section II–4.3, by including the nugget effect in the kriging equations. Section II–4.4 gives a few details about the techniques used for hyperparameter selection in kriging.

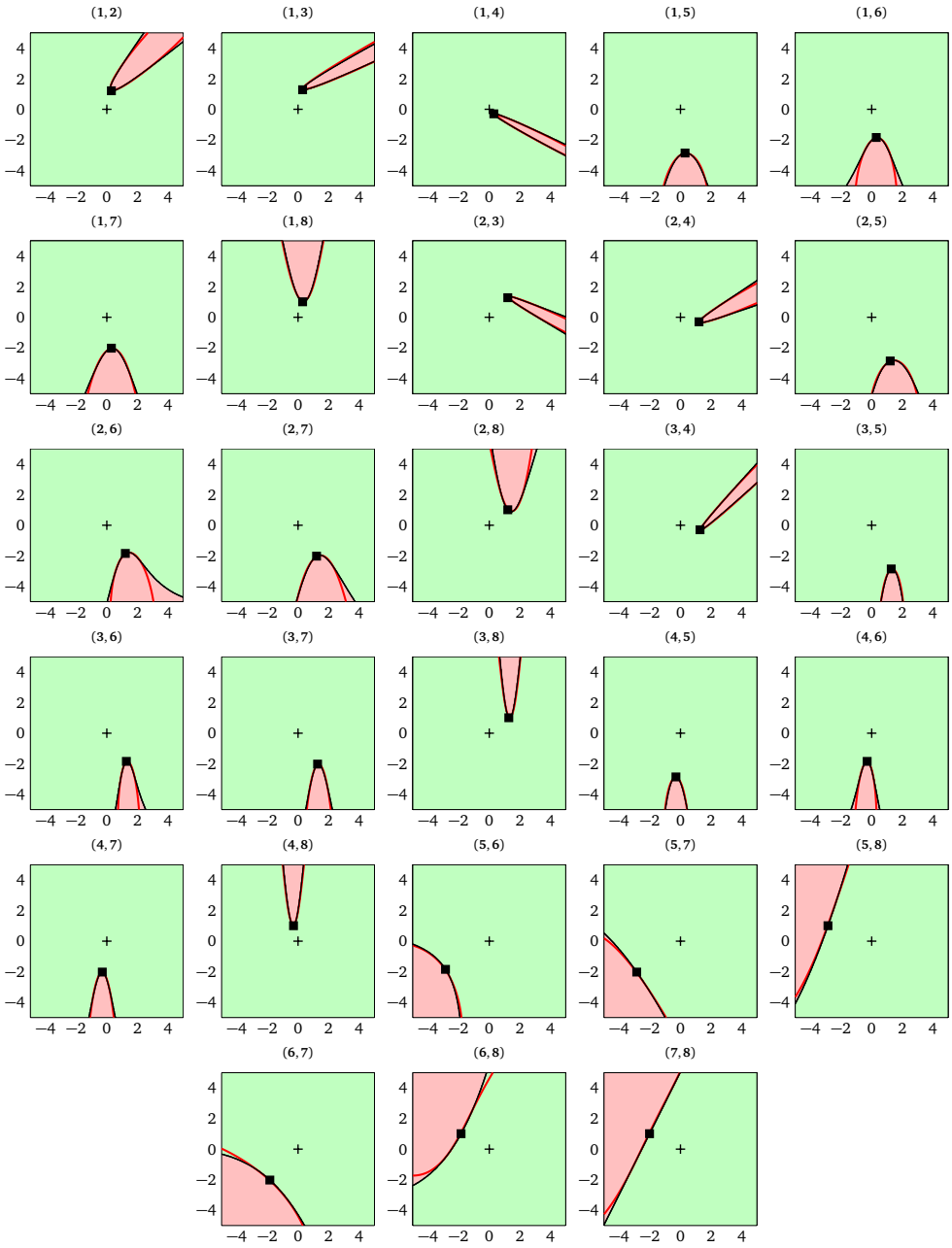

Figure II.12 – Example 1, $\mu_{F_s} = 27.5$. (P^*, u_i, u_j) cross-cuts at MPFP in standard normal space (random variable numbers in their order of appearance in Table I.4). Black square: MPFP, black cross: projection of space origin onto (P^*, u_i, u_j) cross-cut plane, black line: true LSS, green area: safe domain, pink area: failure domain, red line: SVR-based LSS $\{\mathbf{u} : \widetilde{G}_{s_{\text{final}}}(\mathbf{u}) = 0\}$.

Theoretical details about kriging can be found in well-known references in the field (Cressie, 1993; Stein, 1999; Santner et al., 2003; Chilès and Delfiner, 2012). A clear presentation of the main concepts of kriging is made by Vazquez (2005), including intrinsic kriging. For a more concise description, the reader may refer to the works of Dubourg (2011) and Moustapha (2016). A good introduction can also be found in Roustant et al. (2012).

II–4.1 Basics of kriging, simple kriging

As introduced in Section II–1, the objective is again to construct an approximation $\widetilde{y}$ of a true and unknown function $y : \mathcal{X} \to \mathcal{Y}, \mathbf{x} \mapsto y = y(\mathbf{x})$ knowing a set of data pairs $\mathcal{T} = \{(\mathbf{x}_i, y_i) \in \mathcal{X} \times \mathcal{Y}, 1 \leq i \leq N\}$, where $\mathcal{X} \subseteq \mathbb{R}^n$ and $y_i = y(\mathbf{x}_i)$ for $i = 1, \ldots, N$. As for SVM, the presentation will be restricted to a single scalar and real output, i.e. $\mathcal{Y} = \mathbb{R}$.

Kriging is based on the assumption that the unknown function y is a *realization* of a real-valued *random process* $Y(\mathbf{x})$ indexed over $\mathcal{X}$. The set of observed outputs $\{y_i, 1 \leq i \leq N\}$ then appears as respective realizations of the random variables $\{Y(\mathbf{x}_i), 1 \leq i \leq N\}$. We assume that $Y(\mathbf{x})$ is a square-integrable random process. Without loss of generality it is supposed that this random process has a zero mean. If not, we assume that the mean $\mu(\mathbf{x})$ of $Y(\mathbf{x})$ is known and we consider instead the centered process $Z(\mathbf{x}) = Y(\mathbf{x}) - \mu(\mathbf{x})$. Note that the assumption of a known mean is relaxed later for kriging with a trend. $Y(\mathbf{x})$ is therefore fully characterized by its covariance function (or covariance kernel[14]), for any $\mathbf{x}, \mathbf{x}' \in \mathcal{X}$:

$$k(\mathbf{x}, \mathbf{x}') = \mathrm{Cov}\left[Y(\mathbf{x}), Y(\mathbf{x}')\right] = \mathbb{E}\left[Y(\mathbf{x})Y(\mathbf{x}')\right] . \tag{II.128}$$

In kriging the objective is to construct a *predictor* $\widehat{Y}(\mathbf{x})$ of $Y(\mathbf{x})$ at a given point $\mathbf{x} \in \mathcal{X}$. This predictor is a random variable function of $\{Y(\mathbf{x}_i), 1 \leq i \leq N\}$. The kriging predictor is in general chosen in the class of linear predictors and defined as follows:

$$\widehat{Y}(\mathbf{x}) = \boldsymbol{\lambda}(\mathbf{x})^{\mathrm{T}} \mathbf{Y} , \tag{II.129}$$

where $\mathbf{Y} = (Y(\mathbf{x}_1), \ldots, Y(\mathbf{x}_N))^{\mathrm{T}}$ and $\boldsymbol{\lambda}(\mathbf{x}) \in \mathbb{R}^N$ is a vector of unknown weights that depend on the location $\mathbf{x}$. It is important to point out that the assumption of a linear predictor does not imply the linearity of the constructed approximate function $\widetilde{y}(\mathbf{x})$. As for SVMs, the nonlinearity of $\widetilde{y}$ results from the use of a kernel.

We can first notice that the kriging predictor $\widehat{Y}(\mathbf{x})$ has a zero mean and is therefore unbiased:

$$\mathbb{E}\left[\widehat{Y}(\mathbf{x})\right] = \boldsymbol{\lambda}(\mathbf{x})^{\mathrm{T}} \mathbb{E}\left[\mathbf{Y}\right] = \boldsymbol{\lambda}(\mathbf{x})^{\mathrm{T}} \mathbf{0} = 0 = \mathbb{E}\left[Y(\mathbf{x})\right] . \tag{II.130}$$

For a point $\mathbf{x} \in \mathcal{X}$ the weights $\boldsymbol{\lambda}(\mathbf{x})$ of the best predictor in the mean square sense are obtained by minimizing $\mathbb{E}\left[\left(\widehat{Y}(\mathbf{x}) - Y(\mathbf{x})\right)^2\right] = \mathrm{Var}\left[\widehat{Y}(\mathbf{x}) - Y(\mathbf{x})\right]$. The corresponding optimization problem writes as follows:

$$\min_{\boldsymbol{\lambda}(\mathbf{x})} \boldsymbol{\lambda}(\mathbf{x})^{\mathrm{T}} \mathbf{K} \boldsymbol{\lambda}(\mathbf{x}) - 2\boldsymbol{\lambda}(\mathbf{x})^{\mathrm{T}} \mathbf{k}(\mathbf{x}) + k(\mathbf{x}, \mathbf{x}) , \tag{II.131}$$

where $\mathbf{K} = [k(\mathbf{x}_i, \mathbf{x}_j)]_{1 \leq i,j \leq N}$ is the covariance matrix of the random variables $\{Y(\mathbf{x}_i), 1 \leq i \leq N\}$ and $\mathbf{k}(\mathbf{x}) = (k(\mathbf{x}_1, \mathbf{x}), \ldots, k(\mathbf{x}_N, \mathbf{x}))^{\mathrm{T}}$.

The optimality condition of Eq. (II.131) is:

$$\mathbf{K} \boldsymbol{\lambda}(\mathbf{x}) = \mathbf{k}(\mathbf{x}) . \tag{II.132}$$

[14] Contrarily to SVMs, the kernel used in kriging has a probabilistic interpretation. It represents the covariance between $Y(\mathbf{x})$ and $Y(\mathbf{x}')$.

The expression of the predictor $\widehat{Y}(\mathbf{x})$ in terms of $\boldsymbol{\lambda}(\mathbf{x})$ defined in Eq. (II.129), with the optimality conditions on $\boldsymbol{\lambda}(\mathbf{x})$ given by Eq. (II.132), is known as the *primal* formulation of kriging, as opposed to the dual formulation introduced in the following. This formulation was derived under the assumption of a known mean of $Y(\mathbf{x})$, which corresponds to so-called *simple kriging* (SK).

The weights $\boldsymbol{\lambda}(\mathbf{x})$ appearing in Eq. (II.129) need to be calculated for each $\mathbf{x} \in \mathcal{X}$ from Eq. (II.132). *Dual kriging* (Chilès and Delfiner, 2012) avoids solving Eq. (II.132) for each new point $\mathbf{x}$ where the prediction needs to be defined. Assuming that the covariance matrix $\mathbf{K}$ is full rank, and making use of the symmetry property of the covariance matrix $\mathbf{K}$ (and therefore of its inverse $\mathbf{K}^{-1}$), the predictor $\widehat{Y}(\mathbf{x})$ is rewritten as:

$$\begin{aligned}\widehat{Y}(\mathbf{x}) &= \left(\mathbf{K}^{-1}\mathbf{k}(\mathbf{x})\right)^{\mathrm{T}}\mathbf{Y} \\ &= \mathbf{k}(\mathbf{x})^{\mathrm{T}}\mathbf{K}^{-1}\mathbf{Y} \\ &= \mathbf{k}(\mathbf{x})^{\mathrm{T}}\mathbf{C} \\ &= \sum_{i=1}^{N} C_i k(\mathbf{x}_i, \mathbf{x}) \,,\end{aligned} \tag{II.133}$$

where the random vector $\mathbf{C} = (C_1, \ldots, C_N)^{\mathrm{T}}$ is the solution of the following linear system of equations:

$$\mathbf{K}\mathbf{C} = \mathbf{Y} \,. \tag{II.134}$$

The above-defined system needs to be solved only once, for the available realization $\mathbf{y} = (y_1, \ldots, y_N)^{\mathrm{T}}$ of $\mathbf{Y} = (Y(\mathbf{x}_1), \ldots, Y(\mathbf{x}_N))^{\mathrm{T}}$:

$$\mathbf{K}\mathbf{c} = \mathbf{y} \,, \tag{II.135}$$

where $\mathbf{c} = (c_1, \ldots, c_N)^{\mathrm{T}} \in \mathbb{R}^N$. Note that the solution vector $\mathbf{c}$ does not depend on the location $\mathbf{x}$ where the prediction needs to be defined.

The so-called *mean prediction* at location $\mathbf{x}$ can be obtained. In the case of simple kriging it is given by:

$$\begin{aligned}\mu_{\mathrm{SK}}(\mathbf{x}) &= \mathbf{k}(\mathbf{x})^{\mathrm{T}}\mathbf{K}^{-1}\mathbf{y} \\ &= \mathbf{k}(\mathbf{x})^{\mathrm{T}}\mathbf{c} \\ &= \sum_{i=1}^{N} c_i k(\mathbf{x}_i, \mathbf{x}) \,,\end{aligned} \tag{II.136}$$

where $\mathbf{c}$ is the solution of Eq. (II.135). It is important to notice that the mean prediction of the dual formulation of simple kriging has the same expression as that obtained from the representer theorem for SVMs, see Eq. (II.89).

Eq. (II.136) further generalizes as follows in the case of a non-centered random process $Y(\mathbf{x})$ with known mean $\mu(\mathbf{x})$:

$$\mu_{\mathrm{SK}}(\mathbf{x}) = \mu(\mathbf{x}) + \mathbf{k}(\mathbf{x})^{\mathrm{T}}\mathbf{K}^{-1}\left(\mathbf{y} - \boldsymbol{\mu}\right) \,. \tag{II.137}$$

where $\boldsymbol{\mu} = (\mu(\mathbf{x}_1), \ldots, \mu(\mathbf{x}_N))^{\mathrm{T}}$.

In the context of function approximation, it is worth noting that this mean prediction is in general taken as the surrogate model $\widetilde{y}$ for any $(\mathbf{x}) \in \mathcal{X}$:

$$\widetilde{y}(\mathbf{x}) = \mu_{\mathrm{SK}}(\mathbf{x}) \,. \tag{II.138}$$

The variance of the prediction error $\widehat{Y}(\mathbf{x}) - Y(\mathbf{x})$ can also be easily derived. This quantity, known as the *kriging variance*, is given by:

$$\begin{aligned}\sigma^2_{\mathrm{SK}}(\mathbf{x}) = \mathrm{Var}\left[\widehat{Y}(\mathbf{x}) - Y(\mathbf{x})\right] &= \mathbb{E}\left[\left(\widehat{Y}(\mathbf{x}) - Y(\mathbf{x})\right)^2\right] \\ &= \mathbb{E}\left[\widehat{Y}(\mathbf{x})^2\right] - 2\mathbb{E}\left[\widehat{Y}(\mathbf{x})Y(\mathbf{x})\right] + \mathbb{E}\left[Y(\mathbf{x})^2\right] \\ &= \boldsymbol{\lambda}(\mathbf{x})^{\mathrm{T}}\mathbf{K}\,\boldsymbol{\lambda}(\mathbf{x}) - 2\boldsymbol{\lambda}(\mathbf{x})^{\mathrm{T}}\mathbf{k}(\mathbf{x}) + k(\mathbf{x},\mathbf{x}) \\ &= k(\mathbf{x},\mathbf{x}) - \mathbf{k}(\mathbf{x})^{\mathrm{T}}\mathbf{K}^{-1}\,\mathbf{k}(\mathbf{x})\,.\end{aligned} \tag{II.139}$$

The last line is obtained by plugging the optimal weights $\boldsymbol{\lambda}(\mathbf{x})$ obtained from Eq. (II.132) into the equation, assuming again an invertible covariance matrix $\mathbf{K}$ and making use of the symmetry property of the covariance matrix $\mathbf{K}$ (and therefore of its inverse $\mathbf{K}^{-1}$).

The kriging predictor $\widehat{Y}(\mathbf{x})$ is characterized by the following important properties (see, e.g., Chilès and Delfiner, 2012, Chapter 3):

- *Unbiased predictor*: assuming that $Y(\mathbf{x})$ has a known mean, we find that $\widehat{Y}$ is an unbiased predictor of $Y(\mathbf{x})$, i.e. that $\mathbb{E}\left[\widehat{Y}(\mathbf{x})\right] = \mathbb{E}[Y(\mathbf{x})]$ for any $\mathbf{x} \in \mathcal{X}$, see Eq. (II.130) in the specific case of simple kriging. If kriging with a trend is applied, a constraint needs to be added to the optimization problem defined in Eq. (II.131) to ensure the unbiasedness of the constructed predictor, see Section II–4.2.
- *Exact interpolator*: it is easy to prove that $\widehat{Y}$ is an exact interpolator, i.e. that $\widehat{Y}(\mathbf{x}_i) = Y(\mathbf{x}_i)$ for $i = 1, \ldots, N$. If a nugget effect is introduced into the kriging formulation (e.g. to handle noisy data), we will see in Section II–4.3 that this property no longer holds.
- *Kriging variance*: the kriging variance is equal to zero at each $\mathbf{x} = \mathbf{x}_i$ for $i = 1, \ldots, N$. Again this property disappears when a nugget effect is introduced into the kriging formulation. Moreover, the kriging variance in the case of simple kriging does not depend on $\mathbf{y}$.
- *Choice of a Gaussian process for $Y(\mathbf{x})$*: if $Y(\mathbf{x})$ is assumed to be Gaussian, the conditional process $Y(\mathbf{x})|\mathbf{Y} = \mathbf{y}$ is still Gaussian. Under such an assumption the SK prediction mean $\mu_{\mathrm{SK}}(\mathbf{x})$ and variance $\sigma_{\mathrm{SK}}(\mathbf{x})^2$ at location $\mathbf{x}$ respectively coincide with the conditional mean and variance of the process $Y(\mathbf{x})|\mathbf{Y} = \mathbf{y}$. The Gaussian assumption of the process is transmitted to the predictor $\widehat{Y}(\mathbf{x})$ as a linear combination of the Gaussian observations $Y(\mathbf{x}_i)$ for $i = 1, \ldots, N$. This enables easy calculations of exceedance probabilities $\mathbb{P}(\widehat{Y}(\mathbf{x}) < c)$, $c \in \mathbb{R}$, and confidence intervals $[a, b]$ such that $\widehat{Y}(\mathbf{x}) \in [a, b]$ with probability $1 - \alpha$, $a, b \in \mathbb{R}$ and $a < b$.

The choice of a covariance kernel k for a random process is, as for SVMs, of paramount importance in the accuracy of the predicted output. A function $k : \mathcal{X} \times \mathcal{X} \to \mathbb{R}$ is a covariance kernel if and only if it is a symmetric positive definite function, see Eq. (II.71). The usual approach among kriging practitioners is to use *stationary* covariance kernels[15], such as the Gaussian and Matérn kernels introduced in Section II–2.3.1, most often in their anisotropic versions. Such stationary covariance kernels are usually defined in terms of the autocorrelation function R of the process satisfying:

$$k(\mathbf{x}, \mathbf{x}') = f(\mathbf{x} - \mathbf{x}') = \sigma^2 R(\mathbf{x} - \mathbf{x}')\,, \tag{II.140}$$

where $\sigma^2 = f(\mathbf{0})$ is the variance of the process.

With such a definition, the kriging mean and variance respectively rewrite as follows:

$$\begin{aligned}\mu_{\mathrm{SK}}(\mathbf{x}) &= \mu(\mathbf{x}) + \mathbf{r}(\mathbf{x})^{\mathrm{T}}\mathbf{R}^{-1}(\mathbf{y} - \boldsymbol{\mu}) \\ \sigma^2_{\mathrm{SK}}(\mathbf{x}) &= \sigma^2\left[1 - \mathbf{r}(\mathbf{x})^{\mathrm{T}}\mathbf{R}^{-1}\mathbf{r}(\mathbf{x})\right]\,,\end{aligned} \tag{II.141}$$

where $\mathbf{R} = [R(\mathbf{x}_i - \mathbf{x}_j)]_{1 \le i,j \le N}$ is the correlation matrix and $\mathbf{r}(\mathbf{x}) = (R(\mathbf{x}_1 - \mathbf{x}), \ldots, R(\mathbf{x}_N - \mathbf{x}))^{\mathrm{T}}$.

[15] The use of non-stationary kernels in kriging is less popular than stationary ones, see e.g. an example of such use in the work of Xiong et al. (2007).

II–4.2 Kriging with a trend

The mean of the random process $Y(\mathbf{x})$ is in general unknown, and needs to be estimated from the set of training data pairs $\mathcal{T}$. A common assumption is to consider that $Y(\mathbf{x})$ is the sum of two terms, respectively termed *drift* and *residual*:

$$Y(\mathbf{x}) = \mu(\mathbf{x}) + Z(\mathbf{x}) \,, \tag{II.142}$$

where $Z(\mathbf{x})$ is a zero-mean square-integrable random process and $\mu(\mathbf{x})$ is its unknown mean assumed to be expressed as follows:

$$\mu(\mathbf{x}) = \sum_{j=1}^{M} d_j p_j(\mathbf{x}) = \mathbf{p}(\mathbf{x})^{\mathrm{T}} \mathbf{d} \,, \tag{II.143}$$

where $\mathbf{p}(\mathbf{x}) = (p_1(\mathbf{x}), \ldots, p_M(\mathbf{x}))^{\mathrm{T}}$ is a given basis of $M \in \mathbb{N}_{>0}$ real-valued functions, where $p_j : \mathcal{X} \to \mathbb{R}$ for $1, \ldots, M$, and $\mathbf{d} = (d_1, \ldots, d_M)^{\mathrm{T}} \in \mathbb{R}^M$ is a vector on unknown coefficients.

A linear predictor $\widehat{Y}(\mathbf{x})$ satisfying Eq. (II.129) is again sought. Let us first express the random deviation between $\widehat{Y}(\mathbf{x})$ and $Y(\mathbf{x})$:

$$\begin{aligned} \widehat{Y}(\mathbf{x}) - Y(\mathbf{x}) &= \boldsymbol{\lambda}(\mathbf{x})^{\mathrm{T}} \mathbf{Y} - Y(\mathbf{x}) \\ &= \boldsymbol{\lambda}(\mathbf{x})^{\mathrm{T}} (\mathbf{P}\mathbf{d} + \mathbf{Z}) - \big(\mathbf{p}(\mathbf{x})^{\mathrm{T}} \mathbf{d} + Z(\mathbf{x})\big) \\ &= \boldsymbol{\lambda}(\mathbf{x})^{\mathrm{T}} \mathbf{Z} - Z(\mathbf{x}) + \big(\boldsymbol{\lambda}(\mathbf{x})^{\mathrm{T}} \mathbf{P} - \mathbf{p}(\mathbf{x})^{\mathrm{T}}\big) \mathbf{d} \,, \end{aligned} \tag{II.144}$$

where $\mathbf{P} = [p_j(\mathbf{x}_i)]_{1 \le i \le N \,, 1 \le j \le M}$, $\mathbf{Z} = (Z(\mathbf{x}_1), \ldots, Z(\mathbf{x}_N))^{\mathrm{T}}$, and where $\boldsymbol{\lambda}(\mathbf{x})$ and $\mathbf{d}$ are the unknown weights.

The expectation of this deviation reduces to:

$$\mathbb{E}\big[\widehat{Y}(\mathbf{x}) - Y(\mathbf{x})\big] = \big(\boldsymbol{\lambda}(\mathbf{x})^{\mathrm{T}} \mathbf{P} - \mathbf{p}(\mathbf{x})^{\mathrm{T}}\big) \mathbf{d} \,, \tag{II.145}$$

since $\mathbb{E}[\mathbf{Z}] = \mathbf{0}$ and $\mathbb{E}[Z(\mathbf{x})] = 0$ (we assume that the process $Z(\mathbf{x})$ has a zero mean).

The unbiasedness property of $\widehat{Y}(\mathbf{x})$ therefore imposes the following constraint on $\boldsymbol{\lambda}(\mathbf{x})$:

$$\boldsymbol{\lambda}(\mathbf{x})^{\mathrm{T}} \mathbf{P} - \mathbf{p}(\mathbf{x})^{\mathrm{T}} = \mathbf{0}^{\mathrm{T}} \,. \tag{II.146}$$

Under the constraint of no bias the best predictor $\widehat{Y}(\mathbf{x})$ in the mean square sense is obtained by minimizing $\mathbb{E}\Big[\big(\widehat{Y}(\mathbf{x}) - Y(\mathbf{x})\big)^2\Big] = \mathrm{Var}\big[\widehat{Y}(\mathbf{x}) - Y(\mathbf{x})\big]$. The corresponding optimization problem therefore writes as follows:

$$\min_{\boldsymbol{\lambda}(\mathbf{x})} \boldsymbol{\lambda}(\mathbf{x})^{\mathrm{T}} \mathbf{K} \boldsymbol{\lambda}(\mathbf{x}) - 2\boldsymbol{\lambda}(\mathbf{x})^{\mathrm{T}} \mathbf{k}(\mathbf{x}) + k(\mathbf{x}, \mathbf{x}) \quad \text{s.t.} \quad \mathbf{P}^{\mathrm{T}} \boldsymbol{\lambda}(\mathbf{x}) - \mathbf{p}(\mathbf{x}) = \mathbf{0} \,, \tag{II.147}$$

where $\mathbf{K} = [k(\mathbf{x}_i, \mathbf{x}_j)]_{1 \le i,j \le N}$ is the covariance matrix of the random variables $\{Z(\mathbf{x}_i), 1 \le i \le N\}$, $\mathbf{k}(\mathbf{x}) = (k(\mathbf{x}_1, \mathbf{x}), \ldots, k(\mathbf{x}_N, \mathbf{x}))^{\mathrm{T}}$ and $k(\mathbf{x}, \mathbf{x}') = \mathrm{Cov}\big[Z(\mathbf{x}), Z(\mathbf{x}')\big] = \mathbb{E}\big[Z(\mathbf{x}) Z(\mathbf{x}')\big]$.

The optimality conditions are given in the following matrix form:

$$\begin{bmatrix} \mathbf{K} & \mathbf{P} \\ \mathbf{P}^{\mathrm{T}} & \mathbf{0} \end{bmatrix} \begin{pmatrix} \boldsymbol{\lambda}(\mathbf{x}) \\ \boldsymbol{\beta}(\mathbf{x}) \end{pmatrix} = \begin{pmatrix} \mathbf{k}(\mathbf{x}) \\ \mathbf{p}(\mathbf{x}) \end{pmatrix} , \tag{II.148}$$

which is denoted $\overline{\mathbf{K}}\, \overline{\boldsymbol{\lambda}}(\mathbf{x}) = \overline{\mathbf{k}}(\mathbf{x})$ in the following and where $\boldsymbol{\beta}(\mathbf{x}) = (\beta_1(\mathbf{x}), \ldots, \beta_M(\mathbf{x}))^{\mathrm{T}}$ is the vector of Lagrange multipliers introduced to enforce the equality constraint.

The mean prediction at location $\mathbf{x}$ then can be expressed as follows:

$$\begin{aligned}\mu_{\text{UK}}(\mathbf{x}) &= \boldsymbol{\lambda}(\mathbf{x})^{\text{T}}\mathbf{y} \\ &= \overline{\boldsymbol{\lambda}}(\mathbf{x})^{\text{T}}\overline{\mathbf{y}} \\ &= \overline{\mathbf{k}}(\mathbf{x})^{\text{T}}\overline{\mathbf{K}}^{-1}\overline{\mathbf{y}} \\ &= \overline{\mathbf{k}}(\mathbf{x})^{\text{T}}\overline{\mathbf{c}} \\ &= \mathbf{k}(\mathbf{x})^{\text{T}}\mathbf{c} + \mathbf{p}(\mathbf{x})^{\text{T}}\mathbf{d} \\ &= \sum_{i=1}^{N} c_i k(\mathbf{x}_i, \mathbf{x}) + \sum_{j=1}^{M} d_j p_j(\mathbf{x}) \,,\end{aligned} \tag{II.149}$$

where $\overline{\mathbf{y}} = (\mathbf{y}^{\text{T}}, \mathbf{0}_{1\times M})^{\text{T}}$ and where $\overline{\mathbf{c}} = (\mathbf{c}^{\text{T}}, \mathbf{d}^{\text{T}})^{\text{T}}$, $\mathbf{c} \in \mathbb{R}^N$, $\mathbf{d} \in \mathbb{R}^M$ is the solution of the following linear system of equations for the given realization $\mathbf{y}$ of $\mathbf{Y}$:

$$\overline{\mathbf{K}}\,\overline{\mathbf{c}} = \overline{\mathbf{y}} \,, \tag{II.150}$$

assuming that $\overline{\mathbf{K}}$ is invertible. We can notice that the mean prediction now has the same expression as that obtained by means of the semiparametric representer theorem for SVMs, see Eq. (II.91).

After simple calculations the mean prediction can be further expressed as follows:

$$\mu_{\text{UK}}(\mathbf{x}) = \mathbf{p}(\mathbf{x})^{\text{T}}\widehat{\mathbf{d}} + \mathbf{k}(\mathbf{x})^{\text{T}}\mathbf{K}^{-1}\left(\mathbf{y} - \mathbf{P}\widehat{\mathbf{d}}\right) \,, \tag{II.151}$$

where $\widehat{\mathbf{d}} = \left(\mathbf{P}^{\text{T}}\mathbf{K}^{-1}\mathbf{P}\right)^{-1}\mathbf{P}^{\text{T}}\mathbf{K}^{-1}\mathbf{y}$, and the kriging variance is given by:

$$\sigma^2_{\text{UK}}(\mathbf{x}) = \sigma^2_{\text{SK}}(\mathbf{x}) + \mathbf{u}(\mathbf{x})^{\text{T}}\left(\mathbf{P}^{\text{T}}\mathbf{K}^{-1}\mathbf{P}\right)^{-1}\mathbf{u}(\mathbf{x}) \,, \tag{II.152}$$

where $\mathbf{u}(\mathbf{x}) = \mathbf{p}(\mathbf{x})^{\text{T}} - \mathbf{k}(\mathbf{x})^{\text{T}}\mathbf{K}^{-1}\mathbf{P}$ and $\sigma^2_{\text{SK}}(\mathbf{x})$ is defined in Eq. (II.139). For more details, the interested reader may refer to (Dubourg, 2011, Section 1.4) in which the expression of the universal kriging mean prediction and variance are derived for a given autocorrelation function R.

If $M > 1$, the formulation detailed in the present section is known as *universal* kriging (UK). The specific case where $M = 1$ and $p_1 : \mathcal{X} \to \mathbb{R}, \mathbf{x} \mapsto 1$ corresponds to *ordinary* kriging (OK), i.e. to the assumption of an unknown *constant* mean.

The properties of the UK predictor are similar to those of the SK one that are detailed in Section II–4.1. Another interesting property concerns the prediction made far from the points of the training set $\mathcal{T}$ under the assumption of a stationary covariance kernel k decreasing with $\|\mathbf{x} - \mathbf{x}'\|$ (Roustant et al., 2012). $\mu_{\text{UK}}(\mathbf{x})$ tends to the best linear fit $\mathbf{p}(\mathbf{x})^{\text{T}}\widehat{\mathbf{d}}$ for locations where the covariances gathered in $\mathbf{k}(\mathbf{x})$ are small. In addition, the kriging variance $\sigma^2_{\text{UK}}(\mathbf{x})$ becomes large at these locations, reflecting the uncertainty in the estimation of $\mathbf{d}$.

Universal kriging can be placed in the broader context of *intrinsic* kriging (Matheron, 1973). Such a formulation is based on *intrinsic random functions* (IRF) which allow $Y(\mathbf{x})$ to be nonstationary, with the assumption that increments $Y(\mathbf{x}) - Y(\mathbf{x}')$ are second-order stationary. Stationary differences enable a constant drift to be removed (i.e. the unknown constant mean). A wider class of functions includes IRFs of order k whose increments of order k are second-order stationary, which remove a polynomial drift of order up to k (see, e.g., Chilès and Delfiner, 2012). The connection between intrinsic kriging and regularized regression can be made (see, e.g., Vazquez, 2005). Intrinsic kriging hinges on semi-RKHS, evoked in Section II–2.3.1, based on conditionally positive definite kernels.

In practice, ordinary kriging is often preferred to its more general universal counterpart. If no prior information is available about the trend, the safer choice (i.e. one that avoids overfitting) is to consider an unknown and constant mean only (Ginsbourger et al., 2009). The scarce information known from

the available training set is in general not sufficient to make any guess about the trend. As an additional point in favor of ordinary kriging, the number M of functions that are selected in the basis $\mathbf{p}(\mathbf{x})$ may substantially increase the size of the training set $\mathcal{T}$ (its size needs to be at least equal to M). As an example, a second-order polynomial (with interactions) in $\mathbb{R}^n$ requires that $N \geq (n+1)(n+2)/2$, which may be too large from a computational viewpoint. In practical situations, the limits in the choice of the functional basis are those imposed by the size of the training set. For these two reasons ordinary kriging was favored in the works of Dubourg (2011) and Moustapha (2016). Additionally, it is worth noting a few recent attempts to propose some well-chosen function basis for the mean of the process, such as PCE determined by least-angle-regression (Schöbi et al., 2015; Schöbi et al., 2017) and nested polynomial (Perrin et al., 2017). The advantages of using such approaches remains to be demonstrated, in the author's opinion, especially in the context of high-dimensional spaces, small training sets and complex functions to approximate.

II–4.3 Noisy data, relation between kriging and SVR

As pointed out in Section II–4.1, the kriging mean $\mu_{\text{UK}}(\mathbf{x})$ and therefore the constructed approximate model $\tilde{y}(\mathbf{x})$ interpolate the training data. In some situations this property needs to be relaxed. If e.g. the output of the true model y has a stochastic nature, we do not want $\mu_{\text{UK}}(\mathbf{x})$ to interpolate $\mathcal{T} = \{(\mathbf{x}_i, y_i) \in \mathcal{X} \times \mathcal{Y}, 1 \leq i \leq N\}$ where y_i for $i = 1, \ldots, N$ are given realizations of the true model outputs. Another situation appears when the true model output is defined with some usually unknown accuracy (e.g. numerical solution of a finite element problem in structural mechanics). For two input vectors $\mathbf{x}$ and $\mathbf{x}'$ that are very close, the corresponding outputs may substantially differ, due to the numerical error made on the solutions given by the true model (e.g. due to discretization or convergence errors). Interpolating the data makes here no sense, and it is preferable to construct a regularized approximate model, which is close to the available data without being interpolating.

For this purpose a common technique in kriging consists in introducing the so-called *nugget effect* (Forrester et al., 2006). The training set $\mathcal{T}$ is now assumed to be composed of *noisy* observations $y_i = y(\mathbf{x}_i) + \epsilon_i$ of the true outputs $y(\mathbf{x}_i)$ for $i = 1, \ldots, N$ where ϵ_i are zero-mean random variables of respective variances τ_i^2. A common choice consists in considering the N noises ϵ_i as i.i.d. Gaussian random variables with the same variance $\tau^2 = \tau_1^2 = \ldots = \tau_N^2$. Such a choice corresponds to the assumption of a homogeneous level of noise. Under the assumption that the random process $Y(\mathbf{x})$ is Gaussian and that the N Gaussian noises ϵ_i are statistically independent, $Y(\mathbf{x})$ is still Gaussian conditionally on the noisy observations $Y(\mathbf{x}_i) + \epsilon_i$ for $i = 1, \ldots, N$.

In the kriging equations introduced so far (primal or dual form, SK, OK or UK), we only need to replace the covariance matrix $\mathbf{K}$ by $(\mathbf{K} + \tau^2 \mathbf{1})$ where $\mathbf{1}$ is the $N \times N$ identity matrix.[16] The main consequences of such an assumption in terms of properties of the kriging predictor are that the mean prediction is no longer interpolating and that the kriging variance does not vanish at the observation points $\{\mathbf{x}_i, i = 1, \ldots, N\}$.

Let us rewrite the optimality conditions defined in Eq. (II.148) (primal formulation) in the specific case of ordinary kriging (OK) with inclusion of the nugget effect:

$$\begin{bmatrix} \mathbf{K} + \tau^2 \mathbf{1} & \mathbf{1} \\ \mathbf{1}^{\mathrm{T}} & 0 \end{bmatrix} \begin{pmatrix} \boldsymbol{\lambda}(\mathbf{x}) \\ \beta(\mathbf{x}) \end{pmatrix} = \begin{pmatrix} \mathbf{k}(\mathbf{x}) \\ 1 \end{pmatrix}, \tag{II.153}$$

[16] The kriging formulation proposed here differs slightly from the so-called *kriging with nugget effect* used in geostatistics, which also includes the noise variance τ^2 in $\mathbf{k}(\mathbf{x})$ (see, e.g., Roustant et al., 2012). Using τ^2 in both the covariance matrix $\mathbf{K}$ and the covariance vector $\mathbf{k}(\mathbf{x})$ results in an *interpolating* kriging mean predictor.

and the corresponding dual formulation given in Eq. (II.135):

$$\begin{bmatrix} \mathbf{K}+\tau^2\mathbf{1} & \mathbf{1} \\ \mathbf{1}^{\mathrm{T}} & 0 \end{bmatrix} \begin{pmatrix} \mathbf{c} \\ d \end{pmatrix} = \begin{pmatrix} \mathbf{y} \\ 0 \end{pmatrix} . \tag{II.154}$$

The connection between SVR and kriging now becomes obvious. Let us consider the specific case of LS-SVR, whose solution is given by Eq. (II.65) where the Gram matrix should be taken as that associated with a given kernel k, i.e. defined by Eq. (II.70). The linear system of equations to solve in OK is *identical* to that of LS-SVR with a bias term b, with the following identities: $\mathbf{c} \equiv \boldsymbol{\alpha}$, $d \equiv b$ and $\tau^2 \equiv 1/C$. For the same set of kernel parameters and with $\tau^2 = 1/C$, the OK mean prediction is therefore equivalent to the LS-SVR regressor:

$$\widetilde{y}(\mathbf{x}) = \mu_{\mathrm{OK}}(\mathbf{x}) = \sum_{i=1}^{N} c_i k(\mathbf{x}_i, \mathbf{x}) + d \quad \equiv \quad \widetilde{y}(\mathbf{x}) = \widetilde{f}_{\text{LS-SVR}}(\mathbf{x}) = \sum_{i=1}^{N} \alpha_i k(\mathbf{x}_i, \mathbf{x}) + b \, . \tag{II.155}$$

Let us again recall that LS-SVR corresponds to L2-ϵ-SVR with a zero-width ϵ tube, i.e. satisfying $\epsilon = 0$, see Section II–2.2.2. This conclusion can be generalized to universal kriging by considering a function basis $\mathbf{p}(\mathbf{x}) = (p_1(\mathbf{x}), \ldots, p_M(\mathbf{x}))^{\mathrm{T}}$ in the LS-SVR formulation instead of a single constant bias term b. The interested reader may refer to (Matías et al., 2004) for further details about this comparison. However, it is important to point out that no probabilistic interpretation can be given to the LS-SVR solution, contrary to kriging, which defines the variance of the predictor.

II–4.4 Hyperparameter selection

As for SVMs, a central issue in kriging is the choice of the covariance kernel k. A common practice consists in selecting a parametric family for the kernel k, defined in terms of a vector of unknown parameters $\boldsymbol{\theta}$: $k(\mathbf{x}, \mathbf{x}') = k(\mathbf{x}, \mathbf{x}'; \boldsymbol{\theta})$. Under the assumption that this kernel is able to correctly "fit" the true function y to learn, the main numerical task then consists in finding the best values of $\boldsymbol{\theta}$ that achieve the greatest accuracy of the approximate model $\widetilde{y}$ w.r.t. the true function y. Apart from the variogram estimation, which is inapplicable in dimension $n > 3$, there are two main techniques available for parameter selection in kriging, namely maximum likelihood estimation (MLE) and cross-validation (CV).

Let us first consider MLE. The observations $\mathbf{Y}$ follow the multivariate normal distribution:

$$\mathbf{Y} \sim \mathcal{N}_n(\mathbf{P}\mathbf{d}, \mathbf{K}) \, . \tag{II.156}$$

We will restrict the presentation to noise-free kriging for the sake of brevity (see, e.g., Roustant et al., 2012, Appendix A, for noisy kriging). In the case of a stationary covariance kernel k defined in terms of an autocorrelation function R, the covariance matrix is denoted $\mathbf{K}(\sigma, \boldsymbol{\theta}) = \sigma^2 \mathbf{R}(\boldsymbol{\theta})$ where σ^2 is the variance of the process and $\mathbf{R}(\boldsymbol{\theta}) = [R(\mathbf{x}_i - \mathbf{x}_j; \boldsymbol{\theta})]_{1 \leq i,j \leq N}$ is the correlation matrix. The likelihood of the observations writes:

$$\mathcal{L}(\mathbf{d}, \sigma, \boldsymbol{\theta} \mid \mathbf{y}) = \frac{1}{(2\pi\sigma^2)^{\frac{n}{2}} |\mathbf{R}(\boldsymbol{\theta})|^{\frac{1}{2}}} \exp\left[-\frac{1}{2\sigma^2} (\mathbf{y} - \mathbf{P}\mathbf{d})^{\mathrm{T}} \mathbf{R}(\boldsymbol{\theta})^{-1} (\mathbf{y} - \mathbf{P}\mathbf{d}) \right] . \tag{II.157}$$

The MLE estimates of $\mathbf{d}$ and σ^2 are analytically obtained from the first-order optimality conditions of the log-likelihood minimization problem:

$$\begin{aligned} \widehat{\mathbf{d}}(\boldsymbol{\theta}) &= \left(\mathbf{P}^{\mathrm{T}} \mathbf{R}(\boldsymbol{\theta})^{-1} \mathbf{P} \right)^{-1} \mathbf{P}^{\mathrm{T}} \mathbf{R}(\boldsymbol{\theta})^{-1} \mathbf{y} \\ \widehat{\sigma^2}(\boldsymbol{\theta}) &= \frac{1}{N} \left(\mathbf{y} - \mathbf{P}\widehat{\mathbf{d}}(\boldsymbol{\theta}) \right)^{\mathrm{T}} \mathbf{R}(\boldsymbol{\theta})^{-1} \left(\mathbf{y} - \mathbf{P}\widehat{\mathbf{d}}(\boldsymbol{\theta}) \right) . \end{aligned} \tag{II.158}$$

By plugging the expressions of $\widehat{\mathbf{d}}$ and $\widehat{\sigma^2}$ into Eq. (II.157), we obtain an expression of the log-likelihood that only depends on the autocorrelation function parameters gathered in $\boldsymbol{\theta}$:

$$\log \mathcal{L}(\boldsymbol{\theta} \mid \mathbf{y}) = -\frac{n}{2}\left[1 + \log(2\pi)\right] - \frac{n}{2}\log\left(\widehat{\sigma^2}(\boldsymbol{\theta})\,|\mathbf{R}(\boldsymbol{\theta})|^{\frac{1}{n}}\right). \tag{II.159}$$

The MLE estimate of $\boldsymbol{\theta}$ is equivalently given by:

$$\widehat{\boldsymbol{\theta}} = \arg\min_{\boldsymbol{\theta}\in\boldsymbol{\Theta}} \psi(\boldsymbol{\theta}) = \widehat{\sigma^2}(\boldsymbol{\theta})\,|\mathbf{R}(\boldsymbol{\theta})|^{\frac{1}{n}}, \tag{II.160}$$

where $\psi(\boldsymbol{\theta})$ is known as the *reduced* likelihood function and $\boldsymbol{\Theta}$ denotes the domain in which the solution $\widehat{\boldsymbol{\theta}}$ is sought.

A central issue in kriging is to efficiently solve Eq. (II.160). The solution $\widehat{\boldsymbol{\theta}}$ cannot be obtained analytically, and we have to resort to numerical optimization techniques. The correlation matrix $\mathbf{R}(\boldsymbol{\theta})$ is in fact badly conditioned for several values of $\boldsymbol{\theta}$, which makes Eq. (II.160) extremely difficult to solve (see, e.g., Lophaven et al., 2002a; Marrel, 2008). Moreover $\psi(\boldsymbol{\theta})$ is known to have many local minima. Several optimization techniques are available in kriging packages such as DACE (Lophaven et al., 2002b), DiceKriging (Roustant et al., 2012), ooDACE (Couckuyt et al., 2014), UQLAB (Lataniotis et al., 2017). These techniques usually include stochastic optimization in order to identify potential "good" starting points (e.g. by means of genetic algorithms) with the potential subsequent application of a gradient-based search method (e.g. the BFGS algorithm).

In the case of kriging with the nugget effect with the assumption of homogeneous noise, the MLE estimate of the noise parameter τ also needs to be found. A common practice consists in avoiding such an estimation and considering a small value for τ. The main aim of this practice is to prevent the covariance matrix from being ill-conditioned and therefore to ease its inversion. For details about this specific numerical topic the reader may refer to the recent work of Mohammadi et al. (2017), in which a comparison is made between two techniques for the regularization of the covariance matrix: calculation of the pseudoinverse of $\mathbf{K}$ or use of a nugget effect in the kriging formulation such as presented in Section II–4.3.

As an alternative to MLE, cross validation (CV), already introduced in Section II–2.4.1, is a very popular technique for model selection. Exactly as for LS-SVR[17], see Eq. (II.119), the application of LOO-CV in kriging presents the main advantage of providing an exact LOO error obtained from a single training on the whole training set $\mathcal{T}$. The expression of the LOO error in the context of kriging is due to Dubrule (1983). In the case of universal kriging with an unknown homogeneous noise, the LOO error is given by:

$$\begin{aligned}\mathrm{Err}_{\mathrm{LOO},\ell_2} &= \frac{1}{N}\sum_{i=1}^{N}\left(y_i - \mu^{(-i)}_{\text{UK-nugget}}(\mathbf{x}_i)\right)^2 \\ &= \frac{1}{N}\sum_{i=1}^{N}\frac{c_i^2}{\left(\overline{\mathbf{K}}^{-1}\right)_{ii}^2}.\end{aligned} \tag{II.161}$$

where $\mu^{(-i)}_{\text{UK-nugget}}$ is the UK mean prediction obtained by training on $\mathcal{T}\backslash(\mathbf{x}_i, y_i)$,
where $\mathbf{c} = (c_1, \ldots, c_N)^{\mathrm{T}} \in \mathbb{R}^N$ is the solution of:

$$\begin{bmatrix}\mathbf{K} + \tau^2\mathbf{I} & \mathbf{P} \\ \mathbf{P}^{\mathrm{T}} & \mathbf{0}\end{bmatrix}\begin{pmatrix}\mathbf{c} \\ \mathbf{d}\end{pmatrix} = \begin{pmatrix}\mathbf{y} \\ \mathbf{0}\end{pmatrix}, \tag{II.162}$$

[17] It is recalled that the LS-SVR regressor and the kriging mean prediction are identical by construction, see Section II–4.3.

which is denoted $\overline{\mathbf{K}}\,\overline{\mathbf{c}} = \overline{\mathbf{y}}$, and where $\left(\overline{\mathbf{K}}^{-1}\right)_{ii}$ is the i^{th} diagonal element of the inverse of $\overline{\mathbf{K}}$.

In practice, MLE is often preferred to CV to determine the optimal hyperparameters of kriging surrogate models. A comparison between the two techniques was recently performed by Bachoc (2013). The conclusion of this author is that CV performs better than MLE in the case of a misspecification of the parametric family of the covariance kernel, i.e. when the selected parametric covariance kernel differs from the true underlying covariance kernel.

II–5 Surrogate-based RBDO

II–5.1 Design under uncertainty

Design optimization is of prime importance in a wide spectrum of engineering fields. The problem to solve consists in finding the set of *design variables* that minimizes a cost model while satisfying some imposed constraints and design requirements. In real systems to optimize, uncertainties are often present at various levels. The system of interest may be subjected to an uncertain loading, its properties may be not perfectly known due to some uncertainty in the manufacturing process, the numerically-assessed responses may differ to some extent from the true and real ones, etc. Optimal design under uncertainty can be addressed in various frameworks depending on where the uncertainty is introduced in the optimization problem formulation (i.e. cost function or constraints, or both). The two most popular approaches are known as *reliability-based design optimization* (RBDO) and *robust design optimization* (RDO). For a short review of RBDO and RDO the reader may refer to the PhD manuscript of Moustapha (2016). For an overview of other variants which are less well-known than the two approaches mentioned above, the reader may refer to the recent review paper of Lelièvre et al. (2016).

Several formulations can be included in RBDO (Enevoldsen and Sørensen, 1994; Royset et al., 2002; Chateauneuf and Aoues, 2008; Schuëller and Jensen, 2008; Aoues and Chateauneuf, 2010; Valdebenito and Schuëller, 2010; Beck and Gomes, 2012). RBDO most often utilizes the reliability of the system as a constraint, and the objective function is deterministic. We may also include uncertainties in the objective function e.g. when we try to minimize the expected lifetime costs considering the construction cost, maintenance costs and eventual failures[18]. Stochastic subset optimization (SSO) (Taflanidis and Beck, 2008) is also another approach that includes uncertainties in the objective function. In this sampling-based method closely related to subset simulation the objective is to find the optimal design that minimizes the failure probability with potential deterministic constraints on costs.

In RDO, the objective is to find the least sensitive possible design w.r.t. the system variations at the optimal point (Doltsinis and Kang, 2004; Park et al., 2006; Beyer and Sendhoff, 2007; Schuëller and Jensen, 2008). The objective function of RDO is often expressed in terms of the statistical moments of the response, mainly its mean and standard deviation.

The challenges of optimal design under uncertainty are those combining probabilistic analysis and optimal design. Optimal design under uncertainty requires the estimation of the objective function and/or constraints, if these quantities are assumed uncertain. As already indicated in the specific context of reliability, such estimations are in general expensive to evaluate. Moreover, only a limited accuracy can be achieved for these estimations, either due to the limited number of samples used in Monte Carlo methods or to the potential bias of the constructed approximations w.r.t. the true model in surrogate-based analyses. As pointed out e.g. by Medina (2014), this estimation error acts as a noise in

[18] This type of problem is addressed e.g. in the recent paper of Beck and Gomes (2012). The interested reader can find therein a justification of a formulation that includes failure costs.

the objective function and/or reliability constraint, which poses significant difficulties for optimization algorithms. If Monte Carlo methods are used this noise can be reduced, either by lowering the variance of the function estimation (e.g. by increasing the sample size) or by working with *common random numbers* (see, e.g., Taflanidis, 2007, Section 5.1), which limits the *relative* estimation errors by using samples generated with the same seed at each iteration of the optimization algorithm. The techniques related to common random numbers are commonly referred to as exterior sampling approximations (Taflanidis, 2007) or sample average approximations (Royset and Polak, 2004a; Royset and Polak, 2004b). In the work of Royset and Polak on RBDO the sample size is increased, leading to more accurate estimates as the algorithm converges to an optimal solution. Regarding optimization algorithms, the use of gradient-based nonlinear programming algorithms is inapplicable to optimal design under uncertainty. Such a type of algorithm is incompatible with a noisy objective function and/or constraints. Moreover, the gradients of such functions w.r.t. the design variables are most often unavailable. As an alternative, we may consider gradient-free optimization algorithms. Unfortunately, such algorithms tend to be computationally expensive and do not scale well with the number of design variables (Royset et al., 2006).

A presentation of RDBO as addressed in the works of Dubourg (2011) and Moustapha (2016) is given Section II–5.2 along with a brief overview of the main methods applied in this field. In the case of functions which are expensive to evaluate, the use of surrogate models can be interesting to tackle optimal design under uncertainty. Examples of such approaches are given in Section II–5.3, which presents the main concepts of the kriging-based methods developed by Dubourg and Moustapha.

II–5.2 RBDO problem formulation and solving strategies

The scope of the analysis is here restricted to the following RDBO formulation, as considered by Dubourg (2011) and Moustapha (2016):

$$\mathbf{d}^* = \underset{\mathbf{d}\in\mathcal{D}}{\arg\min}\, c(\mathbf{d}) \quad \text{s.t.} \quad \begin{cases} f_j(\mathbf{d}) \leq 0 & \text{for } j = 1, \dots, n_f \\ \mathbb{P}\left(g_k\left(\mathbf{X}(\mathbf{d}), \mathbf{Z}\right) \leq 0\right) \leq \overline{p}_{\mathrm{f},k} & \text{for } k = 1, \dots, n_g \end{cases}, \tag{II.163}$$

where c is the objective function (or cost function) to be minimized w.r.t. the design variables $\mathbf{d} = (d_1, \dots, d_{n_d}) \in \mathcal{D} \subset \mathbb{R}^{n_d}$, $\{f_j, 1 \leq j \leq n_f\}$ are n_f deterministic soft constraints that bound the admissible space in $\mathcal{D}$, $\{g_k, 1 \leq k \leq n_g\}$ are n_g limit-state functions related to the failure modes of interest, $\overline{p}_{\mathrm{f},k}$ are n_g threshold probabilities not to be exceeded by the respective failure probabilities, $\mathbf{X} \sim f_{\mathbf{X}|\mathbf{d}}$ is a random vector indexed on the given design $\mathbf{d}$ and $\mathbf{Z} \sim f_{\mathbf{Z}}$ is another random vector independent of $\mathbf{d}$. $\mathbf{X}$ are called *design* random variables by Dubourg (2011). $\mathbf{Z}$ are called *basic* random variables by Dubourg (2011) and *environmental* random variables by Moustapha (2016). The n_g probabilistic constraints $\mathbb{P}\left(g_k\left(\mathbf{X}(\mathbf{d}), \mathbf{Z}\right) \leq 0\right) \leq \overline{p}_{\mathrm{f},k}$ are usually termed hard-constraints. No uncertainty is accounted for in c, the objective function is supposed to be deterministic. It should be noticed that $\mathbf{d}$ gathers a set of parameters that defines the joint PDF of the random vector $\mathbf{X}$, e.g. the means of its components. It should also be borne in mind that sensitivities of failure probabilities w.r.t. the distribution parameters of $\mathbf{X}$ can be obtained by the methods presented in Chapter I, Section I–4. Each LSF g_k is often expressed in terms of a given model output $\mathcal{M}_k$ (e.g. a FE model) in the following form $g_k(\mathbf{x}(\mathbf{d}), \mathbf{z}) = \overline{g}_k - \mathcal{M}_k(\mathbf{x}(\mathbf{d}), \mathbf{z})$ where $\overline{g}_k$ is a threshold which is not to be exceeded by the model output $\mathcal{M}_k$ and where $\mathbf{x}(\mathbf{d})$ (resp. $\mathbf{z}$) is a realization of $\mathbf{X}(\mathbf{d})$ (resp. $\mathbf{Z}$).

A slightly different problem formulation is adopted by Moustapha (2016), which reformulates the problem defined in Eq. (II.163) in terms of quantiles of the model outputs $\mathcal{M}_k$:

$$\mathbf{d}^* = \underset{\mathbf{d}\in\mathcal{D}}{\arg\min}\, c(\mathbf{d}) \quad \text{s.t.} \quad \begin{cases} f_j(\mathbf{d}) \leq 0 & \text{for } j = 1, \dots, n_f \\ Q_{\alpha_k}\left(\mathbf{d}; \mathcal{M}_k\left(\mathbf{X}(\mathbf{d}), \mathbf{Z}\right)\right) \leq \overline{g}_k & \text{for } k = 1, \dots, n_g \end{cases}, \tag{II.164}$$

where:

$$Q_{\alpha_k}\left(\mathbf{d}; \mathcal{M}_k\left(\mathbf{X}(\mathbf{d}), \mathbf{Z}\right)\right) = \inf\left\{ q_{\alpha_k} \in \mathbb{R} \ : \ \mathbb{P}\left(\mathcal{M}_k\left(\mathbf{X}(\mathbf{d}), \mathbf{Z}\right) \leq q_{\alpha_k}\right) \geq \alpha_k \right\} , \tag{II.165}$$

and $\alpha_k = 1 - \overline{p}_{\mathrm{f},k}$. The choice of such a formulation is motivated by the probability levels $\overline{p}_{\mathrm{f},k}$ that are targeted in the work of Moustapha, which are in the range of 1 to 10% and therefore not very low. In this context it is not necessary to apply any of the reliability assessment techniques presented in Chapter I, the α_k-quantiles can be directly estimated from a Monte Carlo sample of the model outputs corresponding to a given design $\mathbf{d}$: $\{y^{(j)} = \mathcal{M}_k\left(\mathbf{x}^{(j)}(\mathbf{d}), \mathbf{z}^{(j)}\right), 1 \leq j \leq N\}$, where $\mathbf{x}^{(j)}(\mathbf{d})$ and $\mathbf{z}^{(j)}$ for $j = 1, \ldots, N$ are realizations of $\mathbf{X} \sim f_{\mathbf{X}|\mathbf{d}}$ and $\mathbf{Z} \sim f_{\mathbf{Z}}$ respectively. For numerical stability, common random numbers are used for sample generation. The same realizations $\{\mathbf{z}^{(j)}, 1 \leq j \leq N\}$ of $\mathbf{Z}$ are used at each iteration of the optimization algorithm (Moustapha, 2016).

The methods available to solve the RBDO problem defined in Eq. (II.163) are often categorized into three groups (Chateauneuf and Aoues, 2008; Aoues and Chateauneuf, 2010; Valdebenito and Schuëller, 2010): (a) double loop-approaches, (b) single-loop approaches and (c) decoupled approaches.

(a) Double loop-approach

The double loop-approach consists in solving two nested optimization problems: the outer loop explores the design space $\mathcal{D}$ by iterating on different values of $\mathbf{d}$, while the inner one solves the reliability assessment problem. Two main formulations have emerged in this category: the *reliability index approach* (RIA) and the *performance measure approach* (PMA).

The reliability index approach (Enevoldsen and Sørensen, 1994) uses FORM in the inner loop. The constraints expressed in terms of failure probabilities in Eq. (II.163) are replaced by their equivalents in terms of reliability indices. The gradients of the reliability indices w.r.t. the design variables $\mathbf{d}$ need to be assessed accurately in order to ensure a stable convergence in the optimization loop.

An alternative strategy, known as the *performance measure approach* (PMA), was proposed by Tu et al. (1999) to solve the RBDO problem. The reliability problem is solved in a different way to that used in FORM. Instead of minimizing $\frac{1}{2}\mathbf{u}^{\mathrm{T}}\mathbf{u} = \frac{1}{2}\|\mathbf{u}\|$ subject to $G(\mathbf{u}) = 0$, see Eq. (I.34), the reliability index is set to its target value and the LSF is minimized:

$$\mathbf{u}^{*}_{\mathrm{MPTP}} = \underset{\mathbf{u}\in\mathbb{R}^n}{\arg\min}\, G\left(\mathbf{u}\right) \ \text{ s.t. } \ \|\mathbf{u}\| = \overline{\beta} \, , \tag{II.166}$$

where the subscript MPTP stands for minimum performance target point and $\overline{\beta}$ is the target reliability index, i.e. $\overline{\beta} = -\Phi^{-1}(\overline{p}_{\mathrm{f}})$. The spherical constraint introduced is claimed to be easier to handle than that of RIA.[19] Another advantage of PMA is that it only requires the gradient of the LSF w.r.t. the design variables, which may be simpler than obtaining the gradient of the failure probability. For further details the reader may refer to Tu et al. (1999) and Lee et al. (2002).

As an additional comment, the conceptual idea of the double-loop approach may be extended to other methods than FORM for a broader scope of application (e.g. crude Monte Carlo or subset simulation). The reliability constraints of Eq. (II.163) may be assessed by any other method inside the optimization loop. If the design parameters are taken as distribution parameters of $\mathbf{X}$, the sensitivities of the failure probability derived in Section I–4 can be used in a gradient-based optimization approach.

[19] The spherical constraint of Eq. (II.166) is also considered in the so-called inverse-FORM approach (Der Kiureghian et al., 1994) where the goal is to find the value of a given scalar parameter θ of the LSF $G(\mathbf{u}, \theta)$ which ensures a given reliability level.

(b) Single loop-approach

Single loop approaches have been proposed to alleviate the computational burden of nested approaches. The main idea of one class of methods is to replace the reliability constraint by the Karush-Kuhn-Tucker optimality condition at the MPFP in the RBDO formulation. It is assumed that a FORM analysis is applicable, i.e. that the MPFP is unique and can be obtained. Following the idea of Madsen and Hansen (1992), Kuschel and Rackwitz (1997) proposes to solve the following optimization problem:

$$(\mathbf{d}^*, \mathbf{u}^*) = \underset{\mathbf{d}\in\mathcal{D},\mathbf{u}\in\mathbb{R}^n}{\arg\min}\ c(\mathbf{d}) \quad \text{s.t.} \quad \begin{cases} f_j(\mathbf{d}) \leq 0 \quad \text{for} \quad j = 1, \dots, n_f \\ G(\mathbf{u}, \mathbf{d}) = 0 \\ \mathbf{u}^{\mathrm{T}} \nabla_{\mathbf{u}} G(\mathbf{u}, \mathbf{d}) + \|\mathbf{u}\| \|\nabla_{\mathbf{u}} G(\mathbf{u}, \mathbf{d})\| = 0 \\ \overline{\beta} - \|\mathbf{u}\| \leq 0 \end{cases}, \tag{II.167}$$

where the formulation is restricted here to a single LSF for the sake of simplicity, i.e. $n_g = 1$. Note that the original formulation of Kuschel and Rackwitz takes an objective function c as the sum of an initial cost and an expected cost of failure. It is important to note that the optimization problem defined in Eq. (II.167) is *deterministic*, the reliability constraint has disappeared. Such a formulation enables the use of general-purpose non-linear optimization algorithms. However, this type of formulation turns out to be unstable to solve numerically, and the convergence is not easy to obtain. A more robust single-loop formulation was later proposed by Agarwal et al. (2007), in which the n_g inverse FORM problems are solved by means of a Lagrangian formulation. The optimization problem is minimized w.r.t. the design variables $\mathbf{d}$, the vector of standard normal variables $\mathbf{u}_k$ involved in the n_g LSF G_k and the n_g multipliers λ_k corresponding to the respective Lagrangians $\mathcal{L}_k = G_k(\mathbf{u}_k, \mathbf{d}) + \lambda_k(\|\mathbf{u}\|_k - \overline{\beta}_k)$. In the case of a single LSF, the optimization problem writes (Agarwal et al., 2007):

$$(\mathbf{d}^*, \mathbf{u}^*, \lambda^*) = \underset{\mathbf{d}\in\mathcal{D},\mathbf{u}\in\mathbb{R}^n,\lambda\in\mathbb{R}}{\arg\min}\ c(\mathbf{d}) \quad \text{s.t.} \quad \begin{cases} f_j(\mathbf{d}) \leq 0 \quad \text{for} \quad j = 1, \dots, n_f \\ G(\mathbf{u}, \mathbf{d}) \geq 0 \\ \nabla_{\mathbf{u}} G(\mathbf{u}, \mathbf{d}) + \lambda \dfrac{\mathbf{u}}{\|\mathbf{u}\|} = 0 \\ \lambda\left(\|\mathbf{u}\| - \overline{\beta}\right) = 0 \\ \|\mathbf{u}\| - \overline{\beta} \leq 0 \\ \lambda \geq 0 \end{cases}, \tag{II.168}$$

From another perspective, Chen et al. (1997) converted the double-loop into a so-called single-loop single-vector approach, which was further extended to series system RBDO by Liang et al. (2007). In such an approach the design variables $\mathbf{d}$ are taken as the means of the random vector $\mathbf{X}$. Under such an assumption the reliability constraint can be replaced by an approximately equivalent deterministic constraint. The principle of the method consists in iteratively solving the following optimization problem:

$$\mathbf{d}^* = \underset{\mathbf{d}\in\mathcal{D}}{\arg\min}\ c(\mathbf{d}) \quad \text{s.t.} \quad \begin{cases} f_j(\mathbf{d}) \leq 0 \quad \text{for} \quad j = 1, \dots, n_f \\ g(\mathbf{x}(\mathbf{d})) \geq 0 \end{cases}, \tag{II.169}$$

where:

$$\begin{aligned} \mathbf{x}(\mathbf{d}^{(i)}) &= \mathbf{d}^{(i)} - \overline{\beta}\boldsymbol{\sigma}_{\mathbf{X}} \circ \boldsymbol{\alpha}^{(i-1)}, \\ \boldsymbol{\alpha}^{(i)} &= \frac{\boldsymbol{\sigma}_{\mathbf{X}} \circ \nabla_{\mathbf{x}} g\left(\mathbf{x}(\mathbf{d}^{(i)})\right)}{\|\boldsymbol{\sigma}_{\mathbf{X}} \circ \nabla_{\mathbf{x}} g\left(\mathbf{x}(\mathbf{d}^{(i)})\right)\|}. \end{aligned} \tag{II.170}$$

where $\mathbf{x}(\mathbf{d}^{(i)})$ is the approximate MPFP obtained at each iteration i, $\boldsymbol{\sigma}_{\mathbf{X}}$ is the vector of standard deviations of $\mathbf{X}$ and $\circ$ denotes the component-wise multiplication. The method is started with an initial and arbitrary point $\mathbf{x}(\mathbf{d}^{(0)}) = \mathbf{d}^{(0)}$. At the next iterations $i > 0$, the design variables $\mathbf{d}$ are changed and

an updated approximate MPFP is obtained, based on the normalized gradient $\boldsymbol{\alpha}$ of the previous iteration. The single-loop single-vector approach is quite efficient since no reliability constraint is involved. However, the robustness of the method may be considerably affected by the choice of the initial starting point $\mathbf{x}(\mathbf{d}^{(0)})$ (Yang and Gu, 2004) and the nonlinearity of the LSF (Aoues and Chateauneuf, 2010).

(c) Decoupled approach

Another type of method, known as the decoupled approach, consists in performing optimization and reliability analysis sequentially (Der Kiureghian and Polak, 1998). The term decoupled means that the reliability method can be selected independently of the optimization algorithm. In the work of Royset et al. (2001) the RBDO problem is reformulated into a deterministic semi-infinite optimization problem, which enables the application of any optimization algorithm able to solve such problems and any reliability assessment method. Another well-known decoupled approach is the *sequential optimization and reliability assessment* (SORA) method proposed by Du and Chen (2004). In this method the probabilistic constraints are equivalently replaced by deterministic ones by means of inverse FORM (cf. its use in PMA). At each iteration, the SORA algorithm solves a deterministic optimization problem by shifting the design variables based on the MPFP found at the previous iteration, which enforces the reliability constraints. Other decoupled approaches include the sequential approximate programming of Cheng et al. (2006) and the direct decoupling approach of Zou and Mahadevan (2006), as well as several others not listed here for the sake of brevity. The first of these two approaches replaces the probabilistic constraint by a deterministic one, which uses a recurrence-based approximation of the reliability index. In the work of Zou and Mahadevan, the central idea is to consider an equivalent deterministic constraint expressed in terms of a first-order Taylor series expansion of the failure probability w.r.t. the means of $\mathbf{X}$, taken as design variables.

II–5.3 Kriging-based adaptive approaches

Most of the approaches presented in the previous section rely on a FORM approximation of the reliability constraint(s). The necessary assumptions for a valid approximation of the failure probability(ies) may not hold true for some problems (nonlinear LSF, non unique MPFP). This may result in incorrect values of the probabilistic constraint(s) of the RBDO approach and therefore in unsafe designs. Recourse to more robust failure probability assessment techniques is for this reason of great interest. As evoked in Chapter I such an objective can be reached by using the crude Monte Carlo method or some of its variants achieving a reduced variance of the failure probability estimate (e.g. subset simulation). The probabilistic constraint of the RBDO problem can be assessed by a Monte Carlo-like method in the nested framework, see Section II–5.2. This can also be done using other methods such as that of Royset and Polak (2004b), which consists in sequentially increasing the sample size used in the reliability analysis as the optimization algorithm converges towards an optimal design. Although sampling reliability assessment techniques can easily be handled with such RBDO methods, it is worth emphasizing that the associated computational cost is most often too high in practice, except for simple academic problems involving cheap-to-evaluate LSFs. The several calls to the LSFs to obtain the failure probabilities in the RBDO constraints need to be repeated for multiple sets of design parameters, which is unaffordable for real-life RBDO problems on most current computational platforms.

To address this challenge the introduction of surrogate models in RDBO and robust design formulations has been considered as an interesting direction to explore over the past fifteen years. As for surrogate-based reliability analysis, the number of contributions to this field is large and only a few works will be listed here. The solutions proposed are quite diverse, depending on the type of surrogate

models used in the analysis, the quantities that are surrogated (objective function, constraints or both), the type of method involved in the probabilistic estimation, the solver used for optimization and the many ways all these tools are combined together.

Choi et al. (2001) used moving least squares surrogates to solve a PMA-based RBDO problem. An extension of this work was later proposed by the same authors, where the inverse PMA problem was solved by means of an hybrid mean-value method (Youn and Choi, 2004). In the work of Papadrakakis and Lagaros (2002) artificial neural networks were selected in conjunction with importance sampling. RBF artificial neural networks were more recently used by Gomes and Beck (2013), based on FORM solutions of the reliability assessment problems. In the paper of Jin et al. (2003) three types of surrogate models were compared in the context of robust design: polynomial response surfaces, kriging and radial basis functions. Kriging surrogate models have also been used by several researchers to solve RBDO problems (Dubourg et al., 2011; Lee et al., 2011b; Bichon et al., 2012; Moustapha et al., 2016). Lee et al. (2011b) used kriging surrogates with a dynamically selected polynomial trend (called dynamic kriging by these authors), which allows crude MCS estimates of the reliability constraint. In the approach proposed by Bichon et al. (2012) the main idea is to combine the *efficient global optimization* algorithm of Jones et al. (1998) (a gradient-free technique that solves unconstrained optimization problems) and the EGRA method of Bichon et al. (2008) for the reliability analysis. In the works of Dubourg (2011) and Moustapha (2016) a common idea is to alternate between optimization based on the current surrogate model and the enrichment of this surrogate by means of additional training points if the surrogate model is found to be insufficiently accurate, as described in the next section. Some researchers have also had recourse to SVMs in RBDO approaches, see e.g. the work of Basudhar et al. (2008) in which SVMs in classification are used to model the probabilistic constraint, and the more recent work of Lacaze and Missoum (2014) in which kriging is additionally used to approximate the objective function.

To solve the optimization problem of surrogate-based RBDO, the choice is made between two main techniques. The first option consists in using gradient-based algorithms if the gradients w.r.t. the design variables $\mathbf{d}$ are readily available (see, e.g., Choi et al., 2001; Youn and Choi, 2004; Dubourg et al., 2011). Let us recall that these gradients are conveniently obtained if $\mathbf{d}$ is composed of some distribution parameters of the random vector $\mathbf{X}$. The main issue associated with such a technique is that it may only improve the design, without being able to find the optimal one (in other words, we obtain a local optimum instead of the global one). To avoid such an issue, solutions based on stochastic search algorithms have been explored as alternatives, such as evolution strategies (Papadrakakis and Lagaros, 2002; Moustapha et al., 2016) or particle swarm optimization (Gomes and Beck, 2013; Yang and Hsieh, 2013) among other techniques. The main advantage of such gradient-free methods is that they do not require any gradients w.r.t. $\mathbf{d}$. They may also work in the case of discrete design variables. However, their main drawback is that they are quite demanding in terms of the number of calls to the objective or constraint functions. Such methods are by construction actually more explorative in $\mathcal{D}$ than the gradient-based ones.

Two more important ingredients are required for the elaboration of surrogate-based RBDO approaches, in addition to those listed so far (type of surrogate model, method applied for assessing the probabilistic constraint(s), optimization algorithm). First, we need to define the domain in which the surrogate models of the objective and/or constraint functions are trained. This task is not as simple as it seems, since this domain must jointly cover the supports of the PDFs of the random vectors $\mathbf{X}$ and $\mathbf{Z}$, assuming that the PDF of $\mathbf{X}$ depends on the set of design parameters $\mathbf{d}$, see Eq. (II.163). The domain in which the surrogate-based RBDO approach is performed hinges on the so-called augmented reliability problem introduced by Taflanidis and Beck (2008), as presented in Section II–5.3.1. Second, we need to define a strategy to compose the set of training points in this domain in order to build accurate substitutes of the true objective and/or constraint functions. In a naive approach one would fill the whole domain as densely as possible to achieve the required accuracy on all surrogates, e.g. by means of a space-filling technique. Such an approach would result in too high a number of calls to

the expensive-to-evaluate functions. Instead, we start from the premise that for optimization there is no need to be accurate everywhere in the domain. The constructed surrogate models are expected to be accurate only in part of this domain, where the constraints are close to being violated or where the objective function is sufficiently low. In a similar spirit to what was presented for reliability assessment earlier in this chapter, it is proposed to develop *adaptive* approaches for surrogate-based RBDO. The common idea is to start with a fair initial training set, construct an initial surrogate from it, and from there iteratively enrich the training set according to certain criteria, and update the surrogate model until the surrogate-based optimal design can be obtained with sufficient accuracy. Two examples of such approaches are recalled in Section II–5.3.2 (Dubourg, 2011) and Section II–5.3.3 (Moustapha, 2016).

Such adaptive strategies are not specific to RBDO, they are also of great interest in surrogate-based *deterministic* optimization (see, e.g., Queipo et al., 2005; Forrester and Keane, 2009). Several methods have been developed in the specific context of kriging, where advantage is taken of the kriging variance as a measure of the epistemic uncertainty of the constructed surrogates due to the sparsity of the training data. For an overview of adaptive techniques which are not specific to kriging (i.e. methods based on query-by-committee, cross-validation or gradients), the reader may refer e.g. to the recent review of Liu et al. (2017).

In the context of unconstrained optimization, the most popular approach was proposed by Jones et al. (1998) and is known as *expected global optimization* (EGO). The method seeks to solve a kriging-based minimization problem by balancing the search efforts between regions where the mean prediction is minimal (exploitation) and those where the kriging variance is high (exploration). It is based on the so-called *expected improvement* criterion[20] defined by the following integral, which has a closed-form expression (see, e.g., Ginsbourger, 2009, p. 109):

$$\mathbb{E}I(\mathbf{x}) = \int_{-\infty}^{y_{\min}} (y_{\min} - y)\, \varphi\left(\frac{y - \mu_{\widehat{Y}}(\mathbf{x})}{\sigma_{\widehat{Y}}(\mathbf{x})}\right) \mathrm{d}y \,, \tag{II.171}$$

where $y_{\min} = \min_{i\in\{1,\dots,N\}} y_i$. Variants of this criterion were developed later, see e.g. the review of such so-called *infill* criteria made by Picheny et al. (2013).

In the context of constrained optimization, the expected improvement criterion is inapplicable, and several adaptations have been proposed. This includes the adjusted expected improvement (Schonlau et al., 1998), the expected violation (Audet et al., 2000), the expected improvement for contour estimation (Ranjan et al., 2008), the expected feasibility function (Bichon et al., 2008), the constrained EGO formulation (Bichon et al., 2010), the deviation number (Echard et al., 2011), the margin probability function (Dubourg, 2011), see e.g. the short review made by Moustapha (2016). Several of these criteria have been elaborated and applied in a reliability assessment context. The margin probability function and the deviation number will be introduced in Section II–5.3.2 and Section II–5.3.3 respectively, since they were used in the works of Dubourg and Moustapha.

II–5.3.1 Augmented reliability space

This section describes the domain in which the surrogate models are trained in the surrogate-based RBDO approaches developed by Dubourg (2011) and Moustapha (2016), which are respectively recalled in Section II–5.3.2 and Section II–5.3.3. The definition of this domain allows the training set to be sequentially enriched by additional points within the optimization loop. A central idea is to consider a so-called *augmented reliability space* adopting the same philosophy as that proposed by Taflanidis

[20] This criterion can be extended to add more than one point at a time, thanks to the q-$\mathbb{E}I$ criterion, see Ginsbourger et al. (2010).

and Beck (2008) and following the original idea of Au (2005). Basically, the idea is to artificially consider the design variables $\mathbf{d}$ as random, where the notation $\mathbf{D}$ is used for the corresponding random vector. Indeed, the augmented random vector $\mathbf{X}(\mathbf{D})$ has a PDF h that accounts for both an *instrumental uncertainty* in the design choices $\mathbf{D}$ and the assumed aleatory uncertainty in the random vector $\mathbf{X}$. Under such considerations h is expressed as follows:

$$h(\mathbf{x}) = \int_{\mathcal{D}} f_{\mathbf{X}|\mathbf{d}}(\mathbf{x}|\mathbf{d})\,\pi(\mathbf{d})\,\mathrm{d}\mathbf{d}\,, \tag{II.172}$$

where $f_{\mathbf{X}|\mathbf{d}}$ is the PDF of $\mathbf{X}$ given the design parameters $\mathbf{d}$, and π is a *pseudo* PDF for $\mathbf{D}$, which is naturally assumed uniform over the design domain $\mathcal{D}$. An illustration of the definition of this augmented PDF is provided in Figure II.13 for the case of normal distribution with a mean value uniformly distributed over $\mathcal{D}$. The augmented reliability space is spanned by $\mathcal{V} = \mathcal{X}(\mathcal{D})$ in the top left corner of the figure.

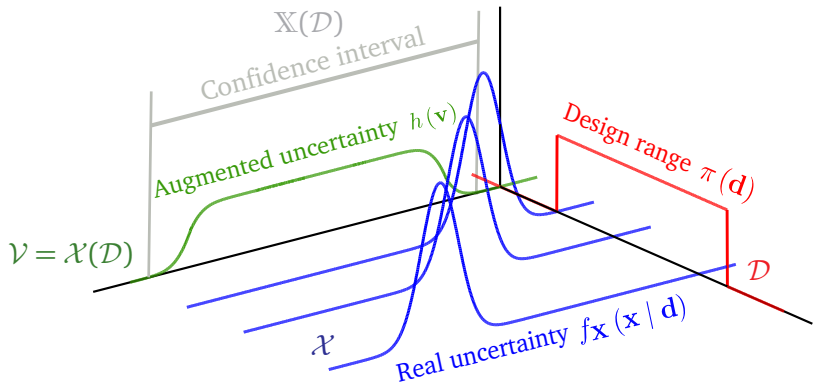

Figure II.13 – Augmented PDF.

For sequential constructions of surrogate models along the optimization process, the additional points that are added to the training set need to cover a sufficiently large confidence region of the augmented PDF h. Specifically, the surrogate models are required to be accurate for potentially extreme choices of the design variables $\mathbf{d}$ (i.e. near their bounds) and extreme values of $\mathbf{X}$ and $\mathbf{Z}$ in the case of small failure probabilities imposed by the reliability constraints. These confidence regions are here denoted $\mathbb{X}(\mathcal{D})$ and $\mathbb{Z}$ for the respective design random vector $\mathbf{X}(\mathbf{D})$ and environmental random vector $\mathbf{Z}$. Assuming that $\mathbf{X}$ and $\mathbf{Z}$ are independent, the confidence region of the random vector $(\mathbf{X}(\mathbf{D}), \mathbf{Z})$ is obtained as a tensor product between $\mathbb{X}(\mathcal{D})$ and $\mathbb{Z}$, i.e. $\mathbb{X}(\mathcal{D}) \times \mathbb{Z}$.

The confidence region $\mathbb{X}(\mathcal{D})$ relative to the design random variable is obtained by the following tensor product (Dubourg, 2011; Moustapha, 2016):

$$\mathbb{X}(\mathcal{D}) = \prod_{i=1}^{n_d} \left[q^-_{x_i|d_i}, q^+_{x_i|d_i} \right], \tag{II.173}$$

where n_d is the number of design parameters and where, for $i = 1, \ldots, n_d$, the lower (resp. upper) quantiles $q^-_{x_i|d_i}$ (resp. $q^+_{x_i|d_i}$) at probability level $\alpha/2$ (resp. $1-\alpha/2$) are defined by:

$$\begin{aligned} q^-_{x_i|d_i} &= F^{-1}_{X_i|d_i^-}(\alpha/2)\,, \\ q^+_{x_i|d_i} &= F^{-1}_{X_i|d_i^+}(1-\alpha/2)\,, \end{aligned} \tag{II.174}$$

where $X_i|d_i$ follows the marginal PDF $f_{X_i|d_i}$ whose associated joint PDF $f_{\mathbf{X}|\mathbf{d}}$ was already introduced in Eq. (II.172), $F^{-1}_{X_i|d_i}$ is the associated inverse CDF, and d_i^- (resp. d_i^+) are lower (resp. upper) bounds of the design variable d_i. Note that the components of $\mathbf{X}|\mathbf{d}$ are assumed to be mutually independent here, which makes $\mathbb{X}(\mathcal{D})$ a rectangular hypervolume.

For the confidence region $\mathbb{Z}$ associated with the environmental random vector $\mathbf{Z}$, two solutions have been proposed. In the work of Dubourg (2011), the random vector $\mathbf{Z}$ is mapped to the standard normal space to allow the application of subset simulation. The confidence region $\mathbb{Z}$ is then defined as follows:

$$\mathbb{Z} = \left\{ \mathbf{z} \in \mathcal{D}_{f_\mathbf{Z}} : \|T(\mathbf{z})\| \leq \beta_0 \right\} , \tag{II.175}$$

where $\mathcal{D}_{f_\mathbf{Z}}$ denotes the support of $f_\mathbf{Z}$, $T : \mathbf{z} \mapsto \mathbf{u}$ is the isoprobabilistic transform and β_0 is a given radius. Another solution is proposed by Moustapha (Moustapha, 2016; Moustapha et al., 2016), since no mapping to the standard normal space is involved in his work. The confidence region $\mathbb{Z}$ is straightforwardly defined by the following rectangular hypervolume:

$$\mathbb{Z} = \prod_{j=1}^{n_z} \left[q_{z_j}^-, q_{z_j}^+ \right] , \tag{II.176}$$

where, for $j = 1, \ldots, n_z$:

$$\begin{aligned} q_{z_j}^- &= F_{Z_j}^{-1}(\alpha/2) , \\ q_{z_j}^+ &= F_{Z_j}^{-1}(1-\alpha/2) , \end{aligned} \tag{II.177}$$

and where $F_{Z_j}^{-1}$ is the inverse CDF of component Z_j of $\mathbf{Z}$. Note that this definition implies that the n_z components of $\mathbf{Z}$ are mutually independent.

II–5.3.2 Proposed adaptive RBDO approach

(a) Adaptive enrichment strategy

We assume that a kriging predictor $\widehat{Y}(\mathbf{x})$ has been trained on a given data set $\mathcal{T} = \{(\mathbf{x}_i, y_i) \in \mathcal{X} \times \mathcal{Y}, 1 \leq i \leq N\}$, as an approximate model of one of the n_g LSF g_k appearing in Eq. (II.163). Let us denote y this specific g_k function for the sake of clarity. The objective is to refine the approximate model around the true limit-state surface $\{\mathbf{x} \in \mathcal{X} : y(\mathbf{x}) = 0\}$, i.e. the zero-level contour of y.

Following the idea of *region of interest* proposed by Picheny et al. (2010), Dubourg (2011) defines the *margin of uncertainty* $\widehat{\mathcal{M}}_{1-\alpha;\,t}$ of the kriging surrogate with confidence level $(1-\alpha)$ associated with the contour level $t \in \mathbb{R}$ as:

$$\widehat{\mathcal{M}}_{1-\alpha;\,t} = \widehat{\mathcal{F}}_{1-\alpha/2;\,t} \setminus \widehat{\mathcal{F}}_{\alpha/2;\,t} , \tag{II.178}$$

where:

$$\widehat{\mathcal{F}}_{\xi;\,t} = \{\mathbf{x} \in \mathcal{X} : \mu_{\widehat{Y}}(\mathbf{x}) \leq t + u_\xi \sigma_{\widehat{Y}}(\mathbf{x})\} , \tag{II.179}$$

and where $u_\xi = \Phi^{-1}(\xi)$ is the ξ-quantile of the standard normal univariate PDF. In the applications made by Dubourg, α is set to 0.05 (i.e. choice of a 95% confidence interval). We are interested in the zero-level contour of the function y, t is therefore set to zero in the following. It is important to notice that $\widehat{\mathcal{F}}_{0.5;\,0} = \{\mathbf{x} \in \mathcal{X} : \mu_{\widehat{Y}}(\mathbf{x}) \leq 0\}$ is the approximate failure domain obtained by kriging. The approximate LSS is defined by $\{\mathbf{x} \in \mathcal{X} : \widetilde{y}(\mathbf{x}) \equiv \mu_{\widehat{Y}}(\mathbf{x}) = 0\}$. The margin of uncertainty therefore represents the subdomain of $\mathcal{X}$ within $u_{0.975} = 1.96$ times the standard deviations of $\widehat{Y}$ on both sides of this approximate LSS.

Since $\widehat{\mathcal{F}}_{\alpha/2;\,0} \subset \widehat{\mathcal{F}}_{1-\alpha/2;\,0}$ the probability that a point $\mathbf{x}$ belongs to $\widehat{\mathcal{M}}_{1-\alpha;\,0}$ is given by:

$$\begin{aligned} \mathrm{MP}(\mathbf{x}) &= \mathbb{P}\left(\widehat{Y}(\mathbf{x}) \in \widehat{\mathcal{M}}_{1-\alpha;\,0}\right) \\ &= \mathbb{P}\left(\widehat{Y}(\mathbf{x}) \in \widehat{\mathcal{F}}_{1-\alpha/2;\,0}\right) - \mathbb{P}\left(\widehat{Y}(\mathbf{x}) \in \widehat{\mathcal{F}}_{\alpha/2;\,0}\right) \\ &= \Phi\left(\frac{u_{1-\alpha/2}\sigma_{\widehat{Y}}(\mathbf{x}) - \mu_{\widehat{Y}}(\mathbf{x})}{\sigma_{\widehat{Y}}(\mathbf{x})}\right) - \Phi\left(\frac{-u_{1-\alpha/2}\sigma_{\widehat{Y}}(\mathbf{x}) - \mu_{\widehat{Y}}(\mathbf{x})}{\sigma_{\widehat{Y}}(\mathbf{x})}\right) , \end{aligned} \tag{II.180}$$

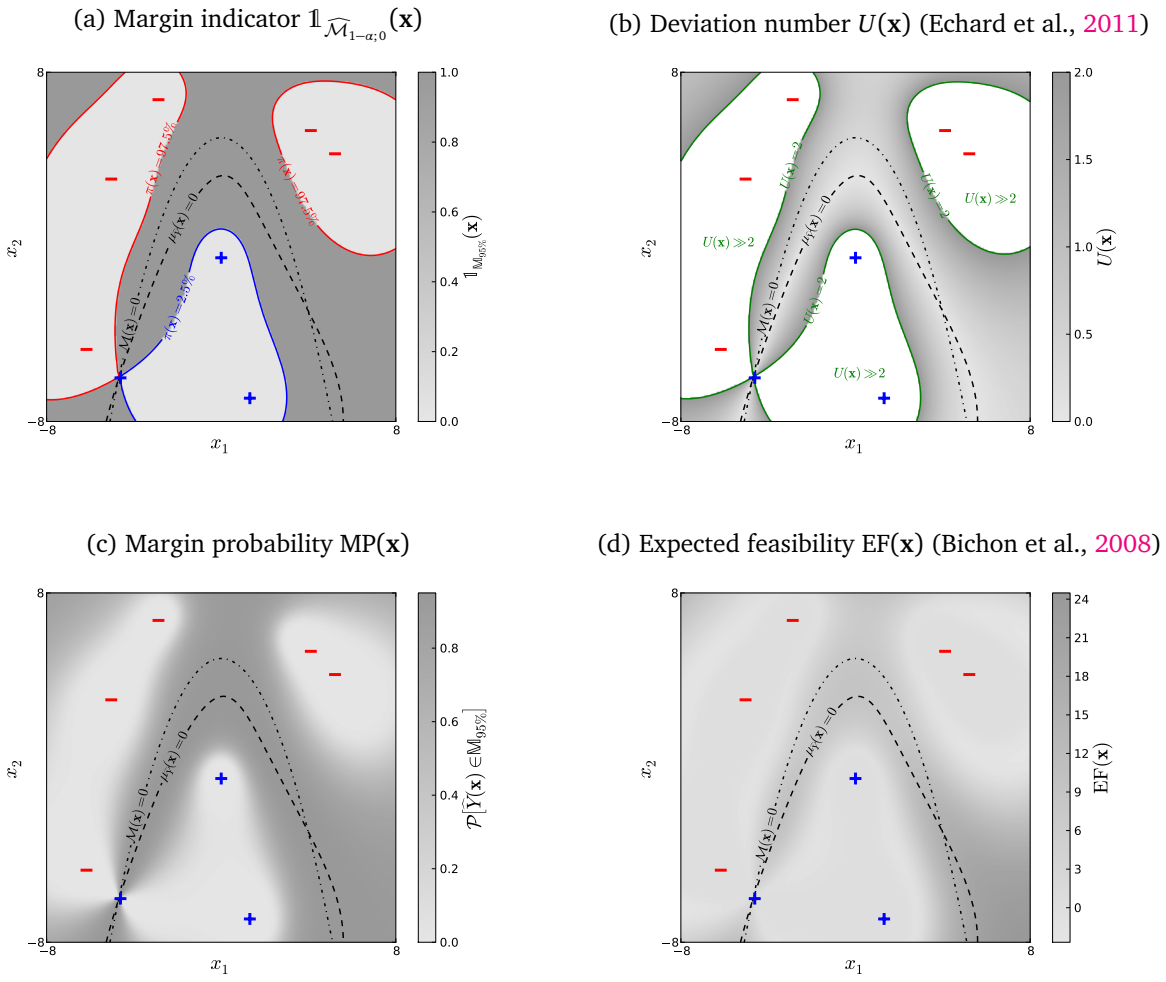

Figure II.14 – Representation of criteria on example 1 of Der Kiureghian and Dakessian (1998) (from Dubourg, 2011).

where $\mathbb{P}$ should be understood as the probability measure w.r.t. the kriging epistemic uncertainty. For illustration purposes, the probability $\mathrm{MP}(\mathbf{x})$ that a point belongs to the margin of uncertainty is represented in Figure II.14, along with the deviation number $U(\mathbf{x})$ of Echard et al. (2011) and the expected feasibility function $\mathrm{EF}(\mathbf{x})$ of Bichon et al. (2008).

The probability that a point $\mathbf{x}$ belongs to the margin of uncertainty such as defined in Eq. (II.180) is used in the following enrichment strategy (Dubourg, 2011; Dubourg et al., 2011), which is carried out for each LSF g_k, $k = 1, \ldots, n_g$.

From a given data set $\mathcal{T} = \{(\mathbf{x}_i, y_i) \in \mathcal{X} \times \mathcal{Y}, 1 \leq i \leq N\}$:

1. Train a kriging predictor $\widehat{Y}(\mathbf{x})$ on $\mathcal{T}$.

2. Define the weighted refinement criterion $C(\mathbf{x}) = \mathrm{MP}(\mathbf{x})\, w(\mathbf{x})$ where $\mathrm{MP}(\mathbf{x})$ is defined in Eq. (II.180) and where $w(\mathbf{x})$ is a weighting PDF. In Dubourg et al. (2011) w is taken as a uniform PDF of a sufficiently large radius β_0 in the standard normal space where the vector $\mathbf{X}$ is mapped to.

3. Sample N_s candidates from $C(\mathbf{x})$, considered as a pseudo PDF by MCMC slice sampler (Neal, 2003).

4. Select N_a additional training points from these N_s candidates by K-means clustering (Lloyd, 1982). Enrich the training set $\mathcal{T}$ with the N_a corresponding data pairs.

5. Loop back to step 1 until (Dubourg et al., 2011):

$$\max\left\{\widehat{\beta}_{1-\alpha/2}-\widehat{\beta}_{0.5}\,;\,\widehat{\beta}_{0.5}-\widehat{\beta}_{\alpha/2}\right\}\leq\epsilon_{\widehat{\beta}}\,, \tag{II.181}$$

where $\widehat{\beta}_\xi$ is the generalized reliability index corresponding to the failure probability assessed on the approximate failure domain $\widehat{\mathcal{F}}_{\xi;0}$:

$$\widehat{\beta}_\xi=-\Phi^{-1}\left(\widehat{P}_{\mathrm{f},\xi}\right)\quad\text{where}\quad\widehat{P}_{\mathrm{f}\xi}=\mathbb{P}\left(\widehat{Y}(\mathbf{x})\in\widehat{\mathcal{F}}_{\xi;0}\right)\,, \tag{II.182}$$

and where $\epsilon_{\widehat{\beta}}$ is a prescribed accuracy level (in the range 0.01 to 0.1 in Dubourg's work). The estimates of the three failure probabilities $\widehat{P}_{\mathrm{f},\alpha/2}$, $\widehat{P}_{\mathrm{f},0.5}$ and $\widehat{P}_{\mathrm{f},1-\alpha/2}$ are assessed by means of a single subset simulation analysis, referred to as *restarted* subset sampling (see Dubourg, 2011, Chapter 3, Section 3.4.2.2).

(b) Kriging-based RDBO approach

The following iterative scheme is proposed for kriging-based RBDO (Dubourg, 2011; Dubourg et al., 2011).

1. Determine the augmented reliability space $\mathbb{X}(\mathcal{D})\times\mathbb{Z}$.

2. Set $s=0$. Choose an initial design $\mathbf{d}^{(0)}$.

3. Fit/refine a kriging predictor with the above proposed adaptive enrichment methodology until the accuracy criterion is below $\epsilon_{\widehat{\beta}}$.

4. Apply one step of the Polak-He algorithm (Polak, 1997, Section 2.6) and update the design parameters:

$$\mathbf{d}^{(s+1)}=\mathbf{d}^{(s)}+s^{(s)}\mathbf{e}^{(s)}\,, \tag{II.183}$$

where $\mathbf{e}^{(s)}$ is the descent direction and $s^{(s)}$ the descent step. This requires the evaluation of the gradient of the failure probability estimate w.r.t. $\mathbf{d}$. These gradients are obtained by subset simulation applied to $\widehat{\mathcal{F}}_{0.5;0}$ if the design parameters $\mathbf{d}$ are distribution parameters of $\mathbf{X}$, which is assumed here, see Section I–4.3.2.

5. Set $s=s+1$.

6. Loop back to step 3 until the convergence of the optimizer is attained.

This adaptive kriging-based RDBO approach is applied to the buckling of imperfect shells in Section III–1.5. As described in Dubourg (2011, Section 4.4.3) the proposed methodology requires some adjustments for enhanced efficiency/accuracy. First, it is necessary to handle the very low failure probabilities which may occur during optimization. This is achieved practically by stopping subset simulation when failure probabilities lower than 10^{-15} are found. Second, some tunings were found beneficial to increase the efficiency and accuracy of the proposed approach. One suggestion of Dubourg is to run the proposed optimization algorithm several times with a decreasing sequence of the accuracy criterion $\epsilon_{\widehat{\beta}}$. It is proposed to start with $\epsilon_{\widehat{\beta}}=1$ and then divide this value by a factor of 2 and so on. Another suggestion is to deliberately reduce the size of the augmented reliability space in order to make the enriching strategy more efficient. The idea is: 1) to center the new augmented reliability space of the next run on the optimal design obtained at the previous run, and 2) to reduce its spread, while maintaining this space inside the initially defined one. In practice, only two to three runs are necessary. The set of training points is reused and enriched at each new run of the optimization algorithm.

II–5.3.3 Proposed adaptive quantile-based RBDO approach

The objective pursued in the work of Moustapha (2016) is to refine the kriging surrogate model such that the quantiles are accurately estimated in regions where the constraints are likely to be violated, see Eq. (II.164). The constraints are expressed in the design domain $\mathcal{D}$ while the kriging surrogate is built in the augmented space $\mathbb{X}(\mathcal{D}) \times \mathbb{Z}$. The trick is to find points in $\mathbb{X}(\mathcal{D}) \times \mathbb{Z}$ which will most improve the surrogate model such that the quantile is in fine more accurate in the regions of interest.

The method proposed by Moustapha (Moustapha, 2016; Moustapha et al., 2016) can be broken down into two main stages.

- The *first stage* aims at sequentially constructing a kriging surrogate in the augmented space with control of overall accuracy achieved on the quantile constraints. Residual model uncertainty is further reduced during the optimization process of the next stage.

- The objective of the *second stage* is to iteratively find the optimal set of design parameters. In this second stage the design is modified by the optimizer and the accuracy of the kriging surrogate model is checked at each iteration of the optimizer. If the accuracy achieved on the quantile constraints is found to be insufficient, the algorithm defines additional training points and the kriging surrogate is updated.

This method was applied to the mass optimization of automotive body structures under crashworthiness constraints (Moustapha, 2016; Moustapha et al., 2016). The objective was to find the best distribution of the metal sheet thicknesses while satisfying frontal impact-related constraints. The application of adaptive surrogate-based optimization was fully justified in this context, since each finite element crash simulation was extremely time-consuming, i.e. about 24 hours for a single model run on 48-cpus in the most computationally intensive application (Euro NCAP frontal impact of a Peugeot 308).

(a) First stage: global adaptive enrichment strategy

The enrichment strategy involved in the first stage of the method is based on the deviation number U of Echard et al. (2011). This criterion was retained for its straightforward evaluation and because other, more elaborate, criteria have not shown any superior performances. The enrichment strategy is recalled here for the specific case of a unique quantile constraint. Handling multi-constraints can be achieved by means of a composite criterion, which ranks the constraints w.r.t. their U-values (see Moustapha, 2016, Eq. (4.35) p. 126). Assuming that a set of data $\mathcal{T} = \{(\mathbf{x}_i, \mathbf{z}_i, \mathcal{M}(\mathbf{x}_i, \mathbf{z}_i)) \in \mathbb{X}(\mathcal{D}) \times \mathbb{Z} \times \mathcal{Y}, 1 \leq i \leq N\}$ is available, the proposed enrichment methodology can be summarized as follows:

1. Build/refine a kriging predictor $\widehat{\mathcal{M}}(\mathbf{x}, \mathbf{z})$ in the augmented space $\mathbb{X}(\mathcal{D}) \times \mathbb{Z}$ as a surrogate of the true model $\mathcal{M}(\mathbf{x}, \mathbf{z})$.

2. Uniformly sample a set of design parameters $\mathcal{C}_{\mathbf{d}} = \{\mathbf{d}^{(j)} \in \mathcal{D}, 1 \leq j \leq m\}$.

3. For each $\mathbf{d}^{(j)} \in \mathcal{C}_{\mathbf{d}}$:

   (a) Generate the sample set $\mathcal{C}_{\mathbf{xz}}^{(j)} = \{(\mathbf{x}^{(k)}(\mathbf{d}^{(j)}), \mathbf{z}^{(k)}), 1 \leq k \leq N_s\}$ of size N_s.
   (b) Compute the set of approximate responses $\mathcal{C}_{\widehat{\mathcal{M}}}^{(j)} = \{\mu_{\widehat{\mathcal{M}}}(\mathbf{x}^{(k)}(\mathbf{d}^{(j)}), \mathbf{z}^{(k)}), 1 \leq k \leq N_s\}$.
   (c) Compute the α-quantiles $\widehat{q}_\alpha(\mathbf{d}^{(j)})$ of the sample set $\mathcal{C}_{\widehat{\mathcal{M}}}^{(j)}$.
   (d) Find the point $(\mathbf{x}_\alpha^{(j)}, \mathbf{z}_\alpha^{(j)}) = \{(\mathbf{x}, \mathbf{z}) \in \mathcal{C}_{\mathbf{xz}}^{(j)} : \widehat{q}_\alpha(\mathbf{d}^{(j)}) = \mu_{\widehat{\mathcal{M}}}(\mathbf{x}, \mathbf{z})\}$, where $\mu_{\widehat{\mathcal{M}}}$ denotes the mean of the kriging surrogate $\widehat{\mathcal{M}}$, see Figure II.15.

(a) Monte Carlo sample sets $\mathcal{C}_{\mathbf{xz}}^{(j)}$ and associated candidates for enrichment

(b) $\mathcal{M}(\mathbf{x},\mathbf{z})$ in the augmented space and resulting quantile $\widehat{q}_\alpha(\mathbf{d})$

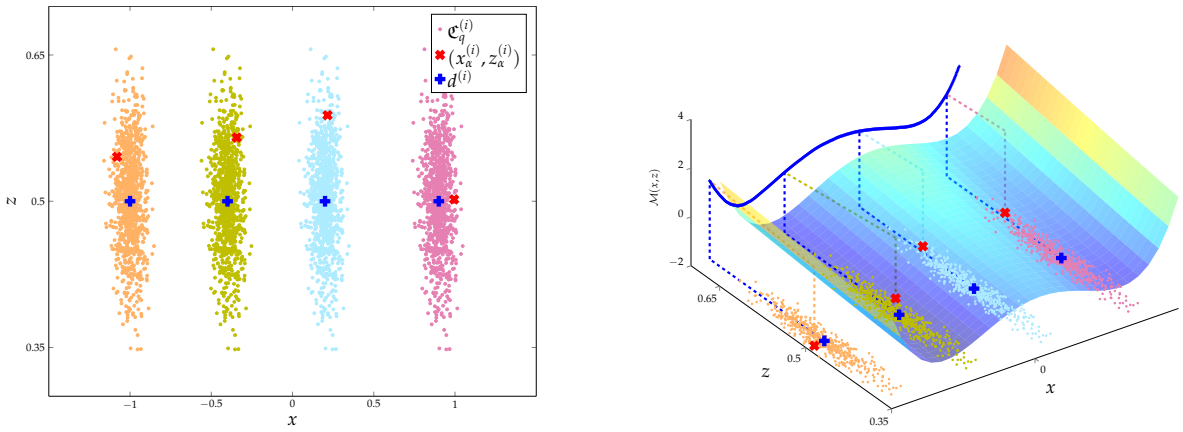

Figure II.15 – Illustration of enrichment in the augmented space (from Moustapha, 2016).

(e) Compute the deviation number U of Echard et al. (2011) at this point:

$$u(\mathbf{d}^{(j)}) \equiv U(\mathbf{x}_\alpha^{(j)}, \mathbf{z}_\alpha^{(j)}) = \frac{\left|\overline{g} - \mu_{\widehat{\mathcal{M}}}(\mathbf{x}_\alpha^{(j)}, \mathbf{z}_\alpha^{(j)})\right|}{\sigma_{\widehat{\mathcal{M}}}(\mathbf{x}_\alpha^{(j)}, \mathbf{z}_\alpha^{(j)})}\,, \tag{II.184}$$

4. Select the new additional point as the one which minimizes the deviation number for all designs $\mathbf{d}^{(j)} \in \mathcal{C}_{\mathbf{d}}$:

$$(\mathbf{x}_{\text{new}}, \mathbf{z}_{\text{new}}) = \underset{\{(\mathbf{x}_\alpha^{(j)}, \mathbf{z}_\alpha^{(j)}), 1 \le j \le m\}}{\arg\min} \; u(\mathbf{d}^{(j)})\,, \tag{II.185}$$

This criterion may be adapted if we wish to take advantage of sending distributed evaluations of the true model $\mathcal{M}$ on multi-core computing resources. In order to define N_{a} new points to be added to the training set simultaneously ($N_{\text{a}} > 1$), Moustapha suggests considering a weighted K-means clustering of the candidates for enrichment, where each point is weighted by $\varphi\left(u(\mathbf{d}^{(j)})\right)$.

5. Loop back to step 1 until:

$$\eta = \frac{\#\mathcal{C}_{d,2}}{\#\mathcal{C}_{\mathbf{d}}} \le \overline{\eta}\,, \tag{II.186}$$

where $\mathcal{C}_{d,2} = \{\mathbf{d}^{(j)} \in \mathcal{C}_{\mathbf{d}} : u(\mathbf{d}^{(j)}) \le 2\}$ and $\overline{\eta}$ is a prescribed accuracy threshold. This convergence criterion is less stringent than the original one defined by Echard et al. (2011), which requires that $u(\mathbf{d}^{(j)}) > 2$ for all $\mathbf{d}^{(j)} \in \mathcal{C}_{\mathbf{d}}$. Here η represents the ratio of points in $\mathcal{C}_{\mathbf{d}}$ for which we tolerate $u(\mathbf{d}^{(j)}) \le 2$. In practice, $\overline{\eta}$ is set in the range [0.15-0.30].

(b) Second stage: optimization with enrichment for quantile accuracy

The second stage aims at finding the optimal design under quantile-constraints, starting from the kriging surrogate obtained in the first stage and considered as globally accurate. The idea is to bring additional information for enrichment, as in the EGO algorithm. The proposed iterative scheme can be summarized as follows (Moustapha, 2016; Moustapha et al., 2016):

1. Determine the augmented space $\mathbb{X}(\mathcal{D}) \times \mathbb{Z}$.

2. Proceed to the first stage with a global adaptive enrichment strategy. Obtain an initial kriging surrogate $\widehat{\mathcal{M}}$.

3. Set $s = 0$. Choose an initial design $\mathbf{d}^{(0)}$.

4. Generate the sample set $\mathcal{C}_{\mathbf{xz}}^{(s)} = \{(\mathbf{x}^{(k)}(\mathbf{d}^{(s)}), \mathbf{z}^{(k)}) \in \mathbb{X}(\mathcal{D}) \times \mathbb{Z}, 1 \leq k \leq N_s\}$, where $\mathbf{X} \sim f_{\mathbf{X}|\mathbf{d}^{(s)}}$ and $\mathbf{Z} \sim f_{\mathbf{Z}}$.

5. Compute the three following sets of approximate responses based on $\widehat{\mathcal{M}}$:

$$\begin{aligned}
\mathcal{C}_{\widehat{\mathcal{M}}}^{(s)} &= \{\mu_{\widehat{\mathcal{M}}}(\mathbf{x}^{(k)}(\mathbf{d}^{(s)}), \mathbf{z}^{(k)}), 1 \leq k \leq N_s\}\,, \\
\mathcal{C}_{\widehat{\mathcal{M}}-}^{(s)} &= \{\mu_{\widehat{\mathcal{M}}}(\mathbf{x}^{(k)}(\mathbf{d}^{(s)}), \mathbf{z}^{(k)}) - 2\sigma_{\widehat{\mathcal{M}}}(\mathbf{x}^{(k)}(\mathbf{d}^{(s)}), \mathbf{z}^{(k)}), 1 \leq k \leq N_s\}\,, \\
\mathcal{C}_{\widehat{\mathcal{M}}+}^{(s)} &= \{\mu_{\widehat{\mathcal{M}}}(\mathbf{x}^{(k)}(\mathbf{d}^{(s)}), \mathbf{z}^{(k)}) + 2\sigma_{\widehat{\mathcal{M}}}(\mathbf{x}^{(k)}(\mathbf{d}^{(s)}), \mathbf{z}^{(k)}), 1 \leq k \leq N_s\}\,,
\end{aligned} \tag{II.187}$$

6. Compute the respective α-quantiles of these sets: $\widehat{q}_\alpha(\mathbf{d}^{(s)})$, $\widehat{q}_\alpha^-(\mathbf{d}^{(s)})$ and $\widehat{q}_\alpha^+(\mathbf{d}^{(s)})$.

7. Proceed to an enrichment of the training set and update the kriging surrogate if:

$$\frac{\widehat{q}_\alpha^+(\mathbf{d}^{(s)}) - \widehat{q}_\alpha^-(\mathbf{d}^{(s)})}{\overline{g}} > \overline{\eta}_q\,, \tag{II.188}$$

   where $\overline{\eta}_q$ is a prescribed threshold. The width $[\,\widehat{q}_\alpha^-(\mathbf{d}^{(s)}), \widehat{q}_\alpha^+(\mathbf{d}^{(s)})\,]$ is taken as a measure of the epistemic uncertainty of the kriging surrogate. The approach shares some similarities with that of Dubourg, see Eq. (II.181). Regarding the choice of $\overline{\eta}_q$, Moustapha suggests starting with a relaxed threshold in the early iterations during the exploration by the optimizer, and then gradually reducing it as the iterations grow and the optimizer starts exploring identified local minima.

   The enrichment procedure is composed of the following steps:

   (a) Compute $\{u_k(\mathbf{d}^{(s)}), 1 \leq k \leq N_s\}$ where:

$$u_k(\mathbf{d}^{(s)}) = \frac{\left|\mu_{\widehat{\mathcal{M}}}(\mathbf{x}^{(k)}(\mathbf{d}^{(s)}), \mathbf{z}^{(k)}) - \widehat{q}_\alpha(\mathbf{d}^{(s)})\right|}{\sigma_{\widehat{\mathcal{M}}}(\mathbf{x}^{(k)}(\mathbf{d}^{(s)}), \mathbf{z}^{(k)})}\,. \tag{II.189}$$

   (b) Select the single new additional point if $N_\mathrm{a} = 1$:

$$(\mathbf{x}_{\mathrm{new}}, \mathbf{z}_{\mathrm{new}}) = \underset{\{(\mathbf{x}^{(k)}(\mathbf{d}^{(s)}), \mathbf{z}^{(k)}), 1 \leq k \leq N_s\}}{\arg\min} u_k(\mathbf{d}^{(s)})\,, \tag{II.190}$$

   or the N_a additional points by K-means clustering with weights $\varphi\left(u_k(\mathbf{d}^{(s)})\right)$ if $N_\mathrm{a} > 1$.

   (c) Update the training set with the additional training data and train a new kriging surrogate $\widehat{\mathcal{M}}$.

8. Find the next design point to explore by means of the (1+1)-CMA-ES optimizer for constrained problems (Arnold and Hansen, 2012):

$$\mathbf{d}^{(s+1)} = \mathbf{d}^{(s)} + \nu^{(s)}\,, \tag{II.191}$$

   where $\nu^{(s)}$ is the mutation. In the (1+1)-CMA-ES algorithm, one parent generates one offspring at each iteration. Such a global search algorithm is quite convenient in the proposed method, since it allows us to check the quantile accuracy for the offspring before moving on. As a global search algorithm, the (1+1)-CMA-ES algorithm is expected to perform better than gradient-based ones. This has been verified e.g. in the bracket structure studied by Moustapha et al. (2016, Section 5.3), where the weight at the optimum is much lower than that obtained by other researchers using gradient-based methods. For details concerning the implementation of the (1+1)-CMA-ES algorithm, the reader may refer to Moustapha (2016, Appendix B).

9. Set $s = s + 1$.

10. Loop back to step 4 until the convergence of the optimizer.

III

Reliability assessment in structural mechanics

Overview, contributions: *Buckling of shells with shape imperfections and crack propagation are well known for their uncertain character, which has been observed experimentally in several works. This chapter presents some of the results obtained in these two fields of structural mechanics:*

- *In the buckling analyses carried out by Noirfalise (2009) and Dubourg (2011), the buckling loads were assessed by means of the asymptotic numerical method as an interesting alternative to more usual incremental-iterative finite element (FE) methods.*
  - *Section III–1.3 presents some of the results obtained by Noirfalise, where random shape imperfections identified from experimental data are accounted for in a reliability analysis. One main contribution of this work is the proposal of two random field models, one based on a random representation of the Fourier coefficients and the other based on a Karhunen Loève series expansion (Noirfalise et al., 2007; Noirfalise et al., 2008). Other interesting contributions made in the finite element formulation are not recalled in this report.*
  - *Section III–1.4 presents the reliability analysis of a cylindrical shell roof subjected to buckling with random shape imperfections and space-variant material and thickness properties studied by Dubourg (Dubourg et al., 2009a; Dubourg et al., 2009b). This problem illustrates the use of FORM and subset simulation in the specific case of multiple MPFPs of equal weights.*
  - *In Section III–1.5, the optimal design of a ring-stiffened cylindrical shell is analyzed using the kriging-based adaptive RBDO approach of Dubourg presented in Chapter II, Section II–5.3.2. This example illustrates the advantage of using an efficient surrogate-based adaptive approach in the context of RBDO with costly-to-evaluate FE problems.*
- *Crack propagation under constant and variable amplitude was studied in the context of reliability assessment.*
  - *In Section III–2.2, crack propagation under constant-amplitude loading is analyzed by considering uncertainty in the Paris-Erdogan crack growth law. This analysis of the problem is based on the experimental data collected by Virkler, which are subject to controversial interpretations. Depending on its formulation, the reliability problem may be sensitive to correlation, which can be assessed in the FORM context using the method proposed in Chapter I, Section I–4.2.2 (a).*
  - *Section III–2.3 presents the main results obtained by Mattrand (2011) concerning crack propagation under random loading. Markov chains and hidden Markov models are proposed and identified from in-flight data recorded in a fleet of fighter aircraft (Mattrand and Bourinet, 2011; Mattrand et al., 2011a). The associated reliability problems are efficiently solved by means of the cross-entropy method presented in Chapter I, Section I–3.3.2 (Mattrand and Bourinet, 2014). The PREFFAS crack closure model, which accounts for load interactions during crack growth, such as retardations and accelerations, is used in this work. Another contribution not detailed in the report is the adaptation brought to this model in order to relax its stationarity assumption, which is incompatible with the non-stationary loads acting on real fighter aircraft.*

Credits: *This chapter is mainly composed of extracts from the PhD works I co-supervised and the associated published papers:*

- *paper of Dubourg et al. (2017) in Section III–1.1 and Section III–1.2,*
- *PhD manuscript of Noirfalise (2009) in Section III–1.3,*
- *PhD manuscript of Dubourg (2011), papers of Dubourg et al. (2009a) and Dubourg et al. (2009b) in Section III–1.4,*
- *PhD manuscript of Dubourg (2011), paper of Dubourg et al. (2017) in Section III–1.5,*
- *paper of Bourinet and Lemaire (2008), book chapter of Bourinet (2017a) in Section III–2.2,*
- *PhD manuscript of Mattrand (2011), papers of Mattrand and Bourinet (2011), Mattrand et al. (2011a), Mattrand et al. (2011b), Bourinet and Mattrand (2013), and Mattrand and Bourinet (2014) in Section III–2.3.*

III–1 Buckling of shells under external hydrostatic pressure

III–1.1 Introduction

Shell structures occupy a predominant part of our landscape (see, e.g., Ramm and Wall, 2004, for a review of their applications). They owe this predominance to their curvature, which allows them to withstand large transverse loading by a membrane-dominated stress state. As a result, they can be used for building large-span shelters such as roofs, fuselages or boat and submarine hulls without requiring too many intermediate supports such as stiffening beams or rims. Nonetheless, like many optimized and therefore slender structures, the strength of thin shells also exhibits significant sensitivity with respect to geometrical, material and other environmental conditions which are typically unknown to some extent.

Early work on the elastic stability of slender structures (such as beams, plates or shells) is often attributed to Euler in 1744, although most of the theoretical concepts for shells in practice today are due to Lorentz, Timoshenko and Southwell in the early nineties. In parallel with theoretical advances, experimental studies revealed embarrassing discrepancies between the predicted buckling loads and those obtained from real tests. Koiter (1945) was certainly the first researcher to point out that these discrepancies are mostly explained by the imperfect geometry, boundary conditions and material properties of the experimental specimens. This premise is now fully acknowledged by the whole community of engineers and scientists in structural mechanics in the light of other studies by Arbocz and Babcock (1969), Singer et al. (1971), and Singer and Abramovich (1995) amongst others. The reader may refer to Bažant (2000) for a review of works in the field of the stability of structures with an emphasis on anelastic structures, and to the recent paper from Elishakoff (2012) for a detailed history of works on the elastic stability of shells.

A key aspect of these imperfections, however, is that they are extremely variable in terms of shape and amplitude. Hence, for the sake of structural safety, designers must account for extreme and fortunately unlikely imperfections. A common practice is to assume a given shape in the calculations, corresponding to the worst case structural strength, and then resort to advanced numerical schemes in order to justify the design. However, this approach, referred to as the *worst case* approach in the following, introduces an unknown degree of conservatism which may not suit the safety requirements imposed by stakeholders.

As suggested early on by Bolotin (1962) in his pioneering works, it is argued that a better solution may be obtained by means of statistical methods and that the design of imperfect shells necessarily falls under a probabilistic formulation. Several imperfection surveys were later carried out in order to assess the statistical properties of imperfections present in both small and large-scale shells. These statistics, such as those gathered in the imperfection data bank (Arbocz, 1982), were then introduced into stochastic buckling analysis by researchers. Elishakoff (1979) was the first researcher to use the random initial imperfections of compressed cylindrical shells in a Monte Carlo analysis. These initial imperfections were expanded in a double Fourier series, and the Fourier coefficients were considered as Gaussian random variables. Such a representation of random imperfections was also used in further studies carried out by the same authors (see, e.g., Elishakoff and Arbocz, 1982; Elishakoff et al., 1987; Arbocz and Hol, 1995; Arbocz and Hilburger, 2005). This double Fourier representation was later investigated by other researchers in an effort to reduce the number of random Fourier coefficients in order to alleviate the cost of the stochastic analysis (Noirfalise, 2009; Kriegesmann et al., 2010; Kriegesmann et al., 2011). In the works of Schenk and Schuëller (Schenk and Schuëller, 2003; Schenk and Schuëller, 2007), the geometric imperfection was modeled as a two-dimensional univariate non-homogeneous Gaussian random field by means of a Karhunen Loève expansion. This representation is also used by Craig and Roux (2008), Noirfalise (2009), and Dubourg et al. (2009b). As an alternative technique, the spectral representation method was applied in several works to model two-dimensional

univariate random fields, see e.g. the work of Stefanou and Papadrakakis (2004) which models homogenous Gaussian random fields representing spatially-varying material properties (Young's modulus and Poisson's ratio) and thickness imperfections. The spectral representation method is also used in conjunction with an autoregressive moving average technique with evolutionary power spectra by Papadopoulos and Papadrakakis (2005) to model non-homogenous Gaussian random fields representing a spatially-varying Young's modulus in addition to geometric and thickness imperfections. A similar approach based on non-Gaussian translation fields was adopted by Papadopoulos and Papadrakakis (2005), putting the emphasis on the influence of the Gaussianity/non-Gaussianity assumption on the results. Recourse to evolutionary power spectra estimated by means of a moving window averaging technique is also found in Broggi and Schuëller (2011) for non-homogenous random fields representing geometric and thickness imperfections. Most of the works reported in the literature have focused on metallic shells with geometric imperfections, possibly combined with spatially-varying material properties and thickness imperfections. A few research studies were also conducted on anisotropic composite shells (Chryssanthopoulos and Poggi, 1995; Kriegesmann et al., 2010; Broggi and Schuëller, 2011; Kriegesmann et al., 2011), characterized by larger imperfections due to their complex manufacturing processes. For a more realistic treatment of imperfections, other sources of random imperfections were additionally incorporated into probabilistic buckling studies, such as those arising from a non-uniform distribution of the axial loading (Papadopoulos and Iglesis, 2007) or those coming from the application of uncertain boundary conditions (Schenk and Schuëller, 2007). It is important to mention that most of the models used to describe the geometric imperfections in the above-cited references were identified from the experimental data available in the imperfection data bank. For thickness imperfections and spatially-varying material properties, the parameters of the random fields are assumed to have specified values, and they are sometimes varied in a parametric analysis.

In early probabilistic studies, buckling loads were computed by means of Koiter's theory (Elishakoff, 1979; Elishakoff and Arbocz, 1982). More refined numerical solutions, based on a multimode analysis, were later used by Elishakoff et al. (1987) and Arbocz and Hilburger (2005). Recourse to a nonlinear finite element (FE) model is often advocated for enhanced accuracy w.r.t. the limit loads. FE-based probabilistic approaches have been carried out using STAGS (Arbocz and Hol, 1995; Schenk and Schuëller, 2003; Schenk and Schuëller, 2007), ABAQUS (Kriegesmann et al., 2010; Broggi and Schuëller, 2011; Kriegesmann et al., 2011) and LS-DYNA (Craig and Stander, 2007; Craig and Roux, 2008) (note that this last code is specifically used in the context of dynamic buckling). In other studies, some researchers implemented specific shell elements for their probabilistic buckling analysis. The TRIC triangular shell element as described by Argyris et al. (2002) is used in the studies performed at the National Technical University of Athens (Stefanou and Papadrakakis, 2004; Papadopoulos and Papadrakakis, 2005; Lagaros and Papadopoulos, 2006; Papadopoulos and Iglesis, 2007; Papadopoulos et al., 2009). In their works, Noirfalise (2009) and Dubourg (2011) used the Büchter and Ramm 8-node shell element (Büchter et al., 1994) for their reliability analysis and reliability-based design optimization. Most of the probabilistic buckling analyses found in the literature assume linear elasticity for metallic shells, which is perfectly appropriate for the studied thin shells taken from the imperfection data bank, such as the so-called A-shells. The nonlinear behavior of shell material is addressed in Papadopoulos and Papadrakakis (2005), Lagaros and Papadopoulos (2006), Dubourg et al. (2009b), and Dubourg et al. (2017). Young's modulus is considered as a random field in the first three references. Yield strength is taken as an additional random field, independent of that of the Young's modulus, by Dubourg et al. (2009b). A random variable probabilistic model is used in the RBDO approach of Dubourg et al. (2017).

In several studies, probabilistic analysis consisted in constructing limit load histograms, in comparison with those obtained experimentally, and analyzing the second-order statistics of these loads. Note that the numbers of samples used in the FE-based Monte Carlo simulations of the reported references are most often in the order of a few hundreds. Another direction followed by researchers has consisted in performing a structural reliability analysis of shells by imposing that their limit loads should be

greater than a prescribed service load. The earliest occurrences of such studies were based on the first-order second-moment method (Elishakoff et al., 1987; Arbocz and Hol, 1995; Arbocz and Hilburger, 2005). The first-order reliability method (FORM) was later used in many works based on analytical models, not listed here for the sake of brevity, or on FE models (see, e.g., Bourinet et al., 2000; Dubourg et al., 2009b). In the specific case of imperfections modeled by random fields, using the subset simulation method (Au and Beck, 2001) is considered as the most suitable solution, as investigated by Noirfalise (2009) and Dubourg et al. (2009b). For the purpose of improving designs, the optimization of shells subject to buckling based on FE models has also been of interest in recent years. In Lagaros and Papadopoulos (2006), the weight of shells with random geometric imperfections and space-variant Young's modulus and thickness was minimized in the framework of reliability-based design optimization. This work was based on a $(5+5)$-evolution strategy optimization algorithm, and the probabilistic constraint was assessed by means of a crude MC with 1000 samples. In Craig and Roux (2008), shells with stochastic imperfections were optimized in a dynamic buckling context. Two optimization studies were performed: the first aimed at minimizing the weight of the shell with constraints on the average peak force and average internal energy, the second aimed at increasing the robustness w.r.t. variations in the normal peak force with the same constraints. The strategy used by Craig and Roux was to construct a quadratic polynomial response surface with a 96-sample MC simulation at each point of the design of experiments.

The following sections compile some results concerning the probabilistic buckling of shells, obtained in the scope of the PhD works of Noirfalise (2009) and Dubourg (2011). In these studies, the main field of application is the stochastic analysis of shells with random imperfections and/or space-variant random material properties and thicknesses. The stability of shells is assessed numerically by means of a non-incremental non-iterative FE method known as the *asymptotic numerical method* (ANM), proposed by Damil and Potier-Ferry (1990) and Cochelin (1994) and briefly recalled in Section III–1.2. Section III–1.3 addresses the buckling of elastic shells of revolution under external hydrostatic pressure with geometrical imperfections, i.e. accounting for deviations from the perfect shell geometry. This section presents some reliability results obtained for shells with random imperfections identified from real measurements in the imperfection data bank. In Section III–1.4 the interest is in the influence of space-variant random material properties and thicknesses on the buckling of shells, accounting for the nonlinear behavior of the constitutive material. The objective is a reliability analysis with certain assumed properties of the random fields. Section III–1.5 illustrates the kriging-based adaptive RBDO approach developed in Section II–5.3.2, where the aim is to optimize the weight of ring-stiffened cylindrical shells representative of those used in submarine pressure hulls.

III–1.2 Elements of shell nonlinear stability analysis

Buckling is a structural instability phenomenon triggered by an excessive load which needs to be identified. This load will be referred to as the *critical* buckling (or collapse) load in the following. In practice it is determined by applying a so-called *load proportionality factor* (LPF) λ which is initialized to zero and then incrementally increased until collapse is observed.

III–1.2.1 Problem formulation

In continuum mechanics, the equilibrium state of a conservative mechanical system is characterized by a zero elementary variation in its total potential energy, denoted E_{t}. This fundamental principle leads to the establishment of the following so-called variational formulation of equilibrium states:

$$\delta E_{\mathrm{t}} = E_{\mathrm{t},\mathbf{u}}(\lambda, \mathbf{u})\,\delta\mathbf{u} = 0\,, \tag{III.1}$$

where $\mathbf{u}$ denotes any admissible displacement of the structure and $E_{\mathrm{t},\mathbf{u}}$ is the first-order functional derivative of the total potential energy that depends on the LPF λ. The infinite set of values of λ and $\mathbf{u}$ satisfying the latter equation is known as the *equilibrium path* of the structure. This path is usually constructed incrementally from a known initial state $\lambda^{(0)}$, $\mathbf{u}^{(0)}$, e.g. the reference state of the unloaded structure for which $\lambda = 0$.

For stable structures, the only state of interest corresponds to a unit value of the LPF λ. Unstable (resp. stable) equilibrium states are characterized by a negative (resp. strictly positive) second-order functional derivative of the total potential energy $E_{\mathrm{t},\mathbf{uu}}$, meaning that they correspond to the local maxima (resp. minima) of this energy.

There exist basically two kinds of instabilities, both potentially leading to buckling and/or premature plastic collapse: *bifurcation points* and *limit points*, see Figure III.1 for an illustration. Regarding bifurcation points, the structure may lose its stability along the equilibrium path, resulting in sudden and large displacements, which often lead to collapse. Limit points occur when the structure is no longer able to withstand loads, due to nonlinear geometrical and/or material effects. For many structures, including shells, these two kinds of points generally interact in a joint manner, one triggering the other and conversely.

Practical detection of these instabilities is a non-trivial task, and it involves the resolution of a perturbed equilibrium problem along with the resolution of Eq. (III.1). For structures with initial geometrical imperfections, and for nonlinear material behaviors, it is commonly admitted that structures fail at their limit load. In such a situation the detection of singular points along the equilibrium path is equivalently replaced by the search for limit load points characterized by horizontal tangents to the equilibrium path, as further developed in the context of the ANM in Section III–1.2.3 (c). Such an assumption is made in the examples presented in Section III–1.4 and Section III–1.5.

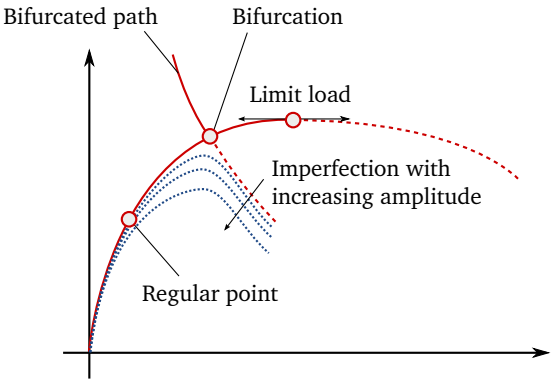

Figure III.1 – Equilibrium paths and stability.

III–1.2.2 General formulation of the static equilibrium equations

In a static analysis, the total potential energy of a structure of volume $\mathcal{V}$ is given by:

$$E_{\mathrm{t}}(\lambda, \mathbf{u}) = \int_{\mathcal{V}} W_{\mathrm{int}}(\boldsymbol{\varepsilon})\,\mathrm{d}v - \lambda\, W_{\mathrm{ext}}(\mathbf{u})\,, \tag{III.2}$$

where W_{int} is the strain energy density in the structure, W_{ext} is the work of external forces and $\mathrm{d}v$ is the infinitesimal volume. $\boldsymbol{\varepsilon}$ stands for the Green-Lagrange strain tensor, defined as:

$$\boldsymbol{\varepsilon} = \boldsymbol{\varepsilon}(\mathbf{u}) = \underbrace{\frac{1}{2}\left(\nabla\mathbf{u} + \nabla^{\mathrm{T}}\mathbf{u}\right)}_{\boldsymbol{\varepsilon}_{\mathrm{l}}(\mathbf{u})} + \underbrace{\frac{1}{2}\nabla\mathbf{u}\,\nabla^{\mathrm{T}}\mathbf{u}}_{\boldsymbol{\varepsilon}_{\mathrm{nl}}(\mathbf{u},\,\mathbf{u})}\,, \tag{III.3}$$

where $\boldsymbol{\varepsilon}_{\mathrm{l}}(\mathbf{u})$, resp. $\boldsymbol{\varepsilon}_{\mathrm{nl}}(\mathbf{u},\mathbf{u})$, denotes the linear, resp. symmetric quadratic bilinear, term of $\boldsymbol{\varepsilon}$ and ∇ the gradient operator. Assuming linear elasticity, the strain energy density W_{int} reduces to the following quadratic form:

$$W_{\mathrm{int}}(\boldsymbol{\varepsilon}) = \frac{1}{2}\,\boldsymbol{\varepsilon} : \mathbf{D} : \boldsymbol{\varepsilon}\,, \tag{III.4}$$

where $\mathbf{D}$ is the elasticity tensor of the material and : denotes the double contraction of tensors.

Introducing the second Piola-Kirchhoff stress tensor $\mathbf{S} = \mathbf{D} : \boldsymbol{\varepsilon}$, the variational formulation of the equilibrium equation rewrites as the following set of equations:

$$\begin{aligned} \delta E_{\mathrm{t}} &= \int_{\mathcal{V}} \mathbf{S} : \delta\boldsymbol{\varepsilon}\,\mathrm{d}v - \lambda\, W_{\mathrm{ext}}(\delta\mathbf{u}) = 0 \\ \mathbf{S} &= \mathbf{D} : \boldsymbol{\varepsilon} \end{aligned} \tag{III.5}$$

where $\delta\boldsymbol{\varepsilon} = \boldsymbol{\varepsilon}_{\mathrm{l}}(\delta\mathbf{u}) + \boldsymbol{\varepsilon}_{\mathrm{nl}}(\mathbf{u},\,\delta\mathbf{u})$.

III–1.2.3 The asymptotic numerical method

The nonlinear problem in Eq. (III.5) is usually solved by means of so-called incremental iterative methods such as the Newton-Raphson algorithm. The present work is based on an original alternative, known as the asymptotic numerical method (ANM) proposed by Damil and Potier-Ferry (1990) and Cochelin (1994).

(a) The idea

It is first proposed to rewrite the nonlinear problem in Eq. (III.5) into the following convenient *quadratic* form:

$$\mathbf{R}(\mathbf{Y},\,\lambda) = L(\mathbf{Y}) + Q(\mathbf{Y},\,\mathbf{Y}) - \lambda\,\mathbf{F} = 0\,, \tag{III.6}$$

where $\mathbf{R}$ is a vector of residuals, L is a linear operator, Q is a bilinear quadratic operator, $\mathbf{F}$ is a known vector and $\mathbf{Y}^{\mathrm{T}} = (\mathbf{u}^{\mathrm{T}}, \mathbf{S}^{\mathrm{T}})$ groups the unknowns of the problem.

A key idea of the ANM then consists in expanding the unknowns $\mathbf{Y}$ and λ over a unique *path parameter* denoted a in the form of the following polynomial series expansions:

$$\left\{\begin{array}{rcl} \mathbf{Y}(a) &=& \mathbf{Y}_0 + a\,\mathbf{Y}_1 + a^2\,\mathbf{Y}_2 + \ldots + a^N\,\mathbf{Y}_N \\ \lambda(a) &=& \lambda_0 + a\,\lambda_1 + a^2\,\lambda_2 + \ldots + a^N\,\lambda_N \end{array}\right. , \tag{III.7}$$

where $(\mathbf{Y}_0,\,\lambda_0)$ describes the initial state of the system, which is presumed to be known. In all the presented applications, the polynomial expansions are truncated after $N = 30$ terms.

Introducing these expansions into Eq. (III.6) and grouping the terms with the same power of a then yields the following succession of linear systems for orders $p = 1, \ldots, N$:

$$\left\{\begin{array}{rcl} L_{\mathrm{t}}(\mathbf{Y}_1) &=& \lambda_1\,\mathbf{F} \\ L_{\mathrm{t}}(\mathbf{Y}_2) &=& \lambda_2\,\mathbf{F} - Q(\mathbf{Y}_1,\,\mathbf{Y}_1) \\ &\vdots& \\ L_{\mathrm{t}}(\mathbf{Y}_N) &=& \lambda_N\,\mathbf{F} - \displaystyle\sum_{p=1}^{N-1} Q(\mathbf{Y}_p,\,\mathbf{Y}_{N-p}) \end{array}\right. , \tag{III.8}$$

where $L_{\mathrm{t}}(\cdot) = L(\cdot) + 2\,Q(\mathbf{Y}_0,\,\cdot)$ is the tangent operator, which is *the same* at all orders.

At this stage, the problem involves one more unknown than the number of available equations, namely the parameter a. Similarly to a classical incremental iterative method, the ANM uses a pseudo arc-length technique by setting:

$$a = (\mathbf{Y} - \mathbf{Y}_0)^{\mathrm{T}} \mathbf{Y}_1 + (\lambda - \lambda_0)\, \lambda_1 \,, \tag{III.9}$$

which completes the system of equations given in Eq. (III.8).

Hence, it can be seen that the initial nonlinear problem in Eq. (III.6) has been genuinely transformed into a set of N *linear systems* by rejecting all nonlinearities to the right-hand side of Eq. (III.8). In addition, the N linear systems composing Eq. (III.8) feature a *single* linear operator L_t, which is *the same* at all orders. When switching to the discrete form of the problem (by means of a classical FE displacement formulation), the resolution of the N linear systems requires *only one* decomposition of the tangent stiffness matrix $\mathbf{K}_{\mathrm{t}}$, which is the discrete counterpart of L_{t}. This latter remark makes the ANM very efficient, as the tangent stiffness matrix $\mathbf{K}_{\mathrm{t}}$ is large in practice.

Eventually, the ANM provides a *continuous* representation of the equilibrium path for any value of λ thanks to the series expansion in a. This is an interesting property with respect to the incremental iterative methods, which need to solve the problem for each value of λ.

(b) Validity of the expansion

Due to the use of finite expansions in Eq. (III.7), the solution becomes invalid for large values of a. Thus, it is proposed to truncate the solution below a maximum value of a, denoted $a_{\max}$. This maximum value is based on a study of the norm of the residual $\mathbf{R}(a) = \mathbf{R}(\mathbf{Y}(a), \lambda(a))$.

Cochelin (1994) proved that it is reasonable to approximate this quantity by the norm of the first omitted term in the expansion, so that:

$$\|\mathbf{R}(a)\| \approx \|a^{N+1}\, \mathbf{R}_{N+1}\| \,. \tag{III.10}$$

Based on this approximation, Cochelin then came up with the following expression for $a_{\max}$:

$$a_{\max} = \left(\epsilon \frac{\|\mathbf{F}\|}{\|\mathbf{R}_{N+1}\|} \right)^{\frac{1}{N+1}} \,, \tag{III.11}$$

where ϵ is the maximum tolerance on the norm of the residual. This tolerance is usually set at a small value (here 10^{-8}) thanks to the normalization of the residual with respect to the right-hand side $\|\mathbf{F}\|$ of Eq. (III.6).

The description of the whole equilibrium path can therefore be made piecewise by repeating the procedure incrementally, i.e. by resetting the initial state of the system to $(\mathbf{Y}_0, \lambda_0)$ to $(\mathbf{Y}(a_{\max}), \lambda(a_{\max}))$. It is worth pointing out that the ANM remains more computationally efficient than its incremental iterative counterparts because it is incremental only. Indeed, incremental iterative methods need to iterate within the increments in order to remain on the equilibrium path, which involves expensive decompositions of the tangent stiffness matrix during the iterative process.

(c) Determination of bifurcation and limit loads

Bifurcations can be detected in the ANM by considering a small virtual displacement perturbation (Boutyour et al., 1995). For a fixed displacement perturbation, singular points correspond to solutions for which the force response tends to zero. The detection of such points is obtained by solving an additional system of equations, which is again formulated in the framework of the ANM, i.e. their unknowns are expressed in terms of series of a path parameter a truncated at an order N, where a

and N are identical to those used in the equilibrium problem. The reader may refer to Baguet (2001, Chapter 4) for a detailed presentation of this highly technical point of prime importance in buckling analysis.

For limit loads their determination can be simply obtained from the parametric approximation of the load proportionality factor. Indeed, limit load points are characterized by a horizontal tangent on the equilibrium path, thus meaning that the derivative of the load proportionality factor with respect to a equals zero at the critical limit load. Hence, the limit LPF is defined as $\lambda_{\text{limit}} = \lambda(a_{\text{limit}})$, where:

$$a_{\text{limit}} = \min \left\{ a \in [0;\ a_{\max}] : \frac{\mathrm{d}\lambda}{\mathrm{d}a} = 0 \right\} . \tag{III.12}$$

Thanks to the chosen polynomial series expansion for the LPF, determining the limit load simply consists in finding the roots of a polynomial of order $(N-1)$ and retaining the lowest positive root that is less than $a_{\max}$, provided it exists.

(d) Sources of nonlinearity

In the works presented in Section III–1, the ANM is applied to geometric nonlinearities extended to large rotations, based on the work of Zahrouni et al. (1999). It can be shown that the corresponding equilibrium equations under such an assumption conveniently fit the quadratic formulation of the ANM given in Eq. (III.6). Two additional sources of nonlinearity are explicitly accounted for within the ANM.

The first source of nonlinearity is due to follower forces resulting from the hydrostatic pressure exerted on shells. Accounting for the specific effects of follower forces in a buckling analysis could be of utmost importance for structural components such as the single-bay of the submarine pressure hull with an overall geometrical imperfection studied in Section III–1.5. From a computational viewpoint, this additional assumption introduces a dependence of the virtual work of external forces on the LPF (see, e.g., Noirfalise, 2009, pp. 81–86). This results in additional terms appearing in the right-hand side forces of Eq. (III.8), on the one hand, and a nonsymmetric tangent operator L_{t} (nonsymmetric tangent stiffness matrix $\mathbf{K}_{\text{t}}$ in the matrix formulation), on the other hand.

The second source of nonlinearity accounted for in this work is due to the assumption of the nonlinear behavior of the constitutive material of shells. A nonlinear elastic Ramberg-Osgood constitutive law characterized by the following stress-strain relationship is considered in the ANM (Zahrouni et al., 1998):

$$E\boldsymbol{\varepsilon} = (1+\nu)\,\mathbf{S}^{\text{d}} - (1-2\nu)\,P\mathbf{I} + \frac{3}{2}\alpha \left(\frac{S_{\text{eq}}}{\sigma_{\text{y}}} \right)^{n-1} \mathbf{S}^{\text{d}} , \tag{III.13}$$

where E is the Young's modulus, ν is the Poisson's ratio, σ_{y} is the yield strength, $P = -\frac{1}{3}\mathbf{S} : \mathbf{I} = -\frac{1}{3}\operatorname{tr}(\mathbf{S})$ is the hydrostatic pressure, $\mathbf{S}^{\text{d}} = \mathbf{S} + P\mathbf{I}$ is the deviatoric part of the stress tensor $\mathbf{S}$, $S_{\text{eq}} = \sqrt{\frac{3}{2}\mathbf{S}^{\text{d}} : \mathbf{S}^{\text{d}}}$ is the von Mises equivalent stress, and α and n are the two Ramberg-Osgood parameters.

Note that plasticity is not considered in the presented works. Even so, it is argued that the structures under consideration do not present any significant local unloading until the collapse load of interest is reached. In such a case, nonlinear elasticity represents a fairly accurate model.

As an additional detail, it is important to mention that large rotations and shear strains in the thin-walled shell structure of interest are accounted for by means of the shell FE formulation. The present approaches resort to a three-dimensional seven-parameter shell formulation proposed by Büchter et al. (1994). This formulation, based on the enhanced assumed strain (EAS) concept, disables the usual locking problems characteristic of shell elements. Such a formulation introduces another set of nonlinear compatibility equations (see, e.g., Baguet, 2001, pp. 43–48).

III–1.3 Elastic buckling of shells with geometrical imperfections

The structural elements of interest in this section are thin-walled cylindrical shells of length $L = 1000$ mm, radius $R = 220$ mm and thickness $t = 0.5$ mm. We consider that the shells have some initial shape imperfections, i.e. there exist unavoidable deviations from the perfect cylinder. The shape and amplitude of these imperfections are defined from the survey conducted by Rhijnsburger (1999) on 27 shells with different sizes and cut-outs. Only the shells with the above-mentioned geometry are considered in the analysis (specimens referenced from zyl113 to zyl121). The circular cut-out present in each of the shells tested by Rhijnsburger is ignored in our analysis. The shells were scanned along their circumference with 60 data points. The distance between the circumferential scans in the axial direction was 20 mm. In the present analysis it is assumed that the shells are constructed of steel with deterministic material properties: Young's modulus $E = 200,000$ MPa and Poisson's ratio $\nu = 0.3$. Material behavior is assumed to be linear elastic. Contrarily to the real shells which were tested under axial compression, the shells here are assumed to be subjected to a uniform external pressure. The cylindrical shells are assumed to be simply supported at both ends (so-called SS3 boundary conditions). Additional constraints are imposed in order to prevent rigid body modes.

The cylinder is discretized with a mesh containing 120 8-node Büchter and Ramm shell elements in the circumferential direction and 25 elements in the axial direction ($\approx 60,000$ d.o.f.)[1]. Bifurcations are detected in the equilibrium path by the ANM as proposed by Boutyour et al. (1995), see Section III–1.2.3 (c). The computational cost of a single FE run, including the determination of the equilibrium path and the detection of bifurcations, was less than 90 min.[2]

III–1.3.1 Identification of random fields from measured imperfections

The initial imperfections, expressed in terms of their radial components, are determined from the experimental measurements w.r.t. a best-fit perfect cylinder (Rhijnsburger, 1999). For each cylindrical shell, the Fourier coefficients are obtained by a double harmonic analysis. Four types of representation are proposed in Rhijnsburger (1999). The type retained here corresponds to a half-wave cosine representation in the axial direction. For a given shell, the radial component $w(x,\theta)$ of the shape imperfection is expressed as follows, for $(x,\theta) \in \mathcal{D} = [0,L] \times [0,2\pi[$:

$$w(x,\theta) = t \sum_{i=0}^{N} a_{i0} \cos\left(\frac{i\pi x}{L}\right) + t \sum_{k=0}^{N} \sum_{l=1}^{N} \cos\left(\frac{k\pi x}{L}\right) [a_{kl} \cos(l\theta) + b_{kl} \sin(l\theta)] \,, \tag{III.14}$$

where t is the thickness, $\{a_{i0}, 0 \le i \le N\}$, $\{a_{kl}, 0 \le k \le N \,, 1 \le l \le N\}$, $\{b_{kl}, 0 \le k \le N \,, 1 \le l \le N\}$ are the coefficients determined from the experimental data by Rhijnsburger (1999) and where the series is truncated after $N = 14$. It is important to notice that the total number of coefficients involved in this expression is equal to $15 + 2 \times 15 \times 14 = 435$.

Two types of random field model are proposed to represent shape imperfections in the objective of a subsequent reliability analysis. The first model consists in considering the Fourier coefficients as random variables in Eq. (III.14), see Section III–1.3.1 (a). In this model, the number of random coefficients accounted for is limited to 35, and a multivariate normal PDF is identified from the experimental data. Selection is made based on criteria representative of the importance of each coefficient in the series.

[1] The convergence of the FE solution of the buckling problem with the ANM is obtained with about 20,000 d.o.f. for the perfect cylinder. It is assumed that the FE mesh with 60,000 d.o.f. is sufficiently refined for accurate solutions in all the problems with shape imperfections involved in the reliability analysis performed later on.

[2] The computations related to this study were performed in 2008. The CPU time of a single FE run with the ANM would be far less than 90 min using more recent computing resources.

The second model is based on a Karhunen Loève (KL) series expansion of the shape imperfections, see Section III–1.3.1 (b). The autocorrelation function is constructed from the measured imperfections, and the integral problem is solved numerically by a Galerkin method using a trigonometric Fourier basis. The random field is assumed to be Gaussian and the KL series is truncated after 12 terms.

(a) Fourier representation with random coefficients

The *random* shape imperfection $W(x,\theta)$ is simply obtained by considering the Fourier coefficients involved in Eq. (III.14) as random variables:

$$W(x,\theta) = t\sum_{i=0}^{N} A_{i0}\cos\left(\frac{i\pi x}{L}\right) + t\sum_{k=0}^{N}\sum_{l=1}^{N}\cos\left(\frac{k\pi x}{L}\right)\left[A_{kl}\cos(l\theta) + B_{kl}\sin(l\theta)\right], \tag{III.15}$$

where $\{A_{i0}, 0\le i\le N\}$, $\{A_{kl}, 0\le k\le N\ , 1\le l\le N\}$, $\{B_{kl}, 0\le k\le N\ , 1\le l\le N\}$ are random variables whose joint distribution is inferred from the measured data.

A reduction in the number of random coefficients considered in the model was performed without altering the accuracy of the shape imperfection representation. The idea is to retain in the representation only those coefficients that are the most important w.r.t. the mean and/or variance of $W(x,\theta)$. An additional selection criterion is based on the contribution of a given coefficient in the covariance matrix related to the whole set of coefficients. Selection is made as follows:

1. We first proceed to a renumbering of the random coefficients by means of a single index $k\in\mathcal{K} = \{1,\dots,435\}$, such that first the A_{i0} and A_{kl} coefficients are placed in ($k\in\{1,\dots,225\}$), and then the B_{kl} coefficients are placed in ($k\in\{226,\dots,435\}$). Let us denote $\boldsymbol{\Xi} = (\Xi_1,\dots,\Xi_{435})^{\mathrm{T}}$ the random vector with the reordered coefficients.

2. We compute the mean $\mu_W(x,\theta)$ and the variance $\sigma^2_W(x,\theta)$ of $W(x,\theta)$ for $(x,\theta)\in\mathcal{D}$. These expressions, detailed in Noirfalise (2009, p. 145), are expressed in terms of the expectations and covariances of the random coefficients $\{\Xi_k, k\in\mathcal{K}\}$, whose sample estimates are known from the data of Rhijnsburger (1999).

3. We additionally compute the Frobenius norm of the covariance matrix $\Sigma_{\boldsymbol{\Xi}\boldsymbol{\Xi}}$ of the random vector $\boldsymbol{\Xi}$:

$$\|\Sigma_{\boldsymbol{\Xi}\boldsymbol{\Xi}}\|_{\mathrm{F}} = \sqrt{\mathrm{tr}\left(\Sigma_{\boldsymbol{\Xi}\boldsymbol{\Xi}}\Sigma^{\mathrm{T}}_{\boldsymbol{\Xi}\boldsymbol{\Xi}}\right)}\,. \tag{III.16}$$

4. For $k\in\mathcal{K}$ let us drop the coefficient Ξ_k in the expression of $W(x,\theta)$ given in Eq. (III.15). We denote $\mu_W^{(-k)}(x,\theta)$, $\sigma^{2\ (-k)}_W(x,\theta)$ and $\|\Sigma_{\boldsymbol{\Xi}^{(-k)}\boldsymbol{\Xi}^{(-k)}}\|_{\mathrm{F}}$ the above-defined quantities with the coefficient Ξ_k omitted.

5. The following error measures are introduced:

$$\begin{aligned}
\epsilon_{\mu}^{(-k)} &= \frac{\sup_{(x,\theta)\in\mathcal{D}}\left|\mu_W(x,\theta) - \mu_W^{(-k)}(x,\theta)\right|}{\sup_{(x,\theta)\in\mathcal{D}}\left|\mu_W(x,\theta)\right|}\,,\\
\epsilon_{\sigma^2}^{(-k)} &= \frac{\sup_{(x,\theta)\in\mathcal{D}}\left|\sigma^2_W(x,\theta) - \sigma^{2\ (-k)}_W(x,\theta)\right|}{\sup_{(x,\theta)\in\mathcal{D}}\left|\sigma^2_W(x,\theta)\right|}\,,\\
\epsilon_{\Sigma}^{(-k)} &= \frac{\|\Sigma_{\boldsymbol{\Xi}^{(-k)}\boldsymbol{\Xi}^{(-k)}}\|_{\mathrm{F}}}{\|\Sigma_{\boldsymbol{\Xi}\boldsymbol{\Xi}}\|_{\mathrm{F}}}\,.
\end{aligned} \tag{III.17}$$

6. The random coefficients selected in the Fourier series are those satisfying:

$$k\in\mathcal{K}_{\mathrm{sel}} = \mathcal{K}_{\mu}\cup\mathcal{K}_{\sigma^2}\cup\mathcal{K}_{\Sigma} \quad \text{where} \begin{cases} \mathcal{K}_{\mu} &= \{k\in\mathcal{K} : \epsilon_{\mu}^{(-k)} \ge \overline{\epsilon}_{\mu}\}\\ \mathcal{K}_{\sigma^2} &= \{k\in\mathcal{K} : \epsilon_{\sigma^2}^{(-k)} \ge \overline{\epsilon}_{\sigma^2}\}\\ \mathcal{K}_{\Sigma} &= \{k\in\mathcal{K} : \epsilon_{\Sigma}^{(-k)} < \overline{\epsilon}_{\Sigma}\} \end{cases}, \tag{III.18}$$

with the following choices for the threshold values: $\overline{\epsilon}_{\mu} = \overline{\epsilon}_{\sigma^2} = 0.03$ and $\overline{\epsilon}_{\Sigma} = 1$.

The selection criteria are shown in Figure III.2. The sets $\mathcal{K}_{\mu}$, $\mathcal{K}_{\sigma^2}$ and $\mathcal{K}_{\Sigma}$ are respectively represented by blue squares in subplots (a), (b) and (c) of this figure. A total of 35 coefficients are selected. It is shown that these coefficients are those associated with axial modes 0 and 2 only, while almost all the circumferential modes are selected, see Figure III.3.

The stochastic model for shape imperfections is therefore expressed in terms of 35 random coefficients. The distribution of the random vector $\boldsymbol{\Xi}_{\text{sel}} = (\Xi_k, k \in \mathcal{K}_{\text{sel}})$ is assumed to be Gaussian (it is recalled that the sample size is small, i.e. only 9 cylinders, which does not leave us other choices). The means and standard deviations of the marginal distributions were estimated from the data, along with the linear correlation between the components of $\boldsymbol{\Xi}_{\text{sel}}$.

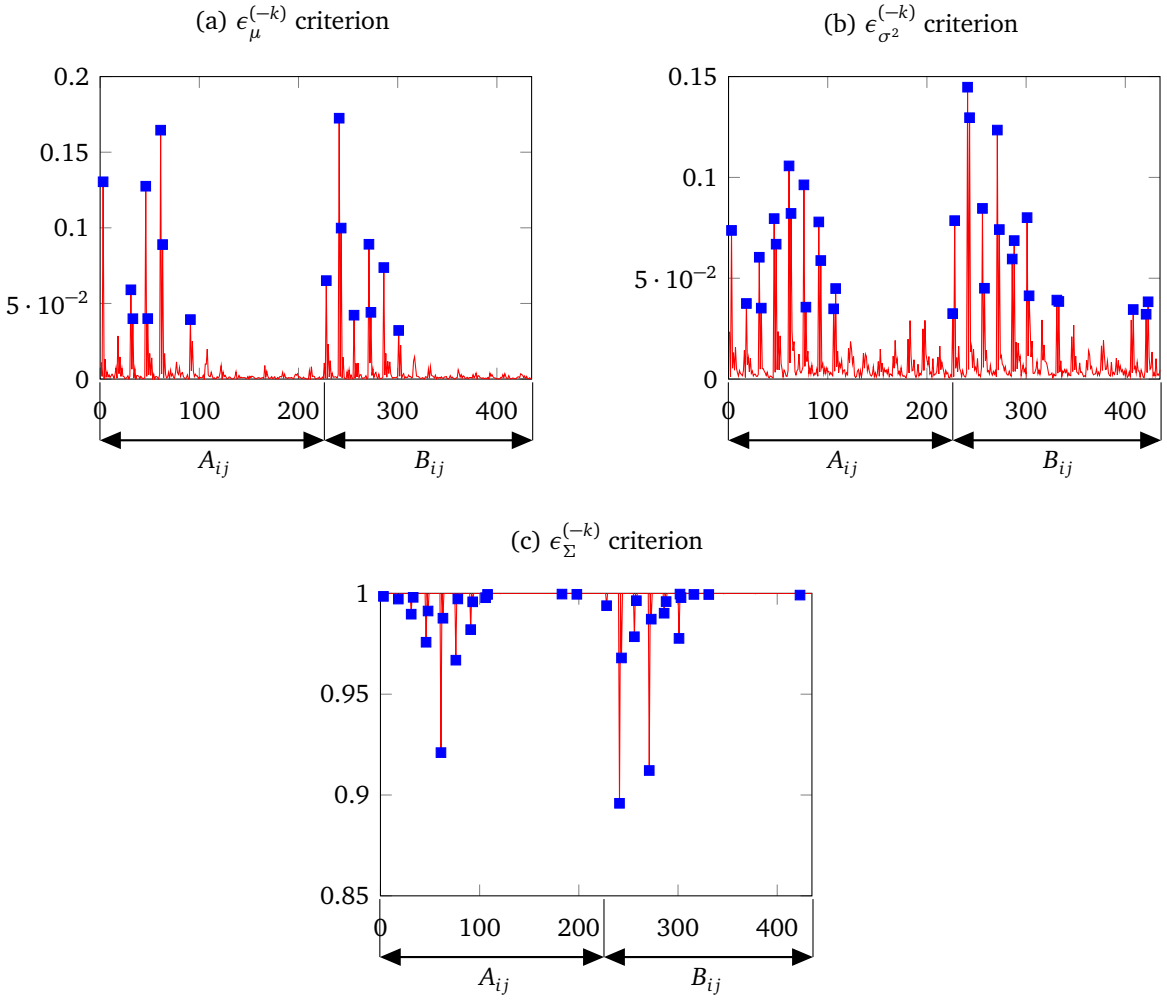

Figure III.2 – Criteria for the selection of random coefficients in the Fourier series.

(b) Stochastic model based on a Karhunen Loève series expansion

The second constructed model is based on a truncated Karhunen Loève (KL) series expansion. The shape imperfection is assumed to be modeled by a Gaussian real-valued second-order random field $W = \{W(\boldsymbol{\tau}), \boldsymbol{\tau} = (x, \theta) \in \mathcal{D}\}$ and we denote in the following by $U = \{U(\boldsymbol{\tau}), \boldsymbol{\tau} \in \mathcal{D}\}$ the zero-mean Gaussian field associated with W such that, for any $\boldsymbol{\tau} \in \mathcal{D}$:

$$U(\boldsymbol{\tau}) = W(\boldsymbol{\tau}) - \mathbb{E}[W(\boldsymbol{\tau})] \, . \tag{III.19}$$

(a) Coefficients A_{ij} (b) Coefficients B_{ij}

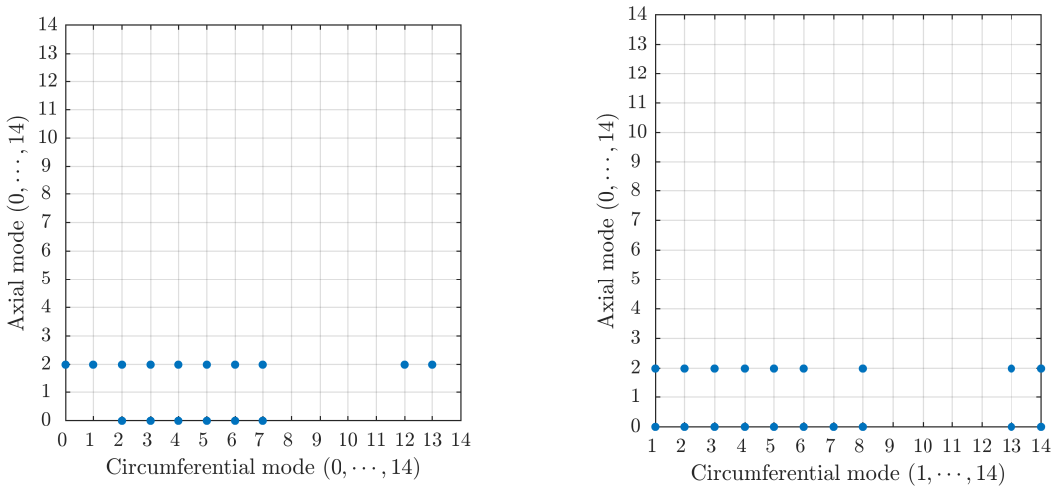

Figure III.3 – Selected random coefficients.

The autocorrelation function of U denoted $R_U : \mathcal{D}\times\mathcal{D} \to \mathbb{R}, (\boldsymbol{\tau},\boldsymbol{\tau}') \mapsto R_U(\boldsymbol{\tau},\boldsymbol{\tau}')$ is defined by $R_U(\boldsymbol{\tau},\boldsymbol{\tau}') = \mathbb{E}\left[U(\boldsymbol{\tau})U(\boldsymbol{\tau}')\right]$ for any $(\boldsymbol{\tau},\boldsymbol{\tau}') \in \mathcal{D}\times\mathcal{D}$.

This random field admits the following expansion for any $\boldsymbol{\tau} \in \mathcal{D}$, referred to as Karhunen Loève (KL) expansion of U:

$$U(\boldsymbol{\tau}) = \sum_{k=1}^{+\infty} \sqrt{\lambda_k}\xi_k\varphi_k(\boldsymbol{\tau})\,, \tag{III.20}$$

where the scalars $\{\lambda_k, k \in \mathbb{N}_{>0}\}$ and the real-valued functions $\{\varphi_k, k \in \mathbb{N}_{>0}\}$ are the solutions of the following homogeneous Fredholm integral equation of the second kind[3] in (λ,φ), for any $\boldsymbol{\tau} \in \mathcal{D}$:

$$\int_{\mathcal{D}} R_U(\boldsymbol{\tau},\boldsymbol{\tau}')\varphi(\boldsymbol{\tau}')\mathrm{d}\boldsymbol{\tau}' = \lambda\varphi(\boldsymbol{\tau})\,, \tag{III.21}$$

and where the random variables $\{\xi_k, k \in \mathbb{N}_{>0}\}$ are given by:

$$\xi_k = \frac{1}{\sqrt{\lambda_k}}\int_{\mathcal{D}} U(\boldsymbol{\tau})\varphi_k(\boldsymbol{\tau})\mathrm{d}\boldsymbol{\tau}\,. \tag{III.22}$$

Under the Gaussianity assumption for the random field which is made here, the random variables ξ_k are mutually independent standard normal random variables. For non-Gaussian random fields, these random variables are zero-mean uncorrelated random variables, i.e. $\mathbb{E}\left[\xi_i\xi_j\right] = \delta_{ij}$, but they are not independent.[4] Note also that the series in Eq. (III.20) converges in quadratic mean and uniformly in $\boldsymbol{\tau}$.

For practical implementation, we resort to a truncated expansion of U, for any $\boldsymbol{\tau} \in \mathcal{D}$:

$$U_M(\boldsymbol{\tau}) = \sum_{k=1}^{M} \sqrt{\lambda_k}\xi_k\varphi_k(\boldsymbol{\tau})\,, \tag{III.23}$$

[3] In other terms Eq. (III.21) expresses that λ_k and φ_k are respectively the eigenvalues and eigenfunctions of the autocorrelation function R_U.

[4] In such problems a Gaussian kernel approximation can be used for modeling the joint PDF of the ξ_k's from a set of observations, as recently proposed by Poirion and Zentner (2014).

where the eigenvalues λ_k are assumed to be sorted in decreasing order. The truncation order M is chosen w.r.t. the ratio $\sum_{k=1}^{M}\lambda_k / \sum_{k=1}^{+\infty}\lambda_k$, which represents an indirect measure of the error in the variance of the random field U due to the truncation (see, e.g., Huang et al., 2001).

The main effort in constructing the KL expansion consists in computing the eigenvalue and eigenfunction solutions of Eq. (III.21). In practice, these solutions are obtained numerically, except for a very few cases for which an analytical solution is available. In this context the eigenfunctions φ_k are expanded on a chosen set of basis functions $\{\Psi_i(\boldsymbol{\tau}), 1 \leq i \leq N\}$, e.g. Fourier, orthogonal polynomial or wavelet basis:

$$\begin{aligned}\varphi_k(\boldsymbol{\tau}) &= \sum_{i=1}^{N} d_{k,i}\Psi_i(\boldsymbol{\tau}) \\ &= \boldsymbol{\Psi}(\boldsymbol{\tau})^{\mathrm{T}}\mathbf{d}_k\,,\end{aligned} \tag{III.24}$$

where $\boldsymbol{\Psi}(\boldsymbol{\tau}) = (\Psi_1(\boldsymbol{\tau}), \ldots, \Psi_N(\boldsymbol{\tau}))^{\mathrm{T}}$ and $\mathbf{d}_k = (d_{k,1}, \ldots, d_{k,N})^{\mathrm{T}}$ is the vector of unknown constant coefficients.

By substituting the expansion of Eq. (III.24) in Eq. (III.21) and by setting the error in Eq. (III.21) to be orthogonal to each basis function Ψ_i, we can obtain the following generalized eigenproblem:

$$\mathbf{A}\mathbf{d}_k = \lambda_k \mathbf{B}\mathbf{d}_k\,, \tag{III.25}$$

where the $N \times N$ matrices $\mathbf{A} = [a_{ij}]_{1\leq i,j\leq N}$ and $\mathbf{B} = [b_{ij}]_{1\leq i,j\leq N}$ are given by:

$$\begin{aligned}a_{ij} &= \int_{\mathcal{D}}\int_{\mathcal{D}} R_U(\boldsymbol{\tau},\boldsymbol{\tau}')\Psi_i(\boldsymbol{\tau}')\Psi_j(\boldsymbol{\tau})\mathrm{d}\boldsymbol{\tau}'\mathrm{d}\boldsymbol{\tau}, \\ b_{ij} &= \int_{\mathcal{D}} \Psi_i(\boldsymbol{\tau})\Psi_j(\boldsymbol{\tau})\mathrm{d}\boldsymbol{\tau}.\end{aligned} \tag{III.26}$$

It is worth noting that the number of terms M in the truncated KL expansion defined in Eq. (III.23) cannot be greater than the selected number of basis functions N.

In the work of Noirfalise (2009), the eigenfunctions φ_k are expanded on a set of basis functions $\{\Psi_{\boldsymbol{\alpha}}(\boldsymbol{\tau}), |\boldsymbol{\alpha}| = \alpha_1 + \alpha_2 \leq p\}$, $p \in \mathbb{N}_{>0}$:

$$\varphi_k(\boldsymbol{\tau}) = \sum_{\boldsymbol{\alpha}\in\mathcal{A}} d_{k,\boldsymbol{\alpha}}\Psi_{\boldsymbol{\alpha}}(\boldsymbol{\tau})\,, \tag{III.27}$$

where $\boldsymbol{\alpha} = (\alpha_1, \alpha_2) \in \mathbb{N}^2$ is a bi-index, $|\boldsymbol{\alpha}|$ denoting its length, and $d_{k,\boldsymbol{\alpha}}$ are the unknown constant coefficients. Given the Fourier representation of U, the most natural choice for $\Psi_{\boldsymbol{\alpha}}$ is the following basis of trigonometric functions:

$$\Psi_{\boldsymbol{\alpha}}(\boldsymbol{\tau}) = \Psi_{\boldsymbol{\alpha}}(x,\theta) = \psi_{\alpha_1}\left(\frac{\pi x}{L}\right)\psi_{\alpha_2}(\theta)\,, \tag{III.28}$$

where, for any $t \in \mathbb{R}$:

$$\psi_0(t) = 1 \quad \text{and, for } m \in \mathbb{N}_{>0}, \quad \psi_{2m-1}(t) = \cos(mt)\,,\ \psi_{2m}(t) = \sin(mt)\,. \tag{III.29}$$

The basis selected by Noirfalise was truncated after $p = 16$ in order to select most important terms in the Fourier series.

The solutions of Eq. (III.25) were obtained by symbolic computations. The problem to solve was found to be very sensitive to rounding errors. The computed eigenvalues λ_k are represented in Figure III.4. Due to the rapid decay of the eigenvalues, the series defined in Eq. (III.23) was truncated after $M = 12$ terms. The first four eigenvectors are represented in Figure III.5.

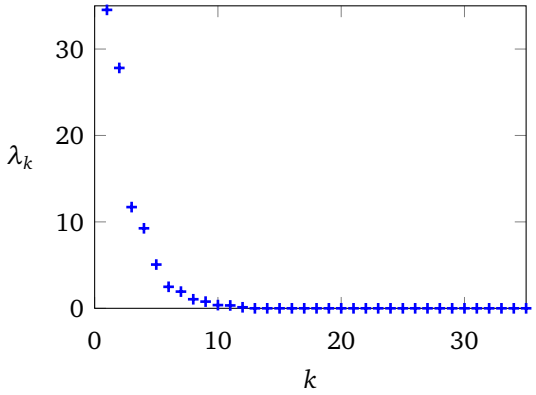

Figure III.4 – Lowest eigenvalues λ_k of the integral equation Eq. (III.25).

(a) 1st eigenvector $\varphi_1(x,\theta)$

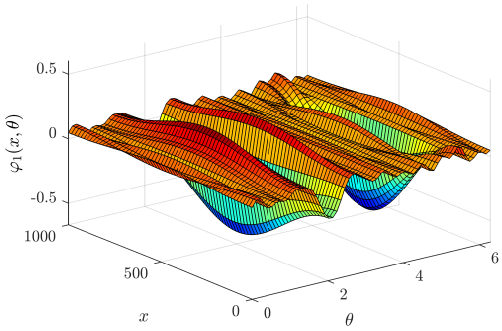

(b) 2nd eigenvector $\varphi_2(x,\theta)$

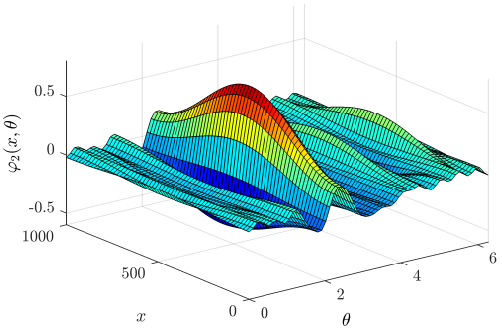

(c) 3rd eigenvector $\varphi_3(x,\theta)$

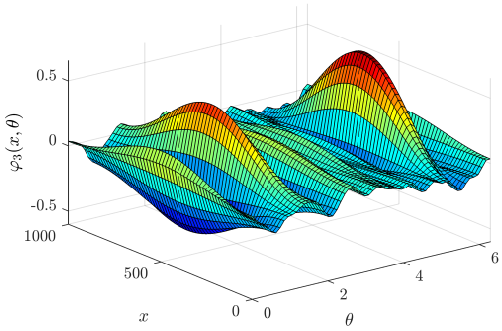

(d) 4th eigenvector $\varphi_4(x,\theta)$

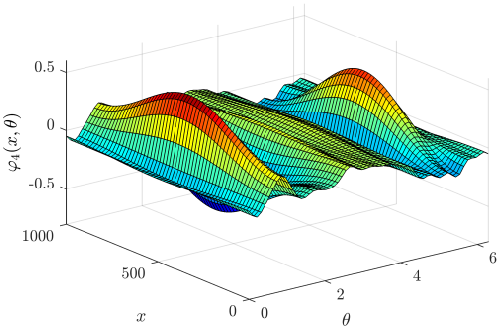

Figure III.5 – Eigenvectors $\varphi_k(x,\theta)$ of the integral equation Eq. (III.25).

III–1.3.2 Reliability assessment by subset simulation

We want to assess the reliability of the thin-walled cylindrical shells analyzed by Rhijnsburger subjected to a prescribed external pressure $p_0 = 1000$ Pa.[5] We assume that these shells have random shape imperfections, modeled by means of one of the two models presented so far: either the random Fourier representation described in Section III–1.3.1 (a) or the truncated Karhunen Loève series expansion described in Section III–1.3.1 (b). The failure probability is given by:

$$p_f = \mathbb{P}\left(p_{cr} \leq p_0\right) , \tag{III.30}$$

where p_{cr} is the buckling pressure of the shell. For the random Fourier representation, $p_{cr} = p_{cr}(\boldsymbol{\Xi}_{sel})$, where $\boldsymbol{\Xi}_{sel} = (\Xi_k, k \in \mathcal{K}_{sel})$ and $\#\mathcal{K}_{sel} = 35$. For the truncated Karhunen Loève series expansion, $p_{cr} = p_{cr}(\boldsymbol{\Xi}_M)$, where $\boldsymbol{\Xi}_M = (\Xi_1, \ldots, \Xi_M)^T$ and $M = 12$. The critical buckling pressures p_{cr} are assessed numerically by bifurcation detection in the ANM, see Section III–1.2.3 (c).

The failure probability is estimated by subset simulation with 10,000 samples per level, see Section I–3.2. The failure probability estimate obtained with the random Fourier representation of the shape imperfection is 5.97×10^{-6} with a coefficient of variation of 0.15. For the truncated Karhunen Loève series expansion, the estimate is 4.47×10^{-6} with a coefficient of variation of 0.16. Each subset simulation analysis requires a total of 60,000 samples. The two failure probability estimates are very close, with a difference in the order of the statistical dispersion. These results allow us to conclude that both models are suitable for the purpose of reliability estimation. The probability estimates $\widehat{\pi}_s$ of π_s at the intermediate levels y_s of the LSF are also represented in Figure III.6 with their 95% confidence intervals where, for $s = 1, \ldots, m = 6$:

$$\pi_s = \prod_{k=1}^{s} p_k = \mathbb{P}\left(p_{cr} \leq p_0 + y_s\right) . \tag{III.31}$$

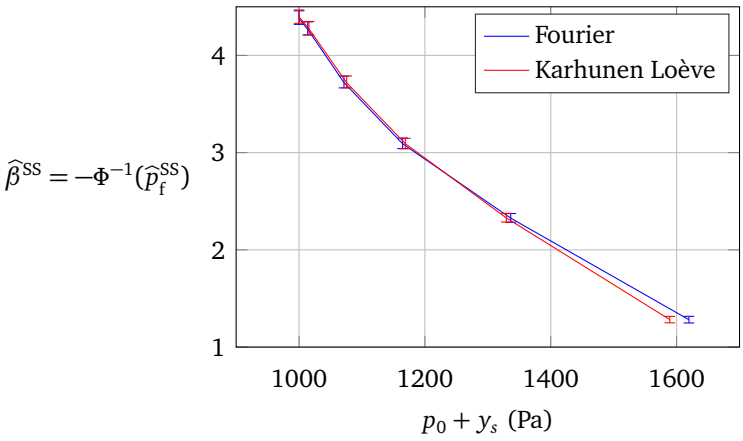

Figure III.6 – Subset simulation results.

III–1.4 Elastoplastic collapse of shells with geometrical imperfections and space-variant material properties / thicknesses

The structure of interest in this section is the cylindrical shell roof illustrated in Figure III.7. This example is inspired by the article of Scordelis and Lo (1964) (see also Ramm and Wall, 2004, pp. 405–406), but the load case and the material properties have been modified (Dubourg et al., 2009a). The dimensions

[5] The buckling pressure of the *perfect* shell determined by the ANM is equal to 2880 Pa.

under consideration are given in Figure III.7. The longitudinal edges are free, while the circumferential edges are simply supported by rigid diaphragms. The roof is subjected to a distributed non-follower vertical load q over its whole upper surface. The constitutive material is assumed to follow a Ramberg-Osgood nonlinear elastic law, as described in Section III–1.2.3 (d). The problem is discretized with a mesh containing 30×30 8-node Büchter and Ramm shell elements ($\approx 17,000$ d.o.f.). Limit loads are computed by differentiating the piecewise polynomial series expansions of the equilibrium path, as explained in Section III–1.2.3 (c).

In the reliability analyses presented here, we assume that the space-variant properties of the roof structure are uncertain over the rectangular domain $[-L/2, L/2] \times [-R\theta/2, R\theta/2]$, where θ denotes the opening angle of the roof in radians. More specifically, the material properties (Young's modulus E and yield strength σ_y) and the shell thickness t are modeled by independent lognormal random fields represented by translated Karhunen-Loève expansions. Moreover, we consider random shape imperfection represented by a random linear combination of the three most critical buckling modes of the perfect structure. The reader may refer to Dubourg et al. (2009a) and Dubourg (2011) for additional details concerning the modeling aspects.

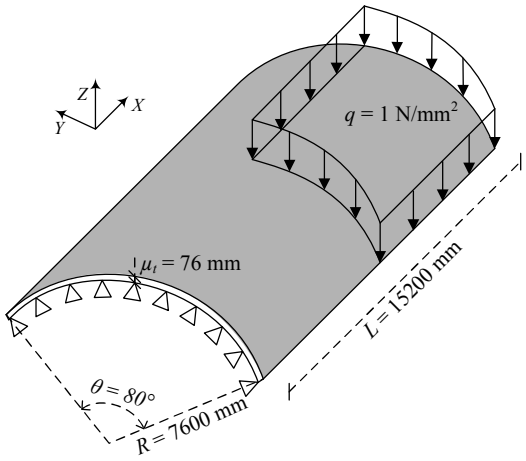

Figure III.7 – A shell roof under a uniformly-distributed vertical load (Scordelis and Lo, 1964).

III–1.4.1 Stochastic model for shape imperfections

The proposed probabilistic model for shape imperfections was deliberately constructed in the absence of real data. The idea is to model the shape imperfection as a random linear combination of the lowest most critical buckling buckling modes of the perfect roof structure. These modes are obtained from a linear buckling analysis (so-called Euler buckling), see the first three modes shown in Figure III.8. The random shape imperfection is expressed in terms of these three modes as follows:

$$\zeta(x,\theta) = \sum_{k=1}^{3} \Xi_{\zeta,k} \mathbf{U}_k(x,\theta)\,, \tag{III.32}$$

where $\{\mathbf{U}_k, 1 \leq k \leq 3\}$ are the displacement fields of the three lowest buckling modes of the perfect structure, and where $\boldsymbol{\Xi}_\zeta = (\Xi_{\zeta,1}, \Xi_{\zeta,2}, \Xi_{\zeta,3})$ is a vector of three independent Gaussian random variables with zero means and standard deviations set to $\sigma_\zeta = 9.5$ mm. These settings respectively ensure that: (a) the mean shape matches the perfect structure, (b) the maximum amplitude of the shape imperfection does not exceed a fraction of the mean thickness. This latter condition is imposed in order to validate

the shell element theory. The standard deviation $\sigma_\zeta = \sigma_{\zeta,1} = \sigma_{\zeta,2} = \sigma_{\zeta,3}$ has been adjusted by Monte Carlo sampling so that the maximum amplitude at ±2 standard deviations matches half of the mean roof thickness $\mu_t/2 = 38$ mm. Such a criterion is met for $\sigma_\zeta = 9.5$ mm.

(a) Mode 1

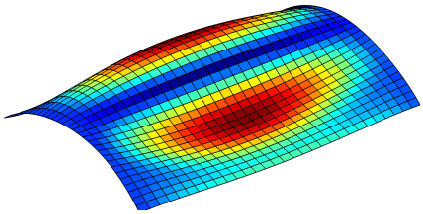

(b) Mode 2

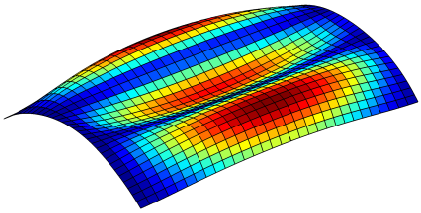

(c) Mode 3

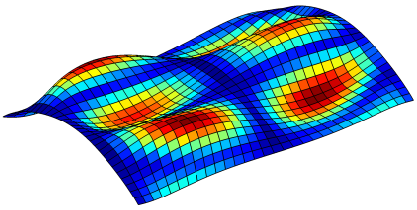

Figure III.8 – The three most critical buckling modes of the shell roof.

III–1.4.2 Stochastic model for space-variant material properties and thicknesses

The three lognormal random fields E, σ_y and h are obtained by transforming the realizations of three independent standard normal random fields, denoted U_E, U_{σ_y} and U_h through the following translation:

$$F(x,\theta) = \exp\left(\lambda_F + \zeta_F U_F(x,\theta)\right) \quad \text{where } F = E, \sigma_y, h\,, \tag{III.33}$$

and where λ_F and ζ_F are respectively the location and scale parameters of the corresponding lognormal distributions whose mean and coefficient of variation are given in Table III.1.

Each underlying standard normal random field U_F is assumed to have the following isotropic squared exponential autocorrelation function:

$$R_{U_F}(\tau,\tau') = \exp\left[\frac{(x-x')^2}{\ell^2} + \frac{R^2(\theta-\theta')^2}{\ell^2}\right], \tag{III.34}$$

Variable		Distribution	Mean	C.o.V.
E	(MPa)	lognormal	200,000	0.03
σ_y	(MPa)	lognormal	390	0.07
h	(mm)	lognormal	76	0.05

Table III.1 – Parameters of the lognormal random fields of the shell roof.

where $\boldsymbol{\tau} = (x, \theta)$, $\boldsymbol{\tau}' = (x', \theta')$, and where the correlation length ℓ is set to 3500 mm. These random fields are represented by means of their truncated Karhunen-Loève expansion:

$$U_{F,M}(\boldsymbol{\tau}) = \sum_{k=1}^{M} \sqrt{\lambda_k} \xi_{F,k} \varphi_k(\boldsymbol{\tau}) \,, \tag{III.35}$$

where $\boldsymbol{\Xi}_F = (\xi_{F,1}, \ldots, \xi_{F,M})$ is a vector of independent standard normal random variates. It is recalled that the M pairs $\{(\lambda_k, \varphi_k), 1 \leq k \leq M\}$ are the solutions of the integral equation defined in Eq. (III.21), corresponding to the greatest eigenvalues λ_k. This equation is solved numerically using the wavelet-Galerkin scheme proposed by Phoon et al. (2002). In this scheme, the set of basis functions $\{\Psi_i(\boldsymbol{\tau}), 1 \leq i \leq N\}$ involved in Eq. (III.24) is composed of wavelet functions. Phoon et al. propose to use the Haar wavelet functions, which are the simplest form of Daubechies' wavelets, with maximum wavelet level m.[6] The main advantage of wavelets over conventional bases is that the integrals appearing in Eq. (III.26) do not require numerical integration. Matrix $\mathbf{A}$ in Eq. (III.25) in fact appears to be the two-dimensional wavelet transform of $R_U(\boldsymbol{\tau}, \boldsymbol{\tau}')$, which can be obtained by the application of the 1D wavelet transform, first on the rows and then on the columns of the matrix containing the values of the autocorrelation function $R_U(\boldsymbol{\tau}, \boldsymbol{\tau}')$ evaluated over an N by N grid (Phoon et al., 2002). The truncation order M of the expansion given in Eq. (III.35) is the same for the three random fields. It is set equal to $M = 30$ so that the relative mean squared error w.r.t. the non-truncated expansion is less than 3.70%.

III–1.4.3 Reliability assessment

The probabilistic model involved in the reliability analysis features 93 independent normal random variables grouped in the vector $\boldsymbol{\Xi} = (\boldsymbol{\Xi}_E, \boldsymbol{\Xi}_{\sigma_y}, \boldsymbol{\Xi}_t, \boldsymbol{\Xi}_\zeta)$. For illustration purposes a realization of the four random fields is illustrated in Figure III.9. The failure probability of the roof is given by:

$$p_f = \mathbb{P}\left(q_{cr}(\boldsymbol{\Xi}) \leq q_0\right) \,, \tag{III.36}$$

where q_{cr} is the buckling load of the shell roof and q_0 is arbitrarily set to 0.18 MPa in order to make the failure probability sufficiently low.[7] Buckling is detected by the ANM as a limit load, i.e. the load corresponding to a path parameter a satisfying Eq. (III.12).

A subset simulation analysis with 5000 samples per level is performed. The failure probability estimate is $\widehat{p}_f^{SS} = 1.27 \times 10^{-4}$ with a coefficient of variation of $\delta_{\widehat{p}_f^{SS}} = 0.12$. A total of 20,000 samples is required in this analysis.

The restarted FORM analysis of Der Kiureghian and Dakessian (1998) presented in Section I–2.1.3 is also applied in order to shed light on the most probable configurations of the random inputs that lead to failure. Four most probable failure points (MPFPs) are identified with the restarted i-HLRF algorithm, tuned as proposed in the original paper by Der Kiureghian and Dakessian (1998), i.e. with $\delta = 0.75, \gamma = 1.1, \epsilon = 0.5$. The four random fields at the first MPFP are represented in Figure III.10. This figure clearly shows that failure occurs in one of the four roof corners when the following conditions are met: Young's modulus, yield strength and thickness are low in the given corner and, additionally, shape imperfections are large in the same corner. Similar configurations are obtained for the three other MPFPs, i.e. in the other three corners. The reliability indices and failure probabilities obtained by FORM for these four MPFPs are listed in Table III.2. The problem of interest is characterized by four MPFPs

[6] In the present application, the maximum wavelet level m is set to 7. The basis $\{\Psi_i(\boldsymbol{\tau}), 1 \leq i \leq N\}$ is therefore composed of $N = 2^m = 128$ elements.

[7] The limit load of the *perfect* structure is found to be equal to $q_{limit} = 0.2676$ MPa.

(a) Young's modulus E (b) Shell thickness t

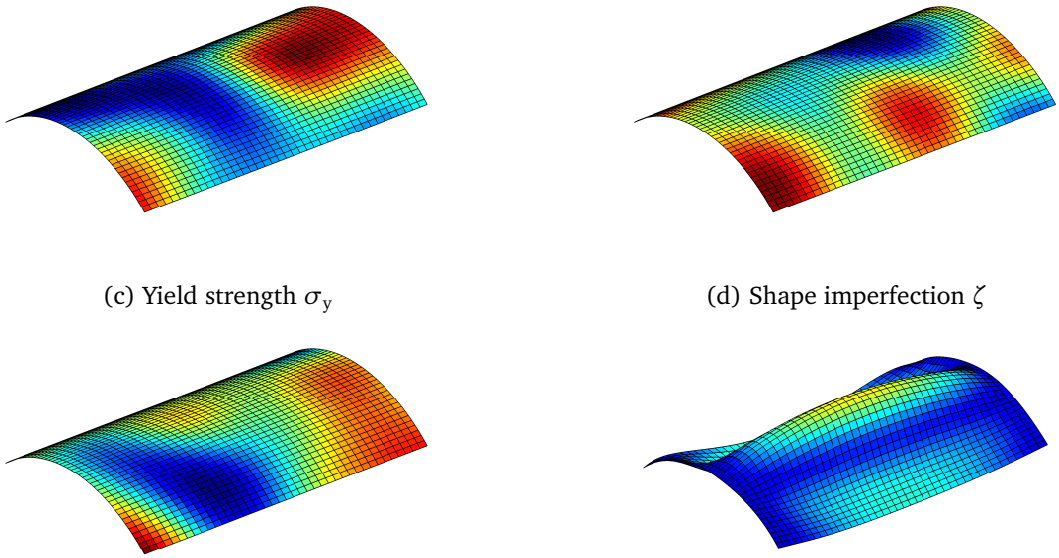

(c) Yield strength σ_y (d) Shape imperfection ζ

Figure III.9 – A given realization of the four random fields.

MPFP	#1	#2	#3	#4
β	4.01	4.01	4.00	4.01
p_f^{FORM}	3.02×10^{-5}	3.02×10^{-5}	3.11×10^{-5}	3.04×10^{-5}

Table III.2 – FORM results at the four MPFPs.

of equal importance, with failure localized in each of the four corners of the roof. These results can be explained by the symmetry w.r.t. x and θ of the three modes $\mathbf{U}_k(x,\theta)$ which are combined linearly in the random shape imperfection model, see Eq. (III.32) and Figure III.8.[8]

The importance factors of the FORM analysis can also be analyzed. These importance factors are represented in Figure III.11 for the first MPFP (similar pie charts are obtained for the three other MPFPs). The quantities represented in the pie chart are the following:

$$\alpha_F^2 = \sum_{i \in \mathcal{I}_F} \alpha_i^2 \,, \tag{III.37}$$

where $\mathcal{I}_F$ denotes the set of indices of the components of $\boldsymbol{\Xi}_F$ in $\boldsymbol{\Xi} = (\boldsymbol{\Xi}_E, \boldsymbol{\Xi}_{\sigma_y}, \boldsymbol{\Xi}_t, \boldsymbol{\Xi}_\zeta)$, and where $F = E, \sigma_y, h$ or ζ. The computed importance factors indicate that the random fields representing the thickness and yield strength are the most influential inputs in the reliability analysis of the shell roof w.r.t. buckling. Random shape imperfection is less important, and the space-variant Young's modulus has no influence on reliability. This type of conclusion was expected from the structural mechanics viewpoint. The mean ratio R/T of the shell is equal to 100, which indicates that the instability is due to the amplification of the shape imperfections, resulting in plastic buckling. This also justifies a posteriori the limit point detection strategy that is used in the ANM, which is well suited to instabilities triggered by material nonlinearities.

[8] The third buckling pattern $\mathbf{U}_3(x,\theta)$ is in fact symmetric w.r.t. x, but only anti-symmetric w.r.t. θ.

(a) Young's modulus E (b) Shell thickness t

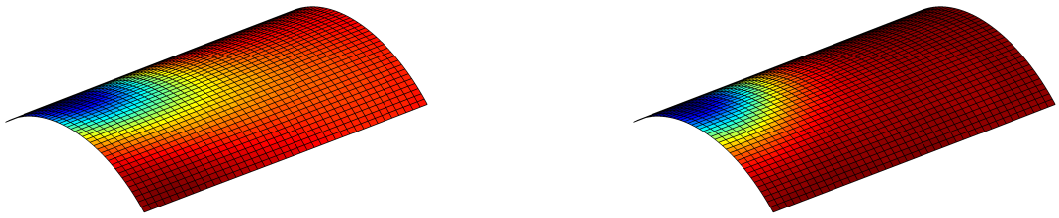

(c) Yield strength σ_y (d) Shape imperfection ζ

Figure III.10 – The four fields at MPFP #1.

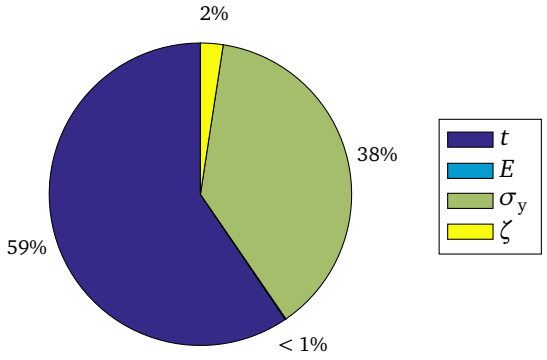

Figure III.11 – FORM importance factors at MPFP #1.

III–1.5 Optimal design of shells with random imperfections

Submarine pressure hulls are mainly composed of structural elements such as ring-stiffened cylinders, cones, elliptical or spherical ends, internal diaphragms, bulkheads and deep frames. At a diving depth I, the pressure hull is subjected to an external hydrostatic pressure $p = \rho_{\text{water}}\, g\, I$, where ρ_{water} is the sea water density (set here equal to 1000 kg/m^3) and $g \approx 10$ m/s^2 is the gravitational constant. Such a loading induces a compression stress state that is mostly membrane-dominated. Buckling therefore constitutes a critical failure mode for submarines.

Design practice is usually based on specific standards and design codes, such as the British Standard 5500 (BS5500) or the more recent Eurocode 3, possibly along with finite-element-based simulations. It often makes use of long-term-experience-based safety factors at various design stages, which potentially implies an unknown degree of conservatism. A key issue for submarine structural designers consists in finding an optimal ratio between the weight of the resistant structure and the buoyancy of the submersible. The tradeoff between the optimal weight and the safety level of the structure is addressed here in the framework of reliability-based design optimization (RBDO).

III–1.5.1 Single bay reference structure

(a) Ring-stiffened shell cylinder

The scope of the present analysis is restricted to a single bay reference structure of a submarine pressure hull, i.e. a shell cylinder with a single inner T-section ring stiffener, whose length is equal to the stiffener spacing. The dimensions of this elementary structure are shown in Figure III.12. In the following, the outer cylinder is referred to as the shell plating, and the web (resp. the flange) designates the vertical (resp. horizontal) part of the T-section ring stiffener. This simplified model with well-chosen boundary conditions is assumed to be representative of the behavior of a central bay of a sufficiently long pressure hull compartment (of infinite length in the present analysis).

The linear elastic stability analysis of this ring-stiffened shell exhibits typical buckling patterns. The three most critical kinds of buckling patterns are known as overall buckling, interframe buckling and frame tripping, and they are basically illustrated in Figure III.13. Actual structures exhibit some unavoidable shape imperfections due to the manufacturing process (mostly cold-bending- and welding-based) and heavy loads connected to the hull. These initial imperfections may trigger buckling or premature plastic collapse at pressures far below those corresponding to elastic buckling, even if these imperfections are of moderate amplitude due to the stringent tolerances used in construction.

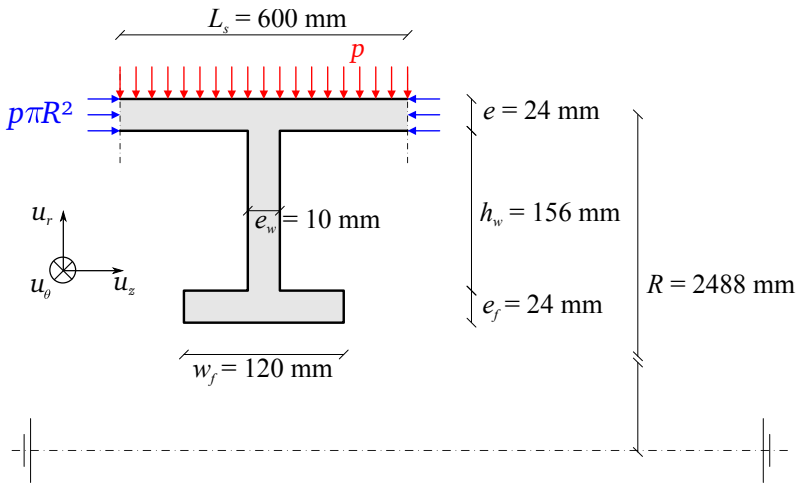

Figure III.12 – Single bay reference structure and initial design.

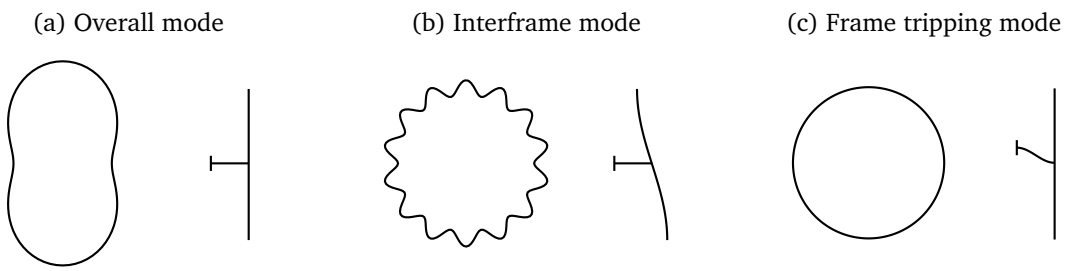

Figure III.13 – Schematic representation of the most critical buckling patterns of a ring-stiffened shell cylinder.

Predicting the collapse pressure for any given imperfect geometry is not straightforward, however, because the structure may feature a considerable degree of interaction between the aforementioned buckling modes. To solve the buckling problem at hand, the designer may resort to closed-form solutions or other semi-numerical methods available in the codes of practice (e.g. the BS5500). Another alternative which is investigated here consists in using an appropriate FE model.

(b) Modeling of shape imperfections

The present analysis is restricted to the effects of overall and interframe shape imperfections. Collapse due to frame tripping is avoided here by imposing some conservative rules taken from BS5500 regarding the proportions of the stiffener web and flange during optimization. The overall (resp. interframe) radial shape imperfection is given by:

$$\begin{aligned} \zeta_n(z,\,\theta) &= A_n\,\cos(n\,\theta)\;, \\ \zeta_m(z,\,\theta) &= A_m\,\cos\left(\pi\,\frac{z}{L_s}\right)\cos(m\,\theta)\;, \end{aligned} \tag{III.38}$$

where n (resp. m) is the number of circumferential waves, which typically ranges from 2 to 6 (resp. 10 to 20), A_n (resp. A_m) denotes the amplitude of the overall (resp. interframe) radial imperfection, and $0 \leq \theta < 2\pi$, $0 \leq z \leq L_s$. In the present analysis, only two modes are considered: $n = 2$ and $m = 14$. These two modes correspond to the most critical buckling patterns of the initial design.[9]

(c) Nonlinear finite element model

Collapse pressures are assessed by means of the ANM, accounting for material and geometric nonlinearities. The constitutive material of the pressure hull is assumed to follow a nonlinear elastic Ramberg-Osgood law, such as described in Section III–1.2.3 (d). Follower forces are taken into account for the hydrostatic pressure field p so that it is always exerted normally with respect to the deformed structure.

Rigid body modes are eliminated in three nodes, as illustrated in Figure III.14a:

- in A, the three translations are set to zero,
- in B, the translation along the z-axis is set to zero,
- in C, the translations along the y- and z-axes are set to zero.

The orthoradial rotations of the two circular ends of the cylinder are set equal to zero in order to fulfill the assumption of repeated adjacent bays. As an additional hypothesis, these two ends are assumed to remain plane and normal to the z-axis during the whole loading process, i.e. the nodes of each end cross-section undergo a constant but unknown overall axial displacement.

In addition to the hydrostatic pressure exerted on the outer cylinder, an axial membrane compressive stress of amplitude $p\,\pi R^2$ is applied, as indicated in Figure III.12. This additional load is due to the hydrostatic pressure exerted on both ends of the pressure hull.

The structure is meshed with 1540 Büchter and Ramm 8-node shell elements featuring about 40,000 degrees of freedom: 70 × 10 elements for the outer cylinder, 70 × 8 for the web of the stiffener and 70 × 4 elements for its flange. The collapse pressure was shown to stabilize for a coarser mesh featuring 15,000 degrees of freedom although it has been raised here in order to accurately represent the highest modal imperfection featuring 14 waves along the circumference, one wave being represented here by $70/14 = 5$ elements. The amplified superimposition of the two shape imperfections considered here is illustrated in Figure III.15.

[9] A finer study would consist in considering a larger spectrum of imperfections, depending on the current design at each iteration of the optimization process.

(a) Nodes for the elimination of rigid body modes (b) Mesh of the perfect structure

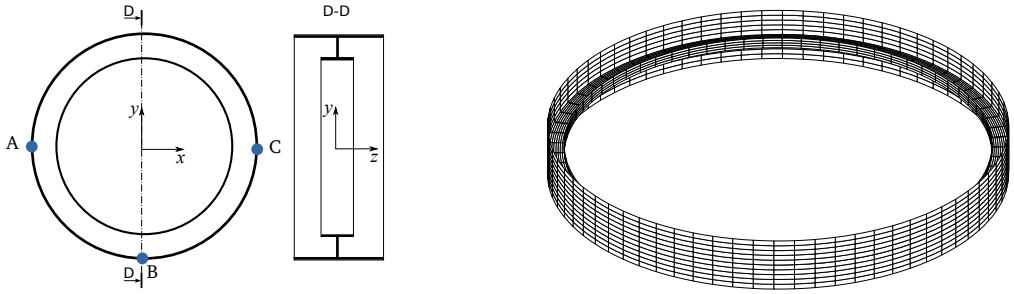

Figure III.14 – FE modeling of the ring-stiffened shell cylinder.

(a) Overall imperfection (b) Interframe imperfection (c) Combined imperfections

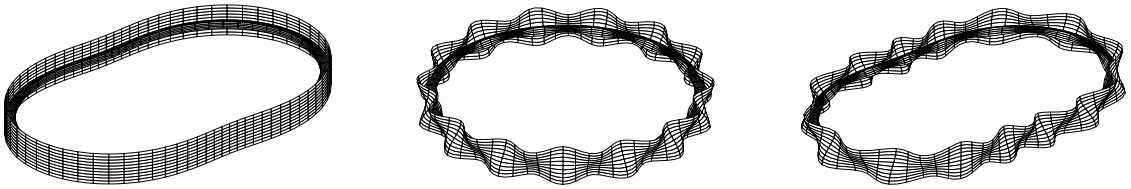

Figure III.15 – Ring-stiffened shell cylinder with amplified imperfections.

(d) Semi-numerical model

In the following, the designs obtained using the ANM-based FE model are compared with those obtained from approximate semi-numerical solutions available in the submarine pressure hull design codes of practice (see Dubourg et al., 2008, for a review). These approximations suppose in general the geometrical imperfection of a given modal shape and, as a consequence, they are not able to account for the possible interactions between buckling modes in case of multimodal (therefore more general) imperfections. The model used to predict the overall plastic collapse pressure $p_{n\,\mathrm{pl}}$ is based here on the Bryant formula embedded in the BS5500. The one used for the interframe plastic collapse pressure $p_{m\,\mathrm{pl}}$ resorts to an interpolated table of numerical solutions derived by the Krylov Shipbuilding Research Institute (KSRI). These two models assume an overall (resp. interframe) modal imperfection of amplitude A_n (resp. A_m).

The final semi-numerical model yielding the plastic collapse pressure of an infinite-length ring-stiffened cylinder with both overall and interframe imperfections is approximated as follows:

$$p_{\mathrm{critical}}(A_n, A_m) = \min\left(p_{n\,\mathrm{pl}}(A_n),\, p_{m\,\mathrm{pl}}(A_m)\right) . \tag{III.39}$$

III–1.5.2 Formulations of the design optimization problem

In this section, two design philosophies are opposed. The first resorts to the so-called worst case approach, which consists in designing for an extreme configuration specified by experts. The second one uses a more comprehensive probabilistic model, and eventually falls under the RBDO formulation.

(a) Objective and constraints

First, the objective of design optimization is to find the set of parameters defining the geometry of the structure $\mathbf{d} = (e, h_w, e_w, w_f, e_f)^T$ that minimizes the ratio between the structural weight and the weight of the displaced water. The latter ratio reads as follows:

$$c(\mathbf{d}) = \frac{\rho_{steel}\, V_{steel}(\mathbf{d})}{\rho_{water}\, \pi\, (R + e/2)^2\, L_s}\,, \tag{III.40}$$

where V_{steel} is the volume of steel composing the ring-stiffened bay and $\rho_{steel} = 7650$ kg/m^3 is the density of steel.

The admissible design space is bounded by the following constraints:

(i) Since the semi-numerical model does not consider the frame tripping collapse mode, it is proposed to use the following conservative safety criteria prescribed in the BS5500:

$$h_w \leq 1.1\sqrt{\frac{E}{\sigma_y}}\, e_w\,, \tag{III.41}$$

$$w_f \leq \sqrt{\frac{E}{\sigma_y}}\, e_f\,. \tag{III.42}$$

These two constraints actually bound the slenderness ratios of the stiffener components.

(ii) The stiffener flange should not be too large with respect to the interframe distance:

$$445 \text{ mm} \leq L_s - w_f\,. \tag{III.43}$$

(iii) The design space is bounded by the following reasonable values:

$$\frac{p\,R}{\sigma_y} \leq e \leq 50 \text{ mm}\,, \tag{III.44}$$

$$w_f \leq h_w \leq 2\,w_f\,, \tag{III.45}$$

$$5 \text{ mm} \leq e_w \leq 25 \text{ mm}\,, \tag{III.46}$$

$$70 \text{ mm} \leq w_f \leq 150 \text{ mm}\,, \tag{III.47}$$

$$15 \text{ mm} \leq e_f \leq 50 \text{ mm}\,. \tag{III.48}$$

The first lower constraint on the hull thickness e means that the circumferential stress in the equivalent non-stiffened cylinder should not exceed the yield strength.

Finally, the predictive models for the collapse pressure (namely the FE model and the semi-numerical solutions) are used to guarantee that collapse does not occur at some prescribed accidental diving depth I_{acc}. This therefore leads to the establishment of the following final constraint:

$$I_{acc}\, \rho_{water}\, g \leq p_{critical}(\mathbf{d})\,. \tag{III.49}$$

It is assumed that the submarine under discussion is designed for an accidental diving depth I_{acc} of 250 m.

Variable		Distribution	Mean	C.o.V.
E	(MPa)	Lognormal	$200,000$	0.05
σ_{y}	(MPa)	lognormal	390	0.05
σ_{u}	(MPa)	lognormal	570	0.03
e	(mm)	lognormal	μ_e	0.03
h_{w}	(mm)	lognormal	$\mu_{h_{\mathrm{w}}}$	0.03
e_{w}	(mm)	lognormal	$\mu_{e_{\mathrm{w}}}$	0.03
w_{f}	(mm)	lognormal	$\mu_{w_{\mathrm{f}}}$	0.03
e_{f}	(mm)	lognormal	$\mu_{e_{\mathrm{f}}}$	0.03
A_2	(mm)	Lognormal	$\frac{1}{3}\,\frac{5R}{1000}$	0.50
A_{14}	(mm)	Lognormal	$\frac{1}{3}\,\frac{L_{\mathrm{s}}}{100}$	0.50

Table III.3 – Probabilistic model for the ring-stiffened shell cylinder.

(b) Worst case approach

The worst case approach basically consists in setting all the demand (resp. capacity) variables to their highest (resp. lowest) possible values and finding the optimal design for this worst-case scenario. In the present context of shell design, this means having recourse to *(i)* prescribed maximum imperfection amplitudes and *(ii)* a destruction diving depth I_{des} that is significantly larger than the accidental diving depth I_{acc}.

Here, the maximum overall imperfection amplitude is taken from the BS5500 recommendations, and is set to $A_{2\,\max} = 5R/1000$. The interframe imperfection amplitude is set to $A_{14\,\max} = L_{\mathrm{s}}/100$. The destruction diving depth is arbitrarily fixed at 340 m.

(c) Probabilistic approach

Arguing that the previous worst case approach introduces an unknown degree of conservatism, it is proposed to turn to a more comprehensive probabilistic model to describe the possible configurations of the hull. This probabilistic model is specified in Table III.3.

Since no data is available, the probabilistic model for the material properties is built from the recommendations available in the JCSS probabilistic modeling code (Vrouwenvelder, 1997). This code also prescribes a linear correlation between the yield strength σ_{y} and the ultimate stress σ_{u} in the form of a Pearson correlation coefficient $\rho = 0.75$, which is taken into account in the present analysis. The right-skewed probabilistic model for the imperfection amplitudes was constructed with an empirical coefficient of variation of 50%, and the mean is such that the previous worst imperfections $A_{2\,\max}$ and $A_{14\,\max}$ matches the 99.5%-quantile of the present probabilistic model. This thus leads approximately to setting the mean value at one third of the latter worst imperfection amplitudes, as indicated in Table III.3.

Given this probabilistic model, the original deterministic design optimization problem is transformed into a reliability-based design problem where safety is measured by means of the following failure probability:

$$p_{\mathrm{f}}(\mathbf{d}) = \mathbb{P}\left(p_{\mathrm{critical}}(\mathbf{d}, \mathbf{X}) \leq I_{\mathrm{acc}}\,\rho_{\mathrm{water}}\,g\right)\,, \tag{III.50}$$

where $\mathbf{X}$ is the random vector that collects all the random variables of the probabilistic model. Optimization is performed w.r.t. the means of the random design variables e, h_w, e_w, w_f and e_f. The single probabilistic constraint ($n_g = 1$) reads as follows:

$$p_f(\mathbf{d}) \leq \Phi(-\beta_0)\,, \tag{III.51}$$

where $\beta_0 = 6$ in the present application (i.e. $p_{f0} \leq 10^{-9}$).

(d) Resolution strategies

The deterministic design optimization problem underlying the worst-case approach is solved here by means of the Polak-He gradient-based optimizer. It uses the two proposed mechanical models for the buckling strength of the structure, namely the semi-numerical (SN) and the ANM-based finite element (FE) models.

The reliability-based design optimization problem underlying the probabilistic approach is solved with the surrogate-based RBDO strategy presented in Section II–5.3.2. Again, two designs are computed with each of the mechanical models.

Once the four optimal designs are found, a reliability analysis is performed in order to compute the safety level of the optimally-designed structures at both the accidental and destruction diving depths, using the probabilistic model of Table III.3. Since the FE model is expensive to evaluate, we resort to the metamodel-based importance sampling technique (Dubourg et al., 2013) with a 5% target coefficient of variation on the failure probability. For the less expensive semi-numerical model, it is proposed to use direct subset simulation in order to compute the whole CDF of the critical pressure, which yields a relationship between the failure probability and the diving depth in a single run for each design.

III–1.5.3 Results

The results are given in Table III.4 and the corresponding designs are illustrated in Figure III.16. First, it should be noticed that the FE-based design is always more cost-optimal than its SN-based counterpart. In fact, this confirms the initial intuition as the semi-numerical solutions involve a set of built-in safety factors that eventually lead to a high (although unknown) degree of conservatism. In the worst-case approach, the relative gain in using a FE model w.r.t. the SN cost is only 2%, whereas it reaches 17% in the RBDO approach.

It should also be noticed that the SN-based design always features a more slender stiffener web than the FE-based designs. This is because the SN-solution lacks an explicit consideration of the frame tripping buckling mode. This lack is such that, in the deterministic worst-case approach, the BS5500 safety constraint regarding this mode and defined in Eq. (III.41) is active at the optimal design. Indeed, in this case the stiffener web is clearly too slender, as illustrated in Figure III.16a.

As expected, the worst-case approach offers a significant degree of safety at the accidental diving depth, and there even remains a little margin at the destruction diving depth, although the failure probability is much greater there ($p_f \approx 10^{-2}$). The probabilistic approach enables the explicit control of the safety level at the accidental diving depth. Due to the high targeted safety level ($p_f < \Phi(-6) \approx 10^{-9}$), the reliability-based optimal designs are of course less optimal than their worst-case counterparts.

The relationship between diving depth and failure probability is illustrated in Figure III.17. The subset sampling technique applied with the semi-numerical model enables the reconstruction of the full CDF. Metamodel-based importance sampling applied to the expensive-to-evaluate finite-element model only yields the failure probability estimates at the two diving depths of interest. It can be seen from Figure III.17b that the failure probability matches the maximum tolerance, set here to $p_f = \Phi(-6) < 10^{-9}$.

Method		Worst case approach		RBDO ($\beta = 6$)	
		FE-based	SN-based	FE-based	SN-based
e	(mm)	21.99	26.56	28.65	35.85
h_w	(mm)	186.01	[a]202.38	181.37	201.66
e_w	(mm)	19.47	[a]8.14	14.44	12.11
w_f	(mm)	119.57	101.22	130.62	146.18
e_f	(mm)	23.97	24.53	29.68	32.77
Cost		0.1960	0.2004	0.2356	0.2847
$\beta(I_{acc})$		4.99	3.81	6.06	6.11
$\beta(I_{des})$		1.40	2.00	4.42	4.99

[a] The frame tripping constraint is active.

Table III.4 – Results for the design optimization of the imperfect infinite-length ring-stiffened shell cylinder.

(a) Worst case approach (b) RBDO ($\beta = 6$)

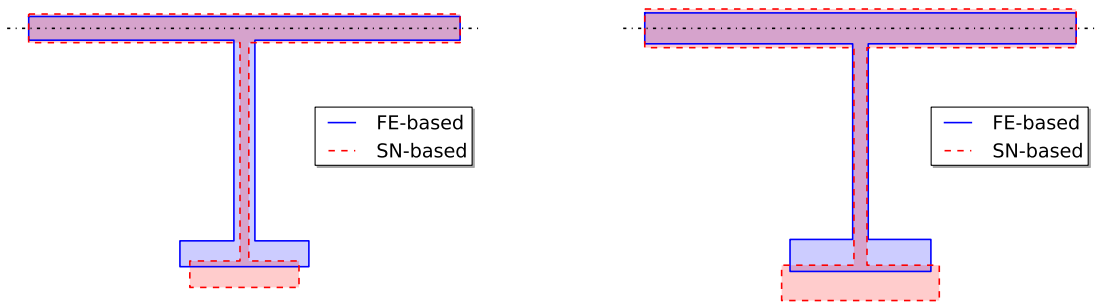

Figure III.16 – Comparison of optimal designs for the imperfect infinite-length ring-stiffened shell cylinder.

(a) Worst case approach (b) RBDO ($\beta = 6$))

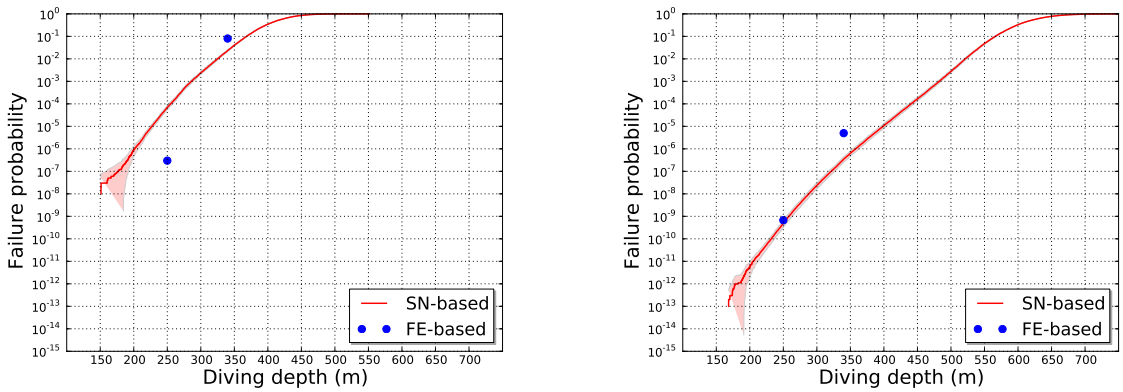

Figure III.17 – Relation between diving depth and failure probability for the imperfect infinite-length ring-stiffened shell cylinder.

The convergence of the surrogate-based RBDO strategy is obtained within 850 calls to the buckling strength models. Note that this is of utmost importance for the FE-based application, due to the large numerical effort required by a single FE analysis (about 10 minutes of CPU time in the present analysis).

III–2 Crack propagation

III–2.1 Introduction

Damage tolerance is of utmost importance for structures designed in various engineering fields, e.g. the nuclear, aeronautical and automotive industries. In damage tolerance it is assumed that some flaws exist, and that they can propagate under time-varying loadings. The models that govern crack propagation are based on the principles of fracture mechanics. Most usual approaches are based on the theory of linear elastic fracture mechanics (LEFM), see, e.g., Nešpůrek (2010) for a short introduction. In LEFM crack propagation is closely related to the stress field around the crack tip. In the works presented in this section we assume that crack propagation is defined through an empirical crack growth law, defined in terms of a so-called stress intensity factor (SIF). SIFs can be assessed by the conventional finite element method or the more elaborate version of such a technique, known as the extended finite element method (Moës et al., 1999). Regarding the crack growth law, the well-known Paris-Erdogan equation is often used for constant-amplitude loading, see Section III–2.2. For variable-amplitude loading, of interest in all real problems, it is of paramount importance to account for the load interactions that may occur during crack growth for accurate fatigue life predictions. The latter case is of interest in the work presented in Section III–2.3, where the PREFFAS crack closure model proposed by Aliaga et al. (1988) is applied.

In damage-tolerant design, a common approach consists in using empirically-derived safety factors a.k.a. scatter factors. Such well-established procedures are assumed to ensure an acceptable, albeit usually unknown, safety level for the designed structures. In practice, several uncertainties arise in any damage tolerance problem. First of all, crack propagation is known to be a rather dispersive phenomenon. Under well-controlled loading conditions, supposedly-identical specimens exhibit highly scattered fatigue lives, as pointed out in several works (Virkler et al., 1979; Ghonem and Dore, 1987; Ichikawa, 1987; Casciati et al., 2007). This uncertainty is mainly epistemic and comes from our lack of knowledge of the complex physics that governs crack propagation at several levels (e.g. at the grain level and below in metallic materials). Secondly, the loads applied to the structures of interest are in general not known very accurately. This uncertainty may be due to the random nature of the loads under consideration (e.g. for wind- or wave-induced loadings). It may also come from the use of the structure, which is uncertain due to varying operating conditions. For example, the loads applied to an aircraft structural element may be uncertain due to the missions assigned to the aircraft, which differ from those accounted for in the design phase. Moreover, these loads are also uncertain due to the aircraft maneuvers and the environmental conditions in which the aircraft operates (winds, gusts, etc). Thirdly, the initial flaws present in the structure from which the cracks emanate are often not accurately determined. These initial flaws are uncertain in terms of locations, sizes and shapes. Quantifying the influence of all these uncertainties on crack propagation is therefore of great interest in damage tolerance. Such an analysis is performed in the framework of *probabilistic fracture mechanics*, which has been developed for several decades (see, e.g., Provan, 1987). In the works presented in this section the focus is put on the *reliability* of structural elements w.r.t. damage tolerance.

In Section III–2.2 the crack propagation experiments carried out by Virkler et al. (1979) under constant amplitude are revisited in the context of the FORM analysis (Bourinet and Lemaire, 2008; Bourinet, 2017a). In the proposed approach the Paris-Erdogan equation is randomized by means of three random input models (inter-specimen scatter approach). For the first two models, the reliability

problem is found to be highly sensitive to the correlation between $\ln C$ and m. The third model includes an additional random input, representative of the model error between the Paris-Erdogan model and the experimental data. It is shown that this latter model avoids a misleading interpretation of the experimental results.

In Section III–2.3 the objective is to specifically account for the stochastic nature of fatigue loading in damage tolerance. The results presented in this section are taken from Mattrand (2011). The analysis performed requires that an appropriate model is available for variable-amplitude crack propagation. Indeed, the model needs to account for the load interactions and retardation/acceleration effects which are likely to occur during crack growth. The work of Mattrand is based on the PREFFAS model developed in aerospace engineering by Aliaga et al. (1988) and briefly recalled in Section III–2.3.1. The random load sequences of max-min stresses are modeled by means of discrete time Markov chains or hidden Markov models, see Section III–2.3.2. The parameters of these models are inferred from in-flight load data recorded in a fleet of fighter aircraft. Section III–2.3.3 presents the reliability assessment of a structural element w.r.t. damage tolerance using the defined models. The reliability problems are solved by means of the cross-entropy method presented in Section I–3.3.2 and adapted to the specific context of Markov chains and hidden Markov models.

III–2.2 Statistical interpretation of the Virker experiment

The experiment carried out by Virkler et al. (1979) in 1979 consisted in recording the crack growth trajectories of 68 samples at 164 equally-spaced measurement points, see Figure III.18, left plot. The test samples were M(T) specimens made of 2024-T3 aluminum alloy of 558.8 mm length, 152.4 mm width and 2.54 mm thickness. The crack was propagated from an initial crack length of 9 mm to a final length of 49.8 mm, after pre-cycling crack growth started from a pre-machined central slit. These specimens were all tested under *constant amplitude* fatigue loading at a maximum stress level $\sigma_{\max} = 48.36$ MPa and a stress ratio $R = 0.2$.

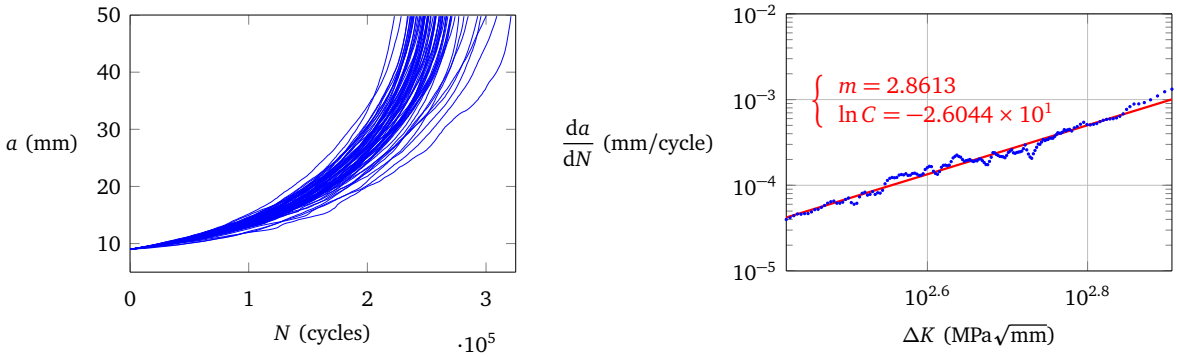

Figure III.18 – Crack length a vs. number of cycles N (left). Determination of m and $\ln C$ from $\mathrm{d}a/\mathrm{d}N$ vs. ΔK curves (right).

For test samples of the same geometry and material properties subjected to the same fatigue loading, the statistical scatter observed experimentally has been addressed by two types of approach in the literature (Ichikawa, 1987):

1. The first approach aims at describing the randomness within the specimen itself a.k.a. *intra-specimen* scatter. Such an approach is commonly based on the following equation:

$$\frac{\mathrm{d}a(t)}{\mathrm{d}t} = X(t)\, f(\Delta K(a(t)); \boldsymbol{\theta})\,, \tag{III.52}$$

where $X(t)$ is a nonnegative random process, f is a (deterministic) crack growth law and $\boldsymbol{\theta}$ is a vector of parameters (see, e.g., Lin and Yang, 1983; Yang and Manning, 1996). $X(t)$ is usually chosen as a stationary lognormal random process, and various approaches can be found in the literature, i.e. either $X(t)$ is assumed to be totally uncorrelated at any two different times (lognormal white noise) or, on the contrary, it is assumed to be totally correlated at all times and therefore replaced by a lognormal random variable (model known as the lognormal random model). It is shown that a totally uncorrelated $X(t)$ leads to the smallest statistical dispersion in terms of the service time required to reach a given crack size, and that a totally correlated $X(t)$ leads to the largest dispersion. Some other models have been proposed with intermediate correlation (Lin and Yang, 1983; Yang and Manning, 1996).

2. The second approach aims at describing the randomness between specimens a.k.a. *inter-specimen* scatter. In this approach, a common practice consists in randomizing the crack growth model, such as the Paris-Erdogan equation:

$$\frac{\mathrm{d}a}{\mathrm{d}N} = C\Delta K(a)^m \,, \tag{III.53}$$

where the model parameters C and m are considered as random. Such an approach is applied here to the Virkler data set.

For each of the 68 trajectories recorded by Virkler et al., a crack growth rate vs. stress intensity factor (SIF) range curve is obtained based on a 5-point moving least squares linear regression, see Figure III.18, right plot. From each trajectory, a pair of values $(m, \ln C)$ is obtained such that:

$$\ln \frac{\mathrm{d}a}{\mathrm{d}N} = \ln C + m \ln \Delta K \,. \tag{III.54}$$

Table III.5 gives the results of a statistical analysis of the 68 pairs $(m, \ln C)$. It is found that the normality hypothesis can be assumed for both m and $\ln C$. Moreover, a linear correlation $\rho = -0.99795$, very close to -1, is observed between m and $\ln C$ due to the linear regression that is used to find these two parameters. Note that these statistical parameters are consistent with those obtained in other references (Ditlevsen and Olesen, 1986; Kotulski, 1998).

Variable	Distribution	Mean	Standard deviation	Correlation
m	normal	2.855	0.166	-0.99795
$\ln C$	normal	-26.056	0.972	

[a] Units consistent with crack length in mm and stresses in MPa.

Table III.5 – Statistical distributions of m and $\ln C$ [a].

In reliability assessment, failure is defined as when the number of cycles N_r to reach the final crack length $a_\mathrm{f} = 49.8$ mm of the Virkler experiment is lower than a given target number of cycles denoted N_s. The LSF is therefore expressed as follows:

$$g(\mathbf{x}) = N_r(m, \ln C) - N_s \,, \tag{III.55}$$

where $\mathbf{x} = (x_1, x_2)^\mathrm{T} = (m, \ln C)^\mathrm{T}$ and where N_r is given by:

$$N_r(m, \ln C) = \int_{a_\mathrm{i}}^{a_\mathrm{f}} \frac{1}{C(\Delta K)^m} \mathrm{d}a \,, \tag{III.56}$$

in which a_i is the initial crack length, $a_\mathrm{f} = 49.8$ mm is the final crack length and ΔK is the SIF range. For the constant-amplitude fatigue loading of M(T) specimens as applied in the Virkler experiment, we have $\Delta K = K_\mathrm{max}\,(1-R)$ where $R = 0.2$ is the stress ratio and K_max is the maximum SIF given by:

$$K_\mathrm{max} = \frac{1 - 0.025\,(a/W)^2 + 0.06\,(a/W)^4}{\sqrt{\cos(\pi a/W)}}\,\sigma_\mathrm{max}\sqrt{\pi a}\,, \tag{III.57}$$

where a is the current crack length, $W = 152.4$ mm is the width of the test specimen and $\sigma_\mathrm{max} = 48.36$ MPa is the maximum applied stress.

The following three test cases are defined for the subsequent reliability studies:

- Case #1: The initial crack length a_i is considered as deterministic and equal to the minimum crack size of the Virkler experiments, i.e. $a_\mathrm{i} = 9$ mm, and N_s is selected as the average value between the 7^th and 8^th lowest numbers of cycles of the Virkler tests:

$$N_s = \frac{237,293 + 237,794}{2} = 237,543.5 \text{ cycles}\,.$$

  This case was proposed and studied by Annis (2017).

- Case #2: The initial crack length a_i is considered as deterministic and equal to 4.4 mm. The target number of cycles N_s is set to 400,000.

- Case #3: The initial crack length a_i is assumed to be exponentially distributed with a mean and a standard deviation both equal to 1.5 mm. The target number of cycles N_s taken is 400,000.

III–2.2.1 Problem 1

This first problem assumes that the random vector $\mathbf{X}$ is composed of the two correlated normal variables m and $\ln C$ with distribution parameters given in Table III.5 for cases #1 and #2. The exponentially-distributed random variable a_i is added to $\mathbf{X}$ as an additional component for case #3. The FORM results obtained for the three cases are gathered in Table III.6. When the stochastic model involves only m and $\ln C$ as random inputs, a very strong sensitivity of β w.r.t. the correlation ρ between m and $\ln C$ is observed: -177.29 for case #1 and -368.22 for case #2. For illustration purposes, lowering ρ by 0.001 would approximately result in a reliability index increase of 0.18 and 0.37 for cases #1 and #2 respectively. When the initial crack length is considered as random (case #3), the FORM solution appears far less sensitive to ρ. Figure III.19 shows how the reliability index β evolves when ρ is varied from -0.99795 to -0.9. It clearly appears that the computed sensitivity $\partial\beta/\partial\rho = -6.7092$ represents the first-order derivative of β at $\rho = -0.99795$.

	Case #1	Case #2	Case #3
a_i (mm)	9	4.4	Exp(1.5, 1.5)
N_s (cycles)	237,543.5	400,000	400,000
β	0.7600	1.8005	1.8399
$p_\mathrm{f}^\mathrm{FORM}$	0.224	3.59×10^{-2}	3.29×10^{-2}
$\partial\beta/\partial\rho^a$	-177.29	-368.22	-6.7092

[a] ρ denotes the correlation between m and $\ln C$.

Table III.6 – Problem 1: FORM results.

We find that the failure probability of 0.224 obtained with FORM for Case #1 does not agree with the experimental data. From the definition of the target number of cycles N_s, we would expect a failure probability in the range $[7/68, 8/68] = [0.103, 0.118]$ since N_s is selected as the average value between the 7^{th} and 8^{th} lowest numbers of cycles of the 68 Virkler tests. The origin of such a difference was investigated by Bourinet and Lemaire (2008). First, it can be shown that the difference is not explained by the nonlinearity of the LSS at the MPFP. A SORM analysis gives $p_{\text{f}}^{\text{SORM-cf}} = p_{\text{f}}^{\text{SORM-pf}} = 0.219$, which is close to the FORM approximation and still far from $[0.103, 0.118]$. The LSS is in fact almost linear in the standard normal space, see Figure III.20. Moreover, it is found that a few samples among the 68 of the experimental data set are not correctly classified by the LSS of the selected model, see Figure III.20. We can find some points with an experimental number of cycles greater than $N_s = 237,543.5$ that belong to the failure domain: (M)T specimens #9, 23, 41, 54, 62, 63 and 66 of the Virkler data set. Besides, the experimental point corresponding to the first experimental test and characterized by a number of cycles lower than N_s is in the safe domain. Although it is very close to the LSS, this is not satisfactory, either. All these issues led Annis (2017) to conclude that FORM and SORM were inappropriate for such a problem, which is untrue. The incorrect approximation obtained by FORM and SORM is in fact due to an inaccurate representation of the LSF, which results here in a slight underestimation of N_r and in fine in quite a significant overestimation of the failure probability. This issue is fixed in Section III–2.2.2 by introducing an extra random variable which is representative of a model error.

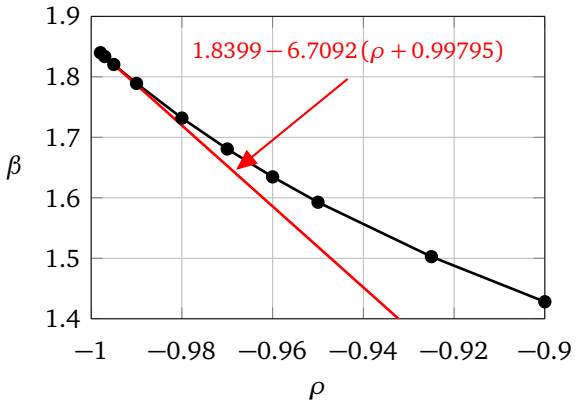

Figure III.19 – Problem 1, Case #3: Reliability index β vs. correlation coefficient ρ between m and $\ln C$.

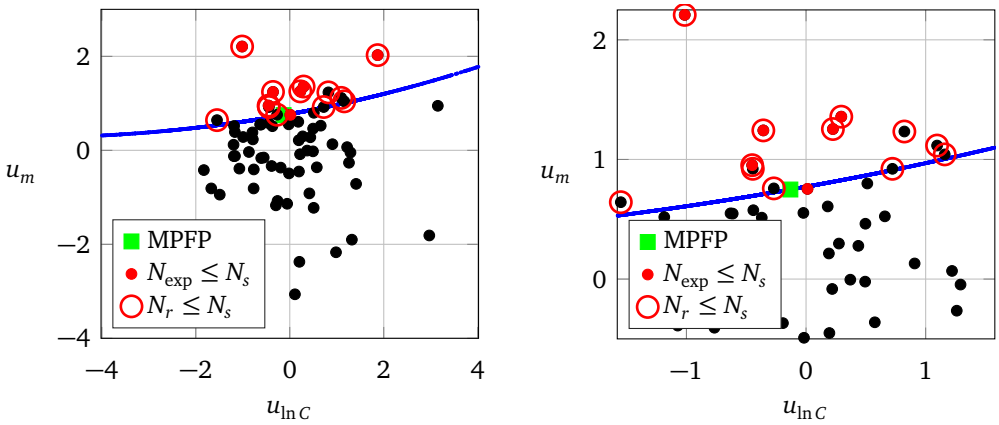

Figure III.20 – Problem 1, Case #1. Blue line: LSS, black dots: Virkler test samples satisfying $N_{\text{exp}} > N_s$, red dots: Virkler test samples satisfying $N_{\text{exp}} < N_s$, red circles: Virkler test samples satisfying $N_r < N_s$. Zoom in right plot.

III–2.2.2 Problem 2

In order to account for a slight underestimation of the number of cycles N_r obtained numerically w.r.t. those found experimentally by Virkler et al., the LSF defined in Eq. (III.55) is modified as follows:

$$g(\mathbf{x}) = k\,N_r(m, \ln C) - N_s\,, \tag{III.58}$$

where $\mathbf{x} = (x_1, x_2, x_3)^{\mathrm{T}} = (m,\, \ln C,\, k)^{\mathrm{T}}$ and k follows a Type-I largest value distribution (a.k.a. Gumbel distribution) with a mean equal to 1.027 and a standard deviation equal to 1.91×10^{-2}. This distribution is identified from a statistical analysis of the ratios $N_{\mathrm{exp}}^{(j)}/N_r(m^{(j)}, \ln C^{(j)})$ for $j = 1, \ldots, 68$ where $N_{\mathrm{exp}}^{(j)}$ is the number of cycles of the j^{th} M(T) specimen of the Virkler data set and $(m^{(j)}, \ln C^{(j)})$ are the 68 pairs $(m, \ln C)$ identified from the experimental crack growth curves. Note that k is assumed to be independent from both m and $\ln C$. The distributions of m and $\ln C$ are those defined in Table III.5. A linear correlation $\rho = -0.99795$ is again assumed between m and $\ln C$.

FORM results with model error are given in Table III.7 for cases #1 and 2. We can easily show that the 8 (=7+1) experimental points that were misclassified in Problem 1 are now correctly placed within the safe and failure domains, see Figure III.21. The failure probability obtained by FORM is now 0.137 and a SORM analysis gives 0.126, which now becomes quite close to the expected range of probability $[0.103, 0.118]$. Regarding sensitivities to correlation, the values obtained in this new problem are again quite high in terms of absolute value: -241.62 for case #1 and -411.16 for case #2. An alternative problem is next proposed which avoids such a high sensitivity to correlation.

	Case #1	Case #2
a_{i} (mm)	9	4.4
N_s (cycles)	237,543.5	400,000
β	1.0947	2.0972
$p_{\mathrm{f}}^{\mathrm{FORM}}$	0.137	1.80×10^{-2}
$\partial\beta/\partial\rho^{a}$	-241.62	-411.16

[a] ρ denotes the correlation between m and $\ln C$.

Table III.7 – Problem 2: FORM results.

III–2.2.3 Problem 3

We now express the linear regression of $\ln C$ on m as follows (Ditlevsen and Olesen, 1986):

$$\widehat{\mathbb{E}}[\ln C|m] = \mathbb{E}[\ln C] + \frac{\mathrm{Cov}[m, \ln C]}{\mathrm{Var}[m]}\,(m - \mathbb{E}[m])\,, \tag{III.59}$$

and we make use of the following residual, which becomes uncorrelated with m:

$$\epsilon_{\ln C} = \ln C - \widehat{\mathbb{E}}[\ln C|m]\,. \tag{III.60}$$

The linear regression of $\ln C$ on m can be expressed from the 68 pairs $(m, \ln C)$ identified from the Virkler data set. This linear regression reads:

$$\widehat{\mathbb{E}}[\ln C|m] = -5.8468m - 9.3623\,, \tag{III.61}$$

and we therefore have:

$$\epsilon_{\ln C} = \ln C + 5.8468m + 9.3623\,. \tag{III.62}$$

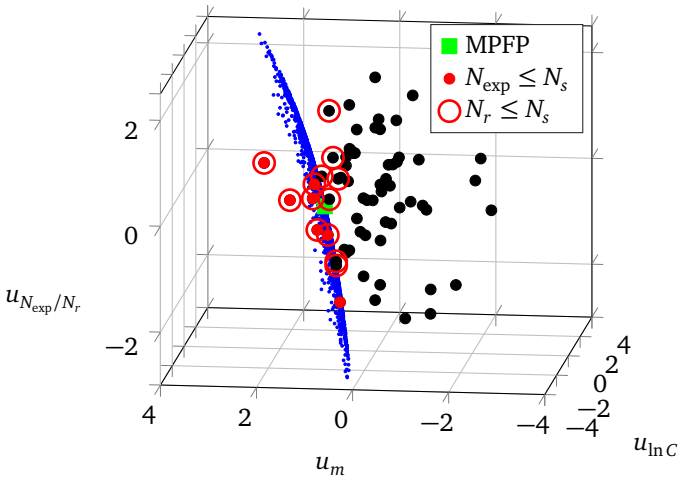

Figure III.21 – Problem 2, Case #1. Blue dot surface: LSS, black dots: Virkler test samples satisfying $N_{\text{exp}} > N_s$, red dots: Virkler test samples satisfying $N_{\text{exp}} < N_s$, red circles: Virkler test samples satisfying $N_r < N_s$. Zoom in right plot.

The distribution parameters of $\epsilon_{\ln C}$ are inferred from the Virkler data set, see values given in Table III.8. The correlation -9.29×10^{-7} between m and $\epsilon_{\ln C}$ is close to zero, which now allows us to express the reliability problem in terms of three independent random variables. The LSF with model uncertainty is rewritten in the following form:

$$g(\mathbf{x}) = k N_r(m, \ln C) - N_s \,, \tag{III.63}$$

where $\mathbf{x} = (x_1, x_2, x_3)^{\mathrm{T}} = (m,\, \epsilon_{\ln C},\, k)^{\mathrm{T}}$ and $\ln C = \epsilon_{\ln C} - 5.8468m - 9.3623$.

Variable	Distribution	Mean	Standard deviation
m	normal	2.855	0.166
$\epsilon_{\ln C}$	normal	-1.20×10^{-6}	6.22×10^{-2}
k	Gumbel	1.027	1.91×10^{-2}

Table III.8 – Problem 3: Statistical distributions of m, $\epsilon_{\ln C}$ and k.

Results obtained by FORM are gathered in Table III.9. The failure probabilities with FORM and SORM are respectively equal to 0.135 and 0.124 for Case #1. These results are almost identical to those obtained in Problem 2. The failure probability obtained with SORM is again close to the expected range $[0.103, 0.118]$. The main difference is that the reliability results are now insensitive to correlation. Near-zero values are obtained for the sensitivity to correlation between m and $\epsilon_{\ln C}$.

III–2.3 Crack propagation under random loading

The modeling of crack growth under *variable amplitude* loading is a central point in the analysis of structures subjected to real fatigue loadings. For accurate live prediction, the selected models needs to account for *load interactions* that may occur during crack growth, see e.g. the description made by Davy (1985) on the main interaction effects and their impact on crack propagation life estimation. Crack retardation after an overload is an example of such effects. If such retardations are not modeled, this could result in large underestimations of fatigue lives.

	Case #1	Case #2
a_i (mm)	9	4.4
N_s (cycles)	237,543.5	400,000
β	1.1050	2.1076
p_f^{FORM}	0.135	1.75×10^{-2}
$\partial\beta/\partial\rho^a$	−0.24	0.68

[a] ρ denotes the correlation between m and $\epsilon_{\ln C}$.

Table III.9 – Problem 3: FORM results.

Such *history effects* in crack propagation can be studied e.g. by means of the extended finite element method, where plasticity-induced crack closure and potential crack face contacts are accounted for in the wake of the growing crack (Elguedj, 2006). The finite element method can also be used to build incremental approaches by means of a phenomenological methodology, see e.g. Pommier (2003) and Pommier (2015). The presented work uses the PREFFAS crack closure model, which was selected for its easy implementation and fast evaluation.[10] The main principles of this model are recalled in Section III–2.3.1. The reader interested in a detailed description of this model may refer to Aliaga et al. (1988) and Schijve (1987) for an additional analysis of its underlying aspects. A description of this model is also available in Mattrand (2011). History effects in crack propagation can be handled by other reference models, e.g. the strip yield model (Wang and Blom, 1991) among others.

III–2.3.1 PREFFAS crack closure model

The PREFFAS model is based on the Elber *crack closure* concept (Elber, 1971), which specifies that a crack does not propagate during the whole loading range but only during part of it, even if the applied loading is of the tension-tension type. An effective crack tip stress intensity factor range ΔK_{eff}, assuming that fatigue crack growth occurs only when the crack is fully opened, is therefore postulated according to the following expression:

$$\Delta K_{\text{eff}} = K_{\max} - K_{\text{op}} = U(R)\left[K_{\max} - K_{\min}\right] = U(R)\Delta K \,, \tag{III.64}$$

where $K_{\max}$, resp. $K_{\min}$, is the maximum, resp. minimum, value of the stress intensity factor K (SIF) during the loading cycle, K_{op} is the opening stress intensity factor, R is the stress ratio and $U(R) = aR + b$ is the Elber effective stress intensity range ratio. In PREFFAS it is often assumed that $a + b = 1$, which gives fairly good results for aluminum alloys and steels used in aircraft structural components. The parameter b is identified from a $R = 0.1$ constant-amplitude test with periodic overloads every 1000 cycles, such that $\sigma_{\text{overload}} = 1.7\sigma_{\max}$. This parameter b is found to be material- and thickness-dependent. It is worth mentioning that this model does not assume any explicit calculation of the plastic zone at the crack tip. These effects, which cover e.g. transitions from plain strain to plain stress at the crack tip, are indirectly accounted for by the way K_{op} is evaluated throughout the cycles and by means of the value which is selected for b (larger b-values correspond to larger plastic zones at the crack tip).

Under Elber's crack closure assumption, the Paris equation is rewritten as follows:

$$\frac{\mathrm{d}a}{\mathrm{d}N} = C_{\text{eff}}\left[K_{\max} - K_{\text{op}}\right]^m = C_{\text{eff}}\,{\Delta K_{\text{eff}}}^m \,, \tag{III.65}$$

[10] The CPU time of the crack growth model is of great concern in reliability assessment, which requires large numbers of model evaluations.

where $C_{\text{eff}} = C_R/U(R)^m$, m is the exponent of the Paris law and C_R is the C-parameter of the Paris law determined from a constant amplitude loading test at stress ratio R.

(a) Opening stress intensity factor K_{op}

The crack opening level at a given cycle i, denoted $K_{\text{op},\,i}$, depends on the previous load history, and calculating its variation cycle-by-cycle is a key feature of the PREFFAS model. All previous cycles $j < i$ need to be considered in order to find the *opening stress intensity factor* at cycle i, noted $K_{\text{op},\,i}$. For each cycle j such that $j < i$, PREFFAS calculates a K-opening value $K_{\text{op},\,i,\,j}$, based on the $K_{\max}$-value at cycle j, noted $K_{\max,\,j}$, and the minimum $K_{\min}$-value occurring between cycle j and the given cycle i, say at cycle k ($j < k < i$), noted $K_{\min,\,k}$, and again in accordance with Elber's assumption:

$$K_{\max,\,j} - K_{\text{op},\,i,\,j} = U(R)\left[K_{\max,\,j} - K_{\min,\,k}\right], \tag{III.66}$$

where $R = K_{\min,\,k}/K_{\max,\,j}$.

According to PREFFAS model, the opening stress intensity factor $K_{\text{op},\,i}$ at cycle i is defined as the maximum of these values $K_{\text{op},\,i,\,j}$, derived from Eq. (III.66):

$$K_{\text{op},\,i} = \max_{j\in\{1,\,\ldots,\,(i-1)\}} K_{\text{op},\,i,\,j}\,. \tag{III.67}$$

Eq. (III.67) assumes that the effects of a crack extension between cycle j and cycle i are neglected, which is a major assumption of the PREFFAS model. This is presumed true if the variable amplitude load spectrum has a "relatively" short recurrence period, i.e. it is repeated a large number of times during crack growth. According to Eq. (III.67), all cycles $j < i$ need to be considered. In practice, it is not required to look at all $K_{\max,\,j}$ and $K_{\min,\,k}$ values in order to estimate $K_{\text{op},\,i}$ in Eq. (III.67). We simply need to consider an increasing series of $K_{\min}$ values and a decreasing series of $K_{\max}$ values. These values work in pairs ($K_{\max,\,j}$, $K_{\min,\,k}$) to estimate the corresponding K-opening values $K_{\text{op},\,i,\,j}$ in Eq. (III.66) (KH-notation used in PREFFAS reference papers).

In addition to the method presented above to assess $K_{\text{op},\,i}$ for each cycle i, the PREFFAS method incorporates the so-called Rainflow effect, in order to lower the effects of small intermediate load variations, which can result in unconservative predictions. The reader is invited to refer to Aliaga et al. (1988) and Schijve (1987) for details of this specific issue and the way it is handled in PREFFAS.

(b) Crack growth and efficiency EF of the load sequence

The crack growth increment Δa in a N-cycle load sequence is then derived from Eq. (III.65):

$$\begin{aligned}\Delta a = \sum_{i=1}^{N} \delta a_i &= C_{\text{eff}} \sum_{i=1}^{N} \left[K_{\max,\,i} - K_{\text{op},\,i}\right]^m = C_{\text{eff}} \sum_{i=1}^{N} {\Delta K_{\text{eff},\,i}}^m \\ &= C_{\text{eff}} \sum_{i=1}^{N} \left[\, F(a)\sqrt{\pi a}\;\Delta\sigma_{\text{eff},\,i}\,\right]^m ,\end{aligned} \tag{III.68}$$

where $F(a)$ is a geometry factor.

Since the effects of a crack extension are neglected in the load sequence, Eq. (III.68) now becomes:

$$\Delta a = C_{\text{eff}}\left[F(a)\sqrt{\pi a}\,\right]^m \sum_{i=1}^{N}\left[\Delta\sigma_{\text{eff},\,i}\right]^m = C_{\text{eff}}\left[F(a)\sqrt{\pi a}\,\right]^m \text{ EF}\,, \tag{III.69}$$

where $\mathrm{EF} = \sum_{i=1}^{N} \left[\Delta\sigma_{\mathrm{eff},\,i}\right]^m = \sum_{i=1}^{N} \left[\sigma_{\max,\,i} - \sigma_{\mathrm{op},\,i}\right]^m$ is a quantity specific to the load sequence, which requires a cycle-by-cycle calculation of $\Delta\sigma_{\mathrm{eff},\,i}$ based on $\sigma_{\min}$, $\sigma_{\max}$ and σ_{op} history levels, in a similar manner as that previously described for the K history levels. EF is called the *sequence efficiency* in PREFFAS.

(c) Equivalent constant amplitude load sequence, σ_{eq} parameter

In the work of Mattrand (2011), the PREFFAS model is used in order to obtain a *constant amplitude* load sequence equivalent in terms of crack extension to the N-cycle variable amplitude load sequence, see Figure III.22. Assuming a given length of N_{fix} cycles for this constant amplitude load sequence and a given stress ratio R_{fix}, the equivalence in terms of crack length writes:

$$\Delta a = C_{\mathrm{eff}}\left[F(a)\sqrt{\pi a}\,\right]^m \mathrm{EF} = C_{R_{\mathrm{fix}}}\left[F(a)\sqrt{\pi a}\,(1-R_{\mathrm{fix}})\sigma_{\mathrm{eq}}\,\right]^m N_{\mathrm{fix}}\,, \tag{III.70}$$

where σ_{eq} is the *unknown* maximum stress of the constant amplitude load sequence.

From Eq. (III.70), we can obtain the expression of σ_{eq}, which is called the *severity* of the load sequence:

$$\sigma_{\mathrm{eq}} = \left(\frac{\mathrm{EF}}{N_{\mathrm{fix}}}\right)^{\frac{1}{m}} \frac{1}{U(R_{\mathrm{fix}})(1-R_{\mathrm{fix}})}\,. \tag{III.71}$$

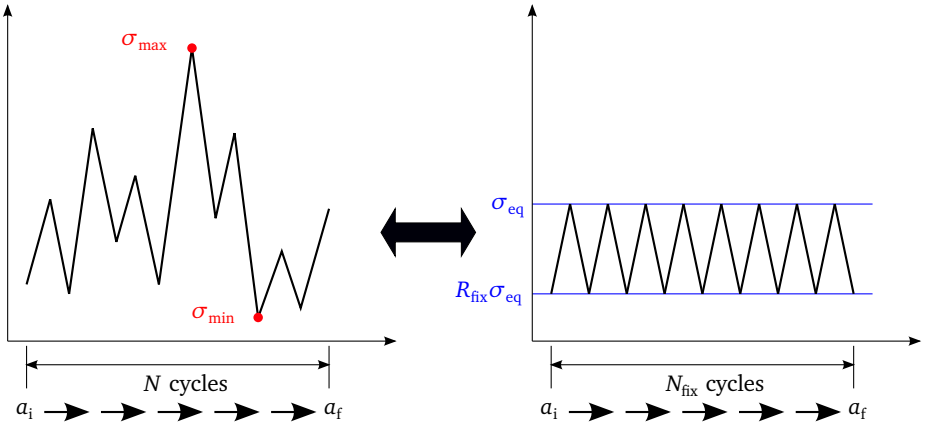

Figure III.22 – Equivalent fatigue loading with the PREFFAS model.

(d) Stationarity assumption of the PREFFAS model

It is worth noting that the effects of crack length and geometry are fully separated from those of the stress history in the PREFFAS model. This separation is made possible thanks to the assumption that the K-levels corresponding to σ-levels are not affected by the crack growth during the applied load sequence. This in fact implies a stationarity assumption during the application of this N-cycle length sequence. However, the loading sequences recorded on real aircraft and used in Section III–2.3.2 are found to be non-stationary, which makes the original PREFFAS model not strictly applicable in such a context. Despite this major limitation, the PREFFAS model was used in the work of Mattrand (2011) due to its main advantages w.r.t. other available models. The PREFFAS model is easy to implement, well validated on many loading test cases, easy to tune due to its small number of parameters and fast to evaluate. Mattrand (2011) also proposed an adaptation of the PREFFAS model, called PREFFAS-m in her PhD manuscript, which no longer assumes stationarity for the loading sequences. This model, not described here for the sake of brevity, enables the evanescence of the history effects and is therefore applicable with *any* realization of a fatigue loading process. The PREFFAS-m model allows the retardation due to

a single overload to vanish, by adaption of the Rainflow. It also enables a variation in the retardation effects, depending on the number of applied overloads. The modified algorithm is given in Mattrand (2011), Appendix B. In the proposed model, the effects of crack length and geometry are no longer separated from those of the stress history. This results in increased computation times compared to the original version of the PREFFAS algorithm. This newly-defined model was not used in the reliability analyses performed by Mattrand. A set of experimental tests was required for the parameter tuning of the PREFFAS-m algorithm, which could not be performed in the context of the PhD work.

III–2.3.2 Random load sequences

In variable-amplitude fatigue design, a common engineering practice is to resort to representative load-time histories or standardized load sequences (see, e.g., Heuler and Klätschke, 2005, for a review). These load sequences are frequently used for comparative tests to help in demonstrating structural integrity and to validate fatigue/crack growth life prediction models. Examples of standardized load sequences in aircraft design are TWIST (stresses in the lower wing skin at the wing root of a transport aircraft) and FALSTAFF (stresses in the lower wing skin near the wing root in a fighter aircraft) (de Jonge et al., 1973; de Jonge, 1973). These load sequences are *deterministic* even though their definition is based on the statistics of real loads experienced in flight. In engineering practice they are repeated several times, up to the failure of the structural component of interest.

In a probabilistic fracture mechanics framework, as assumed here, we need to define *random* models to represent fatigue loading. In such a context a given load sequence corresponds to a realization of the defined random process. Several studies involving random processes have been carried out in the last two decades in order to assess history effects on crack growth life. In most of the reported works, stationary Gaussian random processes are assumed with arbitrary selected parameters, e.g. narrow or wide-banded processes with a given shape for the spectral density. These works were based on experimental tests (Dominguez et al., 1997; Ustilovsky and Arone, 1999; Moreno et al., 2003; Wu and Ni, 2007), crack growth numerical simulations (Domínguez and Zapatero, 1992; Zapatero et al., 1997) or both (Zapatero et al., 2005). The authors mainly conclude that crack growth life dispersion is mostly sensitive to the extreme values encountered in the load history and to the length of the load history, which is repeated until failure.

The modeling of random sequences of turning points (i.e. pairs of min-max amplitudes) has also been investigated in the specific context of a safe life approach based on SN curves. Discrete time Markov chains were selected as suitable processes to represent real random sequences by Krenk and Gluver (1989) and Rychlik (1996). The transition probability matrix used in such approaches keeps the correlation structure between adjacent load levels, belonging to a finite set of discrete load levels which constitutes the state space of the Markov chain. The first objective was to calculate the expected Rainflow matrix (and therefore the expected damage) with loads modeled by such a process, as described by Rychlik (1989) and Olagnon (1994). The reverse problem of finding the transition probability matrix of a Markov chain given an expected Rainflow matrix was tackled by Rychlik (1996). The case of process properties varying over time was later addressed by Johannesson (1999) by means of switching Markov chains, which belong to the broad class of hidden Markov models (HMM). The principle consists in defining an underlying and unobserved regime process (a Markov chain in this work) whose state controls when to change the parameters of the load process and which values of these parameters to use.

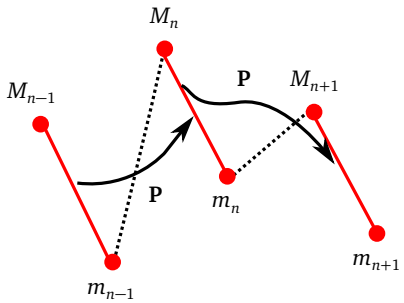

Figure III.23 – Definition of the first-order Markov chain X_n (FMC).

In the work of Mattrand (2011), two main objectives were targeted:

1. The first objective was to construct random load sequences identified from in-flight load data recorded in a fleet of fighter aircraft. An overall set of 27,458 flights was recorded, from which two subsets were identified with distinct flight domains. These two subsets, referred to as groups A and B[11] in Mattrand et al. (2011a), were identified by clustering, and the choice made was corroborated by expert judgment. Two types of models were selected for the random load sequences: first-order Markov chains (FMC) and hidden Markov models (HMM), see Section III–2.3.2 (a) and (b) respectively. The presentation of the work of Mattrand is limited here for the sake of conciseness to the random modeling of flights under a prescribed type of aircraft mission, referred to as given operational requirement in Mattrand and Bourinet (2011) and Mattrand et al. (2011a), i.e. an analysis involving a model specific to a single group of flights, either group A or group B. The extension to aircraft mission variability is addressed in Mattrand et al. (2011a).
2. The second objective was to assess the reliability of a given structural component with an initial crack subjected to a random loading defined by the two proposed models. The solution was obtained using the cross-entropy method presented in Section I–3.3.2 and extended to the specific formalism of Markov chains and hidden Markov models. This analysis and the obtained results are given in Section III–2.3.3. The novelty of the work of Mattrand lies in the use of Markov models as *inputs* of a structural reliability problem, which moreover accounts for cycle interactions in applied loading. This approach differs from the ones developed in other works, which also focused on crack propagation under random loading in a reliability context, see e.g. Zheng and Ellingwood (1998), Beck and Melchers (2004), Moustapha et al. (2013), and Altamura and Straub (2014) among other references.

(a) First-order Markov chains

A *first-order Markov chain* (FMC) with finite state space E is a sequence of E-valued random variables $(X_n)_{n\in\mathbb{N}_{>0}}$ such that the conditional distribution of X_{n+1}, knowing the discrete-time process $(X_m)_{m\leq n}$, is the same as the conditional distribution of X_{n+1} knowing only X_n:

$$\mathbb{P}\left(X_{n+1}=e_{n+1}\,|\,X_n=e_n,\ldots,X_1=e_1\right)=\mathbb{P}\left(X_{n+1}=e_{n+1}\,|\,X_n=e_n\right)\,. \tag{III.72}$$

An original idea of the work of Mattrand (2011) consists in taking $X_n=(M_n,m_n)$ where M_n and m_n denote respectively the peak and trough stresses of the n^{th} cycle, see Figure III.23.

From the definition of X_n, the state space E composed of a finite number of load cycles is defined as follows:

$$E=\left\{\,e_i=(s_k,s_l)\,,\;k,l\in\{1,\ldots,K_c\}\,,\;k>l\,\right\}\,, \tag{III.73}$$

[11] Group A was composed of 24,320 flights recorded on aircraft loaded with two additional on-board fuel tanks. Group B was composed of 3138 flights recorded on lighter aircrafts loaded with at most one additional on-board fuel tank.

where $\{s_k \in c_k, 1 \leq k \leq K_c\}$ are selected stress levels in K_c associated and ordered stress classes $\{c_k, 1 \leq k \leq K_c\}$, see Figure III.24a where the $K_c = 5$ selected classes of the recorded load data referenced as group B in Mattrand et al. (2011a) are represented. The associated normalized[12] stress levels $\{s_k, 1 \leq k \leq K_c\}$ are set to $\{0.039,\ 0.113,\ 0.248,\ 0.507,\ 0.840\}$, by choosing either the mode or the center of each class.

The corresponding load cycle state space E encompasses $\#E = K = K_c(K_c - 1)/2$ cycle states such that a valley m_n systematically follows a peak M_n. Transition probabilities represent probabilities of moving from a given cycle to the following one. The work of Mattrand (2011) assumes a first-order dependence in terms of cycles, which indeed corresponds to a greater order of dependence in terms of load levels, a cycle being composed of two load levels. These probabilities are gathered in a $K \times K$-real transition matrix $\mathbf{P} = [p_{ij}]_{1 \leq i,j \leq K}$ assumed constant over time n (time-homogeneous Markov chain) and which satisfies the following conditions:

$$\begin{cases} 0 \leq p_{ij} \leq 1 & \text{for } i, j \in \{1, \ldots, K\} \\ \displaystyle\sum_{j=1}^{K} p_{ij} = 1 & \text{for } i \in \{1, \ldots, K\} \end{cases} \tag{III.74}$$

where $p_{ij} = \mathbb{P}\left(X_{n+1} = e_j \,|\, X_n = e_i\right)$ and e_i, e_j are load cycle states which belong to the state space E. It is important to point out that some probabilities p_{ij} are zeros by construction, in order to ensure alternating minima and maxima (see Mattrand, 2011, p. 96).

A homogeneous FMC chain is completely defined by its transition matrix $\mathbf{P}$, its initial distribution X_1 describing the starting probabilities of the various cycle states and its length N, which is itself considered as random. The parameters identified from the recorded load data referenced as group B in Mattrand et al. (2011a) are plotted in Figure III.24. The distributions of X_1 and N are easily obtained by standard statistical techniques. The transition matrix $\mathbf{P}$ is obtained by maximum likelihood inference.

(b) Hidden Markov models

As an alternative to FMC, Mattrand (2011) had recourse to *hidden Markov models* (HMMs) identified from the same load data. The HMM model defined by Mattrand (2011) and described in the following presents the main advantage of working with *continuous* stress levels. This continuous description avoids the selection of a unique stress value per class, as is the case in the FMC model. Moreover, it is found to be of great importance for the highest levels of stresses, which may cause a significant amount of retardation in the crack growth. These highest stress levels are modeled here by means of *generalized Pareto distribution* (GPD), which allows the realizations of stresses *larger* than those recorded. HMM models were also found useful for describing the variability of the mission of an aircraft within the fleet (Mattrand et al., 2011a), with a similar idea to that of switching Markov chains. A sequence of flights for a given aircraft is controlled by a HMM which changes the parameters of the FMC or HMM model used to model a single flight load sequence.

Hidden Markov chain models (Rabiner, 1989; Cappé et al., 2005) can be viewed as an extension of the concept of Markov chains for which the observation of X_n is no longer a discrete state but a probabilistic function of this state. Such models are hence described by a bivariate-time process $\{S_n, X_n\}_{n \in \mathbb{N}_{>0}}$ with an observable continuous state space E, see Figure III.25:

[12] All stresses are divided by the maximum stress in the recorded data set.

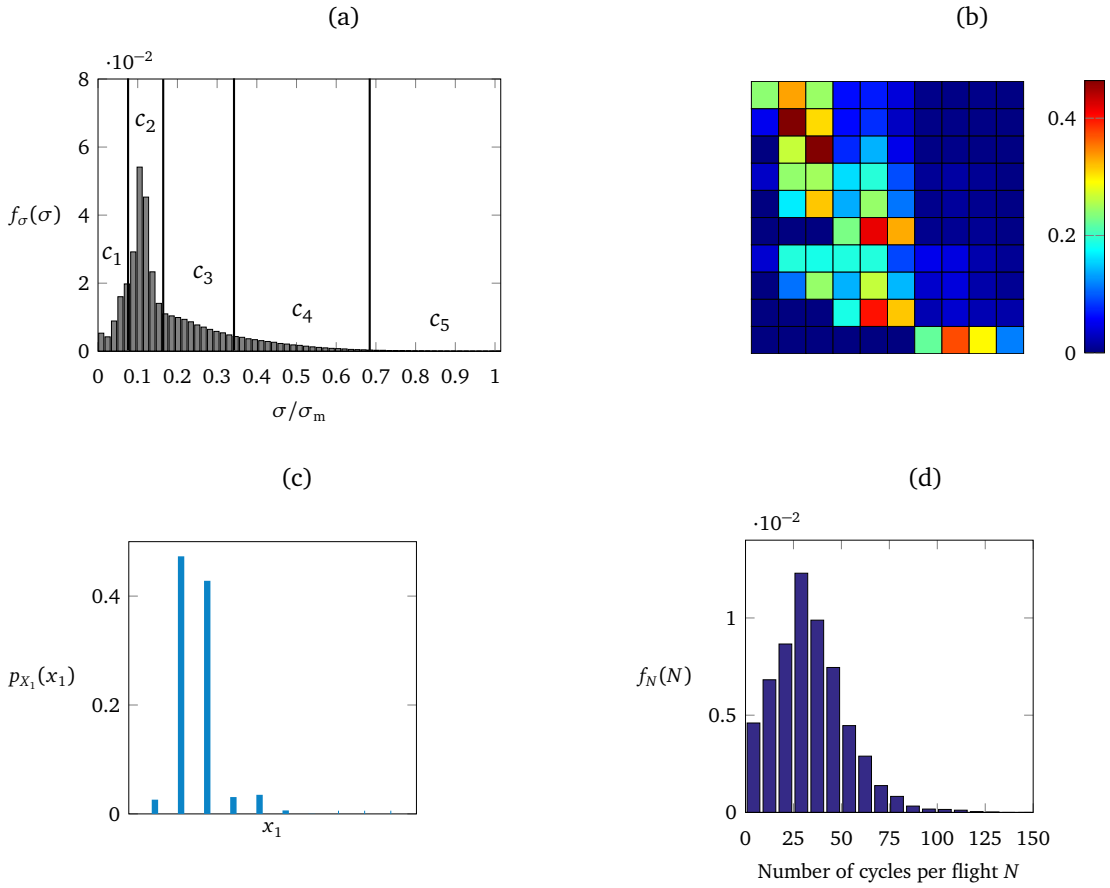

Figure III.24 – Input parameters of the FMC model. (a) Distribution of normalized peak/trough stresses (all stresses divided by the maximum value of the recorded data). (b) Transition matrix $\mathbf{P}$, where the load cycle states are ordered as follows: $\{e_1 = (s_2, s_1),\ e_2 = (s_3, s_1),\ e_3 = (s_3, s_2),\ \ldots,\ e_9 = (s_5, s_3),\ e_{10} = (s_5, s_4)\}$. (c) Distribution of the initial state of the chain X_1. (d) Distribution of the number N of cycles per flight.

- $(S_n)_{n\in\mathbb{N}_{>0}}$ with $S_n = (M'_n, m'_n)$ is a non-observable (hidden) Markov chain with finite state space $E^{\mathrm{h}} = \{\, e_i = (c_k, c_l),\ k, l \in \{1, \ldots, K_c\},\ k > l \,\}$ where $\{c_k, 1 \le k \le K_c\}$ is a selected set of ordered stress *classes*. Note that $\{e_i, 1 \le i \le K\}$ are no longer pairs of stress levels as in the FMC model but pairs of stress classes,
- conditional on S_n, $(X_n)_{n\in\mathbb{N}_{>0}}$ with $X_n = (M_n, m_n)$ is a sequence of independent observable random cycle variables with values in $E = \mathbb{R}^2_{>0}$ such that the conditional distribution of X_n depends only on S_n. The corresponding PDF, which is assumed to exist, is denoted $f_{X_n|S_n}$.

Observed values of M_n and m_n are therefore conditioned by those of M'_n and m'_n. For each time n, a realization of M_n, resp. m_n, is a realization of a random variable with probability distribution $f_{M'_n}$, resp. $f_{m'_n}$. According to the number of stress classes c_k and c_l that can be taken by M'_n and m'_n for $k, l \in \{1, \ldots, K_c\}$, a set of K_c-candidate probability distributions is necessary to define $f_{M'_n}$ and $f_{m'_n}$. The distributions are identified from the recorded stress data, along with their types and parameters, see Figure III.26. Due to the sensitivity of the selected crack growth model to extreme load values (PREFFAS model), the c_{K_c}-load class corresponding to the upper tail of the distribution is modeled by a generalized Pareto distribution (GPD):

$$f_{c_{K_c}}(M_n) = \frac{1}{\beta_0}\left[1 + \xi_0 \frac{(M_n - u_s)}{\beta_0}\right]^{-1-1/\xi_0} \quad \text{for} \quad \xi_0 \neq 0\,, \tag{III.75}$$

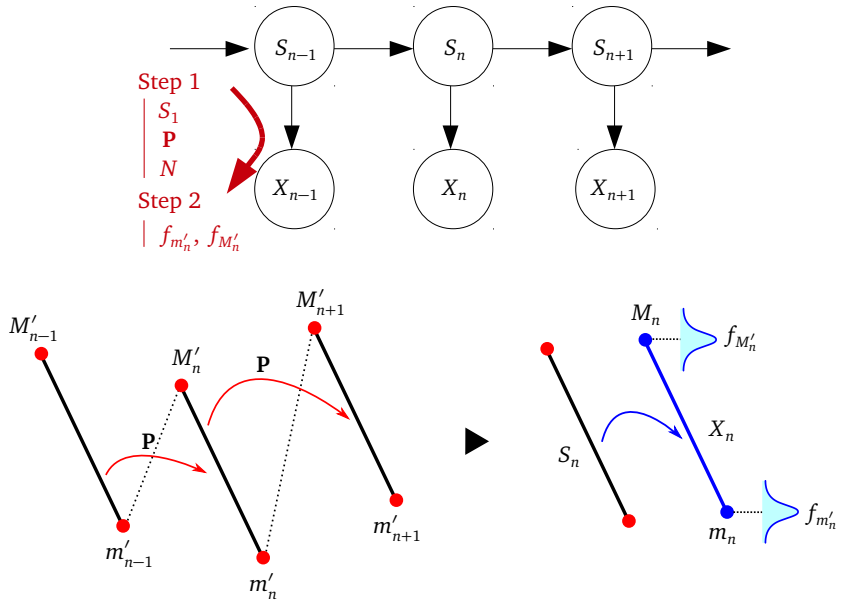

Figure III.25 – Dependence structure of the hidden Markov model (HMM). Hidden chain S_n (initial state X_1, transition matrix **P**, length of chain N), observable process X_n ($f_{m'_n}$: distribution of trough stresses, $f_{M'_n}$: distribution of peak stresses).

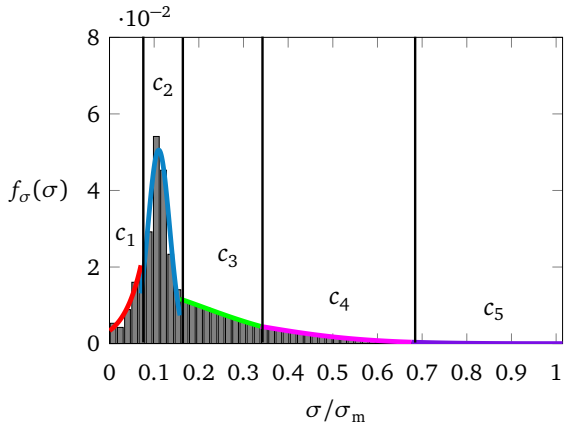

Figure III.26 – Distributions $f_{m'_n}$ and $f_{M'_n}$ of the HMM model. Classes c_1, c_2, c_3, c_4: truncated Gaussian distributions, see detailed parameters in Mattrand et al. (2011a), Table 2. Class c_5: generalized Pareto distribution ($u_s = 0.676$, $\xi_0 = 0.20$, $\beta_0 = 14.7$).

where u_s, β_0, ξ_0 are respectively location, scale and shape parameters, identified by means of the peak-over-threshold method (Davison and Smith, 1990). For the other classes, truncated Gaussian distributions (TGD) are used. The reader may refer to Mattrand and Bourinet (2011) and Mattrand et al. (2011a) which give details about parameter identification.

(c) Validation of the FMC and HMM models

Before their use in a reliability analysis, see Section III–2.3.3, the accuracy of the constructed FMC and HMM models was assessed. The statistical properties of these models were compared to those of the recorded load sequences they were identified from. It was noticed that small deviations between the modeled random load sequences and the recorded loads resulted in large deviations in terms of crack extension, due to the crack growth law (amplification due to m exponentiation in the Paris-Erdogan

equation) and to the interaction effects accounted for by the PREFFAS crack closure model. For this reason a comparison was not made directly in terms of stress levels but in terms of crack growth by means of PREFFAS. The accuracy of the random models is assessed as follows:

- We consider the crack extension Δa of a compact tension (CT) specimen defined in Mattrand et al. (2011a), Section V.B.2, subjected to variable amplitude loads[13]
  (a) simulated from the constructed random models (FMC and HMM),
  (b) randomly and uniformly selected from the load sequences measured in flight.
  Crack propagation is carried out by means of the PREFFAS crack closure model.
- A set of $N_f = \{1,\ 200,\ 500,\ 1000\}$ cumulative flight(s) is generated with FMC and HMM models, in order to analyze the effect of the length of random load sequences on crack growth.
- Such sets are independently repeated $N_{sim} = 10,000$ times. This enables the generation of N_{sim} samples of crack extension Δa for each N_f. The following statistical properties are determined for each sample: first two statistical moments, 0.1, 1, 10, 50, 90, 99 and 99.9 percentiles.
- The accuracy of a given model (FMC or HMM) can be assessed based on the relative error between the statistical moments or percentiles of the crack extensions obtained by simulations of load sequences using this model (subscript sim) and those obtained with experimentally measured load sequences (subscript exp). The relative errors represented in Figure III.27 are defined as $(q_{sim} - q_{exp})/q_{exp}$, where is q is the statistical quantity of interest.

From these results, it is found that the length of the load sequence has a dramatic importance on the accuracy of the crack extension. Crack extensions based on a single flight, i.e. with $N_f = 1$, are incorrectly reproduced with both the FMC and the HMM models. The crack extensions simulated with the random models are biased (FMB, group B), variance is underestimated (25 to 40%) and all the percentiles are far from those obtained with the recorded data. For several cumulative flights the accuracy of the FMC model is not improved, despite some better results on the upper percentiles of group A. By contrast, the accuracy of the HMM model improves as N_f is increased. The variance of the crack extensions simulated with the random models gets closer to that obtained with the recorded data. The percentiles are highly accurate, especially the upper ones corresponding to largest crack extensions. These results clearly point out the superiority of the HMM model w.r.t. FMC. This better accuracy can be attributed to the continuous description of the stress levels, which produces the necessary degree of retardation in the crack growth.

III–2.3.3 Reliability assessment using the CE method

In this section we study the reliability of a M(T) specimen of 150 mm width and 2 mm thickness, made of a 2024-T351 aluminum alloy, under crack growth and subjected to random loading (Mattrand and Bourinet, 2014). Two crack growth models are used: the Paris-Erdogan law, which is characterized by straightforward and fast calculations, and the more elaborate PREFFAS crack closure model, which accounts for interaction effects between cycles, such as crack growth retardations and accelerations.

The only source of uncertainty considered by Mattrand and Bourinet (2014) is that assumed in fatigue loading. The crack growth properties and the initial crack length are considered deterministic for the sake of simplicity. The material properties selected in the two models are: yield strength $\sigma_y =$ 312 MPa, Paris-Erdogan equation model parameters $C = 2.417 \times 10^{-13}$ and $m = 3.42$ (SIF range ΔK

[13] The accuracy of the random load models is analyzed in terms of the stress level σ_{eq} of an equivalent constant amplitude load sequence in Mattrand and Bourinet (2011), as defined in Eq. (III.71). The results presented in Mattrand et al. (2011a) and recalled here in Figure III.27 are quantitatively different from those given in Mattrand and Bourinet (2011), but the conclusions drawn are the same.

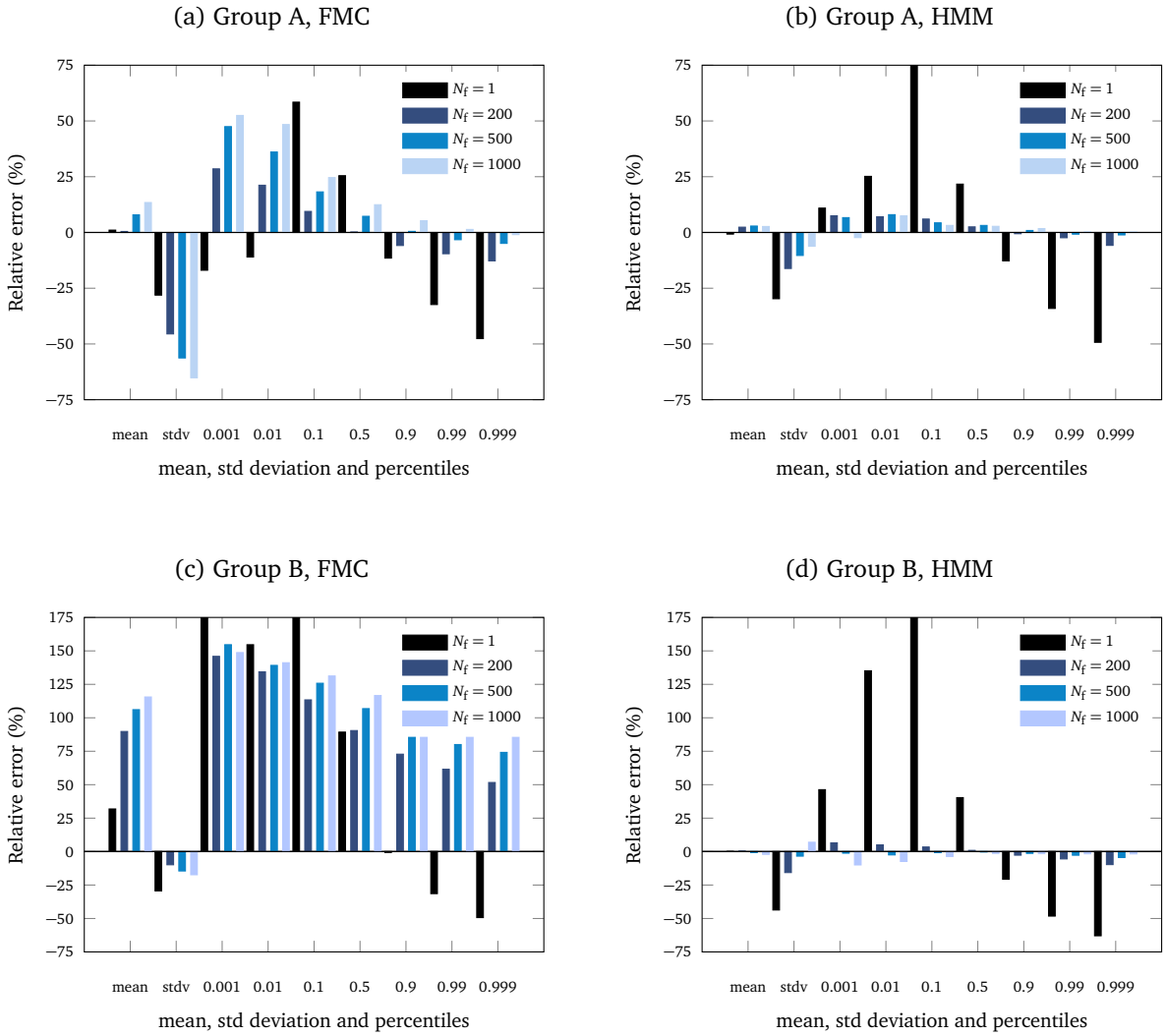

Figure III.27 – Relative error (in %) between statistical properties of Δa-distributions simulated with random models (FMC and HMM) and those of in-flight recorded load sequences.

consistent with MPa$\sqrt{\text{mm}}$ and crack growth rate $\mathrm{d}a/\mathrm{d}N$ with mm/cycle), Elber crack closure parameters $a = 0.45$ and $b = 0.55$. An initial crack length $a_0 = 5$ mm is assumed in all the reliability analyses performed.

For random load sequences, we take as inputs of the reliability problem the FMC and HMM models identified from group B recorded load data, composed of 3138 flights, as defined in Section III–2.3.2. The stress levels are split into $K_c = 5$ classes, which results in $K = 10$ load cycle states. The load cycle states are ordered as follows in the transition matrix $\mathbf{P}$, see Figure III.24b: $\{e_1 = (s_2, s_1),\ e_2 = (s_3, s_1),\ e_3 = (s_3, s_2),\ \ldots,\ e_8 = (s_5, s_2),\ e_9 = (s_5, s_3),\ e_{10} = (s_5, s_4)\}$. In the HMM model, realizations of M_n and m_n are obtained from the set of K_c-probability distributions defined in Mattrand et al. (2011a), see Figure III.26.

The following additional assumptions are made in the definition of the random loading:

- all simulated load sequences are composed of a fixed number of cycles N, which is considered as deterministic,
- it is assumed that all the generated load sequences $x = (x_n)_{1 \leq n \leq N}$ start from the same load cycle $x_1 = e_2 = (s_3, s_1) = (0.248, 0.039)$.

The following LSF is considered in the reliability analyses:

$$g(x) = a_c - a(x)\,, \tag{III.76}$$

where $a(x)$ is the crack length resulting from the application of the load sequence $x = (x_n)_{1\leq n\leq N}$ to the M(T) specimen with initial crack size a_0, and a_c is the critical crack length solution of $K(a_c, \sigma_1) = K_c$, where σ_1 is a given stress level[14] and K_c is the fracture toughness.

Three representative examples are studied: the first two are based on the Paris crack growth model and the third makes use of the PREFFAS model, see Table III.10. For each example, two reliability analyses are performed, the first with the FMC model and the second with the HMM model. The critical crack lengths a_c are arbitrarily selected to obtain sufficiently low failure probabilities, i.e. in the range 10^{-6} to 10^{-3}. In order to meet the assumption of stationary spectra in the PREFFAS model, the whole load sequence must be composed of a randomly-generated load subsequence which is repeated until failure. For this purpose, any N-cycle load sequence applied in example 3 is composed of a randomly-generated load sequence with $N_s = 525$ cycles, repeated $F = 100$ times. The whole applied sequence is therefore composed of $N = 100 \times 525 = 52,500$ cycles.

	Crack growth model	Number of cycles N	Critical crack length a_c (mm)
Example 1	Paris	500	5.09 (FMC) , 5.07 (HMM)
Example 2	Paris	102,000	25.2 (FMC) , 24.9 (HMM)
Example 3	PREFFAS	52,500	9.34 (FMC) , 6.90 (HMM)

Table III.10 – Reliability problems. FMC and HMM models identified from group B load data.

(a) First-order Markov chains

Failure probability p_f with a FMC model for random loading is given by:

$$p_f = \sum_{x\in E^N} \mathbb{1}_{\mathcal{F}_{x,N}}(x)\, p_X(x) = \mathbb{E}_{p_X}\left[\mathbb{1}_{\mathcal{F}_{x,N}}(X)\right], \tag{III.77}$$

where $\mathbb{1}_{\mathcal{F}_{x,N}}(x)$ is the indicator function of the failure domain $\mathcal{F}_{x,N} = \{x \in E^N : a_c - a(x) \leq 0\}$ and p_X is the joint probability mass function of $X = (X_n)_{1\leq n\leq N}$.

According to the first-order Markov property, the joint probability mass function of the homogeneous FMC $X = (X_n)_{1\leq n\leq N}$ writes, by successive conditioning:

$$p_X(x) = \mathbb{P}(X = x) = \mathbb{P}(X_1 = x_1) \prod_{n=1}^{N-1} \mathbb{P}\left(X_{n+1} = x_{n+1} \,|\, X_n = x_n\right). \tag{III.78}$$

which can also be expressed as follows, by making explicit the dependence on the transition matrix $\mathbf{P}$ considered as a parameter:

$$p_X(x) = p_X(x;\mathbf{P}) = \prod_{i,j=1}^{K} {p_{ij}}^{n_{ij}(x)}\,, \tag{III.79}$$

[14] In damage tolerance such as defined in aerospace engineering, this stress level σ_1 can be assumed to be that related to the so-called *limit load* which needs to be sustained at all flight instants during the whole life of the aircraft. If the critical crack length is defined in terms of the peak stress M_n at cycle n, i.e. $a_c = a_{c,n}$ such that $K(a_{c,n}, M_n) = K_c$, the reliability problem becomes *time-variant*, see discussion in Mattrand and Bourinet (2014). To the author's knowledge, there is no alternative to crude MC in order to solve time-variant reliability problems with Markov models as inputs.

where K is the number of defined load cycle states and $n_{ij}(x)$ denotes the number of transitions from cycle e_i to cycle e_j in the load sequence $x = (x_n)_{1\leq n\leq N}$.

The cross-entropy (CE) method introduced in Section I–3.3.2 is used to estimate the failure probability defined in Eq. (III.77). The CE method consists in finding the optimal parameter transition matrix $\mathbf{Q} = [q_{ij}]_{1\leq i,j\leq K}$ solution to the following optimization problem, similar to that introduced in Eq. (I.95):

$$\mathbf{Q}^* = \arg\max_{\mathbf{Q}} \mathbb{E}_{p_X(\cdot;\mathbf{P})}\left[\mathbb{1}_{\mathcal{F}_{x,N}}(X)\ln\left(p_X(X;\mathbf{Q})\right)\right] \quad \text{s.t.} \quad \begin{cases} 0 \leq q_{ij} \leq 1 & \text{for } i,j \in \{1,\dots,K\} \\ \sum_{j=1}^K q_{ij} = 1 & \text{for } i \in \{1,\dots,K\} \end{cases}, \tag{III.80}$$

where constraints are added such that $\mathbf{Q}$ is a transition matrix.

In the context of rare failure events as assumed here, it is necessary to resort once again to importance sampling with a proposal joint probability mass function $p_X(X;\mathbf{R})$, where $\mathbf{R} = [r_{ij}]_{1\leq i,j\leq K}$. Similarly to Eq. (I.96), we can write:

$$\begin{aligned} \mathbf{Q}^* &= \arg\max_{\mathbf{Q}} \mathbb{E}_{p_X(\cdot;\mathbf{R})}\left[\mathbb{1}_{\mathcal{F}_{x,N}}(X)\, W(X;\mathbf{P},\mathbf{R})\ln\left(p_X(X;\mathbf{Q})\right)\right] \\ \text{s.t.} &\quad \begin{cases} 0 \leq q_{ij} \leq 1 & \text{for } i,j \in \{1,\dots,K\} \\ \sum_{j=1}^K q_{ij} = 1 & \text{for } i \in \{1,\dots,K\} \end{cases}, \end{aligned} \tag{III.81}$$

where the likelihood ratio $W(x,\mathbf{P},\mathbf{R})$ is expressed as:

$$W(x;\mathbf{P},\mathbf{R}) = \frac{p_X(x;\mathbf{P})}{p_X(x;\mathbf{R})} = \prod_{i,j=1}^K \left(\frac{p_{ij}}{r_{ij}}\right)^{n_{ij}(x)}. \tag{III.82}$$

The transition probabilities of $\mathbf{Q}^*$ are obtained after straightforward calculations by solving the associated Lagrangian maximization problem w.r.t. q_{ij}:

$$q_{ij}^* = \frac{\mathbb{E}_{p_X(\cdot;\mathbf{R})}\left[\mathbb{1}_{\mathcal{F}_{x,N}}(X)\, W(X;\mathbf{P},\mathbf{R})\, n_{ij}(X)\right]}{\mathbb{E}_{p_X(\cdot;\mathbf{R})}\left[\mathbb{1}_{\mathcal{F}_{x,N}}(X)\, W(X;\mathbf{P},\mathbf{R})\, n_i(X)\right]}, \tag{III.83}$$

where $n_i(x) = \sum_{j=1}^K n_{ij}(x)$ represents the number of transitions starting from state e_i in the load sequence x.

The corresponding estimator $\widehat{q}_{ij}^*$ is given, for $i,j \in \{1,\dots,K\}$, by:

$$\widehat{q}_{ij}^* = \frac{\sum_{k=1}^{N_0} \mathbb{1}_{\mathcal{F}_{x,N}}\left(X^{(k)}\right)\left(\prod_{i,j=1}^K \left(\frac{p_{ij}}{r_{ij}}\right)^{n_{ij}(X^{(k)})}\right) n_{ij}\left(X^{(k)}\right)}{\sum_{k=1}^{N_0} \mathbb{1}_{\mathcal{F}_{x,N}}\left(X^{(k)}\right)\left(\prod_{i,j=1}^K \left(\frac{p_{ij}}{r_{ij}}\right)^{n_{ij}(X^{(k)})}\right) n_i\left(X^{(k)}\right)}, \tag{III.84}$$

where $X^{(1)},\dots,X^{(N_0)}$ are i.i.d. copies of $(X_n)_{1\leq n\leq N}$ sampled from the $p_X(\cdot;\mathbf{R})$ distribution.

In the context of rare failure events, most of the realizations $\mathbb{1}_{\mathcal{F}_{x,N}}\left(x^{(k)}\right)$ are zeros if an insufficient number of samples N_0 is taken. To overcome such an issue we use the multi-level CE method introduced in Section I–3.3.2, see also de Boer et al. (2005) and Ridder (2005). The idea is to build a sequence of reference parameters $\{\widehat{\mathbf{Q}}_s, s \in \mathbb{N}\}$, with $\widehat{\mathbf{Q}}_0 = \mathbf{P}$ and a sequence of LSF levels $\{\widehat{y}_s, t \geq 1\}$ which are iteratively updated. Static smoothing of the solution is applied at each level s. The solution $\widehat{\mathbf{Q}}_s$ is weighted with that of the previous level $s-1$, with a smoothing parameter α set to 0.6. A rarity parameter $\rho = 0.1$ is taken for the determination of the LSF levels $\widehat{y}_s$. A detailed algorithm is given in Mattrand and Bourinet (2014), Section 3.3.

	Method	N_t	$\widehat{p}_f$	c.o.v. (%)
Example 1	MCS	10^7	8.39×10^{-6}	10.9
	MCS	10^8	$\mathbf{7.48 \times 10^{-6}}$	**3.66**
	CE(1000; 4)	4×10^3	7.69×10^{-6}	26.2
	CE(5000; 4)	2×10^4	7.71×10^{-6}	5.82
	CE(20,000; 4)	8×10^4	7.68×10^{-6}	3.13
Example 2	MCS	10^5	$\mathbf{1.10 \times 10^{-3}}$	**9.53**
	CE(1000; 3)	3×10^3	1.11×10^{-3}	10
	CE(2000; 3)	6×10^3	1.11×10^{-3}	5.19
	CE(5000; 3)	1.5×10^4	1.11×10^{-3}	4.77
Example 3	MCS	10^5	$\mathbf{5.31 \times 10^{-4}}$	**13.7**
	CE(1000; 3)	3×10^3	5.06×10^{-4}	17.1
	CE(2000; 3)	6×10^3	4.84×10^{-4}	8.75
	CE(5000; 3)	1.5×10^4	4.84×10^{-4}	4.31

Table III.11 – FMC model. Results of the reliability analyses.

The multilevel CE method is applied to the three reliability problems presented in Table III.10 with the FMC model identified from the load data of group B. The coefficient of variation of the failure probability is estimated by 30 independent runs of the CE method. The results are given in Table III.11, where the number of samples per level N_0 and the number of levels m are given in brackets. The CE results are compared to those obtained by crude MC. Reference results are in bold characters. The total number of samples needed in each analysis is denoted N_t in the table.

As expected, the CE method clearly outperforms crude MC. The total number of samples required by the CE method is much lower than that needed using a crude MC approach for a similar degree of accuracy on p_f The simulation effort is reduced by a factor of about 1000 in example 1, 30 in example 2 and 20 in example 3. Moreover, no significant bias is observed between the averaged failure probability estimates obtained by the CE method and the reference MC estimate, given the statistical accuracy of this estimate.

(b) Hidden Markov models

The CE method applied in the context of FMC and described in Section III–2.3.3 (a) can be extended to HMM models with continuous state space. The joint probability mass function $p_X(x)$ used in the FMC context needs to be replaced by:

$$p_{XS}(x,s) = p_{X|S}(x|s)p_S(s)\,, \tag{III.85}$$

where s and x are respectively realizations of the hidden chain $S = (S_n)_{1\le n\le N}$ and the observable chain $X = (X_n)_{1\le n\le N}$.

Similarly to FMC, see Eq. (III.79), the second term of the product related to the hidden chain S writes:

$$p_S(s) = \prod_{i,j=1}^{K} p_{ij}^{n_{ij}(s)}\,, \tag{III.86}$$

and the first term is given by:

$$p_{X|S}(x|s) = \prod_{n=1}^{N} f_{X_n|S_n}(x_n|s_n) = f_{M'_n}(M_n) f_{m'_n}(m_n)\,, \tag{III.87}$$

where M_n and m_n are realizations of X_n. It is recalled that $S_n = (M'_n, m'_n)$ of the non-observable chain $(S_n)_{1\leq n\leq N}$ corresponds to the n^{th} cycle of the load sequence.

By making explicit the dependence on a parameter transition matrix $\mathbf{P}$ in p_S and on a vector of distribution parameters $\mathbf{u}$ in the PDFs $f_{M'_n}$ and $f_{m'_n}$, we obtain:

$$p_{XS}(x,s;\mathbf{P},\mathbf{u}) = \left(\prod_{n=1}^{N} f_{M'_n}(M_n;\mathbf{u})\, f_{m'_n}(m_n;\mathbf{u})\right)\left(\prod_{i,j=1}^{K} p_{ij}^{n_{ij}(s)}\right). \tag{III.88}$$

The CE optimization problem is derived in a similar manner to that established for FMC in Eq. (III.81). It is expressed as follows:

$$\begin{aligned}(\mathbf{Q}^*,\mathbf{v}^*) &= \arg\max_{\mathbf{Q},\mathbf{v}} \mathbb{E}_{p_{XS}(\cdot;\mathbf{R},\mathbf{w})}\left[\mathbb{1}_{\mathcal{F}_{x,N}}(X)\, W(X,S;\mathbf{P},\mathbf{R},\mathbf{u},\mathbf{w}) \ln p_{XS}(X,S;\mathbf{Q},\mathbf{v})\right] \\ \text{s.t.} &\quad \begin{cases} 0 \leq q_{ij} \leq 1 & \text{for } i,j \in \{1,\dots,K\} \\ \sum_{j=1}^{K} q_{ij} = 1 & \text{for } i \in \{1,\dots,K\} \end{cases},\end{aligned} \tag{III.89}$$

where the likelihood ratio $W(x,s;\mathbf{P},\mathbf{R},\mathbf{u},\mathbf{w})$ writes:

$$W(x,s;\mathbf{P},\mathbf{R},\mathbf{u},\mathbf{w}) = \frac{p_{XS}(x,s;\mathbf{P},\mathbf{u})}{p_{XS}(x,s;\mathbf{R},\mathbf{w})} = \prod_{n=1}^{N} \frac{f_{M'_n}(M_n;\mathbf{u})\, f_{m'_n}(m_n;\mathbf{u})}{f_{M'_n}(M_n;\mathbf{w})\, f_{m'_n}(m_n;\mathbf{w})} \prod_{i,j=1}^{K} \left(\frac{p_{ij}}{r_{ij}}\right)^{n_{ij}(s)}. \tag{III.90}$$

It is worth mentioning that additional constraints need to be added to Eq. (III.89), such as bounds on the distribution parameters $\mathbf{v}$ (see Mattrand, 2011, for details in the specific context of the constructed HMM model). This is of prime importance in numerically solving the optimization problem.

The solution $\mathbf{Q}^*$ and $\mathbf{v}^*$ to Eq. (III.89) can be obtained by the partial differentiation of the associated Lagrangian. The estimator $\widehat{q}^*_{ij}$ of the optimal solution q^*_{ij} writes, for $i,j \in \{1,\dots,K\}$:

$$\widehat{q}^*_{ij} = \frac{\sum_{k=1}^{N_0} \mathbb{1}_{\mathcal{F}_{x,N}}\left(X^{(k)}\right) W\left(X^{(k)},S^{(k)};\mathbf{P},\mathbf{R},\mathbf{u},\mathbf{w}\right) n_{ij}\left(X^{(k)},S^{(k)}\right)}{\sum_{k=1}^{N_0} \mathbb{1}_{\mathcal{F}_{x,N}}\left(X^{(k)}\right)\left(\prod_{i,j=1}^{K} W\left(X^{(k)},S^{(k)};\mathbf{P},\mathbf{R},\mathbf{u},\mathbf{w}\right) n_i\left(X^{(k)},S^{(k)}\right)\right)}, \tag{III.91}$$

where $(S^{(1)},X^{(1)}),\dots,(S^{(N_0)},X^{(N_0)})$ are i.i.d. copies of the HMM model $(S_n,X_n)_{1\leq n\leq N}$ sampled from $p_{XS}(\cdot,\cdot,\mathbf{R},\mathbf{w})$.

The best estimator $\widehat{\mathbf{v}}^*$ of the parameter vector $\mathbf{v}^*$ is obtained by solving the following equation, which results from the partial differentiation of the Lagrangian w.r.t. $\mathbf{v}$:

$$\frac{1}{N_0}\sum_{k=1}^{N_0}\left[\mathbb{1}_{\mathcal{F}_{x,N}}\left(X^{(k)}\right) W\left(X^{(k)},S^{(k)};\mathbf{P},\mathbf{R},\mathbf{u},\mathbf{w}\right) \nabla_{\mathbf{v}} \sum_{n=1}^{N} \ln\left(f_{M'_n}(M_n;\mathbf{v}) f_{m'_n}(m_n;\mathbf{v})\right)\right] = \mathbf{0}. \tag{III.92}$$

The solution of Eq. (III.92) is in general not accessible analytically and the solution $\widehat{\mathbf{v}}^*$ must be therefore obtained numerically.

The multilevel CE method is applied to the three reliability problems presented in Table III.10 with the HMM model identified from the load data of group B.

In examples 1 and 2, the Paris law is not especially sensitive to extreme loads but to load ranges $\Delta\sigma = \sigma_{\max} - \sigma_{\min}$ according to its formulation. The idea followed to solve the HMM-based reliability analysis is therefore to change the distributions in the CE algorithm that mainly affect the load ranges. For this purpose, it is decided only to bias the distribution of the non-observable Markov chain $(S_n)_{1\leq n\leq N}$ with the transition matrix $\mathbf{P}$, and therefore to maintain fixed the set of parameters $\mathbf{u}$ of the

	Method	N_t	$\widehat{p}_f$	c.o.v. (%)
Example 1	MCS	10^8	$\mathbf{1.14 \times 10^{-6}}$	**9.36**
	CE(5000; 7)	3.5×10^4	1.27×10^{-6}	45.8
	CE(20,000; 7)	1.4×10^5	1.13×10^{-6}	13.5
	CE(40,000; 7)	2.8×10^5	1.19×10^{-6}	9.2
Example 2	MCS	10^5	$\mathbf{1.47 \times 10^{-3}}$	**8.24**
	CE(1000; 4)	4×10^3	1.42×10^{-3}	30.4
	CE(2000; 4)	8×10^3	1.35×10^{-3}	14.2
	CE(5000; 4)	2×10^4	1.35×10^{-3}	6.48

Table III.12 – HMM model. Results of the reliability analyses.

distributions $f_{M'_n}(M_n; \mathbf{u})$ and $f_{m'_n}(m_n; \mathbf{u})$ of $X_n|S_n$, i.e. the parameters of the truncated Gaussian distributions (TGDs) and those of the generalized Pareto distribution (TGD) identified for in-flight data and plotted in Figure III.26. Such a strategy presents the main advantage of reducing both the dimension and the complexity of the optimization problem in Eq. (III.89). The parameter $\mathbf{w}$ is kept equal to $\mathbf{u}$ and the first term of the product in the likelihood expression defined in Eq. (III.90) vanishes. The results of the reliability analyses are given in Table III.12. The coefficient of variation of p_f with the CE method is, as with FMC, estimated by 30 independent runs. As with FMC, no significant bias is observed between the averaged failure probabilities obtained using the CE method and the reference solution obtained by crude MC. The efficiency of the CE method is again observed in these two examples. It is especially impressive for very low failure probabilities, as considered in example 1. The required number of samples in this specific case is about 350 times less than the number needed using crude MC for a quasi-similar c.o.v. We should however point out that the efficiency of the CE method is slightly reduced compared with that achieved with the FMC model. The number m of CE levels required to converge appears higher than in the case of FMC: 7 instead of 4 in example 1 and 4 instead of 3 in example 2.

Due to the complexity of the crack propagation model investigated in example 3 (PREFFAS model) and its sensitivity to extreme loads, it is important to vary both the transition matrix $\mathbf{P}$ and the parameters ξ_0 and β_0 of the GPD defined in Eq. (III.75). The threshold u_s of the GPD is maintained fixed to 0.676 in order to not modify the lower bound of the c_{K_c} class of stresses. The parameters of the TGDs are expected to have a lesser impact on crack growth than those of the GPD and they are kept fixed for this reason. The parameter vector $\mathbf{u}$ then reduces to $\mathbf{u} = (\xi_0, \beta_0)$. With such a choice it must be emphasized that the solution to Eq. (III.92) can here only be obtained numerically. The results obtained using the CE method are not fully satisfatory in example 3. Failure probability estimates sufficiently close to the crude MC reference solution of 1.15×10^{-3} estimated with a c.o.v. of 0.0932 can be found only by lowering the smoothing parameter down to 0.2, which results in larger total number of samples N_t compared with the case $\alpha = 0.6$ set initially. Moreover, and even with $\alpha = 0.2$, some estimates obtained from 30 independent runs of the CE Method are too far from the reference failure probability, for a number of samples per level N_0 varying between 1000 and 5000, see Mattrand (2011), Figure 5.6 p. 202. This lack of robustness may have several origins, as investigated in Mattrand and Bourinet (2014). It is the author's belief that this lack of robustness is mainly due the likelihood ratio degeneracy (Chan and Kroese, 2012), which is known to give unreliable failure probability estimates when the number of parameters to estimate becomes large.

The biased transition matrix $\widehat{\mathbf{Q}}^*$ and parameter vector $\mathbf{v}^*$ constitute interesting by-products of the CE method, in addition to the failure probability estimate. These quantities have a similar meaning to the most probable failure point in a FORM analysis. $\widehat{\mathbf{Q}}^*$ and $\widehat{\mathbf{v}}^*$, although unknown, are expected to be close to $\widehat{\mathbf{Q}}_m$ and $\widehat{\mathbf{v}}_m$ obtained in last level $s = m$ of the multilevel CE method. The variations in $(\widehat{\mathbf{Q}}_s - \mathbf{P})$

and $\widehat{\mathbf{v}}_s = (\widehat{\xi}_s, \widehat{\beta}_s)$ for $s \in \{1, 2, 3, m = 4\}$ are respectively represented in Figures III.28 and III.29.[15] It is important to point out that these results are taken from a CE analysis whose failure probability estimate is close to the MC reference. From Figure III.29, we can observe that only the GPD parameters significantly change at first. The tail of the distribution becomes less heavy and, as a consequence, the simulation is composed of fewer high loads. There are therefore fewer retardation effects, which results in larger final cracks and consequently in more failures. Contrarily, we can notice from Figure III.28 that the transition probabilities do not vary significantly until level $s = 2$ is reached. The changes occur at levels $s = 3$ and 4. The GPD then no longer evolves from level $s = 3$ to 4.

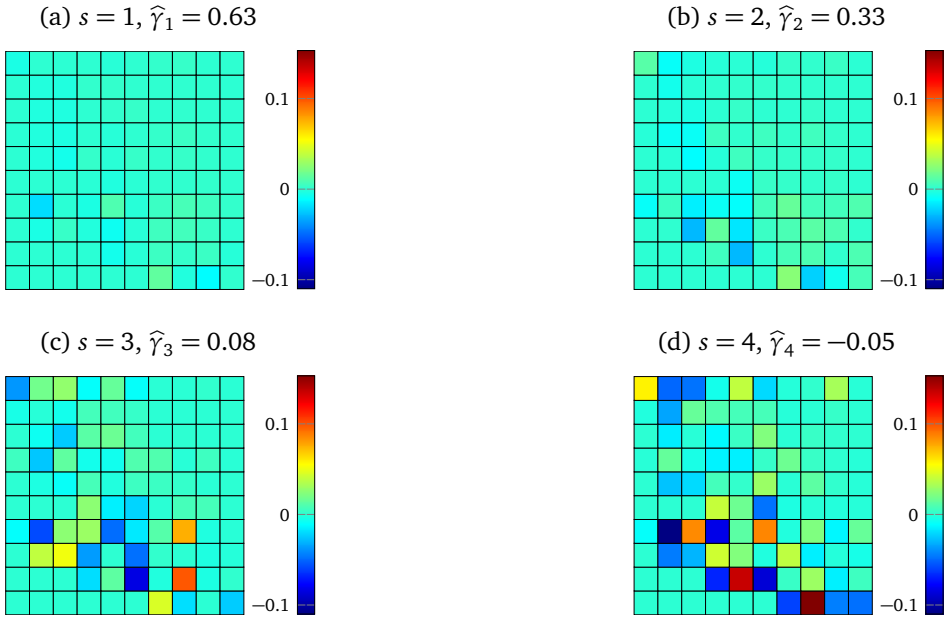

Figure III.28 – Variation in transition matrices $(\widehat{\mathbf{Q}}_s - \mathbf{P})$. $\widehat{p}_{\mathrm{f}}^{\mathrm{CE}} = 1.21 \times 10^{-3}$, $N_0 = 5000$.

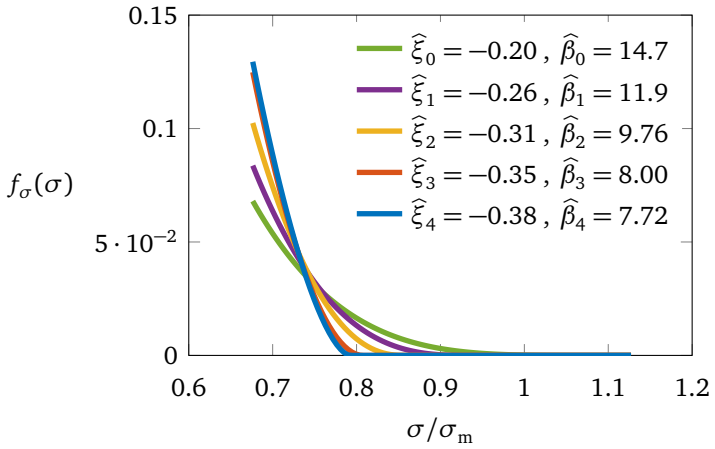

Figure III.29 – Variation in GPD parameters $\widehat{v}_s = \{\widehat{\xi}_s, \widehat{\beta}_s\}$. $\widehat{p}_{\mathrm{f}}^{\mathrm{CE}} = 1.21 \times 10^{-3}$, $N_0 = 5000$.

[15] Such an interpretation was also made was with the FMC model, where the variation in $\widehat{\mathbf{Q}}_s$ with s was analyzed, see Bourinet and Mattrand (2013) and Mattrand and Bourinet (2014).

Concluding remarks, perspectives

This final section makes some concluding remarks and gives potential future research directions.

Reliability assessment

The core of my work has been focused on reliability assessment, and design under uncertainty where reliability is taken as a constraint. The computation of failure probabilities is still a great challenge in engineering, due to the ever-increasing cost of the numerical models involved in the analysis. It is common for a single analysis to take hours or days on multi-core machines, which makes uncertainty propagation analysis at best hard and at worst impossible to solve. The analyst is often confronted with the following dilemma: applying sampling-based techniques known for their robustness at the expense of often too-numerous calls to the numerical models, or applying approximation-based techniques for the sake of efficiency while sacrificing robustness and generality.

From the experience gained in my research work, I believe that subset simulation has been and still is the best choice if several thousands calls to the model are allowed. This method has remarkable properties: it can be applied to models with a large number of inputs (e.g. thousands or more with random processes in structural dynamics) and its efficiency is high compared to a crude MC approach. If only a few hundred calls are possible, recourse to adaptive surrogate-based techniques is of interest, and it has constituted one of the main directions of my research work. The advantage in terms of computational cost, however, needs to be balanced by the following constraints on the models which can be considered in an adaptive surrogate-based analysis: (1) an input space dimensionality which is not too high, and (2) a reasonable shape complexity of the limit-state surface (e.g. a smooth LSS).

Less studied in the literature, reliability assessment based on Markov models has also been addressed in the PhD work of Mattrand. In the case of Markov chain input models, excellent results have been achieved in terms of efficiency w.r.t. crude MC. Those obtained using the proposed hidden Markov models are less impressive. There are still optimization issues, probably due to the high parameter space dimensionality, which would need to be investigated in future works.

Design under uncertainty

Reliability-based design optimization has been addressed by adaptive surrogate-based methods in the PhD works of Dubourg and Moustapha. The problems tackled in these works combine two levels of complexity: the first is associated with the assessment of failure probability under the constraint of the optimization problem, as evoked above, and the second is associated with the search for a minimum cost function. The proposed solving strategies are based on surrogates, with training sets constructed in the augmented reliability space and enriched “on demand”, i.e. when the accuracy of the surrogate

model is found to be insufficient for the application of the optimization algorithm. Optimization was shifted from a gradient-based search technique in the work of Dubourg to a stochastic one in the work of Moustapha, in order to avoid solutions associated with local minima.

The targeted applications were limited to problems with both few design parameters (up to 20) and few random inputs (up to 10). The efficiency achieved in these examples was high, the proposed approaches enabling a reduction in the number of calls to the LSF down to a few hundred. LSF nonlinearity was handled in these approaches by the application of subset simulation for the assessment of the reliability constraint(s), which avoids the usual restrictions imposed by the FORM-based RBDO approaches of the literature. The extension to higher-dimensional problems (both in terms of design parameters and random inputs) is, in my opinion, dependent on advances in surrogate-based techniques.

Surrogate models

Several aspects of surrogate models have been addressed in my works performed so far. I am listing here a few remarks based on experience gained over the studied examples, some of these remarks being more personal beliefs. A few directions to explore are also suggested to improve the construction of surrogate models.

Limits of surrogate models for function approximation

Two types of kernel-based techniques were selected in the work I supervised for the construction of surrogate models: SVM and kriging. The complexity of the machine-learning task strongly depends on the smoothness of the true function we want to approximate. If the function is smooth we may expect to construct an approximation in a high-dimensional space, assuming that a suitable kernel is selected. Unfortunately, this fundamental property may be not met in the functions involved in some practical problems. Two examples of such difficult-to-learn functions are: (1) the LSF considered in the shell buckling problem characterized by four-MPFP studied in Section III–1.4 or even its 16 random input simplified version, introduced as example 3 in Section I–3.4.2, (2) the LSF considered in the electromagnetic compatibility problem presented as example 1 in Appendix A, characterized by sharp peaks at the MPFP.

Choice of a kernel

In usual surrogate-based approaches, the kernel type is chosen a priori and the construction consists in defining the best parameters of this kernel. This was the choice made in the works I supervised or was directly involved in. An isotropic Gaussian kernel was used with SVMs in classification (^{2}SMART method) and regression (ASVR method). The anisotropic version of this kernel was recently applied to SVR. This same anisotropic Gaussian kernel was used in the works of Dubourg and Moustapha based on kriging. The Matérn kernel with $\nu = 3/2$ and $5/2$ was also tested, but did not enable the construction of surrogate models of greater accuracy.

For high-dimensional problems, I consider it mandatory to move to anisotropic versions of kernels, in order to capture the different length scales of the inputs. The price to pay is more parameters to tune and therefore longer training times. Choosing a kernel in the case of nonsmooth problems is in my experience more challenging. The nonsmoothness is most often limited to some inputs, and may be limited to only one subdomain of the whole input space. Two research directions which can possibly be combined are worth investigating: nonstationary kernels and kernels with anisotropic regularities, under the main assumption that these kernels can be tuned with a set of data which is not too large.

Hyperparameter selection

From the works that were carried out, hyperparameter selection was found to be one of the most important aspects of surrogate model construction. My experience has been with SVR mainly, but I presume that the same situation applies to kriging. In the case of SVR, the hyperparameter selection problem has been solved by using an accurate approximation of the generalization error and an exhaustive search for its minimum by stochastic optimization. For SVR based on the ϵ-insensitive loss function, the LOO error approximation of Chang and Lin seems to be a perfect candidate for estimating the generalization error. The stochastic search initially applied by means of the CE method with the isotropic Gaussian kernel is now carried out using the CMA-ES algorithm with anisotropic kernels involving numerous parameters to tune. The stochastic optimization problems to solve are computationally demanding for such anisotropic kernels. One research direction to help cope with the computational burden is to use accelerated computing exploiting graphics processing units (GPUs), as planned in the near future.

Adaptive surrogate-based strategies

In all the works based on surrogate models which are presented in this report, the choice made was to construct surrogate models sequentially, starting from an initial set of data pairs. The idea is to smartly select new points to evaluate in the input space based on the information conveyed by the currently available surrogate model. The choice of the locations of these new points has been found to impact the accuracy of the surrogate models which are constructed. The Gram matrix may become ill-conditioned, depending on the locations of the training points which are selected in the input space. This issue, which is also dependent on kernel choice, needs to be addressed in future works.

SVM or kriging, which to prefer?

The question as formulated may give rise to controversial debate! Both techniques have been used in my works and my only intention here is to pinpoint some important aspects in favor of one technique or the other.

As a first remark, the learning problem in SVM is solved using the regularization parameter C, which is tuned like other parameters, i.e. the kernel parameters and the width of the ϵ-tube in the case of SVR based on the ϵ-insensitive loss function. An equivalent approach with kriging would imply the use of a nugget with the proper identification of the noise parameter τ. In several kriging approaches found in the literature, this parameter is unfortunately not tuned but set a very small constant value.

As a second remark, the SVM formulation requires the choice of a given loss function, which quantifies the deviation between the approximate and true models at the points of the training set. My preference has been for the ϵ-insensitive loss function in SVR-based approaches, while kriging (or LS-SVR) assumes a square loss function. In my experience, I have found that LS-SVR were unable to approximate high-dimensional functions compared to ϵ-insensitive SVR. I therefore assume that the square loss function may not be the perfect candidate for function approximation in high dimensions.

In favor of kriging, one of its main advantages is its variance, which results from the assumption that the function to approximate is a realization of a random process. This variance quantifies the epistemic uncertainty of the constructed surrogates, allowing the derivation of infill criteria used in adaptive approaches. This variance has been used by Dubourg and Moustapha in the context of RBDO. Alternative enrichment strategies have been defined with SVR for reliability assessment, given the absence of a quantity equivalent to the kriging variance for SVR.

The SVM-based approaches developed in my works have been based on a formulation with an unknown bias term b. As pointed out in Chapter II, this approach is similar to ordinary kriging with an unknown constant mean. The extension of the SVM formulation to a set of real-valued functions as a replacement for b, and similarly to universal kriging, has not been investigated. As already mentioned, it is my belief that such an approach is too prone to overfitting in the case of small data sets.

Sensitivity analysis

Some contributions to sensitivity analysis in reliability assessment are presented in this report. Sensitivities to distribution parameters including correlation have been proposed in the FORM context, based on the Nataf transformation. New sensitivities in the standard normal space have also been developed, under the restrictive assumption of uncorrelated random inputs.

Sensitivities in reliability assessment are of prime importance in uncertainty propagation. They allow the analyst to gain an insight into the most influential inputs in the system failure. Moreover sensitivities w.r.t. distribution parameters can also be used in gradient-based RBDO approaches if distribution parameters are taken as design parameters, as considered by Dubourg.

Several perspectives concerning sensitivity analysis are envisaged. The first study to carry out is to extend the proposed sensitivities in the standard normal space to the case of correlated inputs. The derivation of global sensitivities in the context of reliability assessment also deserves some attention, in the same spirit as the work carried out by Wei et al. (2012). Such global sensitivities are expected to bring importance measures representative of the full information contained in the input distributions, which can bring an additional insight into system failure. These sensitivities are currently being studied in the scope of the PhD work of Chabridon. Another research direction which can take advantage of sensitivities is the potential dimension reduction of the input space of the reliability problems to solve. Attempts, not reported here, have been made using sensitivities in the standard normal space for a selection “on the fly” of the most important inputs in the ASVR method.

Applications

The applications covered in my work include: buckling of submarine structures, crack propagation in aircraft structural elements, frontal impact of vehicles, electromagnetic compatibility in wire networks, and vehicle dynamics on rough-profile terrains. Problems of practical interest are often high-dimensional, with inputs expressed as random processes or random fields. The efforts in my future works will still be devoted to the development of efficient methods applicable to problems involving large numbers of random inputs. The solutions will undoubtedly rely on surrogate models, as investigated so far, and take advantage of accelerated computing based on GPUs for faster training. Developments in sensitivity analysis are also extremely necessary, in order to shed light on the most influential inputs in the problems of interest. Attention will be paid to epistemic uncertainty due to scarce statistical information on the inputs, a situation which is often met in engineering. Such epistemic uncertainties need to be propagated throughout the system model, in order to quantify their impact on the results obtained in uncertainty propagation analysis.

Bibliography

Abe S. (2010). Two-class support vector machines. In: *Support Vector Machines for Pattern Classification*. Advances in Pattern Recognition. London: Springer, pp. 21–112.

Agarwal H., Mozumder C.K., Renaud J.E., Watson L.T. (2007). An inverse-measure-based unilevel architecture for reliability-based design optimization. *Structural and Multidisciplinary Optimization*, 33(3), pp. 217–227.

Aizerman A., Braverman E.M., Rozonoér L.I. (1964). Theoretical foundations of the potential function method in pattern recognition learning. *Automation and Remote Control*, 25(6), pp. 821–837.

Aliaga D., Davy A., Schaff H. (1988). *A simple crack closure model for predicting fatigue crack growth under flight simulation loading*. ASTM STP-982. American Society for Testing & Materials, pp. 491–504.

Allen D.M. (1974). The relationship between variable selection and data augmentation and a method for prediction. *Technometrics*, 16(1), pp. 125–127.

Altamura A., Straub D. (2014). Reliability assessment of high cycle fatigue under variable amplitude loading: Review and solutions. *Engineering Fracture Mechanics*, 121–122, pp. 40–66.

Annis C. (2017). *How reliable are first order and second order reliability methods?* Statistical Engineering website, available at `https://statistical-engineering.com/form-sorm/`.

Aoues Y., Chateauneuf A. (2010). Benchmark study of numerical methods for reliability-based design optimization. *Structural and Multidisciplinary Optimization*, 41(2), pp. 277–294.

Arbocz J. (1982). Buckling of Shells: Proceedings of a State-of-the-Art Colloquium, Universität Stuttgart, Germany, May 6–7, 1982. In: ed. by E. Ramm. Springer Berlin Heidelberg. Chap. The imperfection data bank, a mean to obtain realistic buckling loads, pp. 535–567.

Arbocz J., Babcock C.D. (1969). The effect of general imperfections on the buckling of cylindrical shells. *Journal of Applied Mechanics*, 36(1), pp. 28–38.

Arbocz J., Hilburger M.W. (2005). Toward a probabilistic preliminary design criterion for buckling critical composite shells. *AIAA Journal*, 43(8), pp. 1823–1827.

Arbocz J., Hol J.M.A.M. (1995). Collapse of axially compressed cylindrical shells with random imperfections. *Thin-Walled Structures*, 23(1–4), pp. 131–158.

Argyris J., Papadrakakis M., Stefanou G. (2002). Stochastic finite element analysis of shells. *Computer Methods in Applied Mechanics and Engineering*, 191(41–42), pp. 4781–4804.

Arlot S., Celisse A. (2010). A survey of cross-validation procedures for model selection. *Statistics Surveys*, 4, pp. 40–79.

Arnold D.V., Hansen N. (2012). A (1+1)-CMA-ES for Constrained Optimisation. In: *Proc. of the 14th Annual Conference on Genetic and Evolutionary Computation (GECCO'12), Philadelphia, PA, USA, July 07–11, 2012*. ACM, pp. 297–304.

Aronszajn N. (1950). Theory of reproducing kernels. *Transactions of the American Mathematical Society*, 68(3), pp. 337–404.

Au S.-K. (2005). Reliability-based design sensitivity by efficient simulation. *Computers & Structures*, 83(14), pp. 1048–1061.

Au S.-K. (2007). Augmenting approximate solutions for consistent reliability analysis. *Probabilistic Engineering Mechanics*, 22(1), pp. 77–87.

Au S.-K., Beck J.L. (1999). A new adaptive importance sampling scheme for reliability calculations. *Structural Safety*, 21(2), pp. 135–158.

Au S.-K., Beck J.L. (2001). Estimation of small failure probabilities in high dimensions by subset simulation. *Probabilistic Engineering Mechanics*, 16(4), pp. 263–277.

Au S.-K., Beck J.L. (2003). Important sampling in high dimensions. *Structural Safety*, 25(2), pp. 139–163.

Audet C., Denni J., Moore D., Booker A., Frank P. (2000). A surrogate-model-based method for constrained optimization. In: *Proc. 8th Symposium on Multidisciplinary Analysis and Optimization Conferences, Long Beach, CA, USA, September 6–8, 2000*. American Institute of Aeronautics and Astronautics.

Auffray Y., Barbillon P. (2009). *Conditionally positive definite kernels: theoretical contribution, application to interpolation and approximation*. Rapport de Recherche 6835, INRIA.

Bach F. (2009). *High-dimensional non-linear variable selection through hierarchical kernel learning*. Technical Report 0909.0844.

Bach F.R., Thibaux R., Jordan M.I. (2005). Computing regularization paths for learning multiple kernels. In: *Advances in Neural Information Processing Systems 17*. Ed. by L.K. Saul, Y. Weiss, L. Bottou. MIT Press, pp. 73–80.

Bachoc F. (2013). Cross validation and maximum likelihood estimations of hyper-parameters of Gaussian processes with model misspecification. *Computational Statistics & Data Analysis*, 66, pp. 55–69.

Baguet S. (2001). Stabilité des structures minces et sensibilité aux imperfections par la méthode asymptotique numérique. PhD thesis (in French). Université d'Aix-Marseille II, Marseille, France.

Balesdent M., Morio J., Marzat J. (2013). Kriging-based adaptive importance sampling algorithms for rare event estimation. *Structural Safety*, 44, pp. 1–10.

Basudhar A. (2011). Computational optimal design and uncertainty quantification of complex systems using explicit decision boundaries. PhD thesis. University of Arizona, USA.

Basudhar A., Missoum S. (2010). An improved adaptive sampling scheme for the construction of explicit boundaries. *Structural and Multidisciplinary Optimization*, 42(4), pp. 517–529.

Basudhar A., Missoum S., Harrison Sanchez A. (2008). Limit state function identification using support vector machines for discontinuous responses and disjoint failure domains. *Probabilistic Engineering Mechanics*, 23(1), pp. 1–11.

Bažant Z.P. (2000). Stability of elastic, anelastic, and disintegrating structures: a conspectus of main results. *ZAMM - Journal of Applied Mathematics and Mechanics / Zeitschrift für Angewandte Mathematik und Mechanik*, 80(11-12), pp. 709–732.

Beck A.T., Gomes W.J.d.S. (2012). A comparison of deterministic, reliability-based and risk-based structural optimization under uncertainty. *Probabilistic Engineering Mechanics*, 28, pp. 18–29.

Beck A.T., Melchers R.E. (2004). Overload failure of structural components under random crack propagation and loading - a random process approach. *Structural Safety*, 26(4), pp. 471–488.

Bect J., Ginsbourger D., Li L., Picheny V., Vazquez E. (2012). Sequential design of computer experiments for the estimation of a probability of failure. *Statistics and Computing*, 22(3), pp. 773–793.

Bellman R.E. (1961). *Adaptive control processes: a guided tour*. Princeton University Press.

Berveiller M., Sudret B., Lemaire M. (2006). Stochastic finite element: a non intrusive approach by regression. *European Journal of Computational Mechanics*, 15(1–3), pp. 81–92.

Beyer H.-G., Sendhoff B. (2007). Robust optimization - a comprehensive survey. *Computer Methods in Applied Mechanics and Engineering*, 196(33), pp. 3190–3218.

Bichon B.J., Eldred M.S., Swiler L.P., Mahadevan S., McFarland J.M. (2008). Efficient global reliability analysis for nonlinear implicit performance functions. *AIAA Journal*, 46(10), pp. 2459–2468.

Bichon B.J., Eldred M.S., Mahadevan S., McFarland J.M. (2012). Efficient global surrogate modeling for reliability-based design optimization. *Journal of Mechanical Design*, 135(1), p. 011009.

Bichon B.J., Mahadevan S., Eldred M.S. (2010). Reliability-based design optimization using efficient global reliability analysis. In: *Proc. 50th AIAA/ASME/ASCE/AHS/ASC Structures, Structural Dynamics, and Materials Conference, Palm Springs, CA, USA, May 4–7, 2009*.

Bichon B.J., McFarland J.M., Mahadevan S. (2011). Efficient surrogate models for reliability analysis of systems with multiple failure modes. *Reliability Engineering & System Safety*, 96(10), pp. 1386–1395.

Blatman G. (2009). Adaptive sparse polynomial chaos expansions for uncertainty propagation and sensitivity analysis. PhD thesis. Université Blaise Pascal, Clermont Ferrand, France.

Blatman G., Sudret B. (2009). Anisotropic parcimonious polynomial chaos expansions based on the sparsity-of-effects principle. In: *Proc. 10th International Conference on Structural Safety and Reliability (ICOSSAR 2009), Osaka, Japan, September 13–17, 2009*. Ed. by H. Furuta, D.M. Frangopol, M. Shinozuka. CRC Press.

Blatman G., Sudret B. (2010). An adaptive algorithm to build up sparse polynomial chaos expansions for stochastic finite element analysis. *Probabilistic Engineering Mechanics*, 25(2), pp. 183–197.

Blatman G., Sudret B. (2011). Adaptive sparse polynomial chaos expansion based on least angle regression. *Journal of Computational Physics*, 230(6), pp. 2345–2367.

De Boer P.-T., Kroese D.P., Mannor S., Rubinstein R.Y. (2005). A tutorial on the cross-entropy method. *Annals of Operations Research*, 134(1), pp. 19–67.

Bolotin V.V. (1962). *Statistical method in the nonlinear theory of elastic shell*. NASA TT F-85, pp. 1–16.

Bompard M. (2011). Modèles de substitution pour l'optimisation globale de forme en aérodynamique et méthode locale sans paramétrisation. PhD thesis (in French). Université Nice Sophia Antipolis, Nice, France.

Borwein J.M., Lewis A.S. (2000). *Convex analysis and nonlinear optimization : theory and examples*. CMS Books in Mathematics. New York: Springer.

Boser B.E., Guyon I.M., Vapnik V.N. (1992). A training algorithm for optimal margin classifiers. In: *Proc. 5th Annual Workshop on Computational Learning Theory (COLT'92), Pittsburgh, PA, USA, July 27–29, 1992*. ACM Press, pp. 144–152.

Botev Z.I., Kroese D.P. (2012). Efficient Monte Carlo simulation via the generalized splitting method. *Statistics and Computing*, 22(1), pp. 1–16.

Botev Z.I., Kroese D.P., Rubinstein R.Y., L'Ecuyer P. (2013). Chapter 3 - The cross-entropy method for optimization. In: *Handbook of Statistics - Machine Learning: Theory and Applications*. Ed. by C.R. Rao, V. Govindaraju. Vol. 31. Handbook of Statistics. Elsevier, pp. 35–59.

Botev Z.I., Kroese D.P., Taimre T. (2007). Generalized cross-entropy methods with applications to rare-event simulation and optimization. *Simulation*, 83(11), pp. 785–806.

Botev Z.I., L'Ecuyer P. (2011). Semi-parametric importance sampling for rare-event probability estimation. In: *Proc. 8th IMACS Seminar on Monte Carlo Methods, Borovets, Bulgaria, August 29–September 2, 2011*. Ed. by K. Sabelfeld, I. Dimov. De Gruyter.

Bottou L., Lin C.-J. (2007). Support vector machine solvers. In: *Large Scale Kernel Machines*. Ed. by L. Bottou, O. Chapelle, D. DeCoste, J. Weston. Cambridge, MA, USA: MIT Press, pp. 301–320.

Bourinet J.-M. (2014). Reliability assessment with sensitivity-based adaptive SVM surrogates. In: *Proc. 11th International Conference on Structural Safety and Reliability (ICOSSAR 2013), New York, NY, USA, June 16–20, 2013*. Ed. by G. Deodatis, B.R. Ellingwood, D.M. Frangopol. CRC Press, pp. 3297–3304. (8 pages).

Bourinet J.-M. (2015). Reliability assessment with adaptive surrogates based on support vector machine regression. In: *Proc. 1st International Conference on Uncertainty Quantification in Computational Sciences and Engineering (UNCECOMP 2015), Hersonissos, Crete Island, Greece, May 25–27, 2015*. Ed. by M. Papadrakakis, V. Papadopoulos, G. Stefanou, pp. 652–663. (12 pages).

Bourinet J.-M. (2016). Rare-event probability estimation with adaptive support vector regression surrogates. *Reliability Engineering & System Safety*, 150, pp. 210–221.

Bourinet J.-M. (2017a). In: *Risk and reliability analysis: theory and applications*. Ed. by P. Gardoni. Springer Series in Reliability Engineering. Edited Volume in Honor of Prof. Armen Der Kiureghian. Springer International Publishing. Chap. 12: FORM sensitivities to distribution parameters with the Nataf transformation, pp. 277–302. (26 pages).

Bourinet J.-M. (2017b). Anisotropic-kernel-based support vector regression for reliability assessment. In: *Proc. 12th International Conference on Structural Safety and Reliability (ICOSSAR 2017), Vienna, Austria, August 6–10, 2017*. TU Verlag. (10 pages).

Bourinet J.-M., Deheeger F., Lemaire M. (2011). Assessing small failure probabilities by combined subset simulation and support vector machines. *Structural Safety*, 33(6), pp. 343–353.

Bourinet J.-M., Gayton N., Lemaire M., Combescure A. (2000). Reliability analysis of stability of shells based on combined finite element and response surface methods. In: *Proc. 4th International Colloquium on Computation of Shell & Spatial Structures (IASS-IACM 2000), Chania, Crete, Greece, June 5–7, 2000*. Ed. by M. Papadrakakis, A. Samartin, E. Oñate. (20 pages).

Bourinet J.-M., Lemaire M. (2008). FORM sensitivities to correlation: application to fatigue crack propagation based on Virkler data. In: *Proc. 4th International ASRANet Colloquium, Athens, Greece, June 25–27, 2008*. Ed. by P.K. Das. (10 pages).

Bourinet J.-M., Mattrand C. (2013). Damage tolerance and reliability assessment under random Markovian loads. In: *Procedia IUTAM*. Ed. by C. Proppe, J.-M. Bourinet. Vol. 6. IUTAM Symposium on Multiscale Problems in Stochastic Mechanics, Karlsruhe, Germany, June 25–29, 2012. Elsevier, pp. 123–131. (9 pages).

Bourinet J.-M., Mattrand C., Dubourg V. (2009). A review of recent features and improvements added to FERUM software. In: *Proc. 10th International Conference on Structural Safety and Reliability (ICOSSAR 2009), Osaka, Japan, September 13–17, 2009*. Ed. by H. Furuta, D.M. Frangopol, M. Shinozuka. CRC Press. (8 pages).

Boutyour E.H., Cochelin B., Potier-Ferry M. (1995). Détection des bifurcations par des méthodes asymptotiques-numériques. In: *Proc. 2ème Colloque National en Calcul des Structures, Giens, France, 16–19 mai 1995*. 2, pp. 687–692.

Box G.E.P., Draper N.R. (1987). *Empirical model-building and response surface*. Wiley Series in Probability and Statistics. New York, NY, USA: John Wiley & Sons.

Boyd S., Vandenberghe L. (2004). *Convex optimization*. Cambridge University Press.

Breitung K. (1984). Asymptotic approximations for multinormal integrals. *Journal of Engineering Mechanics*, 110(3), pp. 357–366.

Broggi M., Schuëller G.I. (2011). Efficient modeling of imperfections for buckling analysis of composite cylindrical shells. *Engineering Structures*, 33(5), pp. 1796–1806.

Broomhead D.S., Lowe D. (1988). Multivariable functional interpolation and adaptative networks. *Complex Systems*, 2(3), pp. 321–355.

BS5500 (1997). *Unfired fusion-welded pressure vessels*. British Standard Institutions. BS5500.

Bucher C.G. (1988). Adaptive sampling - an iterative fast Monte Carlo procedure. *Structural Safety*, 5(2), pp. 119–126.

Bucher C.G., Bourgund U. (1990). A fast and efficient response surface approach for structural reliability problems. *Structural Safety*, 7(1), pp. 57–66.

Bucher C., Most T. (2008). A comparison of approximate response functions in structural reliability analysis. *Probabilistic Engineering Mechanics*, 23(2–3). 5th International Conference on Computational Stochastic Mechanics, pp. 154–163.

Büchter N., Ramm E., Roehl D. (1994). Three-dimensional extension of non-linear shell formulation based on the enhanced assumed strain concept. *International Journal for Numerical Methods in Engineering*, 37(15), pp. 2551–2568.

Cadini F., Santos F., Zio E. (2014). An improved adaptive kriging-based importance technique for sampling multiple failure regions of low probability. *Reliability Engineering & System Safety*, 131, pp. 109–117.

Cancela H., El Khadiri M., Rubino G. (2009). Rare event analysis by Monte Carlo techniques in static models. In: *Rare Event Simulation using Monte Carlo Methods*. Ed. by G. Rubino, B. Tuffin. John Wiley & Sons, pp. 145–170.

Cappé O., Moulines E., Rydén T. (2005). *Inference in hidden Markov models*. Springer Series in Statistics. New York, NY, USA: Springer, pp. 161–208.

Cardoso J.B., de Almeida J.R., Dias J.M., Coelho P.G. (2008). Structural reliability analysis using Monte Carlo simulation and neural networks. *Advances in Engineering Software*, 39(6), pp. 505–513.

Casciati F., Colombi P., Faravelli L. (2007). Inherent variability of an experimental crack growth curve. *Structural Safety*, 29(1), pp. 66–76.

Cawley G.C., Talbot N., Chapelle O. (2006). Estimating predictive variances with kernel ridge regression. In: *Machine Learning Challenges. Evaluating Predictive Uncertainty, Visual Object Classification, and Recognising Tectual Entailment*. Ed. by J. Quiñonero-Candela, I. Dagan, B. Magnini, F. d'Alché-Buc. Vol. 3944. Lecture Notes in Computer Science. Springer Berlin Heidelberg, pp. 56–77.

Cérou F., Del Moral P., Furon T., Guyader A. (2012). Sequential Monte Carlo for rare event estimation. *Statistics and Computing*, 22(3), pp. 795–808.

Cérou F., Guyader A. (2007). Adaptive multilevel splitting for rare event analysis. *Stochastic Analysis and Applications*, 25(2), pp. 417–443.

Chan J.C.C., Glynn P.W., Kroese D.P. (2011). A comparison of cross-entropy and variance minimization strategies. *Journal of Applied Probability*, 48A, pp. 183–194.

Chan J.C.C., Kroese D.P. (2012). Improved cross-entropy method for estimation. *Statistics and Computing*, 22(5), pp. 1031–1040.

Chang C.-C., Lin C.-J. (2011). LIBSVM: a library for support vector machines. *ACM Transactions on Intelligent Systems and Technology*, 2 (3). Software available at `http://www.csie.ntu.edu.tw/~cjlin/libsvm`, 27:1–27:27.

Chang M.-W., Lin C.-J. (2005). Leave-one-out bounds for support vector regression model selection. *Neural Computation*, 17(5), pp. 1188–1222.

Chapelle O. (2004). Support vector machines: principes d'induction, réglage automatique et connaissances a priori. PhD thesis. Université Pierre et Marie Curie - Paris VI, Paris, France.

Chapelle O. (2007). Training a support vector machine in the primal. *Neural Computation*, 19(5), pp. 1155–1178.

Chapelle O., Vapnik V., Bousquet O., Mukherjee S. (2002). Choosing multiple parameters for support vector machines. *Machine Learning*, 46(1–3), pp. 131–159.

Chateauneuf A., Aoues Y. (2008). Advances in solution methods for reliability-based design optimization. In: *Structural Design Optimization Considering Uncertainties*. Ed. by Y. Tsompanakis, N.D. Lagaros, M. Papadrakakis. CRC Press. Chap. 9, pp. 217–246.

Chen K.-Y. (2007). Forecasting systems reliability based on support vector regression with genetic algorithms. *Reliability Engineering & System Safety*, 92(4), pp. 423–432.

Chen V.C.P., Tsui K.-L., Barton R.R., Meckesheimer M. (2006). A review on design, modeling and applications of computer experiments. *IIE Transactions*, 38(4), pp. 273–291.

Chen X., Hasselman T.K., Neill D.J. (1997). Reliability based structural design optimization for practical applications. In: *Proc. 38th AIAA/ASME/ASCE/AHS/ASC Structures, Structural Dynamics, and Materials Conference, Kissimmee, FL, USA, April 7–10, 1997*.

Cheng G., Xu L., Jiang L. (2006). A sequential approximate programming strategy for reliability-based structural optimization. *Computers & Structures*, 84(21), pp. 1353–1367.

Cheng J., Li Q. (2008). Reliability analysis of structures using artificial neural network based genetic algorithms. *Computer Methods in Applied Mechanics and Engineering*, 197(45–48), pp. 3742–3750.

Cherkassky V., Ma Y. (2004). Practical selection of SVM parameters and noise estimation for SVM regression. *Neural Networks*, 17(1), pp. 113–126.

Chevalier C. (2013). Fast uncertainty reduction strategies relying on Gaussian process models. PhD thesis. University of Bern, Switzerland.

Chevalier C., Bect J., Ginsbourger D., Vazquez E., Picheny V., Richet Y. (2014). Fast parallel kriging-based stepwise uncertainty reduction with application to the identification of an excursion set. *Technometrics*, 56(4), pp. 455–465.

Chib S., Greenberg E. (1995). Understanding the Metropolis-Hastings algorithm. *The American Statistician*, 49(4), pp. 327–335.

Chilès J.-P., Delfiner P. (2012). *Geostatistics: modeling spatial uncertainty*. 2nd ed. Wiley Series in Probability and Statistics. John Wiley & Sons.

Choi K.K., Youn B.D., Yang R.-J. (2001). Moving least square method for reliability-based design optimization. In: *Proc. 4th World Congress of Structural and Multidisciplinary Optimization, Dalian, China, June 4–8, 2001*.

Choi S.-K., Grandhi R.V., Canfield R.A. (2004). Structural reliability under non-Gaussian stochastic behavior. *Computers & Structures*, 82(13–14). Advances in Probabilistic Mechanics and Structural Reliability, pp. 1113–1121.

Chopin N. (2002). A sequential particle filter method for static models. *Biometrika*, 89(3), pp. 539–552.

Chowdhury R., Rao B.N. (2009a). Assessment of high dimensional model representation techniques for reliability analysis. *Probabilistic Engineering Mechanics*, 24(1), pp. 100–115.

Chowdhury R., Rao B.N. (2009b). Hybrid high dimensional model representation for reliability analysis. *Computer Methods in Applied Mechanics and Engineering*, 198(5–8), pp. 753–765.

Chowdhury R., Rao B.N., Prasad A.M. (2009). High-dimensional model representation for structural reliability analysis. *Communications in Numerical Methods in Engineering*, 25(4), pp. 301–337.

Chryssanthopoulos M.K., Poggi C. (1995). Stochastic imperfection modelling in shell buckling studies. *Thin-Walled Structures*, 23(1–4), pp. 179–200.

Chung K.-M., Kao W.-C., Sun C.-L., Wang L.-L., Lin C.-J. (2003). Radius margin bounds for support vector machines with the RBF kernel. *Neural Computation*, 15(11), pp. 2643–2681.

Clarke S.M., Griebsch J.H., Simpson T.W. (2004). Analysis of support vector regression for approximation of complex engineering analyses. *Journal of Mechanical Design*, 127(6), pp. 1077–1087.

Cochelin B. (1994). A path-following technique via an asymptotic-numerical method. *Computers & Structures*, 53(5), pp. 1181–1192.

Cohen S., Intrator N. (2000). *Global optimization of RBF networks*. Preprint.

Cohn D.A. (1996). Neural network exploration using optimal experiment design. *Neural Networks*, 9(6), pp. 1071–1083.

Cohn D., Atlas L., Ladner R. (1994). Improving generalization with active learning. *Machine Learning*, 15(2), pp. 201–221.

Cortes C., Vapnik V. (1995). Support-vector networks. *Machine Learning*, 20(3), pp. 273–297.

Couckuyt I., Dhaene T., Demeester P. (2014). ooDACE toolbox: a flexible object-oriented kriging implementation. *Journal of Machine Learning Research*, 15, pp. 3183–3186.

Craig K.J., Roux W.J. (2008). On the investigation of shell buckling due to random geometrical imperfections implemented using Karhunen-Loève expansions. *International Journal for Numerical Methods in Engineering*, 73(12), pp. 1715–1726.

Craig K.J., Stander N. (2007). Optimization of shell buckling incorporating Karhunen-Loève-based geometrical imperfections. *Structural and Multidisciplinary Optimization*, 37(2), pp. 185–194.

Cressie N.A.C. (1993). *Statistics for spatial data*. John Wiley & Sons.

Cristianini N., Shawe-Taylor J. (2000). *An introduction to support vector machines and other kernel-based learning methods*. New York, NY, USA: Cambridge University Press.

Dai H., Zhang H., Wang W. (2012a). A support vector density-based importance sampling for reliability assessment. *Reliability Engineering & System Safety*, 106, pp. 86–93.

Dai H., Zhang H., Wang W., Xue G. (2012b). Structural reliability assessment by local approximation of limit state functions using adaptive Markov chain simulation and support vector regression. *Computer-Aided Civil and Infrastructure Engineering*, 27(9), pp. 676–686.

Damil N., Potier-Ferry M. (1990). A New method to compute perturbed bifurcations: Application to the buckling of imperfect elastic structures. *International Journal of Engineering Science*, 28(9), pp. 943–957.

Das P.K., Zheng Y. (2000). Cumulative formation of response surface and its use in reliability analysis. *Probabilistic Engineering Mechanics*, 15(4), pp. 309–315.

Davison A.C., Smith R.L. (1990). Models for exceedances over high thresholds. *Journal of the Royal Statistical Society. Series B (Methodological)*, 52(3), pp. 393–442.

Davy A. (1985). Modélisation de la fissuration en fatigue sous chargements d'amplitude variable. Application aux spectres d'avions civils. PhD thesis (in French). Université Technologique de Compiègne, Compiègne, France.

De Stefano M., Der Kiureghian A. (1990). *An efficient algorithm for second-order reliability analysis*. Report No. UCB/SEMM-90/20. Dept of Civil and Environmental Engineering, University of California, Berkeley.

Deheeger F. (2008). ^{2}SMART - Méthodologie d'apprentissage stochastique en fiabilité. PhD thesis (in French). Université Blaise Pascal, Clermont Ferrand, France.

Deheeger F., Lemaire M. (2006). Reliability analysis by support vector machine classification. In: *Proc. 3rd ASRANet International Colloquium, Glasgow, UK, July 10–12, 2006*. Ed. by P.K. Das, M.K. Chryssanthopoulos. ASRANet Ltd.

Del Moral P., Doucet A., Jasra A. (2006). Sequential Monte Carlo samplers. *Journal of the Royal Statistical Society: Series B (Statistical Methodology)*, 68(3), pp. 411–436.

Deng J. (2006). Structural reliability analysis for implicit performance function using radial basis function network. *International Journal of Solids and Structures*, 43(11–12), pp. 3255–3291.

Deng J., Gu D., Li X., Yue Z.Q. (2005). Structural reliability analysis for implicit performance functions using artificial neural network. *Structural Safety*, 27(1), pp. 25–48.

Der Kiureghian A. (1999). *Introduction to structural reliability*. CE229 class notes. Dept of Civil and Environmental Engineering, University of California, Berkeley, USA.

Der Kiureghian A., Dakessian T. (1998). Multiple design points in first and second-order reliability. *Structural Safety*, 20(1), pp. 37–49.

Der Kiureghian A., Haukaas T., Fujimura K. (2006). Structural reliability software at the University of California, Berkeley. *Structural Safety*, 28(1), pp. 44–67.

Der Kiureghian A., Lin H.-Z., Hwang S.-J. (1987). Second-order reliability approximations. *Journal of Engineering Mechanics*, 113(8), pp. 1208–1225.

Der Kiureghian A., Polak E. (1998). Reliability-based optimal design: a decoupled approach. In: *Proc. 8th IFIP WG 7.5 Working Conference on Reliability and Optimization of Structural Systems, Cracow, Poland, May 11–13, 1998*. Ed. by A.S. Nowak. Book Crafters Chelsea, MI, USA, pp. 197–205.

Der Kiureghian A., Zhang Y., Li C.-C. (1994). Inverse reliability problem. *Journal of Engineering Mechanics*, 120(5), pp. 1154–1159.

Ditlevsen O., Madsen H.O. (2007). *Structural reliability methods*. Internet Edition 2.3.7.

Ditlevsen O., Olesen R. (1986). Statistical analysis of the Virkler data on fatigue crack growth. *Engineering Fracture Mechanics*, 25(2), pp. 177–195.

Doltsinis I., Kang Z. (2004). Robust design of structures using optimization methods. *Computer Methods in Applied Mechanics and Engineering*, 193(23), pp. 2221–2237.

Domínguez J., Zapatero J. (1992). Effect of the loading spectrum and history length on fatigue life distribution under random loading. *Engineering Fracture Mechanics*, 42(6), pp. 925–933.

Dominguez J., Zapatero J., Pascual J. (1997). Effect of load histories on scatter of fatigue crack growth in aluminum alloy 2024-T351. *Engineering Fracture Mechanics*, 56(1), pp. 6–76.

Doucet A., de Freitas N., Gordon N., eds. (2001). *Sequential Monte Carlo methods in practice*. Statistics for Engineering and Information Science. New York, NY, USA: Springer New York.

Drucker H., Burges C.J.C., Kaufman L., Smola A., Vapnik V. (1997). Support vector regression machines. In: *Advances in Neural Information Processing Systems 9*. Ed. by M. Mozer, M. Jordan, T. Petsche. MIT Press, pp. 155–161.

Du X., Chen W. (2004). Sequential optimization and reliability assessment method for efficient probabilistic design. *Journal of Mechanical Design*, 126(2), pp. 225–233.

Dubourg V. (2011). Adaptive surrogate models for reliability analysis and reliability-based design optimization. PhD thesis. Université Blaise Pascal, Clermont Ferrand, France.

Dubourg V., Bourinet J.-M., Sudret B. (2009a). Analyse fiabiliste du flambage des coques avec prise en compte du caractère aléatoire et de la variabilité spatiale des défauts de forme et d'épaisseur, et des propriétés matériaux. In: *Proc. 19ème Congrès Français de Mécanique (CFM19), Marseille, France, 24–28 août 2009*. Ed. by C. Rey, P. Bontoux, A. Chrisochoos. Association Française de Mécanique. (6 pages).

Dubourg V., Bourinet J.-M., Sudret B. (2017). Reliability-based design optimization of shells with uncertain geometry using adaptive kriging metamodels. *ArXiv e-prints*.

Dubourg V., Noirfalise C., Bourinet J.-M. (2008). Reliability-based design optimization: an application to the buckling of imperfect shells. In: *Proc. 4th International ASRANet Colloquium, Athens, Greece, June 25–27, 2008*. Ed. by P.K. Das. (10 pages).

Dubourg V., Noirfalise C., Bourinet J.-M., Fogli M. (2009b). FE-based reliability analysis of the buckling of shells with random shape, material and thickness imperfections. In: *Proc. 10th International Conference on Structural Safety and Reliability (ICOSSAR 2009), Osaka, Japan, September 13–17, 2009*. Ed. by H. Furuta, D.M. Frangopol, M. Shinozuka. CRC Press. (8 pages).

Dubourg V., Sudret B. (2014). Meta-model-based importance sampling for reliability sensitivity analysis. *Structural Safety*, 49. Special Issue In Honor of Prof. Wilson H. Tang, pp. 27–36.

Dubourg V., Sudret B., Bourinet J.-M. (2011). Reliability-based design optimization using kriging surrogates and subset simulation. *Structural and Multidisciplinary Optimization*, 44(5), pp. 673–690.

Dubourg V., Sudret B., Deheeger F. (2013). Metamodel-based importance sampling for structural reliability analysis. *Probabilistic Engineering Mechanics*, 33, pp. 47–57.

Dubrule O. (1983). Cross validation of kriging in a unique neighborhood. *Journal of the International Association for Mathematical Geology*, 15(6), pp. 687–699.

Dyn N., Levin D., Rippa S. (1986). Numerical procedures for surface fitting of scattered data by radial functions. *SIAM Journal on Scientific and Statistical Computing*, 7(2), pp. 639–659.

Echard B., Gayton N., Lemaire M. (2011). AK-MCS: An active learning reliability method combining kriging and Monte Carlo simulation. *Structural Safety*, 33(2), pp. 145–154.

Echard B., Gayton N., Lemaire M., Relun N. (2013). A combined importance sampling and kriging reliability method for small failure probabilities with time-demanding numerical models. *Reliability Engineering & System Safety*, 111, pp. 232–240.

Efron B. (1983). Estimating the error rate of a prediction rule: improvement on cross-validation. *Journal of the American Statistical Association*, 78(382), pp. 316–331.

Efron B., Hastie T., Johnstone I., Tibshirani R. (2004). Least angle regression. *The Annals of Statistics*, 32(2), pp. 407–499.

Elber W. (1971). *The significance of fatigue crack closure*. ASTM STP-486. American Society for Testing & Materials, pp. 230–242.

Elguedj T. (2006). Simulation numérique de la propagation de fissure en fatigue par la méthode des éléments finis étendus : prise en compte de la plasticité et du contact-frottement. PhD thesis (in French). Institut National des Sciences Appliquées de Lyon, Lyon, France.

Elishakoff I. (1979). Simulation of space-random fields for solution of stochastic boundary value problems. *The Journal of the Acoustical Society of America*, 65(2), pp. 399–403.

Elishakoff I. (2012). Probabilistic resolution of the twentieth century conundrum in elastic stability. *Thin-Walled Structures*, 59, pp. 35–57.

Elishakoff I., Arbocz J. (1982). Reliability of axially compressed cylindrical shells with random axisymmetric imperfections. *International Journal of Solids and Structures*, 18(7), pp. 563–585.

Elishakoff I., van Manen S., Vermeulen P.G., Arbocz J. (1987). First-order second-moment analysis of the buckling of shells with random imperfections. *AIAA Journal*, 25(8), pp. 1113–1117.

Enevoldsen I., Faber M.H., Sørensen J.D. (1993). Adaptive response surface techniques in reliability estimation. In: *Proc. 6th International Conference on Structural Safety and Reliability (ICOSSAR '93), Innsbruck, Austria, August 9–13, 1993*. Ed. by M. Shinozuka, G.I. Schuëller, J.T.P. Yao. Balkema Publishers, A.A. / Taylor & Francis The Netherlands, pp. 1257–1264.

Enevoldsen I., Sørensen J.D. (1994). Reliability-based optimization in structural engineering. *Structural Safety*, 15(3), pp. 169–196.

Engelund S., Rackwitz R. (1993). A benchmark study on importance sampling techniques in structural reliability. *Structural Safety*, 12(4), pp. 255–276.

Evgeniou T., Pontil M., Poggio T. (2000). Regularization networks and support vector machines. *Advances in Computational Mathematics*, 13(1), pp. 1–50.

Fan R.-E., Chen P.-H., Lin C.-J. (2005). Working set selection using second order information for training support vector machines. *Journal of Machine Learning Research*, 6, pp. 1889–1918.

Faravelli L. (1989). Response-surface approach for reliability analysis. *Journal of Engineering Mechanics*, 115(12), pp. 2763–2781.

Fei S.-W., Wang M.-J., Miao Y.-B., Tu J., Liu C.-L. (2009). Particle swarm optimization-based support vector machine for forecasting dissolved gases content in power transformer oil. *Energy Conversion and Management*, 50(6), pp. 1604–1609.

Forrester A.I.J., Keane A.J. (2009). Recent advances in surrogate-based optimization. *Progress in Aerospace Sciences*, 45(1–3), pp. 50–79.

Forrester A.I.J., Keane A.J., Bressloff N.W. (2006). Design and analysis of "noisy" computer experiments. *AIAA Journal*, 44(10), pp. 2331–2339.

Friedman J.H. (1991). Multivariate adaptive regression splines. *The Annals of Statistics*, 19(1), pp. 1–67.

Gayton N., Bourinet J.-M., Lemaire M. (2003). CQ2RS: a new statistical approach to the response surface method for reliability analysis. *Structural Safety*, 25(1), pp. 99–121.

Geisser S. (1975). The predictive sample reuse method with applications. *Journal of the American Statistical Association*, 70(350), pp. 320–328.

Geman S., Bienenstock E., Doursat R. (1992). Neural networks and the bias/variance dilemma. *Neural Computation*, 4(1), pp. 1–58.

Genton M.G. (2001). Classes of kernels for machine learning: a statistics perspective. *Journal of Machine Learning Research*, 2, pp. 299–312.

Ghanem R.G., Spanos P.D. (1991). *Stochastic finite elements: a spectral approach*. New York, NY, USA: Springer.

Ghonem H., Dore S. (1987). Experimental study of the constant-probability crack growth curves under constant amplitude loading. *Engineering Fracture Mechanics*, 27(1), pp. 1–25.

Ginsbourger D. (2009). Multiples métamodèles pour l'approximation et l'optimisation de fonctions numériques multivariables. PhD thesis (in French). Ecole des Mines de Saint-Etienne, Saint-Etienne, France.

Ginsbourger D., Dupuy D., Badea A., Carraro L., Roustant O. (2009). A note on the choice and the estimation of kriging models for the analysis of deterministic computer experiments. *Applied Stochastic Models in Business and Industry*, 25(2), pp. 115–131.

Ginsbourger D., Le Riche R., Carraro L. (2010). Kriging is well-suited to parallelize optimization. In: *Computational Intelligence in Expensive Optimization Problems*. Ed. by Y. Tenne, C.-K. Goh. Berlin, Heidelberg: Springer, pp. 131–162.

Girosi F. (1998). An equivalence between sparse approximation and support vector machines. *Neural Computation*, 10(6), pp. 1455–1480.

Girosi F., Jones M., Poggio T. (1995). Regularization theory and neural networks architectures. *Neural Computation*, 7(2), pp. 219–169.

Goel T., Haftka R.T., Shyy W., Queipo N.V. (2007). Ensemble of surrogates. *Structural and Multidisciplinary Optimization*, 33(3), pp. 199–216.

Gomes H.M., Awruch A.M. (2004). Comparison of response surface and neural network with other methods for structural reliability analysis. *Structural Safety*, 26(1), pp. 49–67.

Gomes W.J.d.S., Beck A.T. (2013). Global structural optimization considering expected consequences of failure and using ANN surrogates. *Computers & Structures*, 126, pp. 56–68.

Guo Z., Bai G. (2009a). Application of least squares support vector machine for regression to reliability analysis. *Chinese Journal of Aeronautics*, 22(2), pp. 160–166.

Guo Z., Bai G. (2009b). Classification using least squares support vector machine for reliability analysis. *Applied Mathematics and Mechanics*, 30(7), pp. 853–864.

Guyader A. (2011). Contributions à l'estimation non paramétrique et à la simulation d'évènements rares. HDR Report (in French). Université Rennes 2, Rennes, France.

Hansen N. (2016). The CMA evolution strategy: a tutorial. *ArXiv e-prints*.

Hardy R.L. (1971). Multiquadric equations of topography and other irregular surfaces. *Journal of Geophysical Research*, 76(8), pp. 1905–1915.

Hasofer A.M., Lind N.C. (1974). Exact and invariant second-moment code format. *Journal of the Engineering Mechanics Division*, 100(1), pp. 111–121.

Hastie T., Tibshirani R., Friedman J. (2009). *The elements of statistical learning*. Springer Series in Statistics. New York, NY, USA: Springer.

Hastings W.K. (1970). Monte Carlo sampling methods using Markov chains and their applications. *Biometrika*, 57(1), pp. 97–109.

Haukaas T., Der Kiureghian A. (2004). *Finite element reliability and sensitivity methods for performance-based earthquake engineering*. PEER Report 2003/14. Pacific Earthquake Engineering Research Center.

Haykin S. (1998). *Neural networks: a comprehensive foundation*. 2nd ed. Upper Saddle River, NJ, USA: Prentice Hall PTR.

Heinrich A. (2012). Fenchel duality-based algorithms for convex optimization problems with applications in machine learning and image restoration. PhD thesis. Chemnitz University of technology, Germany.

Heuler P., Klätschke H. (2005). Generation and use of standardised load spectra and load-time histories. *International Journal of Fatigue*, 27(8), pp. 974–990.

Hoerl A.E., Kennard R.W. (1970). Ridge regression: biased estimation for nonorthogonal problems. *Technometrics*, 12(1), pp. 55–67.

Hofmann T., Schölkopf B., Smola A.J. (2008). Kernel methods in machine learning. *The Annals of Statistics*, 36(3), pp. 1171–1220.

Hohenbichler M., Rackwitz R. (1981). Non-normal dependent vectors in structural safety. *Journal of the Engineering Mechanics Division*, 107(6), pp. 1227–1238.

Hohenbichler M., Rackwitz R. (1986). Sensitivity and importance measures in structural reliability. *Civil Engineering Systems*, 3(4), pp. 203–209.

Hohenbichler M., Rackwitz R. (1988). Improvement of second-order reliability estimates by importance sampling. *Journal of Engineering Mechanics*, 114(12), pp. 2195–2199.

Homem-de-Mello T. (2007). A study on the cross-entropy method for rare-event probability estimation. *INFORMS Journal on Computing*, 19(3), pp. 381–394.

Homem-de-Mello T., Rubinstein R.Y. (2002). *Rare event estimation for static models via cross-entropy and importance sampling*.

Hornik K., Stinchcombe M., White H. (1989). Multilayer feedforward networks are universal approximators. *Neural Networks*, 2(5), pp. 359–366.

Hosni Elhewy A., Mesbahi E., Pu Y. (2006). Reliability analysis of structures using neural network method. *Probabilistic Engineering Mechanics*, 21(1), pp. 44–53.

Hsu C.-W., Chang C.-C., Lin C.-J. (2016). *A practical guide to support vector classification*. Technical Report. Dept of Computer Science, National Taiwan University, Taipei.

Hu C., Youn B.D. (2011). Adaptive-sparse polynomial chaos expansion for reliability analysis and design of complex engineering systems. *Structural and Multidisciplinary Optimization*, 43(3), pp. 419–442.

Huang S.P., Quek S.T., Phoon K.K. (2001). Convergence study of the truncated Karhunen-Loeve expansion for simulation of stochastic processes. *International Journal for Numerical Methods in Engineering*, 52(9), pp. 1029–1043.

Huang X., Chen J., Zhu H. (2016). Assessing small failure probabilities by AK-SS: an active learning method combining kriging and subset simulation. *Structural Safety*, 59, pp. 86–95.

Hurtado J.E. (2004). An examination of methods for approximating implicit limit state functions from the viewpoint of statistical learning theory. *Structural Safety*, 26(3), pp. 271–293.

Hurtado J.E., Alvarez D.A. (2000). Reliability assessment of structural systems using neural networks. In: *Proc. European Congress on Computational Methods in Applied Sciences and Engineering (ECCOMAS 2000), Barcelona, Spain, September 11–14, 2000*. Ed. by E. Oñate, G. Bugeda, B. Suárez.

Hurtado J.E., Alvarez D.A. (2001). Neural-network-based reliability analysis: a comparative study. *Computer Methods in Applied Mechanics and Engineering*, 191(1–2). Micromechanics of Brittle Materials and Stochastic Analysis of Mechanical Systems, pp. 113–132.

Hurtado J.E., Alvarez D.A. (2003). Classification approach for reliability analysis with stochastic finite-element modeling. *Journal of Structural Engineering*, 129(8), pp. 1141–1149.

Ichikawa M. (1987). Probabilistic fracture mechanics investigation of fatigue crack growth rate. In: *Statistical Research on Fatigue and Fracture*. Ed. by T. Tanaka, S. Nishijima, M. Ichikawa. Vol. 2. Current Japanese Materials Research. Elsevier, pp. 71–89.

Jaakkola T., Diekhans M., Haussler D. (1999). Using the Fisher kernel method to detect remote protein homologies. In: *Proc. 7^{th} International Conference on Intelligent Systems for Molecular Biology*. AAAI Press, pp. 149–158.

Jin R., Chen W., Simpson T.W. (2001). Comparative studies of metamodelling techniques under multiple modelling criteria. *Structural and Multidisciplinary Optimization*, 23(1), pp. 1–13.

Jin R., Du X., Chen W. (2003). The use of metamodeling techniques for optimization under uncertainty. *Structural and Multidisciplinary Optimization*, 25(2), pp. 99–116.

Joachims T. (1999). Advances in Kernel Methods. In: ed. by B. Schölkopf, C.J.C. Burges, A.J. Smola. Cambridge, MA, USA: MIT Press. Chap. Making large-scale support vector machine learning practical, pp. 169–184.

Johannesson P. (1999). Rainflow analysis of switching Markov loads. PhD thesis. Mathematical statistics, Centre for Mathematical Sciences, Lund Institute of Technology, Lund, Sweden.

Johansen A.M., Del Moral P., Doucet A. (2005). *Sequential Monte Carlo samplers for rare event estimation*. Technical Report CUED/F-INFENG/543. Dept of Engineering, University of Cambridge, Trumpington.

Johnson M.E., Moore L.M., Ylvisaker D. (1990). Minimax and maximin distance designs. *Journal of Statistical Planning and Inference*, 26(2), pp. 131–148.

Jones D.R. (2001). A taxonomy of global optimization methods based on response surfaces. *Journal of Global Optimization*, 21(4), pp. 345–383.

Jones D.R., Schonlau M., Welch W.J. (1998). Efficient global optimization of expensive black-box functions. *Journal of Global Optimization*, 13(4), pp. 455–492.

De Jonge J.B. (1973). *Additional information about Falstaff*. Technical Report NLR-TR-79056-U. National Aerospace Laboratory (NLR), Amsterdam.

De Jonge J.B., Schütz D., Lowak H. (1973). *A standardized load sequence for flight simulation tests on transport aircraft wing structures*. Technical Report NLR-TR-73029-U. National Aerospace Laboratory (NLR), Amsterdam.

Kahn H., Harris T.E. (1951). Estimation of particle transmission by random sampling. *National Bureau of Standards Applied Mathematics Series*, 12, pp. 27–30.

Kang S.-C., Koh H.-M., Choo J.F. (2010). An efficient response surface method using moving least squares approximation for structural reliability analysis. *Probabilistic Engineering Mechanics*, 25(4), pp. 365–371.

Karamchandani A., Bjerager P., Cornell C.A. (1989). Adaptive importance sampling. In: *Proc. 5th International Conference on Structural Safety and Reliability (ICOSSAR '89), San Francisco, CA, USA, August 7–11, 1989*. Ed. by A.H.-S. Ang, M. Shinozuka, G.I. Schuëller. ASCE, pp. 855–862.

Katafygiotis L.S., Zuev K.M. (2008). Geometric insight into the challenges of solving high-dimensional reliability problems. *Probabilistic Engineering Mechanics*, 23(2–3). 5th International Conference on Computational Stochastic Mechanics, pp. 208–218.

Kaymaz I. (2005). Application of kriging method to structural reliability problems. *Structural Safety*, 27(2), pp. 133–151.

Kaymaz I., McMahon C.A. (2005). A response surface method based on weighted regression for structural reliability analysis. *Probabilistic Engineering Mechanics*, 20(1), pp. 11–17.

Keerthi S.S. (2002). Efficient tuning of SVM hyperparameters using radius/margin bound and iterative algorithms. *Neural Networks, IEEE Transactions on*, 13(5), pp. 1225–1229.

Keerthi S.S., Lin C.-J. (2003). Asymptotic behaviors of support vector machines with Gaussian kernel. *Neural Computation*, 15(7), pp. 1667–1689.

Kim S.-H., Na S.-W. (1997). Response surface method using vector projected sampling points. *Structural Safety*, 19(1). Asian-Pacific Symposium on Structural Reliability and Its Applications, pp. 3–19.

Kimeldorf G.S., Wahba G. (1970). A correspondence between Bayesian estimation on stochastic processes and smoothing by splines. *The Annals of Mathematical Statistics*, 41(2), pp. 495–502.

Kleijnen J.P.C. (2007). Experimental design for sensitivity analysis, optimization, and validation of simulation models. In: *Handbook of Simulation*. John Wiley & Sons, pp. 173–223.

Koiter W.T. (1945). On the stability of elastic equilibrium (in Dutch). PhD thesis. Delft University, Delft, The Netherlands.

Kotulski Z.A. (1998). On efficiency of identification of a stochastic crack propagation. *Archives of Mechanics*, 50(5), pp. 829–847.

Kouassi A. (2017). Propagation d'incertitudes en CEM : Application à l'analyse de fiabilité et de sensibilité de lignes de transmission et d'antennes. Defended on December 18, 2017. PhD thesis (in French). Université Clermont Auvergne, Clermont Ferrand, France.

Kouassi A., Bourinet J.-M., Lalléchère S., Bonnet P., Fogli M. (2016). Reliability and sensitivity analysis of transmission lines in a probabilistic EMC context. *Electromagnetic Compatibility, IEEE Transactions on*, 58(2), pp. 561–572.

Krenk S., Gluver H. (1989). A Markov matrix for fatigue load simulation and rainflow range evaluation. *Structural Safety*, 6(2), pp. 247–258.

Kriegesmann B., Rolfes R., Hühne C., Kling A. (2011). Fast probabilistic design procedure for axially compressed composite cylinders. *Composite Structures*, 93(12), pp. 3140–3149.

Kriegesmann B., Rolfes R., Hühne C., Tessmer J., Arbocz J. (2010). Probabilistic design of axially compressed composite cylinders with geometric and loading imperfections. *International Journal of Structural Stability and Dynamics*, 10(4), pp. 623–644.

Krige D.G. (1951). A statistical approach to some basic mine valuation problems on the witwatersrand. *Journal of the Chemical, Metallurgical and Mining Society of South Africa*, 52(6), pp. 119–139.

Kroese D.P., Porotsky S., Rubinstein R.Y. (2006). The cross-entropy method for continuous multi-extremal optimization. *Methodology and Computing in Applied Probability*, 8(3), pp. 383–407.

Kroese D.P., Taimre T., Botev Z.I. (2011). *Handbook of Monte Carlo methods*. Wiley Series in Probability and Statistics. New York, NY, USA: Wiley.

KSRI (1998). *Etablissement de la méthode de calcul de la stabilité des coques*. Tech. rep. Krylov Shipbuilding Research Institute.

Kullback S., Leibler R.A. (1951). On information and sufficiency. *The Annals of Mathematical Statistics*, 22(1), pp. 79–86.

Kurtz N., Song J. (2013). Cross-entropy-based adaptive importance sampling using Gaussian mixture. *Structural Safety*, 42, pp. 35–44.

Kuschel N., Rackwitz R. (1997). Two basic problems in reliability-based structural optimization. *Mathematical Methods of Operations Research*, 46(3), pp. 309–333.

Lacaze S., Missoum S. (2014). Reliability-based design optimization using kriging and support vector machines. In: *Proc. 11th International Conference on Structural Safety and Reliability (ICOSSAR 2013), New York, NY, USA, June 16–20, 2013*. Ed. by G. Deodatis, B.R. Ellingwood, D.M. Frangopol. CRC Press, pp. 3305–3312.

Lagaros N.D., Papadopoulos V. (2006). Optimum design of shell structures with random geometric, material and thickness imperfections. *International Journal of Solids and Structures*, 43(22–23), pp. 6948–6964.

Lancaster P., Salkauskas K. (1981). Surfaces generated by moving least squares methods. *Mathematics of Computation*, 37(155), pp. 141–158.

Lanckriet G.R.G., De Bie T., Cristianini N., Jordan M.I., Noble W.S. (2004). A statistical framework for genomic data fusion. *Bioinformatics*, 20(16), pp. 2626–2635.

Lataniotis C., Marelli S., Sudret B. (2017). *UQLab user manual – Kriging (Gaussian process modelling)*. Tech. rep. Report UQLab-V1.0-105. Chair of Risk, Safety & Uncertainty Quantification, ETH Zurich.

Lebrun R. (2013). Contributions à la modélisation de la dépendance stochastique. PhD thesis (in English). Université Paris-Diderot - Paris VII, Paris, France.

Lebrun R., Dutfoy A. (2009a). A generalization of the Nataf transformation to distributions with elliptical copula. *Probabilistic Engineering Mechanics*, 24(2), pp. 172–178.

Lebrun R., Dutfoy A. (2009b). Do Rosenblatt and Nataf isoprobabilistic transformations really differ? *Probabilistic Engineering Mechanics*, 24(4), pp. 577–584.

LeCun Y., Bottou L., Orr G.B., Müller K.-R. (1998). Efficient backprop. In: *Neural Networks: Tricks of the Trade*. Ed. by G.B. Orr, K.-R. Müller. Springer Berlin Heidelberg, pp. 9–50.

Lee I., Choi K.K., Noh Y., Zhao L., Gorsich D. (2011a). Sampling-based stochastic sensitivity analysis using score functions for RBDO problems with correlated random variables. *Journal of Mechanical Design*, 133(2), p. 021003.

Lee I., Choi K.K., Zhao L. (2011b). Sampling-based RBDO using the stochastic sensitivity analysis and dynamic kriging method. *Structural and Multidisciplinary Optimization*, 44(3), pp. 299–317.

Lee J.-O., Yang Y.-S., Ruy W.-S. (2002). A comparative study on reliability-index and target-performance-based probabilistic structural design optimization. *Computers & Structures*, 80(3), pp. 257–269.

Lelièvre N., Beaurepaire P., Mattrand C., Gayton N., Otsmane A. (2016). On the consideration of uncertainty in design: optimization - reliability - robustness. *Structural and Multidisciplinary Optimization*. Special issue on Physical, Model, and Statistical Uncertainty in Structural and Multidisciplinary Optimization.

Lemaire M., Chateauneuf A., Mitteau J.-C. (2010). *Structural reliability*. ISTE.

Levin D. (1998). The approximation power of moving least-squares. *Mathematics of Computation*, 67(224), pp. 1517–1531.

Li B., Der Kiureghian A. (2016). Accelerating subset simulation with a surrogate model. In: *Proc. 2016 IFIP WG 7.5 Working Conference on Reliability and Optimization of Structural Systems, Pittsburgh, PA, USA, May 18–20, 2016*.

Li H.-s., Lü Z.-z., Yue Z.-f. (2006). Support vector machine for structural reliability analysis. *Applied Mathematics and Mechanics*, 27(10), pp. 1295–1303.

Li J., Li J., Xiu D. (2011). An efficient surrogate-based method for computing rare failure probability. *Journal of Computational Physics*, 230(24), pp. 8683–8697.

Li J., Xiu D. (2010). Evaluation of failure probability via surrogate models. *Journal of Computational Physics*, 229(23), pp. 8966–8980.

Liang J., Mourelatos Z.P., Nikolaidis E. (2007). A single-loop approach for system reliability-based design optimization. *Journal of Mechanical Design*, 129(12), pp. 1215–1224.

Lin S.-W., Lee Z.-J., Chen S.-C., Tseng T.-Y. (2008a). Parameter determination of support vector machine and feature selection using simulated annealing approach. *Applied Soft Computing*, 8(4), pp. 1505–1512.

Lin S.-W., Ying K.-C., Chen S.-C., Lee Z.-J. (2008b). Particle swarm optimization for parameter determination and feature selection of support vector machines. *Expert Systems with Applications*, 35(4), pp. 1817–1824.

Lin Y.K., Yang J.N. (1983). On statistical moments of fatigue crack propagation. *Engineering Fracture Mechanics*, 18(2), pp. 243–256.

Liu H., Ong Y.-S., Cai J. (2017). A survey of adaptive sampling for global metamodeling in support of simulation-based complex engineering design. *Structural and Multidisciplinary Optimization*.

Liu P.-L., Der Kiureghian A. (1986). Multivariate distribution models with prescribed marginals and covariance. *Probabilistic Engineering Mechanics*, 1(2), pp. 105–112.

Liu P.-L., Der Kiureghian A. (1991). Optimization algorithms for structural reliability. *Structural Safety*, 9(3), pp. 161–177.

Lloyd S.P. (1982). Least squares quantization in PCM. *IEEE Transactions on Information Theory*, 28(2), pp. 129–137.

López J. (2011). Analysis and convergence of SMO-like decomposition and geometrical algorithms for support vector machines. PhD thesis. Universidad Autónoma de Madrid, Madrid, Spain.

Lophaven S.N., Nielsen H.B., Søndergaard J. (2002a). *Aspects of the Matlab toolbox DACE*. Technical Report IMM-TR-2002-13. Informatics and Mathematical Modelling, Technical University of Denmark.

Lophaven S.N., Nielsen H.B., Søndergaard J. (2002b). *DACE - A Matlab kriging toolbox*.

MacKay D.J.C. (1992). Information-based objective functions for active data selection. *Neural Computation*, 4(4), pp. 590–604.

Madsen H.O., Hansen P.F. (1992). A comparison of some algorithms for reliability based structural optimization and sensitivity analysis. In: *Proc. 4th IFIP WG 7.5 Working Conference on Reliability and Optimization of Structural Systems, Munich, Germany, September 11–13, 1991*. Ed. by R. Rackwitz, P. Thoft-Christensen. Springer Berlin Heidelberg, pp. 443–451.

Marrel A. (2008). Mise en oeuvre et utilisation du métamodèle processus gaussien pour l'analyse de sensibilité de modèles numériques. PhD thesis (in French). Institut National des Sciences Appliquées de Toulouse, Toulouse, France.

Matheron G. (1963). Principles of geostatistics. *Economic Geology*, 58(8), pp. 1246–1266.

Matheron G. (1973). The intrinsic random functions and their applications. *Advances in Applied Probability*, 5(3), pp. 439–468.

Matías J.M., Vaamonde A., Taboada J., González-Manteiga W. (2004). Support vector machines and gradient boosting for graphical estimation of a slate deposit. *Stochastic Environmental Research and Risk Assessment*, 18(5), pp. 309–323.

Mattera D., Haykin S. (1999). Advances in kernel methods. In: ed. by B. Schölkopf, C.J.C. Burges, A.J. Smola. Cambridge, MA, USA: MIT Press. Chap. Support vector machines for dynamic reconstruction of a chaotic system, pp. 211–241.

Mattrand C. (2011). Approche probabiliste de la tolérance aux dommages - Application au domaine aéronautique. PhD thesis (in French). Université Blaise Pascal, Clermont Ferrand, France.

Mattrand C., Bourinet J.-M. (2011). Random load sequences and stochastic crack growth based on measured load data. *Engineering Fracture Mechanics*, 78(17), pp. 3030–3048.

Mattrand C., Bourinet J.-M. (2014). The cross-entropy method for reliability assessment of cracked structures subjected to random Markovian loads. *Reliability Engineering & System Safety*, 123, pp. 171–182.

Mattrand C., Bourinet J.-M., Lemaire M., Bernard P., Fogli M. (2011a). Modeling and simulation of stochastic fatigue load sequences derived from in-flight load data. In: *Proc. 13th AIAA Non Deterministic Approaches Conference, Denver, CO, USA, April 4–7, 2011*. American Institute of Aeronautics and Astronautics. (17 pages).

Mattrand C., Bourinet J.-M., Théret D. (2011b). Analysis of fatigue crack growth under random load sequences derived from military in-flight load data. In: *Proc. ICAF 2011 Structural Integrity: Influence of Efficiency and Green Imperatives, Montréal, Canada, May 29–30, 2011*. Ed. by J. Komorowski. Springer Netherlands, pp. 399–413. (16 pages).

McKay M.D., Beckman R.J., Conover W.J. (1979). A comparison of three methods for selecting values of input variables in the analysis of output from a computer code. *Technometrics*, 21(2), pp. 239–245.

Medina J.C. (2014). Optimization under uncertainty - Adaptive variance reduction, adaptive metamodeling, and investigation of robustness measures. PhD thesis. University of Notre Dame, USA.

Melchers R.E. (1989a). Importance sampling in structural systems. *Structural Safety*, 6(1), pp. 3–10.

Melchers R.E. (1989b). Improved importance sampling methods for structural system reliability calculation. In: *Proc. 5th International Conference on Structural Safety and Reliability (ICOSSAR '89), San Francisco, CA, USA, August 7–11, 1989*. Ed. by A.H.-S. Ang, M. Shinozuka, G.I. Schuëller. ASCE, pp. 1185–1192.

Melchers R.E. (1990). Search-based importance sampling. *Structural Safety*, 9(2), pp. 117–128.

Metropolis N., Rosenbluth A.W., Rosenbluth M.N., Teller A.H., Teller E. (1953). Equation of state calculations by fast computing machines. *The Journal of Chemical Physics*, 21(6), pp. 1087–1092.

Miao F., Ghosn M. (2011). Modified subset simulation method for reliability analysis of structural systems. *Structural Safety*, 33(4–5), pp. 251–260.

Moës N., Dolbow J., Belytschko T. (1999). A finite element method for crack growth without remeshing. *International Journal for Numerical Methods in Engineering*, 46(1), pp. 131–150.

Mohammadi H., Le Riche R., Durrande N., Touboul E., Bay X. (2017). An analytic comparison of regularization methods for Gaussian processes. *ArXiv e-prints*.

Moreno B., Zapatero J., Domínguez J. (2003). An experimental analysis of fatigue crack growth under random loading. *International Journal of Fatigue*, 25(7), pp. 597–608.

Morio J. (2011). Non-parametric adaptive importance sampling for the probability estimation of a launcher impact position. *Reliability Engineering & System Safety*, 96(1). Special Issue on Safecomp 2008, pp. 178–183.

Morio J. (2012). Extreme quantile estimation with nonparametric adaptive importance sampling. *Simulation Modelling Practice and Theory*, 27, pp. 76–89.

MOSEK ApS (2014). *MOSEK optimization toolbox - Version 7.0*.

Most T. (2007). An adaptive response surface approach for structural reliability analyses based on support vector machines. In: *Proc. 11th International Conference on Civil, Structural and Environmental Engineering Computing, St. Julians, Malta, September 18–21, 2007*. Ed. by B.H.V. Topping. Civil-Comp Press.

Most T., Bucher C. (2006). Adaptive response surface approach using artificial neural networks and moving least squares. In: *Proc. 17th International Conference on the Application of Computer Science and Mathematics in Architecture and Civil Engineering, Weimar, Germany, July 12–14, 2006*. Ed. by K. Gürlebeck, C. Könke.

Moustapha M. (2016). Adaptive surrogate models for the reliable lightweight design of automotive body structures. PhD thesis. Université Blaise Pascal, Clermont Ferrand, France.

Moustapha M., Beck A.T., Bourinet J.-M. (2013). Design-point excitation for crack propagation under narrow-band random loading. *International Journal for Uncertainty Quantification*, 3(6). Special issue dedicated to the 1st International Symposium on Uncertainty Quantification and Stochastic Modeling (Uncertainties 2012), pp. 541–554.

Moustapha M., Bourinet J.-M., Guillaume B., Sudret B. (2018). Comparative study of kriging and support vector regression for structural engineering applications. *ASCE-ASME Journal of Risk and Uncertainty in Engineering Systems, Part A: Civil Engineering*, 4(2), p. 04018005.

Moustapha M., Sudret B., Bourinet J.-M., Guillaume B. (2014). Metamodeling for crashworthiness design: comparative study of kriging and support vector regression. In: *Proc. 2nd International Symposium on Uncertainty Quantification and Stochastic Modeling (Uncertainties 2014), Rouen, France, June 23–27, 2014*. Ed. by M. Lemaire, E. Souza de Cursi, pp. 279–286. (8 pages).

Moustapha M., Sudret B., Bourinet J.-M., Guillaume B. (2016). Quantile-based optimization under uncertainties using adaptive kriging surrogate models. *Structural and Multidisciplinary Optimization*, 54(6). Special issue on Physical, Model, and Statistical Uncertainty in Structural and Multidisciplinary Optimization, pp. 1403–1421.

Myers R.H., Montgomery D.C., Anderson-Cook C.M. (2009). *Response surface methodology: process and product optimization using designed experiments*. 3rd ed. Wiley Series in Probability and Statistics. New York, NY, USA: John Wiley & Sons.

Nataf A. (1962). Détermination des distributions dont les marges sont données. *Comptes Rendus de l'Académie des Sciences*, 225, pp. 42–43.

Neal R.M. (2003). Slice sampling. *The Annals of Statistics*, 31(3), pp. 705–767.

Nelsen R.B. (1999). *An introduction to copulas*. Springer Series in Statistics. New York, NY, USA: Springer.

Nešpůrek L. (2010). Stochastic crack propagation modelling using the extended finite element method. PhD thesis. Université Blaise Pascal, Clermont Ferrand, France & Brno University of Technology, Brno, Czech Republic.

Nguyen X.S., Sellier A., Duprat F., Pons G. (2009). Adaptive response surface method based on a double weighted regression technique. *Probabilistic Engineering Mechanics*, 24(2), pp. 135–143.

Niyogi P. (1995). The informational complexity of learning from examples. PhD thesis. MIT, USA.

Noirfalise C. (2009). Analyse fiabiliste de la stabilité des coques minces avec imperfections par la méthode asymptotique numérique. PhD thesis (in French). Université Blaise Pascal, Clermont Ferrand, France.

Noirfalise C., Bourinet J.-M., Fogli M., Cochelin B. (2007). Reliability assessment of imperfect shells subject to buckling based on the asymptotic numerical method. 9th US National Congress on Computational Mechanics (USNCCM9), San Francisco, CA, USA, July 23–26, 2007.

Noirfalise C., Bourinet J.-M., Fogli M., Cochelin B. (2008). Reliability analysis of the buckling of imperfect shells based on the Karhunen-Loève expansion. 5th European Congress on Computational Methods in Applied Sciences and Engineering (ECCOMAS 2008), Venice, Italy, June 30–July 5, 2008.

Olagnon M. (1994). Practical computation of statistical properties of rainflow counts. *International Journal of Fatigue*, 16(5), pp. 306–314.

Orr G.B., Müller K.-R., eds. (1998). *Neural Networks: Tricks of the Trade*. Vol. 1524. Lecture Notes in Computer Science. Springer Berlin Heidelberg.

Orr M.J.L. (1995). Regularization in the selection of radial basis function centers. *Neural Computation*, 7(3), pp. 606–623.

Osuna E., Freund R., Girosi F. (1997). Training support vector machines: an application to face detection. In: *Proc. 1997 Conference on Computer Vision and Pattern Recognition (CVPR '97), Puerto Rico, June 17–19, 1997*. IEEE Computer Society, pp. 130–136.

Paffrath M., Wever U. (2007). Adapted polynomial chaos expansion for failure detection. *Journal of Computational Physics*, 226(1), pp. 263–281.

Pai P.-F. (2006). System reliability forecasting by support vector machines with genetic algorithms. *Mathematical and Computer Modelling*, 43(3–4), pp. 262–274.

Pai P.-F., Hong W.-C. (2006). Software reliability forecasting by support vector machines with simulated annealing algorithms. *Journal of Systems and Software*, 79(6), pp. 747–755.

Papadopoulos V., Giovanis D.G., Lagaros N.D., Papadrakakis M. (2012). Accelerated subset simulation with neural networks for reliability analysis. *Computer Methods in Applied Mechanics and Engineering*, 223–224, pp. 70–80.

Papadopoulos V., Iglesis P. (2007). The effect of non-uniformity of axial loading on the buckling behaviour of shells with random imperfections. *International Journal of Solids and Structures*, 44(18–19), pp. 6299–6317.

Papadopoulos V., Papadrakakis M. (2005). The effect of material and thickness variability on the buckling load of shells with random initial imperfections. *Computer Methods in Applied Mechanics and Engineering*, 194(12–16). Special Issue on Computational Methods in Stochastic Mechanics and Reliability Analysis, pp. 1405–1426.

Papadopoulos V., Stefanou G., Papadrakakis M. (2009). Buckling analysis of imperfect shells with stochastic non-Gaussian material and thickness properties. *International Journal of Solids and Structures*, 46(14–15), pp. 2800–2808.

Papadrakakis M., Lagaros N.D. (2002). Reliability-based structural optimization using neural networks and Monte Carlo simulation. *Computer Methods in Applied Mechanics and Engineering*, 191(32), pp. 3491–3507.

Papadrakakis M., Papadopoulos V., Lagaros N.D. (1996). Structural reliability analysis of elastic-plastic structures using neural networks and Monte Carlo simulation. *Computer Methods in Applied Mechanics and Engineering*, 136(1), pp. 145–163.

Papaioannou I., Betz W., Zwirglmaier K., Straub D. (2015). MCMC algorithms for subset simulation. *Probabilistic Engineering Mechanics*, 41, pp. 89–103.

Park G.-J., Lee T.-H., Lee K.H., Hwang K.-H. (2006). Robust design: an overview. *AIAA Journal*, 44(1), pp. 181–191.

Perrin G., Soize C., Marque-Pucheu S., Garnier J. (2017). Nested polynomial trends for the improvement of Gaussian process-based predictors. *Journal of Computational Physics*.

Phoon K.K., Huang S.P., Quek S. (2002). Implementation of Karhunen-Loeve expansion for simulation using a wavelet-Galerkin scheme. *Probabilistic Engineering Mechanics*, 17(3), pp. 293–303.

Picheny V., Ginsbourger D., Roustant O., Haftka R.T., Kim N.-H. (2010). Adaptive designs of experiments for accurate approximation of a target region. *Journal of Mechanical Design*, 132(7), pp. 77–85.

Picheny V., Wagner T., Ginsbourger D. (2013). A benchmark of kriging-based infill criteria for noisy optimization. *Structural and Multidisciplinary Optimization*, 48(3), pp. 607–626.

Platt J.C. (1998). *Sequential minimal optimization: a fast algorithm for training support vector machines*. Technical Report MSR-TR-98-14. Microsoft Research.

Poggio T., Girosi F. (1989). *A theory of networks for approximation and learning*. Tech. rep. Cambridge, MA, USA.

Poggio T., Mukherjee S., Rifkin R.M., Raklin A., Verri A. (2002). B. In: *Uncertainty in Geometric Computations*. Ed. by J. Winkler, M. Niranjan. Vol. 704. The Springer International Series in Engineering and Computer Science. Springer US. Chap. 11, pp. 131–141.

Poirion F., Zentner I. (2014). Stochastic model construction of observed random phenomena. *Probabilistic Engineering Mechanics*, 36, pp. 63–71.

Polak E. (1997). *Optimization algorithms and consistent approximations*. Springer.

Pommier S. (2003). Cyclic plasticity and variable amplitude fatigue. *International Journal of Fatigue*, 25(9). International Conference on Fatigue Damage of Structural Materials IV, pp. 983–997.

Pommier S. (2015). Development of an incremental model for fatigue crack growth predictions. *Aerospace Lab*, 9, pp. 1–12.

Pronzato L., Müller W.G. (2012). Design of computer experiments: space filling and beyond. *Statistics and Computing*, 22(3), pp. 681–701.

Proppe C. (2008). Estimation of failure probabilities by local approximation of the limit state function. *Structural Safety*, 30(4), pp. 277–290.

Provan J.W. (1987). *Probabilistic fracture mechanics and reliability*. Springer-Verlag Series Engineering Application of Fracture Mechanics. Dordrecht, The Netherlands: Springer.

Queipo N.V., Haftka R.T., Shyy W., Goel T., Vaidyanathan R., Tucker P.K. (2005). Surrogate-based analysis and optimization. *Progress in Aerospace Sciences*, 41(1), pp. 1–28.

Rabiner L.R. (1989). A tutorial on hidden Markov models and selected applications in speech recognition. *Proceedings of the IEEE*, 77(2), pp. 257–286.

Rabitz H., Aliş Ö., Shorter J., Shim K. (1999). Efficient input-output model representations. *Computer Physics Communications*, 117(1), pp. 11–20.

Rackwitz R. (2001). Reliability analysis – a review and some perspectives. *Structural Safety*, 23(4), pp. 365–395.

Rackwitz R., Fiessler B. (1978). Structural reliability under combined random load sequences. *Computers & Structures*, 9(5), pp. 489–494.

Rajashekhar M.R., Ellingwood B.R. (1993). A new look at the response surface approach for reliability analysis. *Structural Safety*, 12(3), pp. 205–220.

Rakotomamonjy A., Bach F., Canu S., Grandvalet Y. (2007). More efficiency in multiple kernel learning. In: *Proc. 24th International Conference on Machine Learning (ICML 2007), Corvallis, OR, USA, June 20–24, 2007*.

Ramm E., Wall W.A. (2004). Shell structures - a sensitive interrelation between physics and numerics. *International Journal for Numerical Methods in Engineering*, 60(1), pp. 381–427.

Ranjan P., Bingham D., Michailidis G. (2008). Sequential experiment design for contour estimation from complex computer codes. *Technometrics*, 50(4), pp. 527–541.

Rannou V., Brouaye F., Hélier M., Tabbara W. (2002). Kriging the quantile: application to a simple transmission line model. *Inverse Problems*, 18(1), pp. 37–48.

Rasmussen C.E., Williams C.K.I. (2006). *Gaussian processes for machine learning*. 2nd ed. Cambridge, MA, USA: MIT Press.

Rhijnsburger M.P.M. (1999). *The initial imperfection databank at the Delft University of Technology: Part VI*. Report M-867. Faculty of Aerospace Engineering, Delft University of Technology, The Netherlands.

Ridder A. (2005). Importance sampling simulations of Markovian reliability systems using cross-entropy. *Annals of Operations Research*, 134(1), pp. 119–136.

Rifkin R.M., Lippert R.A. (2007). Value regularization and Fenchel duality. *Journal of Machine Learning Research*, 8, pp. 441–479.

Robert C.P., Casella G. (2004). *Monte Carlo statistical methods*. 2nd ed. Springer Texts in Statistics. New York, NY, USA: Springer.

Rocco C.M., Moreno J.A. (2002). Fast Monte Carlo reliability evaluation using support vector machine. *Reliability Engineering & System Safety*, 76(3), pp. 237–243.

Rosenblatt M. (1952). Remarks on a multivariate transformation. *The Annals of Mathematical Statistics*, 23(3), pp. 470–472.

Roussouly N., Petitjean F., Salaun M. (2013). A new adaptive response surface method for reliability analysis. *Probabilistic Engineering Mechanics*, 32, pp. 103–115.

Roustant O., Ginsbourger D., Deville Y. (2012). DiceKriging, DiceOptim: two R packages for the analysis of computer experiments by kriging-based metamodeling and optimization. *Journal of Statistical Software*, 51(1), pp. 1–55.

Royset J.O., Der Kiureghian A., Polak E. (2001). Reliability-based optimal structural design by the decoupling approach. *Reliability Engineering & System Safety*, 73(3), pp. 213–221.

Royset J.O., Der Kiureghian A., Polak E. (2002). *Reliability-based design optimization of series structural systems*. Report No. UCB/SEMM-2002/15. Dept of Civil and Environmental Engineering, University of California, Berkeley.

Royset J.O., Der Kiureghian A., Polak E. (2006). Optimal design with probabilistic objective and constraints. *Journal of Engineering Mechanics*, 132(1), pp. 107–118.

Royset J.O., Polak E. (2004a). Implementable algorithm for stochastic optimization using sample average approximations. *Journal of Optimization Theory and Applications*, 122(1), pp. 157–184.

Royset J.O., Polak E. (2004b). Reliability-based optimal design using sample average approximations. *Probabilistic Engineering Mechanics*, 19(4), pp. 331–343.

Rubinstein R. (1999). The cross-entropy method for combinatorial and continuous optimization. *Methodology And Computing In Applied Probability*, 1(2), pp. 127–190.

Rubinstein R.Y. (1976). A Monte Carlo method for estimating the gradient in a stochastic network. Technion, Haifa, Israel. Unpublished manuscript.

Rubinstein R.Y. (1986). The score function approach for sensitivity analysis of computer simulation models. *Mathematics and Computers in Simulation*, 28(5), pp. 351–379.

Rubinstein R.Y. (1997). Optimization of computer simulation models with rare events. *European Journal of Operational Research*, 99(1), pp. 89–112.

Rubinstein R.Y., Kroese D.P. (2007). *Simulation and the Monte Carlo method*. 2nd ed. Wiley Series in Probability and Statistics. John Wiley & Sons.

Rychlik I. (1989). Simple approximations of the rain-flow-cycle distribution for discretized random loads. *Probabilistic Engineering Mechanics*, 4(1), pp. 40–48.

Rychlik I. (1996). Simulation of load sequences from rainflow matrices: Markov method. *International Journal of Fatigue*, 18(7), pp. 429–438.

Sacks J., Welch W.J., Mitchell T.J., Wynn H.P. (1989). Design and analysis of computer experiments. *Statistical Science*, 4(4), pp. 409–423.

Saltelli A., Chan K., Scott E.M. (2008). *Sensitivity analysis*. New York, NY, USA: John Wiley & Sons.

Santner T.J., Williams B.J., Notz W.I. (2003). *The design and analysis of computer experiments*. Springer Series in Statistics. New York, NY, USA: Springer.

Santoso A.M., Phoon K.K., Quek S.T. (2011). Modified Metropolis-Hastings algorithm with reduced chain correlation for efficient subset simulation. *Probabilistic Engineering Mechanics*, 26(2), pp. 331–341.

Saunders C., Gammerman A., Vovk V. (1998). Ridge regression learning algorithm in dual variables. In: *Proc. 15th International Conference on Machine Learning (ICML '98), Madison, Wisconsin, USA, July 24–27, 1998*. San Francisco, CA, USA: Morgan Kaufmann Publishers, pp. 515–521.

Schenk C.A., Schuëller G.I. (2003). Buckling analysis of cylindrical shells with random geometric imperfections. *International Journal of Non-Linear Mechanics*, 38(7), pp. 1119–1132.

Schenk C.A., Schuëller G.I. (2007). Buckling analysis of cylindrical shells with cutouts including random boundary and geometric imperfections. *Computer Methods in Applied Mechanics and Engineering*, 196(35–36), pp. 3424–3434.

Schijve J. (1987). *An evaluation of a fatigue crack growth prediction model for variable-amplitude loading (PREFFAS)*. Report LR-537. TU Delft, Faculty of Aerospace Engineering.

Schöbi R., Sudret B., Marelli S. (2017). Rare event estimation using polynomial-chaos kriging. *ASCE-ASME Journal of Risk and Uncertainty in Engineering Systems, Part A: Civil Engineering*, 3(2). D4016002.

Schöbi R., Sudret B., Wiart J. (2015). Polynomial-chaos-based kriging. *International Journal for Uncertainty Quantification*, 5(2), pp. 171–193.

Schölkopf B., Herbrich R., Smola A.J. (2001). A generalized representer theorem. In: *Computational Learning Theory*. Ed. by D. Helmbold, B. Williamson. Vol. 2111. Lecture Notes in Computer Science. Springer Berlin Heidelberg, pp. 416–426.

Schölkopf B., Smola A.J. (2001). *Learning with kernels: support vector machines, regularization, optimization, and beyond*. Cambridge, MA, USA: MIT Press.

Schonlau M., Welch W.J., Jones D.R. (1998). Global versus Local Search in Constrained Optimization of Computer Models. *Lecture Notes-Monograph Series*, 34, pp. 11–25.

Schuëller G.I., Jensen H.A. (2008). Computational methods in optimization considering uncertainties - an overview. *Computer Methods in Applied Mechanics and Engineering*, 198(1), pp. 2–13.

Schuëller G.I., Stix R. (1987). A critical appraisal of methods to determine failure probabilities. *Structural Safety*, 4(4), pp. 293–309.

Schueremans L., Van Gemert D. (2005). Use of kriging as meta-model in simulation procedures for structural reliability. In: *Proc. 9th International Conference on Structural Safety and Reliability (ICOSSAR 2005), Roma, Italy, June 19–22, 2005*. Ed. by G. Augusti, G.I. Schuëller, M. Ciampoli. Millpress, Rotterdam, pp. 2483–2490.

Scordelis A.C., Lo K.S. (1964). Computer analysis of cylindrical shells. *ACI Journal*, 61, pp. 539–561.

Settles B. (2009). *Active learning literature survey*. Computer Sciences Technical Report No. 1648. University of Wisconsin–Madison.

Shawe-Taylor J., Cristianini N. (2004). *Kernel methods for pattern analysis*. New York, NY, USA: Cambridge University Press.

Shawe-Taylor J., Sun S. (2011). A review of optimization methodologies in support vector machines. *Neurocomputing*, 74(17), pp. 3609–3618.

Simpson T.W., Poplinski J.D., Koch N.P., Allen J.K. (2001). Metamodels for computer-based engineering design: survey and recommendations. *Engineering with Computers*, 17(2), pp. 129–150.

Singer J., Arbocz J., Babcock C.D. (1971). Buckling of imperfect stiffened cylindrical shells under axial compression. *AIAA Journal*, 9(1), pp. 68–75.

Singer J., Abramovich H. (1995). The development of shell imperfection measurement techniques. *Thin-Walled Structures*, 23(1–4), pp. 379–398.

Sklar A. (1959). Fonctions de répartition à n dimensions et leurs marges. *Publications de l'Institut de Statistique de l'Université de Paris*, 8, pp. 229–231.

Smola A.J. (1998). Learning with kernels. PhD thesis. Technischen Universität Berlin, Berlin, Germany.

Smola A.J., Frieß T.-T., Schölkopf B. (1999). Semiparametric support vector and linear programming. In: *Advances in Neural Information Processing Systems 11*. Ed. by M.J. Kearns, S.A. Solla, D.A. Cohn. MIT Press, pp. 585–591.

Smola A.J., Schölkopf B. (1998). *A tutorial on support vector regression*. NeuroCOLT Technical Report NC-TR-98-030. Royal Holloway College, University of London, UK.

Smola A.J., Schölkopf B. (2004). A tutorial on support vector regression. *Statistics and Computing*, 14(3), pp. 199–222.

Smola A.J., Schölkopf B., Müller K.-R. (1998). The connection between regularization operators and support vector kernels. *Neural Networks*, 11(4), pp. 637–649.

Smola A.J., Bartlett P., Schölkopf B., Schuurmans D., eds. (2000). *Advances in large margin classifiers*. Cambridge, MA, USA: MIT Press.

Sobol' I.M. (1993). Sensitivity estimates for nonlinear mathematical models. *Mathematical modelling and Computational Experiments*, 1(4), pp. 407–414.

Soize C., Ghanem R. (2004). Physical systems with random uncertainties: chaos representations with arbitrary probability measure. *SIAM Journal on Scientific Computing*, 26(2), pp. 395–410.

Song S., Lu Z., Qiao H. (2009). Subset simulation for structural reliability sensitivity analysis. *Reliability Engineering & System Safety*, 94(2), pp. 658–665.

Sonnenburg S., Rätsch G., Schäfer C., Schölkopf B. (2006). Large scale multiple kernel learning. *Journal of Machine Learning Research*, 7, pp. 1531–1565.

Spider Toolbox for Matlab, Version 1.71 (2006). Software available at `http://people.kyb.tuebingen.mpg.de/spider/main.html`.

Stefanou G., Papadrakakis M. (2004). Stochastic finite element analysis of shells with combined random material and geometric properties. *Computer Methods in Applied Mechanics and Engineering*, 193(1–2), pp. 139–160.

Stein M.L. (1999). *Interpolation of spatial data. Some theory for kriging*. Springer Series in Statistics. New York, NY, USA: Springer.

Stone M. (1974). Cross-validatory choice and assessment of statistical predictions. *Journal of the Royal Statistical Society: Series B*, 36(2), pp. 111–147.

Sudret B. (2000). *Stochastic finite element methods and reliability*. Report No. UCB/SEMM-2000/08. Dept of Civil and Environmental Engineering, University of California, Berkeley.

Sudret B. (2012). Meta-models for structural reliability and uncertainty quantification. In: *Proc. Asian-Pacific Symposium on Structural Reliability and its Applications, Singapore, Singapore, May 23–25, 2012*.

Sudret B., Der Kiureghian A. (2002). Comparison of finite element reliability methods. *Probabilistic Engineering Mechanics*, 17(4), pp. 337–348.

Suykens J.A.K., Van Gestel T., De Brabanter J., De Moor B., Vandewalle J. (2002). *Least squares support vector machines*. World Scientific Pub. Co.

Suykens J.A.K., Vandewalle J. (1999). Least squares support vector machine classifiers. *Neural Processing Letters*, 9(3), pp. 293–300.

Taflanidis A.A. (2007). Stochastic system design and applications to stochastically robust structural control. PhD thesis. California Institute of Technology, Pasadena, USA.

Taflanidis A.A., Beck J.L. (2008). Stochastic subset optimization for optimal reliability problems. *Probabilistic Engineering Mechanics*, 23(2–3), pp. 324–338.

The MathWorks (2012). *Matlab optimization toolbox user's guide - Version 6.2*.

Tierney L. (1994). Markov chains for exploring posterior distributions. *The Annals of Statistics*, 22(4), pp. 1701–1728.

Tikhonov A.N., Arsenin V.Y. (1977). *Solution of ill-posed problems*. Ed. by D. W. H. Winston Washington. New York, NY, USA: John Wiley & Sons.

Tu J., Choi K.K., Park Y.H. (1999). A new study on reliability-based design optimization. *Journal of Mechanical Design*, 121(4), pp. 557–564.

Tvedt L. (1988). Second order reliability by an exact integral. In: *Proc. 2nd IFIP WG 7.5 Working Conference on Reliability and Optimization of Structural Systems, London, UK, September 26–28, 1988*. Ed. by P. Thoft-Christensen. Springer Berlin Heidelberg, pp. 377–384.

Ustilovsky S., Arone R. (1999). Random fatigue crack growth in aluminum alloys. *International Journal of Fatigue*, 21(Supplement 1), S275–S282.

Valdebenito M.A., Schuëller G.I. (2010). A survey on approaches for reliability-based optimization. *Structural and Multidisciplinary Optimization*, 42(5), pp. 645–663.

Vanderbei R.J. (2006). *LOQO user's manual - Version 4.05*. Technical Report No. ORFE-99-xx. Dept of Operations Research and Financial Engineering, Princeton University, Princeton.

Vapnik V. (1995). *The nature of statistical learning theory*. New York, NY, USA: Springer-Verlag.

Vapnik V., Chapelle O. (2000). Bounds on error expectation for support vector machines. *Neural Computation*, 12(9), pp. 2013–2036.

Vapnik V., Golowich S.E., Smola A.J. (1997). Support vector method for function approximation, regression estimation and signal processing. In: *Advances in Neural Information Processing Systems 9*. Ed. by M.C. Mozer, M.I. Jordan, T. Petsche. MIT Press, pp. 281–287.

Vazquez E. (2005). Modélisation comportementale de systèmes non-linéaires multivariables par méthodes à noyaux et applications. PhD thesis (in French). Université Paris-Sud, Paris, France.

Vazquez E., Walter E. (2003). Multi-output support vector regression. In: *Proc. 13th IFAC Symposium on System Identification (SYSID 2003), Rotterdam, Netherlands, August 2003*, pp. 1820–1825.

Viana F.A.C., Haftka R.T., Steffen V. (2009). Multiple surrogates: how cross-validation errors can help us to obtain the best predictor. *Structural and Multidisciplinary Optimization*, 39(4), pp. 439–457.

Virkler D.A., Hillberry B.M., Goel P.K. (1979). The statistical nature of fatigue crack propagation. *Journal of Engineering Materials and Technology*, 101(2), pp. 148–153.

Vogt M., Kecman V. (2005). Active-set methods for support vector machines. In: *Support Vector Machines: Theory and Applications*. Ed. by L. Wang. Berlin, Heidelberg: Springer Berlin Heidelberg, pp. 133–158.

Vrouwenvelder T. (1997). The JCSS probabilistic model code. *Structural Safety*, 19(3), pp. 245–251.

Wahba G. (1990). *Spline models for observational data*. Society for Industrial and Applied Mathematics.

Walder C., Chapelle O. (2008). Learning with transformation invariant kernels. In: *Advances in Neural Information Processing Systems 20*. Ed. by J.C. Platt, D. Koller, Y. Singer, S. Roweis. MIT Press, pp. 1561–1568.

Walter C. (2015). Moving particles: a parallel optimal multilevel splitting method with application in quantiles estimation and meta-model based algorithms. *Structural Safety*, 55, pp. 10–25.

Wang G.S., Blom A.F. (1991). A strip model for fatigue crack growth predictions under general load conditions. *Engineering Fracture Mechanics*, 40(3), pp. 507–533.

Wang Y., Zhao X., Wang B. (2013). LS-SVM and Monte Carlo methods based reliability analysis for settlement of soft clayey foundation. *Journal of Rock Mechanics and Geotechnical Engineering*, 5(4), pp. 312–317.

Wei P., Lu Z., Hao W., Feng J., Wang B. (2012). Efficient sampling methods for global reliability sensitivity analysis. *Computer Physics Communications*, 183(8), pp. 1728–1743.

Wills A. (2009). *QPC - Quadratic Programming in C - Version 2.0*.

Wu W.F., Ni C.C. (2007). Statistical aspects of some fatigue crack growth data. *Engineering Fracture Mechanics*, 74(18), pp. 2952–2963.

Wu Y.-T. (1994). Computational methods for efficient structural reliability and reliability sensitivity analysis. *AIAA Journal*, 32(8), pp. 1717–1723.

Xiong Y., Chen W., Apley D., Ding X. (2007). A non-stationary covariance-based kriging method for metamodelling in engineering design. *International Journal for Numerical Methods in Engineering*, 71(6), pp. 733–756.

Xiu D., Karniadakis G.E. (2002). The Wiener-Askey polynomial chaos for stochastic differential equations. *SIAM Journal on Scientific Computing*, 24(2), pp. 619–644.

Yang I.-T., Hsieh Y.-H. (2013). Reliability-based design optimization with cooperation between support vector machine and particle swarm optimization. *Engineering with Computers*, 29(2), pp. 151–163.

Yang J.N., Manning S.D. (1996). A simple second order approximation for stochastic crack growth analysis. *Engineering Fracture Mechanics*, 53(5), pp. 677–686.

Yang R., Gu L. (2004). Experience with approximate reliability-based optimization methods. *Structural and Multidisciplinary Optimization*, 26(1), pp. 152–159.

Youn B.D., Choi K.K. (2004). A new response surface methodology for reliability-based design optimization. *Computers & Structures*, 82(2-3), pp. 241–256.

Yuan X., Lu Z., Lu Y. (2009). Support vector machine response surface method based on fast Markov chain simulation. In: *Proc. 2009 IEEE International Conference on Intelligent Computing and Intelligent Systems (ICIS 2009), Shanghai, China, November 20–22, 2009*. Vol. 4. IEEE, pp. 279–282.

Zahrouni H., Cochelin B., Potier-Ferry M. (1999). Computing finite rotations of shells by an asymptotic-numerical method. *Computer Methods in Applied Mechanics and Engineering*, 175(1–2), pp. 71–85.

Zahrouni H., Potier-Ferry M., Elasmar H., Damil N. (1998). Asymptotic numerical method for nonlinear constitutive laws. *Revue Européenne des éléments Finis*, 7(7), pp. 841–869.

Žanić V., Žiha K. (1998). Sensitivity to correlation in multivariate models. *Computer Assisted Mechanics and Engineering Sciences*, 5(1), pp. 75–84.

Žanić V., Žiha K. (2001). Sensitivity to correlations in structural problems. *Transactions of FAMENA*, 25(2), pp. 1–26.

Zapatero J., Moreno B., Domínguez J. (1997). On the use of the strip-yield model to predict fatigue crack growth under irregular loading. *Fatigue & Fracture of Engineering Materials & Structures*, 20(5), pp. 759–770.

Zapatero J., Moreno B., González-Herrera A., Domínguez J. (2005). Numerical and experimental analysis of fatigue crack growth under random loading. *International Journal of Fatigue*, 27(8), pp. 878–890.

Zhang Y., Der Kiureghian A. (1993). Dynamic response sensitivity of inelastic structures. *Computer Methods in Applied Mechanics and Engineering*, 108(1), pp. 23–36.

Zhang Y., Der Kiureghian A. (1994). Two improved algorithms for reliability analysis. In: *Proc. 6^{th} IFIP WG 7.5 Working Conference on Reliability and Optimization of Structural Systems, Assisi, Italy, September 7–9, 1994*. Ed. by R. Rackwitz, G. Augusti, A. Borri. Springer US, pp. 297–304.

Zheng R., Ellingwood B.R. (1998). Stochastic fatigue crack growth in steel structures subject to random loading. *Structural Safety*, 20(4), pp. 303–323.

Zou T., Mahadevan S. (2006). A direct decoupling approach for efficient reliability-based design optimization. *Structural and Multidisciplinary Optimization*, 31(3), pp. 190–200.

Zou T., Mahadevan S., Mourelatos Z.P. (2003). Reliability-based evaluation of automotive wind noise quality. *Reliability Engineering & System Safety*, 82(2), pp. 217–224.

Zuev K.M., Beck J.L., Au S.-K., Katafygiotis L.S. (2012). Bayesian post-processor and other enhancements of subset simulation for estimating failure probabilities in high dimensions. *Computers & Structures*, 92–93, pp. 283–296.

Zuev K.M., Katafygiotis L.S. (2011a). Modified Metropolis-Hastings algorithm with delayed rejection. *Probabilistic Engineering Mechanics*, 26(3), pp. 405–412.

Zuev K.M., Katafygiotis L.S. (2011b). The horseracing simulation algorithm for evaluation of small failure probabilities. *Probabilistic Engineering Mechanics*, 26(2), pp. 157–164.

A

Two challenging problems for surrogate-based reliability analysis

A–1 Example 1

This first reliability problem is studied by Kouassi et al. (2016) in the field on electromagnetic compatibility. It investigates a lossy transmission line of length L, diameter d and attenuation coefficient α such as defined by Rannou et al. (2002), see Figure A.1. The line is placed at a uniform height h (considered as a random variable in the present study) above a perfectly conducting ground plane and loaded at both ends by two impedances Z_0 and Z_L. This line is illuminated at a frequency f by a linearly polarized plane wave with incidence angles ϕ_p (azimut angle) and θ_p (elevation angle). The polarization angle and the magnitude of the electric field $\mathbf{E}$ are denoted θ_e and a_e, respectively.

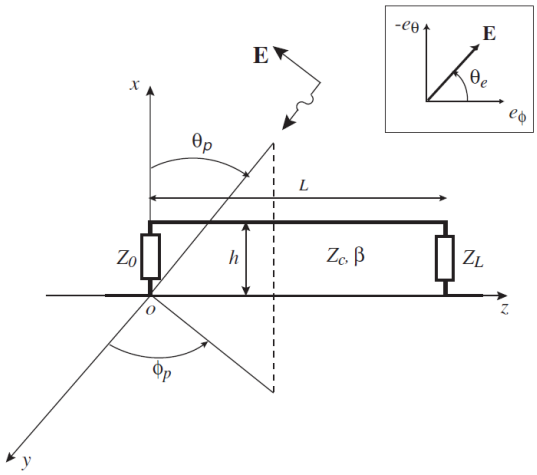

Figure A.1 – Representation of the transmission line studied by Rannou et al. (2002).

The observable of interest is the electric current magnitude I at the end of the line, i.e. in the output load impedance Z_L. This current can be analytically expressed in terms of the $n = 11$ above defined input parameters (Rannou et al., 2002), and its magnitude writes :

$$I = I(\mathbf{x}) = \left| \frac{2ha_e}{I_1} I_2 \left[I_3 \left(I_4 - I_5 \right) + I_6 \right] \right| , \tag{A.1}$$

where $\mathbf{x} = (L, h, d, Z_L, Z_0, a_e, \theta_e, \theta_p, \phi_p, f, \alpha)$,

and where:

$$
\begin{aligned}
I_1 &= (Z_0 Z_C + Z_L Z_C)\cosh(\gamma L) + \left(Z_C^2 + Z_0 Z_L\right)\sinh(\gamma L)\ , \\
I_2 &= \frac{\sin\left(\beta h \cos\theta_p\right)}{\beta h \cos\theta_p}\ , \\
I_3 &= i\beta\cos\theta_p\left(-\sin\theta_e\cos\theta_p\sin\phi_p + \cos\theta_e\cos\phi_p\right)\ , \\
I_4 &= \frac{1}{2}(Z_C + Z_0)\frac{\exp\left[\left(\gamma + i\beta\sin\theta_p\sin\phi_p\right)L\right] - 1}{\gamma + i\beta\sin\theta_p\sin\phi_p}\ , \\
I_5 &= \frac{1}{2}(Z_C - Z_0)\frac{\exp\left[-\left(\gamma - i\beta\sin\theta_p\sin\phi_p\right)L\right] - 1}{\gamma - i\beta\sin\theta_p\sin\phi_p}\ , \\
I_6 &= \sin\theta_e\sin\theta_p\left[Z_C - (Z_C\cosh(\gamma L) + Z_0\sinh(\gamma L))\exp\left(i\beta L\sin\theta_p\sin\phi_p\right)\right]\ ,
\end{aligned}
$$

in which $Z_C = 60\,\mathrm{acosh}(2h/d)$, $\beta = 2\pi f/3\times 10^8$ and $\gamma = \alpha + i\beta$. In these expressions, $i = \sqrt{-1}$ is the imaginary number and $|\cdot|$ denotes the modulus of a complex number.

The LSF is defined by:

$$
g(\mathbf{x}) = I_{\mathrm{cr}} - I(\mathbf{x})\ , \tag{A.2}
$$

where $I_{\mathrm{cr}} = 1.5\times 10^{-4}$ A is a given current magnitude level to be not exceeded.

The input parameters are modeled as mutually independent random variables. The marginal pdfs are defined in Table A.1.

variable X_i	mean μ_{X_i}	c.o.v. δ_{X_i}	distribution / support
$X_1 = L$ (m)	4.2	0.10	lognormal / $\mathbb{R}_{\geq 0}$
$X_2 = h$ (m)	0.02	0.10	lognormal / $\mathbb{R}_{\geq 0}$
$X_3 = d$ (m)	0.001	0.05	lognormal / $\mathbb{R}_{\geq 0}$
$X_4 = Z_L$ (Ω)	1000	0.20	lognormal / $\mathbb{R}_{\geq 0}$
$X_5 = Z_0$ (Ω)	50	0.05	lognormal / $\mathbb{R}_{\geq 0}$
$X_6 = a_e$ (V/m)	1	0.20	lognormal / $\mathbb{R}_{\geq 0}$
$X_7 = \theta_e$ (rad)	$\pi/4$	0.577	uniform / $[0, \pi/2]$
$X_8 = \theta_p$ (rad)	$\pi/4$	0.577	uniform / $[0, \pi/2]$
$X_9 = \phi_p$ (rad)	π	0.577	uniform / $[0, 2\pi[$
$X_{10} = f$ (MHz)	30	0.096	uniform / $[25, 35]$
$X_{11} = \alpha$ (-)	0.0010	0.289	uniform / $[0.0005, 0.0015]$

Table A.1 – Example 1, second-order statistics and distributions.

The results of the reliability analyses are given in Table A.2. All the calculations are performed using the algorithms implemented in FERUM 4.1 (Bourinet et al., 2009). A reference failure probability is obtained by a crude MC approach using 10^9 samples. SS is applied with $N = 2500$ samples at each intermediate level. The FORM and SORM$^{\mathrm{cf}}$ approximations are also given.

Method	Failure probability estimate	# of calls to LSF
MC (reference)	$\widehat{p}_{\mathrm{f}}^{\mathrm{MC}} = 2.24 \times 10^{-4}$ ($\delta_{\widehat{p}_{\mathrm{f}}^{\mathrm{MC}}} = 0.002$)	10^9
SS	$\widehat{p}_{\mathrm{f}}^{\mathrm{SS}} = 2.12 \times 10^{-4}$ ($\delta_{\widehat{p}_{\mathrm{f}}^{\mathrm{SS}}} = 0.184$)	$\approx 10,000$
FORM	$p_{\mathrm{f}}^{\mathrm{FORM}} = 31.83 \times 10^{-4}$	9144
SORM$^{\mathrm{cf}}$	$p_{\mathrm{f}}^{\mathrm{SORM\text{-}cf}} = 1.10 \times 10^{-4}$	(9144+) 77

Table A.2 – Example 1, results.

From these results, it appears that FORM and SORM$^{\mathrm{cf}}$ methods are unable to accurately quantify the failure probability. The FORM failure probability estimate is about one order of magnitude greater than the reference solution. Moreover the FORM result necessitates a large number of calls to the LSF due to the small step size required for convergence of the i-HLRF algorithm (here 0.01). SORM$^{\mathrm{cf}}$ probability estimate is better than FORM but the bias w.r.t. the reference failure probability is still large.

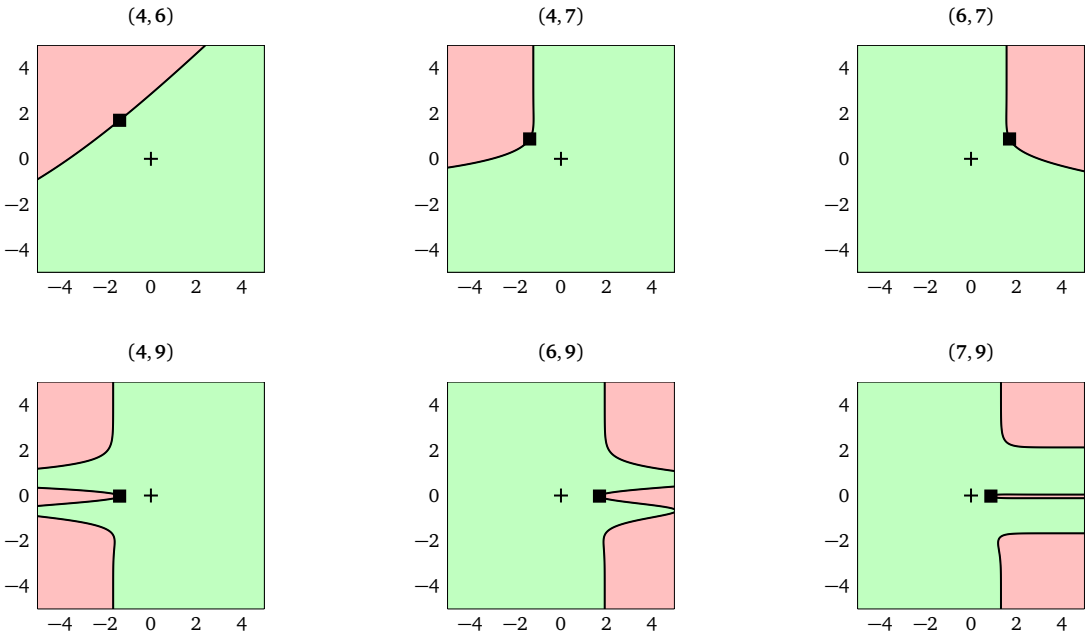

Figure A.2 – Example 1, (u_i, u_j) pairwise cross-cuts passing through the MPFP P^* in the standard normal space. Black square: MPFP, black cross: projection of standard normal space origin onto (u_i, u_j) cross-cut plane, black line: LSS, green area: safe domain, pink area: failure domain. The numbering of the random components of $\mathbf{X}$ is given in the first column of Table A.1.

In order to investigate why FORM and SORM fail in this example, the LSS geometry has been explored by means of (u_i, u_j) pairwise cross-cuts passing through the MPFP P^* in the standard normal space for $i, j \in \{1, \ldots, 11\}$. Some of these cuts obtained are given in Figure A.2. The LSS appears smooth in all pairwise cross-cuts except those involving the azimuth angle ϕ_p of the incident electromagnetic wave (9^{th} component of $\mathbf{X}$). The uncertain azimuth angle ϕ_p induces a very sharp LSS at the MPFP P^* in the $\mathbf{u}$-space (see the three lower subplots of Figure A.2), which explains why FORM and SORM are unable to predict the true failure probability with an acceptable accuracy. This sharpness of the LSS is in fact due to the high sensitivity of the transmission line model to the azimuth angle. Small departures of the angle ϕ_p from 0 and π induce large decreases in the electric current magnitude at the end of the line. This results in a concentration of failure probability close to these two values of azimuth angle.

A–2 Example 2

This second reliability problem is defined in terms of two independent standard normal variates. The LSF at $\mathbf{u} = (u_1, u_2)^{\mathrm{T}}$ is given by:

$$G(\mathbf{u}) = \min_{k \in \{1,2\}} G_k(\mathbf{u}), \tag{A.3}$$

where:

$$G_1(\mathbf{u}) = (u_1 - \epsilon) + \beta_1, \tag{A.4}$$

$$G_2(\mathbf{u}) = \beta_1 \left(1 - \left[\frac{1}{2}\left(\frac{u_1 - \epsilon}{\beta_2} + \left|\frac{u_1 - \epsilon}{\beta_2}\right|\right)\right]^{\gamma}\right), \tag{A.5}$$

and where $\beta_1 = 6$, $\beta_2 = 4.5$, $\gamma = 30$ and $\epsilon = 10^{-6}$.

(a) LSS in the standard normal space

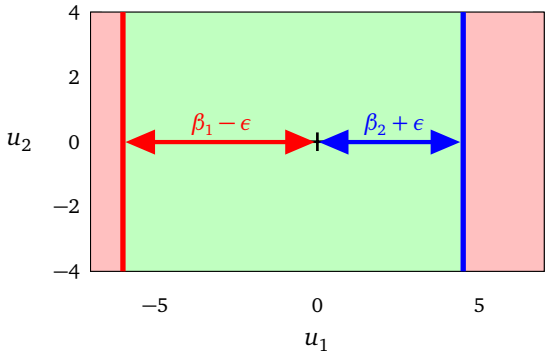

(b) LSF G_1 and G_2 vs. u_1

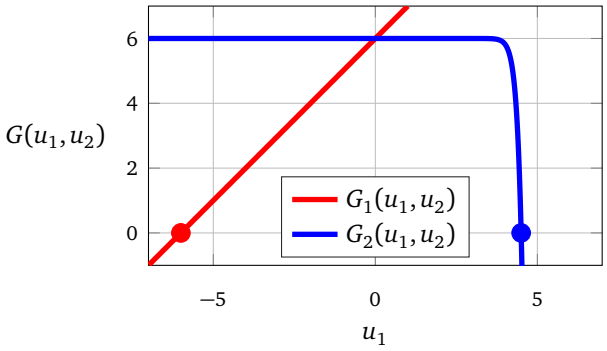

Figure A.3 – Example 2, limit-state surfaces $G_1(\mathbf{u}) = 0$ and $G_2(\mathbf{u}) = 0$ in the standard normal space (left), limit-state functions $G_1(\mathbf{u})$ and $G_2(\mathbf{u})$ vs. u_1 (right). Green area: safe domain, pink area: failure domain.

The reference failure probability is here obtained by means of a directional simulation (DS) with 100 directions evenly distributed over the unit-radius circle centered on the origin of the standard normal space, see the obtained value in Table A.3. The true failure probability writes $p_{\mathrm{f}} = \Phi(-(\beta_1 - \epsilon)) + \Phi(-(\beta_2 + \epsilon)) \approx \Phi(-\beta_2) = 3.40 \times 10^{-6}$.

The failure probabilities obtained using FORM and SORM-cf are given in Table A.3. Starting from the origin of the standard normal space, the MPFP found by FORM is the closest point of the LSS $G_1(\mathbf{u}) = 0$. We therefore obtain $p_{\mathrm{f}}^{\mathrm{FORM}} = p_{\mathrm{f}}^{\text{SORM-cf}} = \Phi(-\beta)$ where $\beta = \beta_1 - \epsilon$, values which are far from the reference solution (almost three orders of magnitude lower than the true failure probability).

SS is applied with 1000 samples per subset level. The SS failure probability estimates obtained from 500 independent runs of the SS method are represented in Figure A.4. It is worth noting that SS explores quasi-exclusively the half-space $\{\mathbf{u} \in \mathbb{R}^2 : u_1 < 0\}$ due to the plateau of G_2 in the half-space $\{\mathbf{u} \in \mathbb{R}^2 : u_1 > 0\}$ (the width of this plateau is controlled by the parameter γ). With a sample size per level set to 1000, there are almost no chances that MCMC samples populate the half-space $\{\mathbf{u} \in \mathbb{R}^2 : u_1 > 0\}$. As a consequence the failure probability estimate obtained using SS is almost always severely biased (again, about three orders of magnitude lower than the true failure probability).

Method	Failure probability estimate	# of calls to LSF
Directional simulation (reference)	$p_{\mathrm{f}}^{\mathrm{DS}} = 3.40 \times 10^{-6}$	1601
FORM	$p_{\mathrm{f}}^{\mathrm{FORM}} = 9.87 \times 10^{-10}$	21
SORM$^{\mathrm{cf}}$	$p_{\mathrm{f}}^{\mathrm{SORM\text{-}cf}} = 9.87 \times 10^{-10}$	(21+) 5

Table A.3 – Example 2, results.

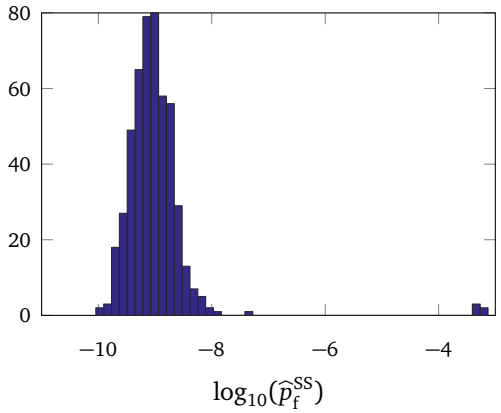

Figure A.4 – Example 2, histogram of the failure probability estimates $\widehat{p}_{\mathrm{f}}^{\mathrm{SS}}$ obtained from 500 independent runs of the SS method.

B

Short bio and academic achievements

B–1 Short bio

First name, last name	**Jean-Marc Bourinet**
Date of birth	February 2, 1969
Civil status	Civil union, 2 children
Address	SIGMA Clermont Campus des Cézeaux - CS 20265, 63178 Aubière cedex, France
Phone	+33 4 73 28 81 16
E-mail	bourinet@sigma-clermont.fr
Google Scholar profile	https://scholar.google.com/citations?user=pzrQbq8AAAAJ
Current position	Associate professor at **SIGMA Clermont** (formerly IFMA) Permanent researcher at **Institut Pascal**, CNRS UMR 6602, M3G Dept, Leader of the Uncertainty Quantification research group
Education	**PhD in Mechanical Engineering**, École Centrale de Nantes (Dec. 1996) Subject: Numerical and experimental approach of damped vibrations of tubes filled with granular materials **Engineering degree**, Naval Architecture, ENSIETA Brest (Sept. 1993)

B–2 Positions held

Jan. 2003 to Aug. 2004	**Centre d'Essais Aéronautique de Toulouse**, DGA, Toulouse, France Appraisal and test manager
Jan. to Dec. 2002	**Centre Technique des Systèmes Navals**, DGA, Toulon, France Design engineer
Jan. to Dec. 2001	**University of California at Berkeley**, Berkeley, CA, USA Visiting scholar, lecturer
Jan. 1997 to Dec. 2000	**Centre Technique des Systèmes Navals**, DGA, Toulon, France Design Engineer
Sep. 1993 to Dec. 1996	**École Centrale de Nantes**, Nantes, France Doctoral student
Apr. to Aug. 1993	**IFREMER**, Plouzané, France Intern
Sep. 1989 to Aug. 1993	**ENSTA Bretagne** (formerly ENSIETA), Brest, France Engineering student

B–3 Teaching

My courses are mainly given to engineering master's students at SIGMA Clermont. I have also taught classes outside my school: 3rd-year courses at École Centrale de Nantes (2005–2008) and specialized master's classes at Centre des Matériaux des Mines ParisTech (2004–2008). Since 2008, I have participated every year in the *Mécanique-Matériaux-Structures-Fiabilité* (MMSF) research master, awarded conjointly by Université Blaise Pascal and SIGMA Clermont. I also teach in professional training programs provided by the École Polytechnique / Executive Education for engineers and researchers. My teaching activities are summarized in the tables below.

I elaborated the complete program content (lectures, tutorials and practical classes) of the following course units: probability and statistics (PRST) given to 1st-year students, finite element method (BMEF) given to 2nd-year students in the Materials and Structures (St2M) department, and uncertainty propagation 1 (APIC) given to 3rd-year students in the same department. I am in charge of these 3 courses (giving lectures in collaboration with the tutorial and practical class teachers, setting exams and assessments, interacting with students).

Level - Type	Title	Lectures	Tutorials	Practicals	#Students	Dates
Ing. 1A - FI	Probability and statistics *	2×16h	2×14h	-	160	Since 2005
Ing. 2A - FI	Finite element method *	16h	12h	14h	48	Since 2004
Ing. 2A - FI	Fatigue, damage, fracture *	6h	-	2×8h	48	2010–2012
Ing. 3A - FI	Uncertainty quantification 1 *	8h	2×2h	2×4h	48	Since 2010
Ing. 3A - FI	Uncertainty quantification 2	4h	-	-	24	Since 2010
Ing. 3A - FI	Non-linear modeling in finite elements *	4h	2×2h	-	48	Since 2010

* : course leader.

Table B.1 – Teaching at SIGMA Clermont.

Establishment	Level - Type	Title	Lectures	Practicals	#Students	Dates
UBP & SIGMA Clermont	M2R MMSF	Reliability, uncertainty, optimization *	15h	-	10 to 20	Since 2008
École Centrale de Nantes	Ing. 3A - FI	Structural reliability	12.5h	7.5h	10 to 20	2005–2008
Centre des Matériaux / Mines ParisTech	MS CoMaDiS	Reliability assessment	15h	-	≈ 10	2004–2008
IUT de Montluçon	M2pro Mécanique	Probabilistic mechanics	10h	-	5 to 10	2004–2008
University of California at Berkeley	Undergraduate	Engineering mechanics - Statics *	28h	-	53	Fall 2001

* : course leader.

Table B.2 – Teaching in other establishments.

Establishment	Participants	Title	#Hours	#Students	Dates
Collège de Polytechnique	Engineers, researchers	Probabilistic safety of structures	7h	≈ 10	2006, 2008
École Polytechnique - Executive Education	Engineers, researchers	Probabilistic methods for uncertainty management in mechanics	7h	≈ 10	2015, 2016

Table B.3 – Professional training.

B–4 Supervision of PhD students and master's thesis students

B–4.1 Ongoing PhD works

- **Vincent Chabridon**
  Uncertainty propagation in costly-to-evaluate models - Application to aerospace engineering
  Start date: October 2015
  Co-supervised with Nicolas Gayton (thesis co-director), Jérôme Morio, ONERA Toulouse (thesis co-director) and Mathieu Balesdent, ONERA Palaiseau
  Collaboration(s)/funding(s): SIGMA Clermont and ONERA grants
- **Mathieu Sallin**
  Approche probabiliste du diagnostic de l'état de santé des véhicules militaires terrestres en environnement incertain (in French)
  Start date: December 2014
  To be defended on January 30, 2018
  Co-supervised with Michel Fogli (thesis director) and David Clair
  Collaboration(s)/funding(s): NEXTER Systems, DGA-TT, CIFRE-Defense grant

B–4.2 Past PhD works

- **Attibaud Kouassi** (current position: engineer at SES-Europe)
  Propagation d'incertitudes en CEM : Application à l'analyse de fiabilité et de sensibilité de lignes de transmission et d'antennes (in French)
  Start date: October 2012
  Defended on December 18, 2017
  Co-supervised with Michel Fogli (thesis co-director), Pierre Bonnet, Institut Pascal (thesis co-director) and Sébastien Lalléchère, Institut Pascal
  Collaboration(s)/funding(s): grant from the French Ministry of National Education
- **Maliki Moustapha** (current position: postdoc at ETH Zurich)
  Adaptive surrogate models for the reliable lightweight design of automotive body structures
  Start date: December 2012
  Defended on January 27, 2016
  Co-supervised with Bruno Sudret, ETH Zurich (thesis director)
  Collaboration(s)/funding(s): PSA Peugeot-Citroën, CIFRE grant
- **Vincent Dubourg** (current position: data scientist at Michelin)
  Adaptive surrogate models for reliability analysis and reliability-based design optimization
  Start date: October 2008
  Defended on December 5, 2011
  Co-supervised with Bruno Sudret, Phimeca Engineering (thesis director)
  Collaboration(s)/funding(s): Phimeca Engineering, DCNS, CIFRE grant
- **Cécile Mattrand** (current position: assistant professor at SIGMA Clermont)
  Approche probabiliste de la tolérance aux dommages - Application au domaine aéronautique (in French)
  Start date: October 2008
  Defended on November 30, 2011
  Co-supervised with Maurice Lemaire (thesis director), Jean-Marc Bourinet (co-encadrant)
  Collaboration(s)/funding(s): DGA, EADS-IW, DGA-CNRS grant

- **Lukáš Nešpůrek** (current position: engineer at Honeywell)
  Stochastic crack propagation modelling using the extended finite element method
  Start date: September 2003
  Defended on November 25, 2010
  Co-supervised with Maurice Lemaire (thesis co-director), Zdeněk Knésl, Brno University of Technology (thesis co-director)
  Collaboration(s)/funding(s): Brno University of Technology, CNOUS grant
- **Claudine Noirfalise** (current position: engineer at Michelin)
  Approche fiabiliste de la stabilité des structures minces imparfaites par la méthode asymptotique numérique (in French)
  Start date: October 2005
  Defended on July 8, 2009
  Co-supervised with Michel Fogli (thesis director)
  Collaboration(s)/funding(s): LMA Marseille, DGA-CNRS grant
- **François Deheeger** (current position: data scientist at Michelin)
  Couplage mécano-fiabiliste : ^{2}SMART - Méthodologie d'apprentissage stochastique en fiabilité (in French)
  Start date: October 2004
  Defended on January 28, 2008
  Co-supervised with Maurice Lemaire (thesis director)
  Collaboration(s)/funding(s): grant from the French Ministry of National Education

B–4.3 Past master's thesis

- **Cécile Mattrand**, IFMA, 2008
  Etude et comparaison des sensibilitées globales et locales en analyse probabiliste
- **Antoine Dumont**, IFMA, 2006
  Analyse mécano-fiabiliste du flambage avec prise en compte d'imperfections géométriques aléatoires

B–5 Industrial research contracts

Ongoing contracts:

- NEXTER Systems (PhD work of M. Sallin 2014–2017)

Past contracts:

- PSA (PhD work of M. Moustapha 2012–2016)
- Phimeca Engineering (2009–2012)
- DCNS (PhD work of V. Dubourg 2008–2011)

B–6 Membership in scientific and professional organizations

I was co-animator and secretary of the French research network *Mécanique Probabiliste des Matériaux et des Structures* under the lead of Prof. M. Lemaire and organized within the Association Française de Mécanique from September 2004 to December 2013. This network has now been renamed *Mécanique et Incertain* (GST MI)

B–7 Collective responsibilities and tasks

Responsibilities at SIGMA Clermont:

- Elected member of the scientific board of SIGMA Clermont (since 2016)
- Elected member of the scientific board of IFMA (2011–2015)
- Defense referent at SIGMA Clermont (2012–2015). Communication with engineering students serving as reservists, participation in local and national meetings
- Administrative management of student internships abroad (2007–2010), ≈140 internships/year
- Administrative management of student internships abroad, St2M department (2006–2010), ≈45 internships/year
- Administrative management of 2nd-year and end-of-study company internships, St2M department (2004–2007), ≈45 internships/year

Collective tasks at SIGMA Clermont:

- Contribution to SIGMA Clermont student placement in internships in France and internationally (since 2004). More than 80 international internships in the industry and 50 in research labs.
- Organization of the specialized elective course on aeronautical design at SIGMA Clermont (2006–2014). Recruitment of outside trainers from industry (Dassault Aviation, DGA), organization of the course program, creation of the assessment process.
- Creation of an outgoing mobility program with the Karlsruhe Institute of Technology for SIGMA Clermont engineering students (2010). This Erasmus semester exchange has been available to students since 2010 (about 2 to 3 students per year)
- Participation in the student recruitment at SIGMA Clermont as examiner (since 2004)

Responsibilities at Institut Pascal:

- Leader of the Uncertainty Quantification (UQ) group in the M3G Department of Institut Pascal (since January 2017)
- Deputy leader of the Probabilistic Mechanics of Materials and Structures (MPMS) research group in the MMS Department of Institut Pascal (2012–2016)
- Elected member of the board of Laboratoire de Mécanique et Ingénieries (LaMI) (2006–2011)

B–8 Code development

FERUM 4.x is an open-source Matlab toolbox for uncertainty propagation in numerical models distributed under the GNU General Public License agreement. Initially developed at UC Berkeley until 2003 (Der Kiureghian et al., 2006), I have modified this toolbox in depth and added several new features to FERUM since 2004. This toolbox is freely accessible at https://www.sigma-clermont.fr/en/ferum.

The methods available in FERUM are: FORM and SORM-cf and -pf, crude MC, IS based on FORM, directional sampling, subset simulation. It also includes the ^{2}SMART adaptive method based on SVM surrogates used in classification. Global sensitivity analysis based on Sobol' indices is also available in FERUM.

This toolbox is immediately comprehensible, easy to use and very accessible for students and researchers who want to explore new solving strategies in uncertainty propagation. Since its initial release in 2009, this toolbox has been downloaded in about 60 countries by more than 1700 users (USA: 210, China: 180, France: 160, Iran: 130, India: 110, Denmark: 70, UK: 70, Germany: 60).

B–9 Editorial and review activities

I am member of the editorial board of Reliability Engineering & System Safety since January 2017.

Review of journal papers for:

- Reliability Engineering & System Safety (RESS)
- Structural Safety (STRUCS)
- Probabilistic Engineering Mechanics (PREM)
- Structural and Multidisciplinary Optimization (SMO)
- Engineering Fracture Mechanics (EFM)
- Computers and Structures (CAS)
- International Journal of Reliability and Safety (IJRS)
- European Journal of Computational Mechanics (EJCM)
- IEEE Transactions on Electromagnetic Compatibility (IEEE Transactions on EMC)

Edition of conference proceedings:

- **IUTAM Symposium on Multiscale Problems in Stochastic Mechanics**, Special Section of Probabilistic Engineering Mechanics (Elsevier), Vol. 37, pp. 123–184, July 2014, http://www.sciencedirect.com/science/journal/02668920/37
- **IUTAM Symposium on Multiscale Problems in Stochastic Mechanics**, Procedia IUTAM (Elsevier), Vol. 6, pp. 1–210, 2013, http://www.sciencedirect.com/science/journal/22109838/6/supp/C

B–10 Organization of scientific events

Conferences:

- Proppe C., Bourinet J.-M., **IUTAM Symposium on Multiscale Problems in Stochastic Mechanics**, Karlsruhe, Germany, June 25–29, 2012, 35 participants, 23 papers presented

Summer schools:

- Bourinet J.-M., Proppe C., **Modeling and Numerical Methods for Uncertainty Quantification (MNMUQ 2014)**, French-German Summer School & École Thématique CNRS, September 1–5, 2014, Porquerolles, France, fundings: French-German University (UFA/DFH), CNRS, AFM, Institut Pascal, ED SPI Clermont and IFMA, 65 participants + 12 lecturers
- Proppe C., Bourinet J.-M., **Uncertainty Quantification in Mechanics and Material Sciences, Theory and Practice**, French-German Summer School, August 22–26, 2011, Pforzheim, Germany, fundings: French-German University (UFA/DFH) and AFM, 38 participants + 12 lecturers

Workshops:

- Lalléchère S. & al., **1st Uncertainty Modeling for ElectroMagnetic Applications Workshop (UMEMA 2015)**, June 29–31, 2015, Saint Nectaire, France
- Bourinet J.-M., Lemaire M., **Journées Méc@Proba - Probabilistic Approaches in Engineering Mechanics**, IFMA, June 4, 2009
- Lemaire M., Bourinet J.-M., **Journées Méc@Proba**, IFMA, January 28, 2008
- Lemaire M., Bourinet J.-M., Fogli M., Mébarki A., **Journées Méc@Proba**, Université de Marne-la-Vallée, January 9–10, 2006

B–11 Organization of sessions and mini-symposia in conferences

International conferences:

- Sudret B., Bourinet J.-M., Mahadevan S., Taflanidis A., "Surrogate models for uncertainty quantification, reliability and sensitivity analysis", 12th International Conference on Structural Safety and Reliability (**ICOSSAR 2017**), Vienna, Austria, August 6–10, 2017 (6 papers presented)
- Sudret B., Chatzi E., Bourinet J.-M., "Non-intrusive surrogate models for uncertainty quantification in high dimensions", 7th European Congress on Computational Methods in Applied Sciences and Engineering (**ECCOMAS 2016**), Crete Island, Greece, June 5–10, 2016 (10 papers presented)
- Sudret B., Bourinet J.-M., Gayton N., "Surrogate models for structural reliability analysis", 25th European Safety and Reliability Conference (**ESREL 2015**), Zurich, Switzerland, September 7–10, 2015 (9 papers presented)
- Sudret B., Bourinet J.-M., Mahadevan S., Missoum S., "Surrogate models for uncertainty quantification, reliability analysis and robust design", 12th International Conference on Applications of Statistics and Probability in Civil Engineering (**ICASP12**), Vancouver, Canada, July 12–15, 2015 (20 papers presented)
- Sudret B., Mahadevan S., Missoum S., Bourinet J.-M., Blatman G., "Meta-models / surrogate models for uncertainty quantification, reliability analysis and robust design", 11th International Conference on Structural Safety and Reliability (**ICOSSAR 2013**), New York, NY, USA, June 16–20, 2013 (23 papers presented)
- Sudret B., Bourinet J.-M., Gayton N., Berveiller M., "Meta-models/surrogate models for uncertainty propagation, sensitivity and reliability analysis", 11th International Conference on Applications of Statistics and Probability in Civil Engineering (**ICASP11**), Zurich, Switzerland, August 1–4, 2011 (13 papers presented)
- Lemaire M., Bourinet J.-M., "Machine learning in structural reliability and probabilistic mechanics" (OS8), 10th International Conference on Structural Safety and Reliability (**ICOSSAR 2009**), Osaka, Japan, September 13–17, 2009 (6 papers presented)

French conferences:

- Gayton N., Bourinet J.-M., Dantan J.-Y., Defaux G., Elachachi S.-M., Gogu C., Yalamas T., Session 3 "Fiabilité et Robustesse des Systèmes Mécaniques", 23ème Congrès Français de Mécanique (**CFM 2017**), Lille, August 28–September 1, 2017 (15 papers presented)
- Gayton N., Bourinet J.-M., Dantan J.-Y., Defaux G., Elachachi S.-M., Gogu C., Yalamas T., Session 12 "Fiabilité et Robustesse des Systèmes Mécaniques", 22ème Congrès Français de Mécanique (**CFM 2015**), Lyon, August 24–28, 2015 (16 papers presented)
- Guillaumat L., Schoefs F., Bourinet J.-M., Session 30 "Incertitudes, Fiabilité et Maîtrise des Risques", 20ème Congrès Français de Mécanique (**CFM 2011**), Besançon, August 29–September 2, 2011 (16 papers presented)

B–12 Participation in scientific committees of conferences

International conferences:

- 3rd International Conference on Uncertainty Quantification in Computational Sciences and Engineering (**UNCECOMP 2019**), Crete Island, Greece, June 24–26, 2019
- 13th International Conference on Applications of Statistics and Probability in Civil Engineering (**ICASP13**), Seoul, South Korea, May 26–30, 2019

- 27th European Safety and Reliability Conference (**ESREL 2017**), Portorož, Slovenia, June 18–22, 2017
- 2nd International Conference on Uncertainty Quantification in Computational Sciences and Engineering (**UNCECOMP 2017**), Island of Rhodes, Greece, June 15–17, 2017
- **TensiNet - COST Action TU1303 Symposium 2016** on Novel Structural Skins, Newcastle, UK, October 26–28, 2016
- 25th European Safety and Reliability Conference (**ESREL 2015**), Zurich, Switzerland, September 7–10, 2015
- 12th International Conference on Applications of Statistics and Probability in Civil Engineering (**ICASP12**), Vancouver, Canada, July 12–15, 2015
- 1st International Conference on Uncertainty Quantification in Computational Sciences and Engineering (**UNCECOMP 2015**), Crete Island, Greece, May 25–27, 2015
- **Uncertainty 2014**, Rouen, France, June 23–27, 2014
- **IUTAM Symposium on Multiscale Problems in Stochastic Mechanics**, Karlsruhe, Germany, June 25–29, 2012

French conferences:

- 2nd Uncertainty Modeling for ElectroMagnetic Applications Workshop (**UMEMA 2016**), Paris, July 4–5, 2016
- 9ème Journées Nationales de la Fiabilité des Matériaux et des Structures (**JFMS 2016**), Nancy, March 31–April 1, 2016
- 8ème Journées Nationales de la Fiabilité des Matériaux et des Structures (**JFMS 2014**), Aix-en-Provence, April 9–10, 2014
- 7ème Journées Nationales de Fiabilité (**JN'Fiab 2012**), Chambéry, June 4–6, 2012
- 6ème Journées Nationales de Fiabilité (**JN'Fiab 2010**), Toulouse, March 24–26, 2010

B–13 Participation in PhD evaluation committees as examiner

- S. Dubreuil, Université Paul Sabatier, Toulouse, December 10, 2014
- O. Pasqualini, Université de Nantes, Nantes, October 28, 2013
- X.-H. Dang, Université Blaise Pascal, Clermont-Ferrand, October 11, 2012
- N. Roussouly, Université Paul Sabatier, Toulouse, December 16, 2011
- S. Kadry, Université Blaise Pascal, Clermont-Ferrand, May 16, 2007
- N. Gayton, Université Blaise Pascal, Clermont-Ferrand, September 26, 2002
- A. Legay, ENS Cachan, Cachan, July 5, 2002

B–14 Invited researchers

Permanent researchers:

- Dr. Sergei Kucherenko, Imperial College, London, UK, September 11–15, 2017
- Prof. Carsten Proppe, KIT, Karlsruhe, Allemagne, April to September 2010

PhD students:

- Maria Steiner, Bauhaus-Universität Weimar, Germany, "Global sensitivity analysis using adaptive LS-SVR surrogate models", October to November 2016
- Sylvain Lacaze, University of Arizona, AZ, USA, "SVC-based reliability assessment", September to December 2012

- Anirban Basudhar, University of Arizona, AZ, USA, "SVC-based reliability assessment", October to December 2010

B–15 Invited and keynote lectures

- Invited lecture, "Adaptive surrogate-based methods for reliability assessment", Uncertainty Modeling for Engineering Applications Workshop (UMEMA 2017), Torino, Italy, November 23-24, 2017
- Invited lecture, "Reliability assessment with SVR adaptive surrogate models", GRK1462 Summer School on Uncertainty in Modeling, Weimar, Germany, September 6, 2016
- Invited lecture, "Méthodes, enjeux et limites pour l'estimation de probabilités d'événements rares - Application aux lignes de transmission", Assemblée Générale du GDR CNRS Ondes, Lyon, France, October 20, 2015
- Invited lecture, "Adaptive SVM surrogate models for reliability assessment", Risk and Reliability Symposium in Honor of Prof. Armen Der Kiureghian, University of Illinois at Urbana-Champaign, IL, USA, October 5, 2015
- Invited lecture, "Strengths and limits of reliability assessment methods - Illustration in the field of electromagnetic compatibility", Uncertainty Modeling for ElectroMagnetic Applications Workshop (UMEMA 2015), Saint Nectaire, France, June 30, 2015
- Keynote lecture, "Reliability assessment with adaptive surrogates based on support vector machine regression", 1st International Conference on Uncertainty Quantification in Computational Sciences and Engineering (UNCECOMP 2015), Crete Island, Greece, May 27, 2015
- Invited lecture, "Reliability assessment based on adaptive Support Vector Machine surrogates", Journée de la Conception Robuste et Fiable - Approches Universitaires et Industrielles (2nde édition), GST AFM Mécanique & Incertain, Paris, France, April 10, 2015
- Invited lecture, "Reliability-based design optimization : bases de l'approche et tentatives d'application à des fonctions coûteuses à évaluer", Journées Optimisation sous Incertitudes & Modèles de Substitution et Optimisation, ONERA, Palaiseau et Toulouse, France, November 12, 2014
- Invited lecture, "Reliability analysis - Application to stochastic damage tolerance", 1st Cenaero Workshop on Damage Tolerant Approaches, Gosselies, Belgium, September 7–8, 2011
- Invited lecture, "Modélisation stochastique d'un chargement d'amplitude variable issue de mesures - Application à l'approche fiabiliste de la tolérance aux dommages", Séminaire Fatigue SF2M "Les chargements de fatigue en conception et validation", Paris, June 16, 2011
- Invited lecture, "Approches probabilistes en mécanique", Séminaire de l'École Doctorale de l'Université Paul Verlaine, Laboratoire de Physique et Mécanique des Matériaux (LPMM), Metz, March 18, 2010
- Invited lecture, "Metamodels in structural reliability and sensitivity analysis", Journées Méc@Proba - Probabilistic Approaches in Engineering Mechanics, IFMA, Clermont Ferrand, France, June 4, 2009
- Invited lecture, "Approche fiabiliste : Exemple d'application en flambage et en propagation de fissures", Sécurité et Sûreté des Structures, Journée IMdR, Paris, October 16, 2007
- Invited lecture, "Methods for reliability estimation and applications using FERUM, from FORM to MC-like simulation", Reliability Seminar, UC Berkeley, Berkeley, CA, USA, July 26, 2007

C List of publications

My scientific publications include 2 book chapters, 13 peer-reviewed journal papers (plus two recently submitted), 30 papers and talks in international conferences, 9 papers and talks in French conferences, and 8 talks in international conferences. The names of the PhD students I co-supervised are underlined in the following list.

C–1 Book chapters

1. **Bourinet J.-M.** (2017a). In: *Risk and reliability analysis: theory and applications*. Ed. by P. Gardoni. Springer Series in Reliability Engineering. Edited Volume in Honor of Prof. Armen Der Kiureghian. Springer International Publishing. Chap. 12: FORM sensitivities to distribution parameters with the Nataf transformation, pp. 277–302. (26 pages).
2. **Bourinet J.-M.** (2014a). In: *Mechanics and Uncertainty*. Ed. by M. Lemaire. John Wiley & Sons. Chap. 2: Modeling uncertainty, reliability analysis - Classification methods (Contribution to), pp. 82–91. (10 pages).

C–2 Peer-reviewed journal papers (submitted)

1. Chabridon V., Balesdent M., **Bourinet J.-M.**, Morio J., Gayton N. (2018b). Reliability-based sensitivity estimators of rare event probability in the presence of distribution parameter uncertainty. *Reliability Engineering & System Safety*. Submitted on November 22, 2017.
2. Steiner M., Lahmer T., **Bourinet J.-M.** (2018). An adaptive sampling method for global sensitivity analysis based on least-squares support vector regression. *Reliability Engineering & System Safety*. Submitted on October 4, 2017.

C–3 Peer-reviewed journal papers

1. Moustapha M., **Bourinet J.-M.**, Guillaume B., Sudret B. (2018). Comparative study of kriging and support vector regression for structural engineering applications. *ASCE-ASME Journal of Risk and Uncertainty in Engineering Systems, Part A: Civil Engineering*, 4(2), p. 04018005.
2. Chabridon V., Balesdent M., **Bourinet J.-M.**, Morio J., Gayton N. (2017a). Evaluation of failure probability under parameter epistemic uncertainty: application to aerospace system reliability assessment. *Aerospace Science and Technology*, 69(Supplement C), pp. 526–537.

3. **Bourinet J.-M.** (2016). Rare-event probability estimation with adaptive support vector regression surrogates. *Reliability Engineering & System Safety*, 150, pp. 210–221.

4. Kouassi A., **Bourinet J.-M.**, Lalléchère S., Bonnet P., Fogli M. (2016). Reliability and sensitivity analysis of transmission lines in a probabilistic EMC context. *Electromagnetic Compatibility, IEEE Transactions on*, 58(2), pp. 561–572.

5. Moustapha M., Sudret B., **Bourinet J.-M.**, Guillaume B. (2016). Quantile-based optimization under uncertainties using adaptive kriging surrogate models. *Structural and Multidisciplinary Optimization*, 54(6). Special issue on Physical, Model, and Statistical Uncertainty in Structural and Multidisciplinary Optimization, pp. 1403–1421.

6. Mattrand C., **Bourinet J.-M.** (2014). The cross-entropy method for reliability assessment of cracked structures subjected to random Markovian loads. *Reliability Engineering & System Safety*, 123, pp. 171–182.

7. Moustapha M., Beck A.T., **Bourinet J.-M.** (2013). Design-point excitation for crack propagation under narrow-band random loading. *International Journal for Uncertainty Quantification*, 3(6). Special issue dedicated to the 1st International Symposium on Uncertainty Quantification and Stochastic Modeling (Uncertainties 2012), pp. 541–554.

8. **Bourinet J.-M.**, Deheeger F., Lemaire M. (2011). Assessing small failure probabilities by combined subset simulation and support vector machines. *Structural Safety*, 33(6), pp. 343–353.

9. Dubourg V., Sudret B., **Bourinet J.-M.** (2011b). Reliability-based design optimization using kriging surrogates and subset simulation. *Structural and Multidisciplinary Optimization*, 44(5), pp. 673–690.

10. Gayton N., Beaucaire P., **Bourinet J.-M.**, Duc E., Lemaire M., Gauvrit L. (2011). APTA: advanced probability-based tolerance analysis of products. *Mechanics & Industry*, 12 (2), pp. 71–85.

11. Mattrand C., **Bourinet J.-M.** (2011). Random load sequences and stochastic crack growth based on measured load data. *Engineering Fracture Mechanics*, 78(17), pp. 3030–3048.

12. Gayton N., **Bourinet J.-M.**, Lemaire M. (2003). CQ2RS: a new statistical approach to the response surface method for reliability analysis. *Structural Safety*, 25(1), pp. 99–121.

13. **Bourinet J.-M.**, Le Houédec D. (1999). A dynamic stiffness analysis of damped tubes filled with granular materials. *Computers & Structures*, 73(1-5), pp. 395–406.

C–4 International conference papers and talks

1. **Bourinet J.-M.** (2017b). Anisotropic-kernel-based support vector regression for reliability assessment. In: *Proc. 12th International Conference on Structural Safety and Reliability (ICOSSAR 2017), Vienna, Austria, August 6–10, 2017*. TU Verlag. (10 pages).

2. Chabridon V., Balesdent M., **Bourinet J.-M.**, Morio J., Gayton N. (2017b). Reliability-based sensitivity analysis of aerospace systems under distribution parameter uncertainty using an augmented approach. In: *Proc. 12th International Conference on Structural Safety and Reliability (ICOSSAR 2017), Vienna, Austria, August 6–10, 2017*. TU Verlag. (10 pages).

3. Steiner M., Lahmer T., **Bourinet J.-M.** (2017b). Investigation of a global adaptive sampling method based on least-squares support vector regression. In: *Proc. GRK International Workshop 2017, Coupled Numerical and Experimental Models in Structural Engineering, Weimar, Germany, April 26–28, 2017*. (8 pages).

4. **Bourinet J.-M.** (2015). Reliability assessment with adaptive surrogates based on support vector machine regression. In: *Proc. 1st International Conference on Uncertainty Quantification in Computational Sciences and Engineering (UNCECOMP 2015), Hersonissos, Crete Island, Greece, May 25–27, 2015*. Ed. by M. Papadrakakis, V. Papadopoulos, G. Stefanou, pp. 652–663. (12 pages).

5. Kouassi A., Lalléchère S., **Bourinet J.-M.**, Bonnet P., Fogli M. (2015). Uncertainty assessment of a coaxial line's capacitance in a stochastic context. In: *Proc. 7th International Conference on Electromagnetics in Advanced Applications (ICEAA 2015), Torino, Italy, September 7–11, 2015*. IEEE, pp. 1526–1529. (4 pages).

6. Moustapha M., Sudret B., **Bourinet J.-M.**, Guillaume B. (2015). Adaptive kriging reliability-based design optimization of an automotive body structure under crashworthiness constraints. In: *Proc. 12th International Conference on Applications of Statistics and Probability in Civil Engineering (ICASP 12), Vancouver, Canada, July 12–15, 2015*. Ed. by T. Haukaas. The University of British Columbia. (8 pages).

7. **Bourinet J.-M.** (2014c). Reliability assessment with sensitivity-based adaptive SVM surrogates. In: *Proc. 11th International Conference on Structural Safety and Reliability (ICOSSAR 2013), New York, NY, USA, June 16–20, 2013*. Ed. by G. Deodatis, B.R. Ellingwood, D.M. Frangopol. CRC Press, pp. 3297–3304. (8 pages).

8. Kouassi A., **Bourinet J.-M.**, Lalléchère S., Bonnet P., Fogli M. (2014a). Fiabilité de fonctionnement et sensibilité CEM pour un problème de ligne de transmission. In: *Proc. 17ème Colloque International et Exposition sur la Compatibilité Electromagnétique (CEM 2014), Clermont Ferrand, France, July 1–3, 2014*. (6 pages).

9. Kouassi A., **Bourinet J.-M.**, Lalléchère S., Bonnet P., Fogli M. (2014b). Safety assessment of a transmission line with EMC requirements. In: *Proc. XXXIth URSI General Assembly and Scientific Symposium (URSI GASS), Beijing, China, August 16–23, 2014*. IEEE. (4 pages).

10. Moustapha M., Sudret B., **Bourinet J.-M.**, Guillaume B. (2014a). Metamodeling for crashworthiness design: comparative study of kriging and support vector regression. In: *Proc. 2nd International Symposium on Uncertainty Quantification and Stochastic Modeling (Uncertainties 2014), Rouen, France, June 23–27, 2014*. Ed. by M. Lemaire, E. Souza de Cursi, pp. 279–286. (8 pages).

11. Moustapha M., Sudret B., **Bourinet J.-M.**, Guillaume B. (2014b). Reliability-based design optimization of an automotive body structure under crashworthiness constraints. In: *Proc. 17th IFIP WG 7.5 Working Conference on Reliability and Optimization of Structural Systems, Huangshan, China, July 3–7, 2014*. (8 pages).

12. **Bourinet J.-M.**, Mattrand C. (2013). Damage tolerance and reliability assessment under random Markovian loads. In: *Procedia IUTAM*. Ed. by C. Proppe, J.-M. Bourinet. Vol. 6. IUTAM Symposium on Multiscale Problems in Stochastic Mechanics, Karlsruhe, Germany, June 25–29, 2012. Elsevier, pp. 123–131. (9 pages).

13. Moustapha M., **Bourinet J.-M.**, Beck A.T. (2012). Design-point excitation for crack propagation under narrow-band random loading. In: *Proc. 1st International Symposium on Uncertainty Quantification and Stochastic Modeling (Uncertainties 2012), Maresias, São Sebastião, SP, Brazil, February 26–March 2, 2012*. Editora Cubo. (14 pages).

14. Sudret B., Dubourg V., **Bourinet J.-M.** (2012). Enhancing meta-model-based importance sampling by subset simulation. In: *Proc. 16th IFIP WG 7.5 Working Conference on Reliability and Optimization of Structural Systems, Yerevan, Armenia, June 24–27, 2012*. Ed. by A. Der Kiureghian, A. Hajian. AUA Press, Yerevan, Armenia. (8 pages).

15. Dubourg V., **Bourinet J.-M.**, Sudret B., Cazuguel M. (2011a). Reliability-based design optimization of an imperfect submarine pressure hull. In: *Proc. 11th International Conference on Applications of Statistics and Probability in Civil Engineering (ICASP 11), Zürich, Switzerland, August 1–4, 2011*. Ed. by M.H. Faber, J. Köhler, K. Nishijima. CRC Press, pp. 703–711. (8 pages).

16. Mattrand C., **Bourinet J.-M.**, Lemaire M., Bernard P., Fogli M. (2011a). Modeling and simulation of stochastic fatigue load sequences derived from in-flight load data. In: *Proc. 13th AIAA Non Deterministic Approaches Conference, Denver, CO, USA, April 4–7, 2011*. American Institute of Aeronautics and Astronautics. (17 pages).

17. Mattrand C., **Bourinet J.-M.**, Théret D. (2011b). Analysis of fatigue crack growth under random load sequences derived from military in-flight load data. In: *Proc. ICAF 2011 Structural Integrity: Influence of Efficiency and Green Imperatives, Montréal, Canada, May 29–30, 2011*. Ed. by J. Komorowski. Springer Netherlands, pp. 399–413. (16 pages).

18. Dubourg V., **Bourinet J.-M.**, Sudret B. (2010a). A hierarchical surrogate-based strategy for reliability-based design optimization. In: *Proc. 15th IFIP WG 7.5 Working Conference on Reliability and Optimization of Structural Systems, Munich, Germany, April 7–10, 2010*. Ed. by D. Straub. CRC Press, pp. 53–60. (8 pages).

19. **Bourinet J.-M.**, Mattrand C., Dubourg V. (2009). A review of recent features and improvements added to FERUM software. In: *Proc. 10th International Conference on Structural Safety and Reliability (ICOSSAR 2009), Osaka, Japan, September 13–17, 2009*. Ed. by H. Furuta, D.M. Frangopol, M. Shinozuka. CRC Press. (8 pages).

20. Dubourg V., Noirfalise C., **Bourinet J.-M.**, Fogli M. (2009b). FE-based reliability analysis of the buckling of shells with random shape, material and thickness imperfections. In: *Proc. 10th International Conference on Structural Safety and Reliability (ICOSSAR 2009), Osaka, Japan, September 13–17, 2009*. Ed. by H. Furuta, D.M. Frangopol, M. Shinozuka. CRC Press. (8 pages).

21. **Bourinet J.-M.**, Lemaire M. (2008). FORM sensitivities to correlation: application to fatigue crack propagation based on Virkler data. In: *Proc. 4th International ASRANet Colloquium, Athens, Greece, June 25–27, 2008*. Ed. by P.K. Das. (10 pages).

22. Dubourg V., Noirfalise C., **Bourinet J.-M.** (2008). Reliability-based design optimization: an application to the buckling of imperfect shells. In: *Proc. 4th International ASRANet Colloquium, Athens, Greece, June 25–27, 2008*. Ed. by P.K. Das. (10 pages).

23. Lemaire M., Deheeger F., **Bourinet J.-M.** (2008). Reliability analysis with an approximate response of the mechanical model: ^{2}SMART method. In: *Proc. 7th International Conference on Reliability of Materials and Structures (RELMAS'2008), Saint Petersburg, Russia, June 17–20, 2008*. Ed. by B. Melnikov, S.V. Petinov, Y.E. Hangu. Polytechnical Publishing House. (3 pages).

24. Nešpůrek L., **Bourinet J.-M.**, Gravouil A., Lemaire M. (2006). Some approaches to improve the computational efficiency of the reliability analysis of complex crack propagation problems. In: *Proc. 3rd ASRANet International Colloquium, Glasgow, United Kingdom, July 10–12, 2006*. Ed. by P.K. Das, M.K. Chryssanthopoulos. ASRANet Ltd. (10 pages).

25. Nešpůrek L., **Bourinet J.-M.**, Gravouil A., Lemaire M. (2005). Probabilistic approach to crack propagation based on XFEM and FORM. In: *Proc. Fatigue Design 2005, Senlis, France, November 16–18, 2005*. CETIM. (7 pages).

26. **Bourinet J.-M.**, Gayton N., Lemaire M., Combescure A. (2001). Plastic collapse of imperfect submarine pressure hulls: a probabilistic approach. In: *Proc. 8th International Conference on Structural Safety and Reliability (ICOSSAR 2001), Newport Beach, CA, USA, June 17–22, 2001*. Ed. by R.B. Corotis, G.I. Schuëller, M. Shinozuka. Balkema. (8 pages).

27. **Bourinet J.-M.**, Gayton N., Lemaire M., Combescure A. (2000). Reliability analysis of stability of shells based on combined finite element and response surface methods. In: *Proc. 4th International Colloquium on Computation of Shell & Spatial Structures (IASS-IACM 2000), Chania, Crete, Greece, June 5–7, 2000*. Ed. by M. Papadrakakis, A. Samartin, E. Oñate. (20 pages).

28. Gayton N., **Bourinet J.-M.**, Lemaire M. (2000). A new tool for response surface approach of structural reliability in reliability and optimization of structural systems. In: *Proc. 9th IFIP WG 7.5 Working Conference on Reliability and Optimization of Structural Systems, Ann Arbor, MI, USA, September 25–27, 2000*. Ed. by A.S. Nowak, M.M. Szerszen. (8 pages).

29. **Bourinet J.-M.**, Le Houédec D. (1997). Vertical vibrations of granular materials between two parallel horizontal walls. In: *Proc. 3rd International Conference on Powders and Grains (Powders and Grains 97), Durham, NC, USA, May 18–23, 1997*. Ed. by R.P. Behringer, J.T. Jenkins. Balkema, pp. 413–416. (4 pages).

30. **Bourinet J.-M.**, Le Houédec D. (1996). Damping of tubes filled with granular materials: a non-conservative dynamic stiffness analysis. In: *Proc. 3rd International Conference on Computational Structure Technology (CST96), Budapest, Hungary, August 21–23, 1996*. Ed. by B.H.V. Topping. Vol. Advances in Finite Element Techniques. Civil-Comp Press, pp. 289–299. (11 pages).

C–5 French conference papers and talks

1. Chabridon V., Gayton N., **Bourinet J.-M.**, Balesdent M., Morio J. (2017c). Some Bayesian insights about the APTA method for statistical tolerance analysis. *Proc. 23ème Congrès Français de Mécanique (CFM 2017), Lille, France, 28 août–1er septembre 2017*. Association Française de Mécanique. (12 pages).

2. Dubourg V., **Bourinet J.-M.**, Sudret B., Cazuguel M. (2012a). Optimisation du dimensionnement au flambement d'une coque résistante de sous-marin sous contrainte de fiabilité. *Proc. 18ème Congrès de Maîtrise des Risques et de Sûreté de Fonctionnement ($\lambda\mu$ 18), Tours, France, 16–18 octobre 2012*. IMDR. (12 pages).

3. Dubourg V., Sudret B., **Bourinet J.-M.**, Cazuguel M. (2011c). Optimisation sous contrainte de fiabilité d'une structure en treillis. *Proc. 10ème Colloque National en Calcul de Structures (CSMA2011), Giens, France, 9–13 mai 2011*. CSMA.

4. Dubourg V., **Bourinet J.-M.**, Sudret B. (2009a). Analyse fiabiliste du flambage des coques avec prise en compte du caractère aléatoire et de la variabilité spatiale des défauts de forme et d'épaisseur, et des propriétés matériaux. *Proc. 19ème Congrès Français de Mécanique (CFM19), Marseille, France, 24–28 août 2009*. Ed. par C. REY, P. BONTOUX, A. CHRISOCHOOS. Association Française de Mécanique. (6 pages).

5. Deheeger F., **Bourinet J.-M.**, Lemaire M. (2008a). Classification par support vector machine pour la conception fiable en mécanique. *Proc. 9ème Congrès de la Société Française de Recherche Opérationnelle et d'Aide à la Décision (Roadef'08), Clermont-Ferrand, France, 25–27 février 2008*. (2 pages).

6. Deheeger F., Pendola M., Lemaire M., **Bourinet J.-M.** (2008b). Apprentissage stochastique pour les calculs de fiabilité de systèmes représentés par des modèles complexes. *Proc. 16ème Congrès de Maîtrise des Risques et de Sûreté de Fonctionnement ($\lambda\mu$ 16), Avignon, France, 6–10 octobre 2008*. IMDR. (8 pages).

7. Noirfalise C., **Bourinet J.-M.**, Fogli M., Cochelin B. (2007a). Analyse fiabiliste de la stabilité des coques minces imparfaites basée sur la méthode asymptotique numérique. *Proc. 8ème Colloque National en Calcul de Structures (CSMA2007), Giens, France, 21–25 mai 2007*. CSMA. (6 pages).

8. Noirfalise C., **Bourinet J.-M.**, Fogli M., Cochelin B. (2007b). Approche fiabiliste de la stabilité des coques minces avec imperfections géométriques aléatoires. *Proc. 18ème Congrès Français de Mécanique (CFM07), Grenoble, France, 27–31 août 2007*. Ed. par J. ETAY, E. HOPFINGER, P. MARTY. Association Française de Mécanique. (6 pages).

9. **Bourinet J.-M.**, Le Houédec D. (1995). Amortissement par matériau granulaire : une approche de type raideur dynamique. *Proc. 12ème Congrès Français de Mécanique (AUM 95), Strasbourg, France, 4–8 septembre 1995*. Vol. 4. Association Universitaire de Mécanique, p. 61-64. (4 pages).

C–6 International conference talks

1. Sallin M., **Bourinet J.-M.**, Clair D., Fogli M., Colin B. (2017). Uncertainty propagation in nonlinear structural dynamics of ground military vehicles. 2nd International Conference on Uncertainty Quantification in Computational Sciences and Engineering (UNCECOMP 2017), Island of Rhodes, Greece, June 15–17, 2017.

2. Steiner M., Lahmer T., **Bourinet J.-M.** (2017a). Investigation of a global adaptive sampling method based on least-square support vector regression. Joint Annual Meeting of GAMM, Weimar, Germany, March 6–10, 2017.

3. Dubourg V., Sudret B., **Bourinet J.-M.** (2012b). Meta-model-based importance sampling for reliability sensitivity analysis. 2012 Joint Conference of the Engineering Mechanics Institute and 11th ASCE Joint Specialty Conference on Probabilistic Mechanics and Structural Reliability (EMI/PMC 2012), South Bend, IN, USA, June 17–20, 2012.

4. Dubourg V., **Bourinet J.-M.**, Sudret B. (2010b). Reliability-based design optimization using hierarchical Gaussian processes surrogates. 4th European Conference on Computational Mechanics (ECCM 2010), Paris, France, May 16–21, 2010.

5. Lebon J., **Bourinet J.-M.**, Yalamas T., Lemaire M. (2009). Efficient methods in fragility curves calculation. Seismic Risk in Moderate Seismicity Area: from hazard to vulnerability (Provence' 2009), Aix en Provence, France, July 6–8, 2009.

6. Noirfalise C., **Bourinet J.-M.**, Fogli M., Cochelin B. (2008). Reliability analysis of the buckling of imperfect shells based on the Karhunen-Loève expansion. 5th European Congress on Computational Methods in Applied Sciences and Engineering (ECCOMAS 2008), Venice, Italy, June 30–July 5, 2008.

7. **Bourinet J.-M.**, Nešpůrek L., Lemaire M. (2007). Reliability approach of crack propagation based on the extended finite element method. International Conference on Computational Fracture and Failure of Materials and Structures (CFRAC 2007), Nantes, France, June 11–13, 2007.

8. Noirfalise C., **Bourinet J.-M.**, Fogli M., Cochelin B. (2007c). Reliability assessment of imperfect shells subject to buckling based on the asymptotic numerical method. 9^{th} US National Congress on Computational Mechanics (USNCCM9), San Francisco, CA, USA, July 23–26, 2007.